Investigation and Evaluation of Rock Mass Characteristics for Development of New TBM Performance Prediction Model in Hard Rock Conditions

Von der Fakultät für Bau- und Umweltingenieurwissenschaften
der Universität Stuttgart
zur Erlangung der Würde eines Doktors der Ingenieurwissenschaften (Dr.-Ing.)
genehmigte Abhandlung

vorgelegt von
ALIREZA SALIMI
aus Babol, Iran

Hauptberichter:	Prof. Dr.-Ing. habil. Christian Moormann
Mitberichter:	Prof. Dr. Jamal Rostami
	Prof. Dr.-Ing. Thomas Marcher

Tag der mündlichen Prüfung: 29.04.2021

Institut für Geotechnik der Universität Stuttgart
2021

Mitteilung 76
des Instituts für Geotechnik
Universität Stuttgart, Deutschland 2021

Herausgeber:
Univ.-Prof. Dr.-Ing. habil. Christian Moormann

Institut für Geotechnik
Universität Stuttgart
Pfaffenwaldring 35
70569 Stuttgart

Schlagwörter: Tunnel Boring Machine (TBM), TBM performance, Penetration rate, Regression analysis, Artificial intelligence algorithm, Classification and regression tree (CART), Genetic programming (GP).

Druck: DCC Kästl e.K., Ostfildern-Kemnat, Stuttgart, Deutschland, 2021

ISBN 978-3-921837-76-6
(D93 – Dissertation, Universität Stuttgart)

Preface

Tunnelling using the Tunnel Boring Machine (TBM) approach has become widely used and is currently an important method employed by the tunnelling industry. The development of TBM technology has made the approach applicable in an increasingly wider range of rock mass conditions. Technically speaking, excavations can now be carried out in almost all rock conditions using this method, given certain economic constraints. The use of TBMs involves major investments and high levels of geological risk. Performance and cutter consumption have a great influence on the successful execution of mechanised tunnelling, especially in hard rock conditions. Furthermore, the method requires accurate predictions of TBM performance and costs, which in turn facilitate the control of risk and enable projects to avoid delays and budget overruns. Penetration rate is a principal measure of TBM performance and is used to evaluate the feasibility of using a machine in a given ground condition and to predict TBM advance rate.

The interaction between the rock mass and the machine is a process of great complexity meaning that estimation of penetration rate is a complex process that not only depends on intact and rock mass properties (strength, fractures, and texture of rock etc.) but also machine specifications, including thrust and torque requirement. Developing a predictive model which can take all these parameters into consideration has been always a challenge. This is the reason for limited success of existing models and lack of a single universal model for TBM performance prediction even after over six decades of use of these machines. In fact, performance predictions and is not straightforward issues and involve major risk assessments, especially in hard rock conditions. In last two decades, many performance predictions models have been offered by various researchers to estimate penetration rate of hard rock tunnel boring machines in new tunnelling projects which can be categorized in two main groups, namely theoretical and empirical methods. Apart from empirical and theoretical models, the use of artificial intelligence (AI) and machine learning (ML) techniques has received widespread attention in TBM performance prediction. Machine learning is a branch of artificial intelligence that consists of developing algorithms able to generalize behaviours from information provided in the form of examples. The flexible nature of the AI techniques makes them powerful tools in approximating and solving engineering problems more specifically when the problem is highly complex and nonlinear. The fact is that ML methods have appeared as alternative techniques to conventional statistical techniques. In this respect, while the domain and common method employed for TBM performance prediction is Artifical Neural Network (ANN), Dr. Salimi has conducted two robust machine learning methods, namely Adative Neuro-Fuzzy Inference System (ANFIS) and Support Vector Regression (SVR) during his PhD program at IGS. However, the results of most of previous studies in this area have been ′black or opaque box′ programs that show high correlation between their predicted rates and actual machine performance but cannot be used in estimating machine performance in other projects. Besides that, although various empirical models and artificial intelligence methods for performance prediction of hard rock TBMs are available, many lacks the correct context of input geotechnical parameters to account for the possible range of variation of such parameters.

The main goal of the present work is to develop a new empirical model in terms of field penetration index (FPI) of a TBM via statistical analysis (regression analysis), as well as artificial intelligence algorithm including tree-based-regression model such as, Classification & Regression Tree (CART) and Genetic Programming (GP) which is known as ′white or transparent box′ solutions for the prediction of TBM performance in hard rock conditions by presenting graph and mathematical equation, respectively. More attention is paid to introduce new models that incorporate rock mass classification systems such as rock mass rating (RMR). In fact, this study is dealing with the new era of data analysis and subsequently this is the first time, these methods have been employed. In the area of rock engineering and data analysis, the suitability of data mining techniques is closely related to the comprehensibility of the obtained model.

The dissertation study begins with a detailed review of the parameters affecting of TBM performance in hard rock conditions and review of the available hard rock TBM performance prediction models. The study conducted by Dr. Salimi compiled a database from seven tunnelling projects with total length of 70.73 km and boring diameter 3.6 m to 10.5 m in different geological conditions representing a really valuable database of TBM field performance in hard rock. This database is subjected to systematic step by step statistical analysis to derive new empirical regression formulas for estimation of field penetration index (FPI). The data was subsequently analysed by artificial intelligence (AI) methods containing CART and GP. A ′graph/mathematical equation′ is offered for improving performance prediction for hard rock TBMs while incorporating rock type in the analysis with special emphasis on application of rock mass classification systems such as rock mass rating (RMR). The results show that the proposed chart/graph via CART offers more accurate results, compared to the previous common models such as CSM, NTNU and Q_{TBM} and the CART model.

Dr. Salami's investigation shows the great potential of the AI method notably CART for estimation of TBM performance in hard rock conditions. Besides that, the thesis of Dr. Salimi indicates that the AI model he developed is a powerful and versatile model for not only understanding the complexity of the rock mass interaction and machine performance since the impact of each variable on the target can be obviously clarified by the addressed tree structure in a CART model but also for estimation of TBM penetration rate with high level of reliability and accuracy.

Stuttgart, April 2021

Univ.-Prof. Dr.-Ing. habil. Christian Moormann

Acknowledgments

The investigation presented in this thesis is a result of the work carried out in the years of 2013-2019 at the Institute of Geotechnical Engineering, University of Stuttgart. No doubt, this research could only be accomplished by the support of number of people to whom I would like to express my gratitude. First and foremost, I would like to express my sincere appreciation to my thesis supervisor Professor Christian Moormann for his guidance, motivation as well as for the significant support during the whole of my Ph.D. study. My gratitude extends to Professor Jamal Rostami for the priceless contribution, direction, and inspiration. His advice on the research has been invaluable and without it, I would never step so far in the academic road. Also, I am grateful to Prof. Thomas Marcher for his valuable comments and guidance through my Ph.D. study.

Here, I would like to especially thank Prof. T.N. Singh and Drs. Prasnna Jain, Amir Asad Fatemi, Andrea Delisio, Masoud Zare Naghadehi, and above all, Dr. Jafar Hassanpour "Associate Professor at the University of Tehran" for sharing their data for developing the TBM database used in this study. Last but not least, I express my appreciation to Prof. Masoud Monejzi for his help in the application of Artificial Intelligence (AI) algorithm. Also, I feel obligated to thank my colleagues at IGS for being such a good team. Particularly from the IGS people: Bernd Zweschper, Patrik Buhmann, Linus Klein, Johannes Aschrafi, Johannes Labenski, Julia Knopp, Farzad Fatemizadeh, Matin Liaghi, Rainer Worbes, Felix Mitlmeier, Shreyas Giridharan, Sujith Gowda, Alessandro Miraldi, Nadja Springer, Birgit Hagenau as well as Dr. Bernhard Westrich. I have all but nice memories and enjoyed good interactions with the team. Moreover, I would like to show my gratitude to "Landesgraduiertenförderungsgesetz" (LGFG) for funding my Ph.D. research. Finally, I am deeply indebted to my wife and long-life partner Dr. Sahar Khodami for her endless love, continual support, and understanding. A special appreciation to my mother Mrs. Halimeh Khatoon Asadi for her unlimited support, love whom God has added an Angel into the Heaven. I am speechless for all the sacrifices you made all throughout my life. I am certain that, Mum would have been extremely proud to see this. I have dedicated this work to you, Mum.

Rest in Peace Mum!

Alireza Salimi

Stuttgart, May 2021

In Memory of My Mother

Halimeh Khatoon (Ashraf)

Asadi

(1943-2020)

“Only a life lived for others is a life worthwhile”, Albert Einstien

Table of Content

Main symbols and abbreviations

Symbol	Unit	Description
AR	m/h	Advance Rate
ARA	m/h	Average Advance Rate
BI	kN/cutter/mm/rev	Boreability Index
$BI_{(1)}$	kN/cutter/mm/rev	Specific Rock Mass Boreability Index
Bi (P_s)	kN/mm	Brittleness Index (Peak Slope Index)
BTS or σ_t	MPa	Brazilian Tensile Strength
d_c	Mm	Diameter of Cylinder
d_{TBM}	M	Machine Diameter
E	Ksi	Elasticity Modulus
FN	kN	Normal Force
F_N	kN/Cutter	Cutting Force per Cutter
FPI	kN/cutter/mm/rev	Field Penetration Index
FPI blocky	kN/mm/rev	Field Penetration Index in Blocky Condition
F_R	kN	Rolling Force
F_S	kN	Side Force
I	m/h	Net Penetration Rate
i_o	mm/rev	Basic Net Penetration Rate
I_T	A	Machine Ampere
Jc	-	Joint Characteristics, Partial Rating in Basic RMR
Js	Cm	Joint Spacing
P	mm/rev	Cutter Penetration per each Cutterhead Revolution
P_c	MPa	Hydraulic Oil Pressure in Cylinder
Po	PW	Power of Machine

Symbol	Unit	Description
P^{o}	MPa	Pressure of Contact Area
q	%	Percentage of Quartz
R	mm	Cutter Radius
ROP	m/h	Rate of Penetration
RPM	rev/min	Cutterhead Rotational Speed
RQD	%	Rock Quality Designation
S	mm	Spacing of Cutters
SER	(m^3/rev)/(kN/cutter)	Specific Excavation Rate
$SIGMA$	MPa	Rock Mass Strength
SP	mm/rev/kN/cutter	Specific Penetration
T	mm	Cutter Tip Width
T_f	kN	Friction Force between Shield and Tunnel Wall
Th	MPa	Total Thrust Force
T_q	kN-m	Cutterhead Torque
T_{tow}	kN	Tow Force or Resistance of Back-up System
U	%	Utilization Rate
UCS or σ_c	MPa	Uniaxial Compressive Strength (Unconfined Compressive Strength)
UCS_{rm}	MPa	Uniaxial Compressive Strength of Rock Mass
U_T	V	Machine Voltage
V_b	m^3	Block Volume
w_f	$m^3 10^{-6}$	Specific Failure Energy
W_f	Nm	Failure Energy
α	°	Smallest Angle between a Fracture Set and the Tunnel Axis
β	°	Angle between the tunnel axis and the dip direction of intersection of foliation and joint set
α_f	°	Dip Angle Discontinuity

Symbol	Unit	Description
α_s	°	Strike Angle Discontinuity
α_t	°	Tunnel Direction
σ_θ	MPa	Tangential Stress at Side Wall
σ_{cm}	MPa	Uniaxial Compressive Strength of Rock Mass
Ψ	-	Power of Pressure Function
ϕ	Rad	Angle of Contact Area Between Rock and Cutter
ν	-	Poisson's ratio

Abbreviations	Meaning
ABR	LCPC Abrasivity Index
ANFIS	Adaptive Neuro-Fuzzy Inference System
AI	Artificial Intelligence
ANN	Artificial Neural Network
AV/AVS	NTNU Abrasion Test
BTCR	Boosted Tree Classifiers and Regression
CAI	Cerchar Abrasivity Index
CART	Classification and Regression Tree
C_C	Cutting Coefficient
CLI	Cutter Life Index
CFF	Core Fracture Frequency
CHAID	Chi-squared Automatic Interaction Detector
CT	Classification Tree
CSM	Colorado School of Mines
DRI	Drilling Rate Index
DT	Decision Tree
EA	Evolutionary Algorithms
E-CHAID	Exhaustive Chi-squared Automatic Interaction Detector
FIS	Fuzzy Inference System
FL	Fuzzy logic
GA	Genetic Algorithm
GP	Genetic Programming
GSI	Geological Strength Index
Gw	Ground Water Condition (Partial Rating in RMR)
Hrs	Number of Working Hours per Day
ICA	Imperialism Competitive Algorithm
$i(t)$	Impurity function
$i(t_p)$	Impurity value for parent node

Abbreviations	Meaning
$i(t_c)$	Impurity value for child node
$i(t_l)$	Impurity value for left child node
$i(t_r)$	Impurity value for right child node
$\Delta i(\mathrm{t})$	Change of impurity
I_G	Gini Index
Jc	Joint Characteristics, Partial Rating in RMR
J_p	Jointing Parameter
J_v	Volumetric Joint Count
K	Number of classes
k	Index of classes
K_s	Rock Mass Fracturing Factor
K_{ekv}	Equivalent Rock Mass Fracturing Factor
K_{s-tot}	Total Rock Mass Fracturing Factor
LCM	Linear Cutting Machine
M	Number of variables in the learning sample
M_1	Critical Thrust
MAD	Mean Absolute Deviation
MAPE	Mean Absolute Percentage Error
MB	Gross Average Cutter Thrust
M_{ekv}	Equivalent Cutter Thrust
MLRA	Multiple linear Regression Analysis
MNLRA	Multiple Non-linear Regression Analysis
MSE	Mean Square Error
N	Number of observations in learning sample
N_c	Number of Cylinder
n_m	Number of Motors

Abbreviations	Meaning
$N_{\min}$	Minimum number of observations parameters
Ns	Number of Shifts per Day
N_{TBM}	Number of Disc Cutters
NTNU	Norwegian University of Science and Technology
PCA	Principal Component Analysis
$p(k\mid t)$	Conditional probability of class k provided we are in node t
P_l	Probability of left node
P_r	Probability of right node
PSO	Particle Swarm Optimization
Q	Rock Mass Quality Index
QUEST	Quick, Unbiased, Efficient Statistical Tree
R^2	Correlation Coefficient
R_C	Rolling Coefficient
R_F	Penetration Index
RFI	Rock Fracture Index
RFRC	Random Forest Regression and Classification
r_{mc}	Average Weight of Cutter Distance from Centre of Rotation
RME	Rock Mass Excavability
RMR	Rock Mass Rating
RMSE	Root Mean Square Error
RSR	Rock Structure Rating
RT	Regression Tree
RTC	Rock Type Code
S	Hoek-Brown Failure Criterion
SSE	Sums of squares error
SA	Sensitivity Analysis
SE	Specific Energy
S_{20}	Brittleness Value

Abbreviations	**Meaning**
SF	Safety Factor
SJ	Sievers' J-value
SRF	Strength Reduction Factor
SVR	Support Vector Regression
T''	Number of terminal nodes in tree
α''	Cost complexity measure/parameter
TBM	Tunnel Boring Machine
t	Index of node
t_l	Child left node
t_r	Child right node
t_P	Parent node
VAF	Variance Account For
VHN	Vickers Hardness Number
VIF	Variance Inflation Factor
X	$[N \times M]$ matrix of variables in learning sample
x_j^R	Best splitting value of variable x_j
Y	$[M \times 1]$ vector of class/response values in learning sample

Abstract

Hard rock tunnel boring has become more or less the standard method of tunnelling for tunnels of various sizes with length over 1.5-2 km, because of several advantages compared to conventional excavation methods. This includes higher possible advance rates and generally improved safety conditions. Prediction of TBM performance is a key factor for planning, cost estimation/control, and selection of proper machine specification to achieve efficient and safe operation. Rate of penetration (ROP) defined as the distance excavated divided by the operating time during a continuous excavation phase is a principal measure of TBM performance and is used to evaluate the feasibility of using the mechanized tunnelling. Machine daily advance rate is estimated by multiplying ROP by machine utilization (U) and hours of work per day.

During the past three decades, numerous TBM performance prediction models have been proposed which can be divided into two distinguished approaches, namely theoretical and empirical ones. Theoretical models analyse cutting forces acting on disc cutter to estimate ROP based on force equilibrium equations. Laboratory cutting tests provide a basic understanding of rock fragmentation and the force-penetration behaviour of rocks are the basis for this class of performance prediction models. The main disadvantage of these models is that they do not completely represent the site parameters relative to rock mass conditions, in particular joints, as the TBM disc cutters would encounter in the field. Empirical models are primarily based on observation of field performance of the TBMs. As such, they do not directly account for cutting force, cutter geometry, cutting geometry, and ability to estimate machine thrust and torque/power relative to detailed cutter head design.

Estimation of penetration rate is a complex process that not only depends on intact and rock mass properties (strength, fractures, and texture of rock) but also machine specifications, including thrust and torque requirements. One should keep in mind that developing a predictive model which can take all these parameters into consideration has been always a problem. This is the reason for the limited success of existing models and lack of a single universal model for TBM performance prediction even after over six decades of use of these machines. To improve the capability of the models for accurately predicting ROP of hard rock TBMs, data from various projects with the different rock mass conditions and machine types have been obtained from pertinent research groups and compiled in a database. This includes the intact rock properties, rock mass characteristics, the corresponding machine operating parameters, and observed performance.

The main goal of this investigation was to develop a new model which incorporates both the intact rock and rock mass properties as well as TBMs specifications (operational and design parameters) to estimate ROP. In particular, following is the list of main accomplishments of the study: a) analysis of the TBM performance to identify the main parameters affecting machine performance and their impact; b) statistical analysis of data to develop new empirical models for prediction of TBM rate of penetration; c) application of artificial intelligence algorithms (Regression tree and Genetic Programming, GP) to improve the accuracy of TBM performance prediction models by offering pertinent graphs and formulas, d) validate the predictive capabilities of the proposed models for application in different geological conditions. The results show that, the proposed models that were generated by statistical regression or use of regression tree offer a quick estimate of TBM performance with reasonable accuracy and efficiency.

The best results seem to be offered by using the regression tree (CART) system where input parameters used in RMR rock mass classification system such as UCS, RQD, Js, and Jc are used to represent the rock mass to predict field penetration index (FPI) which represents the normalized machine performance that incorporates machine size and RPM, cutterload (or by extension cutterhead thrust). The results show that the CART models and the tree that it offers can offer reasonable estimates of the machine performance based on the 61.03 km of data that has been analysed from various rock types and machine sizes and types. Another advantage of CART is that it can be used by anyone for the prediction of the machine performance, in contrast to the other artificial intelligent approaches that require specialized and proprietary computer programs. The accuracy of the proposed CART model in this study is validated/evaluated by comparing the results of its prediction with other world-wide common TBM performance prediction models including, CSM, NTNU, and Q_{TBM}. This comparison was based on available geotechnical information from site investigation and as-built geological data collected during the construction phase of Lot 2 of Zagros water conveyance tunnel (ZWCT) in Iran. The results show that, the CART model which was developed based on a sufficient diverse database of machine performance can provide a more accurate prediction of machine performance compared to other mentioned methods.

Zusammenfassung

Der Hartgesteinstunnelvortrieb hat sich mehr oder weniger als Standardmethode für Tunnel mit unterschiedlichen Durchmessern und Vortriebsstrecken von über 1,5-2 km durchgesetzt, da er im Vergleich zu konventionellen Vortriebsmethoden mehrere Vorteile aufweist. Dazu gehören höhere mögliche Vortriebsraten und allgemein verbesserte Sicherheitsbedingungen. Die Prognose der TBM-Leistung ist ein Schlüsselfaktor für die Planung, Kostenabschätzung/-kontrolle und die Auswahl der richtigen Maschinenspezifikation, um einen effizienten und sicheren Betrieb zu erreichen. Die Vortriebsleistung (ROP), definiert als die gefahrene Strecke geteilt durch die Betriebszeit während einer kontinuierlichen Vortriebsphase, ist ein Schlüsselindikator für die TBM-Leistung und wird zur Beurteilung der Machbarkeit des Einsatzes des maschinellen Vortriebs verwendet. Die tägliche Vortriebsleistung der Maschine wird durch Multiplikation von ROP mit der Maschinenauslastung (U) und den Arbeitsstunden pro Tag geschätzt. In den letzten drei Jahrzehnten wurden zahlreiche Modelle zur Vorhersage der TBM-Leistung vorgeschlagen, die in zwei unterschiedliche Ansätze unterteilt werden können, nämlich in theoretische und empirische Modelle. Theoretische Modelle analysieren die auf das Schild wirkenden Schnittkräfte, um die ROP auf der Grundlage einer Kräftebilanz abzuschätzen. Laborschneidversuche liefern ein grundlegendes und fundamentales Verständnis der Gesteinsfragmentierung. Das Kraft-Durchdringungsverhalten von Gestein ist die Grundlage für Leistungsvorhersagemodelle. Der Hauptnachteil dieser Modelle ist, dass sie die Standortparameter in Bezug auf die Gebirgsverhältnisse wie sie die TBM-Scheibenschneider im Feld antreffen würden, insbesondere die Fugen, nicht vollständig darstellen. Empirische Modelle beruhen in erster Linie auf Beobachtungen der in situ Leistung der TBMs. Als solche berücksichtigen sie nicht direkt die Schneidkraft, die Schneidengeometrie, die Schneidengeometrie und die Fähigkeit zur Abschätzung des Maschinenschubs und des Drehmoments/der Leistung im Verhältnis zur detaillierten Schneidkopfkonstruktion.

Um die Fähigkeit der Modelle zur genauen Vorhersage der ROP von Hartgestein-TBMs zu verbessern, wurden Daten von verschiedenen Projekten mit unterschiedlichen Gebirgsbedingungen und Maschinentypen gesammelt, die die Eigenschaften des intakten Gesteins, die Eigenschaften des Gebirges, die entsprechenden Betriebsparameter der Maschine und die beobachtete Leistung umfassen. Das

Hauptziel dieser Untersuchung war die Entwicklung eines neuen Modells, das sowohl die intakten Gesteins- und Gebirgseigenschaften als auch die TBM-Spezifikationen (Betriebs- und Konstruktionsparameter) zur Abschätzung der ROP einbezieht.

Diese Dissertation ist thematisch in die folgenden Teile unterteilt:

Im **Kapitel 1** werden Grundlagen der Tunnelbohrmaschinen (TBMs) und die Vorhersage der Leistung im Hartgestein sowie die Ziele der Forschung aufgezeigt.

Kapitel 2 beschreibt kurz einen Überblick über die historische Entwicklung des maschinellen Tunnelvortriebs und Vorhersagemodelle. Die Hauptvorteile und die große Bedeutung des TBM-Vortriebs im Untertagebau werden hervorgehoben. Außerdem wird die Klassifizierung von Tunnelbohrmaschinen erörtert und es werden drei Haupttypen von Hartgesteins-TBMs dargestellt.

Kapitel 3 bietet einen umfassenden Überblick über die Parameter, die die TBM-Leistung unter Hartgestein-Bedingungen beeinflussen. Diese sollen als Einführung in die Auswahl der kritischen Parameter und das Verständnis ihrer Auswirkungen auf die TBM-Leistung dienen.

Kapitel 4 enthält einen Überblick über die verfügbaren Modelle zur Vorhersage der TBM-Leistung in hartem Gestein. Er ermöglicht, den Hintergrund der Arbeit zu verstehen und hebt die Hauptkonzepte hinter den vorhandenen Vorhersagemodellen sowie die wichtigsten Einschränkungen dieser Modelle hervor. Dies ermöglicht ein Verständnis der wichtigsten Faktoren und Parameter, sowohl geologisch als auch TBM-bezogen, die eine wichtige Rolle bei der Abschätzung der Leistung von TBMs im Hartgestein spielen.

Kapitel 5 beschreibt die Projekte und die Geologie, die für die Entwicklung der TBM-Feldleistungsdatenbank verwendet wurden, einschließlich des Zagros-Wasserleitungstunnels Los 2 im Iran; des Golab-Wasserleitungstunnelprojekts im Iran; des Ghomrood-Wasserleitungstunnels Los 3 & 4 im Iran; des Maroshi-Ruparel-Wasserversorgungstunnels in Mumbai, Indien; des zweiten Manapouri Tailrace Tunnels in Neuseeland und des Lötschberg Basistunnels in der Schweiz. Für jedes dieser Projekte wird eine kurze Beschreibung der geologischen und bodenkundlichen Bedingungen gegeben.

Kapitel 6 erläutert die TBM-Leistungsdatenbank und die verfügbaren Daten unter verschiedenen Bedingungen. Die Daten sind unterteilt in geologische Parameter (wie z.B. Gesteinsfestigkeit, Bruchgrad der Gesteinsmasse usw.) und TBM-Parameter (wie z.B. gemessene Eindringraten und Vortriebsraten, angewandte Schubkraft usw.). Basierend auf diesen beiden Datensätzen und Analysen wurde ein neues TBM.-Leistungsvorhersagemodell zur Abschätzung der TBM-Leistung auf der Grundlage der

Felsmasseklassifikation (RMR) entwickelt und unter Verwendung von multivariablen Regressionsanalysen vorgestellt.

Kapitel 7: Es wird die Untersuchung von Methoden des maschinellen Lernens vorgestellt, nämlich Genetische Programmierung (GP) und Regressionsbaum, insbesondere Klassifizierungs- und Regressionsbaum (CART), und es werden neue Modelle auf der Grundlage von CART zur Schätzung der TBM-Leistung auf der Basis von RMR-Eingangsparametern vorgeschlagen. Außerdem wird eine neue Formel aus GP-Algorithmen vorgestellt, die RMR-Eingangsparameter verwendet. Die Ergebnisse der vorgeschlagenen Modelle werden durch eine einschlägige statistische Analyse, die die Restfehler darstellt, miteinander verglichen.

Kapitel 8: Präsentiert die Modellbewertung durch verschiedene statistische Indizes, gefolgt von einer probabilistischen Sensitivitätsanalyse, um die entwickelten Modelle zu untersuchen und die Auswirkungen der Eingabeparameter auf die Ausgabeergebnisse zu bewerten. Schließlich wurde die Genauigkeit und Effizienz des CART-Modells durch die drei empirischen Prognosemodelle, einschließlich Colorado School of Mines oder CSM, NTNU und Q_{TBM}, validiert.

Im abschließenden **Kapitel 9** werden die Schlussfolgerungen der Arbeit vorgestellt und die Diskussion über einige Folgearbeiten eröffnet, die in zukünftigen Studien in Angriff genommen werden könnten.

Chapter 1 Introduction

A key factor in the successful application of a Tunnel Boring Machine (TBM) in tunnelling is the ability to develop an accurate penetration rate estimated for determining project schedule and costs as well as selection of proper machine specifications to make tunnelling economical. While the use of hard rock TBM has become the standard method of excavation of tunnels with a length of over 1.5 km in almost all ground conditions, the estimation of machine performance in many of the challenging ground types has not reached a sufficient degree of accuracy. Although many models have been proposed for prediction of rate of penetration (ROP), the accuracy of the models depends on the original database from which they were driven. This is to say that, the errors in prediction caused by lack of accounting for some of the geological parameters are typically high, especially if the model that is used for prediction does not match the ground conditions of the target project.

In general, performance estimation for a TBM refers to estimation of certain parameters which include (Rostami, 2016a):

- Rate of penetration (ROP) which is also referred to as penetration rate (PR) and often expressed in m/h and refers to the linear footage of excavation per unit time, when the machine engages the ground and is in production.

- Utilization rate (U), expressed in percent (%) and representing the ratio of boring time to the total time. Total time could refer to the number of hours worked per workdays, boring days, or calendar days.

- Advance rate (AR), which is the amount of daily advance expressed in m/day and is calculated as:

$$AR = ROP \cdot U \cdot Ns \cdot Sh \qquad (1.1)$$

with Ns being the number of shifts per day and Sh being the number of hours per shift. Currently, three different models including Colorado School of Mines or CSM (Rostami, 1997) and Norwegian University of Science and Technology or NTNU (Bruland, 1998) as well as field penetration index (FPI) (Nelson et al. 1983, Hassanpour 2009, 2011) models are the most recognized TBM performance prediction and prognosis models in use around the world. The CSM model allows the calculation of the cutting forces that need to be applied on a disc cutter in order to reach a certain penetration into the rock. This method offers the advantages of being able to consider the geometry of the problem (the diameter and tip geometry of the disc and the spacing or distance between the grooves) in detail. However, the original CSM model does not consider the natural discontinuities of the rock mass, which have an important influence on the net speed of the TBM. To overcome this shortcoming, Yagiz (2002) and Ramezanzadeh (2005) modified the original CSM model by adding some rock mass properties as input parameters into the model.

Bruland (1998) updated and improved the NTNU model, which was originally proposed in 1978, based on field data mainly collected from Norwegian tunnels. The NTNU method uses some rock drilling indices such as Drilling Rate Index (DRI) estimated from rock brittleness "S_{20}" and hardness index "SJ" in addition to joint conditions to develop the estimated rate of penetration of TBM (Blindheim and Bruland, 1998). The NTNU model requires special specialized tests which are not commonly performed in many projects.

Filed Penetration Index (FPI) has been introduced by Nelson et al. (1983) and has been subsequently used as a means for predicting the performance of TBMs. For instance, Hassanpour et al. (2011) has recently used FPI estimated as a function of *RQD* and *UCS* to develop new equations and charts for TBM performance prediction.

1.1 Motivation

Since the first successful use of tunnel boring machine (TBM) in hard rock in early 1950s, they have been continuously transformed by improving their installed cutterhead power, size of machines, cutter loading capacity, and designs for application in various ground conditions, even some adverse grounds. In the last two decades, many performance predictions models have been developed by various researchers to estimate the penetration rate of hard rock tunnel boring machines (TBMs) in new tunnelling projects. All in all, to answer a basic question, "*How is it possible to accurately estimate TBM rate of penetration (ROP) and assess the interaction between rock mass conditions and the design and operational characteristics of the TBM?*" This is possibly due to the fact that, TBM performance prediction involves understanding the rock fragmentation process in wide range from micro-scale (i.e., the interaction of surface contact of rock material and cutter tip) to macro-scale (including the interaction of rock mass and TBM). As noted by Robbins

(1980): ‘‘*nothing has been more difficult than evaluating the rock mass characteristics and applying the evaluation to a formula predicting penetration rate*" and/or by Nelson (1993): ‘‘*the geotechnical engineering profession clearly does not have a recommended method for quantitative estimation of the effects of rock mass variations on TBM penetration rate*".

As noted earlier, TBM performance prediction models can be divided into two distinguished approaches, namely, theoretical and empirical ones. Although the theoretical models provide a basic understanding of rock fragmentation and explanations into the force-penetration behaviour of rocks, the main shortcoming of these tests is that they do not completely represent the real rock mass conditions as the TBM disc cutters encounter in the field. In such cases where standard laboratory rock cutting facilities are not available, TBM performance may be predicted by using formulas developed to estimate cutting forces for a certain disc cutter, working in a given rock type/strength. The early models were developed by using a single intact rock parameter, mainly uniaxial compressive, and follow-up works involved using other rock strength parameters, namely tensile strength. However, the latest empirical models have considered several rock and rock mass parameters along with machine design and operational parameters to estimate machine performance.

Another group of empirical models attempts to correlate TBM performance to rock mass classifications/features. Among the most commonly used classification/feature systems, Rock Mass Rating (RMR), Rock Mass Quality Index (Q), and Geological Strength Index (GSI) have been used more frequently in TBM performance prediction because of the simplicity and worldwide acceptance of the classification systems in general engineering practices, and in particular, in underground mining and construction. It is worth noting that, the Geological Strength Index (GSI) was first presented in preliminary form by Hoek et al. (1992) and subsequently further developed by Marinos and Hoek (2000, 2001). The GSI can be used for both hard and weak rock masses and is based on an essentially qualitative geological description of the rock mass. The GSI or this system is to provide an estimate of the properties of the rock mass in question (Marinos et al. 2005). This method of quantifying rock mass has been compared to RMR and Q, among other rock mass classification systems and there are formulas linking one to the other in the rock mechanics world. However, GSI is known to work better in weaker rock masses and where RMR and Q cannot quite distinguish the rock mass conditions.

In addition, due to the complexity of TBM performance prediction, beyond mathematical and empirical solutions, artificial intelligence (AI) methods particularly machine learning algorithms, containing artificial neural network (ANN), Fuzzy logic, adaptive neuro-fuzzy inference system (ANFIS) and support vector regression (SVR) have been widely utilized by many researchers (Alvarez Grima et al., 2000; Okubo et al., 2003;

Gholamnejad and Tayarani, 2010; Ghasemi et al. 2014; Salimi et al. 2016a). Mahdevari et al. (2014) used a support vector regression analysis (SVR) to predict penetration rate based on data from the Queens Water Tunnel, in New York City. Machine learning is a relatively new area of science that has been used in a variety of engineering applications and in the past few years, it has been continually under development. Generally, machine learning is a branch of artificial intelligence that investigates how machines can be trained to recognize patterns from a given set of training examples. Over the last decades, a large amount of machine learning methods has emerged and presented. These methods start from very diverse conceptual bases, although all of them have a series of common themes such as, ability to learn and adapt complex patterns; consideration of nonlinear relationships between qualitative and dependent variables; capability of generalization; thus, can be applied to incomplete and noisy data; ability to accommodate both categorical and quantitative data, etc. However, most of these machine learning methods (e.g., artificial neural networks or support vector machines) are difficult to apply as a large quantity of parameters must be fitted and estimated and they behave as "black, hazy or opaque boxes". This means that they can be applied to predict the value of a target variable depending on data, but the rules or implicit patterns within the model cannot be interpreted or the end-users need a computer code and have to be relatively expert in the particular field to employ them. In the area of rock engineering/tunnelling, the suitability of data mining techniques is closely related to the applicability of the resulting model. As a result, this investigation is focused on regression tree and genetic programming which are defined as "white, transparent or translucent box" presenting via a graph and mathematical equation, respectively (Salimi et al. 2016c; Carranza, 2011).

The most commonly used TBM performance prediction models such as, CSM & NTNU models have been developed about 20 years ago, and while there have been some updates and adjustments to the base models, there seems to be a need for new models and approaches. To meet this objective, while there are several TBM performance prediction models introduced within the past two decades, but the growth of TBM manufacturing technology and the existence of some shortcomings in the prediction models have made it necessary to continue the research on the development of new performance prediction models for hard rock TBMs.

1.2 Research Objectives

The main purpose of this study is to improve the predicting capabilities for estimation of TBM performance in various ground conditions. For this purpose, data from various projects with the different rock mass conditions and machine types has been collected from pertinent research groups and compiled in a database.

The term 'hard rock' is not always precisely defined. Table 1.1 shows the classification of rock types in terms of rock strength presented by the International Society of Rock Mechanics (ISRM). The specific parameter used is Uniaxial Compressive Strength, *UCS* (ISRM, 1978; 1979). The research presented in this thesis focuses on 'low strength rock' conditions to extremely high strength which, according to the ISRM classification, fall within the categories low, medium, high, very high, and extremely high strength (*UCS* > 6 MPa) based on the range of the *UCS* values in the TBM field performance database used in this study. Therefore, it can be concluded that, in the current study, the term "hard rock" is colloquial and it only refers to the rocks that are not very soft (i.e., salt, coal. Gypsum, etc.) or very low in strength.

Table 1.1: Classification of rock based on uniaxial compressive strength (ISRM, 1978; 1979)

Definition	UCS (MPa)
Soil	< 0.25
Extremely low strength	0.25 - 1
Very low strength	1 - 5
Low strength	5 - 25
Medium strength	25 - 50
High strength	50 - 100
Very high strength	100 - 250
Extremely high strength	> 250

Obviously, the data collected from the various operation will be inhomogeneous, meaning that there are some parameters missing or incomplete. However, the analysis of available information has been conducted using available analytical tools.

The main goal of the present work is to develop new models based on statistical analysis (Regression analysis), as well as artificial intelligence algorithms (Regression tree and; genetic programming) for the prediction of TBM performance in hard rock conditions. More attention is paid to introduce a model that incorporates rock mass classification systems such as rock mass rating (RMR) or its input parameters into TBM performance prediction. To reach these goals following approach has been taken:

1) Compile a database of field performance of hard rock TBMs and perform an initial qualitative statistical analysis to understand the data and ranges of the critical input parameters. The initial study of the database will also allow the research team to understand the nature of the data, the issue of inhomogeneity, and take measures to reduce the impact of missing data on the outcome. This refers to the proper and methodical screening of the data.
2) Preliminary quantitative statistical analysis including development of histograms, examination of co-variation of different parameters, followed by bi-variate analysis to see the trends and seek normalization of data sets.
3) Application of multivariable regression analysis of independent and objective parameters in linear and non-linear modes to seek the relationship between parameters for introducing new empirical models.
4) Application of machine learning algorithms which are known as "white or transparent box", such as classification and regression tree (CART) to develop a new model (graph). The developed graph allows users to estimate the penetration rate of TBMs. Besides that, genetic programming (GP) is conducted to present a new formula based on GP algorithms.

Figure 1.1 is an illustration of the work-flow research design for this study, including the literature review involved during the course of this research work.

1.3 Thesis layout

The thesis is divided into nine chapters. The present chapter, **Chapter 1**, provides an introduction to the tunnel boring machine (TBM) and prediction of their performance in hard rock conditions, motivation, and objectives of the research are outlined.

Chapter 2 briefly described an overview of the historical development of mechanized tunnelling and predictive models. The main advantages and the great importance of TBM excavation in underground construction are highlighted. In addition, the classification of tunnel boring machines is discussed and three main types of hard rock TBMs are illustrated.

Chapter 3 offers a comprehensive review of parameters affecting TBM performance in hard rock conditions. This would serve as an introduction to the selection of the critical parameters and understanding their effect on TBM performance.

Chapter 4 contains a review of the available hard rock TBM performance predictions models. It allows one to understand the background of the work and highlights the main concepts behind the existing prediction models and the main limitations of these models. This allows for understanding the main factors and parameters, both geology and TBM-related, that play important role in estimating the performance of hard rock TBMs.

Chapter 5 describes the projects used for the development of the TBM field performance database, including Zagros water conveyance tunnel Lot 2 in Iran; Golab water conveyance tunnelling project in Iran; Ghomrood water conveyance tunnel Lots 3 & 4 in Iran; Maroshi-Ruparel water supply tunnel located Mumbai, India; the Second Manapouri Tailrace Tunnel in New Zealand and Lötschberg Base Tunnel in Switzerland. For each of these projects, a brief description of the geological and ground conditions is provided.

Chapter 6 explains the TBM performance database and the available data in different conditions. The data is subdivided into geological parameters (such as rock strength, rock mass fracturing degree, etc.) and TBM parameters (such as measured penetration rates and advance rates, applied thrust force, etc.). Based on these two sets of data, a new TBM performance prediction model for estimation of TBM performance based on rock mass rating (RMR) classification is developed and introduced by using multi-variable regression analyses.

Chapter 7 presents the study of machine learning methods, namely Genetic Programming (GP) and Regression tree in particular classification and regression tree (CART) and new models based on CART for estimation of TBM performance based on RMR input parameters are proposed. Furthermore, a new formula from GP algorithms that uses RMR input parameters is presented. The results of the proposed models are compared and compared through pertinent statistical analysis that represents the residual errors.

Chapter 8 presents the model evaluation through different statistical indices, following by probabilistic sensitivity analysis to examine the developed models and assess the impacts of input parameters on the output results. Finally, the accuracy and efficiency of the CART model has been validated through the three prognosis empirical models, including Colorado School of Mines or CSM, NTNU, and Q_{TBM}.

Chapter 9 presents the conclusions drawn from the work performed and opens the discussion on some of the follow-up work which could be tackled in future studies.

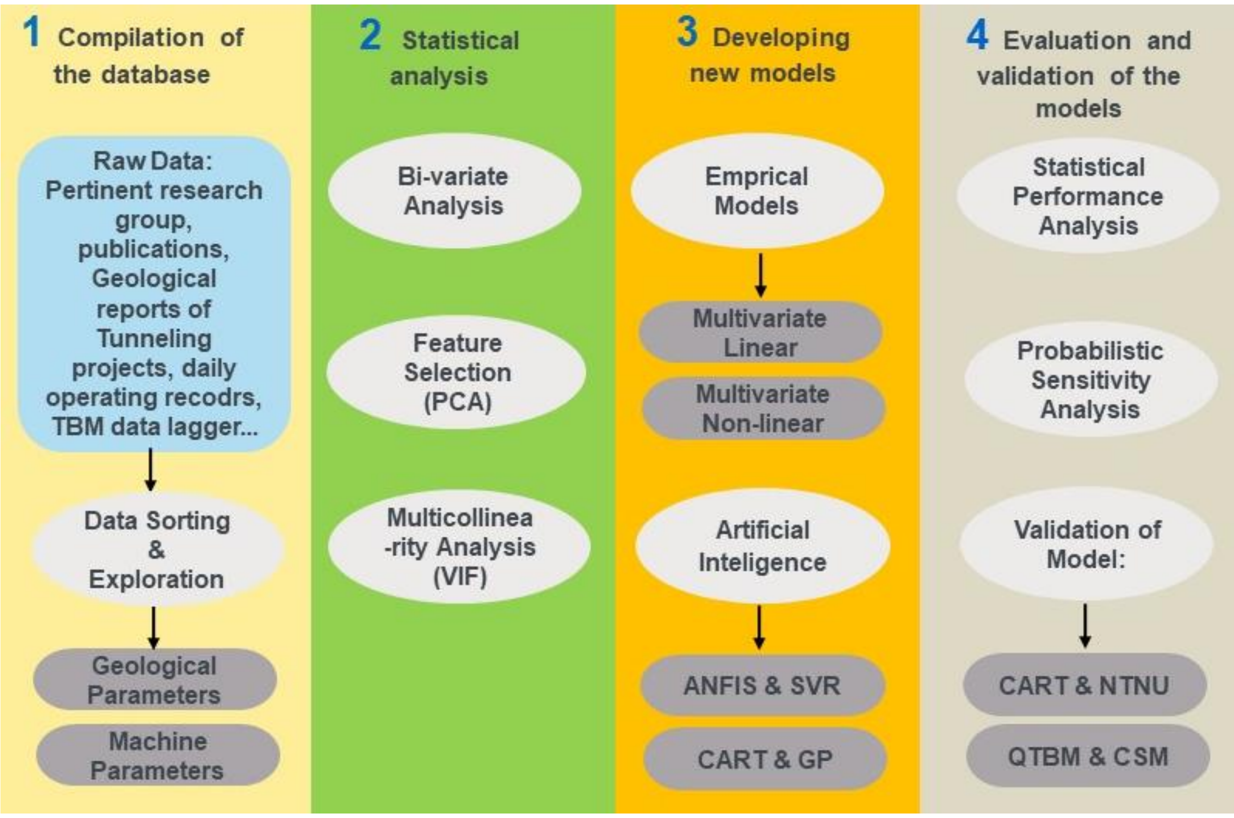

Figure 1.1: Diagram illustrating the research design

Chapter 2 Tunnel Boring Machines (TBM)

2.1 Introduction

Together with bridges and viaducts, tunnel construction is one of the most important branches of Civil Engineering, while there are many precedents of using TBMs in mine developments in the past 50 years. Nowadays, tunnels with increasing complexity (greater length, depth, etc.) and in difficult environments are being constructed for civil purposes (traffic, hydraulic, etc.). This increasing complexity is promoting the use of mechanized tunnelling techniques, which makes it possible to complete tunnel construction in a shorter time and with enhanced safety conditions.

In this chapter, a brief historical overview of the development of mechanized tunnelling techniques is offered. Classification of tunnel boring machine is presented and three main types of TBMs in rock tunnelling are highlighted and compared. The main advantages and importance of TBM excavation in underground construction are noted in this chapter as well.

2.2 History and Development of TBMs

Tunnelling developed rapidly during the industrialization at the start of the 19th century with the building of the railway network. In hard rock, this was by drilling and blasting. The first stage of the developing mechanization of tunnelling therefore was the development of efficient drills for drilling holes for the explosive. There were also attempts to excavate the rock completely by machine (Maidl et al. 2008). The history of the TBMs dates back to 1800's. During the period 1846-1930 more than 100 rock, hard-ground, and soft ground tunnelling machines of various types were designed and patented, e.g., a hammer percussion powered by compressed air used for ramming and boring was first proposed by an English man J.D. Brunton in 1844. In 1849, J. J. Couch of Philadelphia made the first percussion rock drill which was motorized by steam. Later, J. W. Fowle is credited with inventing the first direct action drilling machine in 1874 (Stack, 1995; Kramer et al. 1992).

The first tunnelling machines were not literally TBM in the true impression. They did not work the entire face with their excavation tools, the intention was to break out a groove around the tunnel wall. After cut, the machine was pulled back and the remaining core loosened with explosive or wedges. This was the basic concept of a machine designed and manufactured in 1846 by the Belgian engineer Henri-Joseph Maus for the Mount Cenis tunnel (Figure 2.1). The machine employed with hammer drill chiselling deep annular grooves in the stone, the compressed air to power the drills was to be provided by water powered compressors at the portal and reached to the machine via pipes. As early as 1851, Charles Wilson in the US develop and built a tunnel boring machine, which was patented in 1856 (Figure 2.2) and it was to somehow similar to the modern TBMs. The machine had all the characteristics of a modern TBM and, therefore it can be categorized as the first machine worked by boring the tunnel which the entire face excavated by using cutters. The tools had been organized on rotating cutterhead and the required thrust for cutting was encountered by pressure sideways against the rock. In 1853, the machine underwent various tests and after advancing around 3 m in Hoosac tunnel located in Boston, USA, due to the problems with disc cutters, it was unable to compete with the established Drill & Blast method. After the experience of using TBM at the Hoosac tunnel, in 1875, an improved version of the machine presented which had a completely new design for cutting head; the entire face was not excavated with the cutting tools, and only an external ring and central hole dug up. (Figure 2.3). That was to be obtained by mounting disc cutters at the outer and rotational axis of the cutting wheel. After the maximum cut depth was achieved, the machine had to be pulled back to enable the remaining core to be broken and removed using explosives (Maidl et al. 1996).

In 1866, Cooke and Hunetr from Wales, introduced an exclusive new system, in which, instead of a cutting wheel turning about the tunnel centerline, three drums rotated about a horizontal axis transverse to the tunnel (Figure 2.4). The central drum had a larger diameter and ran ahead of the others, while the outer drums extended the cross-section. In 1863, Frederick E. B. Beaumont applied for a patent for a tunnelling machine equipped with chisels, but unsuccessfully employed for the construction of a water tunnel. Following in 1875, he applied for a patent for a tunnel boring machine with a rotating cutting wheel. Later in 1880, the idea was adapted by Colonol T. English and developed and enhanced for his own machine. It had cylindrical holes in the cutting arms for the drilling tools, which chisel bits screwed. The main advantage of this configuration was that, the bits could be changed without withdrawing the machine from the face. A lower frame built the base frame of the machine with equipment to carry the muck away and drive for the drilling head. An upper frame kept the actual drilling equipment, that was pushed forward by a hydraulic cylinder. It was possible for the first time to push the cutterhead forward without releasing the bracing of the machine to the tunnel walls. Beaumont manufactured two machines to the patent of Colonel T. English in 1881 and applied them to drive the Channel Tunnel. The machine worked well from 1882 till 1883 and altogether 1840 m were excavated on the French side and 1850 m on the English side. The maximum daily advance rate was 25 m which was a phenomenal success for that time (Figure 2.5) (Maidl et al. 2008).

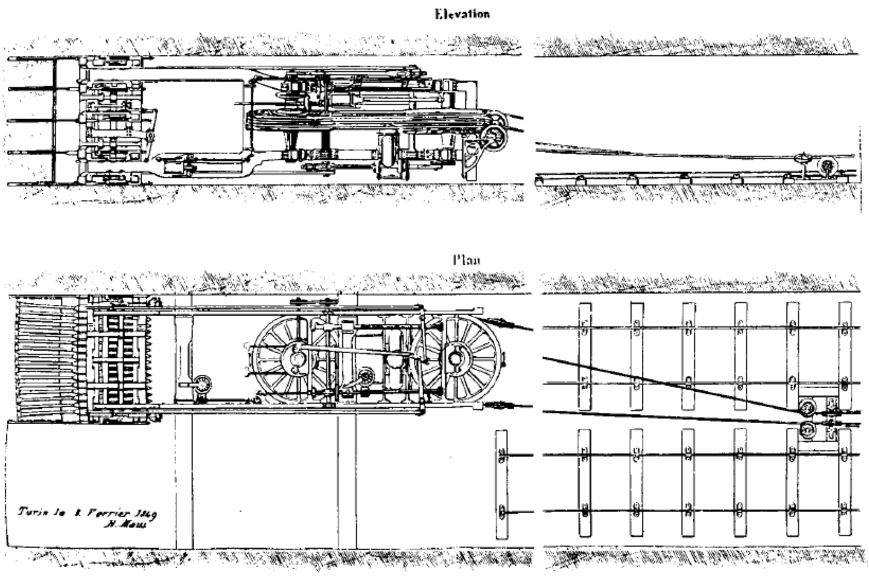

Figure 2.1: Tunneling machine designed by H.J. Maus in 1846 (Stack, 1982)

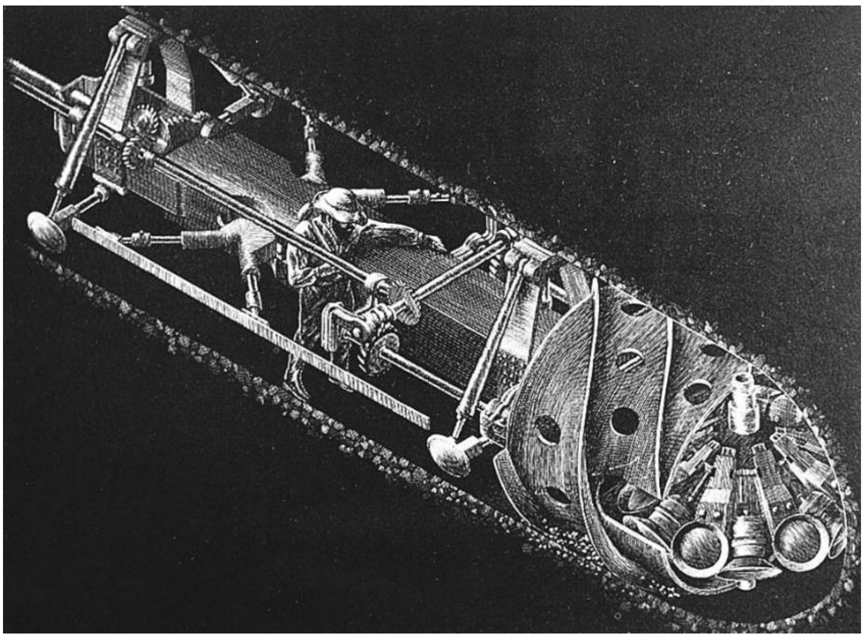

Figure 2.2: First tunnel boring machine by C. Wilson, Hoosac tunnel, 1853 (Maidl et al. 2008)

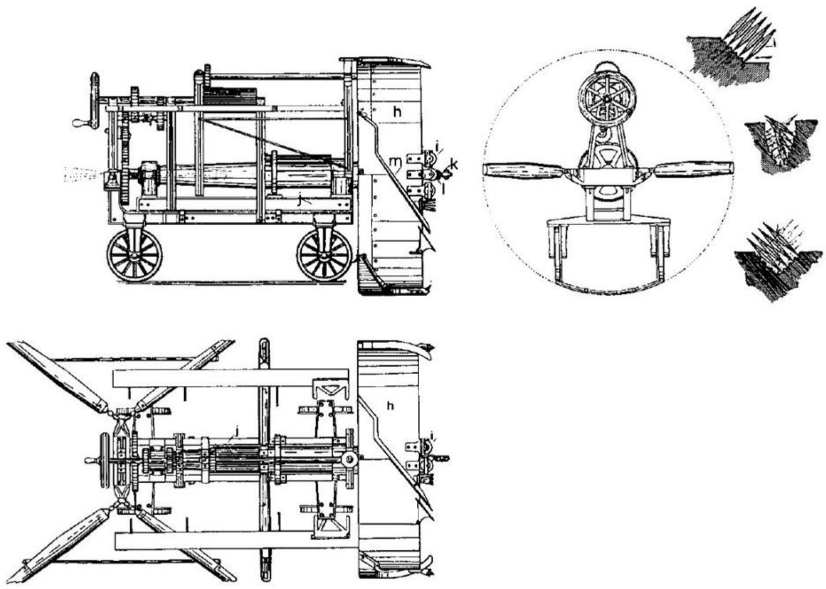

Figure 2.3: Further developed TBM by C. Wilson (Maidl et al. 2008)

There was no further application of tunnelling machine in the next decades, however, they were successfully applied in mining for cutting relatively soft rock, for example, the tunneling machine utilized for driving galleries in potash mines, which the first version in 1916/1917 called “Eiserner Bergmann”.

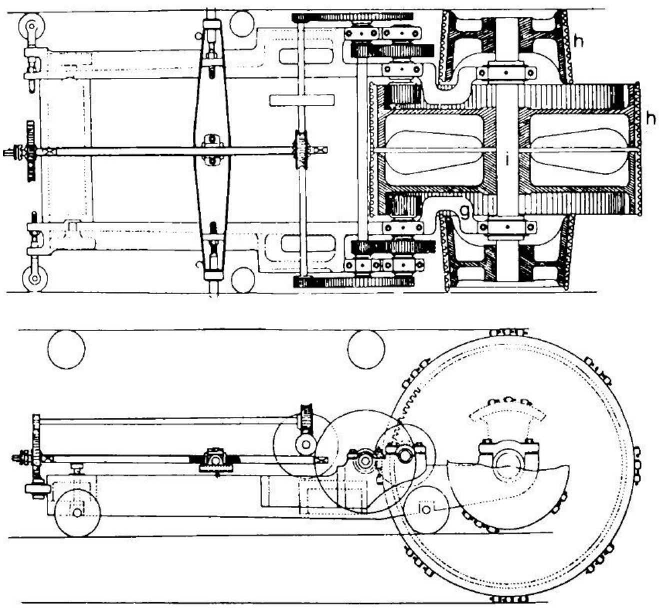

Figure 2.4: Tunneling machine by Cooke & Hunter (Maidl et al. 2008)

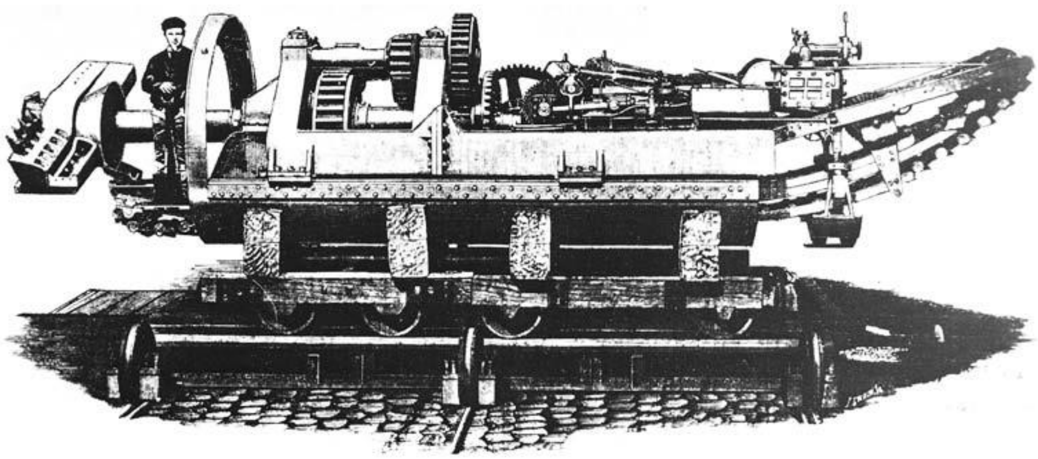

Figure 2.5: Tunnel boring machine by Beaumont, Channel Tunnel; 2.13 m diameter (Maidl et al. 2008)

The first development of modern TBMs was in the 1950s, when the first gripper TBM with disc cutters as the only excavation tool was developed by James S. Robbins (Figure 2.6). With this machine, advance rates up to 30 m/day were achieved in hard rock in the Humber Sewer tunnel project, which represented significant progress at that time (Maidl et al. 2008). The first use of continuous conveyor behind the TBM was conducted in 1963, which the world's largest TBM at the time, a 11.20 m diameter Robbins Main Beam, was built for the Mangla Dam Project. The unique project used a coal mine conveyor developed by James Robbins and Goodman, rather than muck cars, in the industry's first-documented use of continuous conveyors for TBM tunneling. Muck was removed continuously from five TBM tunnels bored at the remote job site, making the prototype a great success (Figure 2.7).

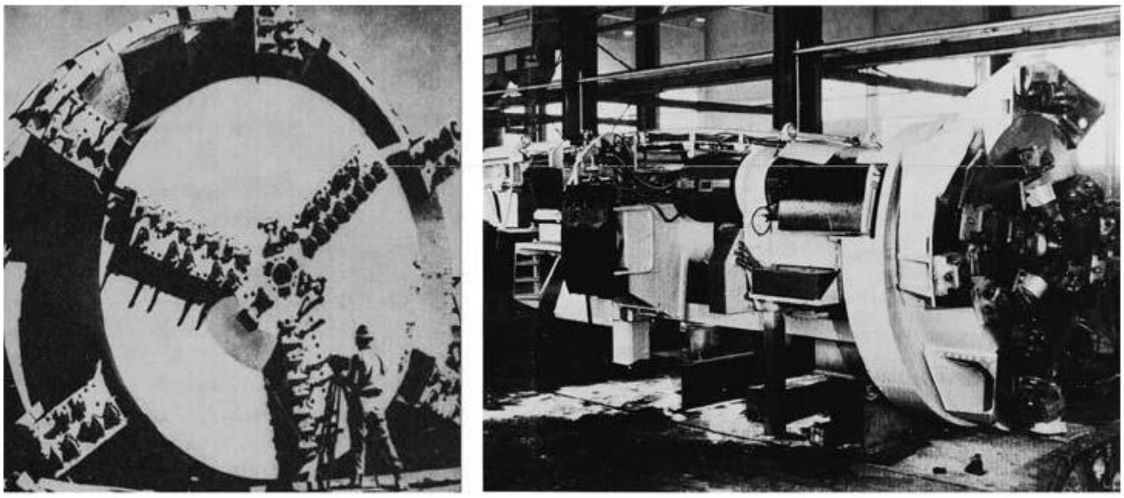

a *b*

Figure 2.6: Tunnel boring machines from Robbins: a) First Robbins TBM (8.0 m diameter); b) First modern gripper TBM (3.3 m diameter) (Robbins, 1976)

Figure 2.7: The first continuous conveyor behind TBM in 1963 (The Robbins Company, n.d.)

The development of earth-pressure balance shields started much later. This technique was first developed by the Japanese company Sato Kogyo Company Ltd. in 1963, after considerable research both in the laboratory and in the field, a unit was finally manufactured by Ishikawajima-Harima Heavy Industries (IHI) in 1966 (Stack, 1995). The development of earth-pressure balance shields was due to the strict environmental regulations and laws already in force in many major cities in Japan. These concerned air and groundwater pollution, the dumping of excavated material, and also health and safety precautions pertaining to compressed air (Maidl et al. 1996; 2012). The precursor to all Earth Pressure Balance (EPB) and Slurry TBMs (For soft ground tunnelling) happened in 1964 which Robbins developed the first compressed air tunnelling machine to successfully excavate a 2.9 km long tunnel below the water table in Paris, France. The design served as the genesis for the EPB and Slurry TBMs (Figure 2.8).

Figure 2.8: Compressed air tunnelling machine, Paris RER metro, 1964 (The Robbins Company, n.d.)

After a delay of about 10 years, in 1960s, the development of tunnel boring machines was also started in Europe by German manufactures such as Demag and Wirth. The early TBMs were mainly intended to bore hard rock. The developing technology for hardening the disc cutters enabled the use of this type of tool in really hard rock.

Encouraged by the successful implementation of a gripper TBM for the Mangla dam project in 1963 with a diameter of 11.17 m, a gripper TBM was also used for the construction of the Heitersberg tunnel (Ø10.65 m) in Switzerland in 1971. The work necessary to secure the rock with steel installation, anchors and mesh-reinforced shotcrete however made the hoped for advance impossible. The required adaptation to the large cross-section was first achieved in 1980 by the modification of the Robbins gripper machine from the Heitersberg tunnel by the Locher und Prader Company to a shielded TBM with segmental lining for the advance of the Gubrist tunnel (Ø11.50 m). Robbins and Herrenknecht had continued to make shield machines of this type in diameters ranging between 11 and 16 m (Maidl et al. 2008). At the end of the 1960s, inclined headings and large tunnel sections were driven for the first time using the reaming method, the development of reamer boring being closely associated with the Murer Company

(Maidl et al. 2008). Drilling tools from deep boring technology such as tungsten carbide insert (TCI) and toothed bits were mounted on rotating cutterheads (Maidl et al. 2008).

As late as 1959, the idea of a fluid-supported tunnel face was successfully tested by Elmer C. Gardner for a sewer tunnel with a diameter of 3.35 m. In 1960 Schneidereit introduced the term active face support through a bentonite suspension. In 1967 the first slurry shield with a cutting wheel and hydraulic mucking was used in Japan. It had a diameter of 3.1 m. In Germany, the first shield with a bentonite-supported tunnel face was developed and used by Wayss & Freytag (Maidl et al. 1996).

In the 70s and 80s, notable signs of progress were directed to TBM tunnelling in brittle, hard rock and bigger excavation diameters. The first double shield TBM was developed in 1972 with the collaboration of SELI, & Robbins companies for the Orichella, Italy. Carlo Grandori developed the concept of the double shield TBM and, in collaboration with Robbins, put it into practice for the building of the Sila pressure tunnel (Ø 4.32 m) in Italy (Figure 2.9). The main intention of the development of this machine was to make the gripper TBM, which had then already proved very effective in appropriate geological conditions, more flexible for use in heterogeneous rock conditions. Since their first use in 1972 and the successful modification of this type of machine, double shield TBMs with customized segmental lining designs have achieved high advance rates under favourable rock conditions and have been made by all the well-known manufacturers, mainly in the medium diameter range. The capability of the double shield TBM design was demonstrated impressively at the end of the 80s in the chalk of the Channel Tunnel, which is favorable for tunnelling (Maidl et al. 2008; 2012). Shielded and double-shield TBMs were introduced in the same period. This made it possible to increase the range of application of TBMs to complex and heterogeneous geological conditions. Today, TBMs with very large diameters (up to 18 m" Bertha, Fig. 2.10a") are being built for use in soft ground tunnelling while the record size in rock tunnelling is about 14.5 m ("Big Becky, Fig. 2.10b") and a lot of efforts have been devoted to increasing the range of application of TBMs to a variety of geological conditions with reduced/acceptable risks. Today's TBMs have advanced computer systems to control and record the excavation parameters. Moreover, they also have advanced guidance systems to minimize deviation from the route.

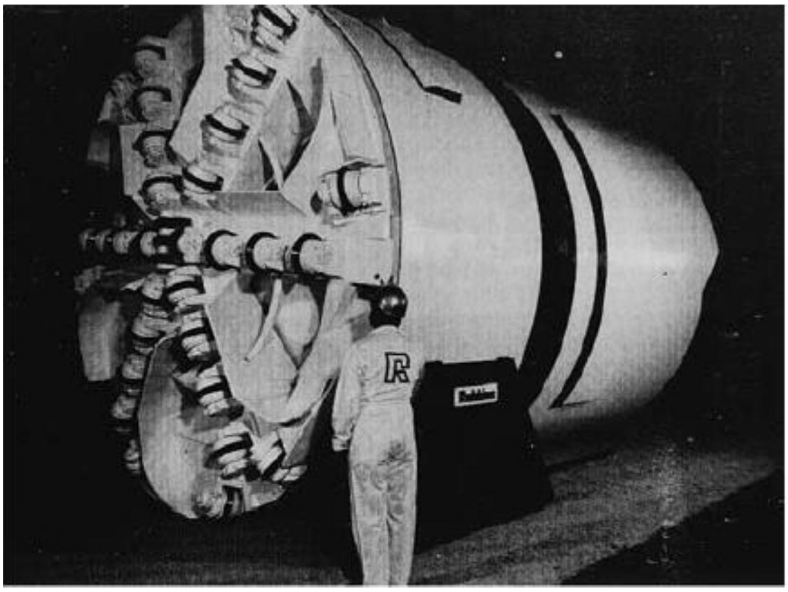

Figure 2.9: Double shield TBM 144-151, Sila pressure tunnel, Ø4.32 m, 1972. (Maidl et al. 1996)

(a) (b)

Figure 2.10: (a)"Bertha", Seattle tunnel project, (TBM-EPB; 17.5 m diameter) USA ; (b) "Big Becky" Niagara tunnel project; (Main Beam TBM; 14.5 m diameter); Ontario, Canada (Tunneltalk.com)

2.3 Classification of Tunnel Excavation Machine

Tunnels are constructed under various types of geological conditions varying from hard rock to very soft sedimentary layers. Various conditions of ground that a TBM may encounter during tunnelling as well as practical issues during an excavation of tunnel necessitates improvement in designing and manufacturing of different TBMs with different capabilities. According to the French Association of Tunnels and Underground

Space (AFTES), "the mechanized tunnelling techniques" (as opposed to the so-called "conventional" techniques) are all the tunnelling techniques in which excavation is performed mechanically by means of teeth, picks, or discs. The problem with the classification of tunnelling machines is that there is no uniform, globally accepted definition and classification for tunnelling machines. However, the term Tunnel Boring Machine (TBM) is now universally adopted for all the machines that have a full-face cutting wheel for excavating a tunnel. The classification to be considered in this study is based on what has been developed by the International Tunnelling Association (ITA) Working Group No.14 "Mechanized Excavation". Tunnel excavation machines can be classified by the methods for excavation (full-face or partial face), the types of cutterhead (rotation or non-rotation), and by the method of securing reaction force (from gripper or segment). Several types of tunnel excavation machine are illustrated in Table 2-1 and Figure 2.11 As can be seen from Table 2-1, Tunnel Boring Machine can be categorized into two main groups including:

- Hard rock machines
- Soft ground machines

Table 2.1: Classification of Tunnel Excavation Machines (ITA, 2000)

<table>
<tr><th rowspan="10">Tunnel Excavation Machine</th><th>Excavation</th><th>Cutting Head</th><th>Reaction Force</th><th colspan="2">TBM Type</th><th>Ground-type</th></tr>
<tr><td rowspan="8">Full face</td><td rowspan="5">Rotation (TBM)</td><td rowspan="2">Gripper</td><td>Open type (I)</td><td>Beam type</td><td>Rock</td></tr>
<tr><td>Closed type or Shield (I)</td><td>Shield</td><td>Rock, soft ground</td></tr>
<tr><td rowspan="3">Segment</td><td>Open type (Π)</td><td>Mechanical excavation type</td><td rowspan="6">Soft ground</td></tr>
<tr><td rowspan="2">Closed type (Π)</td><td>Earth Pressure Balance type (EPB)</td></tr>
<tr><td>Slurry type</td></tr>
<tr><td rowspan="3">Non-Rotation (Shield)</td><td rowspan="3">Segment</td><td rowspan="2">Open type</td><td>Hand Excavation type</td></tr>
<tr><td>Semi-Mechanical Exaction type</td></tr>
<tr><td>Semi-open type</td><td>Blind type</td></tr>
<tr><td colspan="6">Partial Face (Roadheader, Hydraulic Hammer, etc)</td></tr>
</table>

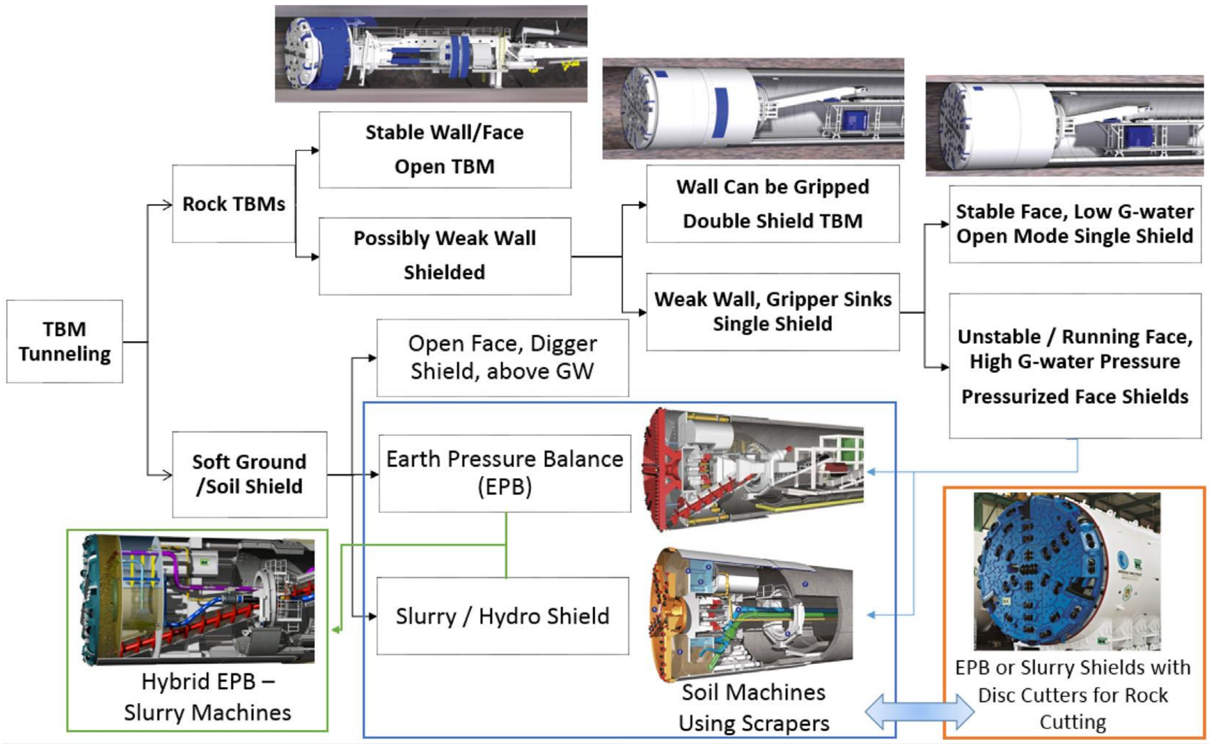

Figure 2.11: General classification of TBMs for various ground conditions (Rostami, 2016a)

In practice, rock tunnelling machines can be grouped into three main categories based on their propelling mechanism:

1. Unshielded or Open TBMs using grippers
2. Single Shield TBMs, pushing off the segments
3. Double Shield TBMs (combination of 1 & 2)

In hard rock tunnelling projects, the type of machine depends on the quality of the surrounding ground and some practical issues. Different types of rock tunnelling machines are shown in Figure 2.12. By considering the purpose of this study, only rock tunnelling machines in this figure are investigated. The open mode rock TBMs can be classified as:

- Unshielded TBMs (open type) with single or double gripper
- Shielded TBMs (single or double or telescopic shield)

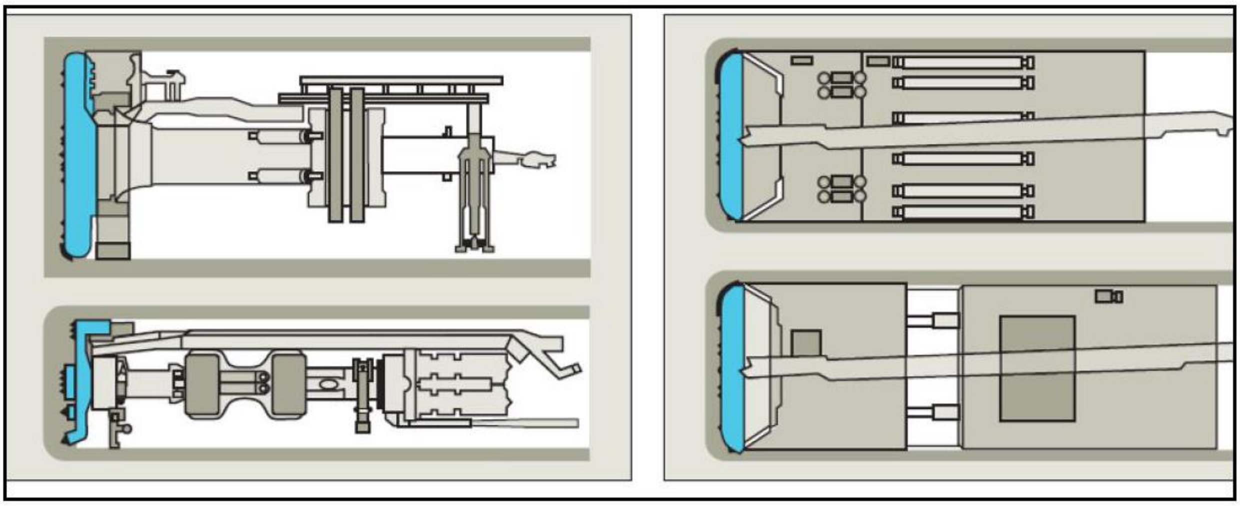

Figure 2.12: Different types of rock tunnelling machine: Left; open TBM with single and double gripper, Right; Single and double shielded machine (Munchener Ruck, Munich Re Group, 2004)

2.3.1 Open TBMs

The gripper TBM, often also widely defined as open TBM, is the classic form of tunnel boring machine. This type of machine is utilized in stable rock conditions with a low flow of water; it needs to be associated with a primary support system for excavation using the conventional method (rock bolts, shot concrete, steel arches, etc). Application of this type in rock with more than 40 MPa has been suggested by the International Tunnelling Association. The problem that may interface in the application of open type is a stand-up time of rock mass. Open type TBMs are designed to have the ability to install various support systems immediately behind the cutterhead. Simultaneous excavation and ground support installation is possible in modern open TBMs. Examples of open type TBM with relevant details are shown in Figures 2.13 and 2.14.

Open type TBM machines are categorized by the single or double gripper. In both types, grippers are utilized to provide thrust force to move forward and press the head against the tunnel face. Thus, the rock mass of the tunnel wall must be competent enough and stable to react to the pressure imposed by grippers. The maximum amount of gripper pressure on the tunnel wall is determined on the basis of compressive strength of rock mass and is usually 2 to 3-fold that of machine thrust. The performance and penetration rate of open machines is directly impacted by the amount, type, and required time to erect supports behind the cutterhead for the given rock conditions.

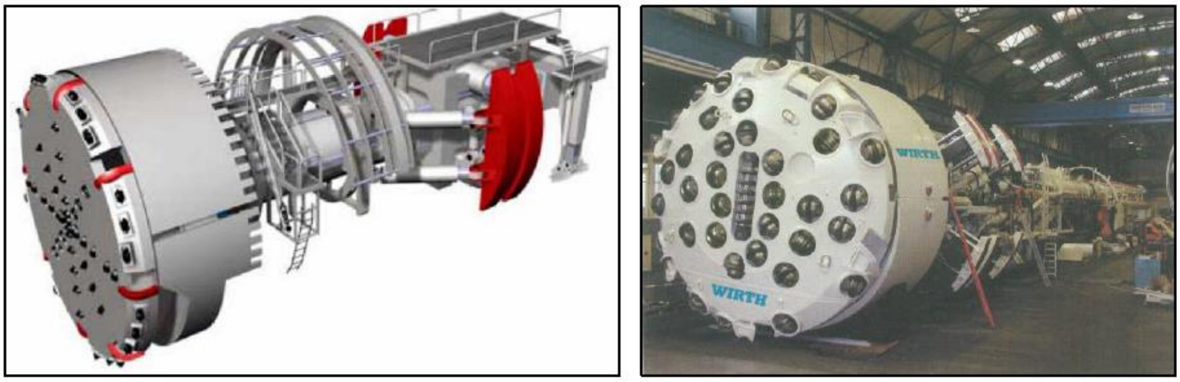

Figure 2.13: Open TBM type: Left; Herrenknecht and Rehm (2006), Right; Wirth Company (Wirth GmbH)

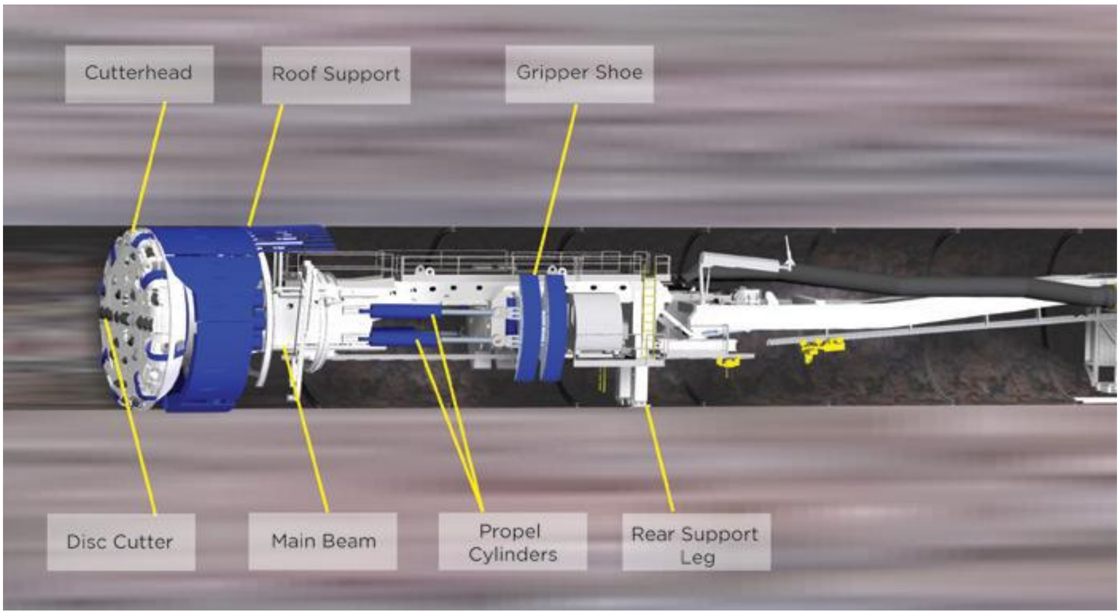

Figure 2.14: Schematic drawing of Open TBM and its components (The Robbins Company, n.d.)

In a single gripper machine, motors are mounted in the front area on the cutterhead support that hosts the gearbox and motors. In double gripper machines, motors are located at the rear end of the machine, behind the rear grippers. To maintain the static stability of double gripper machines and prevent excessive torsion in the cutterhead body, grippers are designed to be close to the cutterhead. This means that there is not enough space for the installation of a support system as compared to single gripper machines. Therefore, the use of a double gripper machine could cause some issues in weak rocks. Also, steering of the open TBMs is different between double gripper (Kelly type) and single gripper (Main beam) TBMs. Machines manufactured by Wirth or Jarva

(Atlas Copco) company, have two sets of grippers and power is transferred through an interior shaft (Kelly), solidly connected to the head and the steering is done by setting the machine in the right course between the strokes and excavating a line during the stroke. The direct is reset as needed for the following strokes. This offers more stable boring and less stress on the head, however; there is no possibility to correct the path during penetration and cycle. The opposite is true for main beam machines where the machine can be steered during excavation by applying differential loading against the opposite grippers and use of the loading by font shoes to direct the machine during the stroke.

2.3.2 Single Shield TBMs

This type of machine is covered by a cylindrical steel shield that starts behind the cutterhead and extends to the rear section of the machine where segments can be erected to cover the tunnel walls. The shield propels forward by activating thrust jacks to push off the segments. Single shield TBMs and its components are shown in Figure 2.15. This type of machine is designed and built for hard rock excavation in unstable ground where there is a high risk of wall cave in and roof falls and offers workspace protection when it is necessary to support the tunnel immediately after excavation. The tunnel is supported by the installation of the precast lining in the rear end of the shield as it propels forward. So, the main task of the shield is to protect the staff and excavation equipment from falling the rock and unstable materials as well as facilitating the conditions to install the required support system. Usually, single shield machines are utilized when there is no possibility to use gripper due to the unfavourable conditions of surrounding rock mass of tunnel. Installation of ground support is done after completion of excavation cycle at tunnel face when a machine is stopped and thrust jacks can be retreated to make room for a new ring of precast concrete segments. Therefore, utilization of the single shield is lower than double shield machines where the excavation and ground support can be done simultaneously. The advance rate of a single shield machine usually is negatively affected by the speed of the installation support system, especially in weak ground conditions.

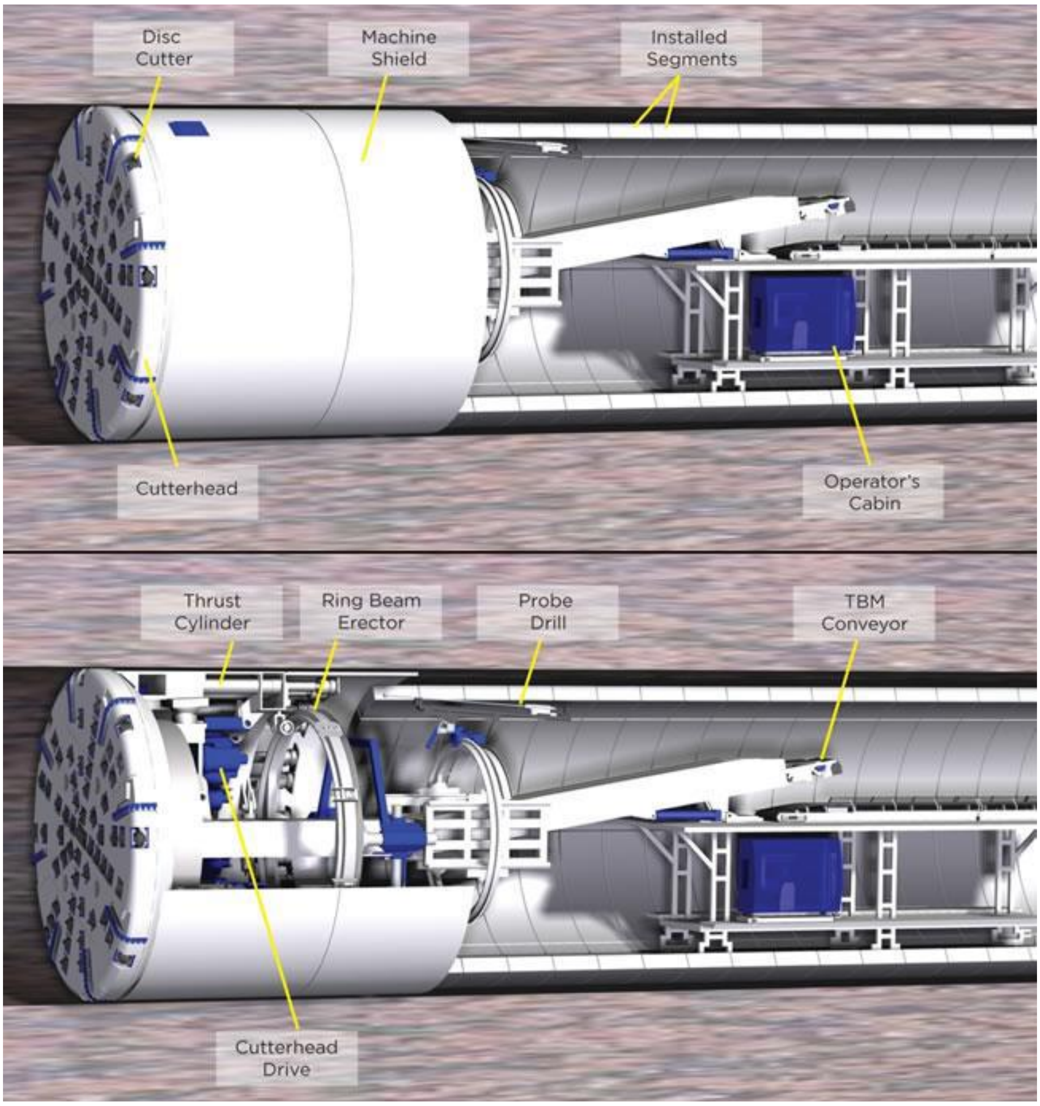

Figure 2.15: Schematic drawing of single shield TBM with different parts (The Robbins Company, n.d.)

2.3.3 Double Shielded TBMs

In 1972, SELI in collaboration with Robbins company developed a new machine for the Orichella project in Italy. The double shield or telescopic shield TBM is a combination of the open and shield TBMs. General shape of this machine and different parts of the double shield machine are shown in Figures 2.16 and 2.17 respectively. It enables, the machine to use grippers in good rock and acts like a single shield TBM for driving in fractured rock with low stand-up time. The double shield TBM consists of two main components, the front shield and the gripper (or rear shield). Both shield parts are connected with each other with telescopic jacks. The machine can either adequately clamp itself radially in the tunnel using the gripping units; or where the geology is bad, can push off the existing lining in the direction of the drive.

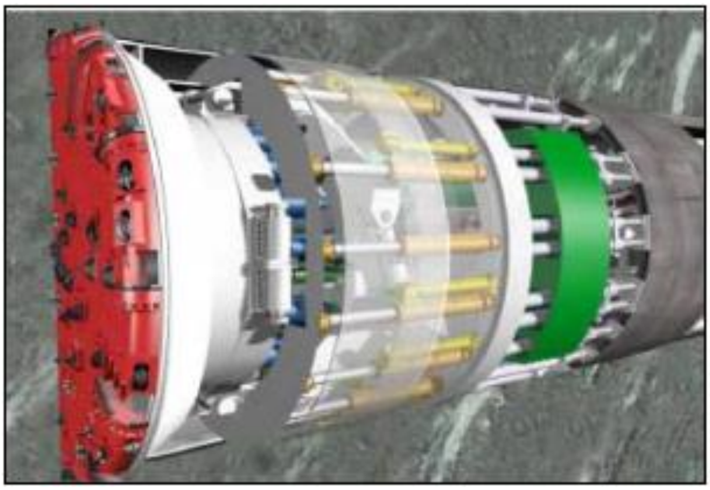

Figure 2.16: 3D view of double shielded TBM (Herrenknecht and Rehm, 2006)

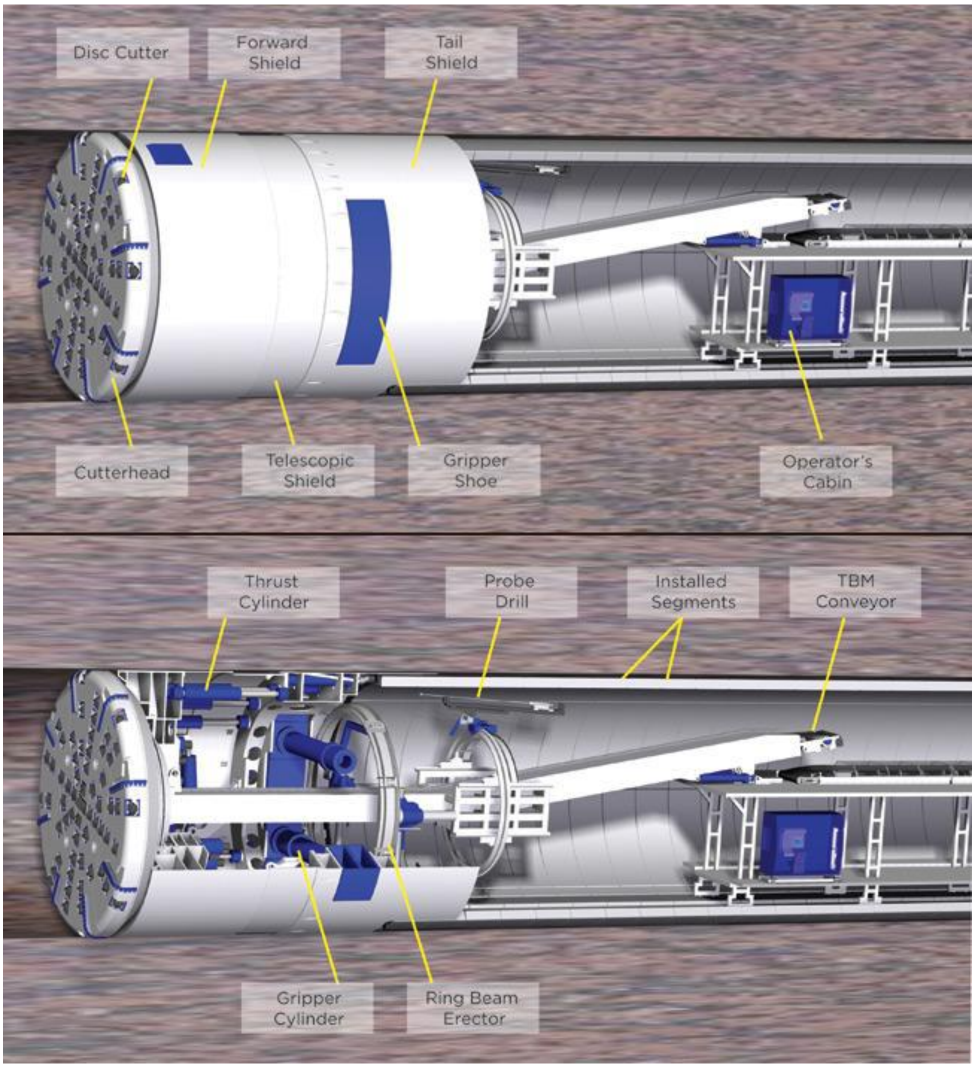

Figure 2.17: Schematic drawing of double shield TBM and its components (The Robbins Company)

The front shield can thus be thrust forward without influencing the gripper shield, so that segmental lining can be installed in the tail/rear shield simultaneously and the machine to move forward when the cycle is complete (without the delay of installing segments). The operation is possible by independent activities associated with excavation and installation of the lining. The double shield TBM has some disadvantages compared to the single shield TBM, including the longer shield that makes it vulnerable to jamming in ground squeezing conditions and material getting into the telescopic joint. Comparison of three types of rock TBMs is illustrated in Table 2.2 based on their advantages and disadvantage. More information about TBM classifications/definitions, application & related subjects can be found in Maidl et al. (1996; 2008; 2012); Stack (1995); DAUB (2005); JSCE (2007); Guglielmetti et al. (2008); Maidl (et al. 2013).

Table 2.2: Comparison of three types of rock TBMs (Barla and Pelizza, 2000)

Open TBM	Single shield TBM	Double shield TBM
Advantages		
Effortless operation	Wide range of application	Wide range of application
Applicability in hard rock	Safety	Safety
High excavation rate	Precast segmental lining	Support system flexibility
Support system flexibility	installation	Simultaneous installation of final support system
Less construction cost	High performance	
Low investment cost	Working in falling ground	Working in falling ground
		Controlling water inflow with closed shield
Disadvantages		
Grippers inability in unstable rock mass	Two work phases	High investment cost
Support installation in weak rock masses	Drive-in weak ground	Complex operation
	Need of precast lining	Need of cleaning the telescopic joint
	High investment cost	
	Complex operation	Possibility of TBM jamming in highly convergent ground
	Need of segment plant	

Chapter 3 Parameters Affecting Performance of Rock TBMs

3.1 Introduction

The rate of tunnelling with TBM can vary between 15 km/year to 15 m/year depending on geological conditions, machine specification, and contractor experience. Major boring problems in TBM operation can appear in both unfavourable or favourable rock mass conditions. In fact, in two boundary conditions of geological settings, perhaps other tunnelling methods, such as blasting, could yield better results as compared to TBM. For example, in 1967 in a TBM manufactured by Robbins Company, bore 7.5 km of a tunnel in 4 months. The tunnel alignment included Shale, with geological and structural was known. Meanwhile, in the former phases of this project, 270 m of the tunnel was driven in glacial sediments and was excavated for 7 months. The advance rate reduction from 2.5 m/h to 0.05 m/h in this project is the exact reason for the great influence of geological conditions of the tunnel on the advance rate of TBM (Barton, 2000). One of the significant technical challenges and achievements in hard rock TBM tunnelling assigned to the construction of the Niagara Tunnel Project (NTP) located in Queenston, Ontario, Canada. A 10.4 km long, 14.4 m diameter tunnel was completed using Main Beam TBM "the largest hard rock TBM in the world" manufactured by Robbins company. The TBM began boring in September 2006 and May 2011 marked the completion of the TBM's drive. During July 2009, the TBM excavated 468 m (1,500 ft) in one month and advanced 153 m (503 ft) in one week overcoming significant geological challenges resulting the machine achieved a world record-breaking month for any TBM 11 m in diameter or larger (The Niagara Tunnel Project (2012).; Perres et al. 2014; Wallis, 2011; Robbins Company).

More recently, after 17 years of construction time, the new Gotthard Base Tunnel was opened on December 2016. With a length of 57 km, it is not only the world's deepest railway tunnel but also a unique masterpiece of engineering, with the highest point lying at 550 metres above sea level excavated by 4 Herrenknecht gripper tunnel boring machines. In late summer 2009, the two Herrenknecht gripper TBM completed the northern Erstfeld-Amsteg section with a length of just over 7 kilometres, fortunately, the geology was almost ideal and this was how the tunnelling record on the Gotthard was set 56 meters just in 24 hours, world record for a hard rock tunnel boring machine of this dimension. On June 16 and September 16, 2009, the construction site teams in the north each reached the destination in Amsteg after 18 months of driving, 6 months earlier than planned. On the way to the Gotthard, lötschberg base tunnel which had been excavated by 2 gripper TBM manufactured by Herrenknecht with the diameter of 9.40 m showed a record of 52 meters in 24 hours. (Herrenknecht AG; Sala & Wick, 2016).

A world record standing for hard rock TBM tunnelling belongs to The Brenner Base Tunnel (BBT). The Brenner Base Tunnel which is "the longest underground rail link in the world when completed in 2026" is being built from the Tulfes portal near Innsbruck to Fortezza in South Tyrol, Italy, for a total of 64 kilometers - 7 kilometers more than the Gotthard Base Tunnel. The tunnel passes through hard rock, including quartz, slate, gneiss, tonalite, and granite. A special feature of the project is the exploratory tunnel, which is driven through the rock in front of the two main tubes. For the exploratory tunnel, Herrenknecht supplied a gripper TBM with a diameter of 7.9 meters. On March 30th 2018, the TBM in the Ahrental exploratory tunnel drove through 10,000 meters of rock in 2.5 years, A new world record: 61.04 meters in 24 hours in quartz phyllite rock (BBT-SE; Skuk & Wegscheider, 2015; Skuk & Schierl, 2017).

In this chapter, a brief description of parameters that impact performance of TBM will be offered. The results of previous studies from different researchers regarding the effects of different geological and geomechanical parameters on TBM performance are also examined. Besides, the principle of the rock fragmentation process in TBM tunnelling and effective parameters is discussed.

3.2 Definitions of Machine Operating Parameters

In order to examine machine performance and effective parameters, it is important to offer a definition of the terms and parameters including, penetration rate, utilization coefficient, advance rate, thrust force, torque, and rotation. Correct understanding and method of calculation of these parameters. Hence, in this section, these parameters are briefly described.

3.2.1 Advance Rate, Penetration Rate, and Utilization

Among the machine performance parameters, the most important one is the advance rate. The advance rate is the ratio between excavated length and total available time. The advance rate of boring machines depends on two major activities in tunnelling, rock excavation and installation of ground support system and completion of the other activities. Rock boring with TBM is represented by penetration rate. Penetration rate is defined as the ratio of the length of tunnel excavated to the actual boring time during a continuous boring cycle which can be calculated using the following formula:

$$ROP(m/h) = \frac{l(m)}{t(h)} \tag{3.1}$$

Or

$$P(mm/rev) = \frac{ROP(m/h) \cdot 1000}{RPM \cdot 60} \tag{3.2}$$

where ROP is the rate of penetration in (m/h); l is boring length (m); t is boring time (h); P is cutter penetration per each cutterhead revolution (mm/rev) and RPM is cutterhead rotational speed (rev/min). Utilization refers to the percentage of the shift time that actual boring activity occurs, i.e., it refers to the ratio between actual penetration time and total available time in percent. Thus, the advance rate of TBM can be calculated as follow:

$$AR(m/h) = ROP(m/h) \cdot U(\%) \cdot Hrs \tag{3.3}$$

Hrs refers to the number of working hours per day. It is worth to note that, installation of the support system (segment installation) and the other operations such as repair and maintenance, other downtimes (electricity breaking off, delay in haulage system, etc.) results in a reduction of the average advance rate. This reduction is defined as the utilization coefficient which can vary between 0 to 55%. TBM utilization depends on job site settings and the contractor's experience.

3.2.2 Thrust

Thrust or propel force of the machine is one of the critical parameters which has a major impact on the performance of TBM. As can be seen from Figure 3.1, by increasing the thrust, rotating the cutterhead, and rolling disc cutters on the tunnel face (rock), different forces act on disc cutters including:

- Normal force F_N

- Rolling force F_R
- Side force F_S

The normal force is defined as a force acting under a disc perpendicular to the face and constitutes the thrust requirement of a machine. The rolling force acts on the disc along the cutting direction and determines the torque and power requirements of a machine to rotate the cutterhead at a certain penetration of the cutters. Side force is usually random since chips can form on either side while the pressure is maintained on the opposite side.

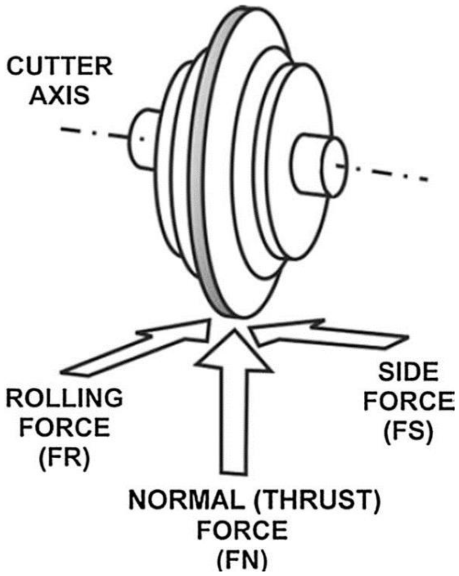

Figure 3.1: Cutting forces acting on a disc (modified from Rostami & Ozdemir, 1993)

The interaction of F_N and F_R, and the penetration is illustrated in Fig.3.2. The changing slope corresponds to a transition in dominance between crushing and chip formation and has been called the "critical thrust": unless the force of this magnitude can be applied, chipping between grooves will not occur. The critical thrust is directly related to rock strength or hardness and increase with cutter spacing and tip width of the disc.

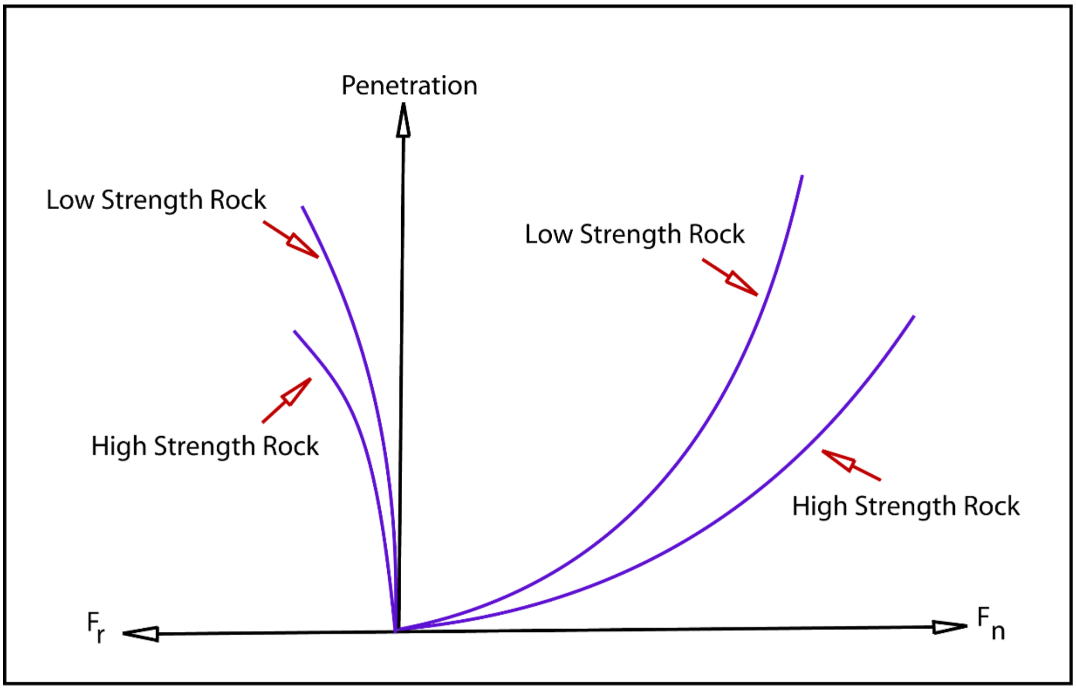

Figure 3.2: Interaction of F_N and F_R with penetration for high and low strength rocks (modified from Nelson, 1993)

Although these force/penetration relationships are known to be non-linear, several parameters have been defined on ratios derived from force/penetration plots. The ratio of F_R to F_N has been defined as the cutting or rolling coefficient (C_C , R_C), and the ratio of F_N to P_{Rev} is defined as the penetration index (R_F) or if measured in the field, it is called Field Penetration Index (FPI) which is calculated as follows:

$$C_C = \frac{F_R}{F_N} \qquad \& \qquad R_F = \frac{F_N}{P_{\text{Rev}}} \tag{3.4}$$

where F_R is rolling force, F_N is the normal force, C_C is cutting coefficient, R_F is penetration index, and P_{Rev} is penetration per revolution.

The thrust force of the machine and cutting force per cutter on the rock are very important parameters in the performance of the machine. Thus, they can be calculated as follow:

$$T_h = \frac{9.81 N_c \cdot \pi \cdot d_c^{\,2}}{4} \cdot P_c \tag{3.5}$$

$$F_N = \frac{T_h - T_f - T_{tow}}{N_{TBM}} \tag{3.6}$$

where T_h is total thrust force, P_C is hydraulic oil pressure in the cylinder (MPa), d_C is the diameter of the cylinder (mm), N_C is the number of the cylinder, F_N is cutting force per cutter (kN/cutter), T_f is the friction force between shield and tunnel wall (kN), T_{tow} is tow force or resistance of back-up system (kN) and N_{TBM} is the number of disc cutters. To calculate the friction force, a series of in situ penetration tests as explained by Bruland need to be employed. This test consists of 4 main steps. As a common practice, the cutter head rotation speed is fixed and simultaneously the excavation thrust force is applied at different levels. The basic testing procedure (start-stop test) can be found in Frenzel et al. (2012). Before performing the test, it should be ensured that the tunnel face is stable and disc cutters are in good condition so that the cutter tip width of mounted cutters is not varying too much. These requirements are often met after daily cutterhead inspections/maintenance. Generally, it is recommended to opt for the base thrust force according to machine consideration with respect to the operator's opinion and then to reduce 10 percent of this force in each step. Subsequently, the value of penetration rate in a specific period of time is determined according to thrust forces in each step and lastly, the average value of torque is also recorded. In addition to the aforementioned steps, it is essential to gather excavation mucks in that step together with the previous and next steps of excavation. The required minimum time for a single test is approximately equal to 30 number of cutter head rotations. In this period of time, it is necessary to maintain the thrust force in a specific value. The friction force follows the contact area between the shield and surrounding rock and is dependent on the rock mass quality and weight of the cutterhead. High friction values caused by low rock mass strength and blocking of the annular gap by rock fragments reduce the applied thrust force respectively the force per cutter significantly. Since different tunnel routes (straight line or curve) and machine types cause varying friction values, this parameter must be considered to ensure comparability of different prediction models. Therefore, a friction stroke has to be performed where the cutterhead rotates in unobstructed space without touching the tunnel face and performing active excavation. During the friction test stroke, the shield of a TBM is in full contact with the surrounding rock mass. But not the entire cutterhead is, since the TBM is not penetrating the face and only gauge cutters are affected by the testing procedure. Consequently, measured values reflect the friction of the shield. Therefore, the cutterhead can be retracted from the tunnel face by approximately 40 cm and then pushed again forward with the average rotation speed and an advance rate of the previous strokes. If the thrust was reasonably constant over a distance of 10 cm, the friction stroke could be finished and the cutterhead could be pushed forward close to the tunnel face without touching it (Frenzel et al. 2012; Wilfing, 2016). The proposed procedure is as follows:

– Retract the cutterhead by 400 mm.

– Rotate the cutterhead at the average speed of the previous strokes.

– Push the cutterhead forward at the average advance rate of the previous strokes.

– If for a distance of 100 mm a reasonably constant thrust force is established, increase the speed and move the cutterhead close to the tunnel face without touching it.

More information about the site penetration test and related subjects can be found in Bruland (2000) and Villeneuve (2005) as well as Gong et al. (2007).

3.2.3 Torque

Torque of TBM cutterhead can be calculated from equations which are proposed by the machine manufacturer. Equation 3.7 is an example of this formula which is introduced by Robbins Company for calculation of open type of TBMs.

$$T_q = \frac{U_T \cdot \sqrt{3} \cdot n_m \cdot Cos\varphi \cdot \eta}{2\pi \cdot 1000 \cdot RPM} \cdot I_T \tag{3.7}$$

By estimation of torque, rolling force can be determined as follow:

$$F_R = \frac{2 \cdot T_q}{r_{mc} \cdot d_{TBM} \cdot N_{TBM}} \tag{3.8}$$

Where T_q is cutterhead torque (kN-m), U_T is machine voltage (v), I_T is amperage (A) $\cos\varphi\eta$ is coefficient of efficiency, n_m is number of motors, d_{TBM} is machine diameter, F_R is rolling force of disc cutter (kN), r_{mc} is the average weight of cutter distance from the center of rotation (r_{mc} = 0.592m), N_{TBM} is number of cutters on cutterhead and RPM is cutterhead rotational speed (rev/min). Torque can be calculated from the rolling force as well to be compared to the available torque on the machine as:

$$T_q = 0.3 \cdot d_{TBM} \cdot F_R \cdot N_{TBM} \tag{3.9}$$

3.2.4 Composite Indices for TBM Performance

In addition to parameters such as, penetration rate, thrust, and torque which can be determined directly during the excavation in tunnel site, there are some parameters which are calculated by the combination of parameters and have been suggested by researchers, for example; power, specific energy, field penetration index and specific excavation rate. These indices can be calculated by the following formulas:

$$Po = \frac{2\pi \cdot RPM \cdot T_q}{60} \tag{3.10}$$

$$SE = \frac{4 \cdot 1000 \cdot Po}{ROP \cdot RPM \cdot 60\pi \cdot d^2_{TBM}} = \frac{400 \cdot T_q}{3 \cdot d^2_{TBM} \cdot ROP} \tag{3.11}$$

or

$$SE = \frac{200 \cdot N_{TBM} \cdot r_{mc}}{3 \cdot d_{TBM}} \cdot \frac{F_r}{ROP} \tag{3.11}$$

$$FPI = \frac{F_n}{P} \quad , \quad SP = \frac{P}{F_n} \tag{3.12}$$

$$SER = A \cdot SP \tag{3.13}$$

where *Po* is power of machine (PW), *SE* is specific energy defined as the energy requirement of disc cutters to cut the unit volume of rock, FPI is field penetration index (kN/cutter/mm/rev), *SP* is specific penetration which is inverse of FPI and *SER* is specific excavation rate defined as the excavation per revolution divided by thrust per cutter to combine *SP* and the tunnel cross-sectional area (m^3/rev)/(kN/cutter).

In equation 3.10, the power of the machine is estimated by torque and RPM . In equation 3.11, in addition to torque, P is applied, and RPM is eliminated. This issue indicates that specific energy (SE) is a function of F_R (torque or power) as well as P .

3.3 Rock Fragmentation Process

Since the introduction of mechanical excavation technology, there have been numerous studies to explain the interaction between rock and mechanical cutting tools as well as the rock fragmentation process. In terms of the developed idea in Colorado School of Mine (Rostami, 1993), rock fragmentation under disc cutter includes different procedures such as; Crushing, Chipping, Fracturing. Each of these phenomena is representing one of the physical properties of rock and in combination with each other indicates the boreability of rock. The indentation tests and numerical modeling results showed that beneath the indenter three different zones can be distinguished, namely, the crushed zone, the fracture zone, and the elastic zone. Given of stresses distribution scheme, three zones can be considered just beneath the disc cutter as can be seen from figure 3.3.

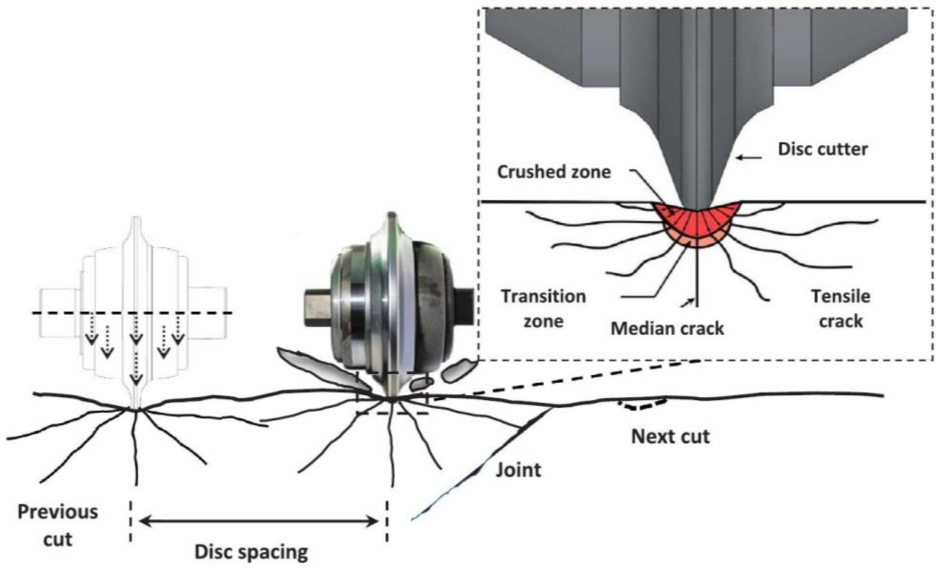

Figure 3.3: Indentation process and different zone (Heydari et al. 2019)

In brief, the process of rock fragmentation (indentation of cutter into rock) can be categorized into two categories:

- Building a highly concentrated stress field and formation of the crushed zone.
- Formation of sub-surface fracture propagation and chipping.

The observations made by nearly all the researchers have confirmed that, as the disc cutter penetrates the rock, it creates a crushed zone or the so-called pressure bubble under a disc cutter. This zone provides the means for the transfer of stresses into the rock medium (Figure 3.3). The exact configuration of this zone is not known, but it is assumed to be circular. This zone consists of some fine-grained crushed rock that is developed due to high-stress concentrations in the area immediately under the cutter. The size of particles increases from the center towards the rock media surrounding the pressure bubble. The extension of this zone is a function of cutter tip geometry and rock properties. The exact pressure distribution in this zone is not clearly/definitely known. Rostmai (2013) has simulated pressure distribution zone in the contact area between the disc and rock surface via finite element model (FEM) code. The results indicated that, the pressure within the contact zone is more concentrated, and the actual pressurized area is smaller than the size of the contact zone that has been assumed by previous models. This indicates that higher stresses could be experienced in this zone, beyond what was previously expected and used in many of the models. Furthermore, rock cutting with a TBM disc cutter has been simulated by Discrete/Finite Element Modelling (Labra et al. 2017). The model has been applied to the simulation of the laboratory test of rock cutting with a single TBM (tunnel boring machine) disc cutter. The results have confirmed a non-uniform contact pressure distribution revealed in experimental investigations and shown that a uniform pressure distribution in theoretical models is a simplified assumption (Figure 3.4). Li et al. (2018) have simulated the cutting processes when a cutter and disc cutter are cutting rock and soil masses using finite element models, ABAQUS software. The simulation demonstrated that, in the penetration process of the disc cutter, the closer the location is to the action area, the bigger the stress is. On the contrary, the further it is from the acting force, the smaller the stress is. In addition, the stress at the two side faces of the cutting edge is strongest, but it is getting smaller gradually towards the middle. Also, it was concluded that, at the initial stage of penetration, stresses concentrate at the contact surface, and the failure zone appears on the rock surface. Because the stress is very high, some parts of the rock mass crush or obvious plastic deformation is created in the failure zone. With penetration depth increasing, the maximum Von Mises stress of the rock increases almost linearly, and plastic strain accumulates constantly, resulting in the stress growing as well.

Also, the effect of confining pressure on the rock breakage efficiency on the TBM cutter has been studied by different researchers (Yin et al. 2014a & b; Innaurato et al. 2011; Ma et al. 2016). It been has proved that, in general, with increasing confining pressure, the crack initiation force and the crushing area gradually increase; in addition, rock fragments form more easily due to the increase of the confining pressure, so the rock breakage efficiency of the TBM cutter is higher. Ma et al. (2011) used the finite element program RFPA^{2D} to study the effect of the limiting stress on the rock fragmentation performance of a TBM cutter and concluded that, the confining pressure can change the direction of crack propagation and the length of the effective crack, which was consistent with the conclusions of Liu et al. (2002), who used the R–T2D (Rock–Tool interaction) program. Ma et al. (2011) also calculated the specific energy (SE) required for different confining pressures and found that when the confining pressure is less than a critical value, the specific energy increases with increasing confining pressure. When the confining pressure is greater than the critical value, the SE decreases as the confining pressure increases.

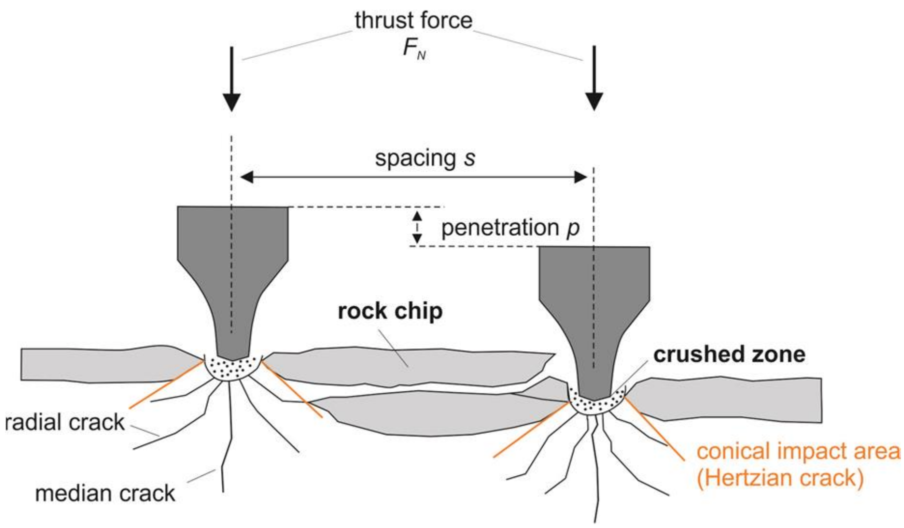

Figure 3.4: Schematic figure of the fragmentation process during rock excavation with disc cutters (Rostami, 1997; Wilfing, 2016)

As can be seen from Figure 3.4, radial cracks are created by the induced stresses in this zone. At the cutter edge, Gong et al. (2005) proved that a conical crack (Hertzian crack) is initiated which agrees with the theory of contact mechanics between a rigid indenter and brittle material. Furthermore, radial cracks and a median crack develop. If these cracks grow and coincide with cracks from adjacent cuts reaching free rock surface, rock chips are formed and chipping takes place. Besides that, Li et al. (2016) studied the effect of the confining pressure on crack propagation during TBM rock breakage using the PFC-2D software. They concluded that the confining pressure plays a negative role in the median crack propagation and that a higher confining pressure consumes more energy. Lin et al. (2018) employed an experimental investigation of jointed rock breaking under a disc cutter with different confining stresses. The results indicated that, peak indentation force increases with the increase in confining stress during the indentation process. The median crack is well developed at low confining stress. However, the median crack is restrained, and the rock chip formation is mainly caused by side crack propagation when the confining stress increases. Moreover, Liu et al. (2015) also used PFC-2D to study the geometric features of the fragments generated by indentation tests under different confining pressures and concluded that the fragment width decreases with increasing confining pressure. The reason for this phenomenon is that the confining pressure increases the deflection angle of the crack initiation, which is consistent with experimental results (Cook et al. 1984) and finite element numerical simulation results (Liu et al. 2002; Ma et al. 2011).

Regarding to chipping, it is not definitely known whether the formation of rock chips is contingent on the development of shear or tension cracks or a combination of both.

Nowadays researchers tend to prefer the mechanical approach of tension cracks since the cutter induces high stresses on a single spot at the tunnel face which is more likely compared to tensile or point load forces than to shear forces (Rostami, 1997; Barton, 2000; Li et al. 2018). Numerical simulation of rock fragmentation process induced by two TBM cutters and optimization of cutter spacing has been investigated by Gong et al. (2006). The results show that, in the beginning, each cutter indents the rock independently and similarly to a single cutter indentation process. The stress field is also independent. After the formation of the crushed zone, cracks are initiated from this zone, and then the side cracks propagate along a certain direction due to the interaction of two cutters. With increasing penetration, the side cracks between two cutters propagate to each other and coalesce, and form the rock chip. The chip formation is greatly dependent on the cutter spacing and the critical cutter load. Also, the critical cutter stress required for chipping increases with increasing cutter spacing. The fact is that, the interaction between the cracks from two adjacent cuts guides the propagation of fractures. When two or more cracks from neighboring cuts meet or cracks reach the free surface, chipping occurs. It is noteworthy that, the length of the cracks is a function of the pressure in the crushed zone. In addition, the cut interaction depends on the spacing between the cuts, the angle, and the extension of cracks between the adjacent cuts. According to fracture mechanics principles, a crack may propagate in any direction which provides the least surface energy and continues to grow as long as the stress intensity is higher than the critical stress factor of rock. This propagation can continue until stress intensity drops below the critical value or the crack meets a free surface (that can be another surface). This means that chips can be formed by cracks at any angle (Xia et al. 2017; Cho et al. 2006 & 2010; Tumac & Balci, 2015).

In practice, during excavation, TBM cutters roll across the tunnel face and continuously expand the crushed zone immediately beneath themselves. Then, cracks are initiated from the crushed zone and propagated downwards and sideways. One or more cracks under the action of the rolling cutter may reach the free surface or propagate to meet the cracks of the neighboring cuts. In these two cases, chipping occurs. The first case is similar to the chip formation of a single cutter indentation process. The latter is the interaction between two adjacent cuts. It is directly relevant to the design of TBM cutterhead and the efficiency of TBM excavation (Figure 3.5) (Gong et al. 2006).

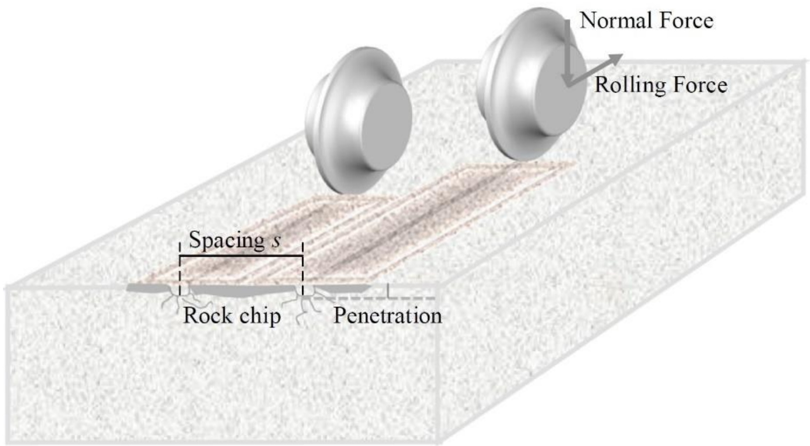

Figure 3.5: Rock chipping by TBM cutters (Zhao et al. 2019)

Snowdon et al. (1982) performed a series of liner cutting tests utilizing the Linear Cutting Machine (LCM). The results showed that, the specific energy of cutting (cutting efficiency) is strongly affected by cutter spacing and cutter force. Also, the influence of cutting geometry on chip formation in the linear cutting tests was investigated by Rostmi and Ozdemir (1993). The results indicate that, the size of the crushed zone immediately under the cutter is affected by cutter tip geometry. Besides that, the cutter spacing, and cutter force affect the induced cracks propagation and rock chip formation between adjacent cuts. Using numerical simulations on the cutter indentation process and rock chipping between adjacent cutters, Gong and Zhao (2007) deduced that the thrust force, the cutter diameter and cutter tip width affect the stress field in rock and then the indentation process.

It is worth to note that, in general, the rock breakage process is closely related to the machine parameters, such as TBM diameter, cutter line spacing, cutter diameter, and tip width, total thrust, and torque- power requirement of the cutterhead.

3.4 Parameters Affecting TBM Performance

During the rock excavation process, many factors affect TBM performance Table 3.1 lists the important factors influencing TBM performance. Some factors directly and some parameters indirectly influence the penetration rate. For example, net penetration is influenced mainly by rock material and rock mass properties and machine parameters such as thrust and cutter spacing. However, if there is a lack of transport capacity, the operator may run the TBM below its capacity instead of pushing it to its limits. The most important factors with major impacts on TBM penetration rate can be classified as follow:

1. Intact rock properties

2. Rock mass properties
3. Ground conditions along the tunnel alignment
4. Machine characteristics (Power, thrust force, torque, shape, and size of disc cutters, etc.)
5. Site management and logistics

Among these parameters, except for the last one; all parameters have a direct impact on the penetration rate of TBM in rock, while the last parameter mainly influences machine utilization.

Table 3.1: Factors influencing TBM performance (Blindheim, 2004)

Geological/Geotechnical	**Machine and Operation**	**Organization**
Rock material properties	TBM specifications	Work arrangements
1.Strength: compressive, tensile, shear	1.Thrust, net and total including friction	1. Available hours, work regulations
2. Crushing strength, toughness strength	2. RPM, rolling speed	2. Shift schedule, buffer time
3. Elasticity, rebound, hardness	3. Torque capacity, installed and usable power	3. Crew organization authority of shift bosses, autonomous groups
4. Anisotropy	4. Number diameter, edge width, material	4. Crew training and experience
5. Porosity	5. Cutterhead diameter, shape, and stiffness	5. Crew remuneration, bonus system
6. Abrasivity	6. Cutter change mode: front or back-loaded	
Rock mass features	7. Re-gripping principle: thrust on walls/roof or on segmented lining	Services
1.Type of weakness planes; joints, fissures, partings, bedding planes		1. Electricity, water etc
2. Spacing		2. Ventilation, cooling
3. Orientation		Safety
4. Persistence		1. Dust control
		2. Fire control
		3. Light, vibrations, noise
Ground conditions	Operation	Management principles
1.Mixed face conditions	1. Thrust and torque	1. Authority of TBM manager, foremen
2. Rock stresses	2. utilization	2. Procurement conditions
3. Fault zones	3. Steering, friction	
4. Water	4. Cutter change sequence	
5. Gas		
Ground control	Backup system	Location
1.Water control measures	Transport system for muck and supplies	1. Tunneling traditions Labor qualifications
2. Rock support measures		2. Supply of goods Local laws, regulations
3. Lining		

3.4.1 Intact Rock properties

Rock material strength is used as an important parameter in many rock classification systems as well as predicting boreability and drillability of rock. Rock strength affects rock behavior under compression. It is certainly true that, when the rolling cutter indents the rock, the stress exerted must be higher than the rock strength. Thus, the rock strength is directly relevant to the performance of TBM. Hence, the Uniaxial Compressive Strength of rock (UCS) is one of the most important engineering properties of rocks. In fact, UCS can be used to evaluate the resistance of the rock against the indentation of the cutting tool into the rock surface. It should be noted that, prediction models relying only on the UCS of intact rock may provide inaccurate results. So, the other intact rock strength tests should be taken into account to increase the accuracy of TBM performance.

Tensile strength is another common rock property that is used in making boreability predictions. Brazilian Tensile Strength (BTS) is generally intended to provide an indication of rock brittleness from a viewpoint of crack propagation between adjacent cutter paths. The fact is that, the compressive strength was used to describe the rock crushing beneath the cutter tip while the tensile strength accounted for the chip formation between adjacent cuts.

It is noteworthy that, great attention should be paid how to the sample failed during UCS or BTS testing. Figure 3.6 illustrates a typical structural and non-structural failure of UCS and BTS samples. Those samples, which were observed to fail along with existing rock defects, such as joints, fractures, bedding, or foliation, must be classified as a structural failure. Where the sample failure was not controlled by any defects and occurred in an "intact" manner, the sample was noted as having failed in a non-structural manner.

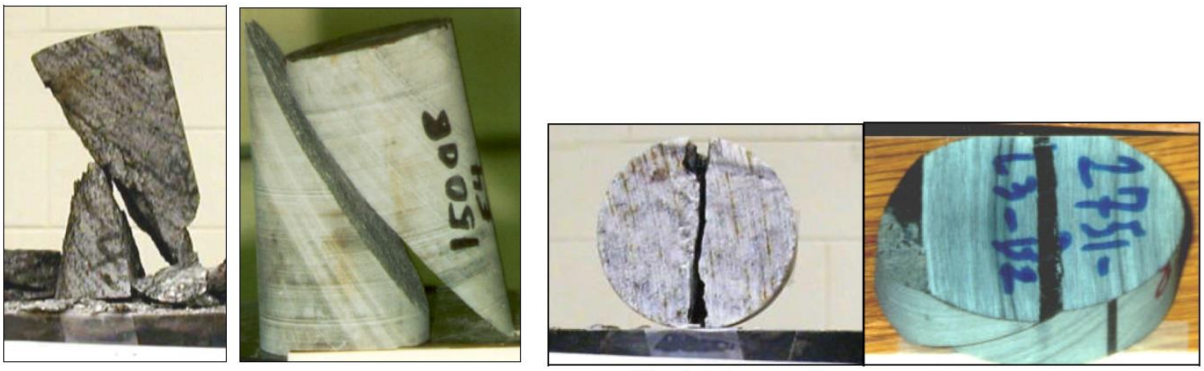

UCS non-structural | UCS Structural | BTS non-structural | BTS structural

Figure 3.6: Failure types for UCS (left) and BTS (right) (Cigla et al. 2001)

Another rock property, which affects boreability is the brittleness or the ductility, which the rock exhibits as subjected to the mechanical forces generated by the cutting action of an excavator. In general, the rock cutting efficiency of any mechanical tool improves with increasing brittleness (ease of fracture initiation and propagation) exhibited by the rock formation. Thus, brittleness is a highly desirable feature of the rock from a boreability standpoint. Even though brittleness is one of the necessary properties of rock, there is no agreement in the engineering rock mechanics community to describe or measure it. There are several different methods used for the determination of rock brittleness; however, two common methods include the Punch penetration test and Brittleness value S_{20} were found to influence brittleness and boreability of rock when evaluating TBM potential performance (Kahraman, 2002; Gong and Zhao 2007; Yagiz, 2009).

Also, the brittleness index of rock has different definitions and it has been investigated by some researchers to estimate the measurement of brittleness index value obtained from uniaxial compressive strength and Brazilian tensile strength. Among them, three common definitions of brittleness indices are presented as follow:

$$B_1 = \frac{\sigma_c}{\sigma_t} \quad , \quad B_2 = \frac{\sigma_c - \sigma_t}{\sigma_c + \sigma_t} \quad , \quad B_3 = \frac{\sigma_c \cdot \sigma_t}{2} \tag{3.14}$$

Where σ_c and σ_t are uniaxial compressive strength and Brazilian tensile strength, respectively. Results of investigations have proved that, by increasing the brittleness index; the indentation process of disc cutter in rock comes easier. Gong and Zhao (2007) investigated the influence of rock brittleness on the rock fragmentation process induced by TBM cutters by utilizing numerical simulation (UDEC). The ratio of uniaxial compressive strength to Brazilian tensile strength (B_1) was adopted to quantify the rock brittleness. The results show that, with the decrease in brittleness index, the size of the crushed zone decreases, and the number and length of the main cracks outside the crushed zone also decrease, this means that, with the increase of the rock brittleness index the cutter indentation process gets easier.

Besides these rock properties, another factor that influences on boreability, as well as the penetration rate of TBM, is abrasivity (cutter life). This parameter is typically expressed in terms of average cutter life in hours, meter travelled on the face, cutters per meters of the tunnel, or cutters per cubic meter of excavated rock. Obviously, increased cutter consumption will impact maintenance time and machine utilization, but this item will not be discussed in this thesis. Abrasiveness is mainly affected by various factors such as mineral composition, the hardness of mineral constituents, and grain characteristics such as size, shape, and angularity. Tool wear is an important parameter in mechanized tunneling and is highly affected by rock abrasiveness. Abrasive wear leads to the removal of material from the tool surfaces while it is moving against the rock. This phenomenon is the function of the hardness difference between interacting bodies. It is caused by direct contact of tool and hard particles in the rock or contacts between tools and particles in between rock and tool. There are numerous tests to identify rock abrasivity. The most commonly used are:

I. The Vickers test, or the Vickers Hardness Number – VHN
II. The Cerchar test, yielding the Cerchar Abrasivity Index – CAI
III. The LCPC abrasimeter test, or the LCPC abrasivity index – ABR
IV. The NTNU abrasion test, offering the Abrasion Value - AV/AVS

3.4.2 Rock Mass Properties

In addition to intact rock properties, joint conditions of rock mass have great effects on machine performance. The main characteristics of rock mass that have a significant influence on TBM performance include:

- Discontinuity spacing
- Joint orientation relative to tunnel axis
- Joint characteristics (conditions)

In the following section, the impacts of these parameters on machine performance are investigated based on previous studies that have been presented by different researchers.

3.4.2.1 Discontinuity Spacing

Undoubtedly, this parameter is the most important property of rock mass which has a great role to play on machine performance. Rock masses are composed of rock material and joints, the existing joint conditions surely can affect the rock breakage process. It is easy to realize that discontinuity can facilitate rock breakage because cracks induced by disc cutters easily develop along the existing discontinuities as compared to extending across the grains. Rock quality designation- *RQD* (Deere et al. 1967), the volumetric joint count- J_v (Palmström, 1995), and joint spacing (Js) are three frequently used parameters to describe the discontinuity spacing. Joint frequency is one of the important parameters in the NTNU model to estimate the penetration rate of TBM. The past investigations by the Norwegian University of Science and Technology (NTNU), decreasing joint spacing means the fracture factor (K_S) increases which has a direct impact and leads to an increased penetration rate of TBM. Figure 3.7 shows the effects of joint spacing on fracture factor (K_S). It should be noted that, the smaller the distance between the fractures, the greater the influence on the penetration rate of the machine.

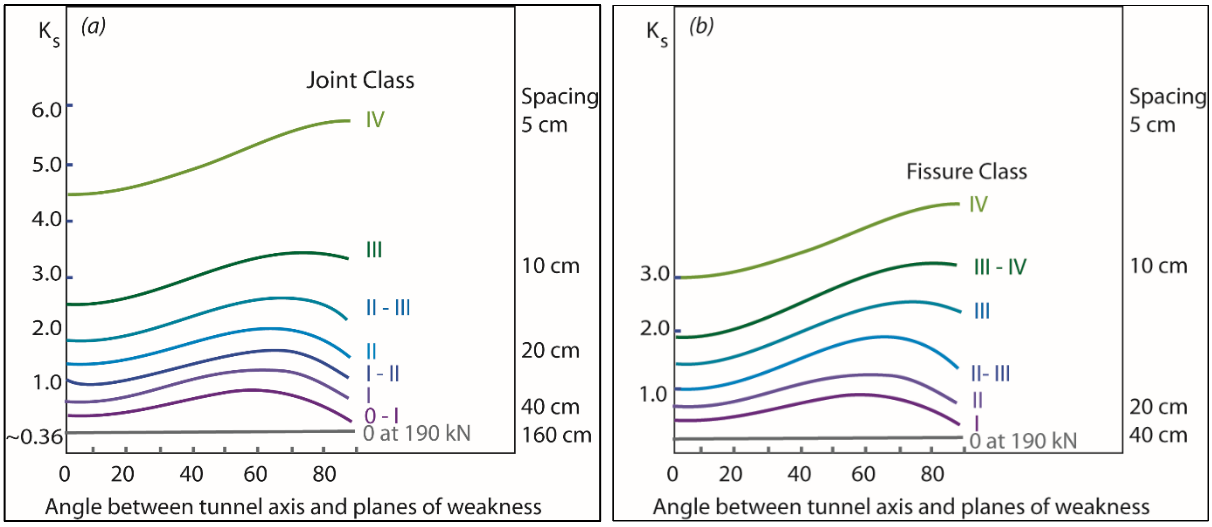

Figure 3.7: Influence of joint spacing and orientation on fracture factor (modified from Movinkel & Johannessen, 1986)

Barton (2000) in the Q_{TBM} model, used modified RQD, namely RQD_0 (it must be oriented in the tunneling direction) for performance prediction of TBM. In this model, RQD_0 has a direct relationship with Q_{TBM} and an inverse relationship with the penetration rate. The effects of joint spacing on TBM performance have been analyzed by Gong et al. (2006). In their investigation, rock indentation by a single TBM cutter is simulated by using the discrete element method (DEM-UDEC). Based on the field observations and statistical analysis of over 250 km of TBM excavated tunnels in hard rock conditions for more than 20 years, Bruland (1998) divided the discontinuities into two sorts, namely joint and fissure, and five classes as listed in Table 3.2. He summarized the effect of every fracture class and its orientation on the TBM penetration rate. For each discontinuity class and its orientation, a fracturing factor graph was drawn and the factor K_S has been estimated as shown in Figure 3.7 above.

Table 3.2: Fractures classes with distance between planes of weakness (Bruland, 1998)

Fracture class (joints = Sp, fissure = St)	Distance between planes of weakness (mm)
0	–
0–I	1600
I–	800
I	400
II	200
III	100
IV	50

The simulated results of Gong et al. (2006) are plotted in Figure 3.8 and have been compared with Brulnad's studies. The simulated values are smaller than the in situ measured values in rock masses with different fissure spacings, and also much smaller than those from in situ measurements in rock masses with different joint spacings. The main reason is that, in numerical modeling, fillings and aperture of the joints are not taken into account, and the simulation also does not consider the continuous boring process. But the shapes of these curves show good agreement.

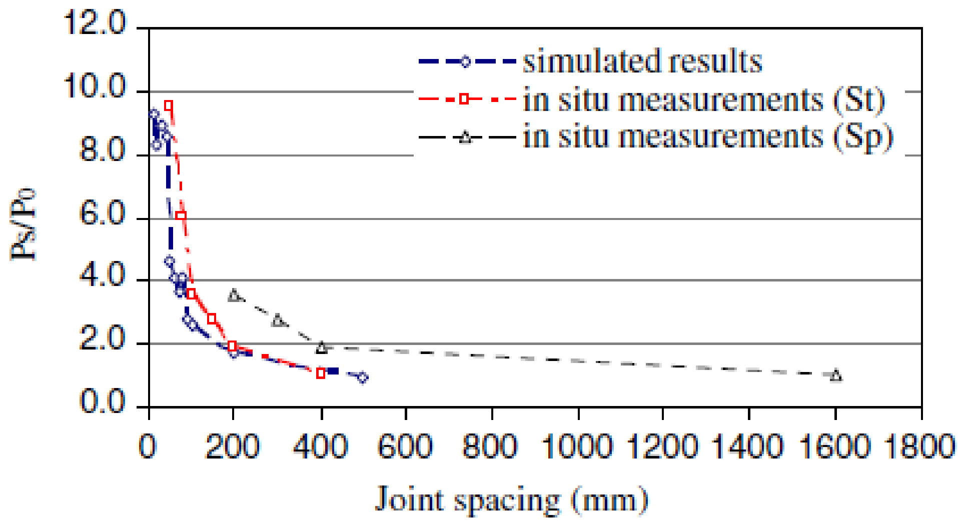

Figure 3.8: Effects of joint spacing on penetration rate (Gong et al. 2006)

In the above plot, P_s denotes penetration rate in different fracture spacings and P_0 denotes penetration rate in rock mass without fractures. It is certainly true that, whatever the ratio of P_s/P_0 is bigger, the effect of joint spacing on penetration rate is greater. This figure is plotted when the angle between the tunnel axis and the fracture plan is 90^0. It is interesting to note that, when joint spacing is 500 mm, its effect on penetration rate is very small while, penetration rate increases at joint spacing less than 100 mm. The main reason is that, when the joint spacing is less than 100 mm, the side cracks can propagate to the joint plan and improve the yield of rock chipping.

3.4.2.2 Joint Orientation

In foliated/bedded rock, foliation can play a significant role in rock fracture propagation between cuts, depending on the foliation direction with respect to the direction of machine advance. In recent years, the influence of the joint orientation on TBM penetration rate is widely observed in tunneling projects. For example, Aeberli & Wanner (1978) observed that, the advance rate of TBM increases with the increase of the angle between the TBM axis and the planes of schistosity in a homogeneous zone of schistose phyllite. In this regard; a 3.5 m diameter sewer tunnel passed through syncline for about 140 m (Figure 3.9) during which the angle between the tunnel axis and foliation planes changed continuously from 60^0 through 0^0 and back to 60^0. When the angle β was 90^0, a PR of about 1 m/hr was recorded, and when 30^0, PR had increased to 2.3 m/hr. Similar phenomena were also observed by Thuro and Plinninger (2003) (Figure 3.10).

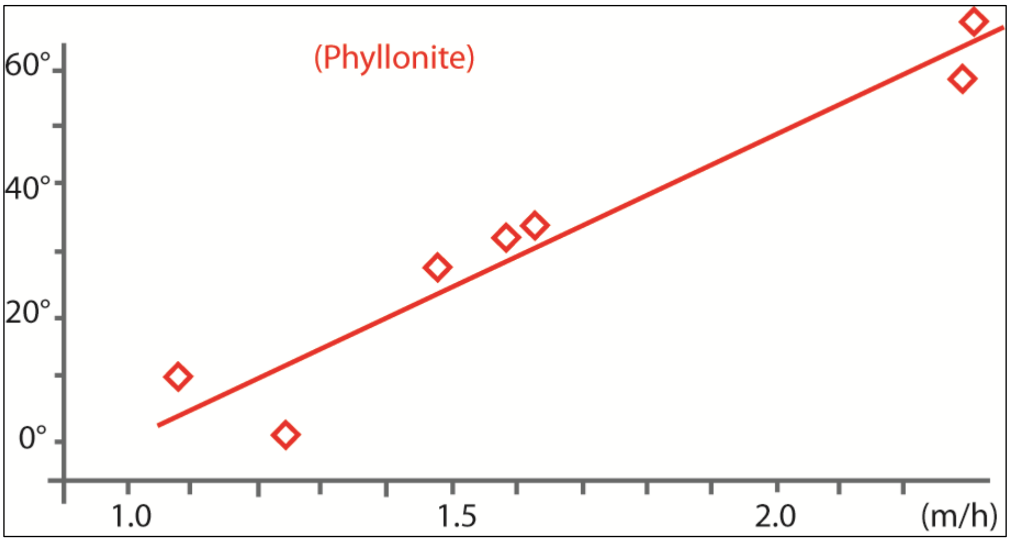

Figure 3.9: Graphic effects of foliation angle on penetration rates (average per day) in a 3.5 diameter TBM tunnel in Switzerland (modified from Aeberli & Wanner 1978)

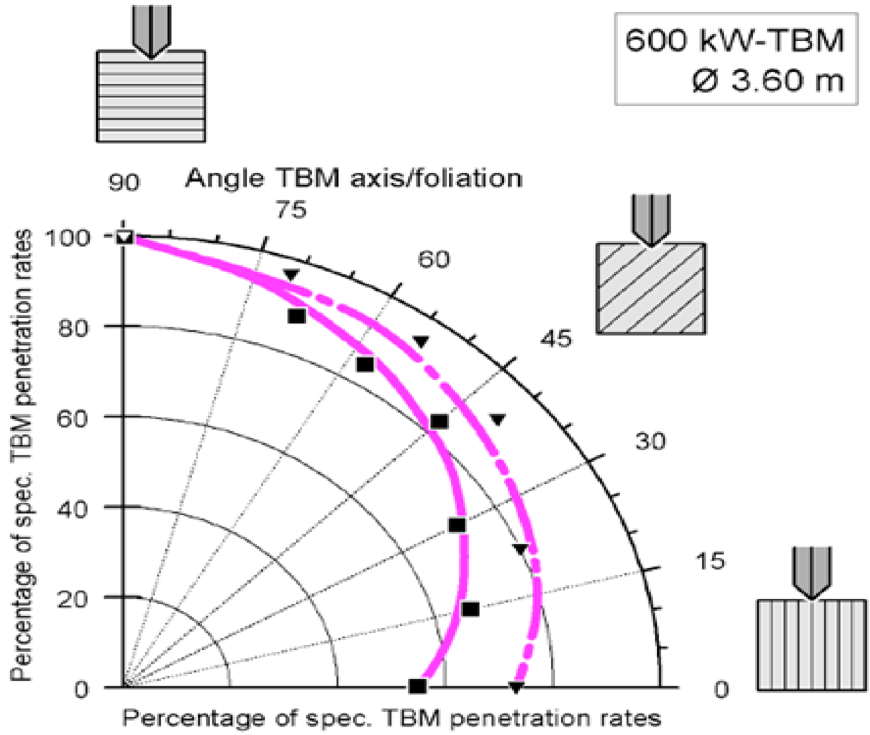

Figure 3.10: Mean values of specific penetration rate in phyllite (continuous line) and phyllite-carbonate-schist inter-stratification (dashed line) versus angle of foliation. Schönberg tunnel (Austria) (Thuro & Plinninger, 2003)

Besides that, a theoretical analysis of the interaction between cutter and rock with a foliation by Sanio (1985) showed a similar tendency. Sanio (1985) used 7 rock types [Salte, Gneiss, Sandstone, and limestone] with varying degrees of anisotropy. The purpose of this study was to develop predictor equations for rocks with bedding or schistosity since anisotropies influence the penetration. The author conducted wedge indentation and full-scale cutting tests on rock samples with certain orientations of the bedding or schistosity. The influence of different orientations on the penetration force has been analyzed by accounting for two different angles (Figure 3.11)

- α' : the angle between the momentary rolling direction of the cutter and the apparent strike of the anisotropy on the tunnel face.
- β' : the angle between the anisotropy planes (bedding, schistosity) and the tunnel face.

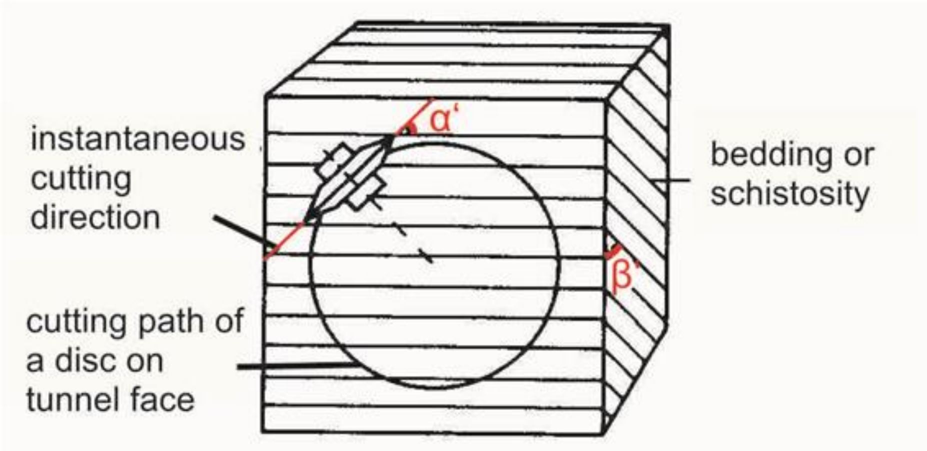

Figure 3.11: Definition of α' & β' determining the orientation of anisotropy planes (Wilfing, 2016; Sanio, 1985)

According to Sanio (1985), penetration rates six times faster were recorded when the tunnel axis impingement angle β was 0^0 compared to 90^0. Bruland (1998) summarized the effects of joint orientation of different classes of joints and showed a similar trend (Figure 3.7). His investigations showed that the maximum penetration rate occurred when the angle was equal to 60^0. For a single joint, whereas the maximum penetration is expected in tightly fissured rocks at $\alpha = 90$ degree. Also, Figure 3.12 shows the influence of bedding planes angle ($\beta = 90 - \alpha$) (normal to tunnel axis) on the penetration rate of the disc cutter. As can be seen, with an increase of angle; the penetration rate decreases significantly (Barton, 2000). β is the angle between foliation and the horizontal plane measured perpendicular to the tunnel face and α is the smallest angle between the foliation and tunnel axis. The definition is also shown in Figure 3.13.

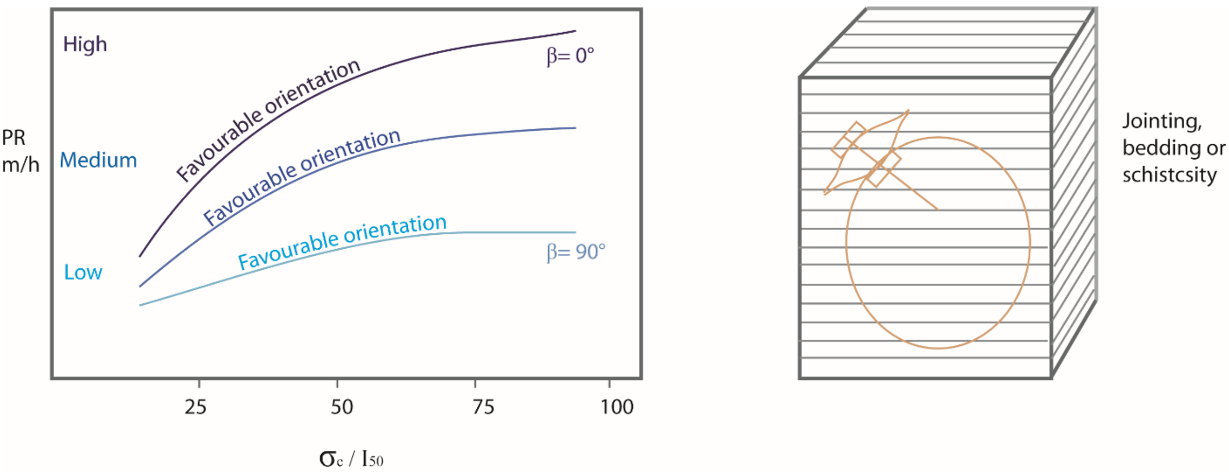

Figure 3.12: Effects of bedding planes angle on penetration rate of disc cutter (modified from Barton, 2000)

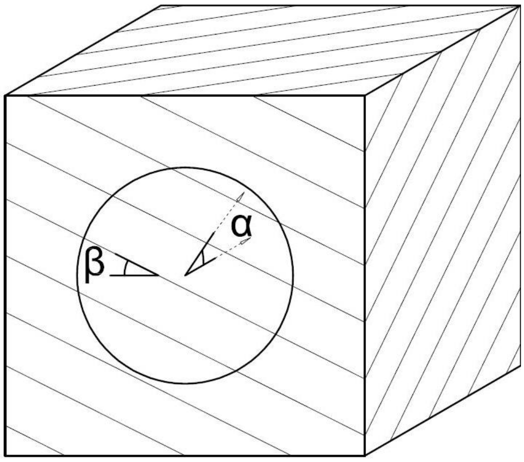

Figure 3.13: Definition of α and β (Entacher, 2013)

The reason for this phenomenon is that, when machine advance is parallel to foliation planes (Figure 3.14); crack propagation is forced to occur across the foliation planes. This reduces machine penetration because of the increased difficulty of rock breakage. When the foliation is perpendicular to the direction of machine advance, rock failure occurs along foliation planes as indicated in Figure 3.15. This case generally, refers to the most favorable boreability as foliation planes assist crack initiation and growth between adjacent cuts.

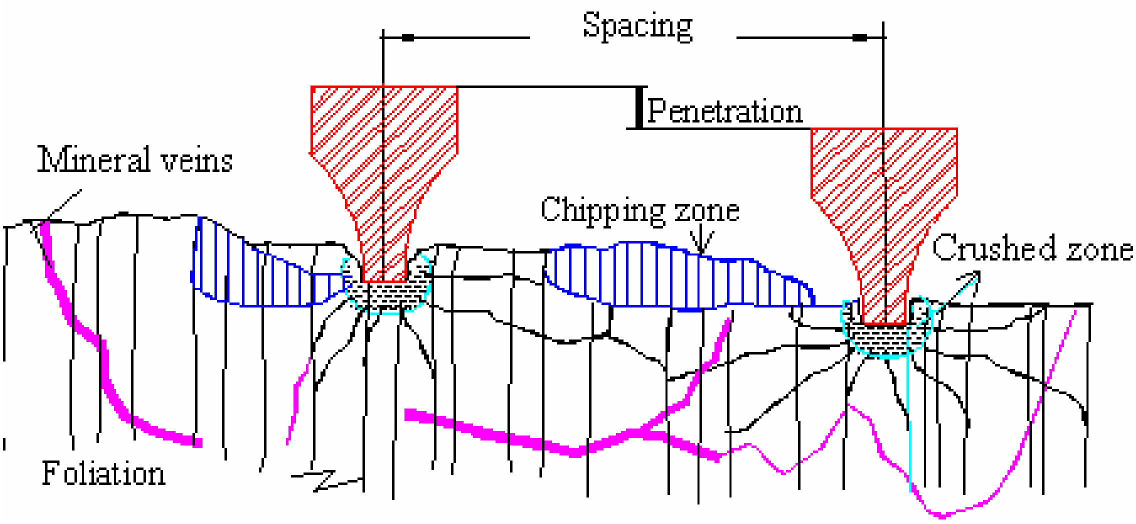

Figure 3.14: Cutting direction parallel to foliation (Yagiz, 2002)

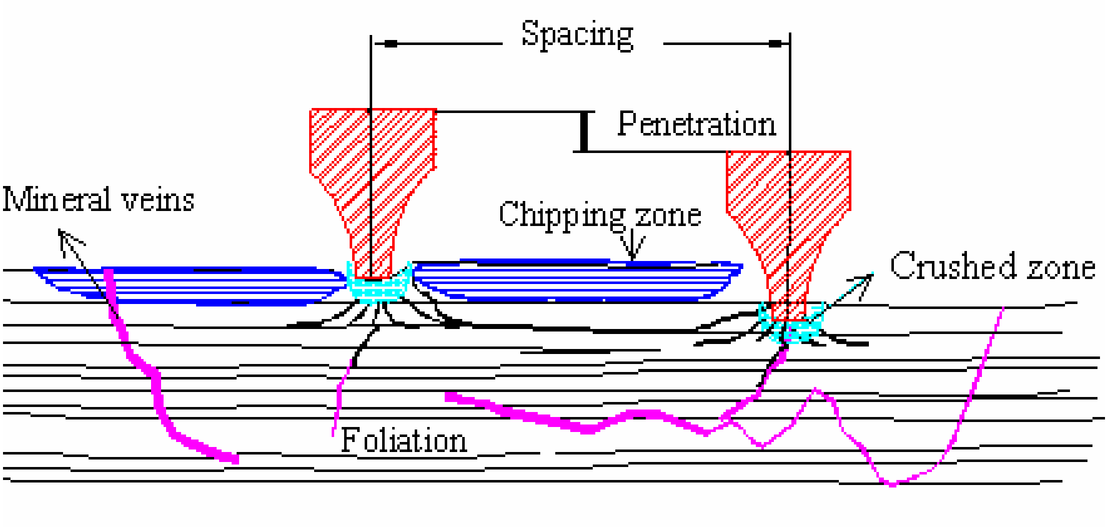

Figure 3.15: Cutting direction perpendicular to foliation (Yagiz, 2002)

Gong et al. (2005) simulated effects of joint orientation on rock fragmentation by TBM cutters with series of two-dimension numerical modelling using the discrete element method (DEM-UDEC). To configure the numerical model, a granite block with a dimension of 1.2 × 1.2 m, a joint spacing of 200 mm was set where the load applied over a 15 mm wide contact area with a fixed spacing of 200 mm had been conducted. The dip angle of the joint was varied between 0° to 90° and the rock chipping process and efficiency for each angle examined. The results demonstrate that, the rock chipping angle increases as the angle between the tunnel axis and the joint plane increases, except when $\alpha = 0°$ and 90°, since the crack initially propagates like in unjointed rock mass. As the angle α increases the penetration rate increases until a reach 60°, then the penetration rate decreases with the increase α . The modelling results conclude that the smaller the angle α , the easier the fragmentation of the rock mass. The results show good agreement with Bruland's result. Moreover, simultaneous effects of joint spacing and joint orientation on the penetration rate of a single disc cutter studied by Bejari et al. (2011) via computational numerical modelling named "Universal Distinct Element Code (UDEC)". To deal with this area of research, seven joint orientation (0°, 15°, 30°, 45°, 60°, 75°, and 90°), on the block of sandstone with the dimension of 1 × 1; 1.5 × 1.5 and 2.5 × 2.5 with three joint spacings, 150, 200, and 300, respectively were considered. The cutter was modelled in a similar method applied by Gong et al. (2005). This was a new contribution since previous studies only considered the effect of one of the joint conditions on rock fragmentation by a disk cutter: either spacing or orientation. The effect of joint spacing and orientation on TBM penetration was investigated by calculating the ratio of the chipping area to chipping stress, which indicates the frequency of chips in terms of cutting force units. The optimum disc spacing of 75 mm in sandstone was considered when calculating the chipping area. For this reason, the chipping area was calculated according to the crack propagation pattern in the rock and the rock cutting type under different joint conditions (Figures 3.16 & 3.17).

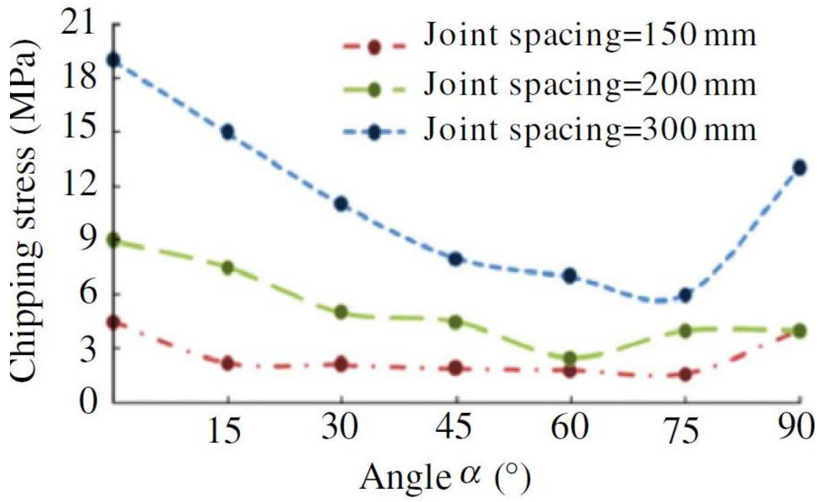

Figure 3.16: Chipping stress versus joint orientation and spacing (Bejari et al. 2011)

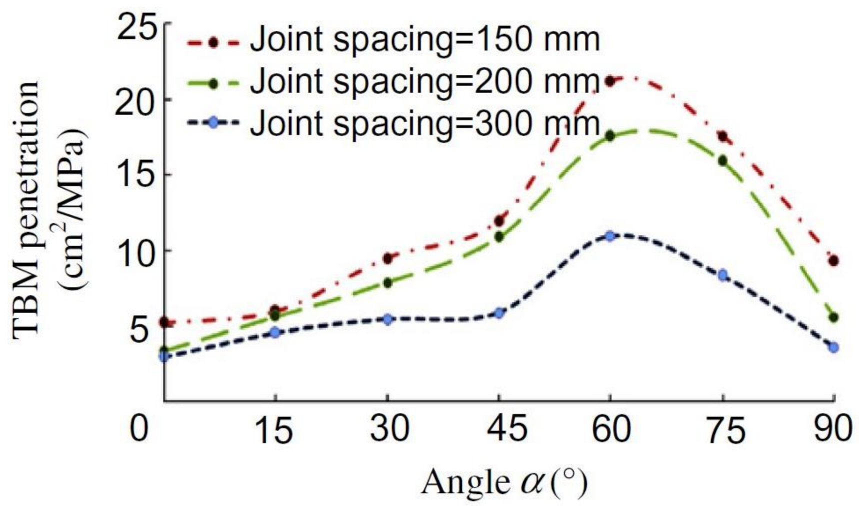

Figure 3.17: Effect of joint orientation and spacing on TBM penetration rate (Bejari et al. 2011)

The study shows that, increasing the joint spacing for a given joint orientation causes the TBM penetration rate to decrease. The gradient of increasing penetration is higher between 45° and 75° than it is between 0° and 30°. In addition, for any joint spacing penetration increases when the joint orientation changes from 0° to 75° but decreases as the joint orientation changes from 75° to 90°.

The results also demonstrate that an optimum joint orientation, from the viewpoint of TBM penetration, is about 60-75° which has a similar tendency with previous investigations. In addition, extensive experimental investigations have been carried out by Lin et al. (2018) to explore the effect of different confining stress (0, 2.5, 5, 7.5, and 10 MPa) on the rock breaking induced by the disc cutter respecting to different joint angles (0°, 30°, 60°, and 90°). The cement mortar sample is taken into account for simulating rock damage, since the main framework of the material is cement and sand, the cement is the adhesive material, and the sand can provide the frictional behaviour of the modelling material. This feature is similar to the actual rock failure. The rock-like specimens with dimensions of 150 ×150 ×30 and to create the existing joint, a mica sheet (70mm long × 30 mm wide ×0.4 mm thick) was inserted into and remained in the specimen. During the curing process, the temperature and humidity were maintained at 25 degrees and 90%, respectively. The dip direction of the joint set was assumed to be identical to the cutting load direction and the distance between the position of indentation and the center of the joint was 55 mm (Figure 3.18).

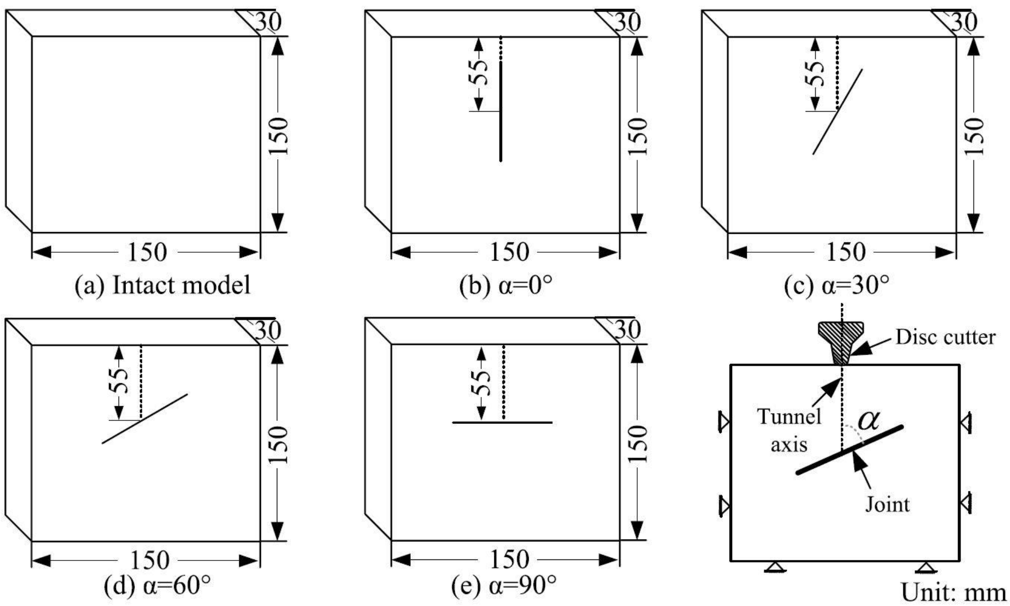

Figure 3.18: Joint geometry in the specimens (Lin et al. 2018)

Figure 3.19 shows the crack propagation and failure modes of rock breaking under the disc cutter when the joint angle is 0° and the confining stress varies from 2.5, 5, 7.5 to 10 MPa. Fig.3.18 displays that the medium cracks initiate from the crushed zone and gradually propagate along the jointed plane. Meanwhile, two cracks initiate at the upper tips of the jointed plane and propagate towards the free surface. With further increase in the indentation depth, the cracks coalesce with the side cracks and finally form rock chips.

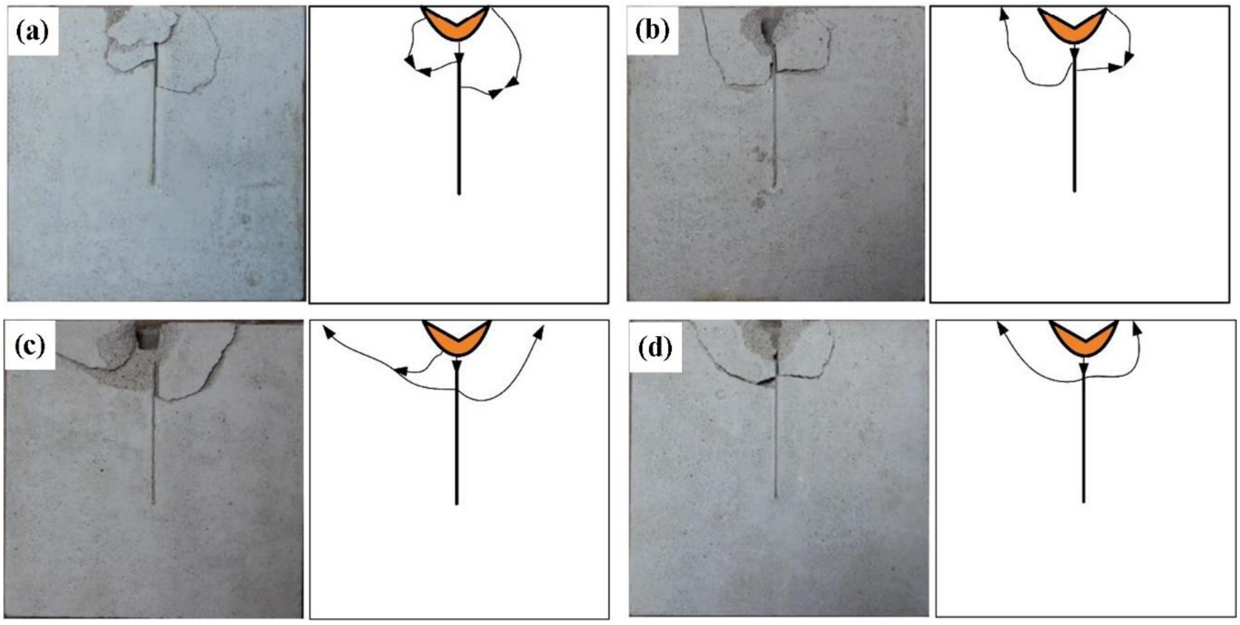

Figure 3.19: Effect of the confining stress on the final failure modes (α = 0°); Confining stress: a=2.5 MPa; b=5 MPa; c=7.5 MPa; d=10 MPa. (Lin et al. 2018)

Figure 3.20 & 3.21 exhibit when α is 30° & 60°, respectively. When the confining stress is low, the cracks propagate along with certain directions; medium and side cracks initiate and propagate from the crushed zone and terminate at the joint plane. Meanwhile, some cracks initiate from the joint plane and propagate upward to the free surface. When those cracks coalesce with the medium and side cracks, the rock chips are formed. However, when the confining stress increases to 7.5 and 10 MPa, the initiation and propagation of the median crack are restrained, as shown in Figs.19c and 19d. It should be noted that, the existence of joints has no obvious effect on the failure mode when the confining stress increases to a certain value.

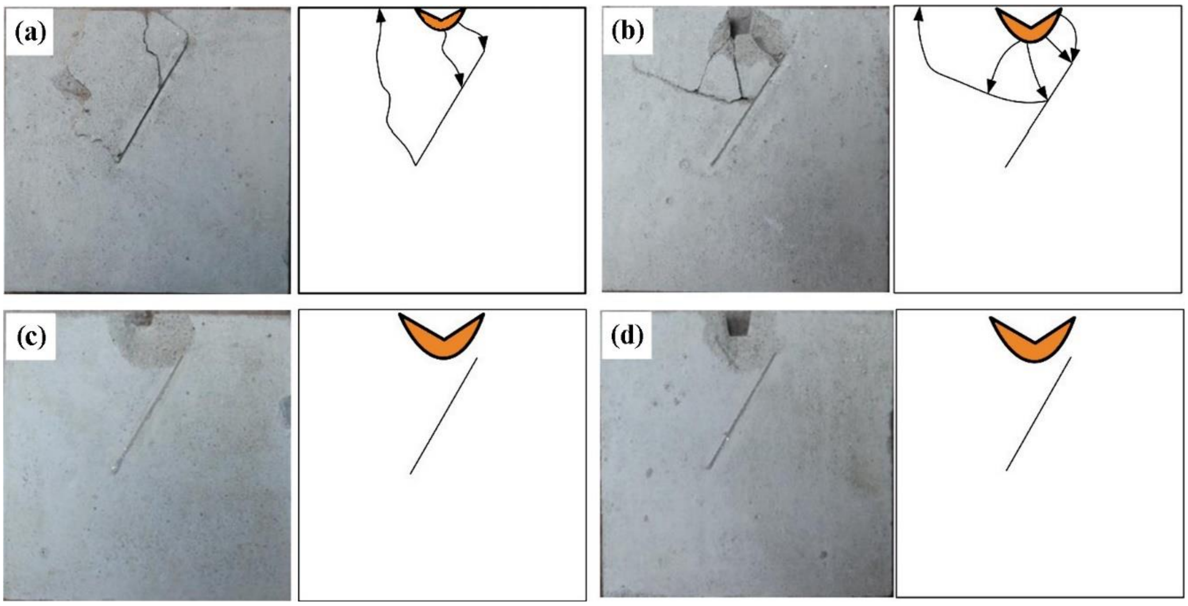

Figure 3.20: Effect of the confining stress on the final failure modes (α = 30°); Confining stress: a= 2.5 MPa; b= 5 MPa; c=7.5 MPa; d=10 MPa. (Lin et al. 2018)

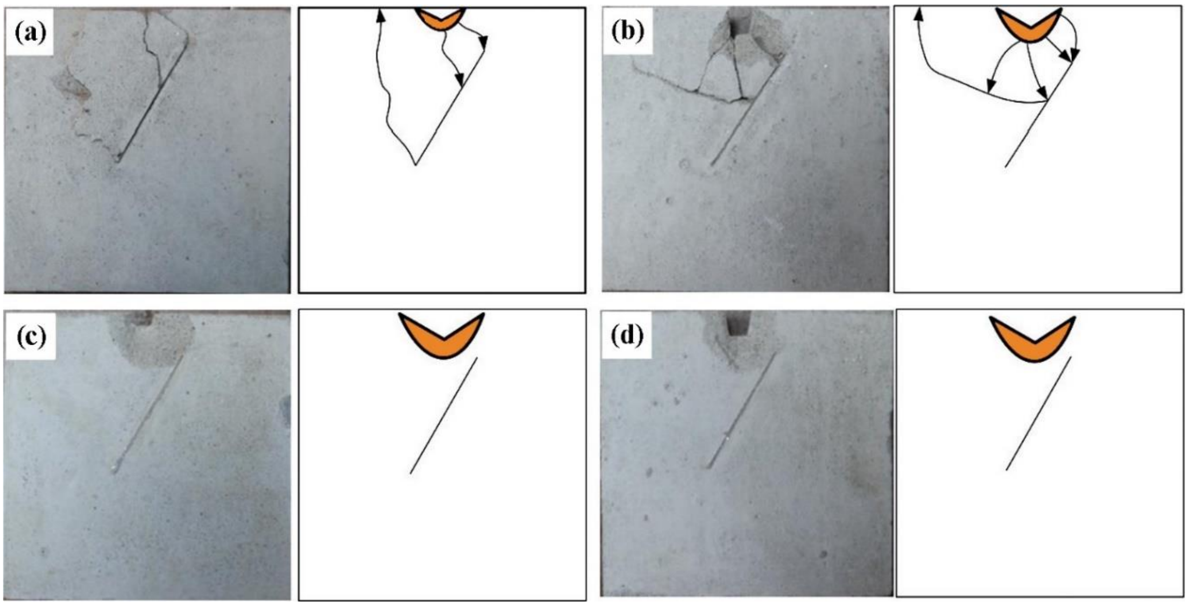

Figure 3.21: Effect of the confining stress on the final failure modes (α = 60°); Confining stress: a=2.5 MPa; b=5 MPa; c=7.5 MPa; d=10 MPa. (Lin et al. 2018)

When the joint angle α increases to 90°, the median crack is initiated immediately in front of the crushed zone, propagates along the induce way, and finally terminates at the joint surface. The side cracks initiate immediately in front of the crushed zone and propagate symmetrically, as shown in Figure.22a and b. The analysis showed that the joint plane significantly affects the rock failure modes when the confining stress is low.

However, when the confining stress increases to a certain value, the presence of the joints has no effect on the failure mode of the specimens.

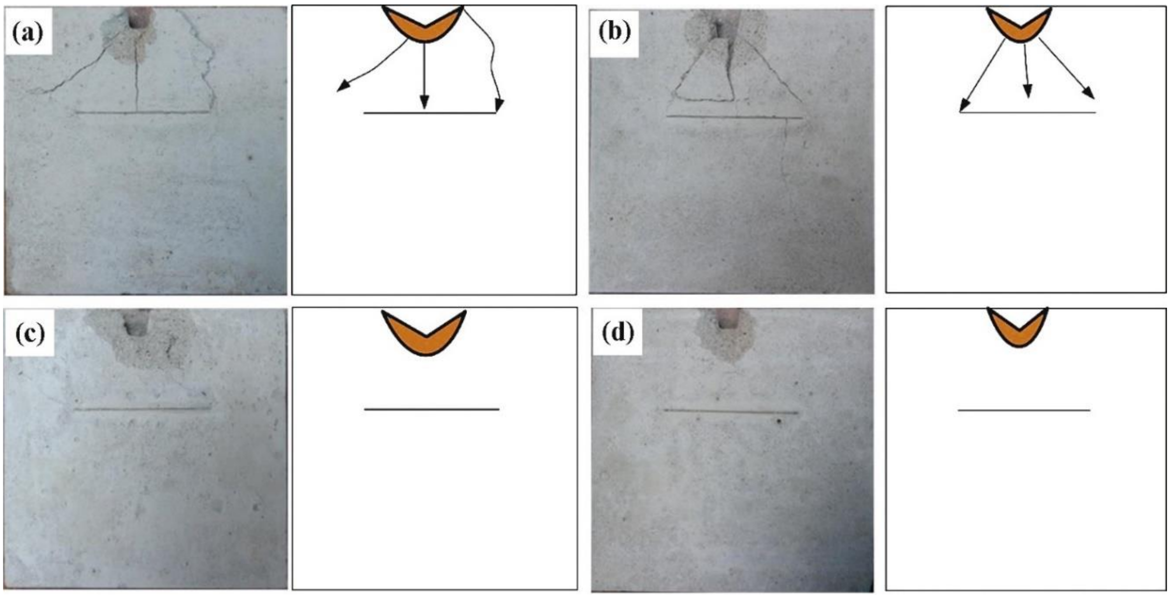

Figure 3.22: Effect of the confining stress on the final failure modes (α = 90°); Confining stress: a=2.5 MPa; b=5 MPa; c=7.5 MPa; d=10 MPa. (Lin et al. 2018)

The failure modes of rock breaking at low confining stress can be summarized as follows:

- when the joint angle is 0°, the crack initiates at the upper tips of the jointed plane and coalesces with the side crack; then, rock chips are formed.
- when the joint angle is 30° and 60°, the crack initiates under the crushed zone and propagates downward the joint plane; then, rock chips are formed.
- when the joint angle is 30° and 60°, the crack initiates at the joint plane and propagates upward the free surface; then, rock chips are formed.
- when the joint angle is 90°, the crack initiates from the crushed zone, propagates towards the joint plane, and finally terminates at the joint plane; then, rock chips are formed.

The change in peak indentation force with different joint orientations and confining stresses is presented in Figure 3.23 where the peak indentation force increases with the increase in confining stress. In particular, when the confining stress is 2.5 MPa, the peak indentation force is significantly different, which indicates that the joint orientation considerably affects the peak indentation force when the confining stress is low. Specifically, when the joint orientation is 30°and 60°, the peak indentation force is lower than that of the other specimens. The experimental results of the final failure modes also prove that the joint orientation has a considerable effect on the rock-breaking process when the confining stress is low. However, there is no obvious difference when confining stress increases to 10 MPa.

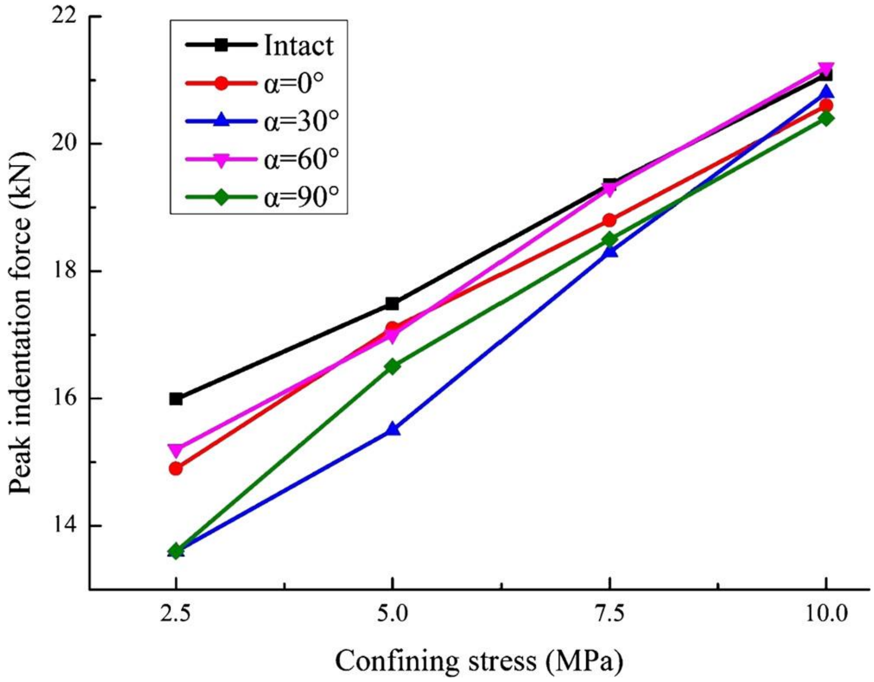

Figure 3.23: Peak indentation force of rock-like specimens with different confining stresses and joint orientations (Lin et al. 2018)

The above analysis indicates that when the confining stress is not notably high, and the rock mass with a certain joint angle is more easily broken. In addition, the peak indentation force increases with the increase in confining stress, which indicates that the TBM cutter requires a high thrust force in a high-confining-stress condition.

Besides that, Zhao et al. (2018) simulated the rock-breaking process of the TBM by the laboratory rolling boring tests on the sandstone specimen with the dimensions of 160 × 160 × 100 mm. Prefabricated joints with different forms are made in rock samples. Specifically, rock mass samples with different joint orientations (α = 0°, 30°, 45°, 60°, and 90°) and a 20 mm joint spacing were selected to study the effect of joint orientation on the cutting efficiency and cutter wear and for the purpose of investigating the influence of joint spacing, rock samples with different joint spacings (10, 20, 30, 40, and 50 mm) and a joint orientation of 45° are prepared for the tests (Figure 3.24). The specific energy is utilized to assess the cutting efficiency of the TBM. In addition to experimental tests, three-dimensional finite element models of rock mass and cutters are established in ANSYS software to study the effect of jointed orientations and jointed spacings on cutting efficiency numerically.

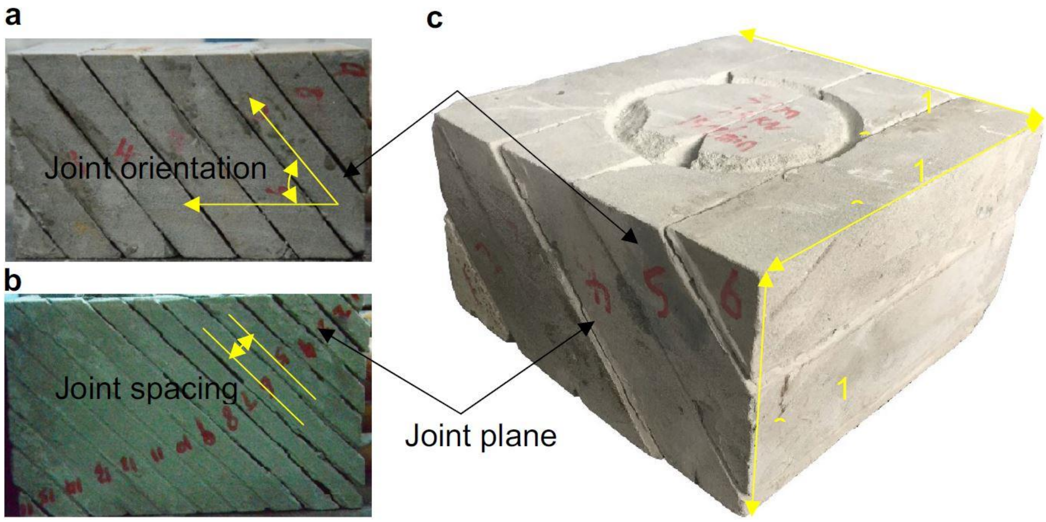

Figure 3.24: Schematic of rock specimens with different orientations and spacings: **a** rock specimens with different orientations (0, 30, 45, 60, 90°) with a 20-mm joint spacing, **b** rock specimens with different spacings (10, 20, 30, 40 50 mm) with a joint orientation of 45°, **c** oblique view of rock specimens with 45° joint orientation and 20-mm joint spacing (Zhao et al. 2018)

It was found that experimental results reach the minimum value when α is approximately 30°. Thus, this angle can be considered as the optimal dip angle for rock-breaking in the experiment. Hence, the phenomena are mainly caused by joint orientation. When disc cutters that are oriented at 0° roll on the surface of rock samples, the penetration process is practically similar to that performed on the intact rock sample until a penetration depth that exceeds the thickness of the rock slice is reached. Therefore, the specific energy and cutter wear are large, and as a result, the cutting efficiency is relatively low under this condition. However, for rock blocks oriented at 30°, the initiation and propagation of cracks exhibit a different mode. At this orientation, tensile cracks firstly occur at the joint plane and then propagate upwards to the free surface. The rock chipping angle (the angle between the tunnel face and rock damage plane) reaches the maximum value (Gong et al. 2006), which is most conducive to the formation of big rock chips. As a result, the minimum specific energy and wear values are achieved, and the cutting efficiency reaches the maximum. However, as α varies from 30° to 90°, the rock chipping angle decreases and hinders crack propagation, as well as chip formation. As the joint orientation increases, a larger normal force is required to cut with the same penetration depth, and fewer rock chips are formed. Therefore, cutter wear and specific energy are increased. When α = 90° the cutting efficiency is reduced to the minimum (Figure 3.25).

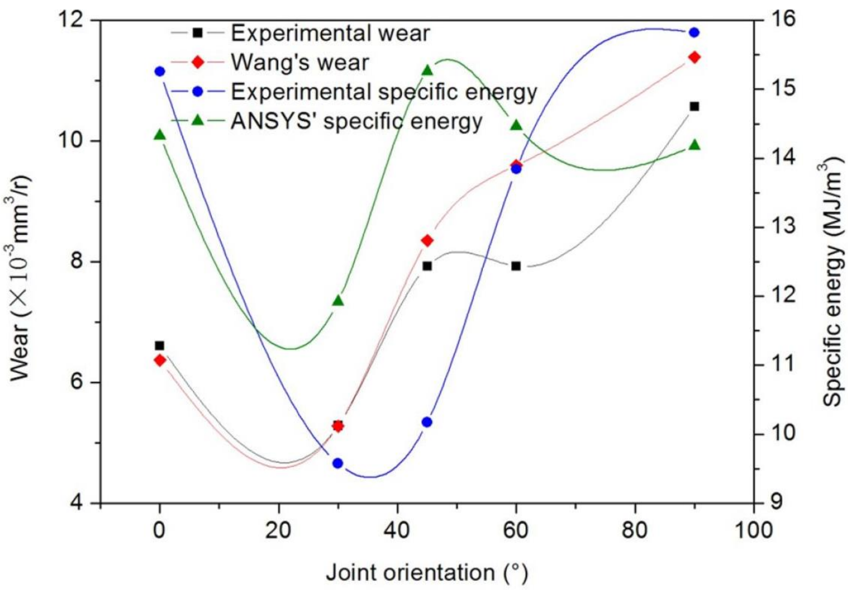

Figure 3.25: Variations of cutter wear and specific energy with joint orientation; joint spacing = 20 mm, normal force = 1.5 kN (Zhao et al. 2018)

In addition, in Fig. 3.25, it was observed that the specific energy obtained using ANSYS software reached a minimum when the joint orientation is approximately 30°, whereas the minimum numerical value is 24.5% larger than the experimental result. However, when the joint orientation is larger than 45°, the trend of numerical results is not in good agreement with that of experimental results. The errors mainly emanate from the lack of information on cutter wear, contact between cutters and rock mass in ANSYS, and measurement error in the tests. Therefore, the finite element simulation can only be used to predict the optimal joint orientation.

Furthermore, the influence of orientation and spacing of joints on the performance of TBM in hard rock by simulation of cutterhead in real dimension has been analysed numerically using PFC-3D (Afrasiabi et al. 2019). To assess the effect of orientation on the TBM penetration, different angles are considered between each joint set related to the advance axis (the spacing is considered constant and equal to 500 mm). The sensitive analysis has been performed on 7 angles (0°, 15°, 30°, 45°, 60°, 75°, and 90°), and the required thrust and torque for 10 cm penetration in different joint orientation have been estimated. Based on Fig. 3.26, the required mean thrust and torque decrease when the α angle between the joint set and advance axis increases. This trend will be changed from angel 60 to 90 and these forces are increased. It is worth noting that, the value of required mean thrust and torque is less than of these values in intact rock, which indicates the effect of jointing on ease of the rock cutting process. Based on these results, the convenience of rock cutting is increased by 30–70% depending on the joint orientation.

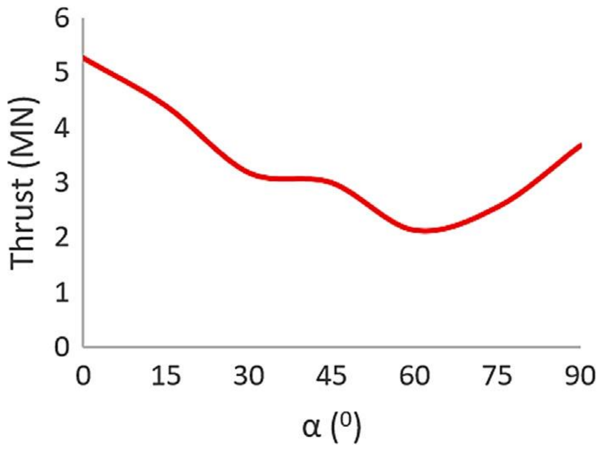

Figure 3.26: Required thrust (left side) and torque (right side) for different orientations (Afrasiabi et al. 2019)

To check the effect of joint spacing on TBM performance, since, in the joint orientation analysis, the zero angle between the joints and advance axis has the least effect on the performance of TBM, this angle has been used to analyse the effect of the joint spacing. The analysis has been performed at 100, 200, 300, 400, and 500 mm spacing (Figure 3.27).

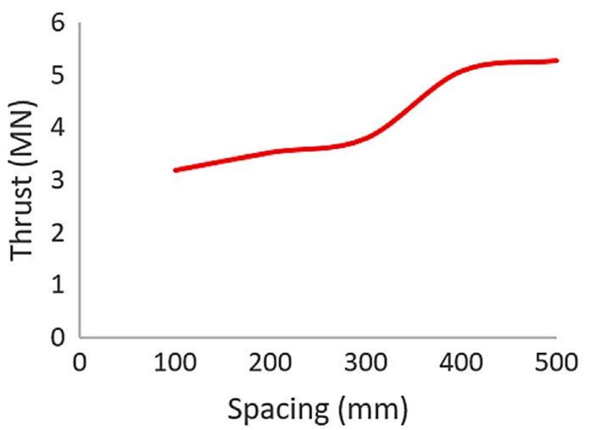

Figure 3.27: Thrust (left side) and torque (right side) required for different spacing (Afrasiabi et al. 2019)

It was found that, the presence of the joints has a significant effect on the performance of TBM as noted by many others, but the amount of this effect varies with different conditions of the joint's orientation and spacing. Based on the results, in the angle 60° (this angle is between joint sets and the advance axis of the tunnel) the best performance of TBM is achieved for single joints at larger spacings of >150-200 mm. On the other hand, by increasing the joint spacing from 100 mm to 400 mm, the positive effect of joint spacing on the TBM performance is reduced, but when the joint spacing is increased more than 400 mm, no change occurs in the machine performance. Therefore, 400mm spacing is considered as a critical spacing of joint on the ease of excavation. Generally, due to the joint orientation and spacing parameters, the ease of cutting in the jointed rock block is increased 30-70 percent (depending on the orientation of the joint), related to the intact rock block.

3.4.2.3 Joint Characteristics (Conditions)

Obviously, joint characteristics have some impact on machine performance. Theoretically, when the joint filled with softer material and has an open aperture, and smoother surface as well as highly weathered conditions, the boreability of rock mass and penetration of cutters become easier. Although, till now there is no comprehensive research to address this conflict, but Khademi et al. (2010) considers joint condition (Jc , partial rating in RMR classification) as an input parameter for prediction of TBM FPI. Jc in RMR is the sum of five factors, including persistence/continuity; aperture; Roughness of discontinuity surface; Infillings, and weathering discontinuity of joint surface. The results showed that, an increase of Jc causes an increase in FPI, meaning rock masses with less weathering become more difficult to bore. However, due to the lack of real proper information, there is no investigation to address this matter in detail and examine the joint characteristics, such as weathering degree or aperture, separately.

3.4.3 Geological Conditions

It is certainly true that, geological conditions such as; faults and underground water inflows have a great role to choose the type of machine, applicability, the performance of the machine, and production rate. Unfavorable ground conditions have a major role in decreasing the utilization of the machine. In brief, rock masses can be classified into four groups in terms of geological conditions including; blocky and jointed rock mass, massive hard rock, squeezing rock mass, and faulted rock mass (Figure 3.28). For more illustration of geological conditions and their effect on machine performance, it is noteworthy that, there is a high risk of tunnel convergence and TBM jamming as well as machine break down in squeezing ground conditions and the need for over-boring, use of lubricators such as bentonite, grease and increasing thrust of longitudinal jacks to remedy the conditions and also need for heavy support. Also, the crossing of fault zones in TBM tunneling represents, in general, a problematic event and is often associated with a slow-down of progress rate when a blockage of the TBM head and wear of disc cutters occurs. In fact, boring through faulted rock mass needs probe drilling, ground improvement, drilling drainage holes (high water pressure present) to mitigate the potential risks. Besides, excavation of high-stress conditions presents many difficulties, such as face instability and TBM jamming due to tunnel convergence. Also, in porous jointed rock masses, excavation is easy, thus penetration rate high but lower advance rate could be experienced due to low utilization rate compared to the massive hard rock where disc cutters wear is an issue and they need to be changed frequently.

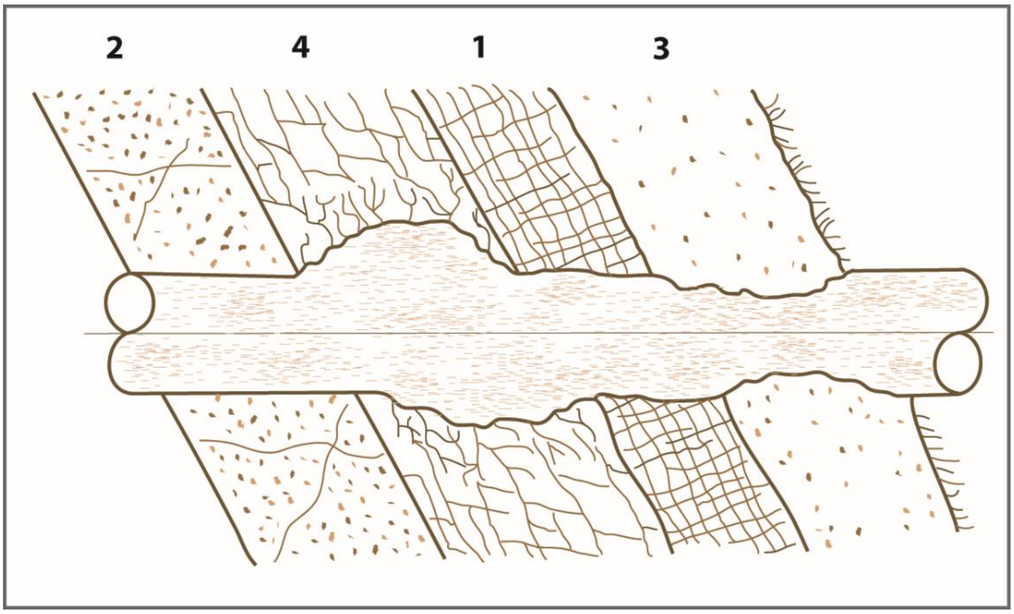

Figure 3.28: Four main types of geological conditions in Tunneling (modified from Barton, 1999); 1- Blocky and jointed rock mass; 2- Massive hard rock; 3- Squeezing rock mass; 4- Faulted rock mass

3.4.3.1 Influence of In-situ Stress

It seems like in-situ stresses have an effective role in machine performance. Klein et al. (1995) analyzed four hard rock tunnels in California. The uniaxial compressive strength (UCS) of the rock ranged from 70 to 489 MPa, TBM diameter raged from 3.4 to 4.3 m, and tunnel lengths varied from 2 to 5 km. These researchers utilized the field penetration index (FPI) as a performance parameter. A high value of FPI indicates the greater difficulty of boring, usually due to high values of thrust needed for a given depth of penetration. The result did not show a satisfactory trend with UCS and the ratio of overburden (σ_v) to the uniaxial compressive strength of rock mass (UCS_{rm}) determined from Hoek & Brown (1980) formula (see Figure 3.15) to examine the impact of rock mass and in situ stresses on FPI.

$$UCS_{rm} = \sqrt{S \cdot UCS^2} \tag{3.15}$$

For high strength intact igneous rock S =1 and for other rock types S was selected from the suggested table by Hoek & Brown (1980). As can be seen from Figure 3.29, with an increase of σ_v / UCS_{rm}, boring of rock mass gets easier. In spite of the above analysis of Klein et al. (1995), Barton (2000) believed that, when rock is massive and highly stressed it will not be easier to bore, unless limited stress-fracturing occurs during the boring process. Tarkoy and Marconi (1991) describe an early case study from the Mont Cenis tunnel, where delays were attributed to 'popping' of the rock during pauses for re-gripping, made very difficult boring somewhat easier. However, in another case at the Star Mine in Idaho, stress-induced slabbing caused problems at the cutterhead, and penetration rates were only about 0.1 m/hr. In this case, the TBM was inadequate for hard quartzite, and TBM tunneling was abandoned.

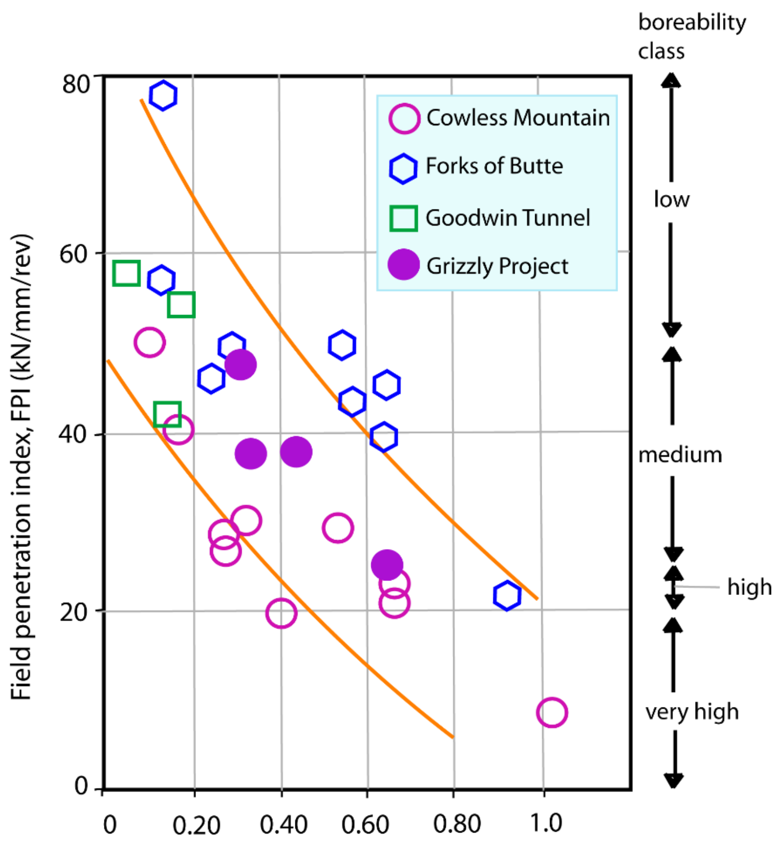

Figure 3.29: Field penetration index versus σ_v / UCS_{rm} for four hard rock tunnels (modified from Klein et al. 1995)

3.4.3.2 Mixed Face Condition

One of the critical parameters in the performance of rock TBM is the presence of hard and weak rocks at the tunnel face. The existence of this kind of conditions at tunnel face means that some disc cutters roll on the stronger rock, while others run on weaker material and at the same depth of penetration, discs running on harder material require higher forces and can fail. This leads to increasing disc cutter change. Also, steering problems are frequently reported in such conditions.

3.4.3.3 Influence of Water Inflows

Water inflows cause various degrees of difficulties in TBM tunneling. Excessive water inflows (underground water) often causes delays and can influence on advance rate of TBM. This parameter has a lower impact on penetration rate but dominates machine utilization.

3.4.3.4 Gas Emission

High gas emission by decreasing the utilization coefficient and cause serious problems with tunnel crew and TBM components such as, decreasing the ability of personnel, reducing the working shift, shutdown of tunneling operations as well as negative effect on electronic devices of the machine. The fact is that, gas emission has a great negative role on the performance of the machine.

3.4.4 Machine Specifications

The machine specifications, such as thrust and power are the key to provide a sufficient amount of forces and torque to support the excavation operation. Machine thrust provides enough force to efficiently penetrate the rock surface. Also, the cutterhead torque and power enable the head to rotate at a designated penetration rate to overcome the rolling resistance. Generally, tougher rocks with less fractures and joints require more thrust and relatively low torque/power (due to low penetration), compared to soft/jointed rock where low thrust and high torque are expected (as a result of high penetration).

3.4.4.1 Cutter Geometry

Cutting tools provide for the transmission of energy generated by the machine to the rock in order to cause fragmentation. As a result, the geometry and wear characteristics of the cutting tool have a significant effect on the efficiency of energy transfer to the rock and the attainable rate of penetration. However, except for the diameter and tip width of the new cutters put on the cutterhead, it is almost impossible to track the real diameter and tip width of the disc cutters during the mining operation as they tend to vary across the face because of the wear process. Moreover, to reduce the frequency of cutter changes in hard and abrasive rocks, larger discs with wider tip have been used which requires higher cutting forces for the given penetration. As such, the impacts of the cutter geometry on the performance of the machine in the field is not well explored, despite the fact that these are the key parameters in CSM performance prediction models for hard rock TBM application.

3.4.4.2 Cutting Geometry

The cut spacing and the depth of cutter penetration into rock per cutterhead revolution define the efficiency of the cutting by disc cutters. As expected, the spacing of cutters has a significant impact on the chipping mechanism and the efficiency of the cutting process. As shown in Figure 3.30, there is an optimum spacing for a given cutter penetration where the interaction between adjacent cuts is maximized. This optimal spacing is usually expressed as the ratio of spacing to penetration (S/P). Above this optimum ratio, ridges start forming and all material between cutters cannot be taken out. At S/P ratios below and above the optimum S/P, cutting less efficient (Figure 3.31) as indicated by higher specific energy. Comprehensive studies and field data analysis have shown that for optimal cutting efficiency, this ratio should be between 10 to 20; with lower ratios in tougher rocks and higher ratios in harder and brittle rocks.

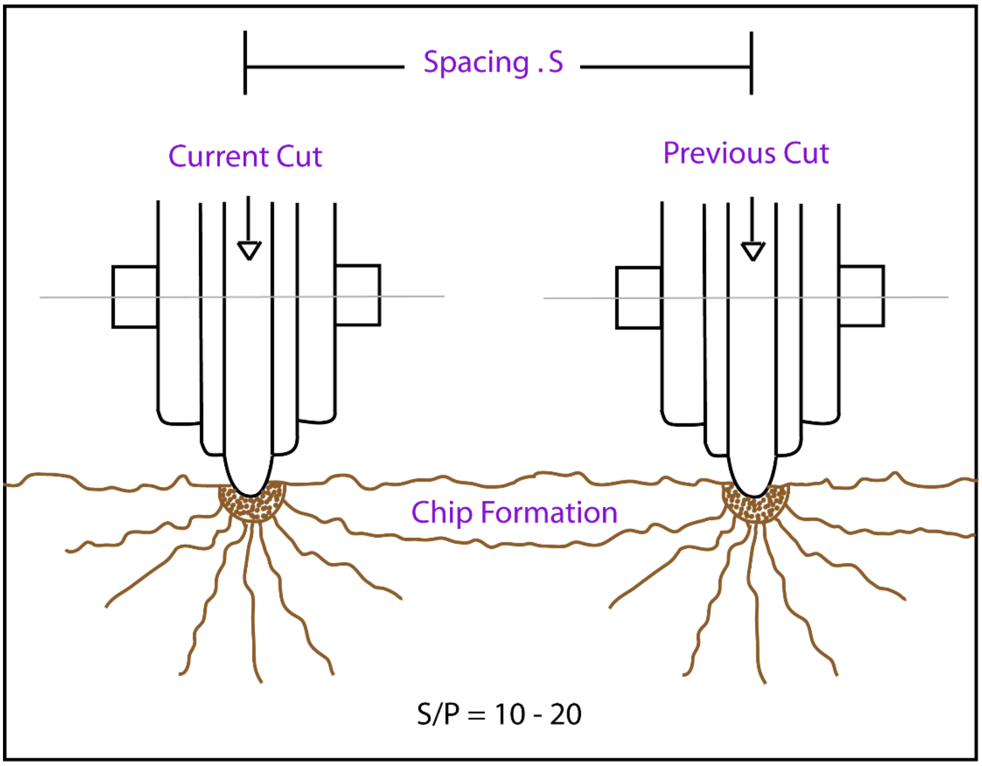

Figure 3.30: Effects of S/P ratio on cutting efficiency (modified from Rostami et al. 1996)

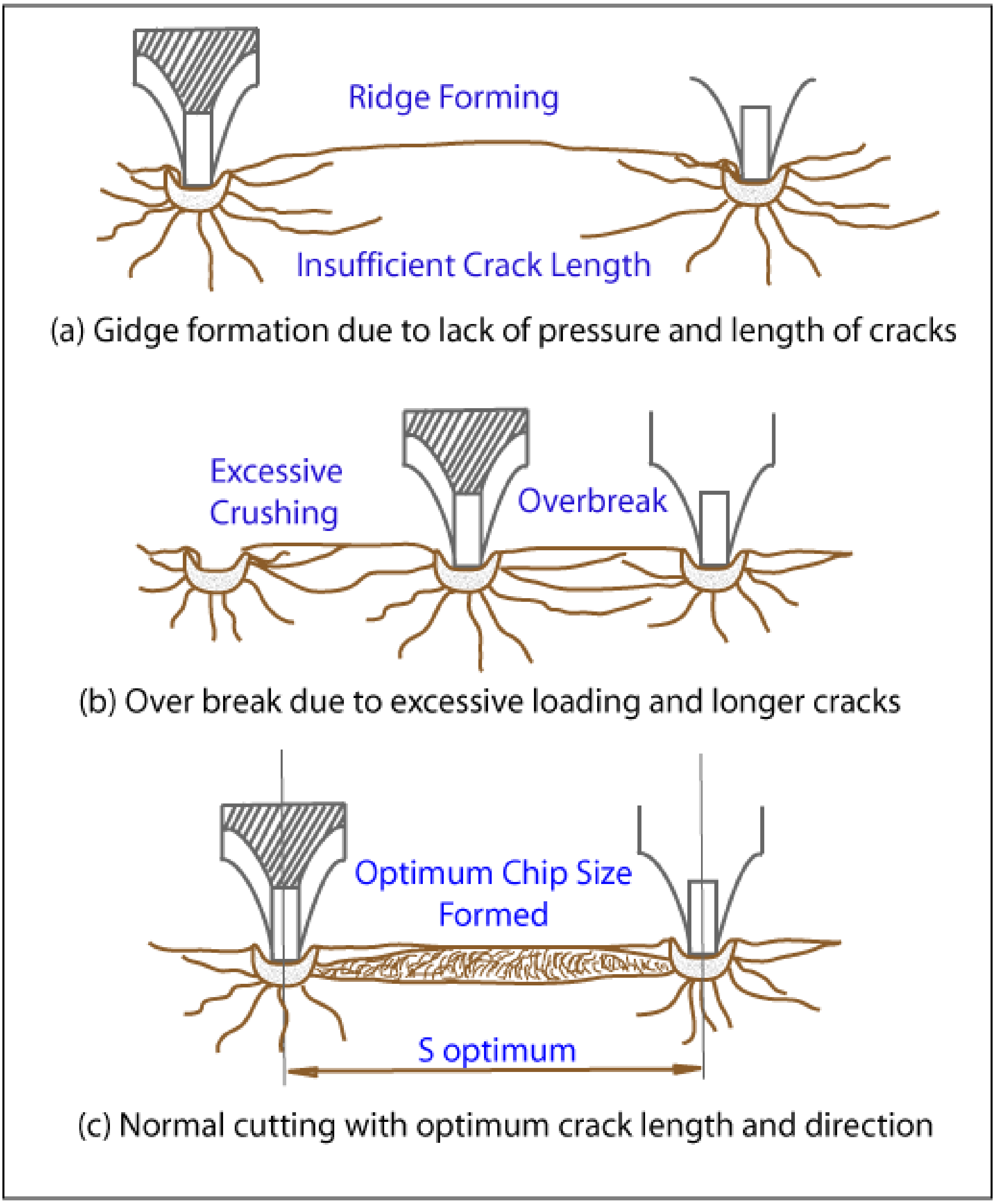

Figure 3.31: Chip formation in different cutting situations (modified from Rostami & Ozdemir, 1993)

3.4.5 Oprational Constraints

In every TBM operation, there are some operational constraints, such as the haulage capacity, ground support requirements, water handling, etc. that limit the productivity of the machine. In addition, other factors such as tunnel grade and curvature impact machine utilization and consequently productivity. All these factors must be taken into account when the application of a mechanical excavator to a particular operation is considered.

Chapter 4 TBM Performance Prediction Models

4.1 Introduction

TBMs have become the method of choice in the tunneling industry, in a variety of tunnel sizes, and ground conditions from soft ground and soil to rock tunnels. The advantages of these machines include the rapid excavation and advance rates compared to alternative methods, while offering a safe working condition. Some of the restrictive issues with the application of TBMs in tunneling projects i.e., inflexibility of machines in coping with variable ground conditions and the high capital cost of the machines have been mitigated in recent years. This was due to the new machine capabilities which allows them to work in various ground conditions. The rise in the cost of skilled labors involved in alternative methods, offsets the initial capital cost of the machine.

The complexity of interaction between rock mass properties and machine means that, performance prediction of TBM and finding the correlation, is not an easy. During the past three decades, numerous TBM performance prediction models have been introduced by many researchers which in some cases were successful with pinpoint accuracy, and in other instances, off by a good margin. A better understanding of machine-rock interaction and a more accurate model for performance estimates of hard rock TBMs has been a subject of interest. As noted before, TBM performance prediction models can be divided into two distinguished approaches, namely, theoretical and empirical models. Table 4.1 is a summary of the advantages and disadvantages of these modeling concepts.

Currently, three different models including Colorado School of Mines (CSM), Norwegian University of Science and Technology (NTNU), and field penetration index (FPI) models are the most recognized TBM performance prediction and prognosis models use around the world. Also, many efforts have been carried out by different researchers to determine the TBM performance based on rock mass classification systems.

In this chapter, some of the TBM performance prediction modes have been examined in more detail in an effort to evaluate their ability to correlate TBM performance and rock mass conditions.

Table 4.1: Advantages/disadvantages of different types of models for performance prediction of rock TBMs (Rostami, 2016a)

Model Type	Advantages	Disadvantages
Theoretical	Flexible with cutter geometry and machine specifications	Unable to easily account for rock mass parameters
	Can be used in tradeoff between thrust and torque optimization	Lack of accounting for joints
	Can be used for cutterhead design and improvements	Can be off by a good margin in jointed rock
	Can explain the actual working condition of discs and related forces	Inability to account for required filed adjustments
Empirical	Proven based on observed field performance of TBMs in the field	Lower accuracy when used in cases when input parameters
		are beyond what was in the original filed performance database
	Accounts for TBM as the whole system	Unable to account for variations in cutter and cutter head
		geometry, i.e., Cutter tip width, diameter, spacing, gage arrangement
	Many of field adjustments (i.e., average cutter conditions) are implied	Extremely sensitive to rock joint properties
	Ability to account for rock joints and rock mass properties	

4.2 TBM Performance Prediction Models

There has been a lot of studies on the development of accurate prediction of machine performance in given ground conditions. Some models are based on one or two rock parameters, while others are based on a combination of comprehensive laboratory, field, and machine data. Figure 4.1 shows a timeline of commonly developed performance prediction models within the last 40 years. The new model which is the outcome of this thesis has been already included. Some of the recent & main TBM performance prediction models (input and output parameters) are also listed in Table 4.2.

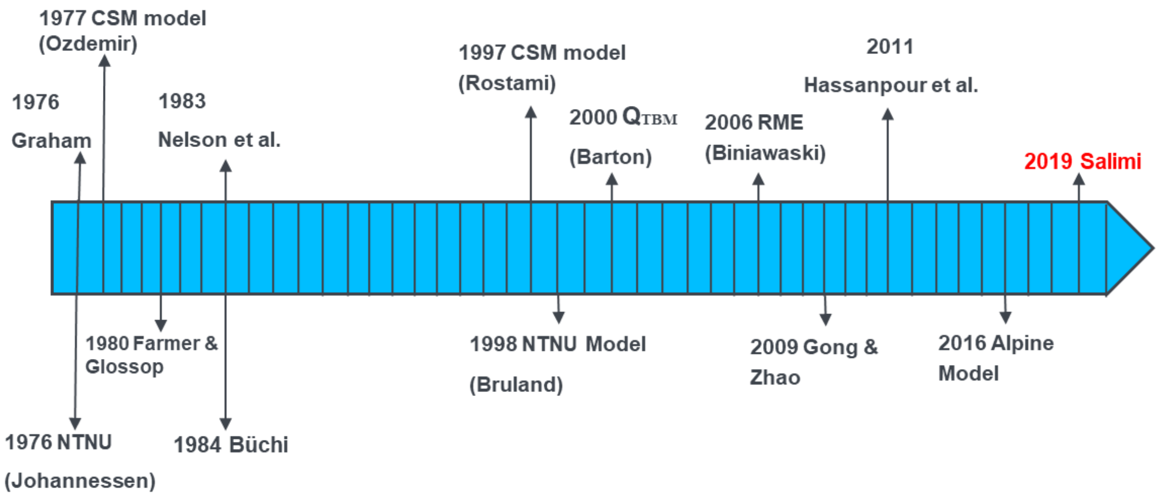

Figure 4.1: Timeline of the common prediction models developed during the last 40 years

Table 4.2: Review of some TBM performance models containing their input & output parameters

Prediction value	**Model**	**Rock mass factors**	**Machine factors**
Penetration rate (m/h) Advance rate (m/h) Some TBM parameters	CSM model (Rostami ,1997)	Uniaxial compressive strength, Tensile strength	Cutter spacing, cutter tip width, cutter radius, cutter force, TBM diameter, RPM
Penetration rate (mm/rev)	Gerhing (1995)	Uniaxial compressive strength, correction factors for joints, specific fracture energy, etc.	Cutter force, F_n
Penetration rate (m/h) Advance rate (m/h)	NTNU (Bruland, 1998)	Uniaxial compressive strength, drilling rate index (DRI), number of joint sets, joint frequency and joint orientation, porosity	Cutter force, RPM, cutter spacing, cutter size and shape, installed cutterhead power
Penetration rate (m/h) Advance rate (m/h)	Q_{TBM} (Barton, 2000)	RQD_0, Jn, Jr, Ja, Jw, SRF, rock mass strength, cutter life index (CLI), quartz content, induced biaxial stress at the face, porosity	Cutter force
Penetration rate (m/h) Advance rate (m/h) Specific energy (kJ/m^3)	RME (Bieniawski et al., 2006)	Uniaxial compressive strength, abrasivity, rock mass jointing at the face, stand-up time, water flows	TBM diameter, Total cutter head thrust, RPM and torque
Boreability index BI (kN/mm/rev)	Gong and Zhao (2009)	Compressive strength, volumetric joint count, brittleness index, angle between main discontinuities and tunnel axis	Cutter force
Field Penetration Index FPI (kN/mm/rev)	Khademi et al., (2010)	Uniaxial compressive strength, RQD, Joint condition, angle between main discontinuities and tunnel axis	Cutter force, RPM
Field Penetration Index FPI (kN/mm/rev)	Hassanpour et al., (2011)	Uniaxial compressive strength and RQD	Cutter force, RPM
Penetration rate (m/h)	Farrokh et al., (2012)	Tunnel diameter, Rock-type code, uniaxial compressive Strength, RQDc	Cutter force, RPM
Penetration rate (mm/rev)	Benato and Oreste (2015)	Uniaxial compression strength, GSI	F_n
Penetration rate (mm/rev)	Alpine model (Wilfing, 2016)	Uniaxial compressive strength, tensile strength, LCPC breakability coefficient, correction factor for joints, etc.	Cutter force, F_n

As can be seen from Table 4.2, the most commonly used input parameters in the previous studies for prediction of TBM performance are: the uniaxial compressive strength of intact rock (used by 70% of the models), distance, and the orientation of discontinuities (used by 50% of the models), the assumed thrust per cutter (used by 40% of the models) and the cutter diameter (used by 30% of the models). One important issue worth noting is, these models established very different approaches, and their input parameters, especially based on rock mass properties, exhibit considerable variation. This makes balanced comparisons problematic. However, in terms of ordinary and common conditions, the results of the models may present satisfactory agreement and results. Following is a brief review of these models, the advantages and disadvantages of the models also discussed.

4.2.1 CSM Model

This model is the most famous theoretical model developed by the Colorado School of Mines (CSM). The first version of this model was developed by Ozdemir (1977) and Ozdemir et al. (1998) using shear failure for performance prediction of V–shape disc cutters. This model was updated by Rostami (1993, 1997) to estimate the cutting force requirement of CCS disc cutters at a given cut spacing and penetration in a rock of known properties based on tensile failure. In fact, the CSM model estimates the cutter forces for a given penetration (mm/rev), based on rock properties, and cutter and cutting geometry.

The formula can be used to estimate forces for a given penetration or maximum obtainable penetration for a given set of machine specifications in a given rock, through iterations. The model is based on a large database of full-scale linear cutting tests performed on rock samples in the CSM laboratory. Full-size cutting tests are performed in several places and take all the parameters affecting the rock cuttability, such as rock strength, toughness, and cutting geometry into account. Obviously, laboratory cutting tests have proven to have some shortcomings when it comes to simulating field conditions, especially the effects of joints and discontinuities. The CSM model does not systematically incorporate rock mass fracturing in the prediction model, but later some modifications have been offered for taking into account the effect of rock mass conditions for the prediction of TBM performance by Cheema (1999) and Yagiz (2002) as well as Ramezanzadeh (2005).

Based on the assumption and deduced functions by Rostami (1997), the total estimated resultant cutting force demonstrated in Fig. 4.2 was derived as follows:

$$F_t = \int_0^{\phi} TRPd\theta = \int_0^{\phi} TRP^o \left(\frac{\theta}{\phi}\right)^{\Psi} d\theta = \frac{TRP^o \phi}{1+\Psi} \tag{4.1}$$

where F_t is total resultant force, T is cutter tip width, R is cutter radius and ϕ is angle of contact area between rock and cutter,

$$P = P^o \left(\frac{\alpha}{\phi}\right)^{\Psi} \quad \text{and} \quad \phi = \cos^{-1}\left(\frac{R-P}{R}\right) \tag{4.2}$$

where P is the pressure of the crushed zone, Ψ is the power of pressure function, P^o is base pressure in the crushed zone at the point directly underneath cutter and α is position angle.

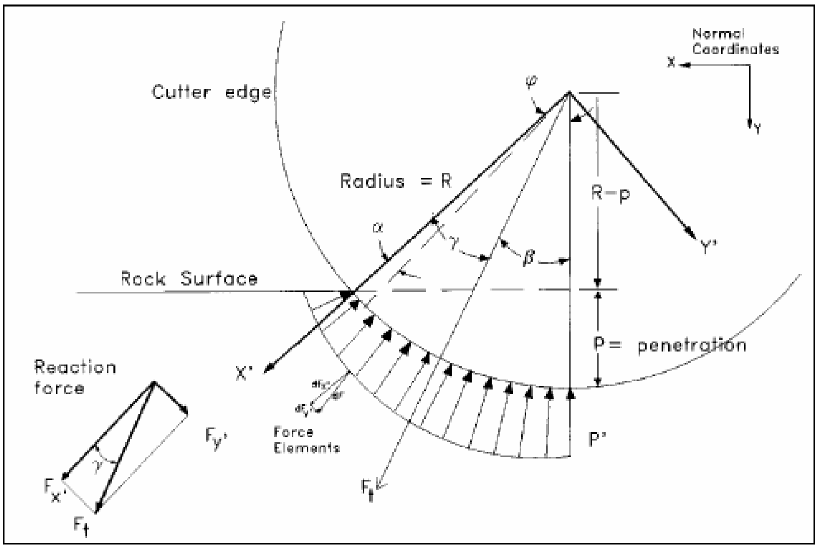

Figure 4.2: General Shape of Pressure Distribution with Power Function (Rostami, 1997)

In these equations, T and R are cutter geometry parameters, which are known. The angle can also be calculated once the penetration is known. The power of the pressure function varies between 0.2 for V-shape and very sharp cutters to -0.2 for wider tip cutters and often can be set to 0.1. The base formula was a force as a product of pressure and area of contact. Yet the equation for estimation of the pressure of crushed zone P^o was derived by regression analysis on available data within the CSM database. As such, this equation was not dimensionally correct and was a linear or polynomial combination of several variables. Therefore, if a logarithmic regression was to be used, the right combination of parameters could be derived. The results of the later analysis performed over an extended database by Rostami (1997) produced equations which are very close to the right dimension, and subsequently were rounded off to offer a dimensionally correct equation. Using the equations derived from regression analysis of measured forces by Rostami (1997), base pressure P^o can be estimated as follows:

$$P^0 = C \sqrt[3]{\frac{S \cdot \sigma_c^{\,2} \cdot \sigma_t}{\phi \cdot \sqrt{R \cdot T}}} \tag{4.3}$$

Where C is constant ~2.12, S is spacing between the cuts, σ_C is the uniaxial compressive strength of rock, and σ_t is the tensile strength of rock.

In either case, to estimate the normal and rolling forces, the following formula can be used:

$$F_n = F_t \cdot \cos\left(\frac{\phi}{2}\right) \text{ and } F_r = F_t \cdot \sin\left(\frac{\phi}{2}\right) \tag{4.4}$$

where F_n is normal force and F_r is rolling force. This is based on the assumption of uniform pressure distribution ($\beta = \phi/2$ angle of the resultant force from the normal) in the contact area, which has been proved to be true.

$$\frac{F_r}{F_n} = \tan\beta = \tan\left(\frac{\phi}{2}\right) \tag{4.5}$$

The following steps to complete the performance prediction with this method are as follows:

1. Calculate the total thrust requirements as: $$T_h = \sum_1^n F_n \approx n \cdot F_n \tag{4.6}$$

2. Calculate torque as: $$T_q = \sum_1^n F_{ri} \cdot R_i \approx 0.3 D_{TBM} \cdot N_{TBM} \cdot F_r \tag{4.7}$$

3. Calculate rotational speed as: $$RPM = \frac{v_{\max}}{\pi \cdot D_{TBM}} \tag{4.8}$$

4. Calculate power requirement of the head: $$HP = \frac{T_q \cdot RPM}{K} \tag{4.9}$$

5. Calculate installed thrust and power by using an efficiency factor η (i.e., $T_h = T_h/\eta$)

where D is TBM diameter, N total number of disc cutters, and V is the linear velocity of the cutters (i.e., 150 m/min = 500 ft/min for 17″ cutters).

For TBM performance estimates, with all parameters fixed in a certain rock type using a specific machine, penetration is the only variable that can be increased till one of the limits (i.e., cutter load, thrust, power, etc.) is reached. In other words, the penetration rate of the machine is the maximum penetration per revolution that can be achieved within the available machine parameters (Rostami, 1997; Hassanpour, 2009).

Discussion

The CSM model is based on linear cutting tests and theoretical force formulations, rather than empirical data, and as such is more capable of adapting to rock conditions that have not previously been encountered. The model is able to be used for the design of cutterhead and evaluation of disk geometry (diameter and tip width) since, it considers the geometry of the problem in its formula including, cutter/ cutting geometry and machine specifications, however, there are many assumptions necessary to relate data obtained from a linear cutting test to the actual performance of a TBM cutter head where the cutters are rolling in a circular fashion and are subjected to imperfect loading due to heterogeneity of the tunnel face. Besides, the main drawback of the CSM model is, it does not originally consider the influence of joints on TBM PR (because it includes just physical/mechanical properties of the intact rock containing UCS, BTS) which has a great role to play as noted by many others.

4.2.2 Modified CSM

As mentioned earlier, in the CSM model; the penetration rate of the machine is the maximum penetration per revolution that can be achieved within the available machine parameters. It established that existing joint conditions certainly affect the rock breakage process and can control the rock breakage. In this regard, some investigations have been conducted to find adjustment factors to enhance and modify the CSM model. In this section, some attempts to mitigate this problem will be introduced and discussed.

A. Modified CSM Model

The first attempt to modify CSM was done at the earth mechanics institute (EMI) of CSM by utilizing existed data to develop adjustment factor FI as follow[1]:

$$F1 = 1.0 + (100 - RQD/150) \qquad \text{when } UCS < 110 \text{ MPa} \tag{4.10}$$

[1] It was adapted from Hassanpour (2009) with some modifications.

$$F1 = 1.0 + (RQD/75) \qquad \text{when } UCS > 110 \text{ MPa} \tag{4.11}$$

B. Cheema (1999)

Cheema (1999) presented a new index as RMBI (Rock Mass Boreability Index) for estimation of boreability of rock masses. In his new model, the conditions of rock mass in the CSM model for the prediction of the performance of TBM was considered for hard schistose rock masses. In this investigation, a database including rock mass specifications and physical properties of intact rock, during the construction of one tunnel in Boston were collected. By analyzing data, the following formula is introduced as:

$$RMBI = 26900 \cdot E^{0.097} \cdot SR^{0.444} \cdot \nu^{-0.066} \qquad (R^2 = 0.85) \tag{4.12}$$

where $RMBI$ is rock mass boreability index (psi), E is elasticity Modulus (ksi), SR is the reduction factor, and ν is Poisson's ratio.

Although there was good agreement between the actual performance of the machine and the suggested formula, but it is worth to note that, this modification was resulted in analyzing of collected data from one tunnel project. Also, joint conditions were not utilized in this equation.

C. Yagiz (2002)

Yagiz (2002) presented two indexes for considering the influence of discontinuities on TBM performance. For this purpose, the data collected from the hard rock TBM tunnel (the Queens Water Tunnel # 3, Stage 2) was analyzed. This tunnel was about 8 km long and was mined in New York City, USA, through hard jointed formations of varying rock types, including biotite-hornblende gneiss intermixed with granite gneiss, amphibolite, pegmatite, and biotite schist. In this investigation, the relationship between geological and rock mechanic properties alignment of tunnel plus actual TBM performance and predicted TBM penetration rate with CSM model was analyzed and finally by utilizing regression analysis; a formula for TBM performance in jointed rock mass was introduced as follow:

$$AR(ft/hr) = 0.859 + RFI + BI + 0.0969\,CSM\,(b - AR) \qquad (R^2 = 0.66) \tag{4.13}$$

As can be seen, in this equation two parameters including RFI -Rock Fracture Index- and BI -Brittleness Index- are used. These parameters are described as follow:

$$RFI = 1.44\log(\alpha) - 0.0187 \cdot Fs \tag{4.14}$$

$$BI = 0.0157 \cdot PTI \tag{4.15}$$

where AR is modified advance rate, $CSM\,(b-AR)$ is basic advance rate based on CSM model, Fs is spacing between the plane of weakness or fracture, α is the angle between planes of weakness to tunnel driven direction and BI is brittleness index calculated from a punch penetration test. In fact, the applicability of the suggested formula is very limited due to its limited original dataset. Although there is a good agreement between the actual performance of the machine and the suggested formula, but this modification comes from analyzing of collected data from one tunnel project. Another weakness of the proposed formula using punch penetration test which is not commonly used in many rock mechanics laboratories which end up in the sophistication of BI estimation. So; it can be used in similar conditions with similar TBM specifications and to mitigate the BI calculation, a proposed conversion formula provided by Yagiz (2009) could be a solution for this problem. Besides that, as can be seen, the penetration rate coefficient for the CSM model in the formula is around 0.1.

As a result, in the proposed equation the other parameters are more important than CSM, and hence; the CSM model can be eliminated without a major impact on the result. This means that the impact of the all the input parameters in the CSM model has been ignored.

D. Ramezanzadeh (2005)

Ramezanzadeh in 2005 analyzed data based on information from 11 projects (more than 60 km) and modified the CSM model as follow:

$$P\,\mathrm{Re}\,v = P\,\mathrm{Re}\,v_{CSM}{}^{0.37}\exp(1.8-0.0031Js-0.0065\alpha) \tag{4.16}$$

where $P\,\mathrm{Re}\,v$ is penetration per revolution, Js is joint spacing and α is the angle between discontinuities to tunnel driven direction.

4.2.3 Gerhing (1995)

The prediction model, proposed by Gehring in 1995, is based on information from preceding literature and the author’s observations in four cases from Voest-Alpine with a certain machine setup (17’’ cutters, 80 mm spacing). From the literature, several curves relating the TBM penetration rate to the intact rock’s uniaxial compressive strength have been drawn (Figure 4.3) by applying the following input parameters (Gehring, 1995):

- Cutter spacing = 80 mm
- Cutter diameter = 430 mm
- Cutter load F_n = 200 kN

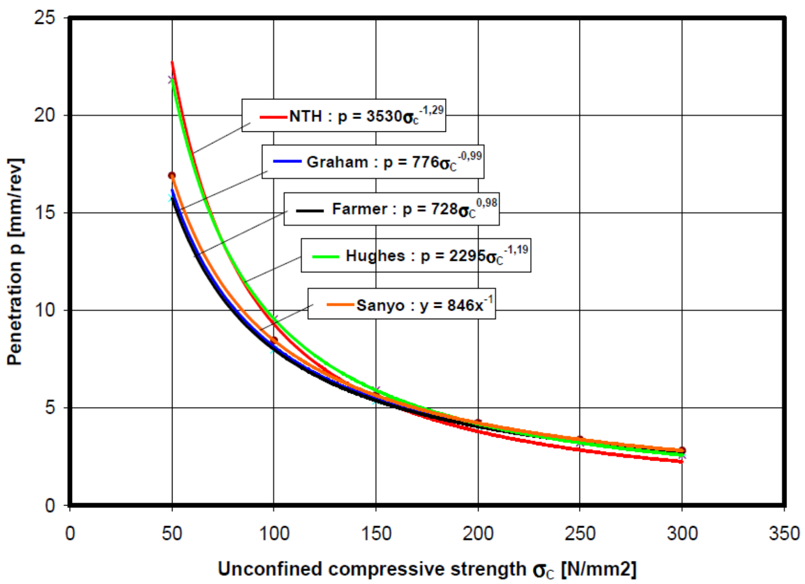

Figure 4.3: TBM basic penetration recalculated from different sources (Gerhing, 1995)

For rock with mean strength in the range of 100 to 250 MPa, the curves can be approximated by a linear relationship, expressed by Equation 4.17 (Delisio, 2014).

$$P(mm/rev) = 4 \cdot \frac{\bar{F}_N}{\sigma_c} \tag{4.17}$$

where P is the penetration per revolution, $\bar{F}_N$ is the mean cutter force, and σ_c is the unconfined compressive strength. Equation 4.17 is then expanded to Equation 4.18 by presenting several correction factors:

$$P(mm/rev) = \frac{K_0, K_1, K_2, K_3 \cdot K_4 K_5 \cdot \bar{F}_N}{\sigma_c} \tag{4.18}$$

where $K_i = K_0.K_1.K_2.K_3.K_4K_5$ are correction factors.

The first correction factor (K_0) is constant and equal to 4.0. This is due to the initial linear relationship expressed by Equation 4.17. The other factors reflect the influence of other parameters and have been derived by comparing Equation 4.18 with the observations made in the four cases analyzed by the author. Specifically, the correction factor K_1 relates to the so-called "specific fracture energy", which is defined as:

$$w_f = \frac{W_f}{\sigma_c} \tag{4.19}$$

where W_f is the fracture energy for a 200 kN cutter load. K_1 can be estimated from w_f by using Figure 4.4.

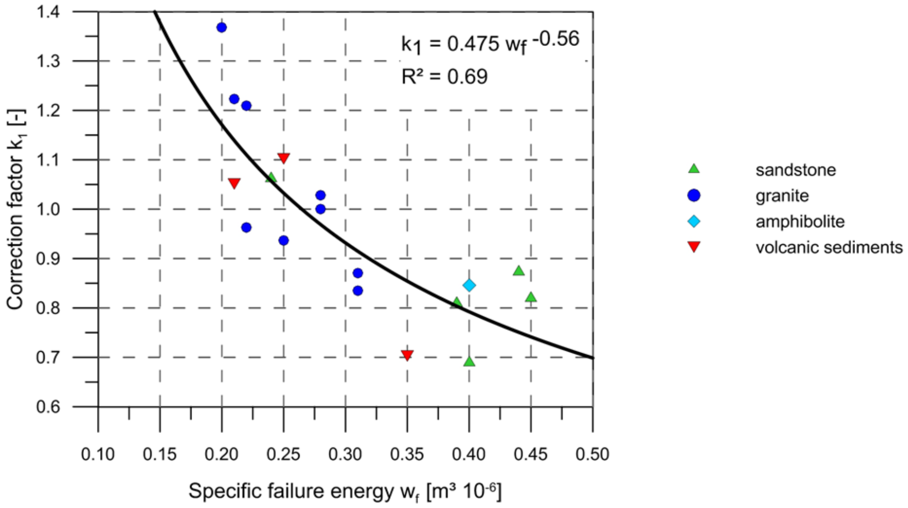

Figure 4.4: Correlation between specific fracture energy w_f and correction factor K_1 (Wilfing, 2016)

The correction factor K_2 is very important as it accounts for the influence of the rock mass discontinuities. The formulation takes into consideration the joint spacing and the inclination of the principal discontinuity planes. The latter is described by an angle α . According to Bruland (1998), the orientation is described by the smallest angle α between the tunnel axis and plane of weakness (Equation 4.20). The proposed K_2 values are listed in Table 4.3 (Delisio, 2014).

Table 4.3: Correction factor K_2 for the Gehring model (Gehring, 1995)

Average joint spacing	**Correction factor K2 as a function of α**			
	0 °	30 °	60 °	90 °
>50 cm	1	1	1	1
10-50cm	1.2	1.3	1.6	1.3
5-10 cm	1.4	1.8	2.3	1.6
< 5 cm	1.7	2.3	3	2

$$\alpha = \sin^{-1}(\sin\alpha_f \cdot \sin(\alpha_t - \alpha_s)) \quad (4.20)$$

where α is the smallest angle between tunnel axis and discontinuity, α_f is dip angle discontinuity, α_s is strike angle discontinuity, and α_t is tunnel direction [all in degree °]. Finally, the factor K_3 accounts for the state of stress at the face, but no correlation formula or diagrams are provided. K_4 is correction factor regarding to cutter diameter which is not equal to 432 mm (17″). He performed a regression analysis for constant section cutters with diameters of 432 mm (17′′) and cutter tip widths of 15.875 mm (5/8′′). Field data showed that the relation between cutter diameter and penetration rate is linear displayed in Equation 4.21.

$$K_4 = \frac{430}{d_c} \tag{4.21}$$

where d_c is the cutter diameter. The last correction factor, K_5 is related to cutter spacing ≠ 80 mm. This correction factor is based on research at the NTNU concerning the relation between cutter spacing and penetration (Wilfing, 2016). The suggested correlation diagram for K_5 considers the influence of cutter spacing ≠ 80 mm, depending also on the cuttability of the rock.

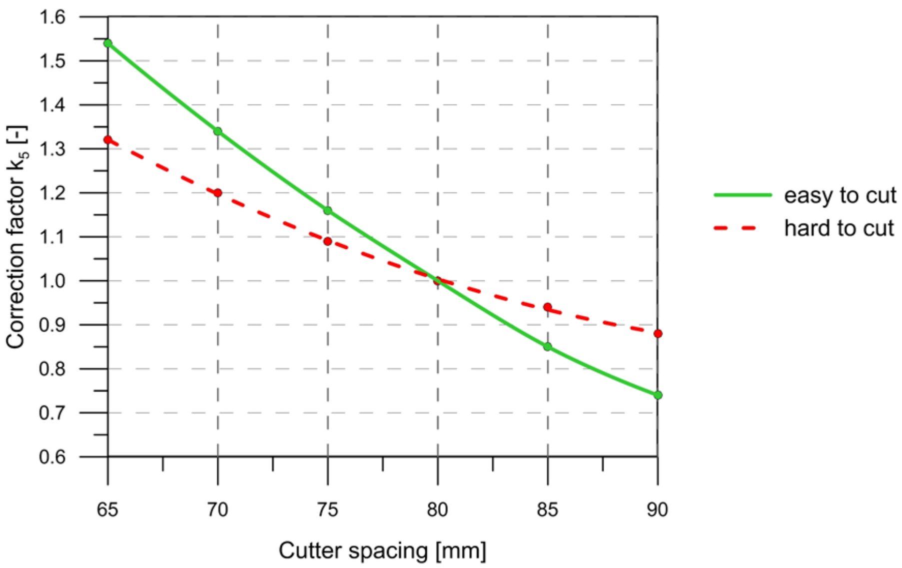

Figure 4.5: Correlation diagram of correction factor K_5 and cutter spacing as a function of drillability (Wilfing, 2016)

Discussion

The fact is that, the principal approach of the model seems very objective and reasonable. The model and respected formula has a transposable and modular structure and contains a simple linear function with independent correction factors that takes into consideration of rock mass properties, as well as different cutterhead types and associated geometries. But, as noted by Wilfing (2016), it considers spacing and orientation only of the major plane of weakness and not of intersecting discontinuity systems, which might not reflect actual rock mass characteristics. Furthermore, only spacing less than 50 cm were considered to impact on TBM penetration rate. By contrast, the NTNU model counts for spacing up to 160 cm. In addition, as expressed by Gerhing (1995), another limitation of the model is that, it is based on a limited number of cases (four tunnels) which cover a small range of lithologies (granite, amphibolite, sandstone, and agglomerate) in the range $\sigma_c/\sigma_t = 10$ to 15.

4.2.4 Alber (2000)

The empirical model of Alber (2000) is focused on the probabilistic estimation of penetration rate, utilization, and an advance rate of TBM. In this model, the advance rate is affected by two factors including boreability and stability of rock mass. Boreability has a direct relationship with penetration rate, while behavior of rock mass upon excavation (ground support) as well as machine maintenance, cutter change, drainage system, backup system and so on which results in decreasing the utilization coefficient. The penetration rate of TBM in this model is expressed in terms of rock mass strength (σ_{cm}) which includes both σ_c and discontinuity features and covers thus the main rock mass characteristics that influence the penetration rate of a TBM. The uniaxial rock mass strength (σ_{cm}) estimated by characterizing a rock mass with the RMR-System (Bieniawski, 1989) and using the Hoek-Brown failure criterion (Eq. 4.22). Using the RMR index has the advantage that discontinuity spacing, surface condition, and groundwater inflow are already included.

$$\sigma_{cm} = \sigma_c \cdot \sqrt{S} \tag{4.22}$$

where σ_{cm} is rock mass strength (MPa), σ_c is uniaxial compressive strength (MPa), and S is Hoek-Brown failure criterion calculated by:

$$S = \exp\left(\frac{RMR - 100}{9}\right) \tag{4.23}$$

In this model, in order to compare the penetration rate of TBMs with different specifications, Alber introduced a specific penetration rate SP defined as:

$$SP = \frac{P(cm)}{RPM \cdot F_N}$$
(4.24)

where P is penetration depth (cm/min), RPM is cutterhead rotation head (rotation/minute) and F_N is cutter thrust. This relationship (Eq.4.24) is depicted in figure 4.6b. As expected, the specific penetration of TBM increases as the uniaxial rock mass strength decreases. This holds true down to a rock mass strength of about 15 MPa. Rock masses in the low range of strength are often dominated by closely spaced discontinuities. The formation of rock chips between two discs may be hindered in those very blocky rock masses. Single blocks may be ripped out of the face and reground. In summary, the penetration rate may rise considerably in weak rock masses.

Although estimation of the TBM utilization rate is so difficult because it depends on many factors; Alber assumes that, utilization rates were mainly seen as a function of support installations (mainly through for open TBMs). In fact, the necessary ground support is a function of the rock mass behavior upon excavation. Hence, the respective behavior depends on the ratio of rock mass strength to induced stresses at the tunnel wall. This ratio is expressed by the Factor of Safety FS :

$$FS = \frac{\sigma_{cm}}{\sigma_\theta} \tag{4.25}$$

where FS is a factor of safety, σ_{cm} is rock mass strength (MPa), and σ_θ is tangential stress at the sidewall (MPa).

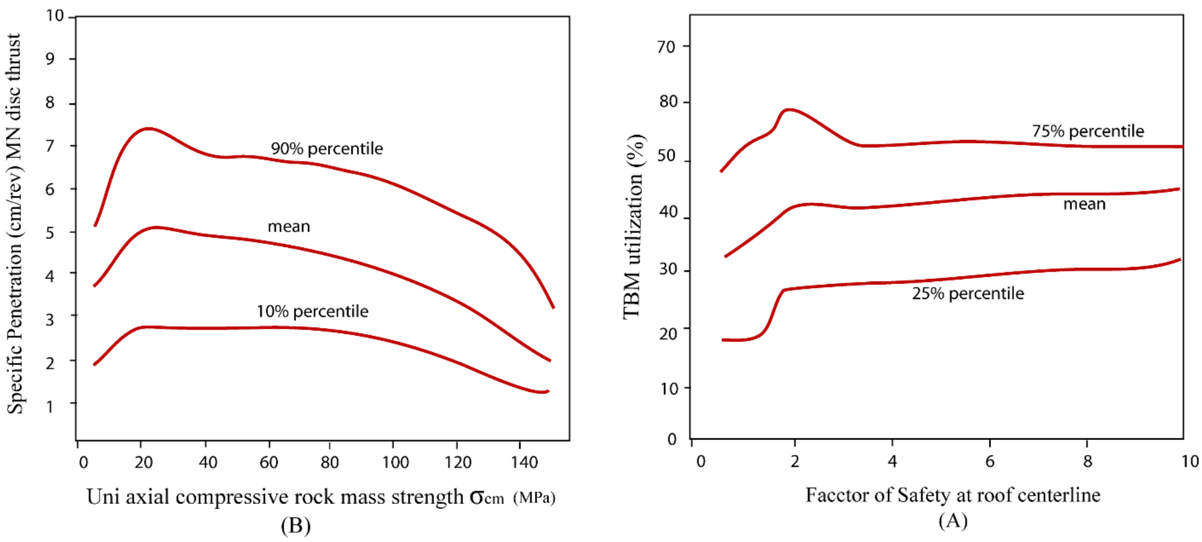

Figure 4.6: A) TBM utilization as a function of the factor of safety at roof centreline; B) Relationship between specific penetration rate and uniaxial compressive rock mass strength (modified from Alber, 2000)

The relation between the Factor of Safety at the roof centerline and the TBM utilization was found by Alber by the analysis of more than 100 km TBM tunnels. Figure 4.4a shows this relationship. As may be seen in this figure, in stable rock mass behavior the TBM utilization ranges from 25 to 50% and averages at 40%. For *FS* between 1.25 and 2, the average utilization decreases to 35%. For *FS* < 1.25, the TBM's utilization is well below 35% and may even drop to zero in tunnel sections in which *FS* approaches zero. Thus, the finding about the relations between the strength of a rock mass and the specific penetration of a TBM as well as between rock mass behavior and TBM-utilization allows estimating TBM advance rates. In this regard, by considering the variability in rock mass strength, Alber suggests classifying rock masses in three broad groups of low, medium, and high rock mass strength, respectively. Also, it seems necessary to classify the rock mass behavior into three groups, namely, stable, friable, and squeezing behavior. So, a rock mass to be tunneled by a TBM may thus be described by three behavioral classes (Table 4.4), which gives nine possible combinations of tunneling conditions or advance classes. For practical tunneling purposes, it is sufficient to classify a rock mass in those nine classes. By analyzing the variability of respected parameters, the probability functions can be estimated for each class of advance rate. (Fig. 4.7). Based on this figure, the end-user can assess the minimum and maximum, as well as the most probable advance rate for the given ground conditions.

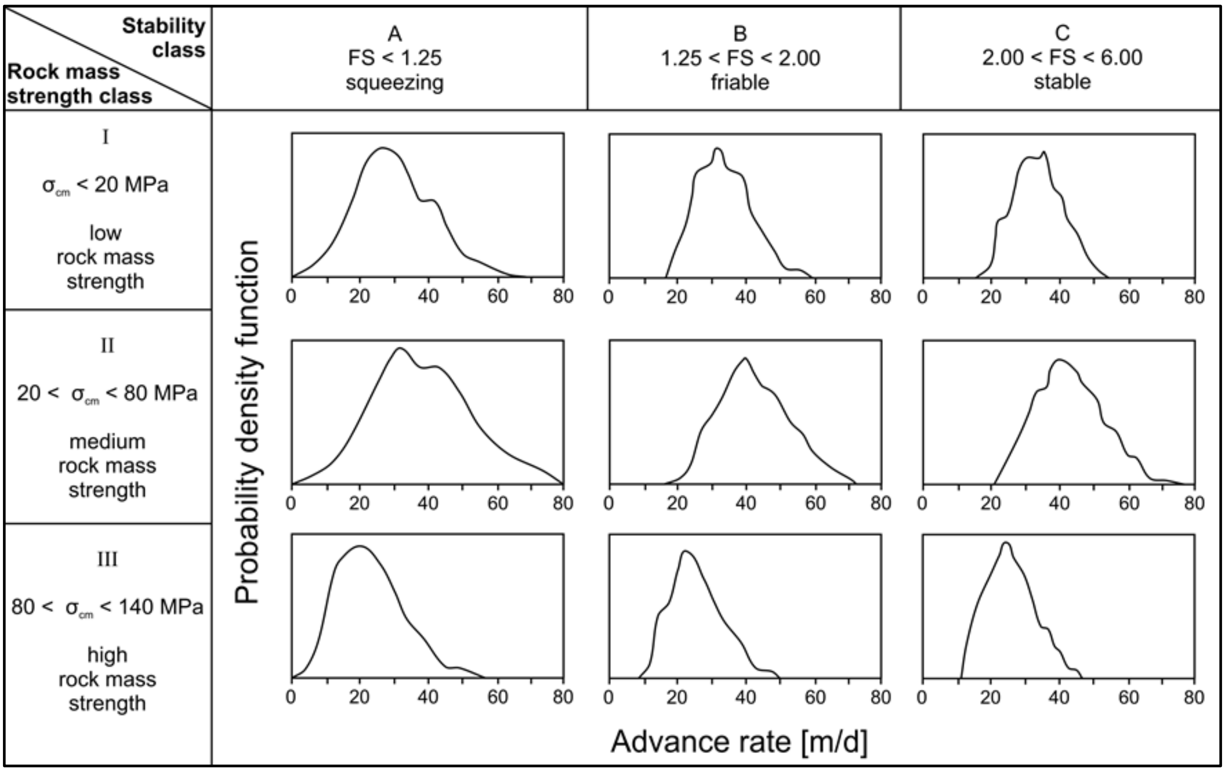

Figure 4.7: Probability functions of the nine recommended advance rate classes (Wilfing, 2016; Alber, 2000)

Discussion

The prediction model proposed by Alber is not commonly utilized in practical approaches, since the determination of the parameters encounter uncertainties. Besides, the results only assess a range of advance rates. As such, the model is not a very useful way to reflect the operating issues in the field.

Table 4.4: Classification of the rock mass factors influencing the main tasks in TBM tunnelling

Task: Penetration		**Task: Support**	
Rock mass strength class	Characteristics value	Stability class	Characteristics value
I low rock mass strength	σ_{CM} < 20 MPa	A squeezing	FS < 1.25
II medium rock mass strength	20 MPa < σ_{CM} < 80 MPa	B friable	1.25 < FS < 2
III high rock mass strength	80 MPa < σ_{CM} < 140 Mpa	C stable	FS > 2

4.2.5 Yagiz (2008)

Yagiz in 2008 presented a model to predict the penetration rate of TBM in hard rock conditions. To achieve this aim, the database composed of actual measured TBM penetration rate and rock properties was established using the data collected from hard rock TBM tunnel (the Queens Water Tunnel # 3, Stage 2). In terms of this investigation, the best correlation was achieved between *PSI* and *ROP* (r = 0.58). The results of this investigation are demonstrated in Figure 4.8 and Table 4.5.

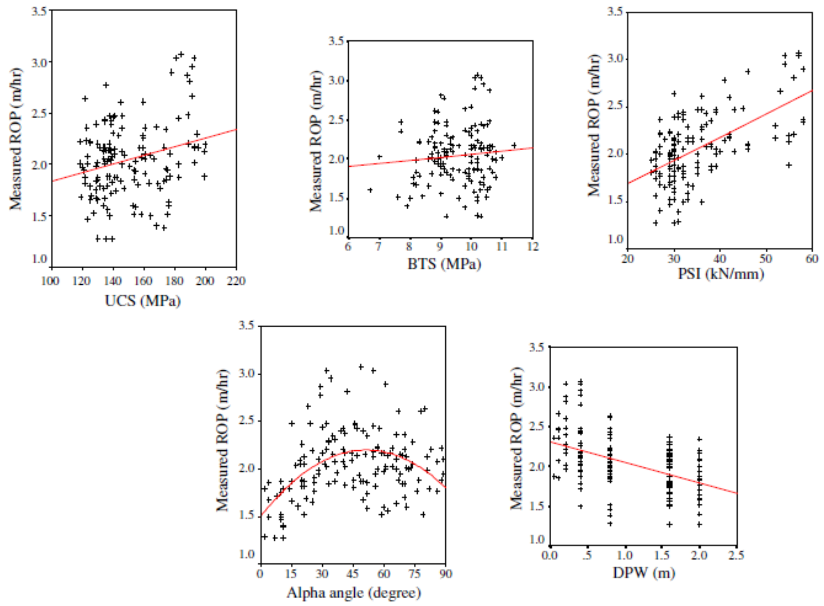

Figure 4.8: Correlation between Rock properties and ROP (Yagiz, 2008)

Table 4.5: Relations between rock properties and measured ROP with achieved equations

Relations of rock properties with ROP	An empirical equation	Coefficient of correlation r
Measured ROP vs. PSI	$ROP = 1.19 + 0.0247PSI$	0.58
Measured ROP vs. DPW	$ROP = 2.31 - 0.260DPW$	0.45
Measured ROP vs. a	$ROP = 1.50 - 0.0003 \cdot \alpha^2 + 0.0273 \cdot \alpha$	0.47
Measured ROP vs. UCS	$ROP = 1.413 + 0.0042 \cdot UCS$	0.26

Measured ROP vs. BTS	$ROP = 1.66 + 0.040 \cdot BTS$	0.1

It is worth to note that, although the UCS of the rock is one of the most crucial parameters for TBM performance estimation; however, as the rock mass demonstrates heavily joint, faults, UCS and BTS of intact rock cannot be enough alone for predicting machine performance, because intact rock strengths are barely representing the actual rock mass condition in the field. As can be seen that from table 4.4, the relationship between UCS and BTS of rock with the ROP was found very weak with a correlation coefficient (r) of 0.26 and 0.10 respectively. Finally, by utilizing the multivariable regression analysis equation 4.26 was suggested (r = 0.82).

As can be seen from the below equation, in the performed statistical analysis; BTS was excluded due to a very weak correlation with measured ROP .

$$ROP(m/h) = 1.093 + 0.029\,PSI - 0.003UCS + 0.437\log(\alpha) - 0.219\,DPW \tag{4.26}$$

Discussion

It should be mentioned that, the introduced equation is just related to the conditions of Queens Water Tunnel and belonged TBM; hence it can't be a reliable model to predict the performance of the machine. Furthermore, the proposed formula using a punch penetration test, which is commonly applied and used in North America, but not available in many rock mechanics laboratories around the world. Also, sensitivity analysis and examination of the effects of variation in the input parameters on the results indicate that, the model dedicated to the changes of PSI which end up in alteration of penetration will be substantial if the parameter is not appropriately calculated (Fatemi et al. 2016).

4.2.6 Gong and Zhao (2009)

Gong and Zhao in 2009 have presented a model to predict the performance of TBM with the analysis of collected database including Rock mass properties, TBM specifications and the corresponding TBM performance during the construction of two tunnels in Singapore nominal T05 (12.6 km in length with a finished diameter of 3.6 m) and T06 (9.6 km in length with a finished diameter of 3.3 m) excavated through Granite with different weathering grades. In this study, to develop a model, nonlinear regression analysis was used to carry out the multi-variables regression analysis. The best combination of rock mass parameters to predict the performance of the machine is as follow:

$$BI_{(1)} = 37.06UCS^{0.26}\,Bi^{-0.1}\,(0.84e^{-0.05J_v} + e^{-0.09\sin(\alpha+30)}) \tag{4.27}$$

where $BI_{(1)}$ is specific boreability index (kN/cutter/mm/rev) which is equivalent to FPI, UCS is rock uniaxial compressive strength (MPa), Bi is rock brittleness index (UCS / BTS), J_v is volumetric joint count, and α is the angle between the tunnel axis and the joint plane. In this study, to eliminate the influence of machine specifications and TBM operation parameters; a specific rock mass boreability index (SRMBI) defined as a boreability index at the PR equal to 1 mm per revolution, was proposed to evaluate the rock mass boreability in different rock mass conditions. The relationships between the rock mass boreability index, the specific rock mass boreability index, and TBM PR are estimated as follows:

$$BI \approx BI_{(1)} P^{-0.75} \tag{4.28}$$

where BI is the rock mass boreability index, $BI_{(1)}$ is the specific rock mass boreability index, and P is the penetration per revolution. Also, the parametric studies of the new model showed that the rock uniaxial compressive strength and the volumetric joint count have predominantly effects on the penetration rate.

Discussion

The main limitation of the model is that, it is based only on one tunnel project where an EPB machine is used to excavate granite. Therefore, the other rock types such as sedimentary formations are missing. All machine parameters (e.g., cutter diameter, cutter tip width, cutter spacing) are considered constant. Hence, the model might not be applicable to predict the penetration in tunnel projects that are not in granite, and not using 17" cutters. In addition, the brittleness index (Bi) in this model is obtained by dividing uniaxial compressive strength by tensile strength, resulting in substantial interdependence of these two variables and therefore, the model sensitivity to brittleness index is low, perhaps due to its dependence on compressive strength. This subject reflects the marginal impacts of Bi associated with respected results (Fatemi et al. 2016).

4.2.7 Farrokh et al. (2012)

Farrokh et al. (2012) have presented a new model based on an analysis of a comprehensive database of more than 300 TBM projects records. In order to develop a new equation, two separate databases were compiled from the review of various technical sources. The first database (general database) was assembled with the objective of developing a new performance model. The second database was developed to support model validation work. The general database contains different levels of information which define the tunnel, rock mass conditions, and TBM performance parameters over the full length of a tunnel drive, within discrete geological zones, or short tunnel reaches. The general database contains over 300 data sets. Besides, to verify the predictive capability of existing or new models, a testing database including 17 hard rock TBM projects with a total length of 73.6 km was selected and then evaluated. These projects provided detailed information for TBM performance in each geological zone. TBM diameter for these projects ranged from 2.6 m to 11.8 m. Figure 4.9 shows a histogram of TBM diameters in the database. As can be seen, the 3-6 m diameter range is common for a large number of projects, and it is the most popular range in the database. The graphs in Figs. 4.10-11 and 12 show tunnel diameters related to TBM characteristics and performance.

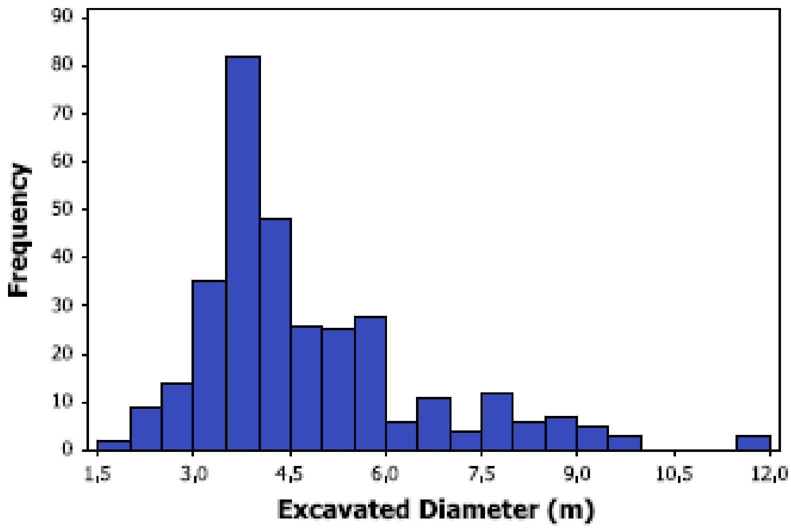

Figure 4.9: Histogram of tunnel diameter in the database (Farrokh et al. 2012)

In this study, Core fracture frequency (CFF) data was the only rock mass parameter that was available for all the records from and some of the records of the general database. Basically, this factor is in close relationship with *RQD* and refers to the frequency of rock mass fractures. Table 4.6 shows the approximate relationship between CFF and *RQD* and the numerical codes used for subsequent analyses. Besides, due to different rock textures (cementation and grain size and shape) affect the penetration rate, seven rock type categories, as proposed by Hoek and Brown (1980) and Stevenson (1999), were utilized. These rock types are listed in Table 4.7. The first four classes are for ''Sedimentary Rocks.'' The fifth, sixth, and seventh classes are for ''Metamorphic Rocks, Granitic Rocks, and Volcanic Rocks'', respectively. It should be noted that, Gneiss (GN) is inherently metamorphic, but it is typically closer to granite in terms of its behavior, especially where foliation is less pronounced. For this reason, it was categorized as GN in this analysis.

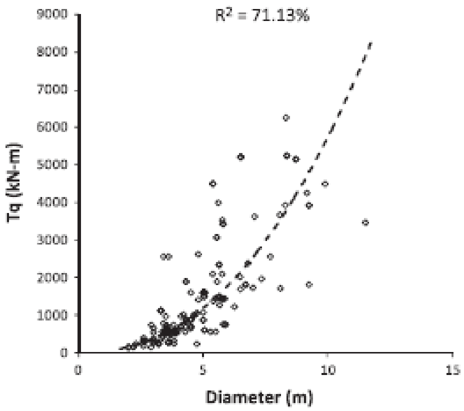

Figure 4.10: Relationship between installed torque and tunnel diameter (Farrokh et al. 2012)

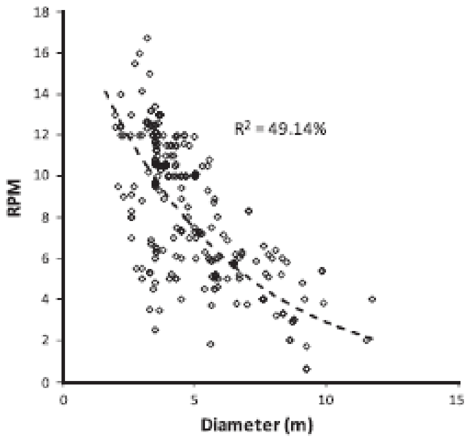

Figure 4.11: Relationship between nominal RPM and tunnel diameter (Farrokh et al. 2012)

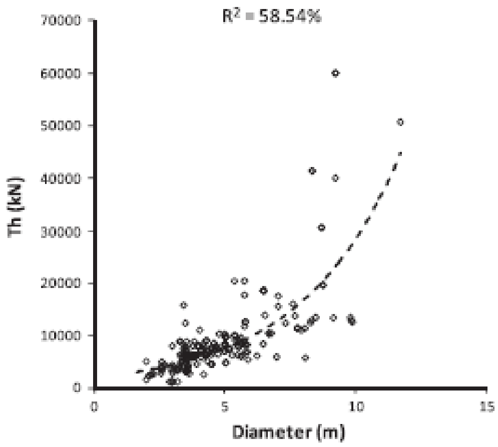

Figure 4.12: Relationship between installed thrust and tunnel diameter (Farrokh et al. 2012)

Table 4.6: CFF categorization (Farrokh et al. 2012)

CFF	Code	Description	Corresponding RQD range
Less than 8 fractures/m	S or 1	Low frequency	90–100
8–12 fractures/m	M or 2	Medium frequency	60–90
12–16 fractures/m	H or 3	High frequency	<60

Table 4.7: Rock-type categorization in database (Farrokh et al. 2012)

Rock type	Code
Claystone, mudstone, marl, slate, phyllite, argillite	C
Sandstone, siltstone, conglomerate, quartzite	S
Limestone, chalk, dolomite, marble	L
Karstic Limestone	K
Metamorphic rocks such as gneiss and schist	M
Coarse igneous such as granite and diorite	G
Fine volcanic such as basalt, tuff, and andesite	V

As can be seen from Figure 4.13, when the rock type is taken into consideration in the analysis, a good relationship can be established between rock strength and $PR/P\,\mathrm{Re}\,v$. The graphs show that in general a higher $PR/P\,\mathrm{Re}\,v$ is achieved in sedimentary rocks, and a lower $PR/P\,\mathrm{Re}\,v$ is achieved in igneous rocks.

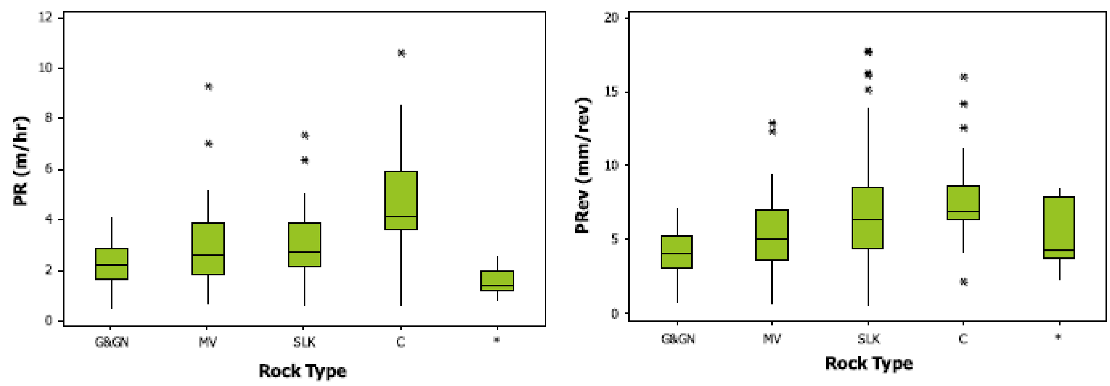

Figure 4.13: Correlation between PR/PRev and other parameters (Farrokh et al.2012)

Finally, multivariable regression analysis with $PR/P\,\mathrm{Re}\,v$ as the objective parameter was performed. To correct for normality in the regression model, Ln($P\,\mathrm{Re}\,v$) and Ln(PR) were used as response and new equations were introduced as follows:

$$P\,\mathrm{Re}\,v = Exp\,(0.41 + 0.404\cdot D - 0.027D^2 + 0.0691\cdot RT_C - 0.00431\cdot UCS + 0.0902\cdot RQD_C + 0.000893\cdot F_n) \qquad (R^2=63\%) \qquad (4.29)$$

$$PR = \frac{Fn^{0.186}\cdot RQD_C{}^{0.133}\cdot RT_C{}^{0.183}\cdot RPM^{0.363}\cdot D^{5.47}\cdot \exp(0.046\cdot D^2)}{5.64\cdot UCS^{0.248}\cdot \exp(1.58D)} \qquad (R^2=58\%) \quad (4.30)$$

where D is tunnel diameter in m, RTc is rock type numerical code (1 for G and GN, 2 for MV, 3 for SLK, 5 for C), UCS is uniaxial compressive strength in MPa, RQD_C is RQD numerical code (Table 4.6), and F_n is disc cutter normal force in kN.

Discussion

Although the correlation coefficient of the proposed model is comparatively low, the introduced models offer better accuracy than existing models. It is worth noting that, in addition to some effective factors such as UCS and F_n this model considers two factors that have a major influence on PR. It is obvious that, different rocks have a different texture (grain size, cementation, and shape) that should be considered, hence in the proposed model seven rock types categories which was presented by Hoek and Brown (1980) and Stevenson (1999) were considered. In this regard, the results show that, in general, a higher $PR / P\mathrm{Re}v$ is achieved in sedimentary rocks and lower $PR/PR\mathrm{e}v$ is achieved in igneous rock. In addition to rock texture, tunnel diameter also is taken into account. It is interesting to note that, maximal power and the maximal torque, as well as maximal RPM, depend mainly on the diameter of the tunnel. In fact, the RPM (revolution per minute) is limited by the size of the tunnel. It means that, the cutterhead RPM is inversely proportional to cutterhead diameter. In general, it can be stated that the penetration rate decreases with increasing TBM diameter. However, the proposed model may produce higher errors in estimating PR values in highly jointed (fractured) rock masses due to lack of accounting for RQD value or lack of other rock mass parameters such as joint orientation or joint conditions.

4.2.8 Benato and Oreste (2015)

Benato and Oreste in 2015 presented a new model which can be used to estimate the penetration-per-revolution for TBM tunneling. An analysis has been performed on several TBM operating Parameters of TBMs used for the excavation of two tunnels (overall length of about 6 km) in metamorphic rock in the Western Alps. The penetration of the disks per revolution of the head (the depth of pass p) was obtained from the net propelling speed, while the contact force acting on each disk (F_N) was obtained from the total force applied to the head. Basic geomechanical parameters (GSI "Geological Strength Index" of the rock mass and the compressive strength σ_C of the intact rock) were correlated with the mean $p-F_N$ Values of each section. Finally, multivariable regression analysis was performed, and a new equation was introduced as follows:

$$P \cong \frac{5}{8}\cdot[(F_N-14)+(0.0132-0.00009\cdot\sigma_C)\cdot(100-GSI)^2] \tag{4.31}$$

where P is the penetration per revolution (mm/rev), F_N in the contact force on the disc (in tons$_f$), σ_C is the uniaxial compressive strength of intact rock (MPa) and GSI is the Geological Strength Index.

Discussion

One main limitation of the model is that, it is based on only two tunnels excavated in metamorphic rocks and the other rock types such as sedimentary are missed. In addition, in the proposed model, the rock mass conditions are taken into account by GSI which is based on the visual impression on the rock mass and the surface characteristics of discontinuities. Meaning that, the effect of joint spacing is not considered directly; as shown by many researchers for having a key role to play on TBM performance. Another problem, is the issue of the machine size which not addressed in this model. Ignoring machine size can interject huge errors in the analysis of machine performance when comparing different projects.

4.2.9 NTNU Model

The NTNU model has been originally introduced in the later 1970s and continuously revised and improved, as new tunneling data and TBM modifications become available. The 1998 version of the NTNU model (Bruland, 1998) is based on data from about 230 km of bored tunnels. Contrary to many other models the uniaxial compressive strength is not considered as a significant factor in this model. In fact, the boreability is expressed by drilling rate index DRI, which is a combination of rock brittleness value “S_{20}”and Siever’s miniature drill test (SJ). The SJ value expresses rock surface hardness. The brittleness test “S_{20}”value includes the effect of rock brittleness and therefore grain size and grain boundary strength.

Input parameters of this model can be divided into two main groups including rock/rock mass parameters, and machine parameters. These parameters also depend on various individual factors which include as follow:

Rock Mass Factors:

- Fracturing degree which describe based on rock fracture class (spacing between the joints) and orientation of planes of weakness with tunnel axis
- Drillability, represented by the drillability index (DRI)
- Abrasiveness, represented by Cutter Life Index (CLI) and quartz content in percentage
- Porosity which important in some rocks

Machine Factors:

- Cutter thrust
- Cutter spacing
- Cutter diameter
- Cutterhead speed (rev/min)
- Installed cutterhead power

Among all rock mass parameters, the degree of fracturing is the most important penetration rate parameter for tunnel boring. In the NTNU model, all parameters which are related to rock mass represented by **Equivalent Fracturing Factor (**K_{ekv}**),** and all machine parameters represented by **Equivalent Thrust (**M_{ekv}**) (kN/cutter)**. In NTNU model basic penetration rate is calculated as follow:

$$i_o(mm/rev) = \left(\frac{M_{ekv}}{M_1}\right)^b \tag{4.32}$$

where i_o is penetration rate of disc cutter (mm/rev), M_1 is critical thrust (the thrust needed to bore 1.0 [mm/rev]). This parameters and penetration coefficient (b) depends on Equivalent Fracturing Factor or K_{ekv} (Fig. 4.14). Therefore, as mentioned earlier, in equation 4.32 penetration rate depends on two major factors including the Equivalent Fracturing factor and Equivalent thrust.

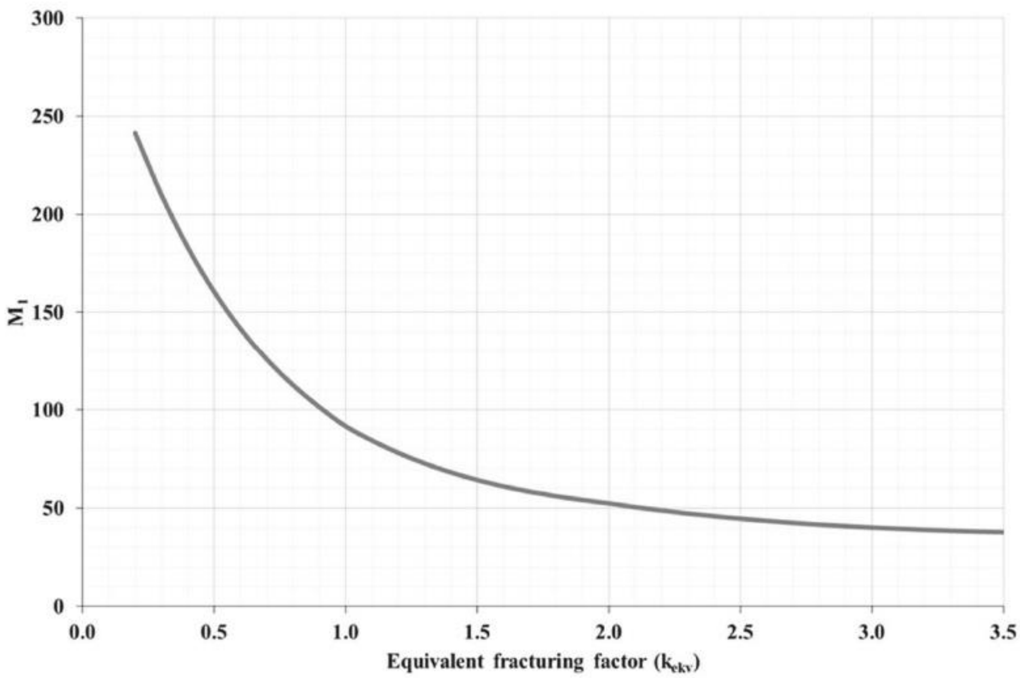

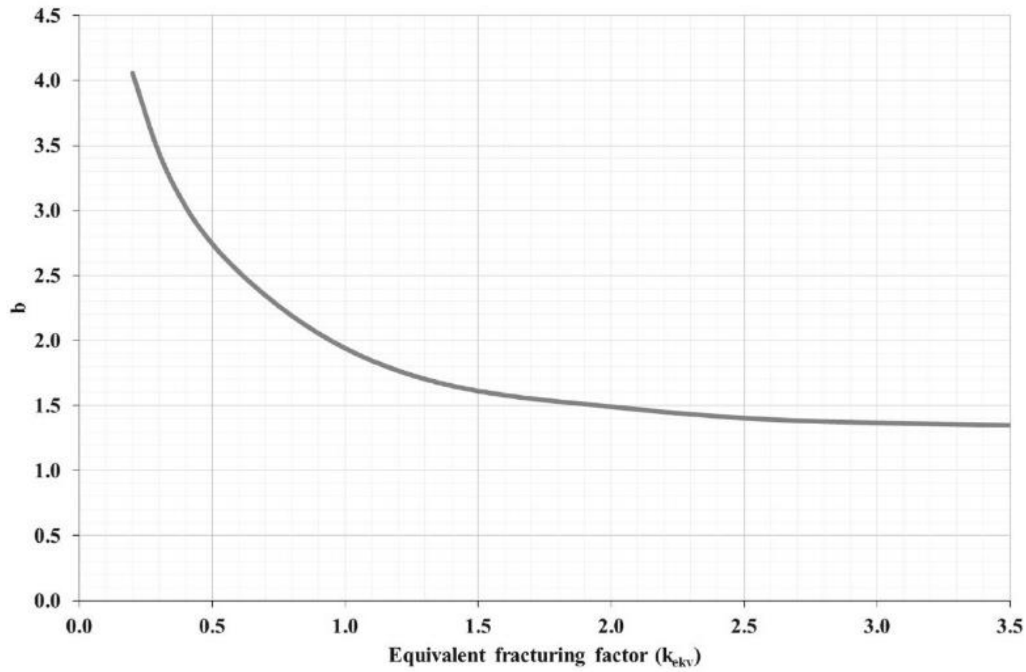

Figure 4.14: Relationship between critical thrust (M_1) and Penetration coefficient (b) with Equivalent Fracturing Factor or K_{ekv}, respectively (Macias, 2016)

4.2.9.1 Equivalent Fracturing Factor

Equivalent fracturing factor is the combination of some parameters like type of discontinuity, fracturing degree, angle between tunnel axis and the planes of weakness as well as rock drillability index which estimated as follow:

$$K_{ekv} = K_{s-tot} \cdot K_{DRI} \cdot K_{por}$$
(4.33)

where K_{s-tot} is total fracturing factor, K_{DRI} and K_{por} are the coefficient which depends on drillability index and porosity of the rock. K_{por} can be calculated from Figure 4.15. K_{DRI} is the correlation factor for DRI≠50 which can be estimated from Figure 4.18.

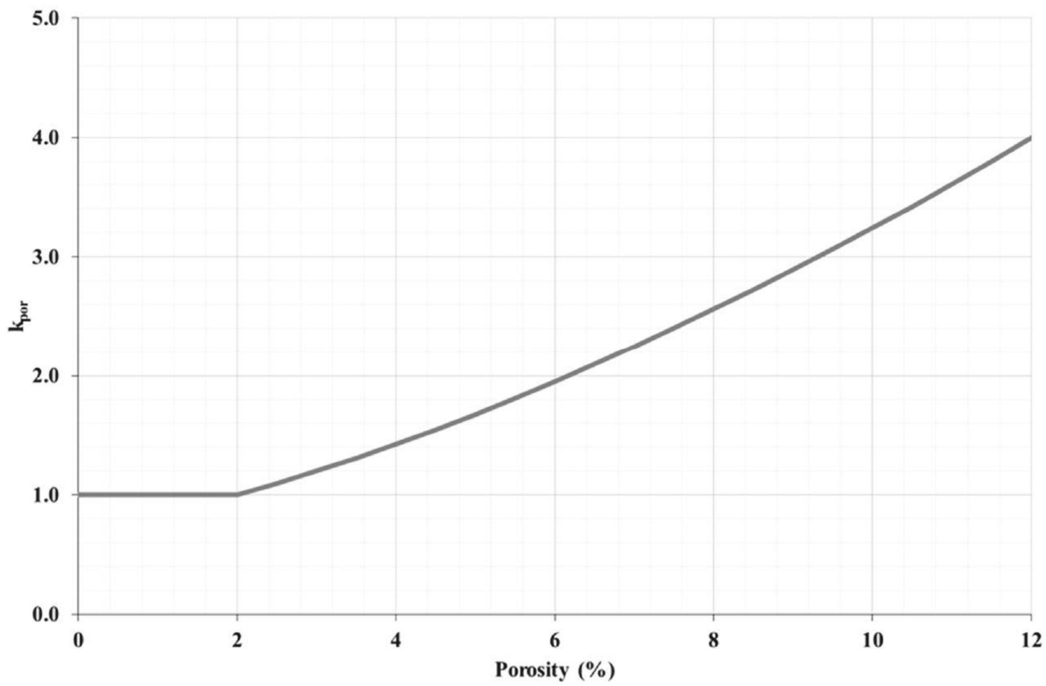

Figure 4.15: Correlation coefficient for K_{por} (Macias, 2016)

Also, the value of K_{s-tot} (when there are more than one joint set and maximum three joint sets) can be calculated as follow:

$$K_{s-tot} = \sum_{i=1}^{n} K_{si} - (n-1) \times 0.36 \tag{4.34}$$

where K_{si} is fracturing factor for set no.i, and n is the number of fracturing sets.

In order to estimate K_{si}, it is necessary to determine the fracture class. In fact, rock mass fracturing is characterized by a degree of fracturing (type and spacing) and the angle between the tunnel axis and the planes of weakness. In the NTNU system, discontinuities are classified into two major groups including joints (includes continuous joints that can be followed all around the tunnel profile, they can be open like bedding joints in granite or filled with clay or weak minerals such as; calcite, chlorite, or similar minerals) and fissures (includes non-continuous joint-can be followed partly around the tunnel profile-filled joints with low shear strength and bedding planes fissures such as in mica schist or mica gneiss). The degree of fracturing is systematically fractured rock mass is divided into class for practical use (see table 4.8).

Table 4.8: Fracture classes with distance between the planes of weakness (Macias, 2016)

Fracture class (Sf)	Average spacing between fractures (cm)	Range class (cm)	Degree of fracturing
0	∞	480 - ∞	Non-fractured
1	320	240 - 480	Extremely low
2	160	120 - 240	Very low
3	80	60 - 120	Low
4	40	30 - 60	Medium
5	20	15 - 30	High
6	10	7.5 - 15	Very high
7	5	4 - 7.5	Extremely high

The next step to determine K_{si} is a calculation of Alpha angle (α) (the angle between the plane of weakness and the tunnel axis) which can be calculated as follow:

$$\alpha = \sin^{-1}(\sin\alpha_f \cdot \sin(\alpha_t - \alpha_s)) \tag{4.35}$$

where α is the smallest angle between tunnel axis and discontinuity, α_f is dip angle discontinuity, α_s is strike angle discontinuity, and α_t is tunnel direction [all in degree °]. By calculation of fracture classes and the angle between the plane of weakness and the tunnel axis, the fracturing factor for each set of discontinuity can be determined by Figures 4.16 & 4.17.

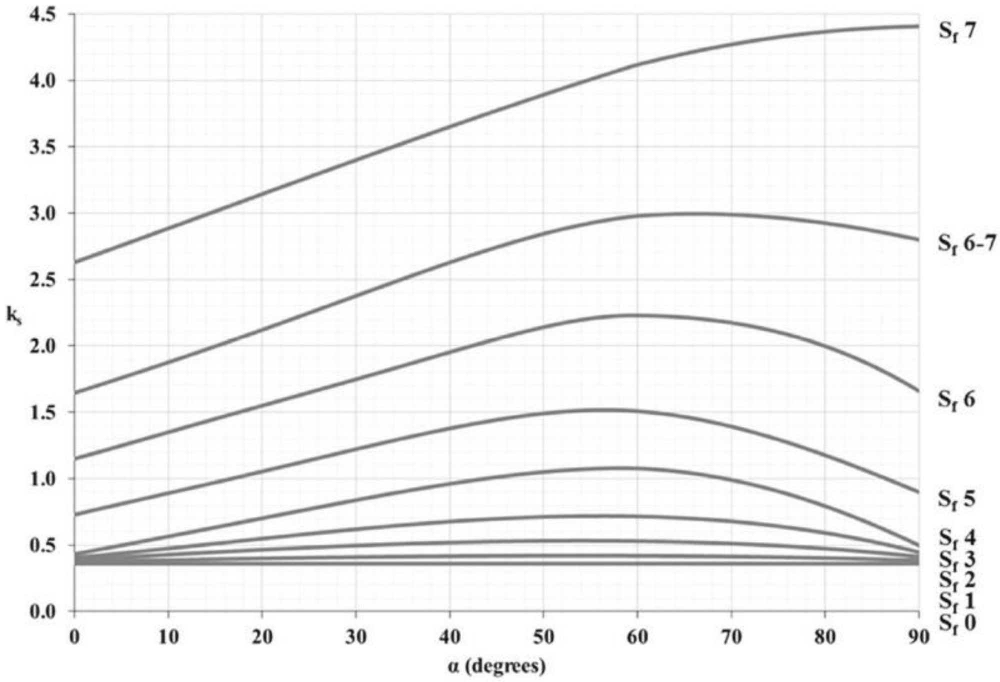

Figure 4.16: Rock mass fracturing factor (K_s) as a function of the angle between the tunnel axis and the fractures. (Macias, 2016)

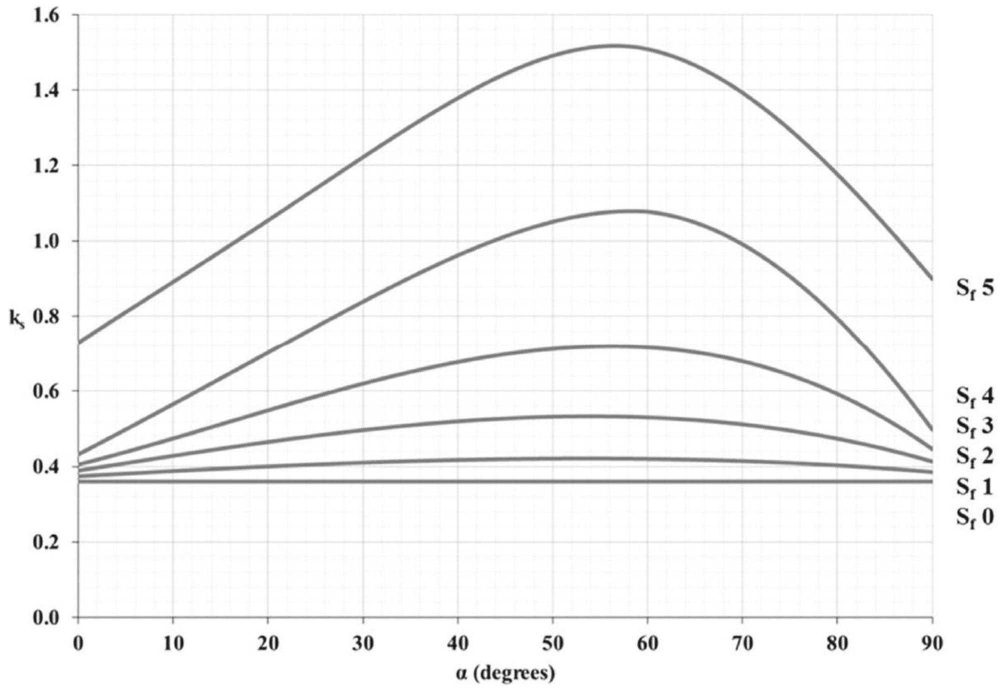

Figure 4.17: Rock mass fracturing factor (K_s) as a function of the angle between the tunnel axis and the fractures (for detailed calculations of rock masses with low degrees of fracturing) (Macias, 2016)

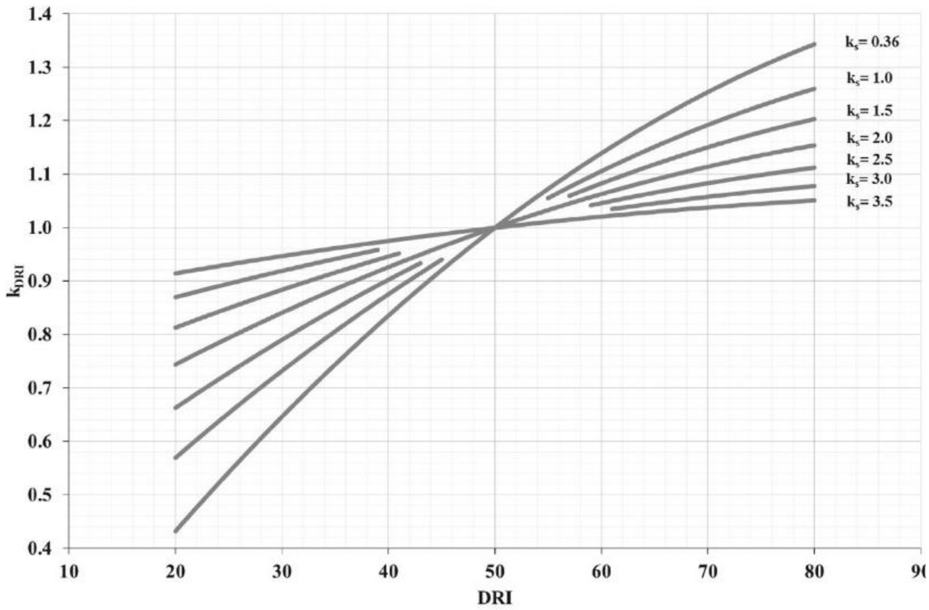

Figure 4.18: Correction factor for DRI≠50 value (Macias, 2016)

Drilling Rate Index

Rock drillability is evaluated on the basis of the drilling rate index-DRI. As it is expressed earlier, DRI is a combination of rock brittleness value "S_{20}" and Siever's miniature drill test (SJ). Here these two tests briefly are described.

Swedish Brittleness S_{20}

The brittleness test method, utilized by NTNU/SINTEF, was originally developed in Sweden by Matern and Hjelmer (1943). The original test was initially intended for the determination of strength properties of aggregates, but several modified versions of the test have later been developed for various purposes. The version of the S_{20} test developed for the determination of rock drillability has been used since the end of the 1950s. The brittleness test gives a measure of the ability of the rock to resist crushing from repeated impacts (Figure 4.19). The volume of test material corresponds to 500 grams of specific gravity 2.65 g/cm^3 of the fraction 16 – 11.2 mm. The Brittleness Value (S_{20}) is defined as the percentage of material passing the 11.2 mm sieve after 20 impacts of a 14 kg weight, taken as the mean value of 3-4 parallel tests (Bruland and Nilsen, 1995).

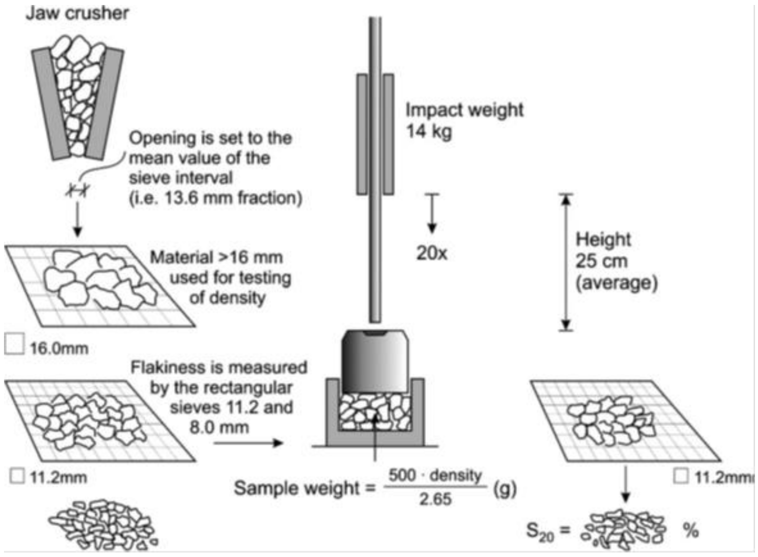

Figure 4.19: Outline of the Brittleness Value (S_{20}) test (Bruland, 1998)

The S_{20} is influenced by the mineralogical composition of the rock as well as grain size and grain binding, but also to a great extent by the degree of weathering/alteration, microfracturing, and foliation. Classification of rock brittleness is shown in table 4.9.

Table 4.9: Classification of rock brittleness, or the ability to be crushed by repeated impacts (Dahl et al. 2011)

Category – brittleness	**S_{20}-value (%)**	**Cumulative percentage (%)**
Extremely high	≥ 66.0	95–100
Very high	60.0–65.9	85–95
High	51.0–59.9	65–85
Medium	41.0–50.9	35–65
Low	35.0–40.9	15–35
Very low	29.1–34.9	5–15
Extremely low	≤ 29	0–5

Siever's Miniature Drill Test (SJ)

This test was originally developed by Sievers in 1950. SJ constitutes a measure of the rock surface hardness or resistance to indentation. SJ is defined as the mean value of the measured drillhole depths in 1/10 mm, after 200 revolutions of the 8.5 mm miniature drill bit, see Figure 4.20. The standard procedure is to use a pre-cut surface of the sample which is perpendicular to the foliation of the rock. SJ is hence measured parallel to the foliation. The SJ test is normally performed as 4–8 drilling tests, depending on variations in the texture of the sample. The SJ values may however in some specific cases show a variability, which necessitates more than 8 drillings in order to achieve a representative average value. Classification of rock surface hardness " SJ " is shown in table 4.10.

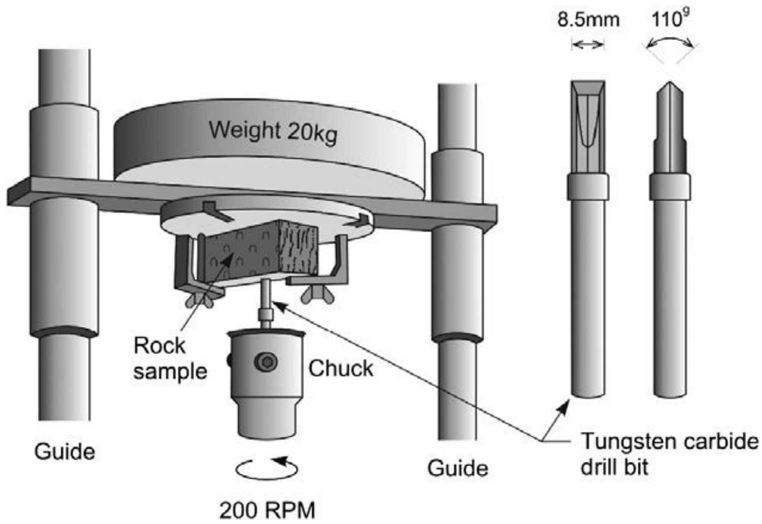

Figure 4.20: Outline of the Sievers' J-Value (SJ) miniature drill test (Dahl et al. 2011)

Also, it should be mentioned that, SJ is influenced by the same factors as the S_{20}. The mineralogical composition has however normally the most significant influence on the surface hardness and hence on the SJ .

Table 4.10: Classification of rock surface hardness, or resistance to indentation (Dahl et al. 2011)

Category – surface hardness	SJ value (mm/10)	Cumulative percentage (%)
Extremely high	≤ 2.0	0–5
Very high	2.1–3.9	5–15
High	4.0–6.9	15–35
Medium	7.0–18.9	35–65
Low	19.0–55.9	65–85
Very low	56.0–85.9	85–95
Extremely low	≥ 86.0	95–100

4.2.9.2 Equivalent Thrust

As it was expressed before, in the NTNU model all machine parameters represented by Equivalent Thrust (M_{ekv}) is calculated as follow:

$$M_{ekv} = M_B \cdot K_a \cdot K_d \tag{4.36}$$

where M_B is the gross average thrust per cutter, not the available thrust capacity of the machine, but the actual thrust used (kN/cutter), K_a is a correction factor for average cutter spacing as given in Figure 4.21 and K_d is a correction factor for cutter diameter as given in Figure 4.22.

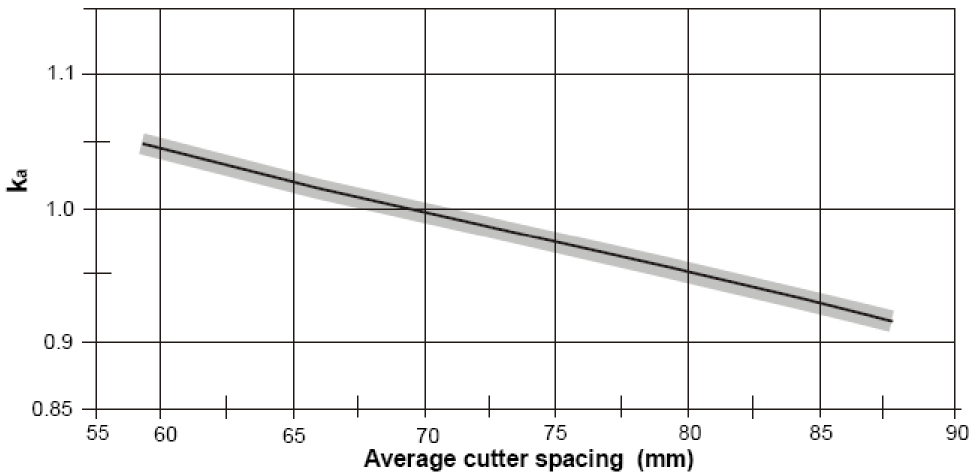

Figure 4.21: Correction factor K_a for mean spacing of the cutters (Bruland, 1998)

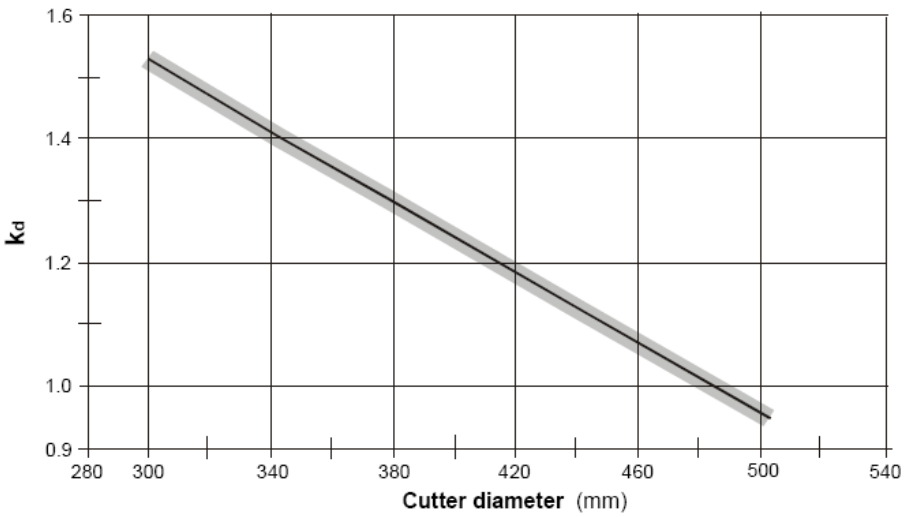

Figure 4.22: Correction factor K_d for the size of cutters (Bruland, 1998)

4.2.9.3 Penetration Rate

In the NTNU model, after estimation of two major factors including equivalent fracturing factor and equivalent thrust; the basic penetration rate i_0 in mm/rev can be calculated from Figure 4.23. As can be seen, the basic penetration rate is known as mm per cutterhead revolution is independent of TBM diameter. Net penetration rate I based on m/h is calculated by the following equation:

$$I = i_o RPM \frac{60}{100} \cdot K_{rpm} \tag{4.37}$$

where RPM is cutterhead revolution per minute and K_{rpm} is the correction factor for applied cutterhead rpm which can be found in Figure 4.24. As remarked by Macias (2016), the cutterhead velocity correction factor is based on limited information and must be applied with caution. The optimal cutterhead velocity appears to be influenced by rock drillability, rock mass fracturing, and/or thrust level. Low values of and applied cutter thrust indicate a lower optimal cutterhead velocity.

Also, the procedure to achieve penetration values is shown in Figure 4.25 graphically.

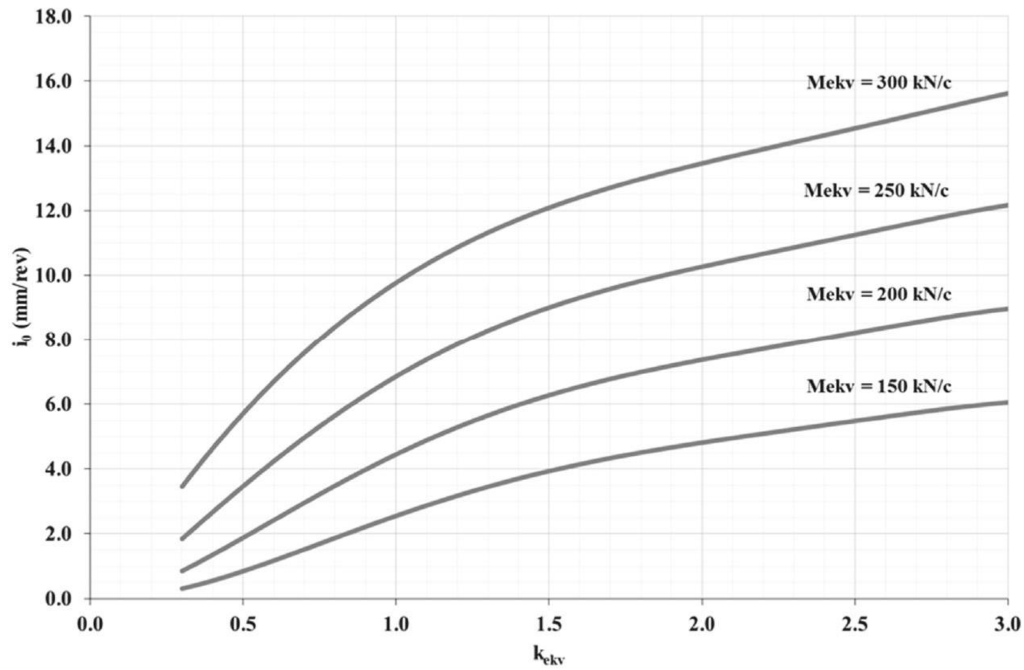

Figure 4.23: Estimation of penetration rate based on rock mass properties and machine (Macias, 2016)

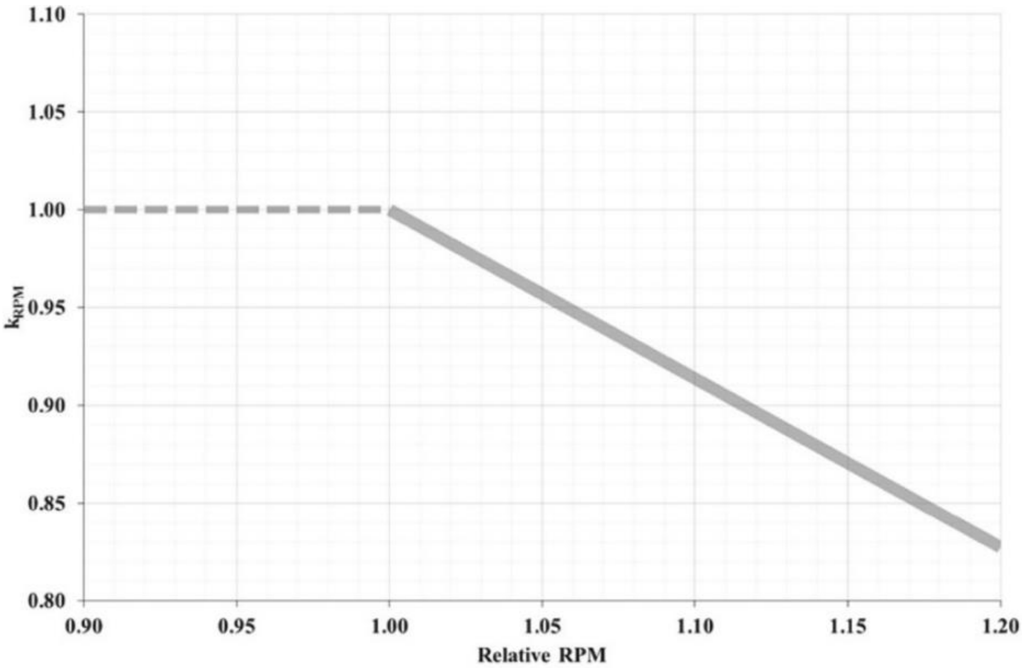

Figure 4.24: Correction factor for cutterhead velocity (rpm) illustrating where it differs from the recommended value (Macias, 2016)

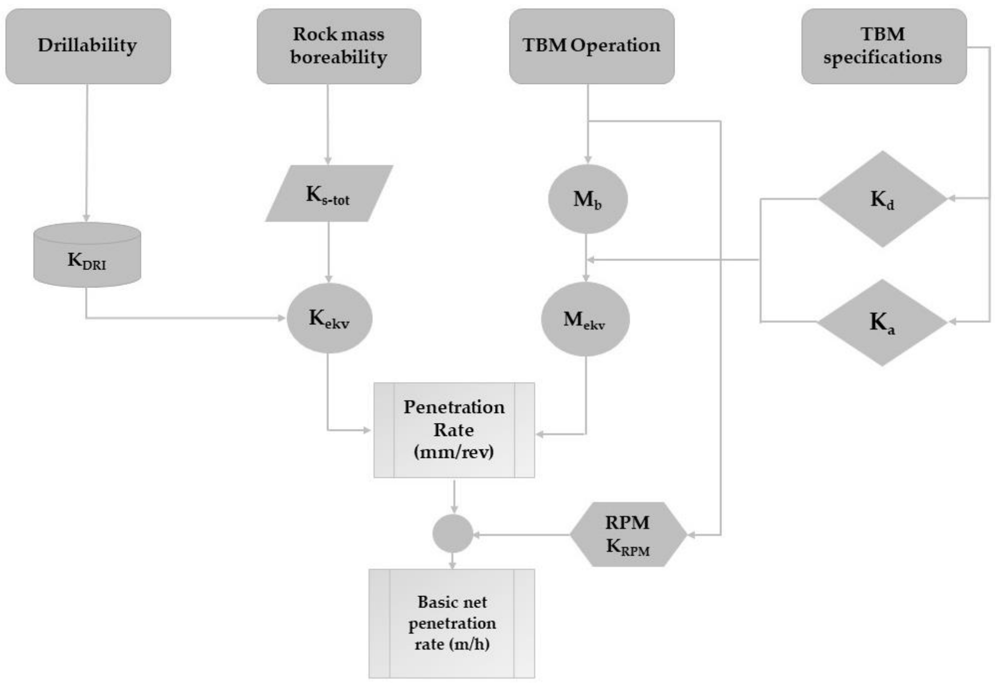

Figure 4.25: Flow chart of the procedure of predicting penetration rate in the latest version of NTNU (modified from Macias, 2016)

Discussion

The NTNU model is based on a vast database of TBM performance in a variety of geological settings and machine conditions. The model also focuses on whole-system processes, rather than single cutter processes, and their effect on machine performance and can therefore better take rock mass properties into account. However, extrapolation of machine performance into geological conditions that have not been encountered could be unreliable, as with all empirically based models. The main limitation of the model is related to some input parameters originated from NTNU/SINTEF drillability test and related tests are available through a limited number of laboratories, and therefore not commonly recorded and available by the typical geotechnical site investigations unlike other test methodologies such as UCS & BTS . As noted by Macias (2016), the machine type assumed by the model is a hard rock TBM (open or shield). However, the model is based on data derived from a large number of open TBM types tunneling in rock mass conditions summarized in the foregoing. No distinction is made between machine types. Also, a cutter diameter of 483 mm (19 inches) and 508 mm (20 inches) are currently used in hard rock tunneling and the NTNU model incorporates cutter diameter by makes no distinction between cutter ring design or quality and assumes in all cases that cutter ring quality is tailored to the rock conditions.

4.2.10 Hassanpour et al. (2011)

Hassanpour et al. (2011; 2009a, 2009b) developed an empirical prediction model based on a database including four different tunnels in medium to hard rock (shale, limestone, tuff, schist, gneiss, gabbro, diorite) totaling 158 data points. They recognized the Field Penetration Index (FPI), defined as the ratio between the average cutter load and the penetration rate (Barton, 2000; Klein et al. 1995), as the TBM performance parameter having the best correlation with the observed rock mass conditions. They also highlighted the important effect that the rock mass fracturing degree has on the rock mass boreability and developed an equation for the estimation of FPI based on the uniaxial compressive strength of intact rock and the Rock Quality Designation (RQD).

$$FPI = \exp(0.008 \cdot \sigma_C + 0.015 \cdot RQD + 1.384) \quad (4.38)$$

where σ_c is the uniaxial compressive strength of intact rock and RQD is the Rock Quality Designation.

Based on Equation 4.30, the authors developed charts for FPI estimation (Figure 4.26) and for rock mass boreability prediction (Figure 4.27). In the other words, the new boreability classification system based on FPI has been presented. In this model, six rock mass boreability classes from the most difficult for boring or B-0 class (Tough) to easiest for boring or B-V class (excellent) were defined (Table 4.11). It is worth to note that, higher values of FPI are usually recorded in strong and massive rock masses typically higher than 70 KN/cutter/mm/rev. On the other hand, in poor quality rock masses, there is no need to apply high thrust values (contrary to massive strong rock masses) and therefore FPI values are small and typically less than 10 KN/cutter/mm/rev.

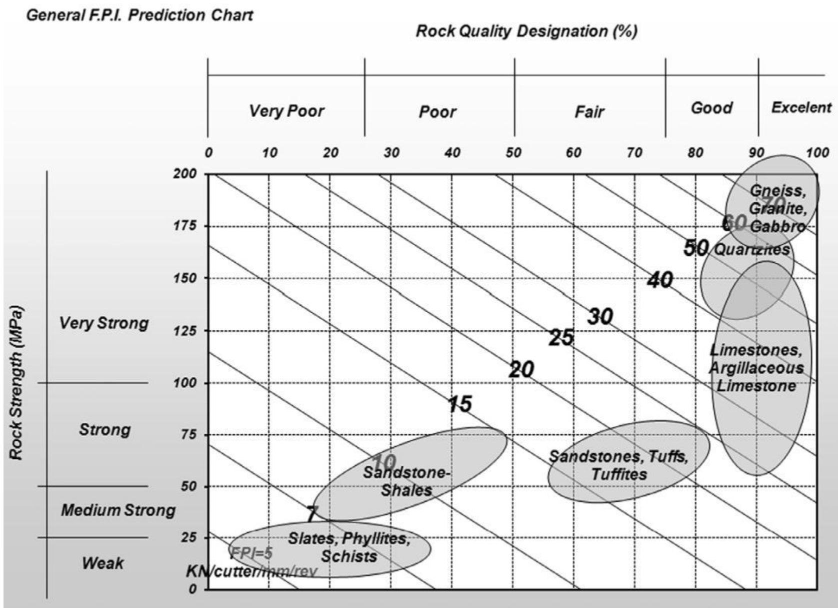

Figure 4.26: Empirical chart for the estimation of FPI (Hassanpour et al. 2011)

Table 4.11: Summary of ground conditions for various boreability classes, Hassanpour et al. (2011)

Boreability class	FPI range (kN/mm/rev)	Rock mass boreability	Stability condition	TBM excavability (relative difficulty of ground for TBM use)	Example
B-0	> 70	Tough	Completely stable	Tough	Very strong and massive quartzitic veins, intrusive and metamorphic rocks
B-I	40–70	Fair-tough	Stable	Fair	Massive igneous and metamorphic rocks
B-II	25–40	Good-fair	Minor instabilities	Good	Blocky and jointed Tuffs, Tuffites, Limestones
B-III	15–25	Good	Only local structural instabilities	Very good	Alternations of Sandstones, limestones and Shales
B-IV	7–15	Very good	Some major instabilities	Good	Alternations of thin-bedded Shale and Sandstone layers

B-V	< 7	Excellent	Collapse, gripper problems, squeeze, etc.	May be problematic	Highly foliated and schistose metamorphic rocks (Slate, Phyllite, Graphite schist), Shale, Marlstone, thick fault zones

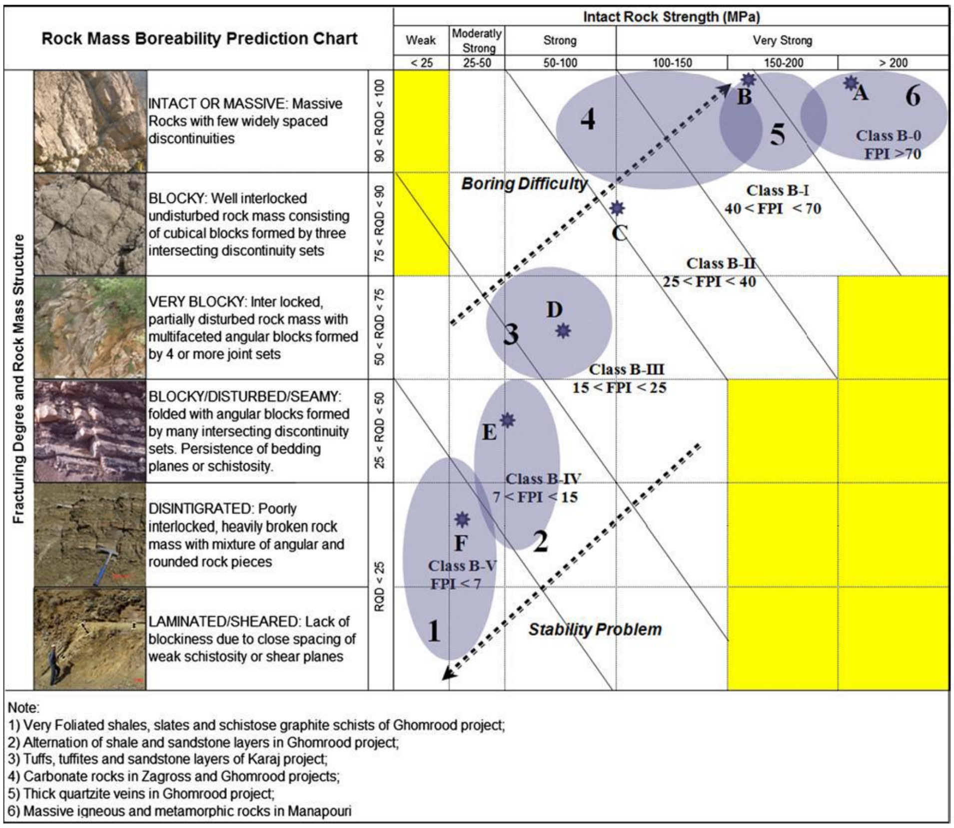

Figure 4.27: Rock mass boreability prediction chart based on FPI (Hassanpour et al. 2011)

The conclusion is then made that low TBM advance rates may be observed in high strength, massive rock due to low boreability/penetration rates. On the contrary, low advance rates are experienced in more fractured/unstable grounds due to stability problems and increased support requirements.

Discussion

The Formula and associated chart introduced by Hassanpour et al. (2011) are very applicable/constructive and reflect the practical approach in an early stage of tunnel design and construction, since it has been developed based on two commonly available inputs including, *UCS* and *RQD* which are most often available in many tunneling projects around the world. Besides, the model considers the most influential operational machine parameters, containing thrust and RPM. Also, the variations of parameters consisted of various rock types such as sedimentary and igneous with a different range, and as such, it can be used to assess TBM performance in different types of rocks. In addition, the usage of FPI to be representative of rock mass boreability makes it possible to compare and apply the model on different tunnels with different diameters. However, as noted by authors, the model shows better results when FPI is less than 70 (kN/cutter/mm/rev), and for the strong massive rock masses with *UCS* approximately, more than 200 (MPa), it displays a higher error, the reason could be the *RQD* limitation since, it is an index with the maximum value of 100 which indicates the discontinuity spacing/frequency. Perhaps, this is why Gong & Zhao (2009) and Delisio (2014) considered J_v being representative of joint frequency in their developed models.

4.2.11 Delisio et al. (2013; 2014)

Delisio et al. (2013; 2014) developed a new empirical equation for the prediction of TBM performance in blocky rock conditions which is the only FPI introduced for blocky conditions. The term "blocky rock conditions" is associated in the literature to face instabilities in blocky/jointed rock masses, where the combined effect of rock mass structure and in-situ stresses may lead to a degradation process of the tunnel face that may become "blocky".

To quantify the performance of TBMs in two rock tunneling projects including the Lötschberg Base tunnel and Manapouri second tail race tunnel, FPI was selected to represent the TBM performance. As noted by the authors, if the excavation face is not regular and flat, as in the case of a blocky face, not all the cutters are in contact with the rock. So, a transfer of loading from those cutters, which are not in contact with the face may take place, with a concentration of loading on the neighboring cutters in contact with the rock. In this case, the entire thrust force is distributed over a smaller number of discs and the force acting on each single cutter cannot be considered to be constant anymore. For this reason, the thrust per cutter (F_n) is substituted by the total applied thrust force for the calculation of the FPI (Equation 4.39).

$$FPI_{blocky} = TF/P \tag{4.39}$$

where TF is the total applied thrust force, i.e., as measured at the thrusting cylinders, expressed in kN, and P is penetration rate per cutterhead revolution (mm/rev). The authors developed an equation for the estimation of FPI_{blocky} based on the uniaxial compressive strength of intact rock and the volumetric joint count (J_V) (Equation 4.40).

$$FPI_{blocky} = e^{6.04} \cdot J_V^{-0.82} \cdot \sigma_C^{0.17} \tag{4.40}$$

where J_V is the volumetric joint count (joint/m^3) and σ_c is the uniaxial compressive strength (MPa). The correlation between volumetric joint account (J_V) and uniaxial compressive strength with FPI$_{blocky}$ is depicted in Figure 4.28. As can be seen, in terms of the regression coefficient (R^2) of the two relationships, it is clear that stronger correlation exists between the FPI$_{blocky}$ and the volumetric joint count than between the FPI$_{blocky}$ and the uniaxial compressive strength.

This means that the variability of FPI$_{blocky}$ is better explained by J_V rather than σ_c .This indicates that, when dealing with blocky rock masses, the fracturing of the rock seems to be the most important factor influencing the TBM performance.

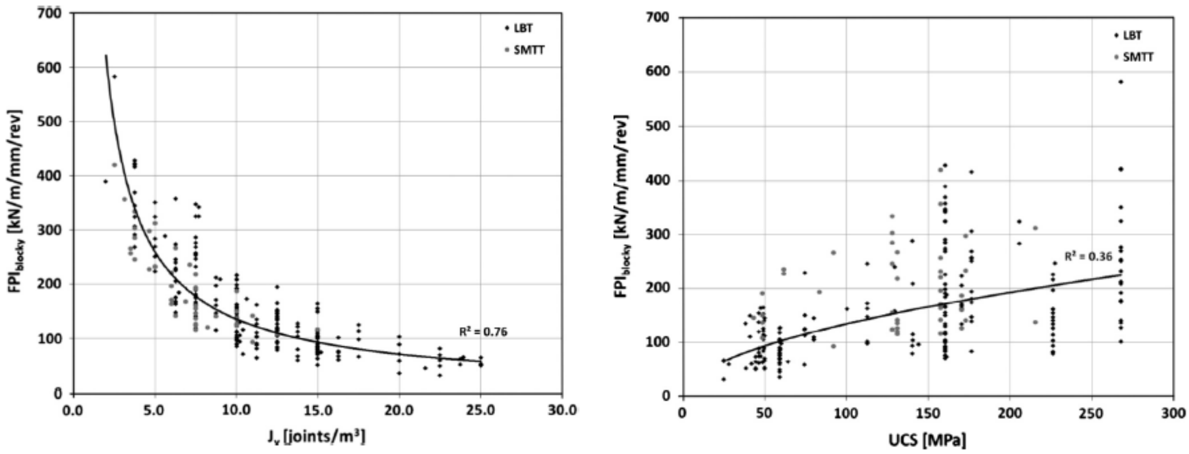

Figure 4.28: Correlation between FPI$_{blocky}$ with J_V and σ_c (Delisio and Zhao, 2014)

The developed database is composed by data of gripper/open TBMs. To such that, the authors noted that the friction force which builds-up between machine and surrounding ground is much lower with respect to shielded machines, but the front shoes of the machine are pressed against the walls and can impose a substantial amount of pressure and thus friction. In addition, when different TBMs with different sizes are used the installed/ applied thrust force strongly depends on the size of the machine being considered. For this reason, the total thrust force has been scaled by the TBM diameter D . One could consider the ratio TF/D as a sort of ''thrust density''. However, machines of the same size may have a different number of cutters on the cutterhead. Based on these statements, the ''expanded'' Field Penetration Index for blocky rocks, becomes as follow:

$$FPI_{blocky} = \frac{(TF - f)/D}{P} \tag{4.41}$$

where f (kN) is the friction force to be subtracted from the applied thrust (TF) and D is the TBM diameter. Also, the authors noted that, for gripper TBMs, the friction f can be estimated by considering about 20% of the machine weight which by considering the weight of machines (1000 tons); a friction f of about 2000 kN. Furthermore, to make a comparison with other prediction models using the original FPI formulation, the author proposed the following equation:

$$FPI = \frac{D}{c} \cdot FPI_{blocky} \tag{4.21}$$

where D is the TBM diameter and c is the number of cutters installed on the cutterhead. Finally, the following equation is presented to estimate penetration per revolution and the rate of penetration in blocky rock conditions.

$$P_{blocky} = \frac{(TF - f)D}{FPI_{blocky}} = \frac{(TF - f)}{D \cdot e^{a} \cdot J_V{}^{b} \cdot UCS^{c}} \tag{4.43}$$

$$ROP_{bocky} = \frac{P_{blocky} \cdot 60 \cdot RPM}{1000} \tag{4.44}$$

where P_{blocky} is the penetration per revolution, expressed in mm/rev and ROP_{blocky} is the rate of penetration in m/h and a, b, c are 0.604, -0.82, 0.17, respectively. The author also mentioned that, the applied thrust force and RPM need to be reduced in blocky conditions to limit excessive cutterhead/cutter wear, and extensive cutterhead vibrations. To address this matter, an attempt is made to express the TBM thrust force and cutterhead RPM as a function of the volumetric joint account to obtain an indication of the needed reduction of TF and RPM. Therefore, the Equation 4.45 is presented to compute a suitable value of thrust force.

$$\frac{TF}{D} = -523 \cdot \ln(J_V) + 2312 \pm 328 \tag{4.45}$$

Also, two different relationships for the calculation of an adjusted RPM in blocky rock conditions (during operation) are introduced due to the difference between the recommended RPM (6.0 for LBT and 5.1 for the SMTT). One should note that these are site/TBM specific formulas and not universal for use in other projects.

$$\begin{aligned} RPM_1 &= -0.8 \cdot \ln(J_V) + 6.9 \pm 0.5 \\ RPM_2 &= -1.7 \cdot \ln(J_V) + 7.0 \pm 0.7 \end{aligned} \tag{4.46}$$

Discussion

The main limitation of the proposed model is that the model is only evolved and developed based on two tunnels excavated mainly old crystalline gneiss, granodiorite, granite rock types (massive hard rock). Also, the model has been developed for blocky rock conditions and cannot be employed for other geology conditions, although the author proposed a formula to compare other prediction models using original FPI formulations.

4.2.12 Alpine model (Wilfing, 2016)

The Alpine model derived from the research project group "ABROCK" which has been formed in 2006 and was the collaboration between five universities (Technische Universität München, Montanuniversität Leoben, Universität Innsbruck, ETH Zürich, EPF Lausanne), clients, contractors, TBM manufacturers, and TBM experts. ABROCK approaches the analysis and prediction of TBM performance by improving the existing prediction model of Gehring (1995) and consequently develop a new model called the "Alpine model" which improved and validated by two correction factors ($K_1 \& K_2$) in Gehring's model. The factor for specific failure energy includes the term of rock toughness, whereas the factor for rock mass fabric describes characteristics of discontinuity systems. To achieve the aims and enable the investigations on the influence of toughness as well as a discontinuity on the boreability (penetration rate), extensive laboratory and in-situ penetration tests were conducted. To define the toughness of rock, different approaches such as, the ratio of uniaxial compressive strength to Brazilian tensile strength (B_1, B_2, B_3); ratio of uniaxial compressive strength to point load index (σ_c / I_s), LCPC breakability coefficient (LBC), and LCPC abrasivity coefficient (LAC) were employed. A database of TBM field performance from two hard rock tunneling projects including Koralm tunnel project in Austria (by double shield TBM with a diameter of around 10 m, length of study area 13 km) and Røssåga tunnel project in Norway (by open gripper TBM with the diameter of around 7 m, with the length of the study area, the first 2.5 km) has been used to develop the model. The geology of the study area for the Koralm tunnel project consisted of schistose gneisses and mica schist, but also cutting the unit of fine and coarse-grained gneisses and for Røssåga tunnel comprised mica schist (calcareous), granite and quartzite.

In addition to extensive laboratory tests which has been performed on several different rock samples from 25 locations to primarily investigate the deformation behavior of rocks under load in terms of rock toughness, more than 28 penetration tests on-site (start-stop test) as well as geological back-mapping at the Koralm tunnel and the Røssåga hydropower project were performed and analyzed to validate the results of penetration prediction models. The emphasis was on conducting penetration tests at construction sites to analyze the interaction of tunnel boring machines and excavated rock mass, as well as the influence of discontinuities on the performance and penetration rate of hard rock TBMs. In addition to the actual test, a detailed geological mapping and sample acquisition were done at each chainage where penetration tests have been conducted.

Several examinations were conducted to obtain the best definitions to classify rock toughness and the best correlation was achieved by the ratio of LBC to Brazilian tensile strength (BTS) with a threshold equal to 5 and named $T_{LBC} = LBC/BTS$, since it defines rock toughness by the ratio of LBC & BTS. Ratios higher than five are related to tough rocks, whereas lower ratios correspond to brittle rocks. Since the relation between the normal force and resulting penetration is not a linear function, the original FPI was transferred to the point, at which the relationship becomes linear. This was the fact at the threshold of subcritical penetration, which is set at 3 mm/rev (FPI_{3mm}) in that study. The relationship between FPI_{3mm} with uniaxial compressive strength (UCS), Brazilian tensile strength (BTS), and LCPC breakability coefficient (LBC) and performed penetration tests at the Koralm tunnel reveals that, the two geotechnical rock properties affect the "critical stress" (the stress under the disc cutter at 3 mm/rev penetration rate called critical stress) are the BTS & LBC. Therefore, these parameters were considered for further analysis to develop a model. The actual relation between the applied force and resulting penetration can be described by a linear function with a certain y-intercept specified by the threshold of subcritical penetration. The magnitude of the offset highly depends on the LCPC breakability and subordinated on the Brazilian tensile strength, whereas uniaxial compressive strength, failure and destruction work, and point load strength revealed no significance. Though, the LBC appears to be much more accurate for the determination of the y-axis offset in terms of critical stress under the cutter. A regression analysis reveals that the relation of stress and penetration can be described either by an exponential or linear function. Since both regressions resulted in similar coefficients, the linear function was considered for the sake of simplicity. Although LBC shows a very high correlation, the parameter bears one weakness. The test is not used as a standard laboratory test during pre-investigations of tunnel projects up to now (Figure 4.29).

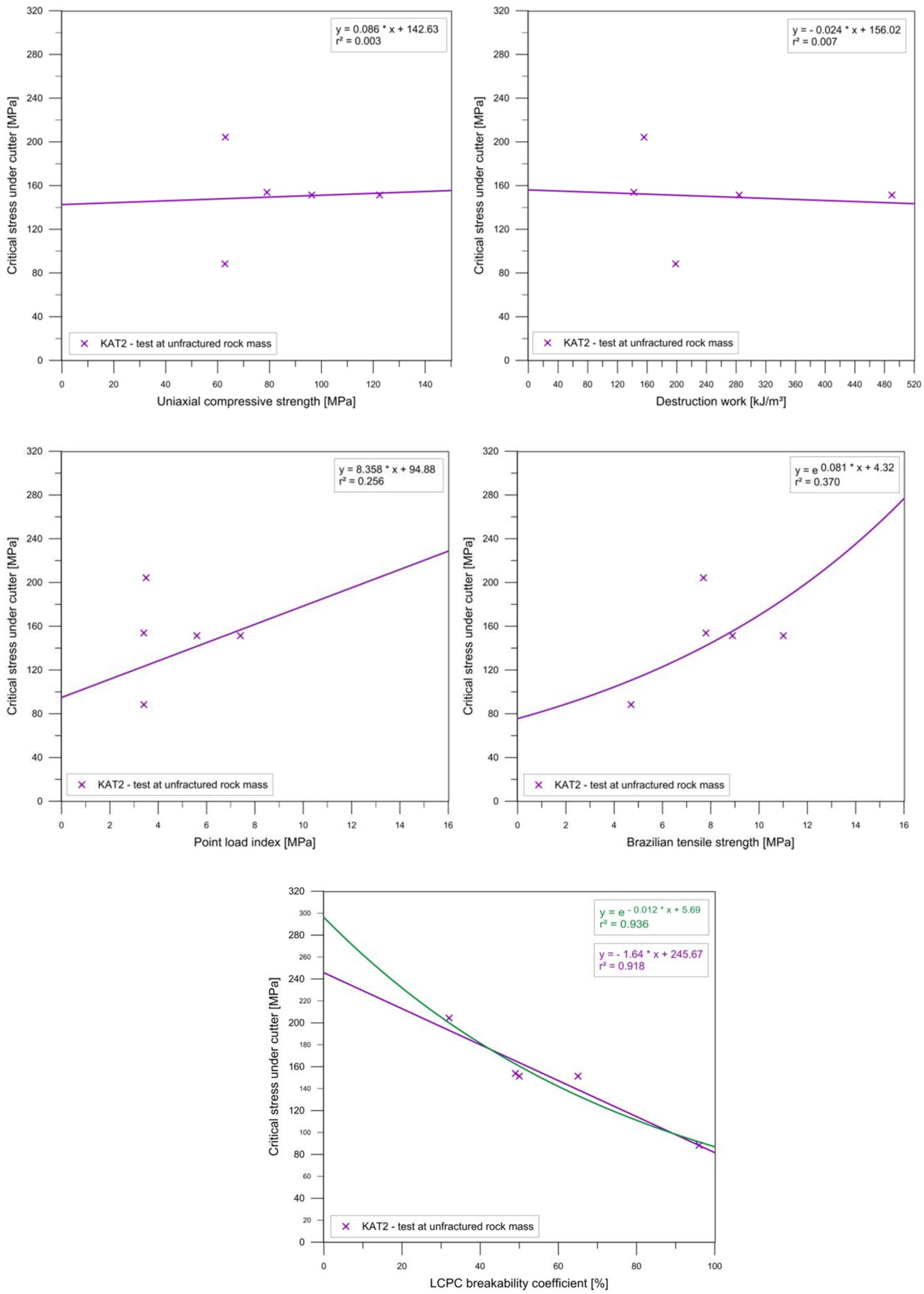

Figure 4.29: Stress under disc cutter at subcritical penetration plotted against uniaxial compressive strength, destruction work, point load index, Brazilian tensile strength, and LCPC breakability coefficient (Wilfing, 2016)

To allow further analysis on the y-intercept in terms of penetration prediction models, the above-mentioned regression functions are back-transformed to the normal force per cutter. Since the Brazilian tensile strength and the LBC result in moderate and significant correlation, the y-intercept at subcritical penetration was determined for both parameters, resulting in Equations 4.47 & 4.48.

$$b_{BTS(3mm)} = e^{0.08 \cdot \sigma_t + 4.1} = y - \text{intercept}_{BTS(3mm)} \tag{4.47}$$

$$b_{LBC(3mm)} = -1.3 \cdot LBC + 194.7 = y - \text{intercept}_{LBC(3mm)} \tag{4.48}$$

where $b_{BTS(3mm)}$ is y-intercept BTS approach at penetration 3 mm/rev, σ_t is Brazilian tensile strength (MPa), $b_{LBC(3mm)}$ is y-intercept LBC approach at penetration 3 mm/rev and LBC is LCPC breakability coefficient (%). The incorporation of suggested y-intercepts into the Gehring model is achieved by transforming the linear function. Since the parameter is based on the threshold of subcritical penetration, the value of 3 mm/rev penetration rate must be accounted for in the new prediction model and results in a basic linear equation depending on the "slope a" and the "y-intercept b".

$$F_N = a \cdot (p - 3) + b \tag{4.49}$$

where F_N is normal force per cutter (kN), p is penetration rate (mm/rev), a is the slope of the line and b is the y-intercept of the line. The y-intercept has been defined above by two possibilities. The slope of the force-penetration graph appears to depend on rock mass parameters such as discontinuities and in-situ stress. These parameters are already included in the Gehring model by correction factors that reduce the slope of the basic Gehring function.

Also, it is well-recognized that, the discontinuity pattern in a rock mass (spacing & orientation) plays a significant extent in TBM penetration rate. Due to, in original Gerhing's model, only the major plane of weakness with spacing less than 50 cm was taken into account, the improved obtained by extending the table 4.3 to distances between planes of weakness up to 160 cm, since K_2 is based on observation by Bruland, K_2 was directly substituted by K_{s-tot}. The total fracturing factor results in much higher value of K_{s-tot} = 3.3 as it considers spacing up to 160 cm, the interaction of different discontinuity sets among each other, and single marked joints like faults. Finally, a newly developed modified Gehring model, so-called "Alpine Model", is proposed that includes the important parameter of the y-intercept.

$$P = \frac{F_N - b_{BTS/LBC}}{\sigma_c} \cdot K_0 \cdot K_2 \cdot K_i + 3 \tag{4.50}$$

Where P is penetration rate (mm/rev), F_N is normal force per cutter (kN), $b_{BTS/LBC}$ is y-intercept BTS or LBC approach, σ_c is uniaxial compressive strength, K_0 is basic penetration factor = 4.0, K_2 is a correction factor for discontinuity pattern and K_i is further correction factors for geotechnical/machine properties. More information about the model and respected procedures can be found in a Ph.D. thesis written by Wilfing (2016).

Discussion

The 'Alpine model' strongly improves the existing version of 1995 by Gehring, since the y-intercept is of major importance to reflect the actual relation between the applied force and resulting penetration. However, one must bear in mind that these findings rely only on one tunnel project with a very narrow range of rock types (schistose gneiss, fine-/coarse grained gneiss, siliceous marble). Further investigation with several more rock types such as limestone with sedimentary layering, homogeneous granite, etc. is inevitable and must be validated by further data. Besides that, the LCPC test is rarely used in the tunnel industry compared to other tests such as, UCS or BTS , and as a such, LBC (LCPC breakability coefficient) is not commonly available in many tunneling projects.

4.3 TBM Performance and Rock Mass Classification

One of the useful methods to predict and estimate TBM performance is, utilizing the relationship between geomechanical parameters, such as strength parameters of rock mass and parameters which are related to rock mass classifications with machine performance. Until now, many efforts have been conducted by different researchers. In this section, some classification methods which were utilized in TBM performance analysis will be briefly reviewed.

4.3.1 Cassinelli et al. (1982) & Innaurato et al. (1991)

Cassinelli et al. (1982) used a correlation between Rock Structure Rating (RSR) system and actual TBM performance to evaluate TBM penetration rate. The tunnel with 2 km long and section of 5.2 m^2 excavated in granitic gneiss in the western Alps, Italy was investigated. The authors presented the following equation for evaluation of TBM PR:

$$PR = -0.0059RSR + 1.59 \tag{4.51}$$

The RSR was originally developed for the determination of the appropriate steel rib tunnel wall support. Afterward, Innaurato et al. (1991) investigated the potential application of the first four parameters in the Q-system $(RQD/J_n)\cdot(J_r/J_a)$ with the performance of TBM was analyzed. The penetration rate, rock strength (σ_c), Q-value, and RSR correlations shown in Figure 4.30 were derived from measurements in 3.5 m diameter tunnels, 3000 m long in three lithological types including an Oolitic limestone, a grey limestone, and dolomite. Also, the authors modified Cassinelli's (1982) model by including the uniaxial compressive strength (σ_c) in the model as follow:

$$PR = \sigma_c^{-0.437} - 0.047RSR + 3.15 \tag{4.52}$$

The fact is that, Innaurato's formulation considers the effect of both the intact rock and of the rock mass, but the latter is characterized with a by now infrequently used geomechanical quality index which is rarely available in the geotechnical characterization of a tunnel. In addition, the penetration rate is estimated without any reference to the force acting on discs which has a major impact on penetration rate.

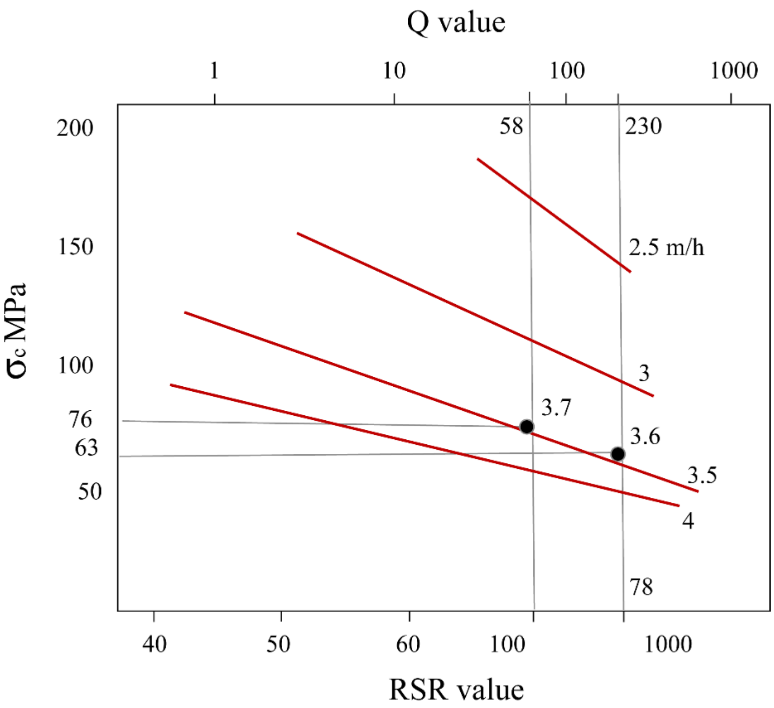

Figure 4.30: Correlation of PR with σ_c, RSR and approximate Q-value for 3.5 m diameter tunnel (modified from Innaurato et al. 1991)

Discussion

The fact is that, Innaurato's model considers the effect of intact and rock mass, but the latter is characterized by an infrequently used geomechanical quality index which is rarely available in the geotechnical characterization of a tunnel. Moreover, the penetration rate is estimated without any reference to the force F_N acting on each disc in which caused a huge error in the assessment of TBM PR as indicated by many researchers before.

4.3.2 Mitani et al. (1987)

Mitani et al. in 1987, analyzed data from two small diameter TBM tunnels predominantly granite, sandstone, slate, and porphyry. The authors showed quite a significant relationship between penetration rate (m/hr) and P- wave velocity V_P (km/s) obtained from refraction seismic measurements performed along the tunnel wall. The data trend is shown in Figure 4.31.

$$PR \approx 5.6 - 0.8V_p \tag{4.53}$$

By the combination of two equations (4.53 and 4.54), (the relationship between seismic velocity and Q-value which has been presented by Barton, 1991) then the following approximate trend for PR (m/hr) can be derived from equation 4.55 (Barton, 2000).

$$V_P \approx 3.5 + \log(Q) \tag{4.54}$$

$$PR \approx 2.7 - 0.8\log(Q) \tag{4.55}$$

Note that, this simple empirical relationship gives PR values in excess of 2.7 m/hr when Q-value is less than 1.0, and smaller values when Q-value is more than 1.0. When no joints are present and Q =1000, a PR value of 0.3 m/hr is anticipated. It would be more realistic if the rock is also hard and abrasive as well as being massive (Barton, 2000).

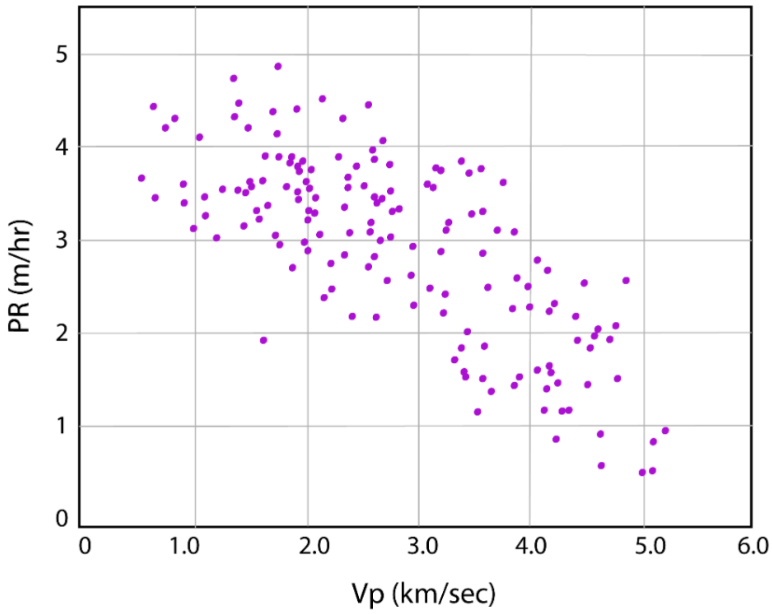

Figure 4.31: Correlation between PR and V_p at two small diameter TBM tunnels in Japan (modified from Mitani et al. 1987)

4.3.3 Palmström (1995)

Palmström (1995) developed another model base on the Rock Mass index (RMi). This model is to be considered the closest relation to the NTNU model with its parameters but has some differences. The NTNU model uses the drilling rate index (DRI)-which requires some special laboratory equipment to determine DRI- to present the properties of intact rock. Instead of using DRI as representative of intact rock properties, the correlation between the DRI and the compressive strength of rock material can be used as follow:

$$DRI = E \cdot \sigma_C{}^{0.6} \tag{4.56}$$

where E is a factor representing various groups of rocks. It has the following values:

- E = 1000 for most non-schistose, hard rock (compressive strength σ_c > 40 MPa)
- E = 750 for metamorphic schists (σ_c = 30 - 150 MPa)
- E = 500 for argillaceous rocks (σ_c = 10 - 100 MPa)

The system for applying the RMi to evaluate the TBM boring capacity is shown in Figure 4.32.

Palmström (1995) believes that, K_S (fracture factor) in the NTNU model does not fully include the effect of the three-dimensional occurrence of joints; this issue can be solved by considering block volume (V_b). The correlation between block volume (V_b) and jointing factor (Ks) which has been found by Palmström as follow:

$$K_S = 1.6 C_0 \times V_b^{-0.33} \tag{4.57}$$

where V_b is the block volume in m³ and C_0 is a factor representing the orientation of the main joint set with tunnel axis. C_0 can be estimated from Table 4.12.

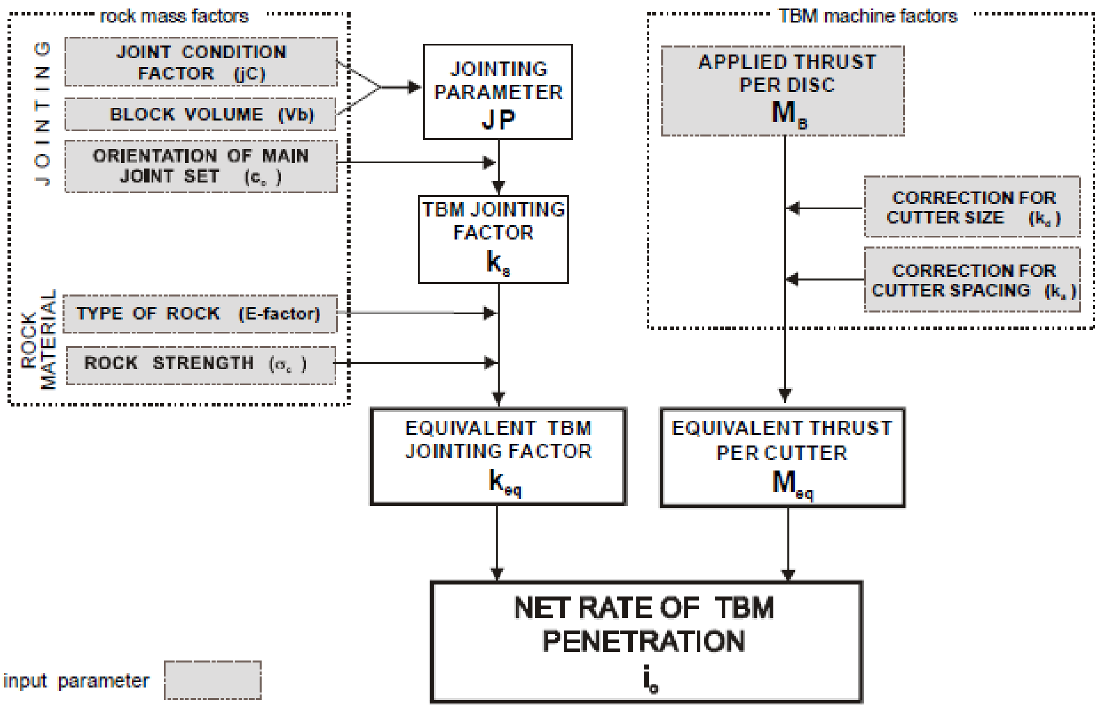

Figure 4.32: Layout of a method to predict TBM penetration using RMi parameters (Palmström ,1995)

Table 4.12: Rating of the joint orientation factor for TBM (Palmström, 1995)

Angle between tunnel axis and joint set	0-15 o	15-30 o	30-45 o	45-75 o	75-90 o
Average value of C_0	1	1.25	1.5	1.75	2

Also, Equation 4.57 can be expressed in terms of J_P (jointing parameters) as follow:

$$K_S = 0.43 \sqrt{C_0 \cdot J_p} \tag{4.58}$$

In the NTNU model for the calculation of machine performance parameters, it is necessary to covert fracturing factor (K_s) to equivalent fracturing factor (K_{ekv}). On the basis of Palmström's suggestion, it can be expressed as following equations:

$$K_{DRI} = 0.14\sqrt{DRI} \tag{4.59}$$

$$K_{ekv} = K_S \cdot K_{DRI} \tag{4.60}$$

$$DRI = E \cdot \sigma_C^{-0.6} \tag{4.61}$$

$$K_{ekv} = \frac{0.06 C_0 \sqrt{E}}{J_P \cdot \sigma_C^{0.3}} \tag{4.62}$$

In order to estimate TBM performance by this model, other steps are exactly similar to the NTNU model which was described in detail before. Also, the above parameters are discussed in section 4.2.9. in the description of the NTNU method.

4.3.4 Grandori et al. (1995)

Grandori et al. in 1995 by analyzing the data from two tunnels in Hong Kong estimate the relationship between IMS classification with TBM performance. The first tunnel was 7.4 km long with 3.6 m diameter in predominantly fine and coarse granites, granodiorites, and intrusive dykes, and the second tunnel was 5.4 km long also in granites were excavated. It should be mentioned that, the IMS classification is on the basis of joint spacing and weathering degree. In very approximate terms, the five IMS joint spacing-weathering classes can be compared to Q-value in the following manner:

Table 4.13: Adaption of two classification systems (IMS, Q) (Barton, 2000)

IMS class	1	2	3	4	5
Q-value	≥ 50	≈ 10	≈ 1	≈ 0.1	≤ 0.01

These analyses are shown in Figures 4.33. As can be seen from Figure 4.33 in the first tunnel; it showed consistent trends for PR, U, and AR and average cutter thrust F with IMS classification. It can be seen that, machine utilization as well as average cutter thrust decrease with the decrease of rock mass quality. In the second tunnel (Figure 4.34), the PR value is seen to fall in the poorest rock classes due to difficulties with the grippers. While in the first tunnel; only the advance rate falls in the lowest classes due to reduced utilization and increased rock support needs. Note how the utilization falls successively with lower rock mass qualities, likewise, the necessary thrust grows for achieving generally faster penetration rates.

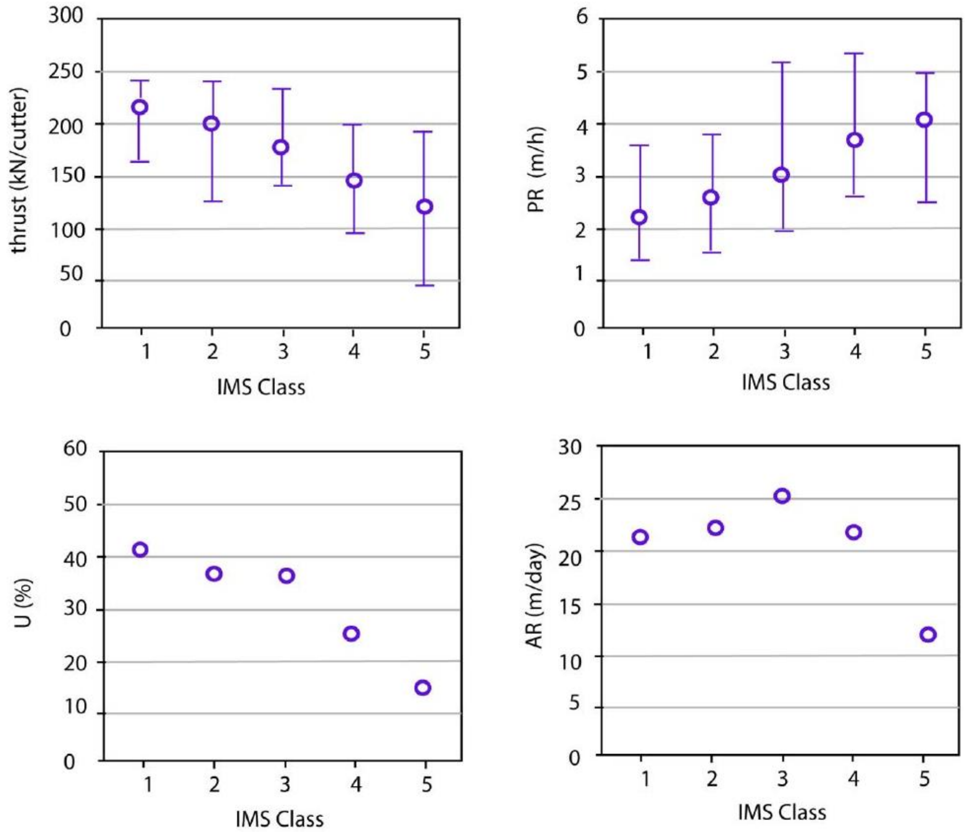

Figure 4.33: Relationship between IMS classification with machine performance parameters in 7.4 km long tunnel in Hong Kong granites, granodiorites, and intrusive dykes (modified from Grandori et al. 1995)

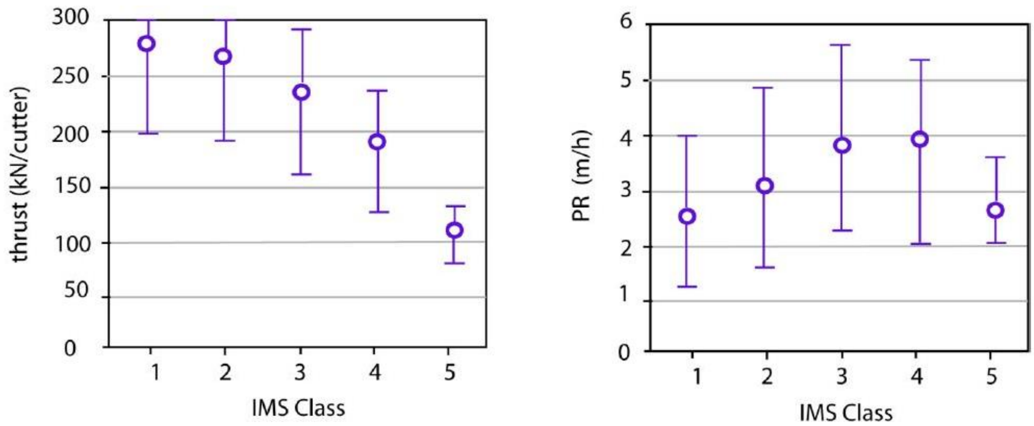

Figure 4.34: Relationship between IMS classification with machine performance parameters in 5.4 long tunnel in Hong Kong granites (modified from Grandori et al. 1995)

4.3.5 Sundaram et al. (1998)

Sundaram et al. (1998), analyzed the correlation between five machine performance parameters (included; Field penetration index, penetration rate, specific energy, torque, and utilization coefficient) with some rock mass parameters which were collected in a tunnel with 2825 m, excavated in medium to coarse-grained granite with σ_C = 130 to 246 MPa (mean 182 MPa). The results of this investigation are shown in Table 4.14. The four strongest correlation coefficients for the field penetration index were the volumetric joint account Jv (Palmström, 1982) from which RQD was estimated, the ratio RQD / J_n, $Q^{'} = (RQD / J_n) \cdot (J_r / J_a)$ and the Q-value itself. These correlations are indicated in Figure 4.35 together with joint spacing (Js) and Schmidt rebound (R). Also, it should be noted that, RQD derived from J_v showed a good correlation with field penetration rate, but insufficient sensitivity below an RQD of about 75% (Barton, 2000).

Table 4.14: Correlation values (r) of machine parameters with average rock mass properties

Machine parameters	Schmidt rebound value R	Discontinuity alteration	Aperture	Infill material	Roughness	Joint orientation	RQD
FPI	0.33	0.53	0.22	0.17	-0.35	-0.19	0.72
ROP (mm/rev)	-0.29	-0.043	-0.16	-0.21	0.23	0.21	-0.54
Specific energy	-0.21	0.2	0.15	-0.04*	-0.21	0.28	0.26
Torque	-0.09*	0.12	-0.01*	-0.09*	-0.19	0.15	0.11
Utilization	0.15	0.29	0.25	0.09*	-0.20	0.11*	0.37

Machine parameters	Fissure	Joint volume	Continuity	Rock mass alteration	Joint spacing	Strength estimate	(RQD /Jn)	(RQD/ Jn).(Jr/Ja)	Q-value
FPI	0.61	-0.76	-0.55	0.55	0.64	0.56	0.70	0.69	0.68
ROP (mm/rev)	-0.55	0.63	0.46	-0.43	-0.52	-0.43	-0.57	-0.55	-0.54
Specific energy	0.23	-0.24	-0.24	0.19	0.27	0.20	0.23	0.24	0.30
Torque	-0.05*	-0.06*	-0.07*	0.15	0.10	0.17	0.11	0.14	0.12
Utilization	0.34	-0.37	-0.34	0.25	0.32	0.24	0.38	0.39	0.46

* Insignificant correlation

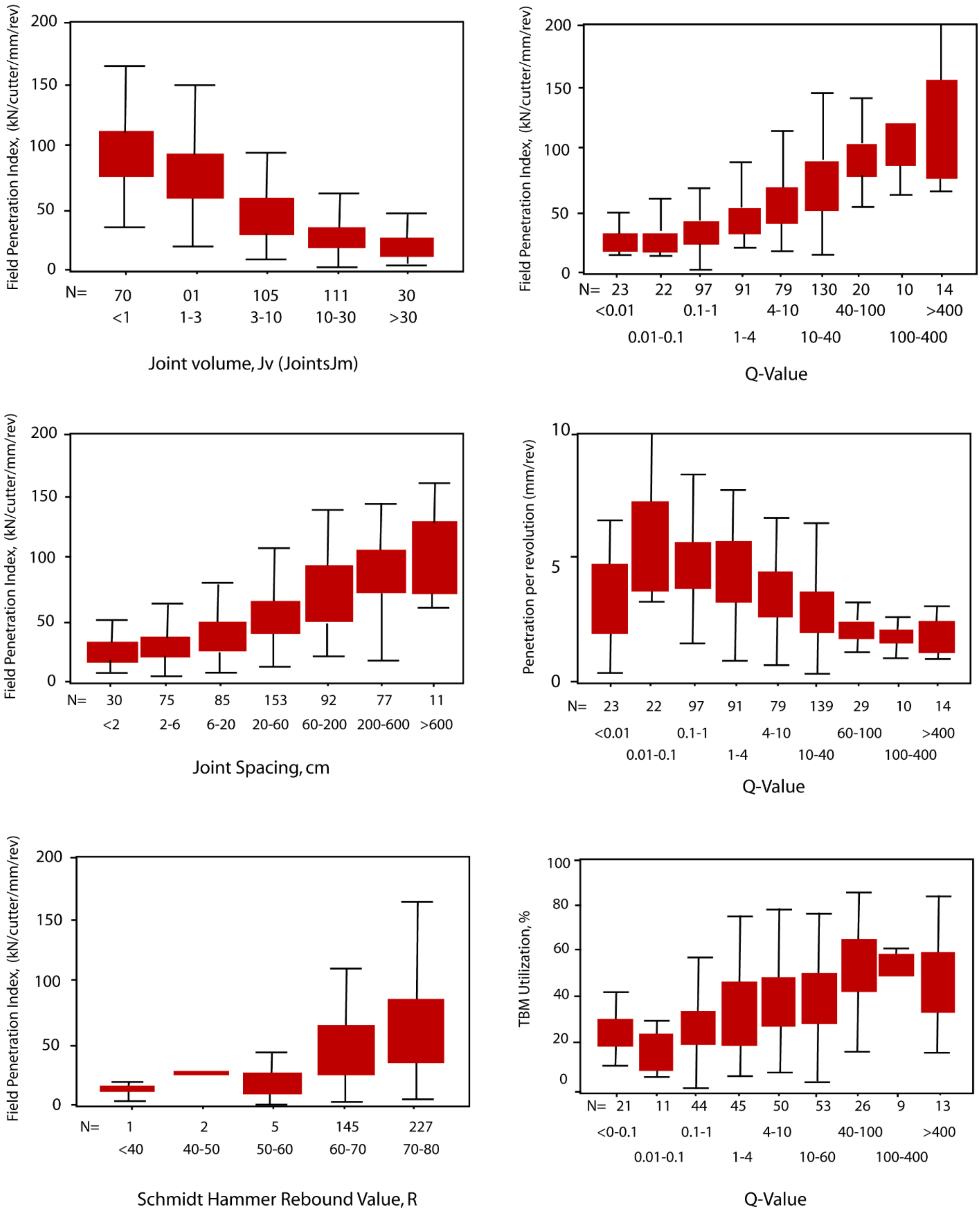

Figure 4.35: Correlation between TBM performance parameters with Q-value, J_v, joint spacing, R (modified from Sundaram et al. 1998)

4.3.6 Barton (2000)

The Q_{TBM} model (Barton, 2000) is based on an expanded Q-system in which the factors relevant to TBM performance have been introduced, such as the orientation of joints or joint structures, the strength and abrasiveness of the rock, and so on. The model starts from the observation that, when dealing with TBM tunneling, both extremely good (Q up to 1000) and extremely bad conditions (Q down to 0.001) are unfavorable for TBM advance, one slowing the average progress due to multiple cutter changes and low penetration rate, the other stopping the machine for long periods and requiring heavy "pre-treatment" and support. Starting from these considerations, Barton (2000) identified general trends for the penetration rate (PR) with uninterrupted boring, and the actual advance rate (AR), as a function of the rock mass quality (Figure 4.36).

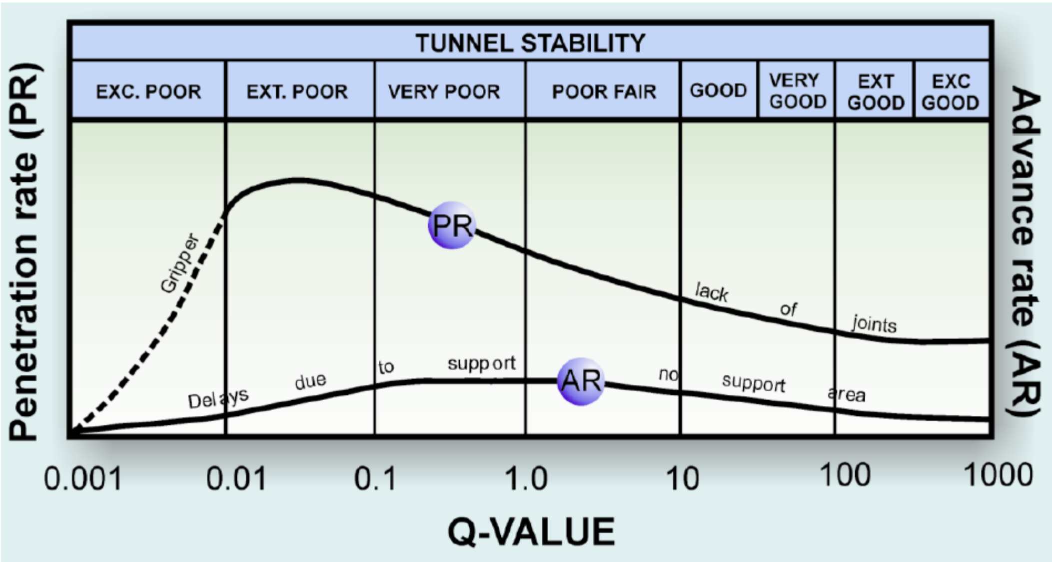

Figure 4.36: Conceptual relation between Q index, penetration rate (PR) and advance rate (AR) (Barton, 2000)

The Q_{TBM} (Equation 4.63) is based on the familiar Q-parameters but has additional rock-machine-rock mass interaction parameters. Together, these factors give twelve potential orders of magnitude for the Q_{TBM} range.

$$Q_{TBM} = \frac{RQD_0}{J_n} \cdot \frac{J_r}{J_a} \cdot \frac{J_w}{SRF} \cdot \frac{SIGMA}{F^{10}/20^9} \cdot \frac{20}{CLI} \cdot \frac{q}{20} \cdot \frac{\sigma_\theta}{5} \tag{4.63}$$

where RQD_o is RQD (%) interpreted in tunneling direction; J_n, J_r, J_a, J_w are joint parameters in Q-system; SRF is the strength reduction factor, $SIGMA$ is the rock mass strength expressed as:

$$SIGMA_{cm} = 5 \cdot \gamma \cdot Q_c^{1/3} \tag{4.64}$$

and Q_c is equal to:

$$Q_C = \frac{\sigma_C}{100} Q_0 \tag{4.65}$$

where Q_0 is oriented along the tunnel axis; F is the average cutter load (tnf) through the same zone, normalized by 20 tnf; CLI is the cutter life index; q is the quartz content (%); σ_θ is the induced biaxial stress on tunnel face in the same zone, normalized to an appropriate depth of 100 m (Barton, 2000; Delisio, 2014).

The relationship between PR (m/hr), AR (m/hr), and Q_{TBM} is shown in Figure 4.37.

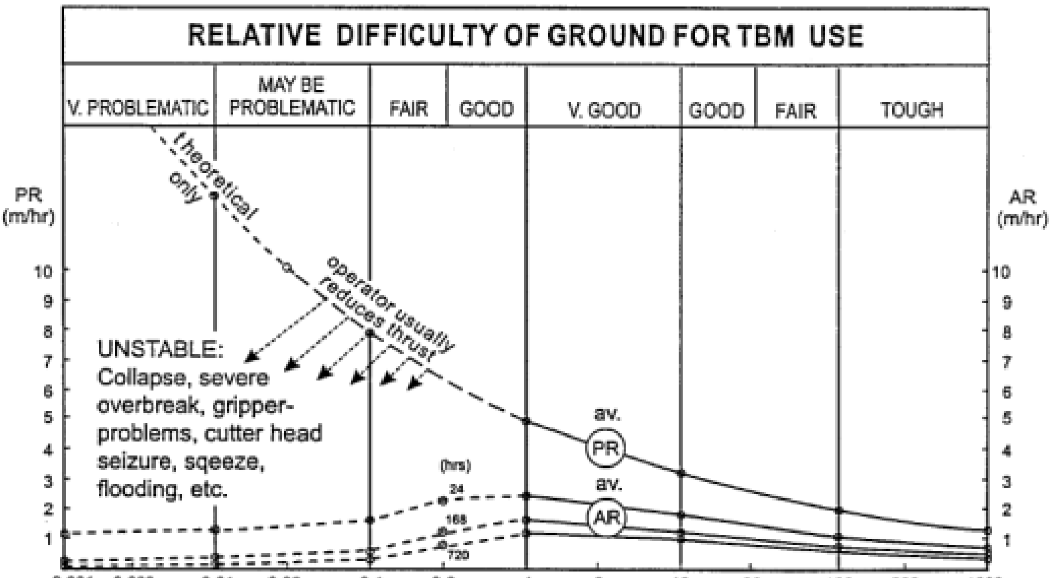

$$Q_{TBM} = \left[\frac{RQD_0}{J_n} \times \frac{J_r}{J_a} \times \frac{J_w}{SRF} \times \frac{SIGMA}{F^{10}/20^9} \times \frac{20}{CLI} \times \frac{q}{20} \times \frac{\sigma_\theta}{5} \right]$$

Figure 4.37: Suggested relationship between PR, AR, and Q_{TBM} (Barton, 2000)

Usually, PR is related to AR with the utilization factor U (Equation 4.66), defined as the ratio between the machine utilization time and the total shift time.

$$AR = PR \cdot U \tag{4.22}$$

Barton (2000) introduced an alternative format for AR (Equation 4.67):

$$AR = PR \cdot T^m \tag{4.23}$$

where T is the time (hours) and m is a negative gradient (LT^{-2} - deceleration) that expresses the decelerating average advance rate which is observed as the unit of time (hours, days, weeks, months) increases (Figure 4.38). Barton (2000) observed this trend by the analysis of 145 tunnel case histories totaling more than 1000 km.

The gradient m includes the abrasiveness of rock via the cutter life index CLI , and so includes the cutter wear. It also includes the percentage of quartz (%), rock porosity, and tunnel dimension via the tunnel diameter (Equation 4.68).

$$m \approx m_1 \left(\frac{D}{5}\right)^{0.20} \cdot \left(\frac{20}{CLI}\right)^{0.15} \cdot \left(\frac{q}{20}\right)^{0.10} \cdot \left(\frac{n}{2}\right)^{0.05} \tag{4.68}$$

where m_1 is a factor depending on the Q-value, D is the tunnel diameter, CLI is the cutter life index, q is the quartz content (%) and n is the porosity. Suggested m_1 values are listed in Table 4.15.

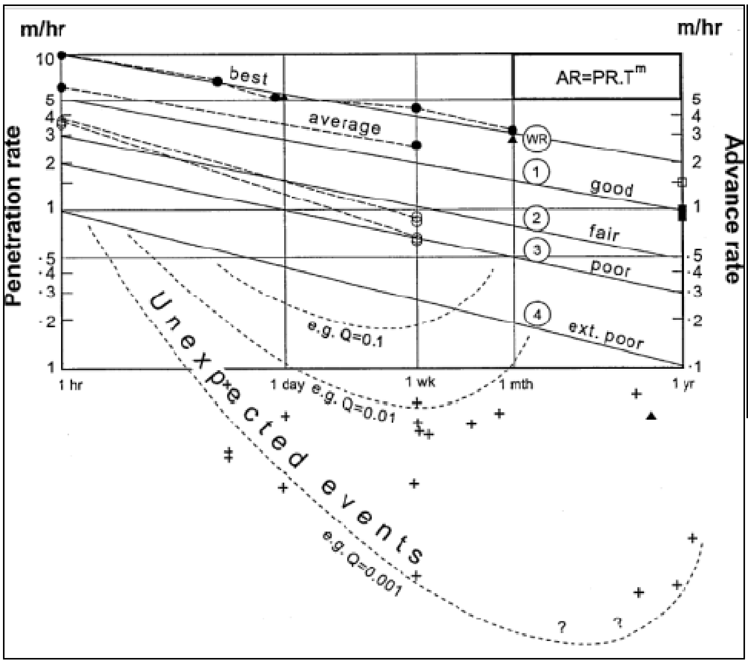

WR	(best performance)	m = -0.13 to -0.17
1	(good)	m = -0.17
2	(fair)	m = -0.19
3	(poor)	m = -0.21
4	(ext. poor)	m = -0.25

Figure 4.38: Decelerating average advance rate observed as the unit of time (day, week, month) and tunnel length increase (Barton, 2000)

Table 4.15: Decelerating gradient m_1, and its approximate relation with Q-value (Barton, 2000)

Q	0.001	0.01	0.1	1	10	100	1000
m_1	-0.9	-0.7	-0.5	-0.22	-0.17	-0.19	-0.21
Unexpected events or expected bad ground. Many stability and support related delays and gripper problems. Operator reduces the thrust force (i.e., the cutter load F). This increases Q_{TBM}.				Most variation of m may be due to rock abrasiveness. CLI, quartz content and porosity are important factors. PR depends on Q_{TBM}.			

Note: the subscript (1) is added to m for evaluation of Equation (4.68)

The development of a relationship between PR, AR, and Q_{TBM} was based on a process of trial and error using case records from literature. The following relationships are obtained (Barton, 2000):

$$PR \approx 5{Q_{TBM}}^{-0.2} \tag{4.69}$$

$$AR \approx 5{Q_{TBM}}^{-0.2} \cdot T^{m} \tag{4.70}$$

Finally, the time T to bore a length of tunnel L with an average advance rate of AR is obviously L/AR. Therefore, Equation 4.71 can be derived.

$$T = \left(\frac{L}{PR}\right)^{\frac{1}{1+m}} \tag{4.71}$$

Discussion

Although the proposed equations are rather simple, and the concepts behind the theory mediate and attribute in the right direction, but the model has many input parameters, consisted of parameters of the Q system in addition to input parameters for the NTNU TBM prognosis mode. Besides that, technical points of view the implementation of the model is complicated and expensive in practice. Also, the model involves and utilized some parameters which are not commonly assessable outside of Norway, for example, the cutter life index (CLI). In this regard, as pointed out by Wilfing (2016), Q_{TBM} did not gain acceptance in the construction industry in Central Europe.

4.3.7 Sapigni et al. (2002)

Sapigni et al. (2002) related the TBM performance to the Rock Mass Rating (RMR) based on the analysis of three tunnels (the Maen, Pieve, and Varzo tunnels for a total length of 14 km and 733 sets of data) in the Alps driven in medium to hard metamorphic rocks. They also identified a correlation between RMR and Q (Figure 4.39), thus indirectly relating the TBM performance to Q (Einstein et al. 2006).

As represented in Figure 4.40, a quadratic relationship between the penetration rate (expressed in m/hr) and RMR is derived. The relation follows a bell-shaped curve. However, a high dispersion of the data is noted which is attributed to (Delisio, 2014):

- Cumulative analysis of different rocks (less significant effect).
- Intrinsic feature of penetration data which arises from the difficulty of maintaining a constant thrust (significant effect).

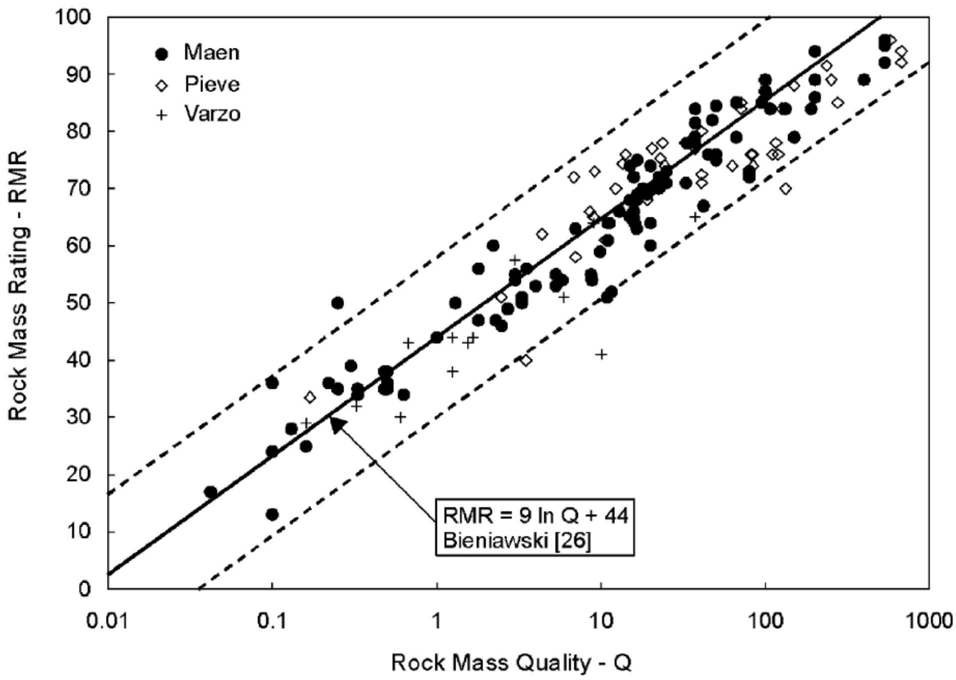

Figure 4.39: Correlation between RMR and Q values logged in the three tunnels considered in the study. Dotted line includes 80% of the 111 case histories analysed by Bieniawski (Bieniawski, 1989) (Sapigni et al. 2002)

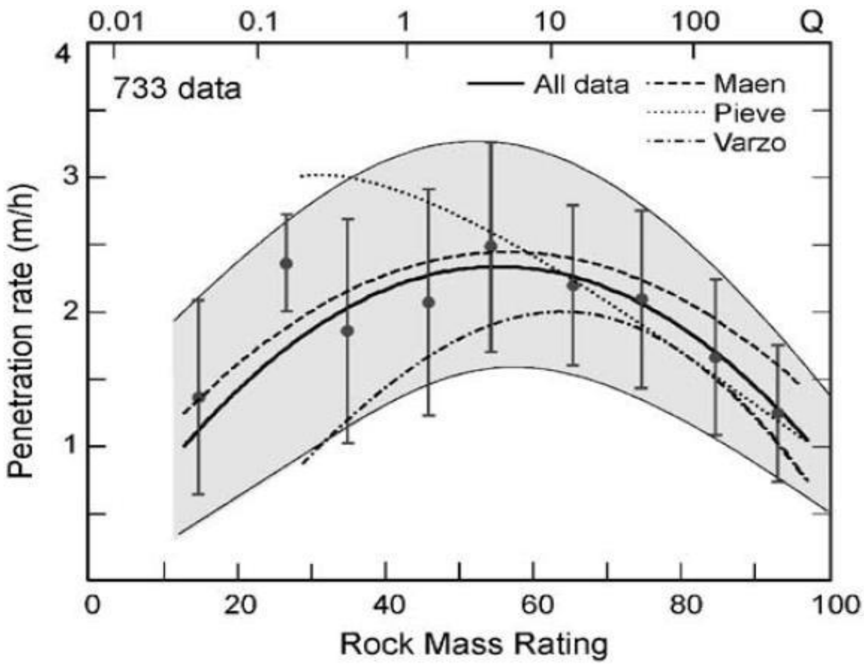

Figure 4.40: Correlation between penetration rate and RMR for the three tunnels considered in the analysis. The excavated rocks include serpentinite, metabasite, chlorite schist, talc, schist. calc schist, metagabbro, mica schist, metadiorite, metagranite, and gneiss. (Sapigni e al. 2002)

Sapigni et al. (2002) stated that the correlation depicted in Figure 4.40 is significant in terms of the shape of the curve, but it cannot be used for numerical predictions. The RMR does not account for rock-machine interaction parameters, so any empirical relationship based on this system is inevitably limited to the rock-machine combinations considered in the original dataset. The work is very interesting because the authors also provide a relationship between the TBM utilization factor, defined as the fraction of total construction time in which the TBM has been used for boring, and RMR (Figure 4.41). The three lines in Figure 4.41 show that even in favorable conditions the utilization coefficient is less than 55% and that values as low as 5-10% may be observed in poor rock mass conditions.

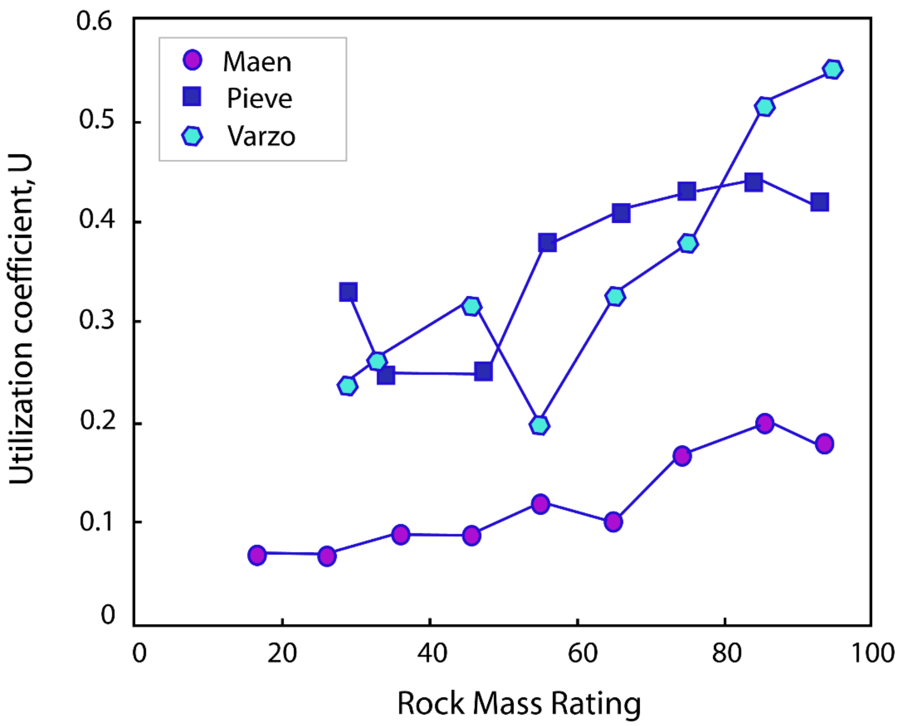

Figure 4.41: Correlation between TBM utilization factor derived from daily average data and RMR (modified from Sapigni et al. 2002)

Finally, Sapigni et al. (2002) highlighted the strong dependence of TBM performance on the rock type. Even considering the same TBM and the same RMR class, lower penetration rates are experienced in stronger rocks, indicating that rock-related factors (jointing, tensile strength, joint or fabric orientation) may dominate the mechanism of rock crushing and chip formation in hard rock. They concluded that the conventional RMR system is inadequate for TBM performance prediction. They suggested a logical development as to define a normalized RMR index with reference to the basic factors affecting penetration rate, for example, uniaxial compressive strength, tensile strength, brittleness, abrasiveness, hardness, etc., which are factors controlling rock resistance to cutter penetration and fracture propagation.

4.3.8 RME Model (Bieniawski et al. 2007a; 2007b; 2006)

The Rock Mass Excavability (RME) Indicator is presented by Bieniawski et al. (2006) is based on five basic input parameters as listed in Table 4.16 with the aid of a methodology called "Linear Discriminant Analysis" the authors found that the parameters with the strongest influence on the TBM advance rate (AR) are the rock abrasiveness (expressed via the Drilling Rate Index), the joint spacing and the stand-up time (Bieniawski et al. 2006).

In addition, the authors also included in the model the uniaxial compressive strength of intact rock and the water inflows because of the great effect that they may have on TBM performance (Bieniawski et al. 2006). Excavability is defined as the rate of excavation expressed in machine performance in meters per day. A weighted distribution was then performed to associate a rating to each parameter.

Table 4.16: Input parameters and rating for the RME index (Bieniawski et al. 2006)

Uniaxial compressive strength of intact rock (0–25 points)									
σ_c (MPa)	< 5	5-30	30-90	90-180	> 180				
Rating	4	14	25	14	0				
Drillability — Drilling rate index (0–15 points)									
DRI	< 80	80-65	65-50	50-40	< 40				
Rating	15	10	7	3	0				
Discontinuities in front of the tunnel face (0–30 points)									
Homogeneity		Number of joints per meter					Orientation with respect to tunnel axis		
Homogeneous	Mixed	0-4	4-8	8-15	15-30	> 30	Perpendicular	Oblique	Parallel
Rating 10	0	2	7	15	10	0	5	3	0
Stand-up time for TBM excavated tunnels (0–25 points)									
Hours	< 5	5-24	24-96	96-192	>192				
Rating	0	2	10	15	25				
Groundwater inflow (0–5 points)									
Liter/sec	>100	70-100	30-70	10-30	< 10				
Rating	0	1	2	4	5				

With the exception of the stand-up time, all the remaining four parameters may be determined from standard site exploration programs. The stand-up time may be estimated from the well-known RMR chart (Figure 4.42) which relates it to the unsupported active span, as a function of the RMR (Bieniawski, 1989).

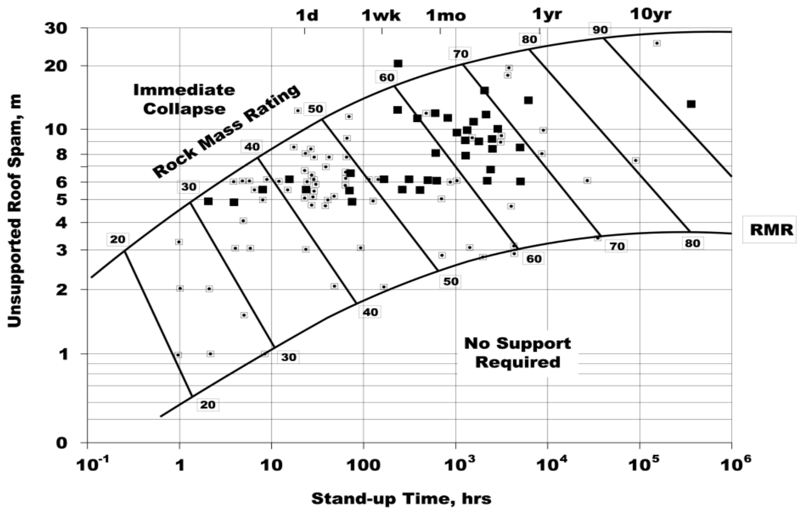

Figure 4.42: Stand-up time as a function of RME and unsupported span (Bieniawski, 1989)

The data used to derive the chart of Figure 4.35 were all from drill and blast tunnels. Therefore, a correlation for TBM tunnels has been introduced (Alber, 1996):

$$RMR_{TBM} = 0.8 \cdot RMR_{D\&B} + 20 \tag{4.72}$$

The authors correlated the RME to the average rate of advance ARA, computed as the ratio between the length of a given tunnel section and the total time needed to excavate that section. The dataset was composed by data coming from three tunnels excavated by double shield machines. The proposed relationship is represented in Figure 4.43 (Delisio, 2014).

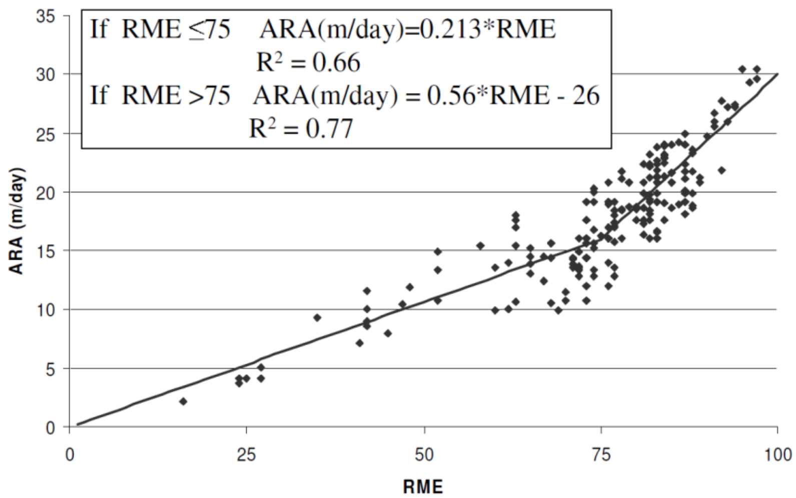

Figure 4.43: Correlation between ARA and RME (Bieniawski et al. 2006)

The above correlation is valid for tunnel diameter around 10 m. For different tunnel dimensions, a coefficient F_D has to be applied to ARA.

$$F_D = -0.007D^3 + 0.163D^2 - 1.2859D + 4.5158 \tag{4.73}$$

The correlation between ARA and RME for different tunnel diameters is represented in Figure 4.44.

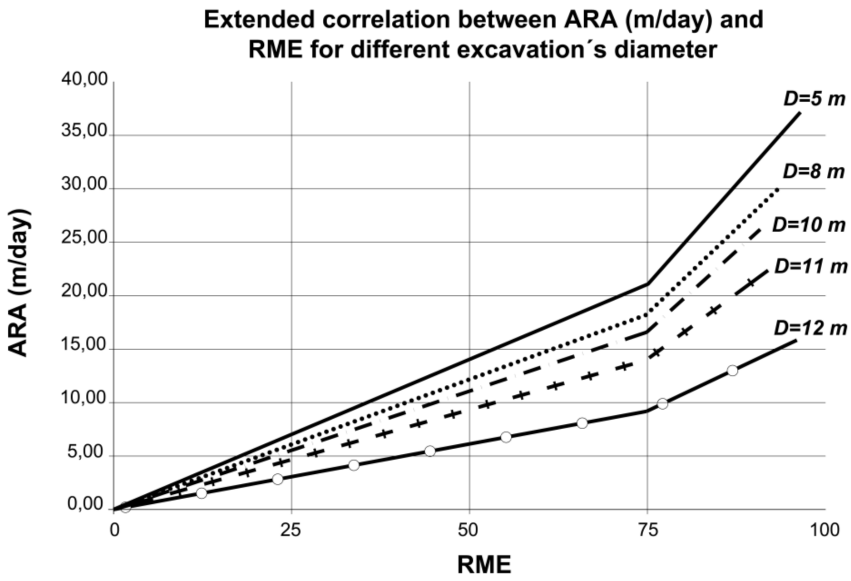

Figure 4.44: Correlation between ARA and RME for different tunnel diameters (Bieniawski et al. 2007a)

Then, based on the TBM performance observed during the excavation of the Guadarrama tunnels (Spain), Bieniawski et al. (2007a) introduced other correction factors which incorporate the length of the tunnel already excavated and the effect of the crew skills. The adjusted ARA becomes:

$$ARA_R = ARA_T \cdot F_D \cdot F_L \cdot F_C \tag{4.74}$$

where ARA_T is the predicted value of ARA from the correlation with RME, F_D is the correction factor for the tunnel diameter, F_L is the correction factor for the already excavated length (Table 4.17), and F_C is the correction factor for the crew skills (Table 4.18).

Table 4.17: Correlation factor for tunnel excavated length (Bieniawski et al. 2007a)

Tunnel length excavated (km)	Adaptation factor (F_L)
0.5	0.68
1	0.8
2	0.9
4	1
6	1.08
8	1.12
10	1.16
12	1.2

Table 4.18: Correlation factor for the efficiency of the tunnel crew (Bieniawski et al. 2007a)

Effectiveness of the crew handling TBM and terrain	Crew factor (F_C)
Less than efficient	0.88
Efficient	1
Very efficient	1.15

Besides that, the authors also compared the performances of double shield TBMs and gripper TBMs for the two cases of σ_c < 45 MPa and σ_c > 45 MPa (Figures 4.45 and 4.46) based on a dataset of 49 tunnel sections of the San Pedro tunnel (Spain). It was concluded that, for σ_c < 45 MPa, double shield TBMs always provide better results than open TBMs. For σ_c > 45 MPa and RME > 75, the use of gripper TBMs gives the best performance. If 65 < RME < 75, double shield TBMs and open TBMs provide similar results. Finally, if 50 < RME < 65, double shields generally register better performances than open machines (Bieniawski et al. 2007a; 2007b).

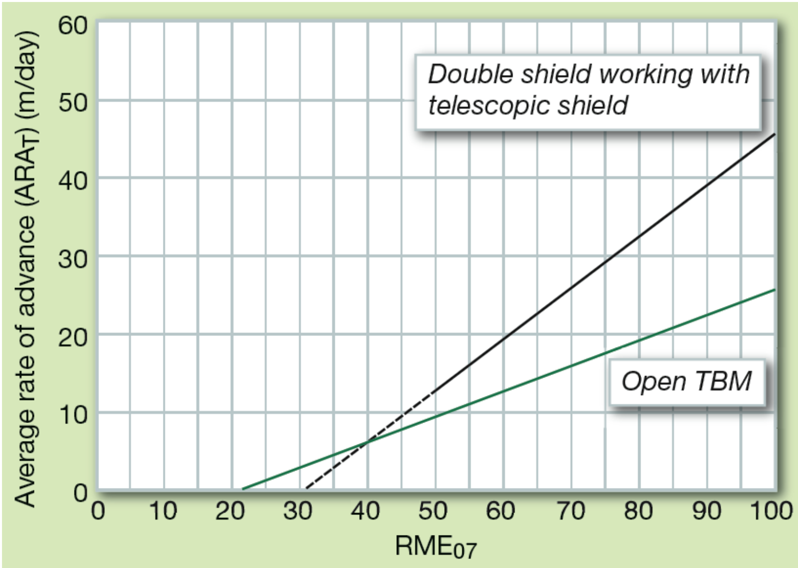

Figure 4.45: Comparison of the performance of double shield and open TBMs for $\sigma_c < 45$ MPa (Bieniawski et al. 2007a)

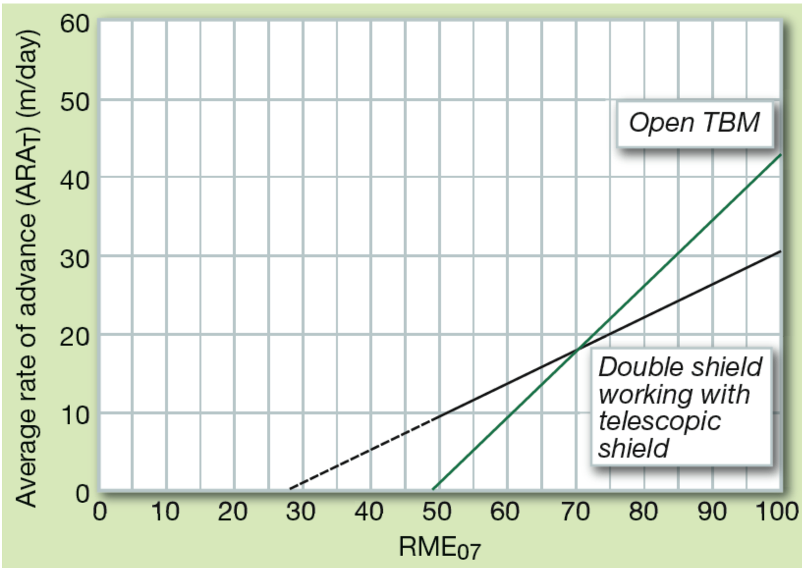

Figure 4.46: Comparison of the performance of double shield and open TBMs for $\sigma_c > 45$ MPa (Bieniawski et al. 2007a)

Discussion

The RME index is very similar to the better known RMR, and it can therefore be obtained quite easily on the basis of elements that are generally known from the geotechnical characterization of the rock masses encountered along with the tunnel layout. However, force (F_N) acting on disc cutters is not considered. Such a force, as noted by Rostami

(1996), can have a very important effect on the performance of TBM. Furthermore, the estimation of the stand-up time involves uncertainties in the model. This parameter needs to be estimated from an RMR chart, which has been developed and presented by Bieniawski for drill and blast tunneling, although an equation established from case studies must be used to convert $RMR_{D\&B}$ to RMR_{TBM} proposed by Alber (1996).

4.3.9 Khademi et al. (2010)

Khademi et al. (2010) have presented a model to predict the performance of TBM by employing a multiple linear-regression analyses on field data collected from 8.5 km of the bored section of Zagros long tunnel in a sedimentary rock which is located in Iran, an attempt was made to provide a predictor equation of the TBM field penetration index (FPI) by use of RMR rock mass classification system. The range of UCS in this study was 20 to 150 MPa; RQD, 30-95%; RMR Jc rating of 10-22. The relationship between FPI and the five basic RMR input parameters plus tunnel depth and the angle of the joints with tunnel axis (Alpha) was conducted. It should be mentioned that, in this investigation, the α angle plays an alternate role for adjustment factor for discontinuity orientation in RMR_{89} system. Also, the tunnel depth is an indicator of in situ and, consequently confining stress on tunnel face was considered as input parameters. According to regression analysis, tunnel depth and groundwater (Gw) condition showed meaningless correlations with the FPI and eliminated. Figures 4.47 and 4.48 illustrate the correlations between the individual independent variables and the actual measured FPI in this investigation.

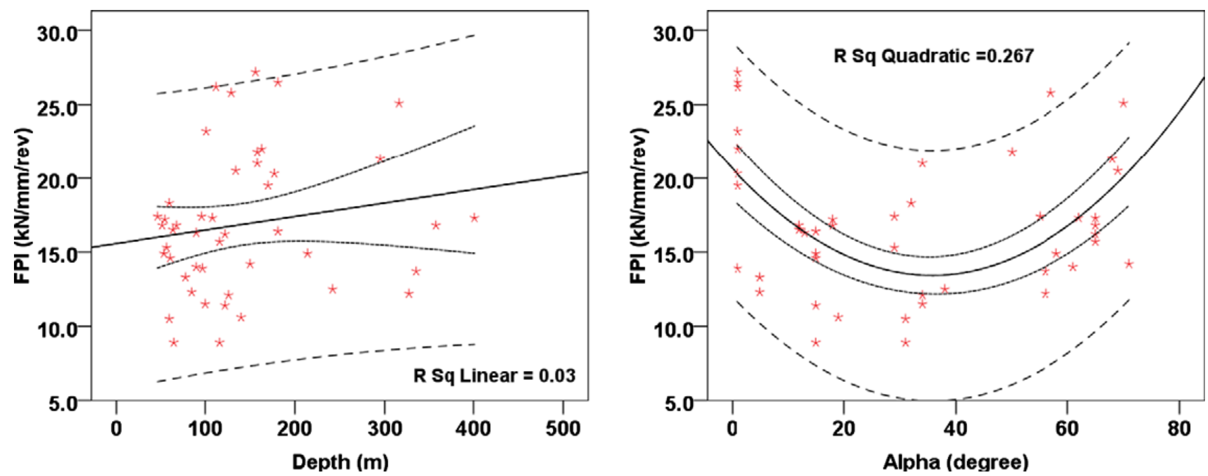

Figure 4.47: The relationship between measured FPI and two additional parameters (tunnel depth and α angle), (Khademi et al. 2010)

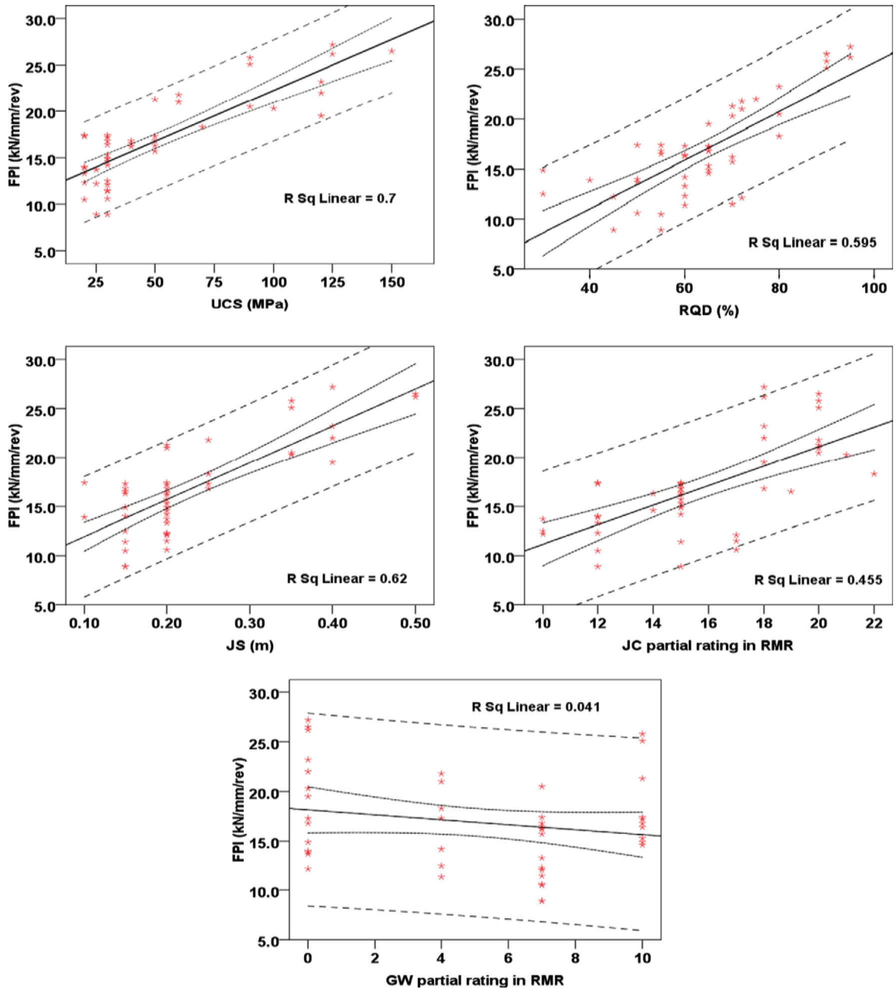

Figure 4.48: The relationship between measured FPI and RMR five input parameters (Khademi et al. 2010)

Also, inter-correlation between the UCS and joint spacing (Js) led to exclusion of Js from the subsequent analysis thus; new equation was introduced as follows (R = 0.87):

$$FPI = 4.161 + 0.091 UCS + 0.077\, RQD + 0.117\, Jc + 1.077 \log(\alpha) \tag{4.75}$$

Discussion

It should be mentioned that, the main problem of the introduced equation is that; it is just related to the conditions of Zagros Tunnel and a double shield TBM; hence it can't be a reliable model to predict the performance of the machine in different geological conditions. In addition to this limitation, the bivariate analysis shows that UCS by itself accounted for 70% of the variation of the FPI. Adding three more parameters led to only a marginal increase in R^2 from 0.7 to 0.77. This means that the effects of the additional parameters were largely overshadowed by UCS . This matter has been also assessed by

Fatemi et al. (2016) which the results of sensitivity analysis demonstrated that, the greatest sensitivity belongs to compressive strength. Despite great changes in the nature of the joints, lower sensitivity was detected due to perhaps the score of joint conditions in the RMR classification system, and the low range of variations of these parameters in the original database. Therefore, it is natural that the model sensitivity to this parameter is low. In this model, the log (alpha-α) is also presented in the equation, and owing to the log function, despite the changes of alpha from 1° to 70°, the range of variations in output results is very minimal. Thus, the model sensitivity to alpha is low, as is the case with Jc, where even the 100% change in the value of Jc shows minor effects on FPI.

4.4 Conclusion Remarks

Various approaches for predicting the penetration rate of hard rock tunnel boring machines (TBMs) have been studied by researchers since the early stages of TBM applications in the 1950s. These studies ended up in the development of several prediction models for predicting TBM performance with versatile inputs/tests. Among the geological/geotechnical factors, on one side, there are parameters associated with the intact rock strength such as the uniaxial compressive strength, the drilling rate index, the tensile strength, etc.; on the other side, there are parameters related to the rock mass conditions, and notably to the rock mass fracturing, which may be expressed and presented via the RQD, the volumetric joint count, the joint spacing and orientation, etc.

Based on the common understanding and definition of the phenomenon, it can be concluded that the TBM advancement in hard rock masses may be explained, to some extent, by these recursive rock/rock mass parameters. If the attention is now focused on the TBM side, the machine factors generally used for performance estimation include the cutter spacing, the cutter tip width, the cutter diameter, the average thrust per cutter, and the cutterhead rotation speed (RPM). In the majority of the cases, the combined ground parameters and machine parameters are employed to describe/predict the TBM performance in terms of penetration rate. Table 4. 19 offers a brief review and discusses the capabilities of some of the more commonly used TBM performance prediction models.

In brief, estimation of TBM PR must include the affective parameters including rock material and rock mass parameters, machine characteristics, and operational parameters as well as in-situ boundary conditions. However, developing a predictive model which can take into account all these parameters all together has been always a hard nut to crack. This is why over three decades after its conception; no single universal model has been proposed for TBM performance prediction. However, according to the literature survey and previous investigations in this respect, some of the most important TBM prognosis models include CSM (Rostami, 1997), NTNU (Bruland, 1998), Q_{TBM} (Barton, 2000), and Hassanpour et al. (2011).

The brief and non-exhaustive description and explanation of the most relevant TBM performance prediction models presented in this chapter may help to define the background of the work described in the next chapters. Specifically, this overview highlights the most important rock/rock mass factors and TBM factors which are commonly used for performance estimation and recursive in many described models. The conclusions derived from the cases analyzed in the previous studies are also important.

Table 4.19: Overview of TBM performance prediction models and their advantages and disadvantages

Prediction model	Required input parameters		Output	Advantage	Limitations
	Rock mass parameters	Machine parameters			
CSM	UCS, BTS, (CAI)	Cutter load capacity, cutter spacing, cutter diameter, cutter tip width, TBM thrust, and torque.	PR, AR, U	adaptability to rock conditions not previously encountered, used for design of cutterhead	Based only on intact rock properties
Gehring	UCS, correction factors for joints, specific fracture energy, etc.	Cutter force, Fn	P	Easy to apply, independent correction factors	Spacing and orientation of the major plane of weakness, limited number of cases (Tunnels)
NTNU	DRI, no. of joint sets, joint frequency and joint orientation, CLI,	Cutter thrust, cutter spacing, cutter diameter	PR, AR, U	Accounting for both rock mass & TBM specifications	Determination of input parameters needs special tests; Database is mainly limited to strong rocks
Q_{TBM}	RQD_0, Jn, Jr, Iw, SRF, rock mass strength, (CLI), quartz content, induced biaxial stress	Average cutter load, TBM diameter	PR, AR, U	Relying on good database	Many input parameters, needs uncommon tests, some inputs parameters are overlapped, complex relationships
RME	UCS, abrasivity, rock mass jointing at the face, stand-up time, water flows	TBM diameter, Total cutter head thrust, RPM and torque	PR, AR	Easy to apply	Force on disc cutters is not considered, Lack of some basic parameters (e.g., tunnel diameter), Limited database
Yagiz (2008)	DPW, rock brittleness, UCS, α	-	PR	-	Limited database (one tunnel project), requires special/uncommon test "punch penetration test"

Prediction model	Required input parameters		Output	Advantage	Limitations
	Rock mass parameters	Machine parameters			
Gong & Zhao (2009)	UCS, Jv, Bi, α	Cutter force	BI	Eliminate the influence of the operative uncertainties on the rock mass boreability	Limited database (one tunnel project)
Khademi et al. (2010)	UCS, RQD, Joint condition, α	Cutter force, RPM	FPI	Capability to be used across different TBM diameters	Limited database (one tunnel project), UCS by itself accounted for 70% of the variation of the FPI
Hassanpour et al. (2011)	UCS and RQD	Cutter force, RPM	FPI	Easy to apply, capability to be used across different TBM diameter rely on good/various database	Higher error in strong massive rock masses "i.e., UCS more than 200 MPa"
Farrokh et al. (2012)	Tunnel diameter, Rock-type code, UCS, RQDc	Cutter force, RPM	PR	Relying on good database	The proposed model may produce higher errors in estimating PR values in highly jointed (fractured) rock masses
Delisio, 2014	UCS, Jv	Cutter force, RPM	FPI_{blocky}	Mitigating the lack of the model/investigations for blocky rock conditions	Limited database (only two tunnel projects); limited application, i.e., blocky rock conditions
Alpine model	BTS, LCPC breakability coefficient, correction factor for joints, etc	Cutter force, Fn	FPI_{3mm}	Mitigating the shortages of Gerhing's model	Rely only on one tunnel project, requires uncommon test

Chapter 5 Geological Description & Data Collection

5.1 Introduction

In this chapter, the selected and available projects used as base cases for the new TBM performance prediction model, including Zagros water conveyance tunnel Lot 2 in Iran, Ghomrood water conveyance tunnel Lots 3 & 4 in Iran, Golab conveyance water tunnel in Iran, Karaj-Tehran water conveyance tunnel Lot 1 in Iran, Maroshi-Ruparel water supply tunnel Mumbai in India, Manapouri second tailrace tunnel in New Zealand and Lötschberg Base Tunnel in Switzerland are presented, brief geological description of the projects are expressed. Furthermore, descriptive statistics of the generated database for this study are represented.

5.2 Geological Description

In order to develop a more accurate TBM performance prediction model that can be applied in different geological conditions, data from various projects with the different rock mass conditions have been obtained from pertinent research groups and compiled in a database. The database on TBM field performance contains different levels of information which define the tunnel, rock mass conditions, and TBM performance parameters over the full length of a tunnel drive, and some within discrete geological zones or short tunnel reaches. The database contains data on 7 tunnel projects and includes over 621 data sets. This database includes bored tunnel records with a total length of over 70.73 km.

The tunneling projects used in this investigation are listed as follow:

- Zagros water conveyance tunnel, Lot 2 in Iran (Hassanpour, 2009; Hassanpour et al. 2009; Hassanpour et al. 2016).
- Ghomrood water conveyance tunnel, Lots 3 & 4 in Iran (SCE Company, 2004; Hassanpour, 2009; Hassanpour et al. 2011).
- Karaj-Tehran water conveyance tunnel, Lot 1 in Iran (SCE Company, 2006; Hassanpour, 2009; Hassanpour et al. 2010).

- Golab conveyance water tunnel in Iran (Fatemi, 2016; Fatemi et al. 2016; ICE 2009).
- Maroshi-Ruparel water supply tunnel, Mumbai India (Jain et al. 2014; Jain 2014).
- Manapouri second tailrace tunnel, New Zealand (Watts et al. 2003; Hassanpour et al. 2011; Delisio, 2014)
- Lötschberg Base Tunnel in Switzerland (Delisio et al. 2013; Delisio 2014).

The main characteristics of these TBM tunnelling projects are summarized in Table 5.1 and 5.2. Figure 5.1 shows the geographical distribution of project sites.

Table 5.1: Main characteristics of tunnelling projects

No	Projects	Tunnel Length (km)	Available data (km)	TBM type	TBM diameter (m)
1	Ghomrood water conveyance tunnel, Lots 3 & 4 (Iran)	21.5	15	Double shield (Wirth)	4.525
2	Manapouri second tailrace tunnel (New Zealand)	10	9.7	Main beam open TBM (Robbins, Kvaerner-Markham)	10.5
3	Golab conveyance water tunnel (Iran)	10	8	Double shield (Wirth)	4.495
4	Maroshi-Ruparel water supply tunnel Mumbai, (India)	12.24	5.83[1]	Hard rock Gripper TBM (Wirth)	3.6
5	Zagros water conveyance tunnel, Lot 2 (Iran)	26	15[2]	Double shield (Herrenknecht)	6.73
6	Karaj-Tehran water conveyance tunnel, Lot 1 (Iran)	15.9	8.7	Double shield (Herrenknecht)	4.65
7	Lötschberg Base Tunnel (Switzerland)	36.4	8.5[3]	Gripper TBM (Herrenknecht)	9.43

[1]Maroshi- Vakola; [2]The first 5.3 km used for model development, remaining 9.5 km employed for model evaluation/validation; [3]Steg lateral adit, Main southern.

Table 5.2: Geological characteristics of tunnelling projects

No	Projects	Geological zone	Formation	Lithology	Max. depth (m)
1	Ghomrood tunnel, Lots 3 & 4	Sanandaj-Sirvan metamorphic belt	Jurassic metamorphic rocks (low to medium grade) and Cretaceous Limestone	Limestone, Shale and Sandstone, Slate, Phyllite, Schist with quartzitic veins	700
2	Manapouri tunnel	-	Paleozoic metamorphic and igneous rocks of the Fiordland Complex	Gneiss, Calc-silicate and quartzite and the intrusive rocks (Gabbro and Diorite)	1200
3	Golab tunnel	Sanandaj-Sirjan	Sedimentary and Igneous rocks of Eucen to Jurassic	Periodic series of argillite shale and metamorphic sandstone, schist and amphibolite	-
4	Maroshi-Ruparel tunnel	Deccan traps (Lava flows of Basaltic rocks)	Upper traps (Upper Cretaceous to Lower Eocene)	Fine compact basalt, Porphyritic basalt, Amygdaloidal basalt, Pyroclastic rocks (Tuff, Tuff breccia) and Intertrappeans (Shale)…	82
5	Zagros tunnel, Lot 2	Zagros Simply folded zone	Carbonate-Argillaceous rocks of Pabdeh, Gurpi and Ilam Formations	Limestone, Shale and Limy Shales	650
6	Karaj-Tehran tunnel, Lot 1	Central Alborz	Pyroclastic rocks of Karaj formation	Tuffs, Shaly and Sandy Tuffs, Agglomerate	600
7	Lötschberg Base Tunnel	-	Autochthon Gampel-Baltschieder and Aar Massif	Crystalline Gneiss, Granodiorite and Granite, Granitic Gneiss, Amphibolite	1950

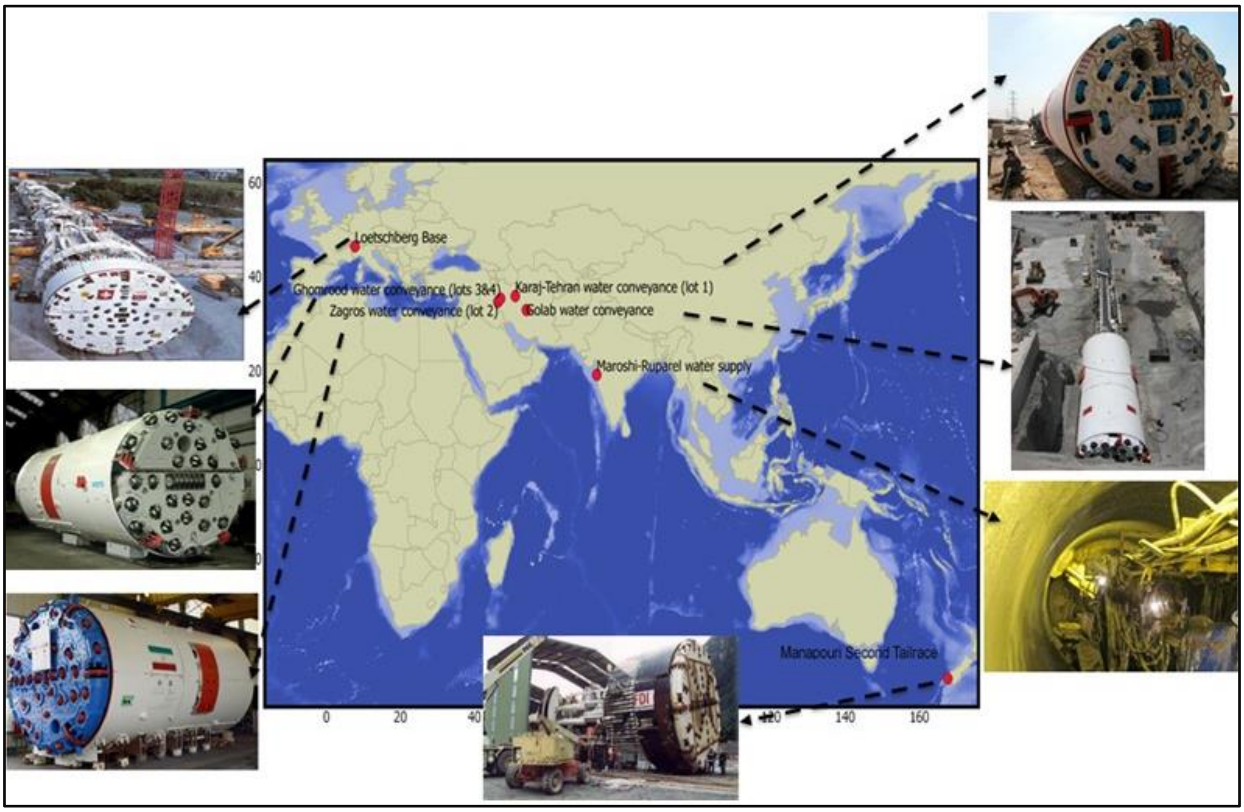

Figure 5.1: Geographical distribution of the hard rock TBM projects used in this study

5.2.1 Zagros Water Conveyance Tunnel (Lot 2)

Zagros water conveyance tunnel, with a total length of 49 km and a diameter of 6.73 m, has been designed to transfer 70m^3/s of water from the Sirvan River in the south of the city of Nowsood to Dasht-e-Zahab plain. The tunnel was divided into three sections: 1A (14 km) as the northeast section, 1B (9 km) as the middle section, and lot 2 (26 km) as the southwest section (Figure 5.2). By April 2008, about 5.3 km of lot 2 (26 km) of this section had been completed. At the southwest portal, a double-shield TBM was launched from a 200-m starter tunnel excavated by the drill and blast method. The tunnel is lined with pre-cast concrete segments with a hexagonal arrangement and thickness of 25 cm. The maximum rock cover in section 2 is about 1000 m, with an average of about 300 m. Maximum and average overburdens in the bored section are 200 and 150 m, respectively. The area around the tunnel is located in Zagros Mountain in western Iran. The main geological formations outcropped in the project area (in the first 6 km of the tunnel) include various carbonate and argillaceous rock units. The oldest geological unit along the tunnel alignment is the grey limestone of Illam formation (ch: 03 + 710 to ch: 04 + 927) that is located in the core of the A2 anticline (Figure 5.3).

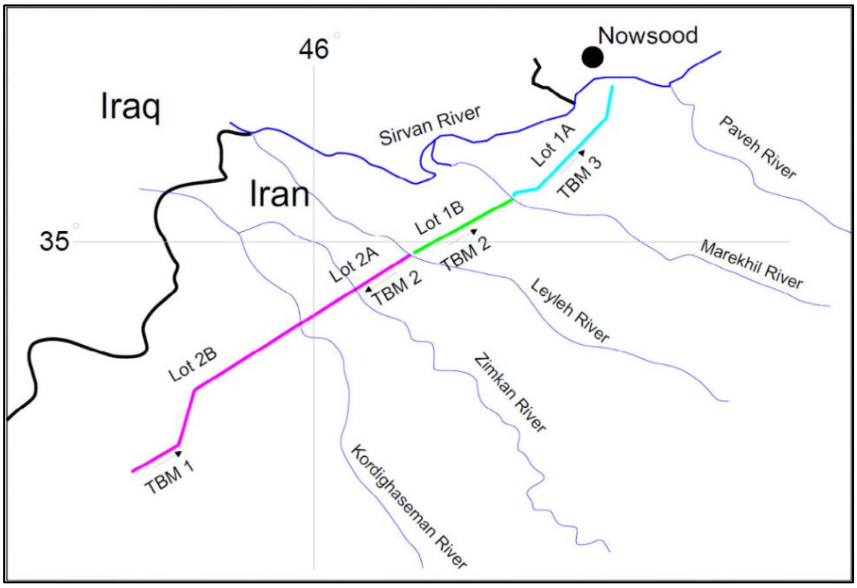

Figure 5.2: Details of Zagros water conveyance tunnel scheme, west of Iran (Hassanpour et al. 2016)

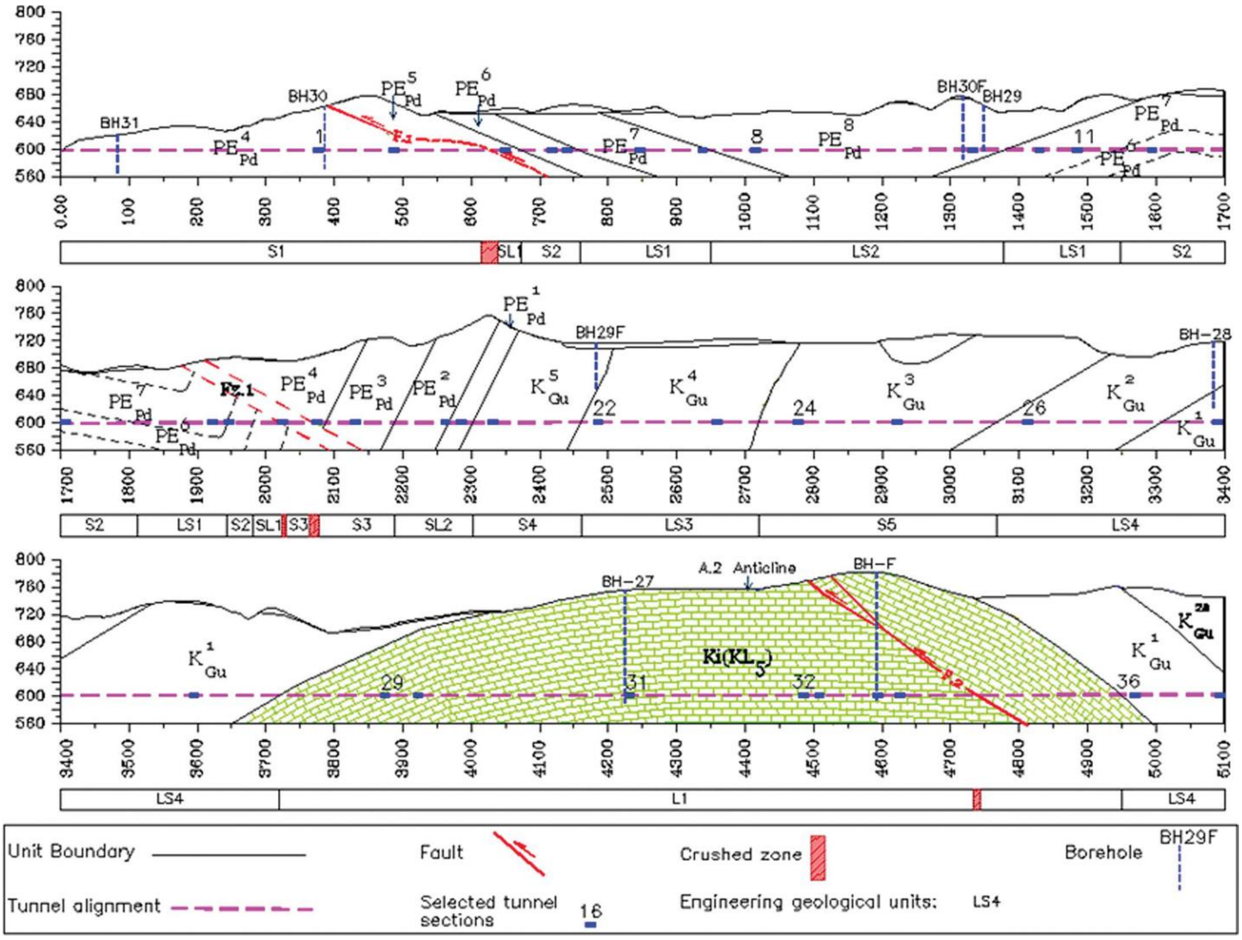

Figure 5.3: Tunnel profile with engineering geological units of Zagros tunnel lot 2 (Hassanpour, 2009)

Overlying this unit is the Gurpi formation, which consists of alternating limy shale and argillaceous limestone (ch: 02 + 300 to ch: 03 + 710). The youngest unit is the Pabdeh formation (ch: 00 + 000 to ch: 02 + 300), which is composed of alternations of dark-gray shale and greenish-grey argillaceous limestone. During geological studies in the project area, 14 predominant stratigraphic units were identified along the excavated section of tunnel alignment (Table 5.3). These units are different members of the above-mentioned formations. The geological section in Figure 5.3 shows the distribution of these rock units along the mined section of the tunnel.

Table 5.3: Engineering geological units identified along tunnel alignment of Zagros lot 2 (Hassanpour, 2009)

No.	**Engineering geological unit**	**Equivalent stratigraphic units**		**Main lithology**
1	S1	Pabdeh (Paleogene)	PE_{Pd}^{4a}	Shale
2	SL1		PE_{Pd}^{5}	Argillaceous limestone
3	S2		PE_{Pd}^{6}	Shale
4	LS1		PE_{Pd}^{7}	Limy shale
5	LS2		PE_{Pd}^{8}	Limy shale
6	S3		PE_{Pd}^{3}	Shale
7	SL2		PE_{Pd}^{2}	Argillaceous limestone
8			PE_{Pd}^{1}	Argillaceous limestone
9	S4	Gurpi (Upper Cretaceous)	K_{Gu}^{5a}	Shale
10	LS3		K_{Gu}^{4}	Limy shale
11	S5		K_{Gu}^{3}	Shale
12	LS4		K_{Gu}^{2}	Limy shale
13			K_{Gu}^{1}	Limy shale
14	L1	Ilam (Upper Cr.)	Ki ($K1_5$)	Limestone

Structurally, the area around the tunnel is moderately folded and gently faulted. As shown in Figure 5.3, the tunnel in the bored section has passed through some minor synclines and anticlines. There are no important faults in the bored section of the tunnel route, but some minor faults and shear zones have been identified as crossing the tunnel line. The thicknesses of these fault zones are estimated through back mapping of the tunnel and it is recognized that they generally range between 10 and 25 m. In the shale layers, usually, more than three joint sets with low values of average spacing can be observed in the tunnel. This is in addition to foliation and bedding planes. In limestone layers, the quality of surrounding rocks changes to less fractured rock masses with more systematic and fewer joint sets (typically two conjugate joint sets and bedding planes) and higher values of spacing. Due to the folded structure of the tunnel route and the existence of some minor faults along the tunnel, the tunnel route can be divided into some structural zones. The orientation of bedding planes and related structures (joint sets) changes in a wide range in these structural zones. Results of petrographic analyses show that, considering mineralogy and texture, there are four main lithotypes in tunnel alignment. These lithotypes include (1) limestone, (2) argillaceous limestone, (3) limy shale, and (4) shale. The first two lithotypes are competent and more brittle rocks with well-developed joint systems and the latter two are incompetent rocks with more plastic behaviour and weathered features at outcrops. To measure the physical and mechanical properties of these lithotypes, many laboratory tests were performed on samples taken from boreholes, tunnel faces, and surface exposures. The main petrographic, physical, and mechanical characteristics of these lithotypes are summarised in Table 5.4. To determine drillability indices 12 sets of tests have also been performed by the SINTEF laboratory (Trondheim, Norway) on samples taken from different boreholes on the tunnel alignment. The summary results of these tests are also presented in Table 5.4 (Hassanpour, 2009).

Table 5.4: Main characteristics of lithotypes in Zagros tunnel, lot 2 (Hassanpour, 2009)

No	Lithotype	Major minerals	Quartz content (%)	Porosity (%)	UCS (MPa)	Tensile strength (MPa)	Drilling rate index (DRI)	Cutter life index (CLI)
1	Limestone	Calcite, clay minerals	< 5	10-12	100-150	8-10	55-60	75-85
2	Argillaceous limestone		< 5	5-8	50-100	6-8	60-65	70-75
3	Limy shale	Clay minerals, calcite	5-15	8-10	20-50	4-6	65-70	60-70
4	Shale		10-15	5-10	15-30	3-5	70-75	50-60

A TBM was launched from a 200 m starter tunnel excavated by the drill and blast method. In this project, a double-shield TBM manufactured by Herrenknecht has been selected to provide for safer operation in adverse geological zones identified along the tunnel route. The cutterhead is laced with 42 17 inch or 432 mm diameter disc cutters with a load capacity of 267 kN. The other main specifications of the machine are listed in Table 5.5.

Table 5.5: Main specifications of TBM used in Zagros tunnel lot 2 (Hassanpour, 2009)

Parameter	Value
Machine diameter	6.73 m
Cutter diameter	432 mm
Number of disc cutters	42
Disc nominal spacing	90 mm
Max. Operating cutterhead thrust	28,134 kN at 350 bar
Cutterhead power	2100 kW
Cutterhead speed	0-11
Cutterhead torque (nominal)	4450 kN.m at 9 rpm
Thrust cylinder stroke	1700 mm
Conveyor capacity (approx.)	690 t/h
Total TBM weight (approx.)	573 ton

To obtain the required data for the analysis of TBM performance, results of studies performed during the pre-construction phase and construction phase have been compiled into a database. During the construction phase and through back-mapping of the tunnel, predicted geological and geomechanical properties of the rock mass along the tunnel were examined by a detailed investigation of tunnel faces. In addition to sampling from surface outcrops and boreholes in the pre-construction phase, during back-mapping of the tunnel, many samples were taken from the muck and tunnel face to perform tests such as point load index test and petrographic analysis (Hassanpour, 2009; Hassanpour et al. 2009). Average values of rock mass parameters (and intact rock properties) have been used to determine geomechanical conditions of the identified engineering geological units by some empirical rock mass classification systems including, RMR (Bieniawski, 1989), GSI (Hoek et al. 1995, Hoek, 2007) and Q-system (Barton et al. 1974) which are illustrated in Figure 5.4. Also, the changes in RQD_0 respecting tunnel sections is presented in Figure 5.5. Since the dominant and widely used intact rock properties for the estimation of TBM performance is *UCS*, the changes of this parameter in respected tunnel sections are illustrated in Figure 5.6. As can be seen from the figure, the diversity of *UCS* in related sections are between 15 till 150 MPa which can be categorized within low strength to very high strength according to the International Society of Rock Mechanics (ISRM, 1978; 1979). In the construction phase, machine performance data and operating parameters (such as applied thrust, RPM, torque, etc.) were also recorded continuously in special sheets and analysed separately. Variations of TBM penetration rate (ROP), applied total thrust, and RPM regarding to selected tunnel sections are demonstrated in Figures 5.7. As can be seen from the figure, the minimum and maximum ROP are around 1 and 3.5 (m/h), respectively.

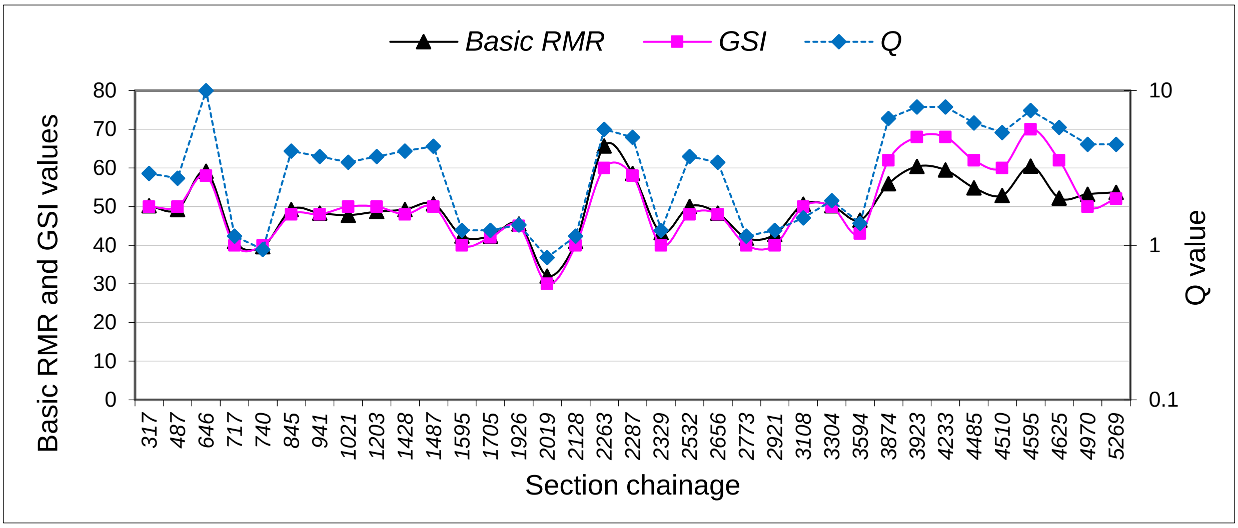

Figure 5.4: Variation of basic RMR, GSI, & Q in selected tunnel sections in Zagros lot 2

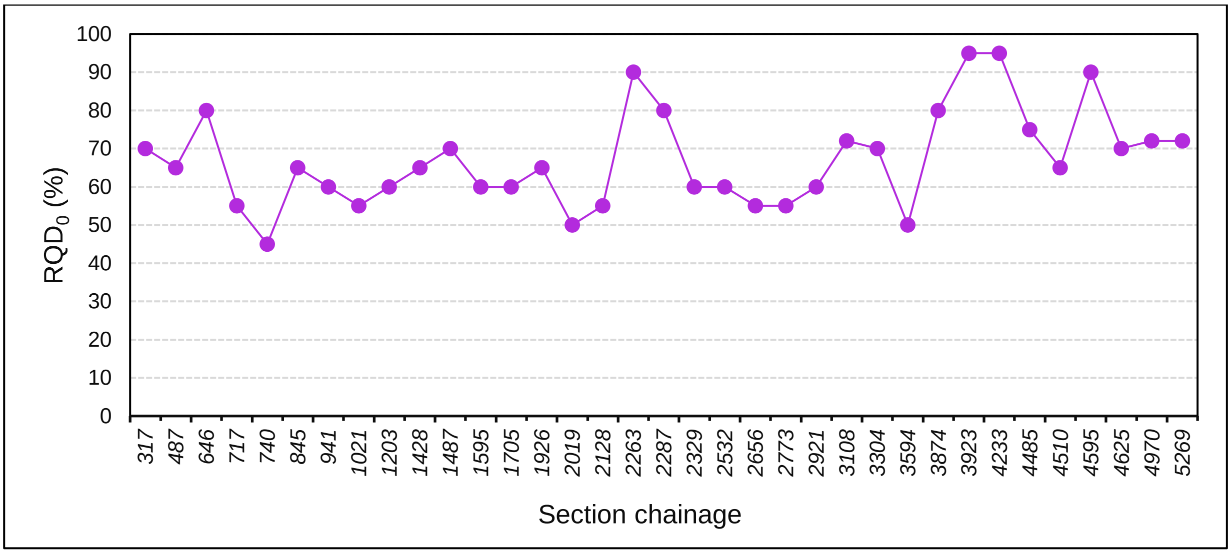

Figure 5.5: Variation of RQD_0 in selected tunnel sections in Zagros lot 2

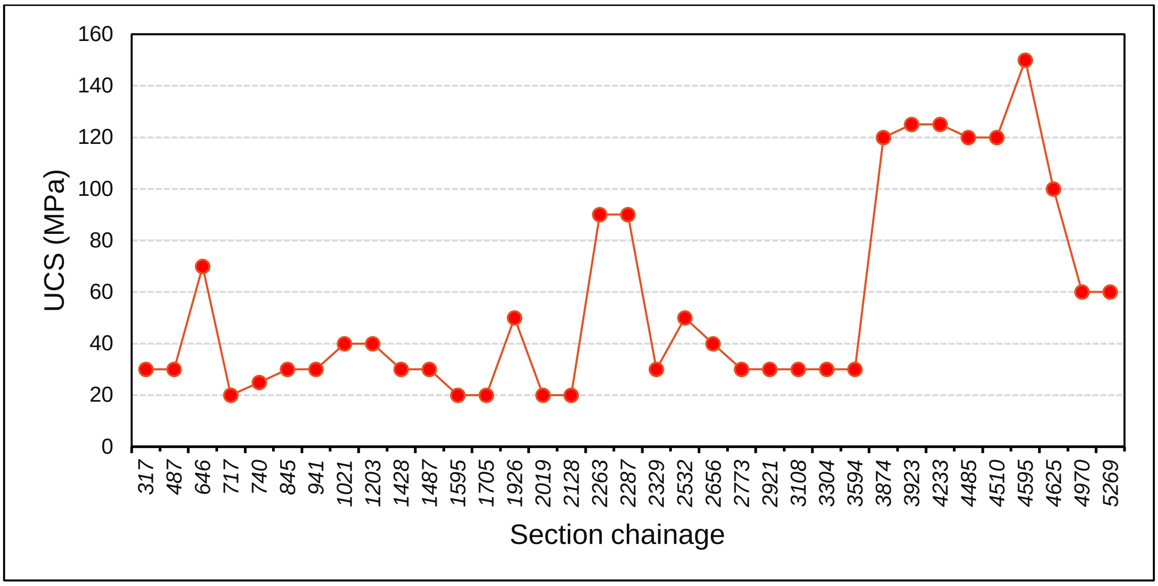

Figure 5.6: Variation of *UCS* in selected tunnel sections in Zagros lot 2

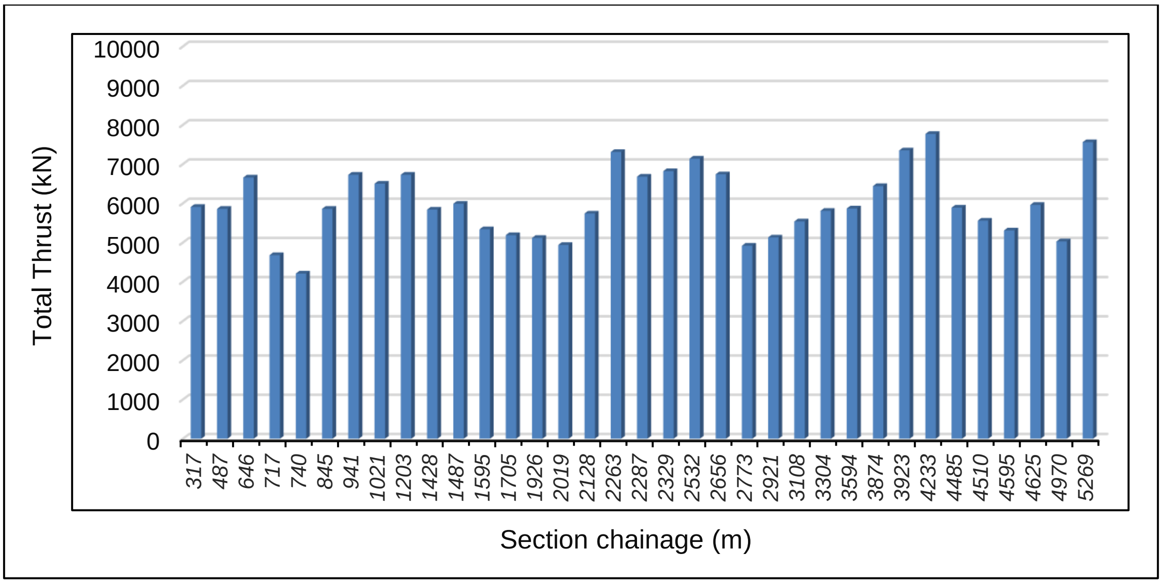

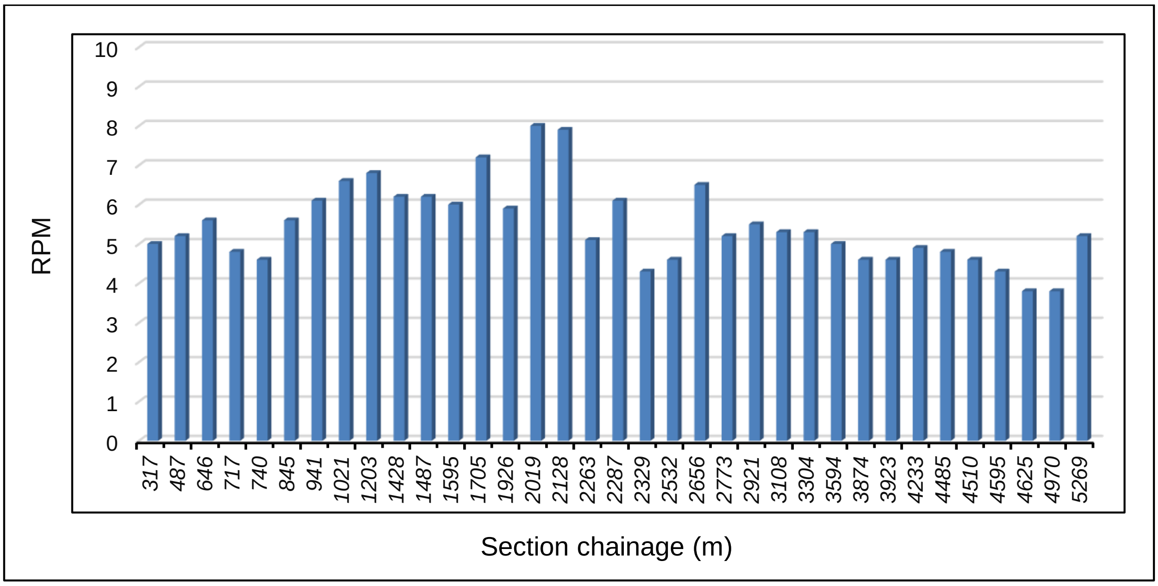

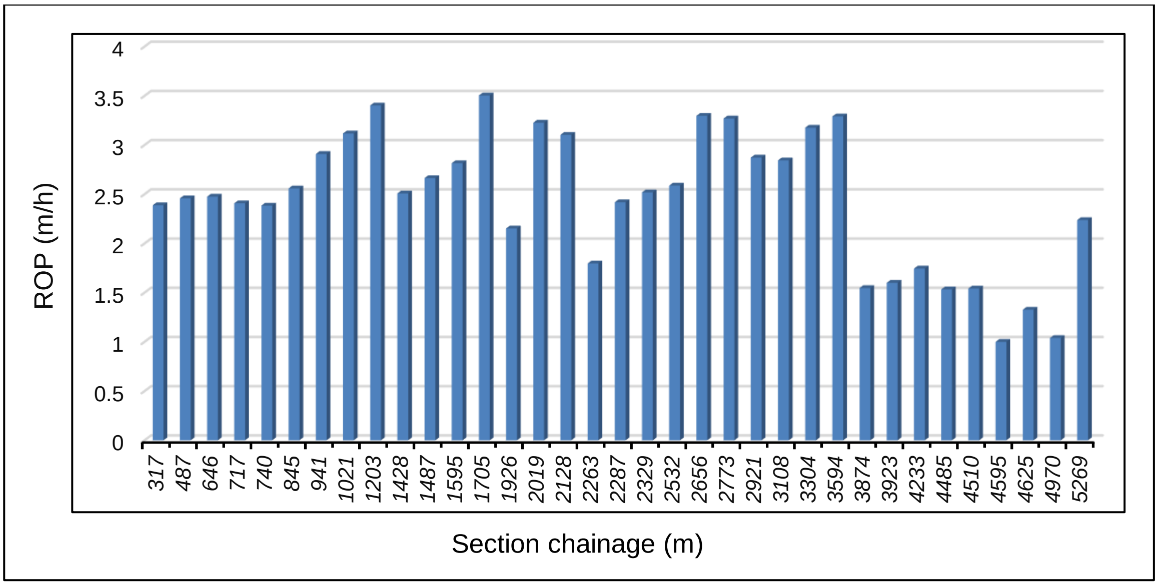

Figure 5.7: Variations of total thrust, RPM, and rate of penetration (ROP) in selected tunnel sections in Zagros lot 2

5.2.2 Ghomrood Water Conveyance Tunnel (Lots 3 & 4)

The Ghomrood water conveyance tunnel is one of the components of a water management system in central Iran. This involves a 36 km tunnel from the Dez river to the Golpayegan reservoir (Figure 5.8). The tunnel was originally divided into four parcels, each about 9 km, and was put out to bid as design/build contracts in 2002. Combined parcel 3-4 of this project totalling 18 km at the exit end of the tunnel with a portal access had been excavated via double shield TBM manufactured by Wirth with a diameter of 4.38 was excavated at a grade of 0.134% and finished in winter 2009 with a concrete segmental lining to a diameter of 3.8 m. Machine specifications of TBM is listed in Table 5.6.

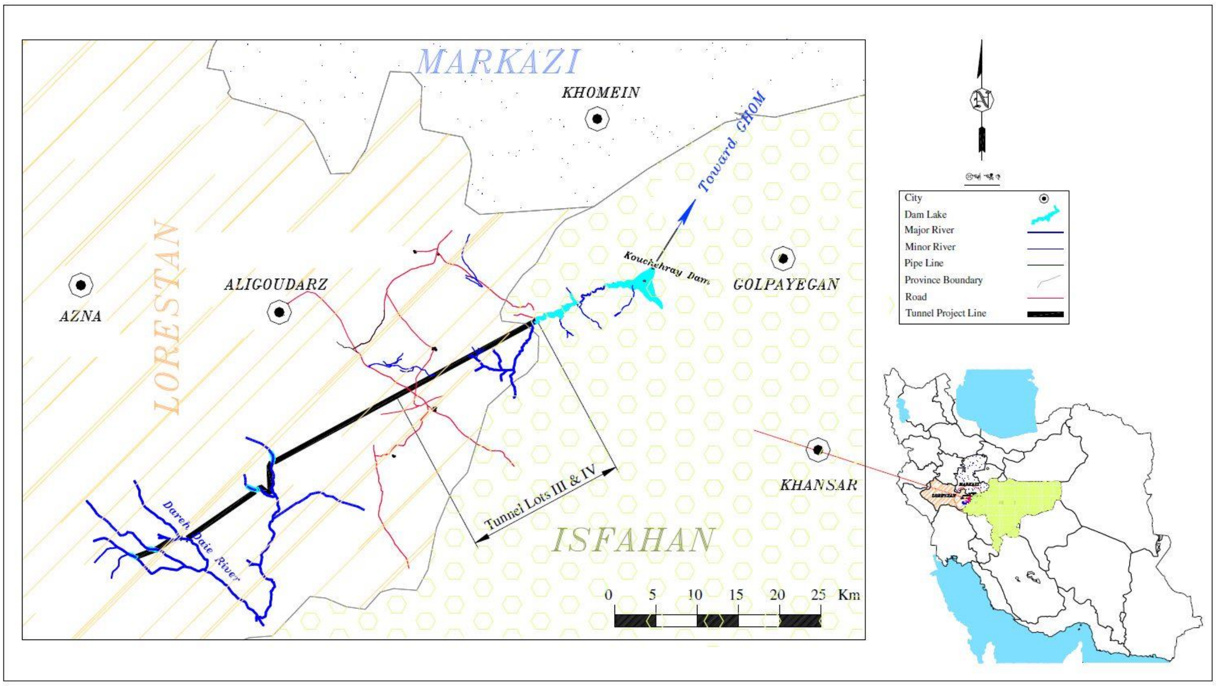

Figure 5.8: Geographical location of the Ghomrood project (Farrokh & Rostami, 2008)

Table 5.6: Main specifications of TBM used in Ghomrood tunnel lot 3 & 4 (Hassanpour, 2009)

Parameter	Value
Machine diameter	4.53 m
Cutter diameter	432 mm
Number of disc cutters	36
Disc nominal spacing	75 mm
Max. Operating cutterhead thrust	18,000 kN
Cutterhead power	1120 kW
Cutterhead speed	0-12
Cutterhead torque (nominal)	802 kN.m at 10rpm
Thrust cylinder stroke	1400 mm
Total TBM weight (approx.)	255 ton

The area under study is located in the Sanandaj-Sirjan formation of the geological divisions of Iran. This formation consists of a series of asymmetric foldings and faults and is gone through mild to high metamorphisms. The lithology of this area consists of a sequence of Jurassic–Cretaceous formations. The Cretaceous formation consists of massive limestone and dolomite while the Jurassic formation mainly consists of slate, schist, and metamorphic shale and sandstone units. The majority of the rock mass is considered to be of weak to fair quality (SCE Company, 2004; Farrokh & Rostami, 2008; Hassanpour, 2009). The geological conditions along the tunnel alignment are illustrated in the cross-sectional profile in Fig. 5.9. To collect the required data for the analysis of TBM performance, a similar methodology which applied for to data-compilation of Zagros tunnel lot 2, had been employed, meaning pre-construction and construction investigations such as back-mapping of the tunnel face, etc. In brief, according to geological investigation (Figure 5.9), the lithology encountered along the tunnel can be categorized into three main units including:

- The northeast part of Chal-Hendeh mountain (Tunnel outlet area) which contains Sandstone and Shale that have been altered into metamorphic Slate and Phyllite (Jsh1 unit)
- Elevated and calcareous (limy) section of Chal-Hendeh mountain which is the most sophisticated part in terms of lithology, including Carbonate facies (Klm1 & Klm)
- The southeast part of Chal-Hendeh mountain which includes Jurassic units (Jsh1 & Jsh2) located below the Cretaceous limestones with fault boundary. In terms of lithology, the section near to the mountain is not different from the first part, but in the southwest, this section changed from Slate form to Schist, which causes its lithology changed more to quartzite graphite schists. Another difference is related to the abundance of quartz veins and quartzite layers which quartz veins in the north-eastern part of the mountain have a maximum frequency of around 10% with the maximum thickness around 0.5 m whereas, in south-western, the frequency increased to 20 to 30% and the thickness sometimes is even more than 10m.

Results of petrographic analyses indicate that, considering mineralogy and texture, there are six main lithotypes in tunnel alignment. These lithotypes include (1) clay-limestone, (2) limestone, (3) Shale & Slate (4) Low metamorphosed fine Quartzite Sandstone, (5) graphite schist, and (6) Quartzite. The main petrographic, physical, and mechanical characteristics of these lithotypes are summarised in Table 5.7.

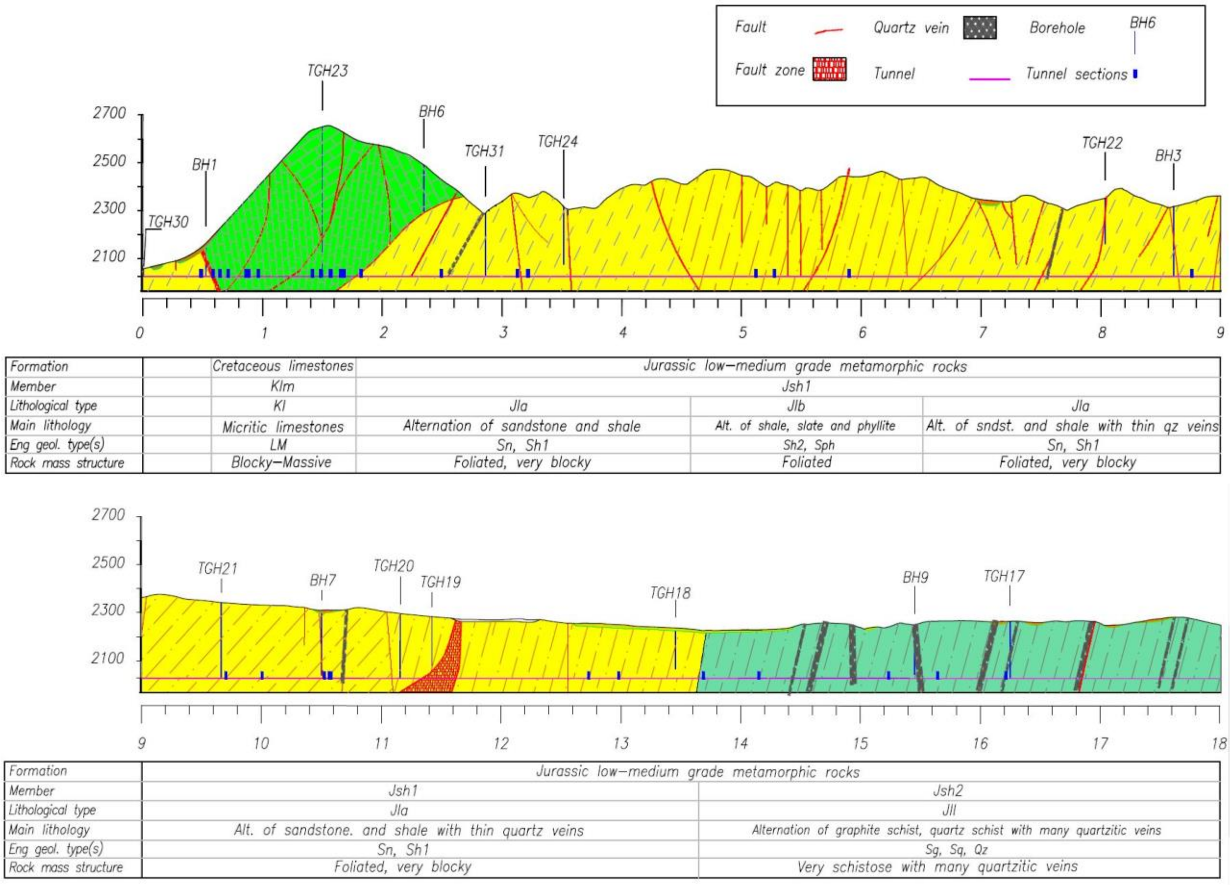

Figure 5.9: Geological section through the Ghomrood tunnel excavated alignment, Lot 3 &4 (Hassanpour, 2009)

Table 5.7: Main characteristics of lithotypes in Ghomrood tunnel (Hassanpour, 2009)

No	Lithotype	Major minerals	Quartz content (%)	Porosity (%)	UCS (MPa)
1	Clay limestone	Calcite, clay minerals, opaque minerals	< 5	< 5	130-150
2	Massive limestone	Calcite, clay minerals	< 5	< 5	150-175
3	Slate/Shale	Phyllosilicate minerals (clay, mica, and chlorite), fine quartz, feldspars, iron oxide minerals, and opaque minerals	5-10	< 2	20-30
4	Low metamorphosed fine Quartzite Sandstone	quartz, feldspars, Phyllosilicate minerals (chlorite & mica), iron oxide minerals and opaque minerals	> 60	5-10	50-100
5	Graphite Schist	fine feldspars, mica & quartz, opaque minerals	5-10	< 2	20-30
6	Quartzite	quartz, opaque minerals	> 90	< 2	> 150

It is worth to note that, average values of rock mass parameters (and intact rock properties) have been utilized to determine and assess the geomechanical conditions of the identified engineering geological units by some empirical rock mass classification systems including, RMR (Bieniawski, 1989), GSI (Hoek et al. 1995) and Q-system (Barton et al. 1974) which are illustrated in Figures 5.10. The changes of RQD_0 related to selected bored tunnel sections is also depicted in Figure 5.11 which ranges between 10 to 100 and based on Deere et al. (1967), it can be classified as very poor rock to excellent rock quality. Besides that, the diversity of commonly used intact rock properties for estimation of TBM performance (UCS), relative to tunnel sections is also illustrated in Figure 5.12 graphically to reflect the variation of compressive strength in bored sections of the tunnel. Furthermore, during the construction phase, machine performance data, and operating parameters (such as applied thrust, RPM, torque, etc.) were also recorded continuously in special sheets and analysed independently. As a such, the variations of TBM penetration rate (ROP), applied total thrust, and RPM are depicted in Figures 5.13.

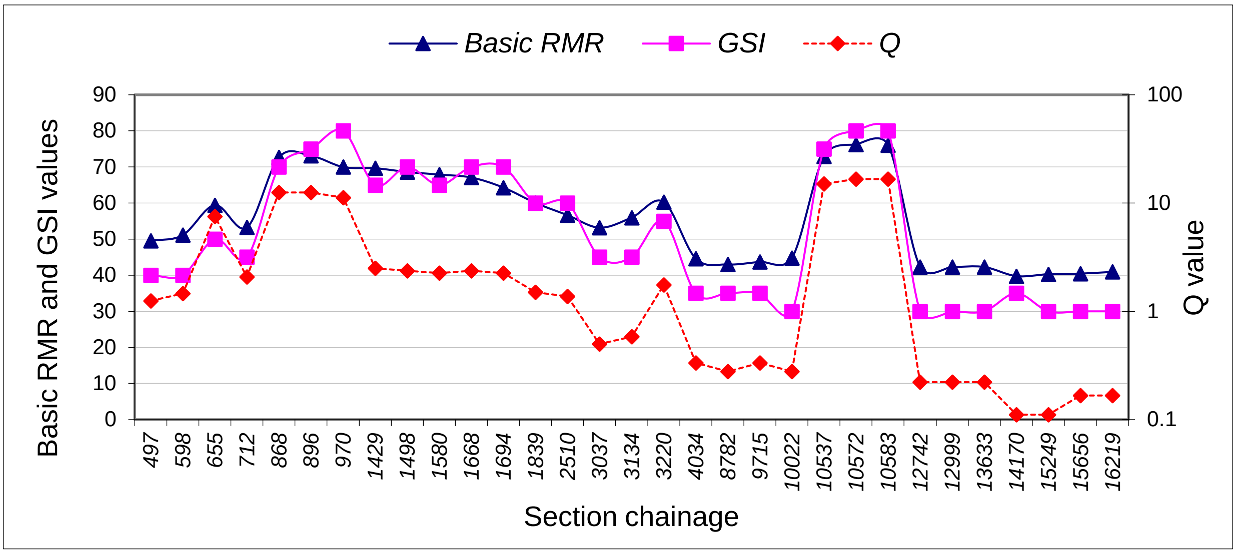

Figure 5.10: Variations of basic RMR, GSI & Q value in selected tunnel sections in Ghomrood tunnel lot 3 & 4

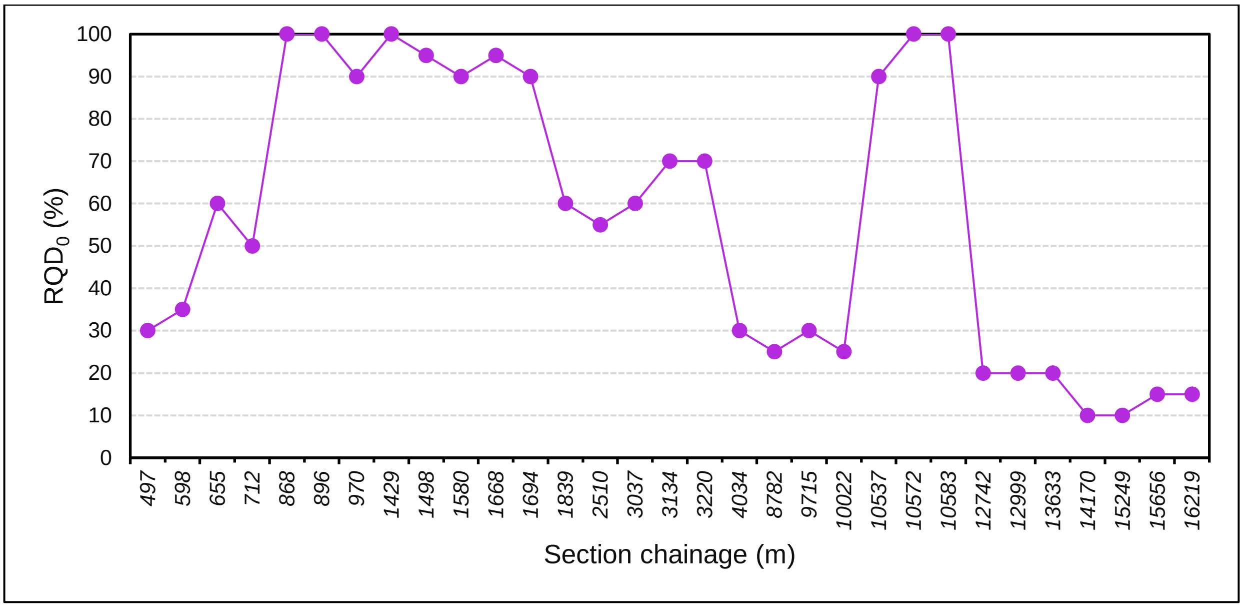

Figure 5.11: Variations of RQD_0 (%) in selected tunnel sections in Ghomrood tunnel lot 3 & 4

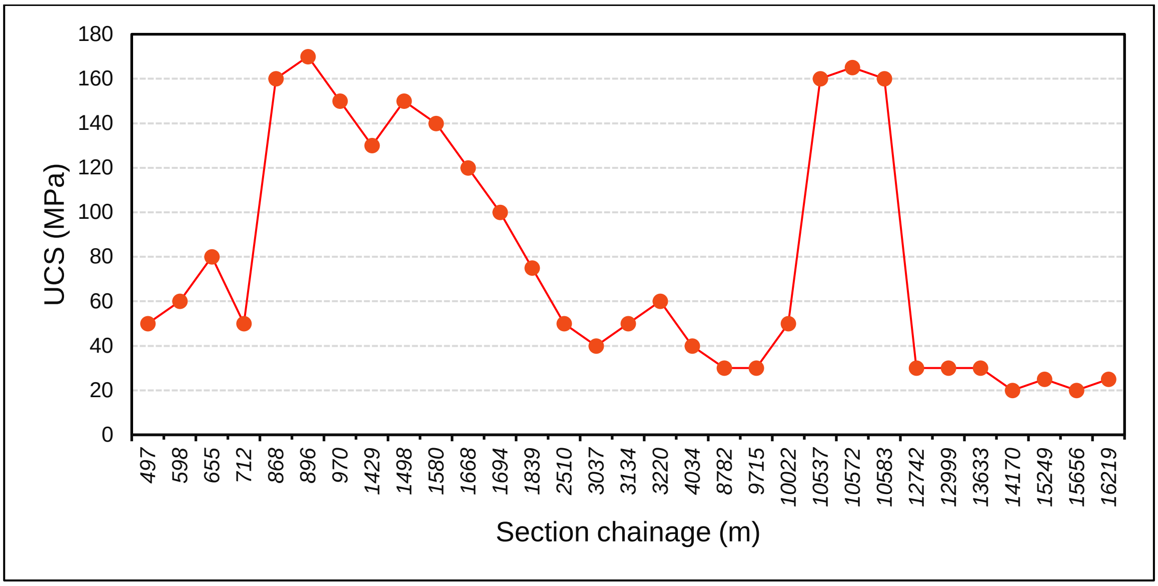

Figure 5.12: Variations of *UCS* in selected tunnel sections in Ghomrood tunnel, Lot 3 & 4

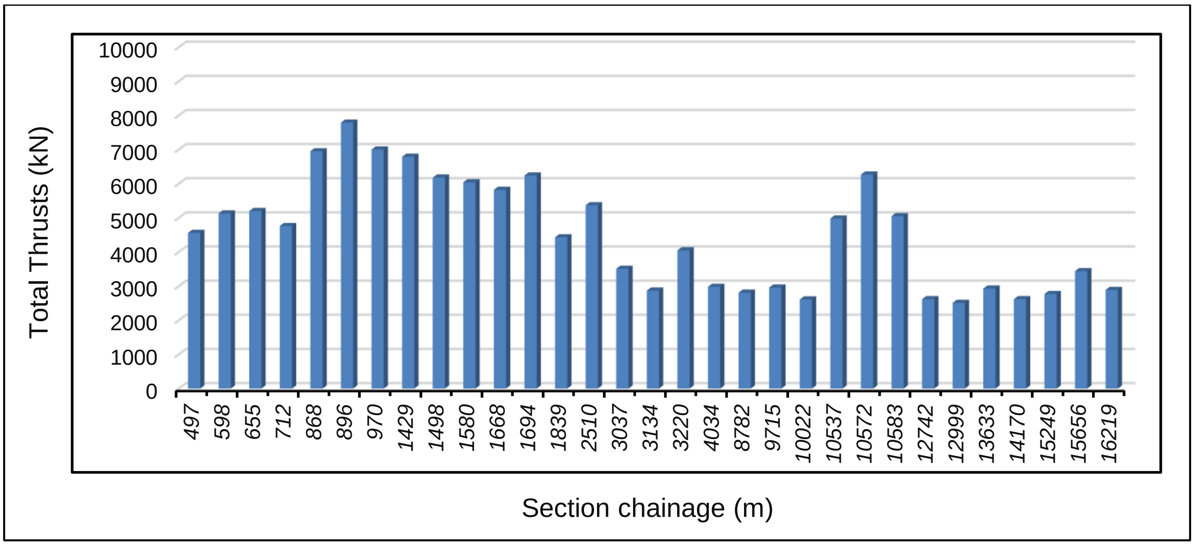

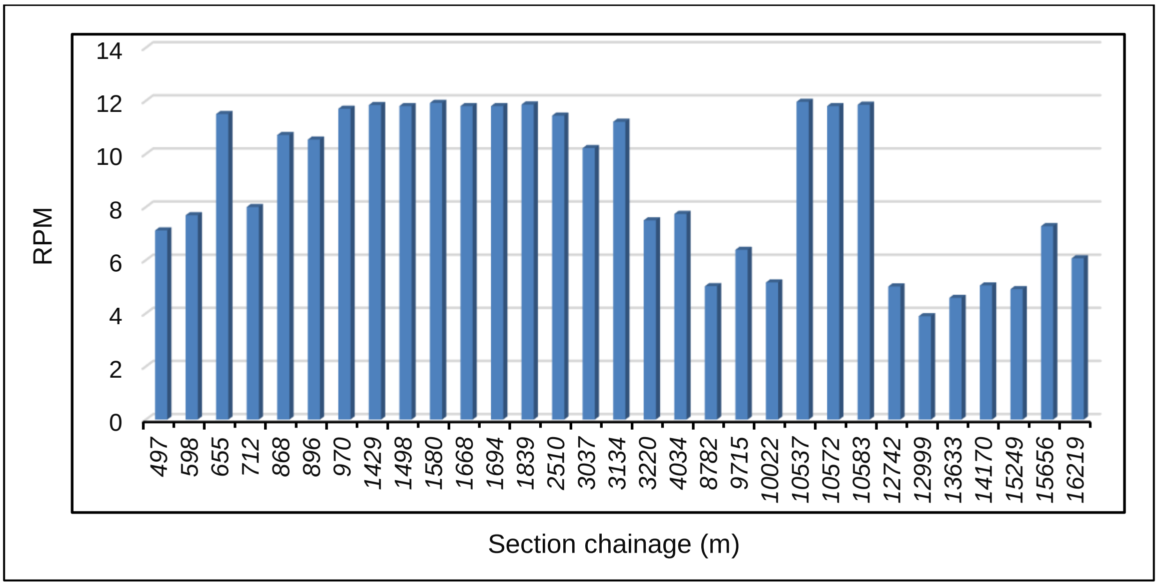

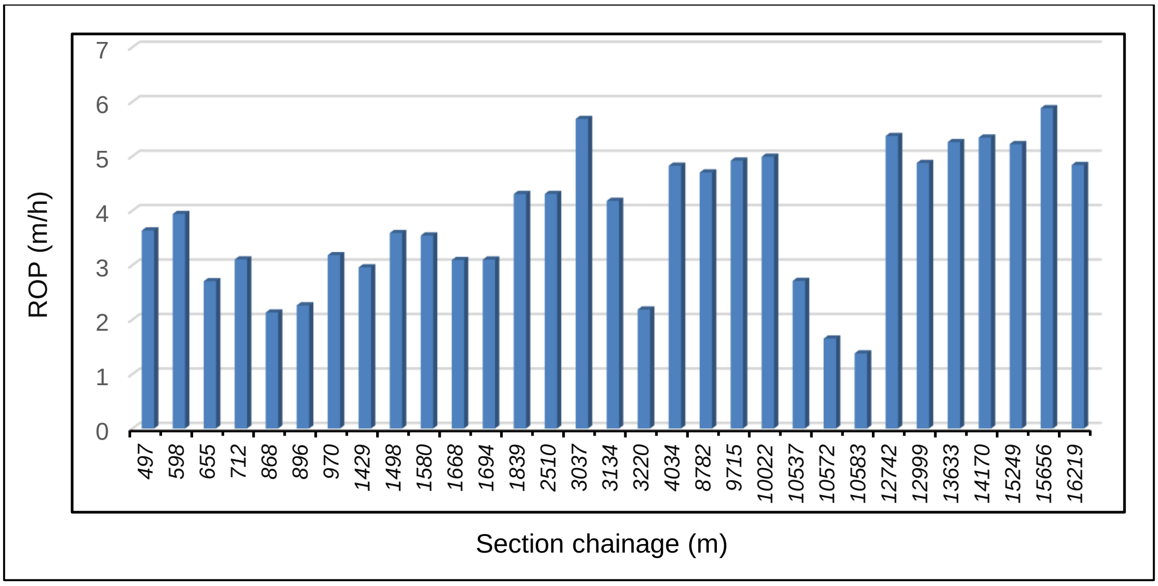

Figure 5.13: Variations of total thrust, RPM, and rate of penetration (ROP) in selected tunnel sections in Ghomrood tunnel lot 3 & 4

5.2.3 Karaj-Tehran Water Conveyance Tunnel

The Karaj-Tehran Water Conveyance Tunnel has been designed to transfer 16 m^3/s of water from the Karaj (Amir-Kabir) Dam northeast of Karaj City to Tehran City (Figure 5.14). The tunnel was divided into two sections: Lot 1 or ET-K (16 km) at the southeast end and Lot 2 or K-P (14 km) at the northwest end of the project area. Lot 1 of the project started in 2006 and had been excavated by double-shield TBM manufactured by Herrenknecht, finished by 2009. Machine specifications of TBM is listed in Table 5.8. The available data for this project includes the first 8.7 km of Lot 1.

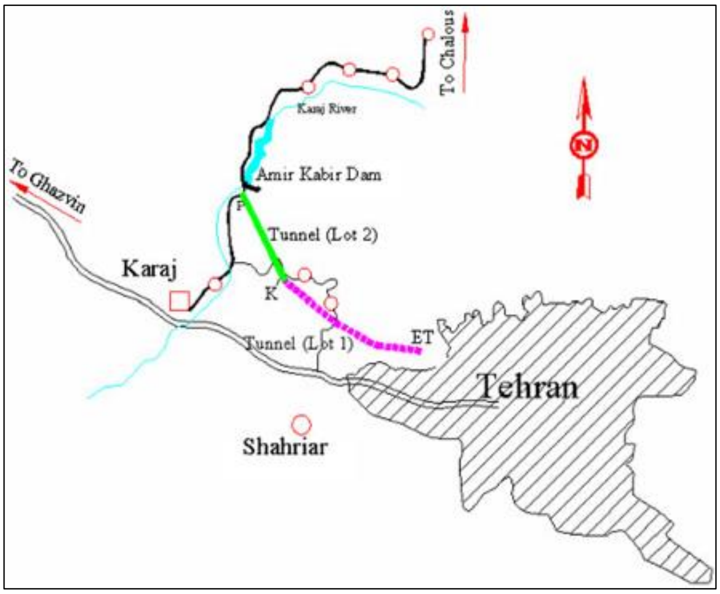

Figure 5.14: Details of Karaj water conveyance tunnel scheme, northwest of Tehran (Hassanpour, 2009)

Table 5.8: Main specifications of TBM used in Karaj-Tehran water Conveyance Tunnel, lot 1 (Hassanpour, 2009)

Parameter	Value
Machine diameter	4.65 m
Cutters diameter	432 mm
Number of disc cutters	31
Disc nominal spacing	90 mm
Maximum operating cutterhead thrust	16,913 kN
Cutterhead power	1,250 kW
Cutterhead speed	0-11 rpm
Cutterhead torque (nominal)	1,029 kNm (11 rpm)
Thrust cylinder stroke	1,400 mm
Conveyor capacity (approx.)	200 m3/h
TBM weight (approx.)	170 ton

The maximum overburden in section Lot- 1 is 670 m, with an average of about 400 m. The elevation of K' and ET points at the two ends of the section are 1,582 m and 1,560 m, respectively, with a slope of 0.013 % toward the outlet portal. Geological units of this area comprise a sequence of Karaj formations having a variety of pyroclastic rocks, often interbedded with sedimentary rocks. The characteristic rock types are green vitric to crystal lithic tuff, tuff breccias, sandy and silty tuffs with shale, siltstone, and sandstone (Hassanpour et al. 2010). The engineering geological profile of the tunnel (Fig. 5.15) shows the distribution of rock units along the bored section of the tunnel. During the geological studies in the project area, 14 predominant stratigraphic units were identified along the tunnel alignment. Table 5.9 lists 11 stratigraphic units encountered in the bored section of the tunnel.

Table 5.9: Stratigraphic and engineering geological units identified along the Karaj-Tehran tunnel (Hassanpour, 2009)

No	Stratigraphic units	Lithology	Engineering geological units
1	U14	Undifferentiated rocks of U11 to U13 units	Gta1
2	U13	Sandstone, green vitric tuff, and siliceous tuff	Gta2
3	U12	Light cream lithic and vitric tuff	
4	U11	Sandstone and micro-conglomerate	Gta3
5	U10	Siliceous green tuff and sandstone	
6	U9	Green vitric and lithic tuff and siltstone	Sts2
7	U8	Siliceous green tuff and sandstone	
8	U7	Massive green tuff	Sts1
9	U6	Tuffy siltstone	
10	U5	Sandstone and micro-conglomerate	
11	U4	Alternation of thin-bedded shale, siltstone, and sandstone	Tsh
-	-	Intense faulted zone, crushed zone	Cz

The area along the tunnel is moderately folded and intensively faulted. Further, some minor faults and shear zones have been observed at the tunnel face. As shown in the geological cross-section (Fig. 5.15), the bored section of the tunnel has passed through a wide syncline (Azgilak syncline) and anticline (Vardij anticline), and some thrust faults with different length of influence zone. Due to the folded structure of the area and the existence of some thrust faults, the tunnel route can be divided into several structural zones. The orientation of bedding planes and related structures (joint sets) changes in different structural zones. The most important thrust faults in the area are the Poorkan-Vardij and North Tehran faults. Although the alignment has been chosen to avoid these two major faults, the first 3 km of the tunnel have passed through the zone of influence of these two major faults, resulting in many delays due to instabilities in the tunnel walls. In addition, some minor faults and shear zones have been identified as crossing the tunnel line. The thickness of the fault zones is thought to be generally between 10 and 50 m.

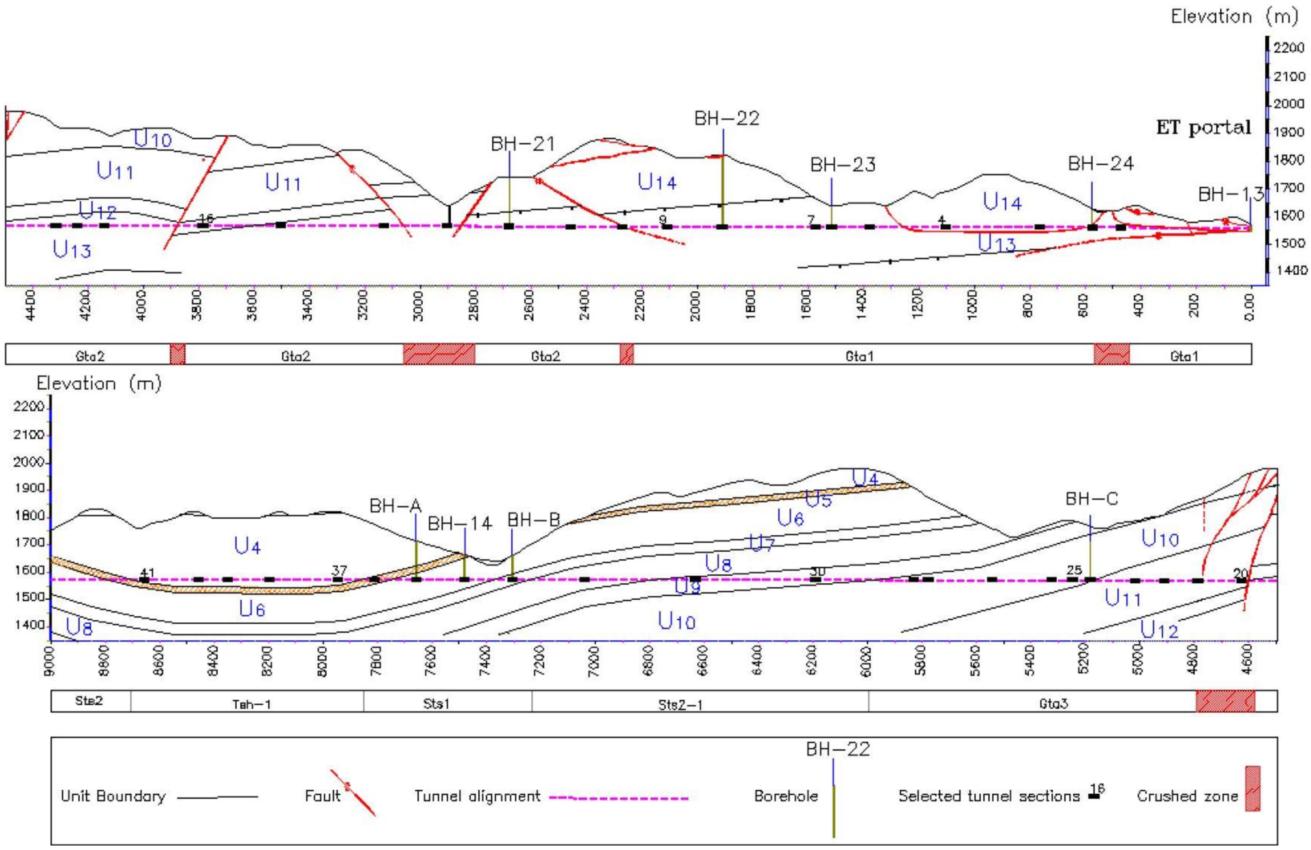

Figure 5.15: Geological cross-section along the Karaj-Tehran tunnel (Hassanpour, 2009)

The bored section of the tunnel can be subdivided into 7 segments (engineering geological units) with uniform characteristics related to TBM performance, tunnel stability, and groundwater inflow. This was based on studies of outcrops; core boxes and also results of laboratory and field tests. The main petrographic, physical, and mechanical characteristics of these lithotypes are summarised in Table 5.10.

Average geomechanical characteristics of the engineering geological units in the area were assessed using some empirical rock mass classification systems, RMR (Bieniawski 1989), GSI (Hoek et al. 1995, Hoek 2007) and Q-system (Barton et al. 1974) which the results of calculation of different rock mass classification parameters are depicted in Figure 5.16. Besides that, the diversity of UCS & RQD_0 which are representative of intact and rock mass properties in each selected section of bored tunnel are shown in Figures

5.17 & 5.18, respectively. As shown in Figure 5.17, the average *UCS* ranges between 30 and 150 MPa. Also, data obtained from the back mapping of the tunnel was used to analyse TBM performance and also to verify design assumptions. In addition, machine performance data and operating parameters (such as applied thrust, RPM, torque, etc.) were recorded continuously by the data acquisition system. The respected ROP, total thrust, and RPM of selected bored tunnel sections are presented in Figure 5.19.

Table 5.10: Main characteristics of lithotypes in Karaj-Tehran tunnel (Hassanpour, 2009)

No	Lithotype	Major minerals	Quartz content (%)	Porosity (%)	UCS (MPa)	BTS (MPa)
1	Vitric tuff	Feldspars, clay minerals, calcite, quartz	5	1-10	30-100	5-10
2	Lithic tuff	Rock fragments, feldspars, clay minerals, chlorite, quartz	15	3-6	50-80	6-8
3	Siliceous tuff	Silica, feldspars, clay minerals, quartz	30	1-3	80-160	8-12
4	Sandstone, microconglomerate	Feldspars, clay minerals, calcite, chlorite, quartz	20	1-5	40-80	6-8
5	Siltstone, shale	Clay minerals, calcite, quartz, chlorite	10	1-5	30-50	5-6

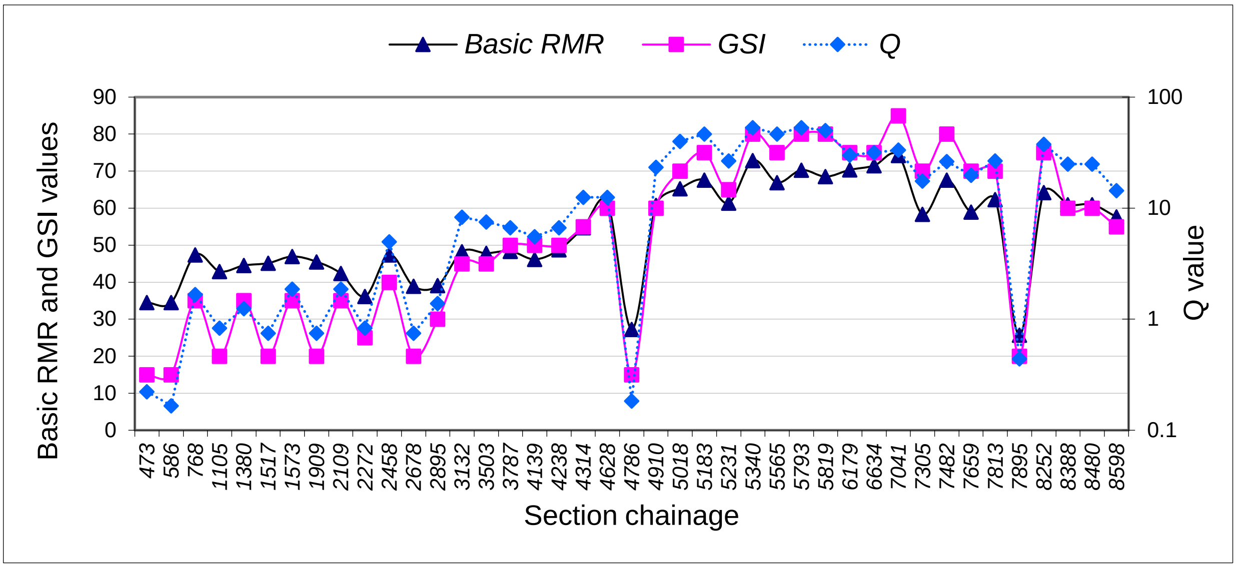

Figure 5.16: Variations of basic RMR, GSI & Q value in selected tunnel section in Karaj-Tehran water conveyance tunnel

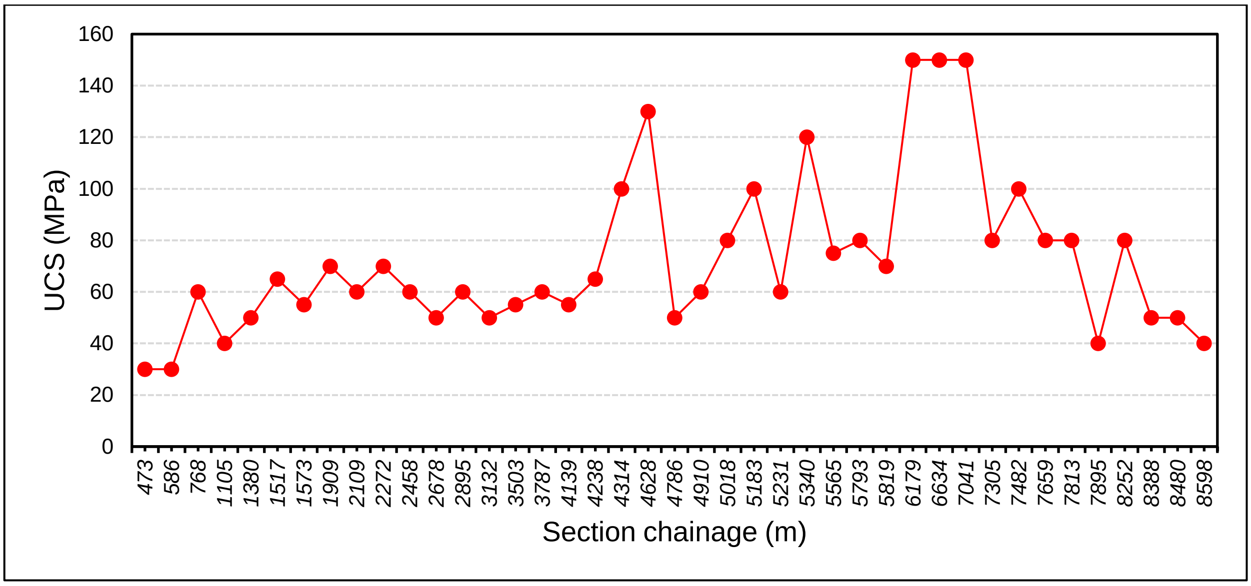

Figure 5.17: Variations of *UCS* in selected tunnel section in Karaj-Tehran water conveyance tunnel

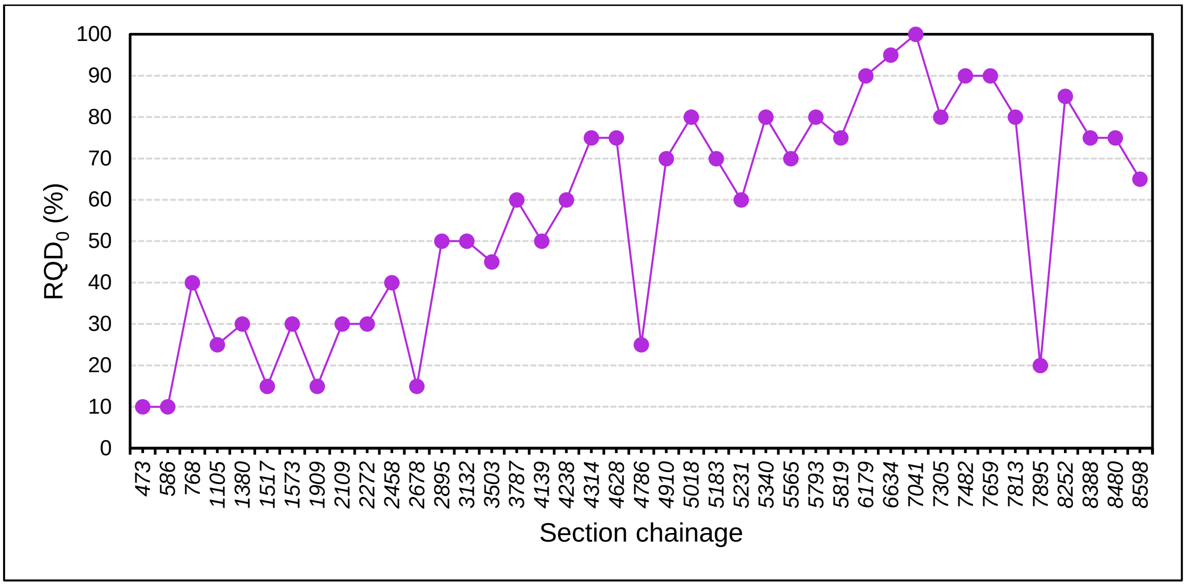

Figure 5.18: Variations of RQD_0 in selected tunnel section in Karaj-Tehran water conveyance tunnel

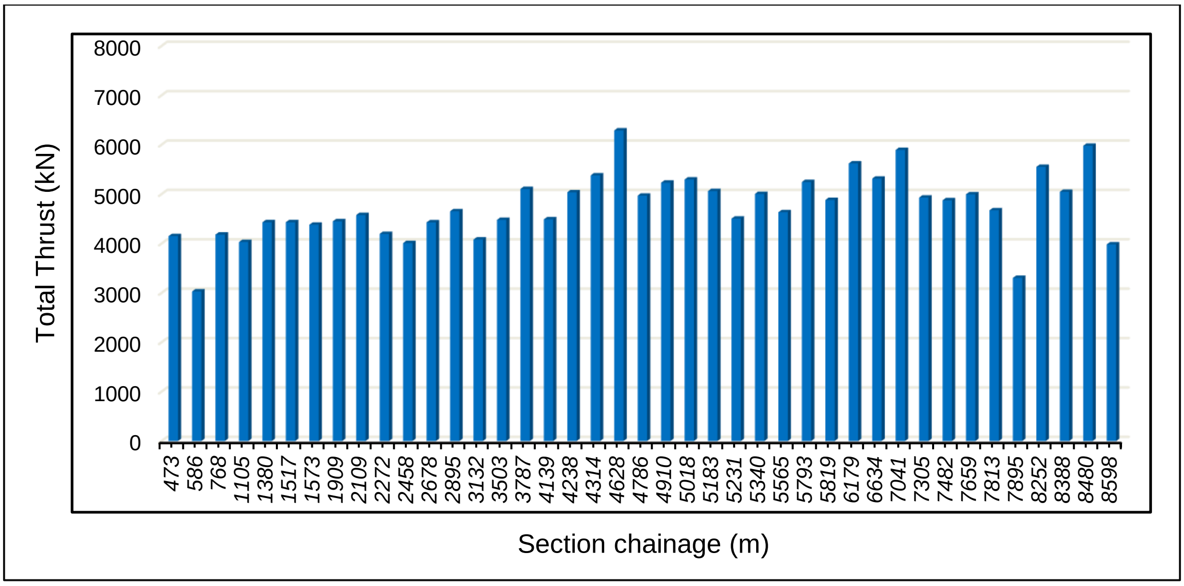

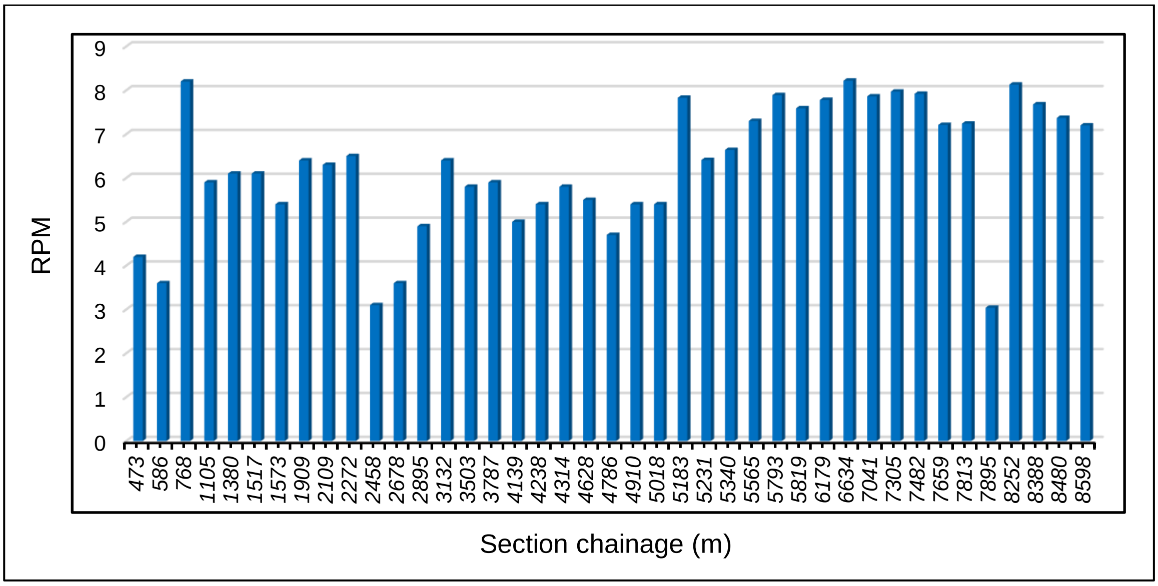

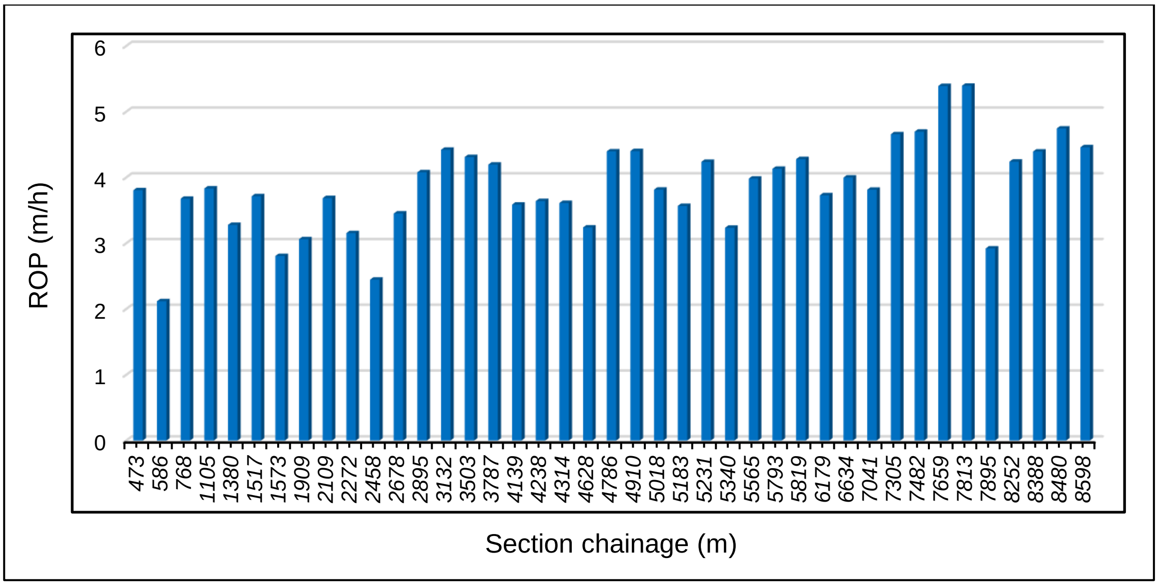

Figure 5.19: Variations of total thrust, RPM, and rate of penetration (ROP) in selected tunnel section in Karaj-Tehran water conveyance tunnel

5.2.4 Golab Water Conveyance Tunnel

Golab water transfer tunnel was introduced with the aim of transferring Zayandehrud river water to Kashan in Iran. This project with an approximate length of 11.5 km includes the main tunnel, an access tunnel, a water intake tunnel, and a pumping station cavern. After passing through the 10 km main tunnel, water is transferred to the pumping station cavern by a water intake tunnel, and finally, it is pumped through the 1.5 km pipeline in the access tunnel to the refinery at the portal (See Figure 5.20). The tunnel is excavated from the inlet to the outlet with a negative dip angle. The machine used in the Golab tunnel was a double-shield TBM with a 4.495 m diameter manufactured by Wirth. The cutterhead was laced with 35 discs cutters, 432 mm in diameter. The cutterhead was designed with six (6) cutters as the center cluster, 26 single face cutters, and 3 are gage cutters. Overall specifications of the machine are shown in Table 5.11.

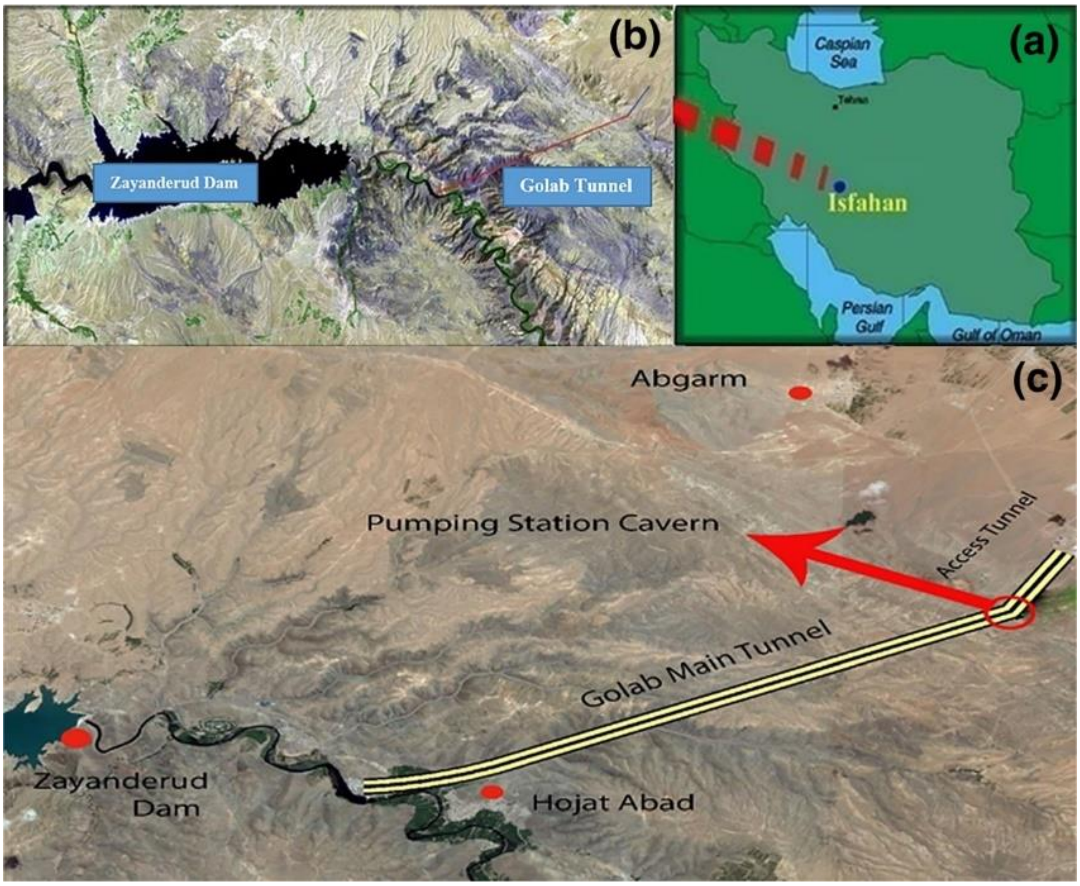

Figure 5.20: (a) Location of the project, (b) A large-scale view of the project, (c) small-scale view of the project indicating various components of Golab water transfer tunnel (Fatemi, 2016)

Table 5.11: Main specifications of TBM used in Golab water Conveyance tunnel (Wirth TBM- TB 458 E/TS) (Fatemi, 2016)

Parameter	Value
Machine diameter	4.495 m
Number of disc cutters	35
Disc cutter diameter	432 mm
Disc nominal spacing	75 mm
Max. Cutterhead rotational speed	12 rpm
Max. Cutterhead torque	80 kNm at 12 rpm
Max. Thrust force	20000 kN
Total machine power	1750 kW
Cutterhead power	1120 kW

The tunnel path is surrounded by numerous faults. These faults have been identified by the surface exploration of outcrops. Given the considerable depth of the tunnel, predicting the location of these faults along the tunnel route based on surface surveying is not very accurate. Therefore, to determine the exact location of faults intersecting the tunnel an as-built geological map has been developed. This map has been used in the database of machine performance to represent the ground conditions (Fatemi, 2016). The back-mapping shows that rock masses along the tunnel route can be divided into several zones based on different geological characteristics and geomechanical properties of the units. Table 5.11 shows a list of engineering geological units and their approximate length in the bored tunnel. From the geological aspect, Golab's main tunnel is situated in the metamorphosed zone of Sanandaj-Sirjan. The starting part of the tunnel which is located in the shear zone of Chadegan mostly contains metamorphic rocks including different types of Schists and some igneous rocks. Besides, the middle part of the tunnel includes an intermittent set of slightly metamorphic argillaceous shales which in some cases were converted to slates and Phyllites. The end part of the tunnel is located in the intersection area of the main tunnel and the access tunnel generally consists of limestone and conglomerate. Figure 5.21 also indicates the longitudinal profile of the tunnel. Engineering geological studies were conducted to determine the geomechanical properties of different units along the tunnel. Also, 10 boreholes were drilled along the tunnel route and some tests were carried out on samples taken from boreholes as well as tunnel face. Ground characteristics of various engineering geological units are summarized in Table 5.12.

Table 5.12: Engineering geological units along Golab alignment (Fatemi, 2016)

No.	Lithology	Stratigraphic units	Engineering geological units	Chainage (m)
1	Quartz Muscovite Biotite chlorite Schist	$J_{1met}^{M.Sch}, J_{1met}^{Sch}, J_{1met}^{Gr.Sch}, J_{1met}^{Ch.Sch}, J_{1met}^{Ac.Sch}, J_{1met}^{Bi.Sch}, J_{1met}^{Q.M.Sch}$	Met-Sch	4070.75
2	Gray Massive Limestone		Li	109.83
3	Low Metamorphosed Greenish Gray Shale	J_{3set}^{Sch}	Met-Sh	1147.22
4	Very Weak Black Phyllite	J_{2Met}^{Phy}	Met-Phy	1069.54
5	Very Weak Greenish Slate	J_{2Met}^{SI}	Met-SI	672.45
6	Fine to Medium Grain Igneous Rocks	$Mo - Di, Di, Dol, To, AP$	Ig	1737.63
7	Metamorphosed Igneous Rocks	$Gr - G_{met}, Dol_{met}, Vol_{met}$	Met-Ig	422.2
8	Schistose Meta Sandstone	J_{2met}^{St}	Met-Sa	299.56
9	Argillaceous Limestone	K_{km}, K_{km}^{bgr}	Ar-Li	126.14
10	Red Conglomerate	Pcg, Pcr	Cg.r	57.62
11	Gray Conglomerate with Limy Sandstone	Ec, Ec^{L-S}, Ecs^{L-S}	Cg-Li. Sn	130.9
12	Crushed Zone		CZ	13.41
13	Fracture Zone		FZ	113.75

Database of Golab tunnel TBM performance includes the geotechnical information as well as TBM operating parameters gathered by the machine's PLC system. Average geomechanical characteristics of the engineering geological units in the area were assessed using some empirical rock mass classification systems, such as *RQD* (Deere et al. 1967), RMR (Bieniawski 1989), GSI (Hoek et al. 1995, Hoek 2007), and Q-system (Barton et al. 1974) which the results of calculation of different rock mass classification parameters regarding to each lithology are summarized in Table 5.13. Figure 5.22 presents the total thrust, RPM, and ROP related to some selected tunnel sections in the Golab water conveyance tunnel.

Table 5.13: Main physical & mechanical characteristics of lithotype encountered along the Golab tunnel (Fatemi, 2016; Imensazan Consulting Engineering "ICE", 2009)

Lithology	UCS (MPa)	$I_{s\,(50)}$ (MPa)	RQD (%)	RMR_{basic}	GSI Value	Q value	Porosity (%)
Met- Sch	12-17	1.5 - 3	25-35	40-45	35-40	0.4-0.95	4.5- 8.5
Li	50-60	2 - 4.5	70-80	49-57	44-52	1.2-2.2	0.5 - 2.5
Met-Sh	2 - 6.5	0.83 - 0.1	20-25	28-33	25-30	0.9-0.17	5.5 - 10.8
Met-Phy	7-12	0.65 - 1.5	20-30	34-40	30-35	0.18-0.25	4.2 - 6.5
Met-SI	4-8	0.2 - 1	20-25	32-37	28-34	0.15-0.25	7.7 - 10.4
Ig	108- 130	5.8 - 7	75-90	72-76	62-65	8.5-20.5	0 - 0.15
Met-Ig	60 – 65	3.5 - 5.5	50-70	60-68	65-60	3.5-7.5	0.1 - 0.5
Met-Sa	25 – 30	1.8 - 3	35-50	48-52	45-49	0.8-1.4	6 - 8.5
Ar-Li	10 - 13.5	1 - 2.2	45-55	48-53	43-48	0.3-1	7.1 - 8.8
Cg.r	21 – 31	2-4	50-60	46-55	44-52	0.8-1.5	1.5 - 2.51
Cg-Li. Sn	71.5 - 85	4.1 - 5	90-100	60-67	48-54	1.8-4	0.43 - 0.75

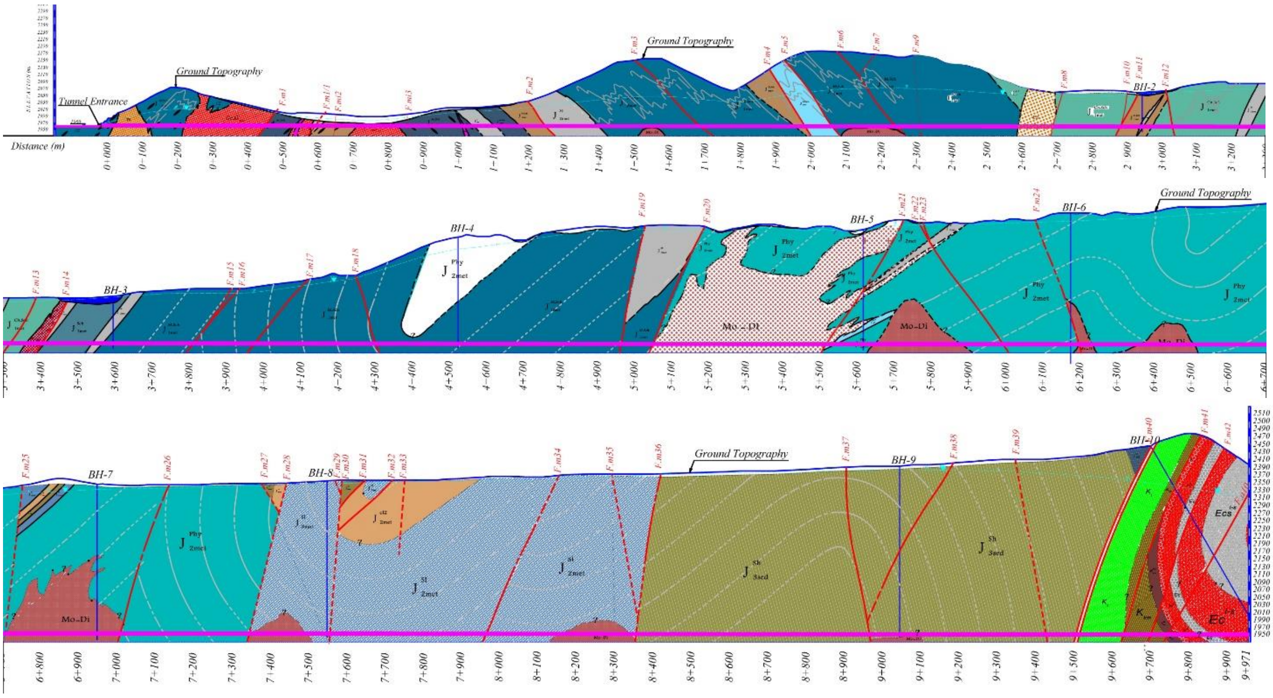

Figure 5.21: Profile of engineering geological units along Golab tunnel (Fatemi, 2016)

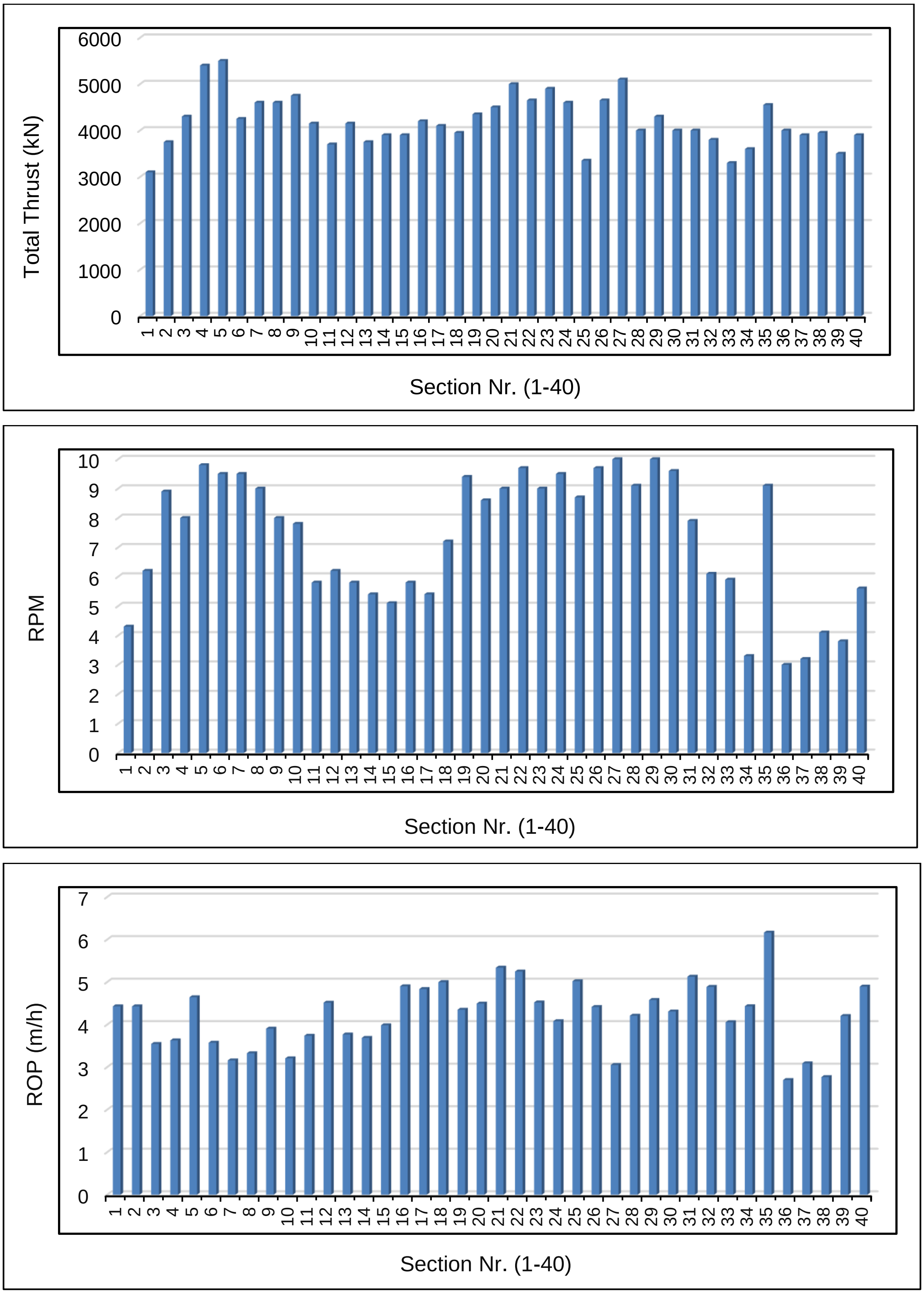

Figure 5.22: Variations of total thrust, RPM and ROP in some selected tunnel sections in Golab water transfer tunnel

5.2.5 Maroshi-Ruparel Water Supply Tunnel

To improve the water supply to Vakola, Mahim, Dadar and Malbar Hill of Greater Mumbai, a 12.24 km long tunnel between Maroshi and Ruparel College is being excavated by TBM. The tunnel is divided into three sections, i.e., Maroshi–Vakola (5.834 km long), Vakola–Mahim (4.549 km long), and Mahim–Ruparel Col-lege (1.859 km long) (Figure 5.23). The longest tunnel between Maroshi and Vakola has been completed. WIRTH TB-II-320H and TB-II-360H TBMs (Hard rock, Open type) were used for the excavation of Maroshi–vent hole and Vakola–vent hole tunnel sections, respectively. These are refurbished full-face hard rock TBMs and refurbishment was carried out under the supervision of the equipment manufacturer. Main TBMs specifications are given in Table 5.14 & 5.15 respectively.

The tunnel boring was extremely challenging between Maroshi and Vakola section due to heavy water seepage, varying rock strata conditions, and the presence of various weak zones. The rock mass conditions were assessed by precise judgment using forward probing and "3D" geological logging of tunnel walls. Studies indicate that in Deccan traps, variations in rock types, flow contacts, rock strength, and volumetric joint amount with the presence of weak zones have predominantly affected the penetration rate and stability of tunnels.

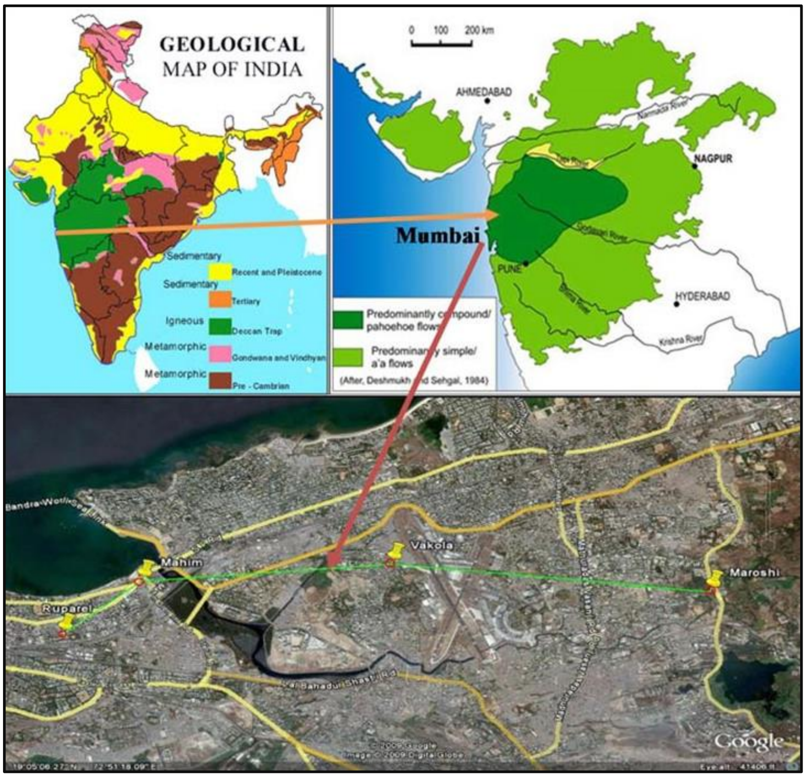

Figure 5.23: Location map of the study area, Maroshi-Ruparel tunnel (Jain, 2014)

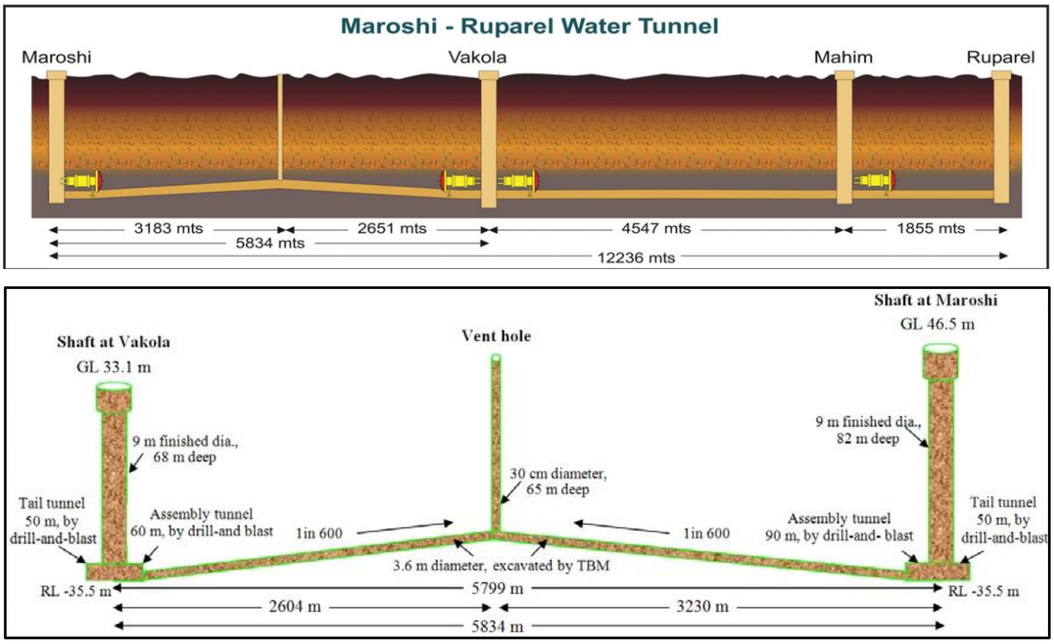

Figure 5.24: Plan map of Maroshi–Ruparel College tunnel and shafts (Jain, 2014)

Table 5.14: Main specifications of TBM Maroshi-Vent hole stretch (Wirth / TB-II-320H), (Jain, 2014)

Parameter	Value
Machine diameter	3.6 m
Cutter diameter	432 mm
Number of disc cutters	31
Disc nominal spacing	62 mm
Maximum operating cutterhead thrust	3828 kN (220 bar)
Cutterhead speed	0-14 rpm
Cutterhead torque	225 kNm (225 bar)
Thrust cylinder stroke	1,100 mm
Muck handling capacity	5 m/h
TBM weight (approx.)	107 ton

Table 5.15: Main specifications of TBM Vakola-Vent hole stretch (Wirth / TB-II-360 H) (Jain, 2014)

Parameter	Value
Machine diameter	3.6 m
Cutter diameter	432 mm
Number of disc cutters	31
Disc nominal spacing	62 mm
Maximum operating cutterhead thrust	3828 kN (220 bar)
Cutterhead speed	0-12 rpm
Cutterhead torque	185 kNm (185 bar)
Thrust cylinder stroke	1,100 mm
Muck handling capacity	5 m/h
TBM weight (approx.)	107 ton

Geologically, the entire Mumbai area is occupied by Deccan basaltic flows and the associated pyroclastic and the plutonic rocks of the Upper Cretaceous to Palaeogene age classified as Sahyadri Group. Deccan basalt of Mumbai Island is considered to be the youngest basalt of the Eocene age. Overall, the geology around Mumbai indicates the presence of ultrabasic, basic, and acid differentions with intertrappean beds, agglomerates, and tuffs. The ultrabasic differentiates are of limited occurrence. Acid rocks include quartz trachyte. The agglomerate and tuff include reworked materials as indicated by the current bedding as well as graded bedding. The lava pile of Mumbai is intruded by columnar jointed, medium-grained doleritic dykes. The rock types encountered during tunnelling are fine compacted basalt, porphyritic basalt, amygdaloidal basalt, and pyroclastic rocks, namely tuff and tuff breccia with layers of red boles and intertrappean beds consisting of different types of shales. The thickness, presence, and structural characteristics of fine compacted basalt, porphyritic basalt, and amygdaloidal basalt vary in different flows, depending on properties of magma, cooling history, and geological conditions at the time of formation, which make these rock types suitable or unsuitable for engineering structures. Vesicles and amygdales increase toward the top of a flow unit which in turn merges into the bole at some places. The red bole is overlain by the massive strata of the next younger flow unit. Vesicular basalt with empty gas cavities and amygdaloidal basalt with gas cavities filled with secondary minerals like zeolites, carbonate minerals, and secondary silica, i.e., agate, etc., do not have a regular pattern of jointing and are massive, while compacted basalt with no gas cavities is usually jointed. The lava flows show various types of structures such as joints, fractures, vesicles, veins, breccias clasts, mafic-dykes, and amygdule with different shapes like a circular, elliptical, and irregular boundary. Due to the emplacement of the traps upon the eroded surfaces of the earlier rock strata, minor undulations in the flow were also observed. The general flows contact dip varies between 30°and 45°in N020°-N040°and N200°-N220°directions. Some flow contacts were open, filled with weathered, altered, or soft materials while some were tight and commonly coalescent. Open flow contacts provide passage for water and weathered materials. Weathered or soft materials are generally deposited during the time internal between two flows. The angle between the tunnel axis and the flow contact was 80°and penetration rate was less at flow contact. The advance rate was low in the case of open flow contact zones while it was high in tight flow contact zones. The sequences of flows are different in different chainages of tunnel indicating they do not have a regular structure like ideal sedimentary rocks. In sedimentary rocks, beds having plane surface stops and bottoms, constant dip, uniform thickness, and wide lateral extent, such a disparity in sequences could validly be interpreted as a fault. It has now been well established that Deccan trap basalt flows do not have such regular structure, and have limited the lateral extent and stretch out over short distances. There is variation in thicknesses, i.e., flows usually have a different thickness in different parts. Its tops and bottoms are not regular plane surfaces with constant dip but irregular surfaces. As a result, it is almost invariable that the flow sequence in boreholes, which were drilled during the investigation does not normally match. This disparity however does not indicate faulting as it would be in the case of beds with regular structural behaviour. Hence, the possibility of the occurrence of a fault between boreholes need not be apprehended merely because the flow sequence in boreholes does not match, as this disparity is the outcome of the structural irregularity of the basalt flows. Traps show two or more sets of vertical joints. Horizontal joints are parallel to the top or bottom surfaces. Two sets of columnar joints were observed in thicker flows. Fractures were identified and they were generally parallel to the prominent joint directions. Conchoidal fracturing of rock mass was a common feature. Generally, amygdaloidal basalt and tuff breccia were massive while in porphyritic basalt the spacing of joint sets was more than 2 m and in fine-grained jointed compacted basalt, it varied from 10 cm to 30 cm. Generally, the TBM penetration rate was greater in fine compacted basalt than that in the porphyritic basalt. Veins are extension fracture that was filled with mineral deposits of quartz, calcite, and zeolites of different dimensions. They were generally sheet-like or tabular or regular in shape. Veins have major influences on cavability and fragmentation and may be weaker or stronger than the wall rock. In the tunnels, generally, calcite and zeolite veins were mapped. About 32 cm to 3.5 m thick mafic dykes were mapped in the Vakola shaft area. The dyke exhibits prominent columnar joints, which were formed due to differential volume changes in cooling and contracting magma. No curviplanar (fold) structure was observed during the geological “3D” logging of the tunnel wall (Jain, 2014). The mineralogical content of basaltic rocks was analysed for each rock type. Major mineral composition of fine-grained basalt and porphyritic basalt constitutes plagioclase (40-45%), pyroxene (15-20%), glass (10-15%), iron oxide (8-10%), and secondary calcite (7-10%), and groundmass was composed of plagioclase, pyroxeneand glass. The mineral contents of the amygdaloidal basalt and tuff breccia are plagioclase (35%), devitrified glass (30%), pyroxene (20%), and oxide phase (15%), and groundmass was composed of glass, chlorite, calcite, and zeolite. Cutter abrasion in basalts and breccia was less due to less quartz and low silica percentage. Basalt generally has a composition of SiO_2(45-55%), total alkalis (2-6%), TiO_2 (0.5-2%), FeO (5-14%) and Al_2O_3 (14% or more). The content of CaO is commonly about 10% and that of MgO is usually in the range of 5-12%. A detailed engineering geological investigation, as well as laboratory investigation, were carried out in the tunnels and related core samples to acquire the geological and/or geotechnical details for rock mass quality assessment. Laboratory rock strength test results of core samples are given in Table 5.16.

Table 5.16: Laboratory rock strength results of core samples (Jain, 2014)

Rock type	UCS (MPa)	$I_{s\,(50)}$	BTS (MPa)	Brittleness index
Fine compact basalt	33.35-115.90	-	2.57-13.31	8.26-15.12
Porphyritic basalt	115.87-143.33	-	8.76-15.26	8.31-15.78
Amygdaloidal basalt	54.10-65.70	-	-	-
Tuff breccia	26.43-50.20	1.33-3.44	1.5-3.2	4.60-11.5
Tuff	15.68-24.28	0.5-1.25	1.6-3.8	4.12-15.17
Flow contact zone	12.40-31.87	-	-	-
Intertrappeans (shale)	28.30-34.35	-	4.90-6.10	4.63-7.10

Various rock types encountered during tunnelling which are illustrated graphically in Figures. 5.25 and 5.26. In this project, the rock mass was characterized using RMR classifications (Bieniawski, 1989). RMR values were calculated after geological mapping and measurements of discontinuity data. In the Maroshi–vent hole section, 1160 m lengths fell in the good rock mass category, while 1098.5 m, 453 m and 375 m lengths fell in fair, very good, and poor rock mass categories respectively. In the Vakola–vent hole section, 1510.5 m length was of good rock mass category, while 998 m, 60 m, and 22 m lengths were of fair, very good, and poor rock mass categories respectively. Generally, the rock conditions were fair to good except at or near the flow contacts where poor to fair rock mass conditions were observed. For medium quality rock masses (RMR of 40-75), the maximum TBM performances (penetration rate and advance rate) were achieved while lower penetration was for poor and very good rock masses.

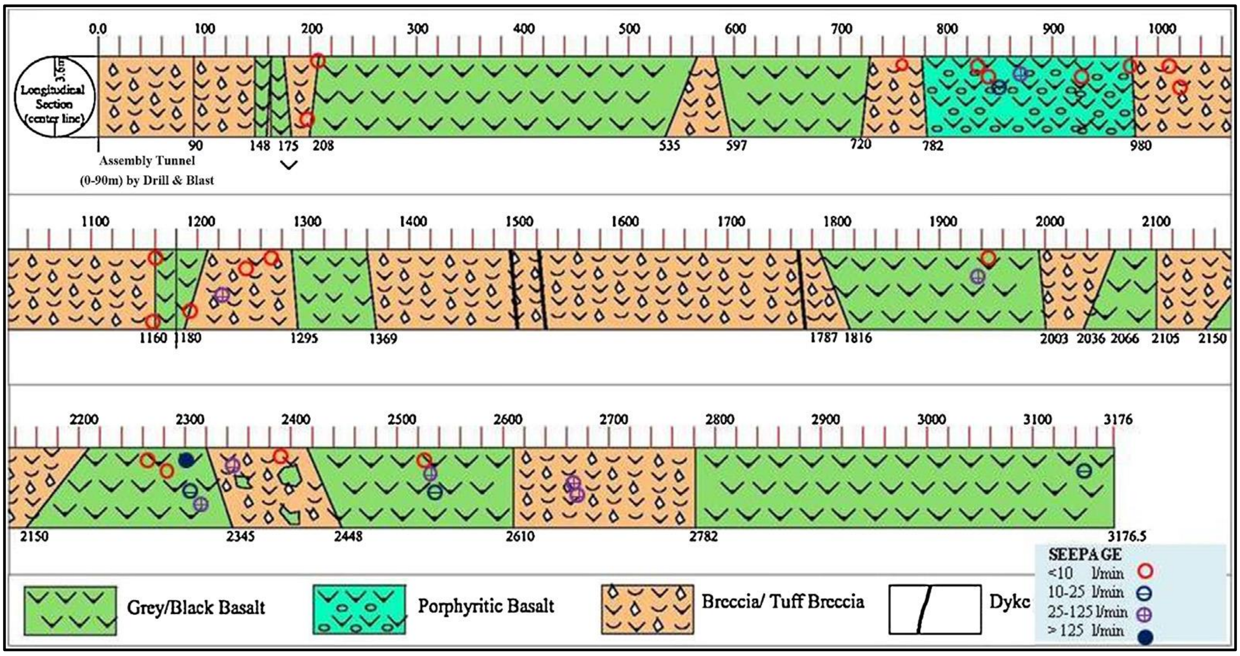

Figure 5.25: Lithological mapping along the tunnel from Maroshi to vent hole (Ch. 90-3180 m) (Jain, 2014)

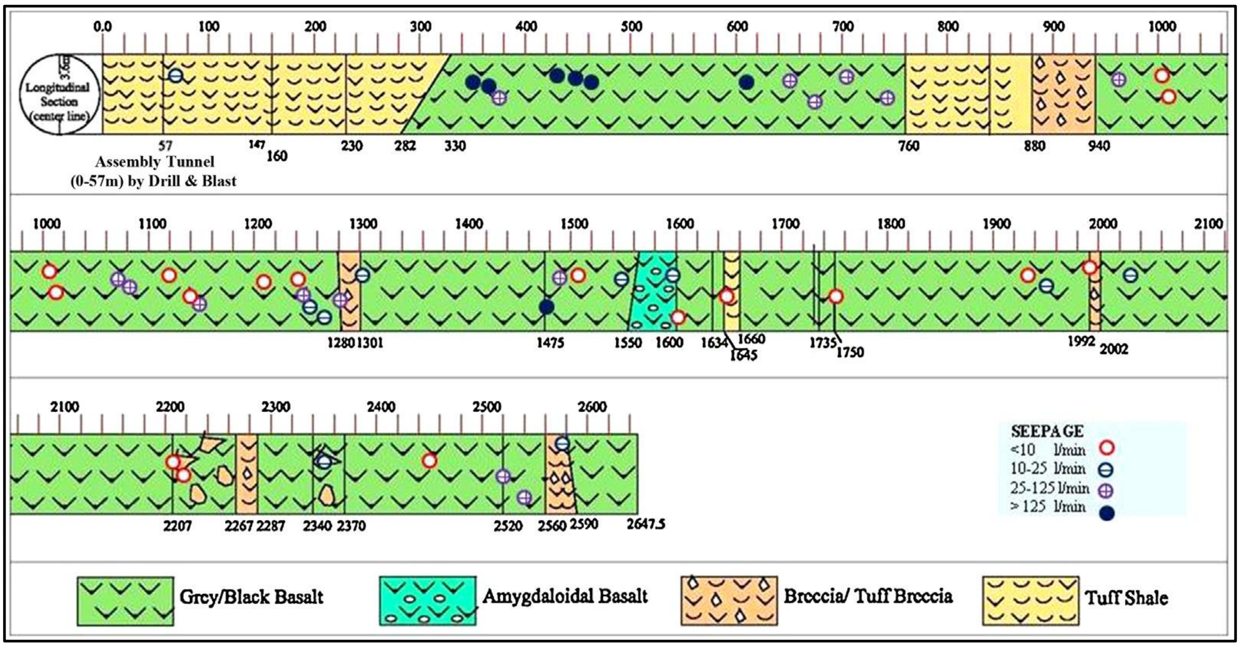

Figure 5.26: Lithological mapping along the tunnel from Vakola to vent hole (Ch. 57–2645 m) (Jain, 2014)

About 3534 m lengths, of the tunnel, was excavated in basalts (compacted basalt-3341 m, porphyritic basalt-193 m). The UCS of the intact basalt varied from 33.35 MPa to 143.33 MPa and the rock mass fell in fair to good rock mass categories. A total of 35.0 m was excavated in the amygdaloidal basalt. In addition, a total of 1617 m of tunnel length (tuff breccia-1257 m, tuff-360 m) was excavated in tuff breccias and tuff. Also, there were sedimentary beds known as intertrappean beds associated with the Deccan trap lava flows. They were predominantly made up of argillaceous and carbonaceous shales. The fine-grained variety of shale had good compressive strength, i.e., up to 34.35 MPa, but it was thinly bedded. Approximately 90 m of tunnel length was excavated in the intertrappean shales, which was about 2% of the total length. The assessment of 'RMR' and 'Q' and 'GSI' in selected tunnel sections are shown in Figure 5.27 & 5.28. It is worth to be noted that, RMR has been estimated directly from the tunnel sites and related core samples, and the other rock mass classifications including, Q and GSI have been measured via related converting equations which can be found in Singh & Goel (2011). Detailed engineering geological mapping, geological logging of drill holes, rock mass permeability values, in-situ testing, and laboratory test results, rock mass was evaluated in which the variations of respected UCS and RQD_0 regarding to each tunnel sections are presented in Figures 5.29 to 5.32 respectively. Also, machine performance data and operating parameters (such as applied thrust, RPM, torque, etc.) were recorded continuously and analysed separately. The respected ROP, total thrust, and RPM of selected bored tunnel sections for each tunnel are presented in Figure 5.33 & 5.34.

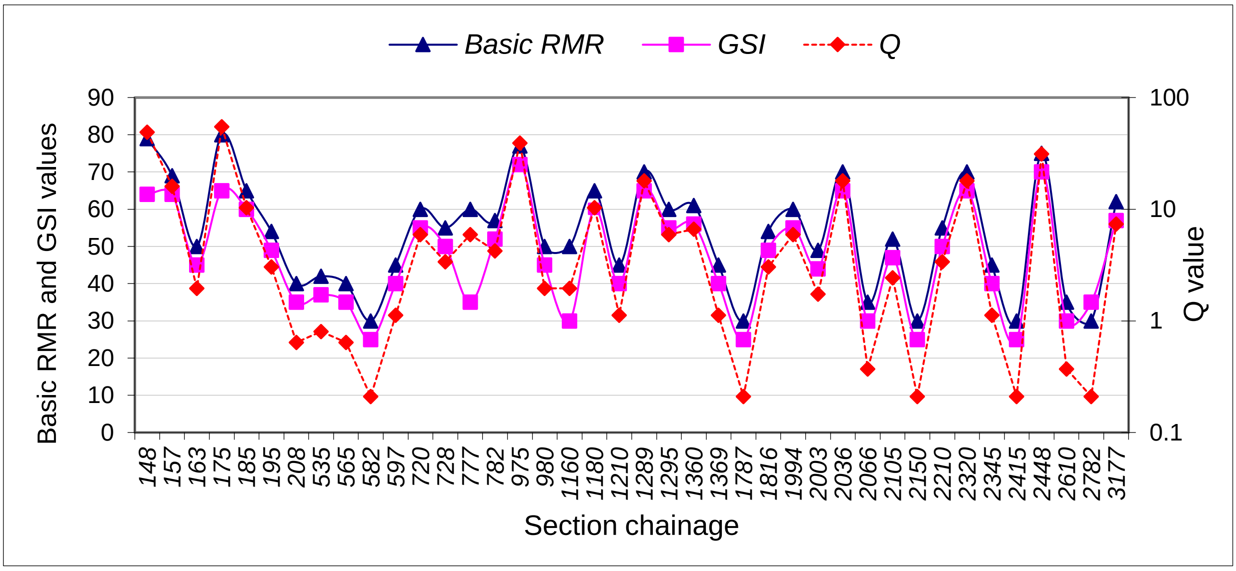

Figure 5.27: Variations of basic RMR, GSI & Q value in selected tunnel sections in Maroshi to vent hole Tunnel

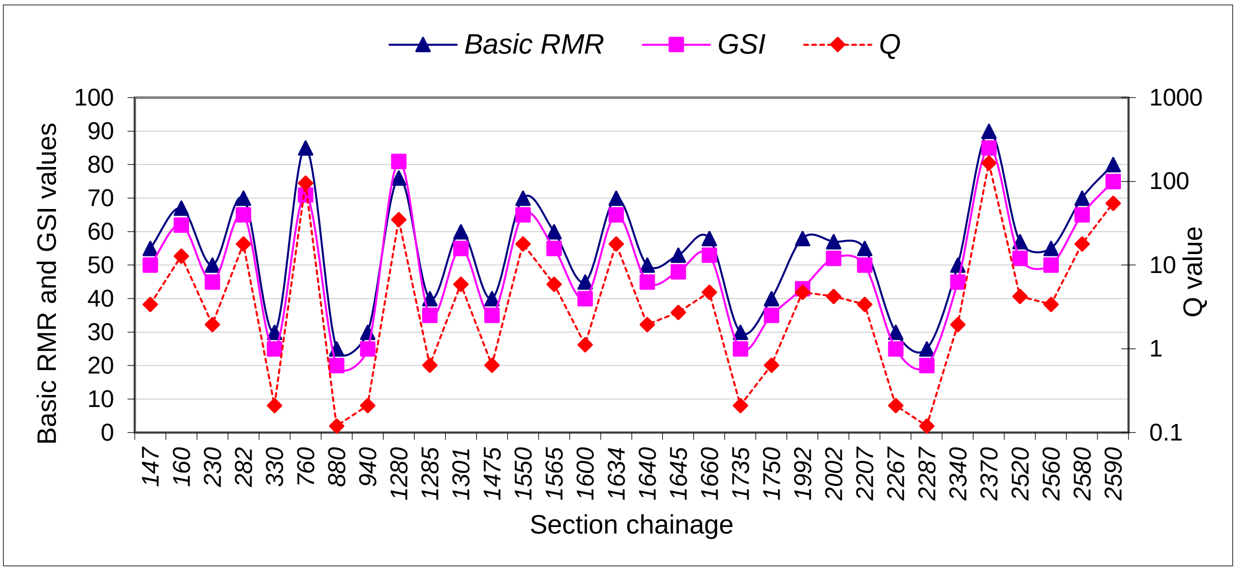

Figure 5.28: Variations of basic RMR, GSI & Q value in selected tunnel sections in Vakola to vent hole Tunnel

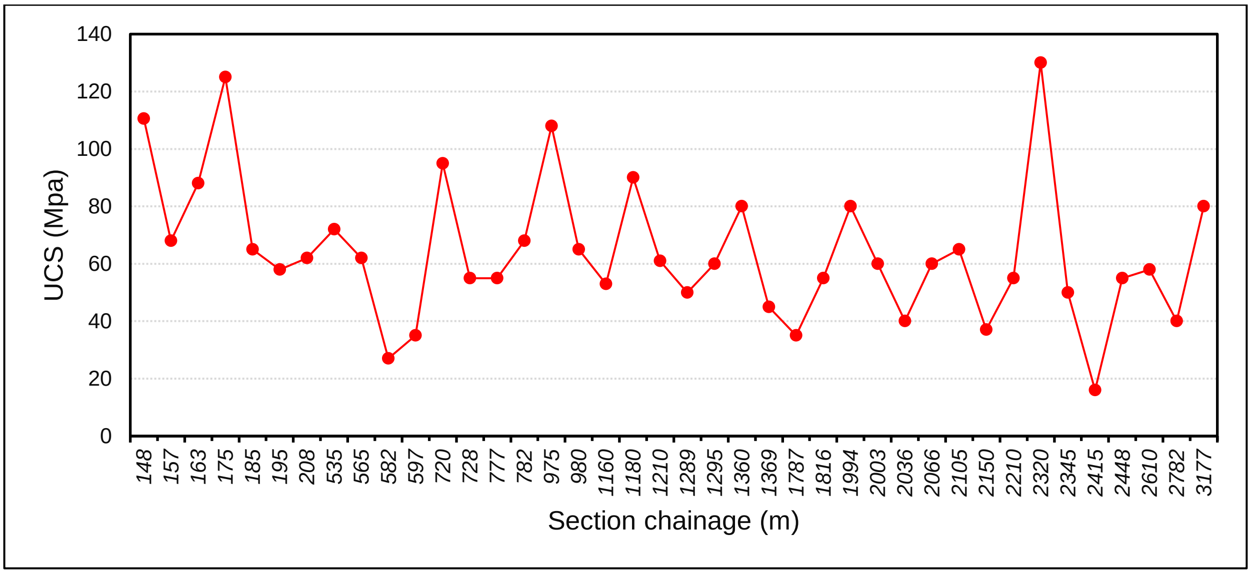

Figure 5.29: Variations of *UCS* in selected tunnel sections in Maroshi to vent hole Tunnel

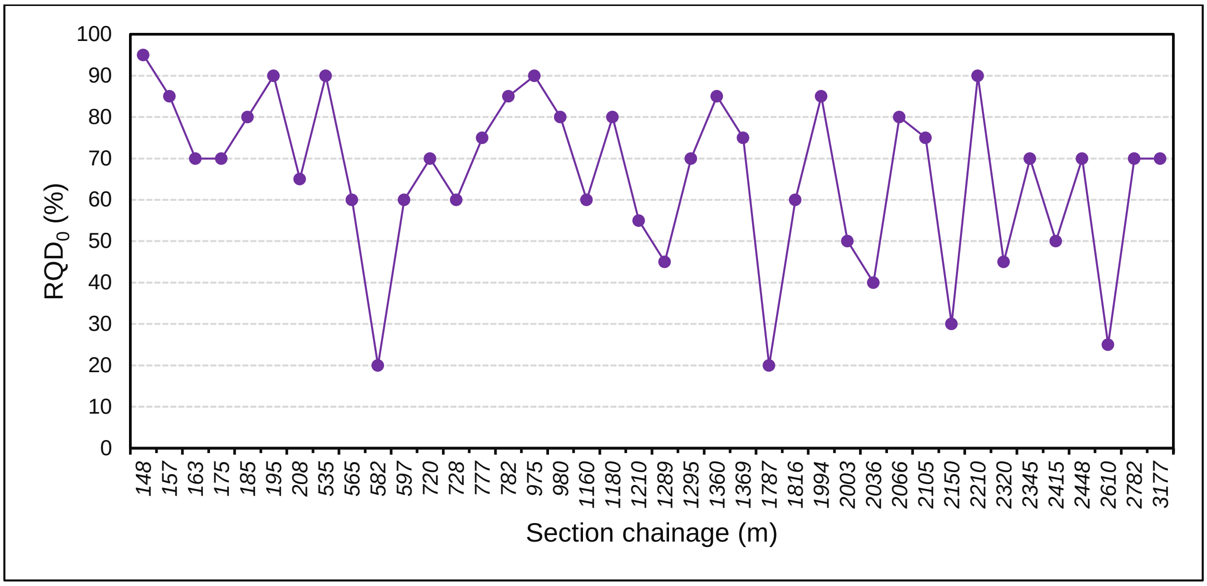

Figure 5.30: Variations of RQD_0 in selected tunnel sections in Maroshi to vent hole Tunnel

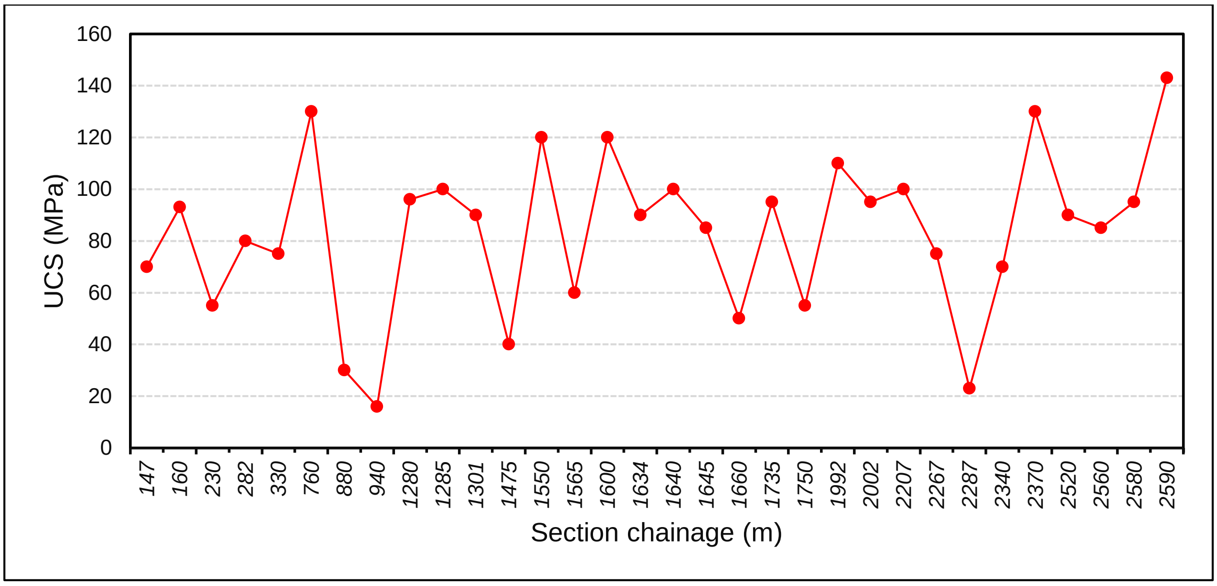

Figure 5.31: Variations of UCS in selected tunnel sections in Vakola to vent hole Tunnel

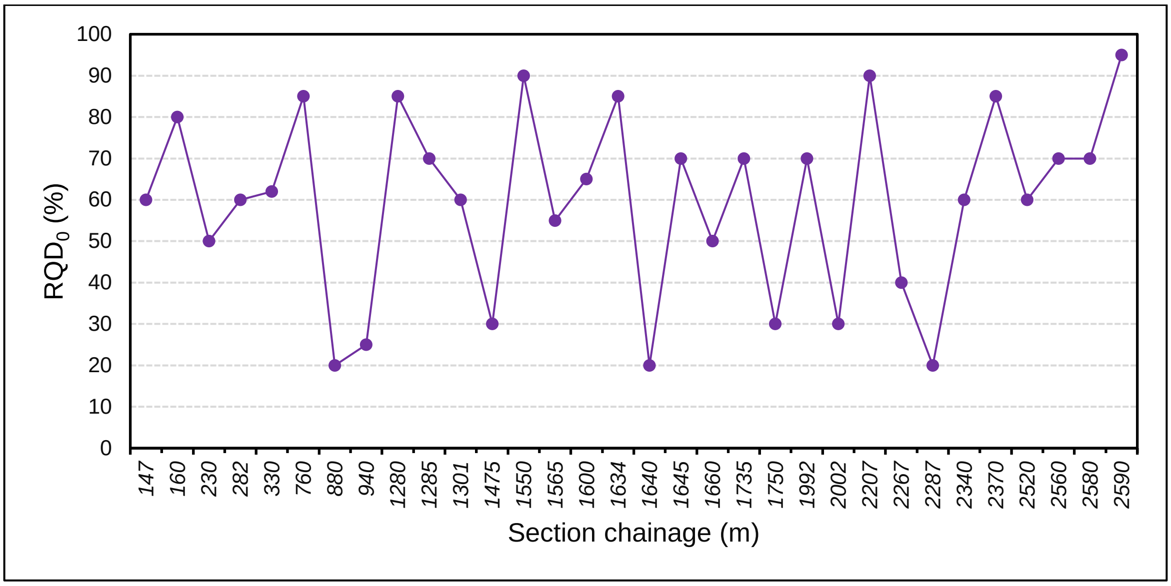

Figure 5.32: Variations of RQD_0 in selected tunnel sections in Vakola to vent hole Tunnel

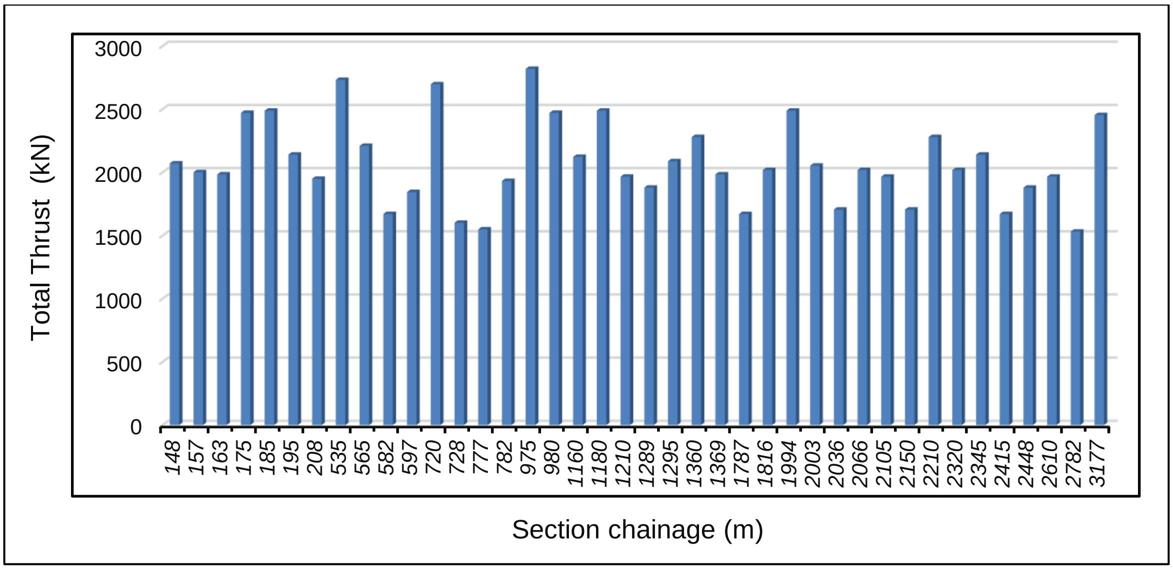

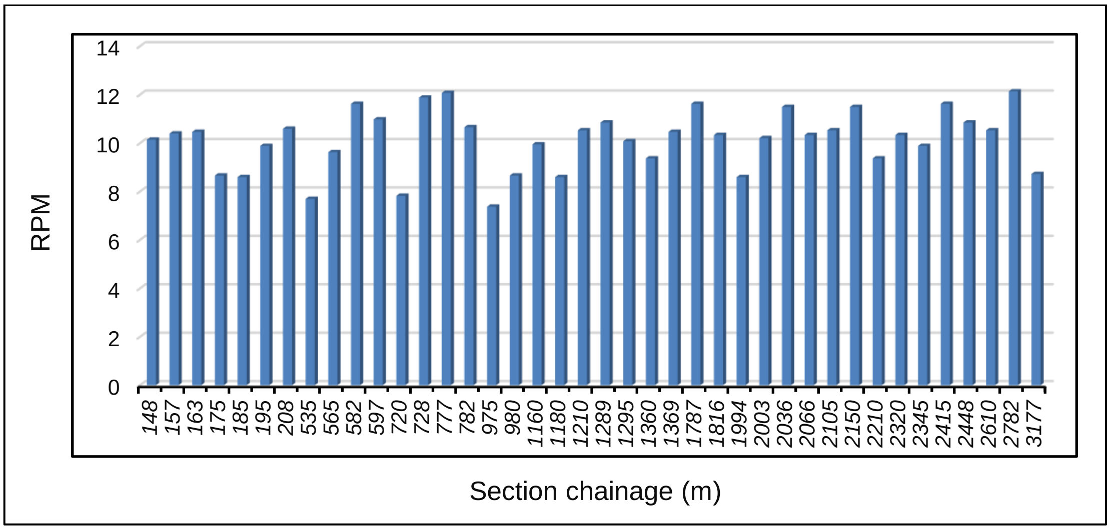

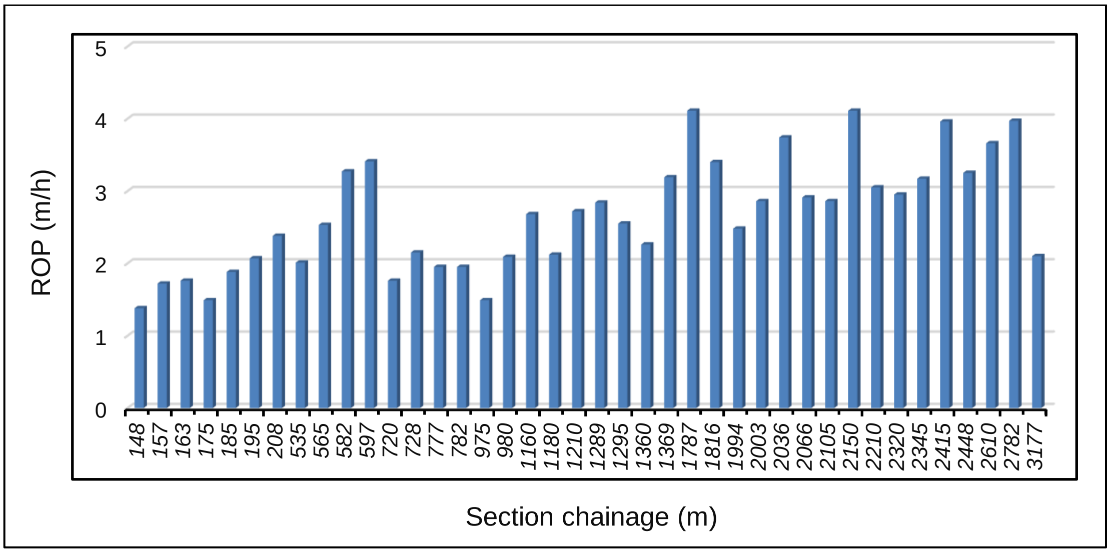

Figure 5.33: Variations of total thrust, RPM and ROP in selected tunnel sections in Maroshi to vent hole Tunnel

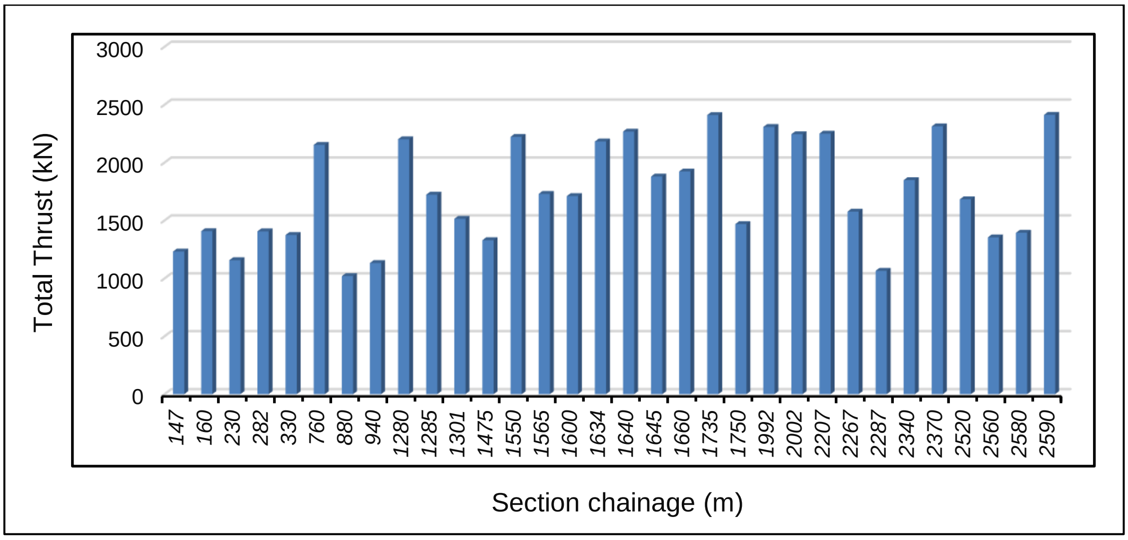

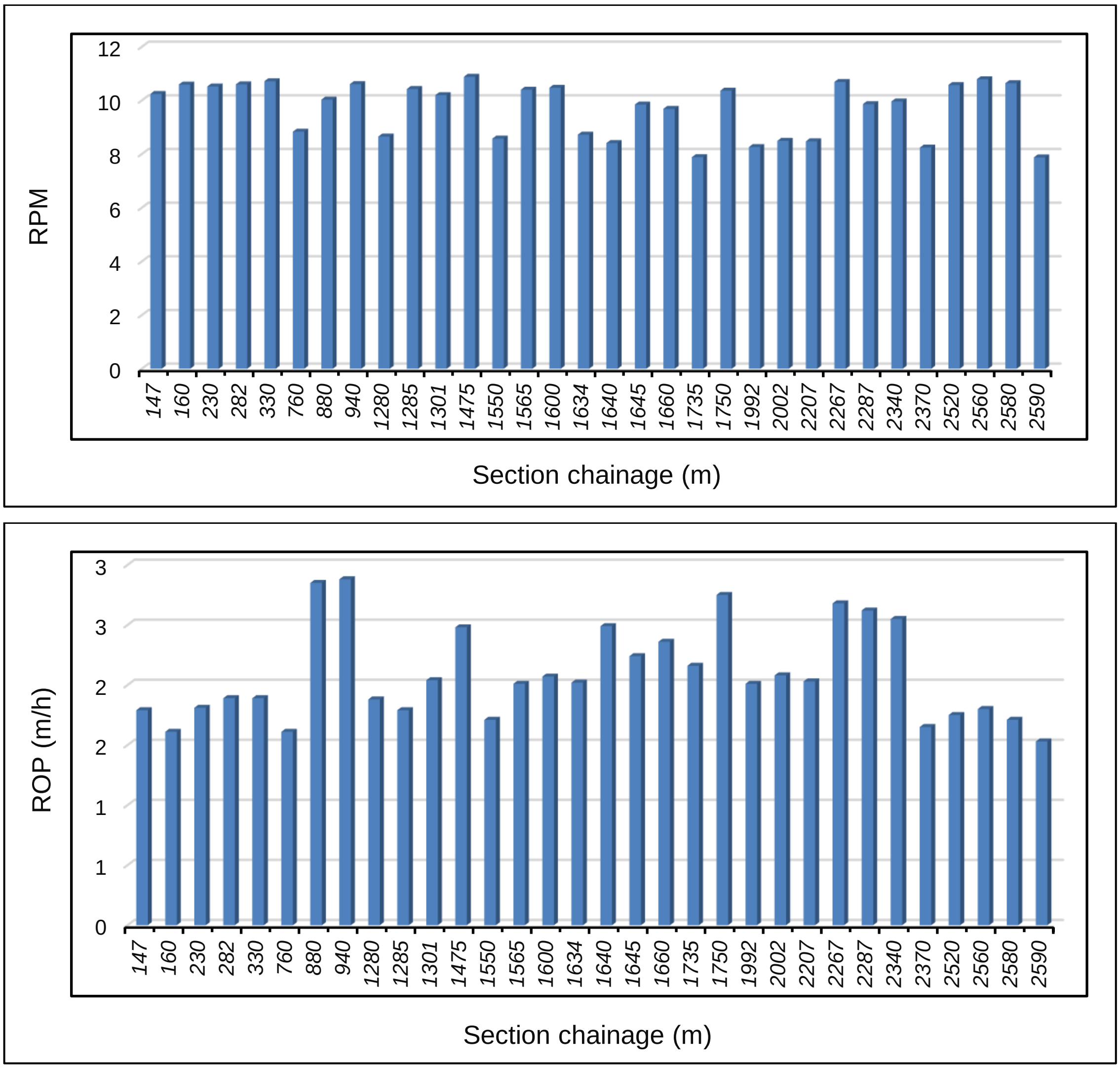

Figure 5.34: Variations of total thrust, RPM and ROP in selected tunnel sections in Vakola to vent hole Tunnel

5.2.6 Manapouri Second Tailrace Tunnel

The Second Manapouri Tailrace Tunnel (SMTT), located in the Fiordland region of Southern New Zealand (5.35), was constructed between 1997 and 2002 as part of a 700 MW hydropower project of Meridian Energy Ltd, New Zealand (Deere et al., 2004; Maidl et al., 2008; Papke and Heer, 1999; Delisio, 2014). The 9.6 km long, 10 m diameter tunnel was constructed near an existing tailrace tunnel (Tunnel No. 1) to increase the power output of the existing Manapouri Power Station. With the exception of a few hundred meters at either portal, a TBM was used to excavate Tunnel No. 2 (Watts et al. 2003). The tunnel connects the existing power station at Lake Manapouri to the outlet portal located in the "Deep Cove Area", formed by a low relief delta of the Lyvia River.

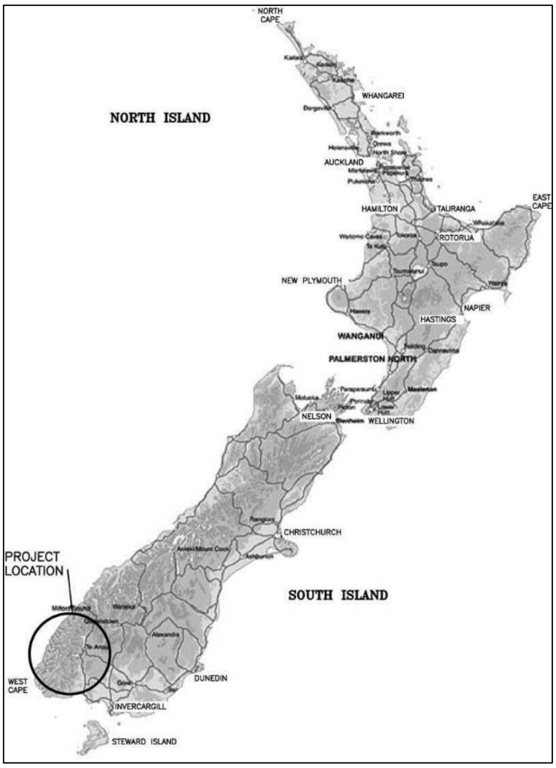

Figure 5.35: Location of the Second Manapouri Tailrace Tunnel (SMTT) project (Deere et al. 2014)

As shown on the geological profile in Figure 5.36, the TBM part of the tunnel was subdivided into four reaches during the design phase.

- Reach 1 (1’770 m long, from Tm 10+00 to Tm 27+70) was excavated in mixed meta-sediments, primarily consisting of non-banded and banded gneiss and inter-bedded meta-sedimentary calc-silicate rocks.
- Reach 2 (2’530 m long, from Tm 27+70 to Tm 53+00) consists of hard rock such as gabbro/diorite and diorite gneiss, but also contains banded gneiss with some inter-bedded calc-silicate rocks.
- Reach 3 (1’880 m long, from Tm 53+00 to Tm 71+00) is mainly constituted by banded gneiss, amphibolite, and amphibolite-gneiss with only minor amounts of pegmatite and granite.
- Reach 4 (3’600 m long, from Tm 71+00 to Tm 107+00) intercepts banded and non-banded massive gneiss with inter-layers of calc-silicate and intruded pegmatite and granite, which are more prevalent in this reach.

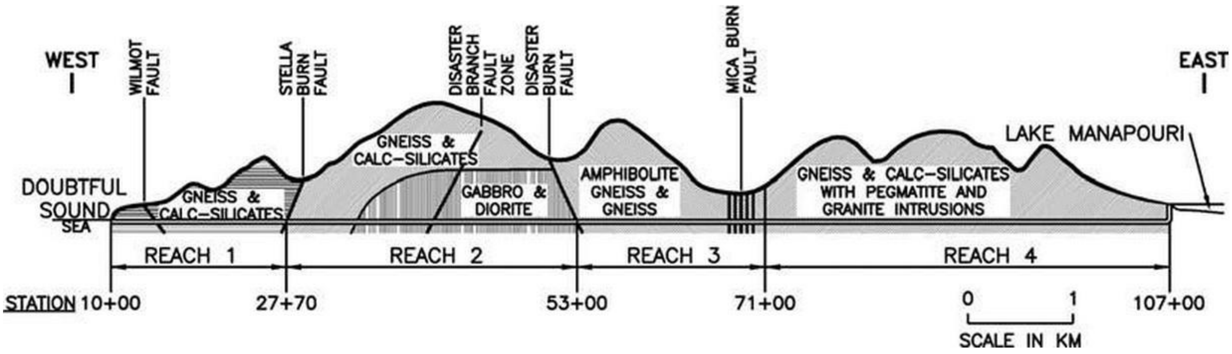

Figure 5.36: Geological longitudinal profile along the SMTT (Delisio, 2014)

The surface geology along the tunnel alignment is shown in Figure 5.37. Several large, regional-scale faults were identified from the construction of Tunnel No.1 and from surface geological mapping. From the west portal at Deep Cove, towards the east portal at Lake Manapouri, a first fault zone of crushed and sheared rock, named “Wilmot Fault” is encountered between Station 14+52 and 15+04 (Reach 1). The “Stella Burn Fault” is then met at Station 26+95. It consists of a zone of blocky/seamy rocks cut by several sheared zones over a length of approximately 90 m. After around 1’300 m, the “Disaster Branch Fault” is encountered. It can be described as a wide fault zone consisting of crushed/sheared/shattered rock with a well-defined hanging wall striking approximately 45° off the tunnel alignment. The “Disaster Burn Fault” is located in Reach 3 and intercepts Tunnel No.2 for around 14 m between Station 54+14 and 54+28. It is formed by sheared and crushed material, representing the poorest conditions found in Tunnel No.2. Finally, the last major fault named “Mica Burn Fault” is encountered between Station 67+04 and 68+24. Although this is the largest fault zone encountered, it was characterized by relatively good tunnelling conditions (Delisio 2014; Watts et al. 2003; Deere et al. 2004).

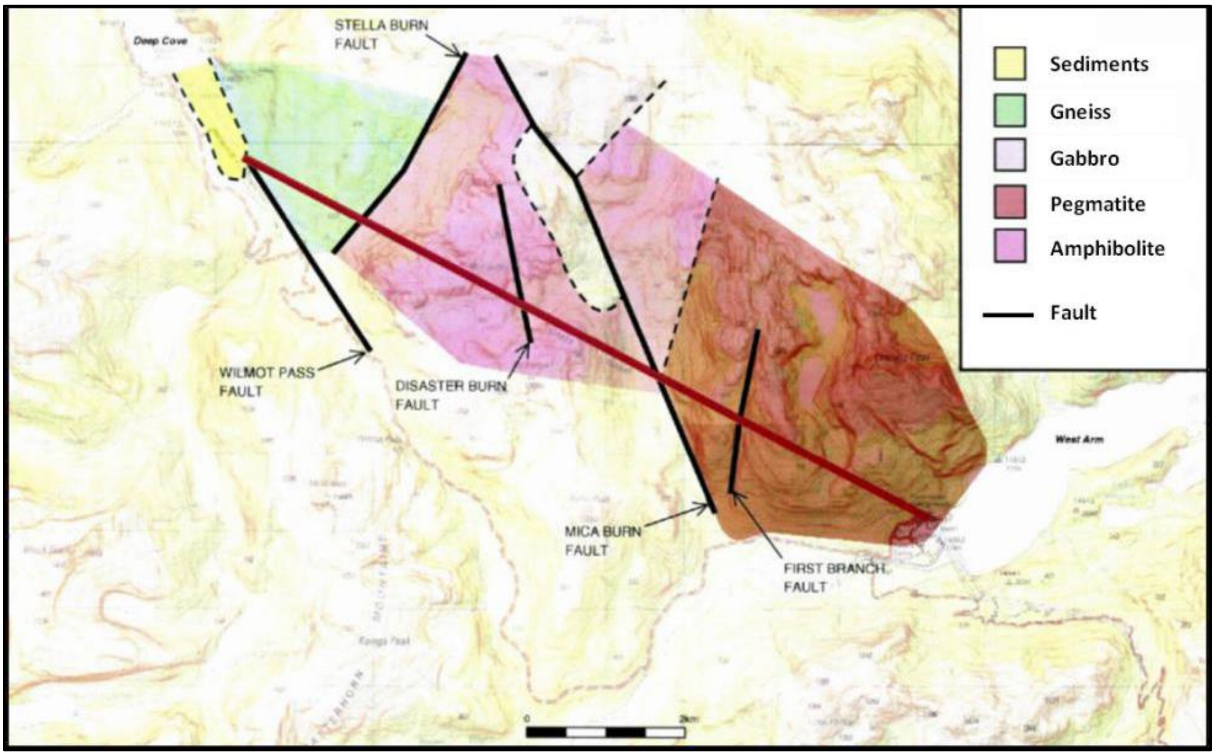

Figure 5.37: Surface geology along the SMTT alignment (Delisio, 2014)

The rock encountered along the tunnel alignment includes, gneiss with an average *UCS* of 140.1 MPa and ranging from 45 to 379 MPa. Gneiss was the dominant rock type in the tunnel (5.175 m or 83%). Also, the fine-grained gneiss makes up nearly 20% or 354 m of the rock excavated in Reach 1 and 8.8% or 223 m of rock excavated in Reach 2. The calc-silicates is around 730 m or 7.5% with the average *UCS* of 171 MPa and ranged from 41 to 309 MPa. Another rock type is Amphibolite with an average *UCS* of 131 MPa which ranged from 20 to 273 MPa. This rock type was present in the tunnel for 920m or 9.5%. Besides that, pegmatite with the average *UCS* of 174 MPa and ranging from 50 to 225 MPa presents 950 m or 9.7% of the excavated rock in the tunnel. Another rock type is gabbro/diorite with an average *UCS* of 161 MPa which ranged from 89 to 228 MPa. 1988 m or 20.2% of the tunnel excavated in this rock type (Deere et al. 2004; Watts et al. 2003). A summary of the mechanical properties of the rocks encountered at the SMTT is reported in Table 5.17, in terms of uniaxial compressive strength (σ_C) and Brazilian tensile strength (σ_t). A Robbins gripper TBM of 10.05 m diameter was used for tunnel excavation. The main machine specifications are listed in Table 5.18.

Table 5.17: Intact rock parameters in each reach of the SMTT (Watts et al. 2003; Delisio, 2014)

Rock type	σ_C **(MPa)**			σ_t **(MPa)**		
	N. of test	**Mean**	**S.D.**	**N. of test**	**Mean**	**S.D.**
Gneiss	295	140.1	49.7	283	9.8	3.3
Calc-silicate	58	171	64.9	43	8.4	3.6
Pegmatite	41	174	53.8	32	8.3	3.2
Gabbro/Diorite	70	161	32.8	59	8.9	2.2
Amphibolite	63	131	52.6	59	8.8	3.6

Table 5.18: Main specifications of the SMTT TBM (Deere et al. 2004)

Parameter	**Value**
Machine diameter	10.5 m
Recommended normal operating force	18156 kN
Max. Thrust	27101 kN
Number of disc cutters	68
Cutterhead Speed (RPM)	5.07
Max. Torque	9860 kNm
Cutter diameter	17" (432 mm)
Nominal cutter spacing	90 mm
Cutterhead power	3465 kW (11*315 kW)
Thrust cylinder stroke	1.83 m
Conveyor capacity (approx.)	1500 ton

The field data collected at the Second Manapouri Tailrace Tunnel (New Zealand) has been included in a TBM performance database. The compiled TBM performance database is subdivided into two parts. The first one includes some TBM performance parameters such as the penetration per revolution (P), the TBM boring time (t_{boring}), the rate of penetration (ROP), and the average of some other TBM operational parameters, such as the applied thrust force, torque, and RPM, which were registered by the onboard TBM data acquisition system. The second category of data includes the geological/geotechnical parameters obtained from site investigation and laboratory testing. These comprise some intact rock parameters, such as uniaxial compressive strength (UCS), Brazilian tensile strength (BTS), and some rock mass parameters such as joint spacing, *RQD*. The Rock Mass Rating (RMR), the Rock Quality Index (Q), and the Geological Strength Index (GSI) have also been back-calculated (Watts et al. 2013; Hassanpour, 2009; Hassanpour et al. 2011; Delisio, 2014). Figure 5.38 shows the average of basic RMR, Q, and GSI in some selected tunnel sections.

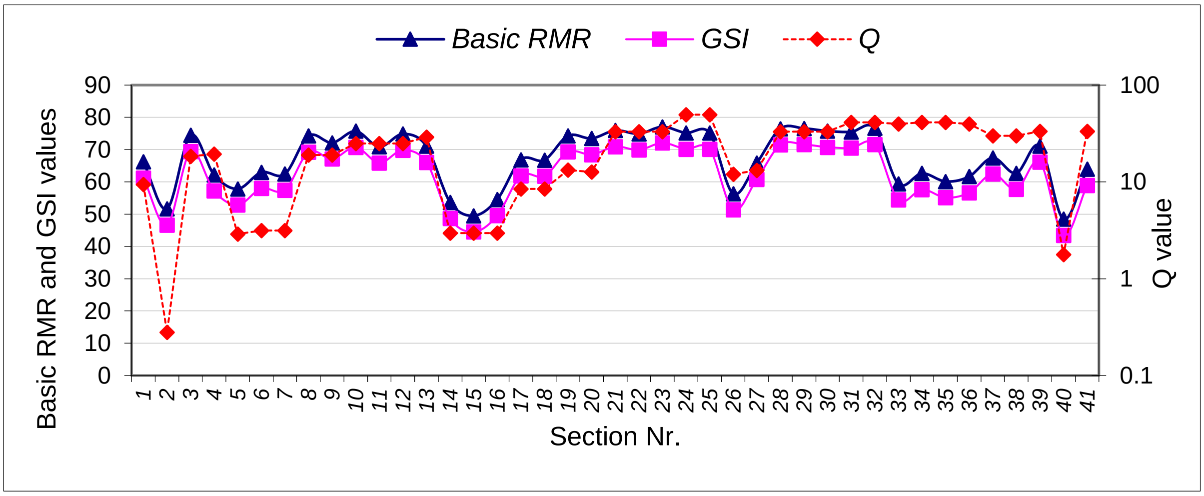

Figure 5.38: Variations of basic RMR, GSI & Q value in some selected tunnel sections in SMTT

Besides that, variations of respected *UCS* and *RQD* regarding to some selected tunnel sections in SMTT are depicted in Figures 5.39 & 5.40 respectively. Also, the average of thrust force, RPM, and ROP associated with some selected tunnel sections are illustrated in Figure 5.41.

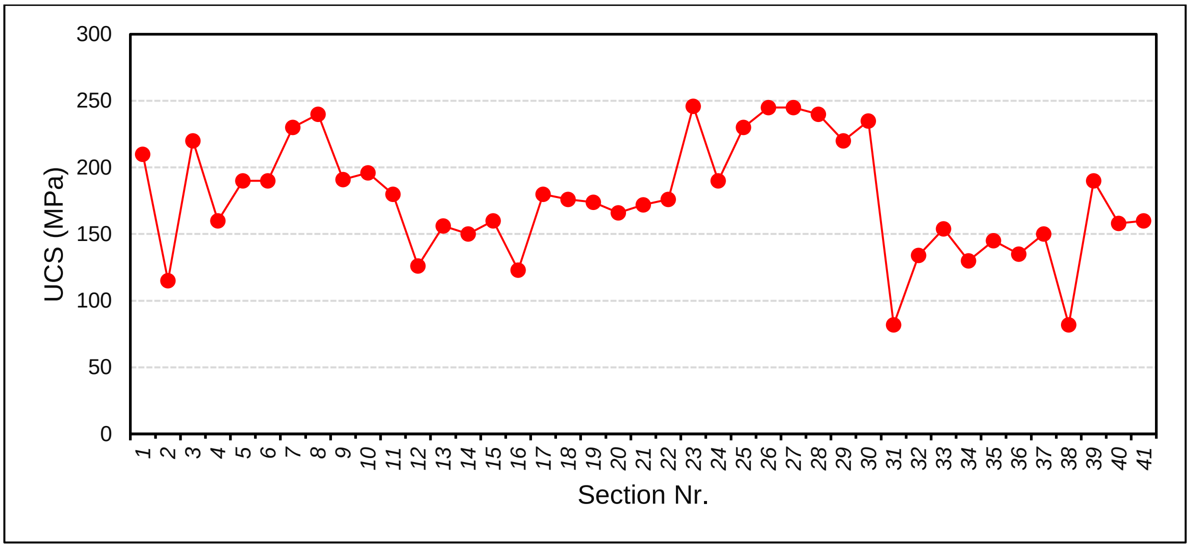

Figure 5.39: Variations of *UCS* in some selected tunnel sections in SMTT

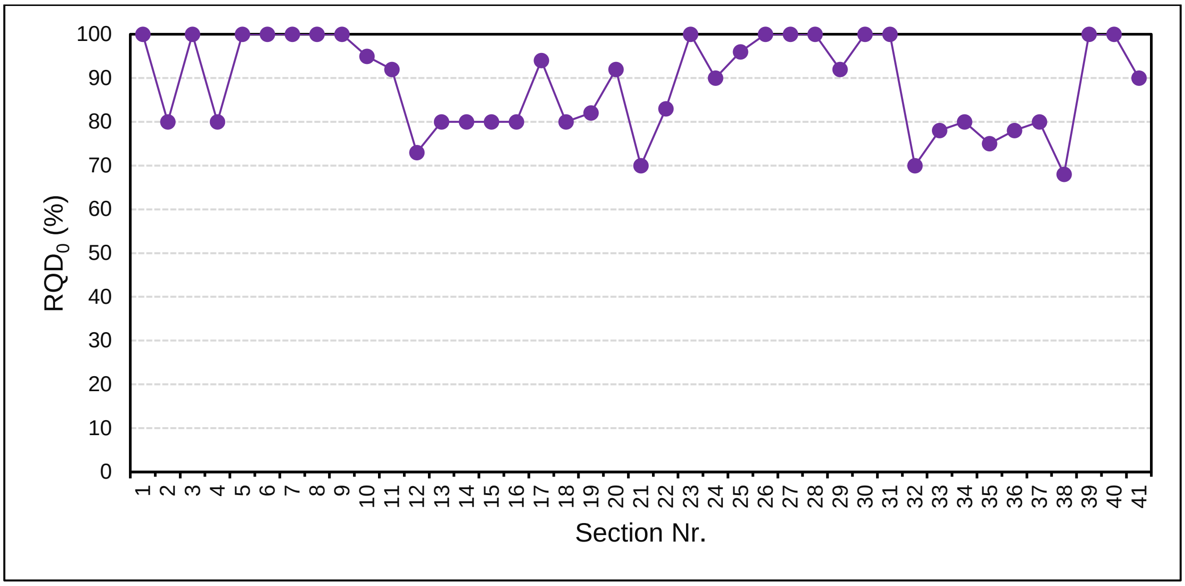

Figure 5.40: Variations of RQD_0 in some selected tunnel sections in SMTT

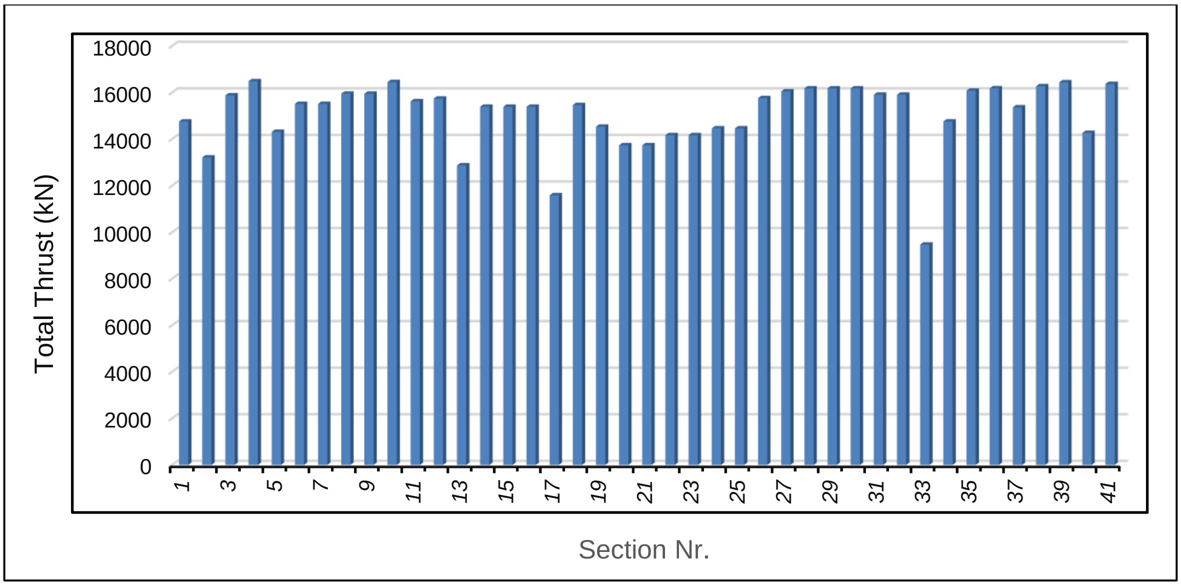

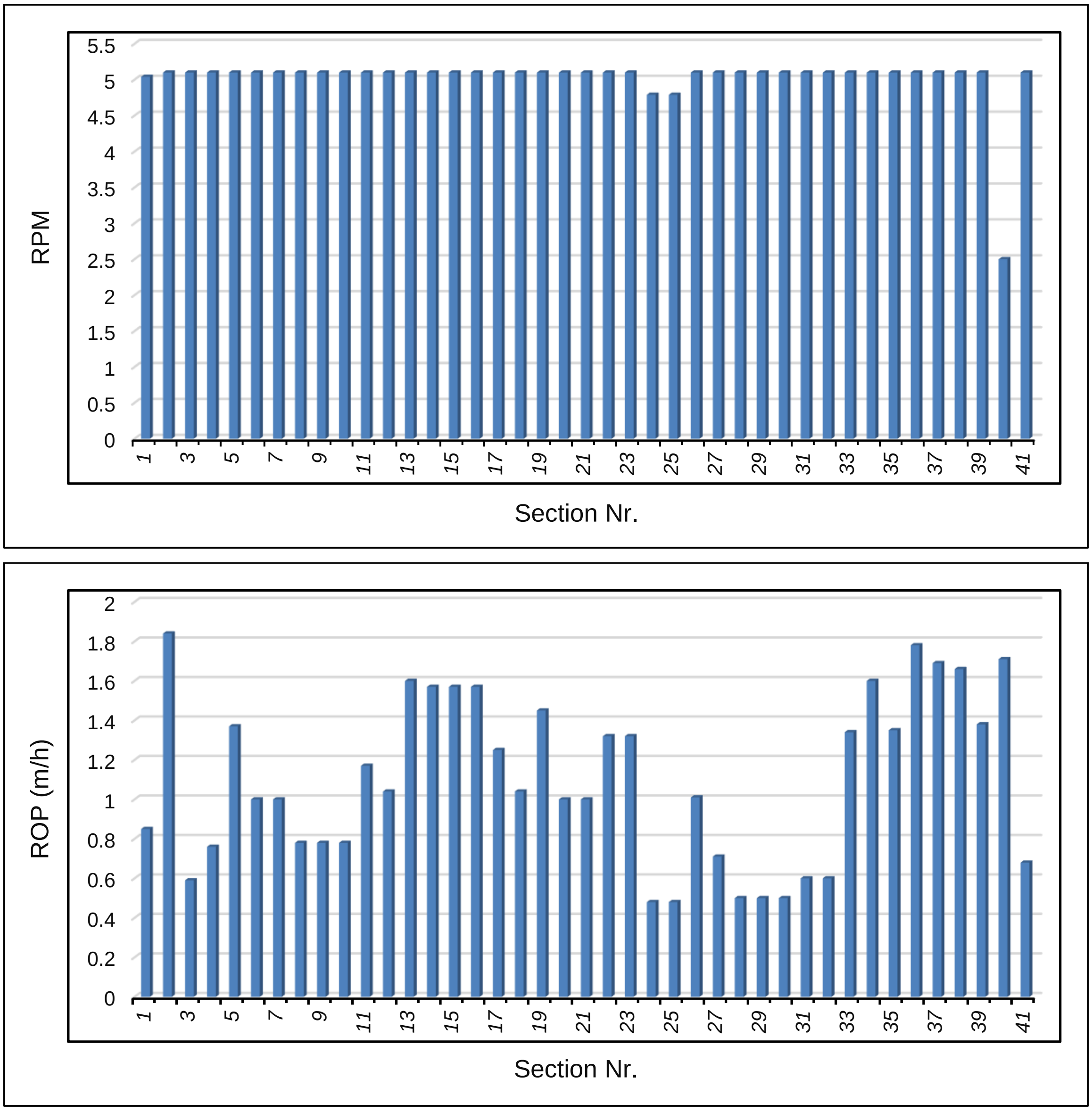

Figure 5.41: Variations of total thrust, RPM & ROP in some selected tunnel sections SMTT

5.2.7 Lötschberg Base Tunnel

The Lötschberg Base Tunnel (LBT) is part of the so-called New Rail Alpine Routes project (NEAT in German) whose objective is to modernize the Swiss railways and to switch heavy traffic from road to rails. The NEAT, with a budget of about 30 billion Swiss francs, consists of the Lötschberg Base Tunnel, the Gotthard Base Tunnel, and the Ceneri Tunnel (Figure 5.42).

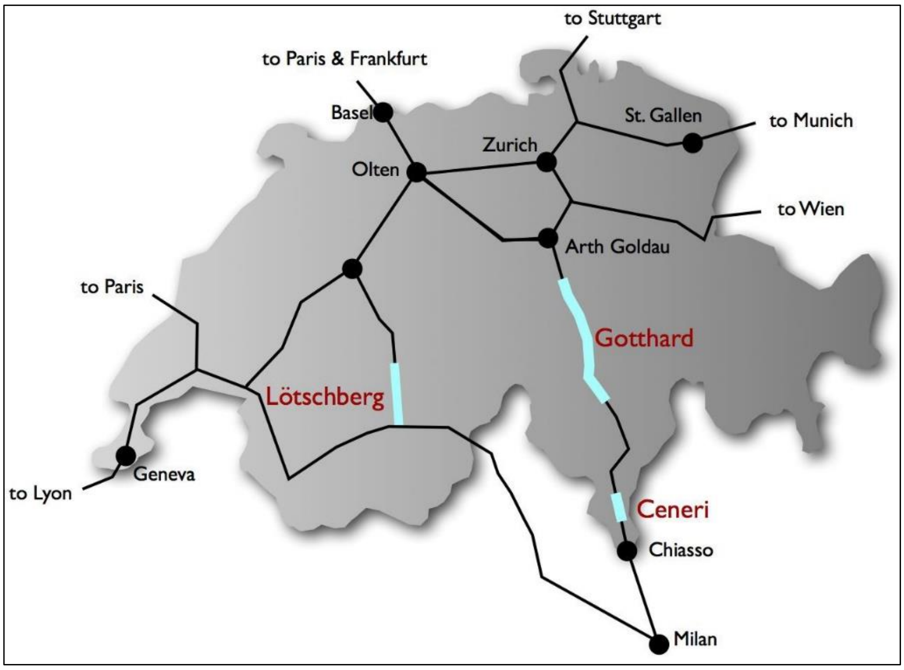

Figure 5.42: Overview of the NEAT project with location of the Lötschberg Base Tunnel, the Gotthard Base Tunnel, and the Ceneri Tunnel (Delisio, 2014)

The LBT was the first work of the project and was constructed between 1999 and 2006. It is a high-speed railway tunnel linking Frutigen in the Kander Valley and Raron in the Rhône Valley (Figure 5.42). Combined with the Simplon Tunnel (constructed between 1904 and 1919), the LBT provides a direct link between Germany and Italy through Switzerland. The LBT is 36.4 km long and consists, in most parts, of two tubes with a separation of 40 m, linked at every 333 m through transversal bypasses. The southern part of the LBT, for a total length of about 18.5 km, has been excavated by two gripper TBMs with a diameter of 9.43 m. The first machine started to excavate at the Steg lateral adit before reaching the main west tube after around 3 km. From this point on (Lötschen link), the TBM proceeded along the main route for around 6 km up to Ferden. The second machine directly started with the excavation of the main east tube (Raron Sector) and, starting from Raron, it proceeded towards north for around 10 km. The main construction sections of the LBT are represented in Figure 5.43.

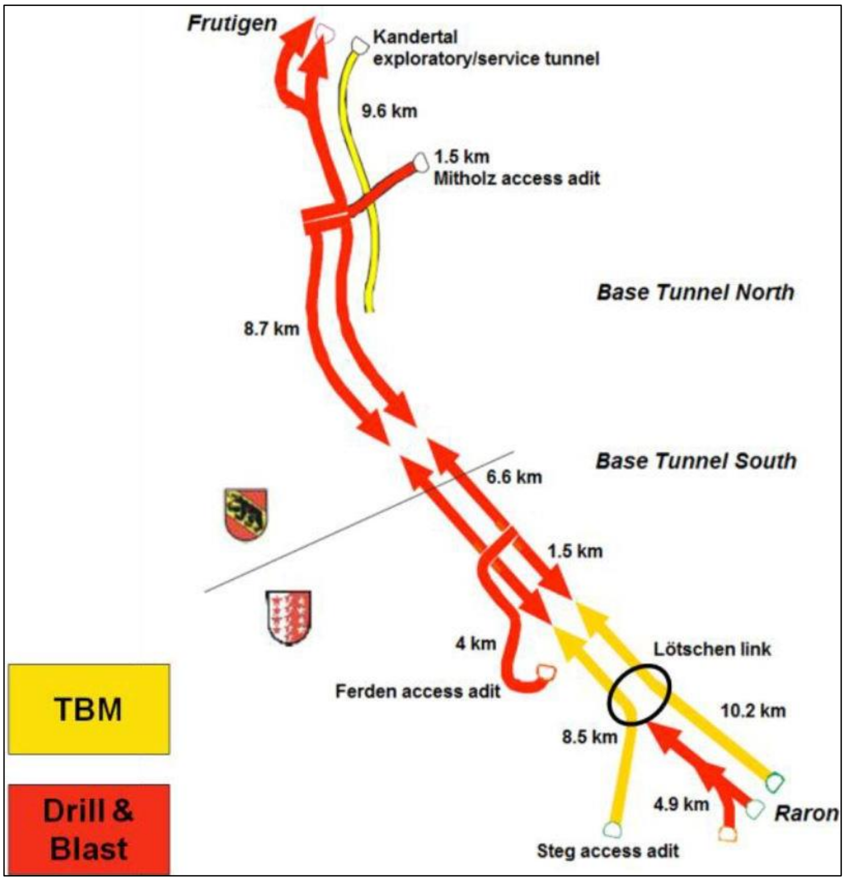

Figure 5.43: Main construction sections of the LBT and indication of the adopted excavation method (Delisio, 2014)

The southern part of the LBT, excavated by TBMs, is located in two distinct tectonic formations called Autochthon Gampel-Baltschieder and Aar Massif. These are, respectively, composed of sedimentary and crystalline rocks. As presented in Figure 5.44, moving from south (right) to north (left), the first part of the tunnel is intersected by a zone of loose rock which precedes the southern old crystalline sector "SOC" of the Aar Massif. This is composed by crystalline gneiss and shows a well-defined folded structure. After around 500 m from the portal, a complicated Triassic folded zone "Tr", mainly composed of dolomite, schist, and gypsum, starts. This area is then followed by the Autochthon Gampel-Baltschieder, composed of several lithological units: the Lias zone "Li" (limestone and shale), the Dogger zone "Dog" (slate, limestone, and marl) and finally the Malm zone "Ma" (limestone). Large-scale folds characterize this part of the rock mass (Delisio 2014; Ziegler et al. 2008). After about 2800 m from the south portal, the contact between the Autochthon Gampel-Baltschieder and the Aar Massif is met. This contact between sedimentary and crystalline rocks represents the major tectonic disturbance of the region named Rote Kuh – Gampel fault. From this point on, the excavation proceeded into the Aar Massif, which is formed by three main lithological units: the Baltschieder granodiorite “BG” (gneiss and granodiorite), the Central Aar granite “CAG” (fine to coarse-grained granite), and the northern old crystalline sector “NOC” composed of amphibolite, granitic – gneiss, and massive/schistose gneiss, the latter containing different proportions of sericite, biotite, and chlorite. The depth of cover along the alignment increases from 0 to 1950 m, reaching its maximum in the granitic gneiss at Tm 5600 from the south portal (Raron). Consequently, the in-situ stresses can be substantial (Delisio, 2014; Delisio et al. 2013; Ziegler et al. 2008).

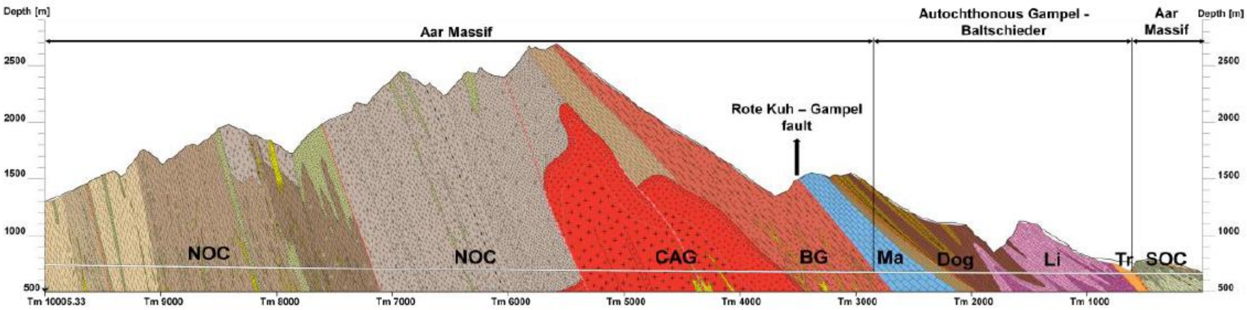

Figure 5.44: Longitudinal geological profile along the main southern Lötschberg Base Tunnel axis (Delisio, 2014); SOC = southern old crystalline; Tr = Trias zone; Li = Lias zone; Dog = Dogger zone; Ma = Malm zone; BG = Baltschieder Granodiorite; CAG = Central Aar Granite; NOC = northern old crystalline sector

The Steg lateral adit is located in the Autochthon Gampel-Baltschieder and the Aar Massif, and is connected to the main tunnel axis at Tm 3059 from the south-west portal (Figure 5.45). Moving from south to north in the access tunnel, the sediments of the Autochthon Gampel-Baltschieder (Malm zone “Ma” and Dogger zone “Dog”) are first met. Around Tm 600 from the Steg portal, the Rote Kuh – Gampel fault is again encountered and the Aar Massif begins with the Baltschieder granodiorite zone “BG”. The Central Aar granite “CAG” is finally encountered in the northern part, around Tm 2000. The maximum overburden depth along this route is 1330 m (Delisio, 2014; Delisio et al. 2013).

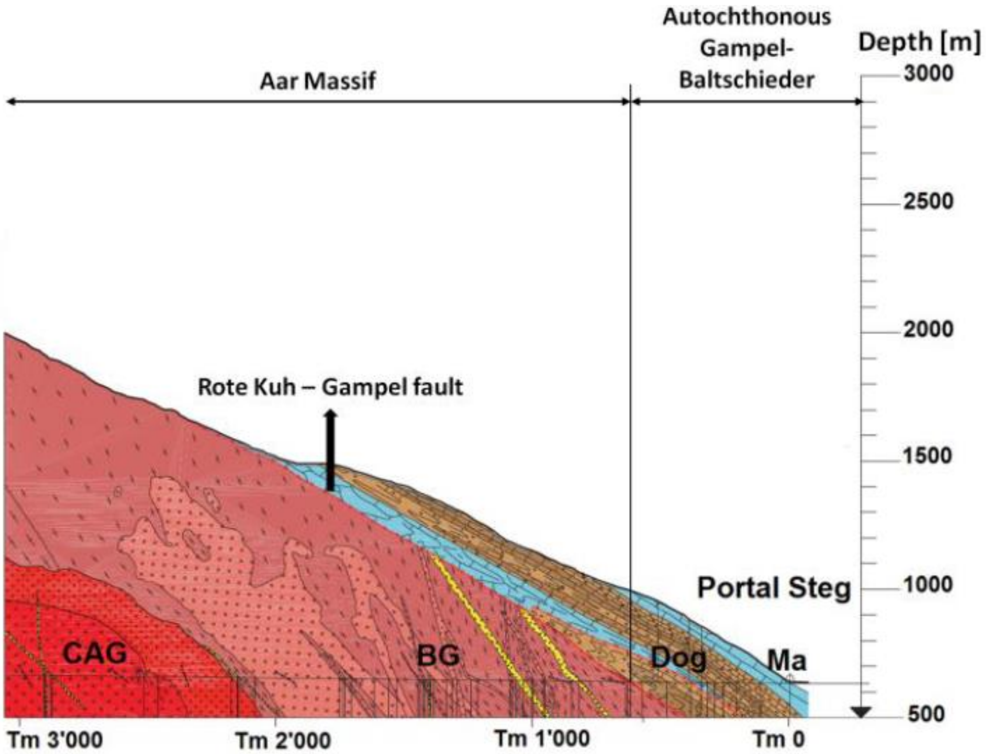

Figure 5.45: Longitudinal geological profile along the Steg lateral adit (Delisio, 2014); Dog = Dogger zone; Ma = Malm zone; BG = Baltschieder Granodiorite; CAG = Central Aar Granite

A summary of the mechanical properties of the intact rock found along the tunnel alignment is reported in Table 5.19. For the four main rock types, the mean uniaxial compressive strength (σ_C) ranges between 100 and 220 MPa, the mean Brazilian tensile strength (σ_t) between 11 and 19 MPa, approximately, and the mean Cerchar Abrasiveness Index (CAI) between 3.3 and 5.2. This generally defines the excavated material as a very strong and highly abrasive rock. In the case of rocks with well-developed foliation (banded gneiss and schistose gneiss), the foliation planes lead to rock anisotropy, causing a variation of the uniaxial compressive strength of the intact rock along with different loading directions. At the tunnel level, the direction of loading is defined by the angle between the tunnel axis and the weak structural planes. In most cases, this angle ranged between 60° and 70°, causing the uniaxial compressive strength to be reduced down to 30-50% of its maximum value, which occurs when the direction of loading is parallel to the foliation planes (Delisio 2014; Hassanpour, 2011; Singh et al. 1989). Two gripper TBMs manufactured by Herrenknecht were used to excavate the southern Steg and Raron lots of the LBT. The main machine specifications are listed in Table 5.20. The machine used in Raron was essentially the same.

Table 5.19: Average mechanical properties of the main rock types in the Aar Massif. σ_C = uniaxial compressive strength; σ_t = Brazilian tensile strength; CAI= Cerchar abrasiveness index (Delisio, 2014)

Rock type	**σ_C (MPa)**			**σ_t (MPa)**			**CAI (-)**		
	No. of test	**Mean**	**S.D.**	**No. of test**	**Mean**	**S.D.**	**No. of test**	**Mean**	**S.D.**
Old crystalline gneiss	26	107.7	29.4	16	11.4	1.7	25	3.3	0.6
Granodiorite and Granite	17	146.7	34.7	16	11.2	1.8	16	4.8	0.6
Granitic Gneiss	25	221.1	54.4	19	14.2	1.0	23	5.2	0.6
Amphibolite	5	184.3	46.3	4	18.7	1.1	6	3.8	0.1

Note: the uniaxial compressive strength of schistose rocks is measured perpendicular and parallel to the foliation planes

Table 5.20: Main specifications of the LBT TBMs (Raron / Steg TBMs) (Delisio, 2014)

Parameter	**Value**
Machine diameter	9.43 m
Max. Thrust force	16,000 kN
Max. Revolutions per minute (RPM)	6.00
Max. Torque	8825 kNm
Number of cutters	60
Cutter diameter	17" (432 mm)
Nominal cutter spacing	90 mm
Max. Cutter force	267 kN

The data compilation/dataset is composed of two main categories. The first one includes machine performance parameters recorded during the construction of the two main tubes and the Steg access adit. The principal data of this category are the actual penetration rate, the boring time, and the average of some machine operational parameters such as the total applied thrust force, the RPM, and the torque. The second category comprises geological/geotechnical parameters obtained from site investigations, laboratory tests, and tunnel perimeter/face mappings during construction. These data include rock mass jointing (described by both joint spacing and volumetric joint count), intact rock and rock mass properties (uniaxial compressive strength, Brazilian tensile strength, CAI, etc.), as well as the estimated rock mass classifications using Rock Mass

Rating (RMR), Tunneling Quality Index (Q) and Geological Strength Index (GSI). For instance, Figure 5.46 illustrates the variations of basic RMR, Q, and GSI in some selected tunnel sections, while Figure 5.47 shows the variations of respected thrust force, RPM, and ROP in some selected tunnel sections.

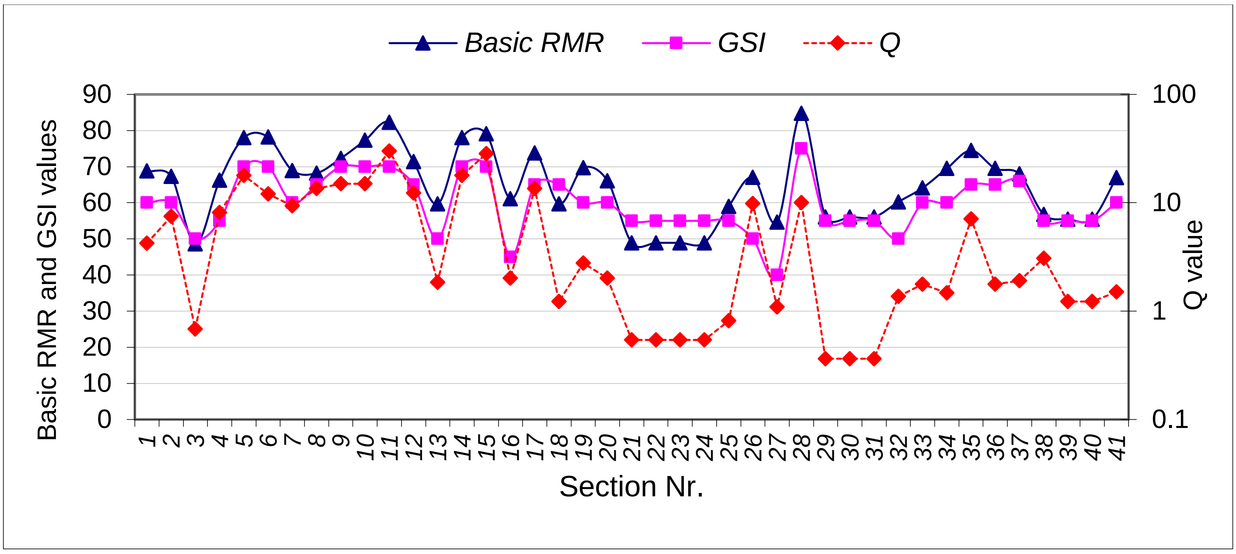

Figure 5.46: Variations of basic RMR, GSI & Q value in some selected tunnel sections in LBT tunnel

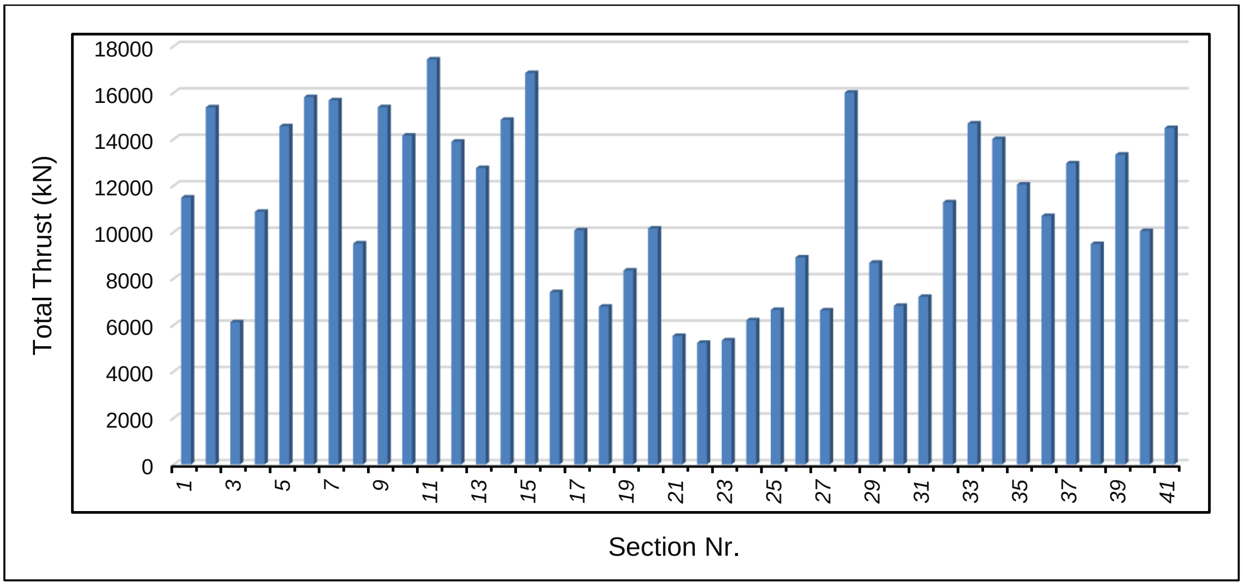

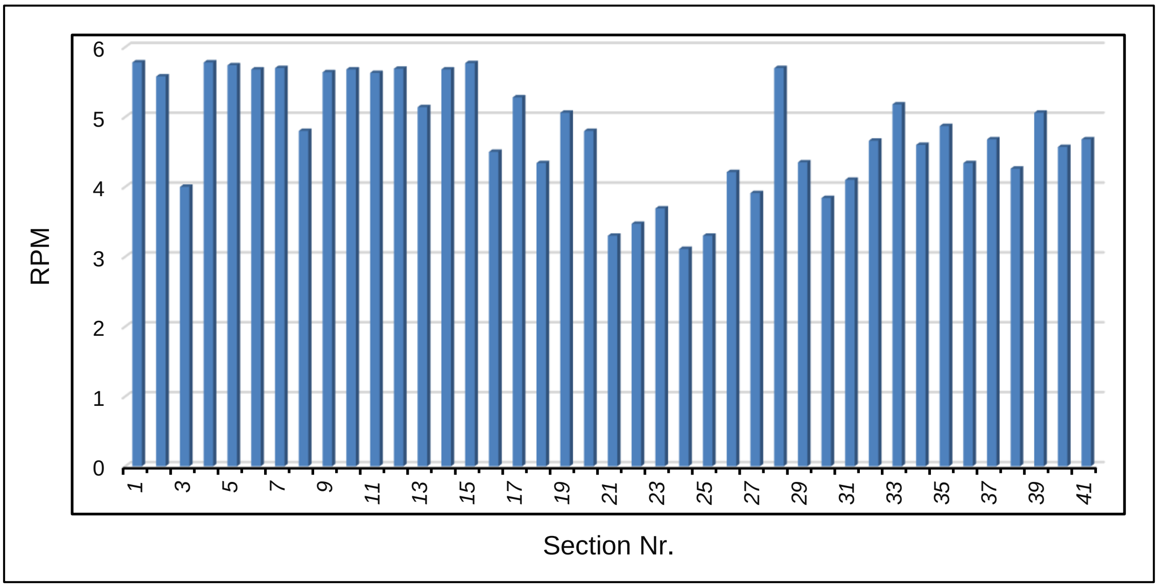

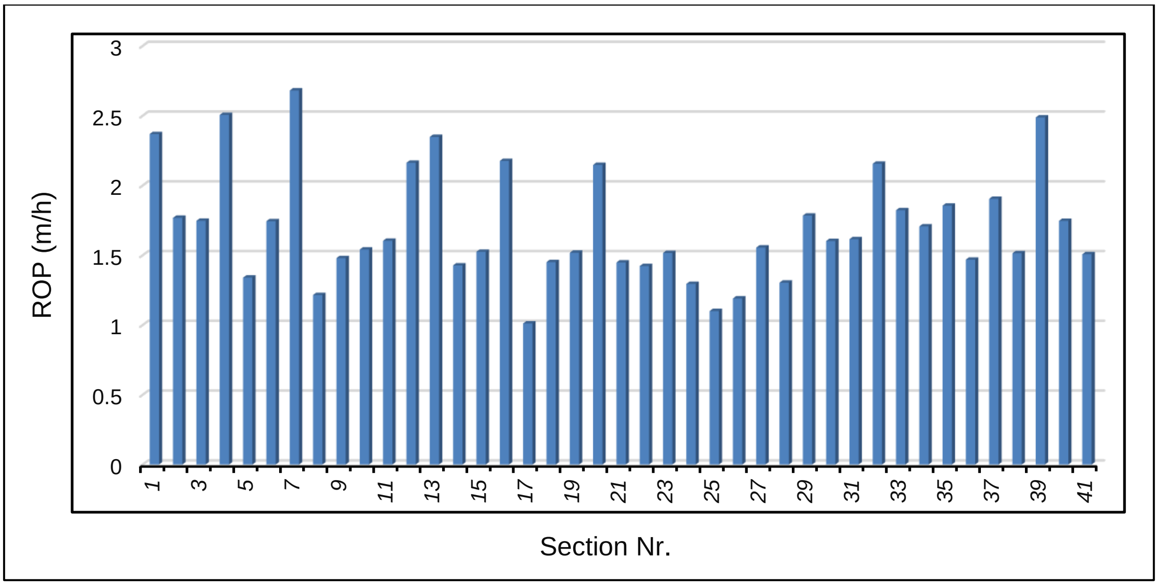

Figure 5.47: Variations of total thrust, RPM and ROP in some selected tunnel sections in LBT

5.3 Data Collection (TBM Field Performance Database)

In this study data on geological and ground conditions, TBM operational parameters, and machine performance represented by the rate of penetration were collected during pre-construction and construction phases. During the construction phase and through back-mapping of the tunnel, predicted geological and geomechanical properties of rock mass along the tunnels were examined by a detailed investigation of the tunnel face. During the construction phase and through back-mapping of the tunnel, predicted geological and geomechanical properties of rock mass along the tunnels were examined by a detailed investigation of the tunnel face. In this stage, information such as rock type, rock mass fracturing, joint condition, characteristics of fault zones, weathering/alteration characteristics, groundwater condition, and rock stability information were recorded on mapping sheets. In addition, during back-mapping of the tunnel, many samples were taken from the muck and tunnel face to perform tests such as point load index and petrographic analysis. In the construction phase, machine performance data, and operating parameters such as applied thrust, RPM, torque, and rate of penetration (ROP) were also recorded continuously in special sheets and analyzed separately. It is worth to be mentioned that, there were some limitations on the accessibility of geological features in the tunnels through the observation of the walls, notably in DS-TBMs. Therefore, an attempt was made into select parts of the tunnels where sufficient and reliable geological data were available. Data were collected from the following general locations within the tunnels:

- Locations where exploration borings extended to the tunnel level.
- Tunnels sections where the rock face was inspected during geological back-mapping.
- Places where extrapolation of surface geological parameters to tunnels level were possible with a high degree of reliability.

As would be expected, the format and the extent of reported TBM operational parameters and geological data varied significantly from project to project. As such, one important issue to be noticed in this process is the missing data for different parameters in different records. Due to the difficulty of dealing with volumes of detailed data in several separate databases for different projects, it was necessary to reduce the number of data sets to a manageable number. Heterogeneity of the data was also an issue which was caused by using different protocols for recording TBM performance data for different tunnel job sites.

In brief, the data for developing new models were organized in a special database including 580 (61.03 km) tunnel sections of seven selected projects where the ground conditions and machine performance were reliable and could be verified. A tunnel section is a part of the tunnel that has been excavated in a working shift and its two ends have been studied by direct observations and geological measurements, sampling, and laboratory tests. In this respect, the main data collected during the construction phase, include TBM performance parameters, operational parameters, and geological parameters.

The data sets included two main categories. The first category contained machine performance parameters such as, net boring time, length of mined section as well as the average of machine operational parameters like thrust, RPM, applied torque, and power throughout the section. These parameters were gathered from the daily operating records and TBM data logger "Automatic recording on PLC". In addition, the most important performance parameters containing average penetration rate (ROP), penetration per revolution (P) and field penetration index FPI have been estimated using the formula as shown below:

$$ROP = \frac{L_b}{t_b} \;,\; P = \frac{ROP \cdot 1000}{RPM \cdot 60} \;,\; FPI = \frac{F_n}{P} \quad , \quad F_n = (T_h - F_f) / N_{cutters} \tag{5.1}$$

where ROP is the rate of penetration (m/h), L_b is boring length (m), t_b is boring time (h), P is cutter penetration per revolution (mm/rev), RPM is cutterhead rotational speed (rev/mm), FPI is Field Penetration Index expressed in (kN/cutter/mm/rev), F_n is cutter load or normal force, T_h is the applied thrust of the machine, and F_f is the estimated friction between the machine and the ground. To estimate the frictional force, machines were placed in two groups as reported in Table 5.1. The TBM field performance database is composed of both gripper/open and double shield TBMs. In open type TBM the friction force which builds up between machine and surrounding ground is much lower than shielded machines. In some cases, the front shoes of the machine are pressed against the walls and can impose high pressure on the walls and thus high friction. However, for the most part, the friction of the machine can be included in the calculations by subtracting 20% machine weight from the total thrust force applied by the thrust cylinders (Delisio and Zhao, 2014). For shielded TBMs, the friction force builds-up between the shield and surrounding ground, and hence is significantly higher than open machines, especially for double shield TBM. Previous studies have used 20% weight of the machine in non-squeezing grounds, or 20% of the rock load against the shield in low to medium level squeezing conditions. For highly squeezing conditions the value of friction forces could be higher than the machine thrust, leading to jamming. In such conditions, the use of an arbitrary percentage of the weight of the machine is misleading. Further investigations are needed when shield TBMs are being utilized to assess the friction between the shield and respected ground conditions (Maidl et al. 2008 & 2012; Hassanpour, 2009; Hassanpour et al. 2016).

The second part of the database included some geological parameters such as lithology and petrographical characteristics, intact rock properties (Compressive strength, porosity and…), discontinuity characteristics such as spacing, surface condition, weathering/alteration, groundwater, and also results of calculation of some rock mass parameters (like RQD, RMR, Q, and GSI) in selected tunnel sections based on tunnel rock face observation, analysis of muck materials (chips analysis), sampling and testing in laboratory and study of surface outcrops and boreholes. A descriptive statistical distribution of variables in the database and input parameters for the generated model is summarized in Table 5.21. Since the parameters including joint condition (Jc) and groundwater condition (Gw) in RMR systems are qualitative (descriptive), the partial rating of these parameters are used in this analysis. Also, it is important to note that, where multiple joint sets were identified, different strategies could be adopted to incorporate their impact. One approach is to focus on the critical joint set which can have the highest impact (most assist or hinder) on TBM penetration rate. Another approach is to use a combination of the joints as prescribed by the NTNU system and using K_{s-tot}. The last approach was to compute an average α angle for all existing joint sets. This approach has some downsides since it assumes an arithmetic averaging of the joint orientation to represent the cumulative impact of the joints. The approach used in this study was the first one i.e., using the critical joint set, which was selected to be the set with the highest frequency and minimum joint spacing.

Table 5.21: Descriptive statistics of the generated database for model development used in this study

Variable	N	Min.	Max.	Mean	Std. Deviation	Variance
UCS (MPa)	580	6	267.9	97.41	68.79	4732.18
Js (cm)	580	0.34	200	31.59	29.3	858.53
RQD (%)	580	10	100	66.45	24.15	583.28
Jc (partial rating in RMR)	580	5	30	16.54	5.36	28.74
Gw (partial rating in RMR)	580	0	15	11.67	3.39	11.55
RMR basic	580	25	90	57.56	13.24	175.47
Q	580	0.11	165.85	7.53	12.82	164.5
GSI	580	15	85	52.66	13.54	183.46
P (mm/rev)	580	1.63	38.87	7.53	4.68	21.96
ROP (m/h)	580	0.48	6.2	2.62	1.32	1.75
FPI (kN/cutter/mm/rev)	580	1.43	145.6	25.83	21.27	452.71

As can be seen from Table 5.2, the database covers three main types of rock including, Igneous rocks (37%), Metamorphic rocks (35%), and Sedimentary rocks (28%). The distribution of different rock types is illustrated in Figure 5.48. The distribution pattern of the intact and rock mass properties including, UCS, Js, RQD, Jc, basic RMR, Q, and GSI value in 2D are depicted in Figure 5.49.

The two-dimensional space graphs from the data variabilities displayed in Figure 5.49 show that in the comparison of RQD and UCS, the highest distribution of the data laid beyond 20 value for both parameters. Meanwhile, the Js variables are mainly dominated between 5-50 cm when compared with the RQD. The UCS however showed high fluctuations when depicted with Js and Jc in which the UCS parameter showed the highest distribution when compared with the Js at the range of 5 -100 cm whereby Js of 5-150 cm are in correlation with the Jc over 9 value. Analyses of the RQD and Jc indicates that the Jc parameters less than 9 value fell as not in the domain region when compared with RQD. The same pattern can be seen inspecting Jc and Js where $Jc > 9$ value are dominantly correlated with the Js over 5 cm. Regarding to rock mass classification, GSI compared with basic RMR and Q values illustrate a linear correlation between GSI over 30 value and basic RMR higher than 40 value, whereas the Q value laid majorly between 0.5 and 50 value.

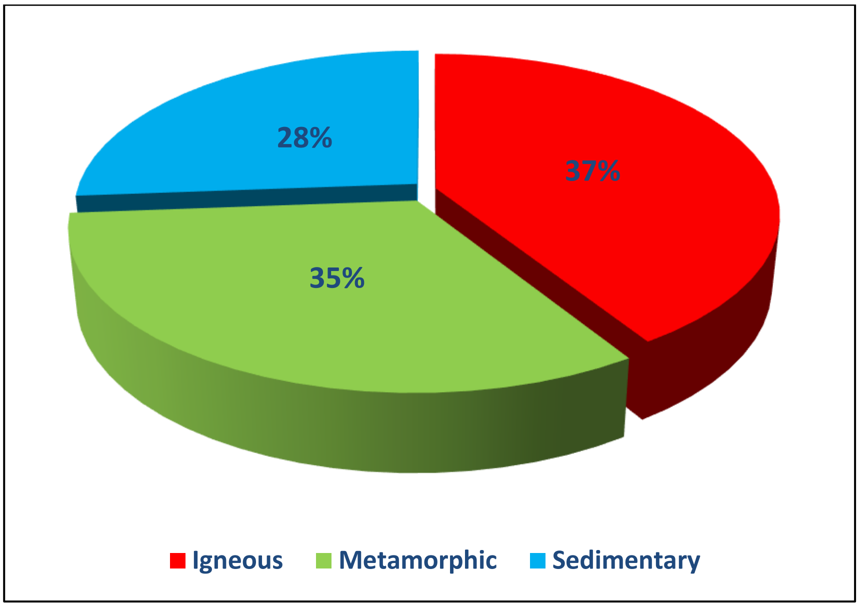

Figure 5.48: The percentage distribution of different rock types in this investigation

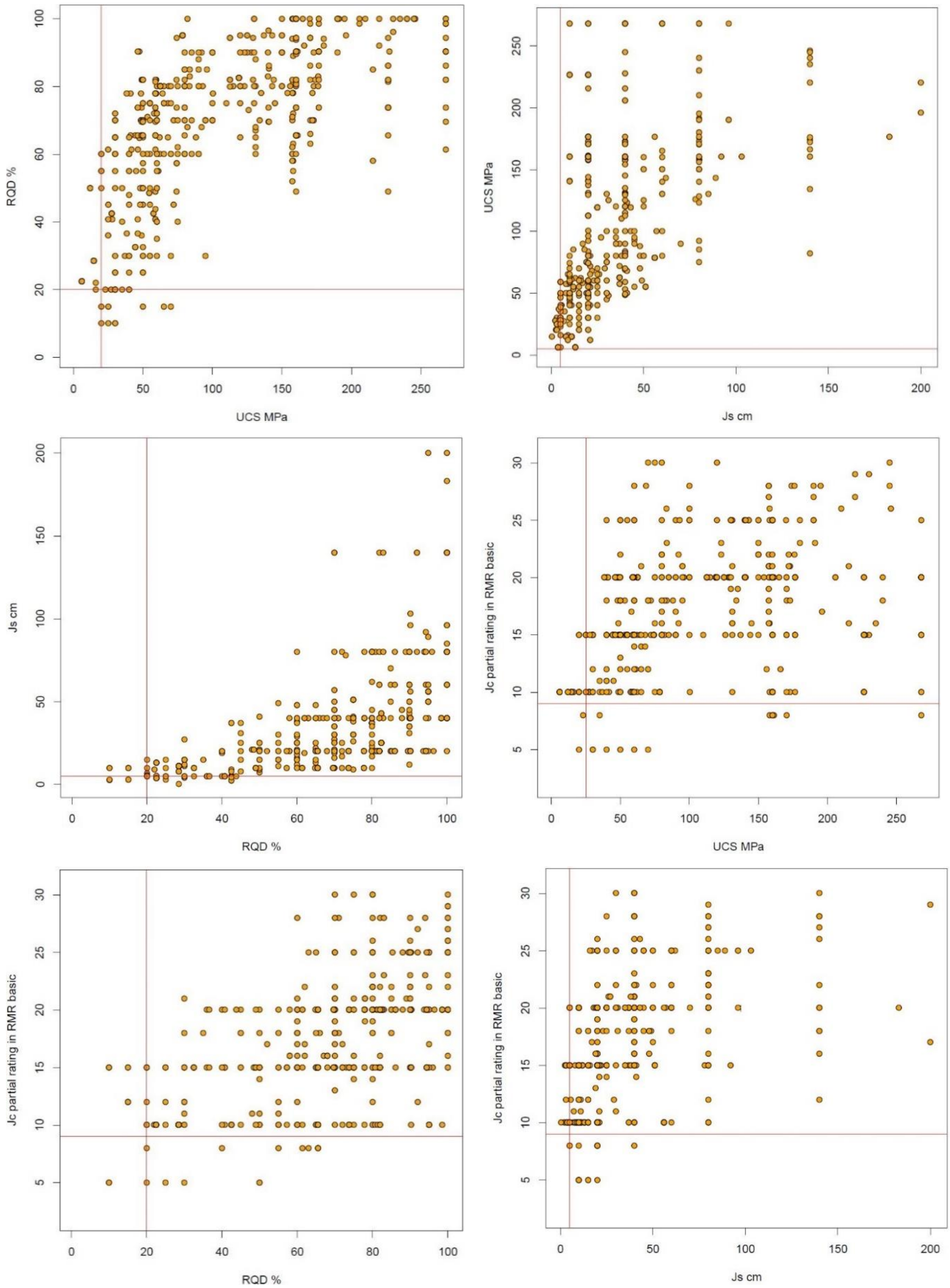
RQD %
UCS MPa
UCS MPa
Js cm
Js cm
RQD %
Jc partial rating in RMR basic
UCS MPa
Jc partial rating in RMR basic
RQD %
Jc partial rating in RMR basic
Js cm

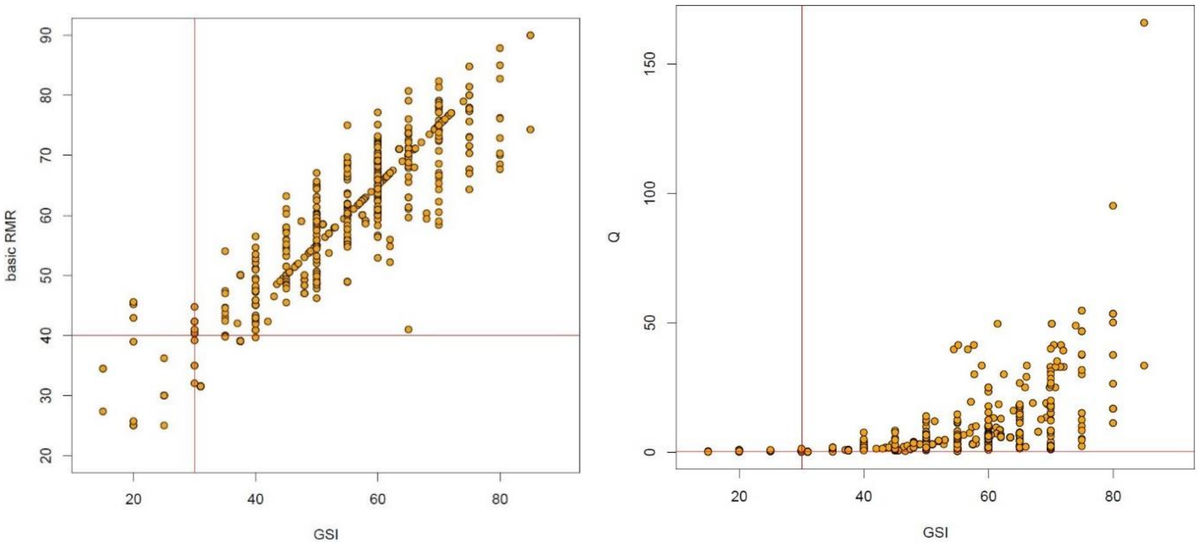

Figure 5.49: Distribution pattern of variables for this study presented in 2-dimensional space

Chapter 6 Developing New Empirical Models

6.1 Introduction

Geotechnical and geological parameters have the greatest impact on the performance of hard rock tunnel boring machines (TBMs). This includes the rock and rock mass properties that affect the rate of penetration (ROP) as well as the machine utilization that is heavily dependent on ground support type and related machine downtime and delays. However, despite the widespread use of TBMs and established track records, accurate estimation of machine performance is still a challenge, especially in complex geological conditions. During the past three decades, numerous TBM performance prediction models have been introduced based on theoretical, empirical, and semi-empirical investigations.

This chapter covers the discussion of the pertinent analysis on the machine performance versus geotechnical parameters, including a series of bi-variate analyses conducted to evaluate the relationship between common rock mass classification systems, including RMR, Q, and GSI, and their input parameters with TBM performance. The preliminary bivariate analysis is followed by principal component analysis (PCA) was performed to identify the critical input parameters, leading to developing new empirical equations based on linear and non-linear regression for the prediction of TBM performance.

6.2 Rock Mass Classification Systems & TBM Performance

Over the years, many rock mass classification systems have been presented in mining and civil engineering (see Table 6.1). According to Bieniawski (1989), a rock mass classification scheme is intended to classify the rock masses, provide a basis for estimating deformation and strength properties, supply quantitative data for support estimation and present a platform for communication between exploration, design, and construction groups. With the widespread use of TBMs in tunnelling in the past two decades, there have been many attempts to use these classification systems to estimate machine performance in various rock masses compared to their original purpose. The fact is that, also, these models are commonly employed in many empirical design practices and planning in rock engineering contrasting with their original intent and applications. A good example is the usage of available rock mass classification systems in the estimation of TBM performance in different tunnelling projects. This is because of the simplicity and worldwide acceptance/availability of the classification systems in general engineering practices, such as underground mining and construction. To deal with this conflict, many investigations have been conducted to assess the applicability of rock mass classification systems in TBM performance prediction.

Table 6.1: Some rock classification and characterization systems (revised from Palmström, 1995; Edelbro et al. 2006)

Name	Form and Type [a]	Main applications and remarks	Author and first version
Terzaghi rock load classification system	Descriptive and behaviouristic form Functional type	Tunnels with steel support (unsuitable for modern tunnelling)	Terzaghi (1946)
Lauffer's stand-up time classification	Descriptive form General type	For input in tunnelling design (conservative)	Lauffer (1958)
New Australian tunnelling method (NATM)	Descriptive and behaviouristic form tunnelling concept	For excavation and design in incompetent ground (utilized in squeezing ground condition)	Rabcewicz (1964, 1965)
Rock classification for rock mechanical purposes	Descriptive form General type	For input in rock mechanics	Patching and Coates (1968)
Unified classification of soils and rocks	Descriptive form General type	Based on particles and blocks for communication	Deere et al. (1969) in Deere and Deere (1988)
Rock Quality Designation (RQD)	Numerical form General type	Based on core logging; used in other classification systems	Deere et al. (1967)
Size-strength classification	Numerical form Functional type	Based on rock strength and block diameter, used mainly in mining	Franklin (1975)
Rock Structure Rating (RSR)	Numerical form Functional type	For design of (steel) support in tunnels (not useful with steel fibre shotcrete)	Wickham et al. (1972)
Rock Mass Rating (RMR)	Numerical form Functional type	For design of tunnels, mines, and foundations	Bieniawski (1973)
Q Classification System	Numerical form Functional type	For design of support in underground excavation (tunnel, large caverns)	Barton et al. (1974)

Name	Form and Type [a]	Main applications and remarks	Author and first version
Mining RMR (MRMR)	Numerical form Functional type	Rock support in mining	Laubscher (1975) in Laubscher (1977)
Typological classification	Descriptive form General type	For use in communication	Matula and Holzer (1978)
Unified rock classification system	Descriptive form General type	For use in communication	Wiliamson (1980)
Basic geotechnical classification (BGD)	Descriptive form General type	For general applications	ISRM (1981)
Slope Mass Rating (SMR)	Numerical form Functional type	Forecast stability problems and support techniques for slopes	Romana (1985)
Geological Strength Index (GSI)	Numerical form Functional type	Indicates the strength of rock masses, input to engineering applications	Hoek (1994)
Rock Mass Index (RMi)	Numerical form Functional type	Rock engineering, general characterization, design of support	Palmström (1995)

[a] Glossary:
- Descriptive form: input to the system is mainly based on descriptions;
- Numerical form: input parameters are given numerical ratings according to their character;
- Behaviouristic form: input is based on rock mass behaviour in a tunnel;
- General type: system is worked out to serve as a general characterization;
- Functional type: the system is structured for a special application (for example, for rock support).

There are new models and rock mass classification systems particularly adapted for the application of TBM projects. Innaurato et al. (1991) developed a new model for estimation of TBM penetration rate based on the intact rock (presented by uniaxial compressive strength) and rock mass characteristics by Rock Structure Rating (RSR). The model considers the effect of intact and rock mass properties, but the latter is defined by an infrequent geotechnical quality index which is not commonly available in the tunnelling projects. Barton (2000) introduced a new model based on Q-system, namely Q_{TBM} which includes many additional input parameters related to TBM tunnelling. They include all original Q system input parameters as well as NTNU boreability indices. Sapigni et al. (2002) correlated TBM performance parameters including penetration rate (PR) and FPI to the RMR classification system. The estimated PR often has more errors since it does not include the force cutterload (F_N) acting on a disc, nor cutterhead RPM into account. Rock Mass Excavability (RME) has been introduced by Bieniawski et al. (2006) and is directly linked to the performance of TBM. The new system incorporates the intact and rock mass characteristics pertinent to TBM tunnelling. The fact is that, the RME index is quite similar to RMR and quite easy to apply. However, the cutterload is not taken into account which can have a significant impact on PR as noted before. Some follow-up studies by Hassanpour et al. (2009, 2011, 2013) have linked FPI to geosocial parameters, namely UCS and RQD, or alternatively using UCS and GSI. The use of FPI allows for accounting for the machine size and thrust and thus offers reasonably good results. A quick review of the related literature reveals that the rate of success of these attempts has been limited and there is no consensus nor accepted formula or model that can use the original rock mass classification systems and related ratings in TBM performance estimates. This could be attributed to the original intent of such classification methods for the evaluation of rock stability and design of ground support measures (Rostami, 2016b). The summary of empirical correlations for TBM performance factors versus the rock mass classification systems is summarized in Table 6.2.

Table 6.2: List of selected empirical TBM performance prediction models based on rock mass classifications

Correlations (TBM performance prediction)	References
$PR = -0.0059 RSR + 1.59$	Cassinelli et al. (1982)
$PR = \sigma_c^{-0.437} - 0.047 RSR + 3.15$	Innaurato et al. (1991)
$PR = 5 \cdot Q_{TBM}^{-0.2}, Q_{TBM} = \frac{RQD_0}{J_n} \cdot \frac{J_r}{J_a} \cdot \frac{J_w}{SRF} \cdot \frac{SIGMA}{F^{10}/20^9} \cdot \frac{20}{CLI} \cdot \frac{q}{20} \cdot \frac{\sigma_\theta}{5}$	Barton (2000)
$SP = 250 \cdot \sigma_{cm}^{-0.66}, \sigma_{cm} = \sigma_c \cdot \exp\left(\frac{RMR - 100}{18}\right)$	Ribacchi and Lembo-Fazio (2005)
$ARA = 0.422 RME_{07} - 11.61$	Bieniawski et al. (2007a, b)
$FPI = 4.161 + 0.091 UCS + 0.077 RQD + 0.117 Jc + 1.077 \log(\alpha)$	Khademi et al. (2010)
$FPI = 0.053 BRMR^2 - 4.205 BRMR + 92.068$	Hassanpour et al. (2011)
$FPI = 4.619 e^{0.023 GSI}$	Hassanpour et al. (2011)
$FPI = 15.309 Q^{0.304}$	Hassanpour et al. (2011)

PR = penetration rate; σ_c = rock material uniaxial compressive strength; RSR = rock structure rating; ARA = average rate of advance; FPI = field penetration index; Jn, Jr, Ja, Jw and SRF are original parameters of Q-system, RQD_0 is oriented-RQD in tunnelling direction, SIGMA = rock mass strength; F = average cutter load; CLI = cutter life index; q = quartz content; = average biaxial stress on tunnel face; RME = rock mass excavibility; BRMR = basic rock mass rating; GSI = geological strength index.

6.3 Composite Indices for Representing TBM Performance

Various TBM performance indices have been introduced and used by many researchers to assess the boreability of a rock mass. This includes FPI and Specific Penetration (SP) which are the composition of penetration per revolution (which accounts for TBM size and RPM) and cutterload (which represents machine thrust). The purpose of using SP (Alber, 2000) or FPI (Nelson et al. 1983) is to combine the thrust and cutterhead rate of rotation with the penetration rate. Stevenson (1999) introduced a Specific Excavation Rate (SER) as the excavated volume per revolution divided by thrust per cutter to combine SP and the tunnel cross-sectional area. Also, the specific rock mass boreability index (SRMBI), defined as boreability index of 1 mm/rev in a given ground expressed by Gong et al. (2007). Table 6.3 summarizes various parameters related to machine performance and their definitions.

Among the indices, the FPI developed by Nelson et al. (1983) has been successfully applied to the determination of the correlation between rock mass characteristics and TBM performance. It is good to note that, usually, stronger and less fractured rock masses are more difficult to cut by TBM and require higher thrust levels to achieve a certain depth of penetration. So, higher values of FPI are usually seen in strong and massive rock masses. In contrast, there is no need to apply high thrust values for excavation of poor-quality rock masses (weaker and more fractured) due to crack initiation and propagation are enhanced by pre-existing fractures (Gong et al. 2006). It means that, the values of FPI are low (Hassanpour et al. 2011). Therefore, FPI has been selected to represent rock mass boreability due to its simplicity and scalability to various machine sizes.

Table 6.3: Summary of various parameters related to machine performance and their definition

Parameter	Symbol	Typical unit	Formula
Penetration rate	PR	m/h	-
Penetration per revolution	PRev	mm/rev	$(1000 \cdot PR)/(60 \cdot RPM)$
Specific penetration	SP	(mm/rev)/(kN/cutter)	$P\mathrm{Re}v / F_n$
Field penetration index	FPI	(kN/cutter)/(mm/rev)	$F_n / P\mathrm{Re}v$
Specific excavation rate	SER	(m3/rev)/(kN/cutter)	$A \cdot SP$
Boreability index	BI	kN/cutter/mm/rev	-
Filed penetration index in blocky rocks	FPI_{blocky}	kN/(mm/rev)	F_n / PR
Specific rock mass boreability index	$BI_{(1)}$	-	$BI \approx BI_{(1)} P\,\mathrm{Rev}^{-0.75}$

A : tunnel area; F_n : Normal force on disk cutter; RPM: cutter head rotation per minute.

6.4 Evaluation and Analysis of TBM Operational Parameters and Performance with Rock Mass Properties

During tunnel excavation with a TBM, the thrust and torque produced by the machine to break the rock vary depending on the properties of intact and rock masses. Therefore, it is necessary for the TBM operators to control the penetration rate and rotational speed of the cutterhead to maximize the production/penetration rate of the machine for the given ground conditions. The relationship between thrust and RPM which are important TBM operational parameters, with TBM performance and rate of penetration (mm/rev) at Lötschberg Base Tunnel (LBT) is shown in Figure 6.1. A similar tendency has been observed in the other tunneling projects used in this study. The reason for the low correlation can be attributed to the influence of the operational attributes of the TBM that is managed by the operator. In hard rock formation, TBM runs thrust-limited, while in the soft ground it runs torque/power-limited. In hard rocks, TBM applies higher thrust to penetrate, while in soft rock more power is required for rolling force, needed for TBM for deeper penetration for a given level of thrust (Cheema, 1999).

Typically, in soft rocks penetration rate was higher, whereas in hard rock penetration lower at the same thrust levels and for the same machine it may appear than at higher thrust levels lower penetration rate is achieved, if one ignores the rock strength. The study of available data shows that, higher thrust and torque were used in the excavation of harder rock and the cutterhead speed and penetration rate were low. Conversely, the penetration rate and cutterhead rotation speed were higher in softer rock, at low thrust levels. However, the performance characteristics of TBMs were varying not only according to whether the rock was soft or hard, but also according to the condition of fracturing and many other characteristics of the rock mass, in addition to the experience, reaction, and skill of the operator.

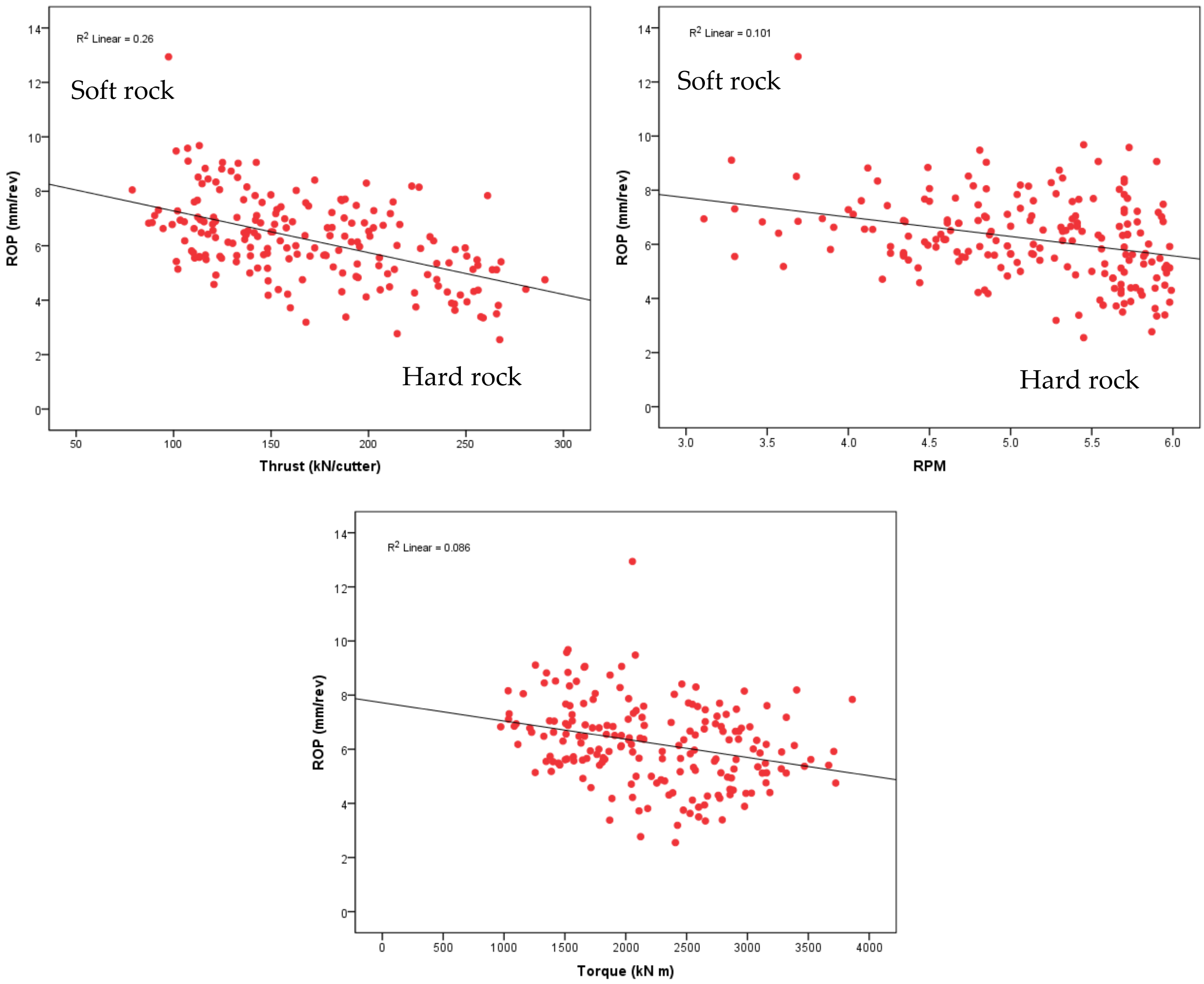

Figure 6.1: Relationship between rate of penetration (ROP, mm/rev) with TBM thrust, RPM & Torque in Lötschberg Base Tunnel

The analysis undertaken here consists of comparing the rock strength (*UCS*) with the operating parameters and excavation characteristics of the machine at the excavated section in the LBT project (Figure 6.2). It shows that, the thrust increases with increasing *UCS* of the rock as well as torque. Also, as it was expected, the rate of penetration (ROP, mm/rev) decreased as *UCS* increased. The fact is that, the uniaxial compressive strength

(*UCS*) is the most widely used rock property for performance prediction because of the easy availability of *UCS* test results.

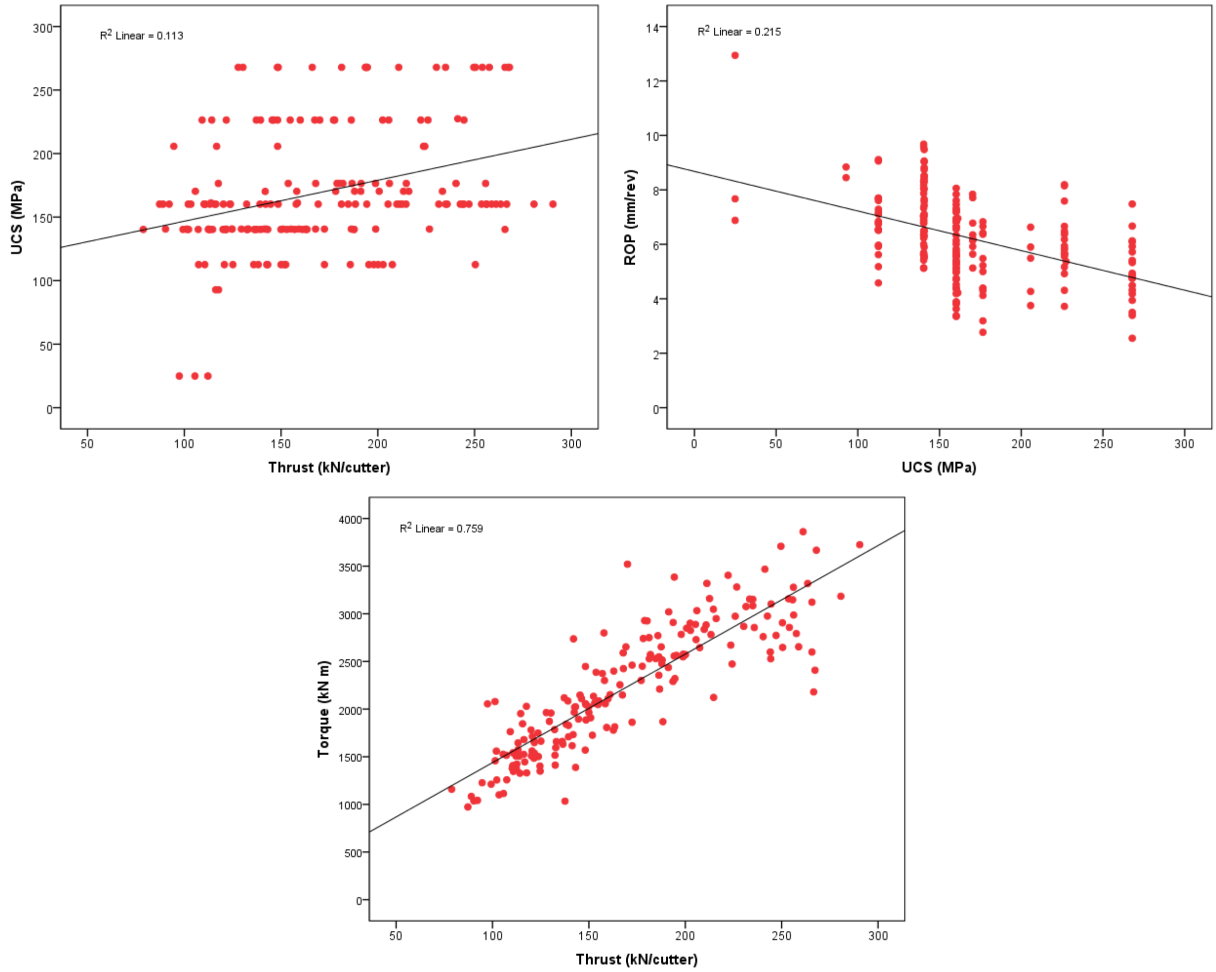

Figure 6.2: Plot of *UCS* -Thrust, ROP-*UCS* with and Torque-Thrust for Lötschberg Base Tunnel

Furthermore, relations between cutter-head rotation per minute (RPM) with *UCS* and with thrust are shown in Figure 6.3. For these relations, it can be concluded that, speed of the cutterhead (RPM) increases with increasing *UCS* value as well as with increasing thrust. Similar trends have been also observed in other projects used in this study.

It is well established that, the degree of fracturing in rock masses has a great influence on TBM performance and operational parameters. In this respect, the relations between *RQD* which is the representative of rock mass fracturing degree with TBM operational and performance in the LBT project are displayed in Figure 6.4. As can be seen, in general, there is a better correlation between machine operational parameters with rock mass properties, i.e., *RQD* as compared to intact rock such as, *UCS* .

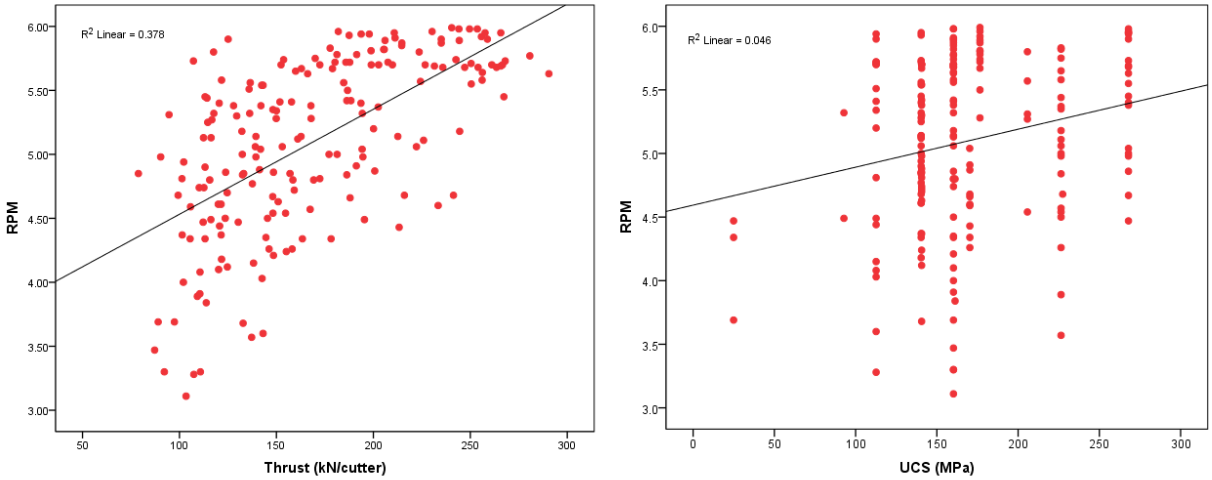

Figure 6.3: Relationship between RPM with thrust and *UCS* in Lötschberg Base Tunnel

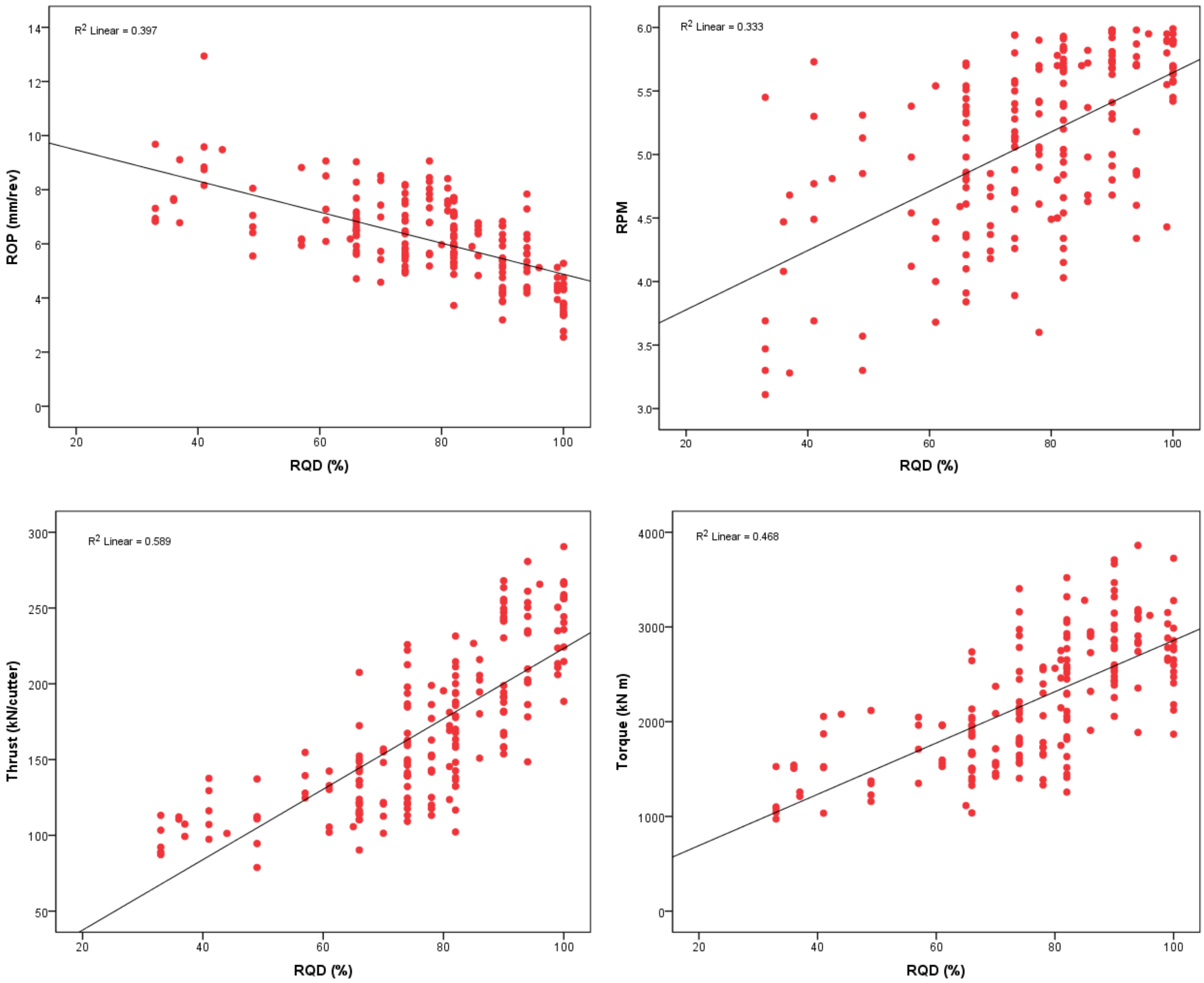

Figure 6.4: Relationship between *RQD* with ROP, Thrust, RPM and Torque in Lötschberg Base Tunnel

6.5 TBM Performance Estimation & Rock Mass Rating (RMR) Classification

Among different rock mass classification systems, RMR, Q, and GSI classifications are the most commonly used methods in many empirical design practices and planning in rock engineering. More information about each of these classification methods can be found in Singh and Goel (2011). It is good to note that, according to the result of Hassanpour et al. (2010; 2011) basic RMR shows a better correlation with machine performance than RMR_{89}. The basic RMR classification system is determined from the sum of ratings (weighting) that is outlined by a table for calculation of rock load and tunnel support selection (Bieniawski, 1973). Therefore, the RMR basic has been considered. The distribution curve and frequency histogram of rock mass classifications including basic RMR, Q, and GSI in the database grouped by rock type is depicted in Figure 6.5. The relationships between FPI and basic RMR, Q, and GSI classifications grouped by rock types are depicted in Figure 6.6.

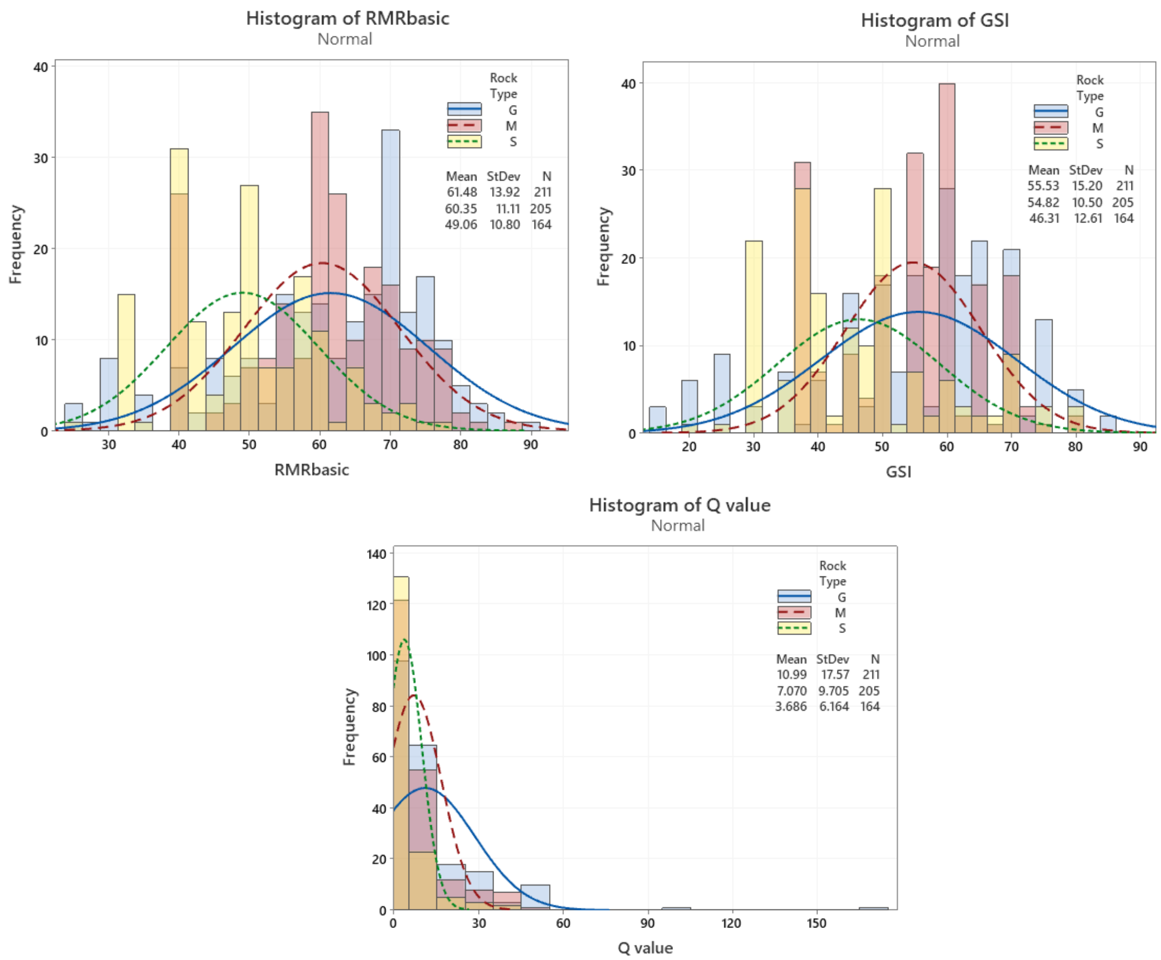

Figure 6.5: Distribution curve and frequency histogram of rock mass classifications in the database (G: Igneous rocks, M: Metamorphic rocks, S: Sedimentary rocks)

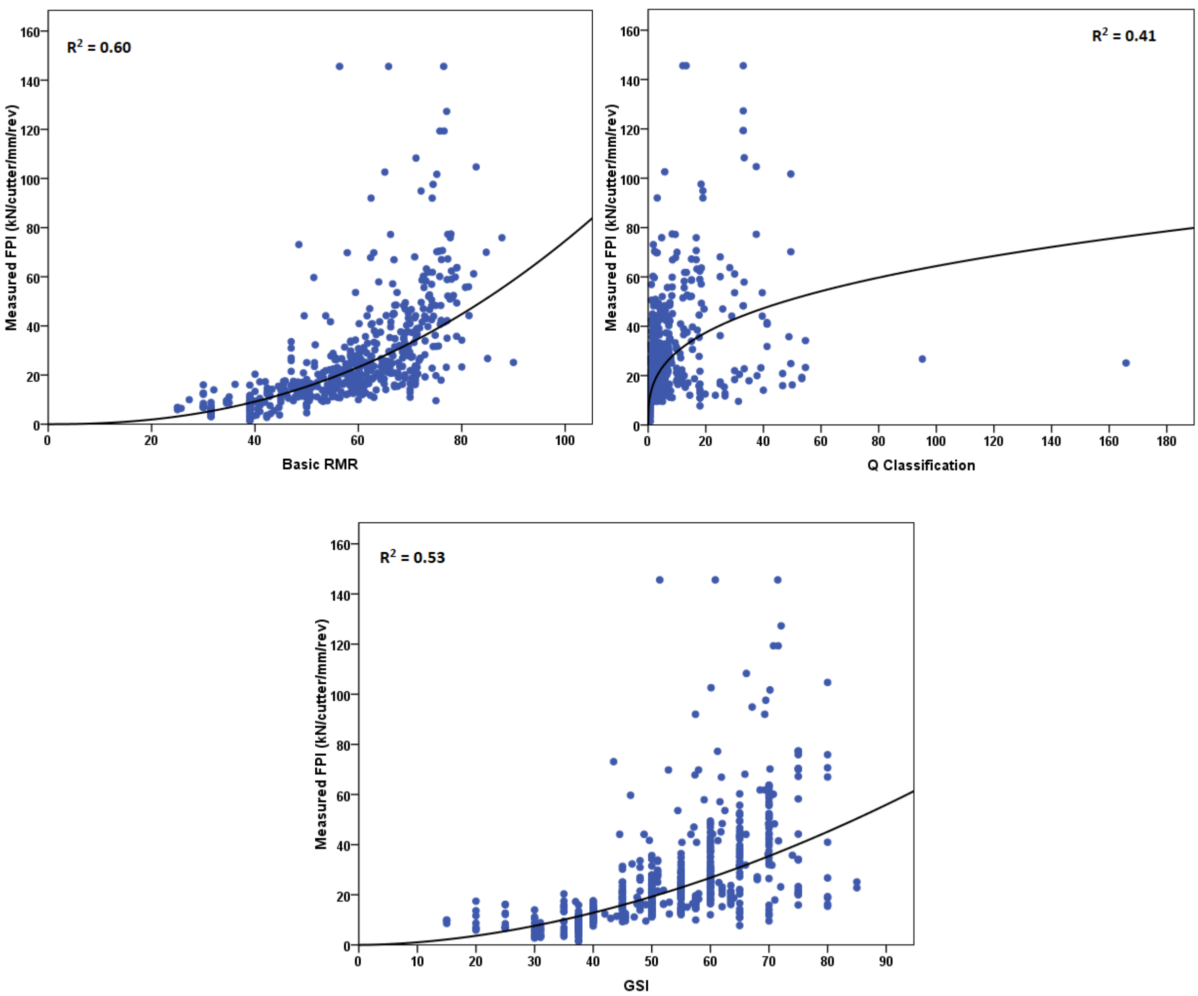

Figure 6.6: Correlation between basic RMR, GSI, Q and measured FPI

Overall, when comparing the most commonly used rock mass classification systems, RMR shows a better correlation with TBM penetration rate, possibility due to the use of intact rock compressive strength as an input parameter. This matter has also been also observed by previous investigations (Hassanpour et al. 2009, 2011; Salimi et al. 2016a; b). Besides, RMR is frequently used in the tunnel design process and reported from the logging of cores in the site investigation reports as well as back mapping of the tunnels. As such, input parameters of the RMR system are often available for various projects, including seven tunnelling projects used in the current study.

It should be noted that, the TBM utilization is mainly influenced by ground condition, support design, and cutter replacement, and in other words, the rock mass quality is tightly associated with tunnel stability, based on which these classification systems have been developed. Zhao (2007) expressed the correlation between rock mass to TBM utilization, which was found to be better than the correlation to the TBM penetration rate.

Also, parameters in these classifications were related to support the design and they were not selected to describe rock mass boreability.

As can be seen from Fig.6.6, the correlation between basic RMR and FPI is better than the others, however at a low correlation factor (R^2 = 0.60). So, it was subsequently decided to investigate the possibility and capability of using input parameters of RMR in developing a new weighing scheme for TBM applications. Fig.6.7 illustrates the correlations between the five individual independent variables in the basic RMR and the actual measured FPI. Also, the figure includes the coefficient of determination (R^2) which is an indicator of correlation strength.

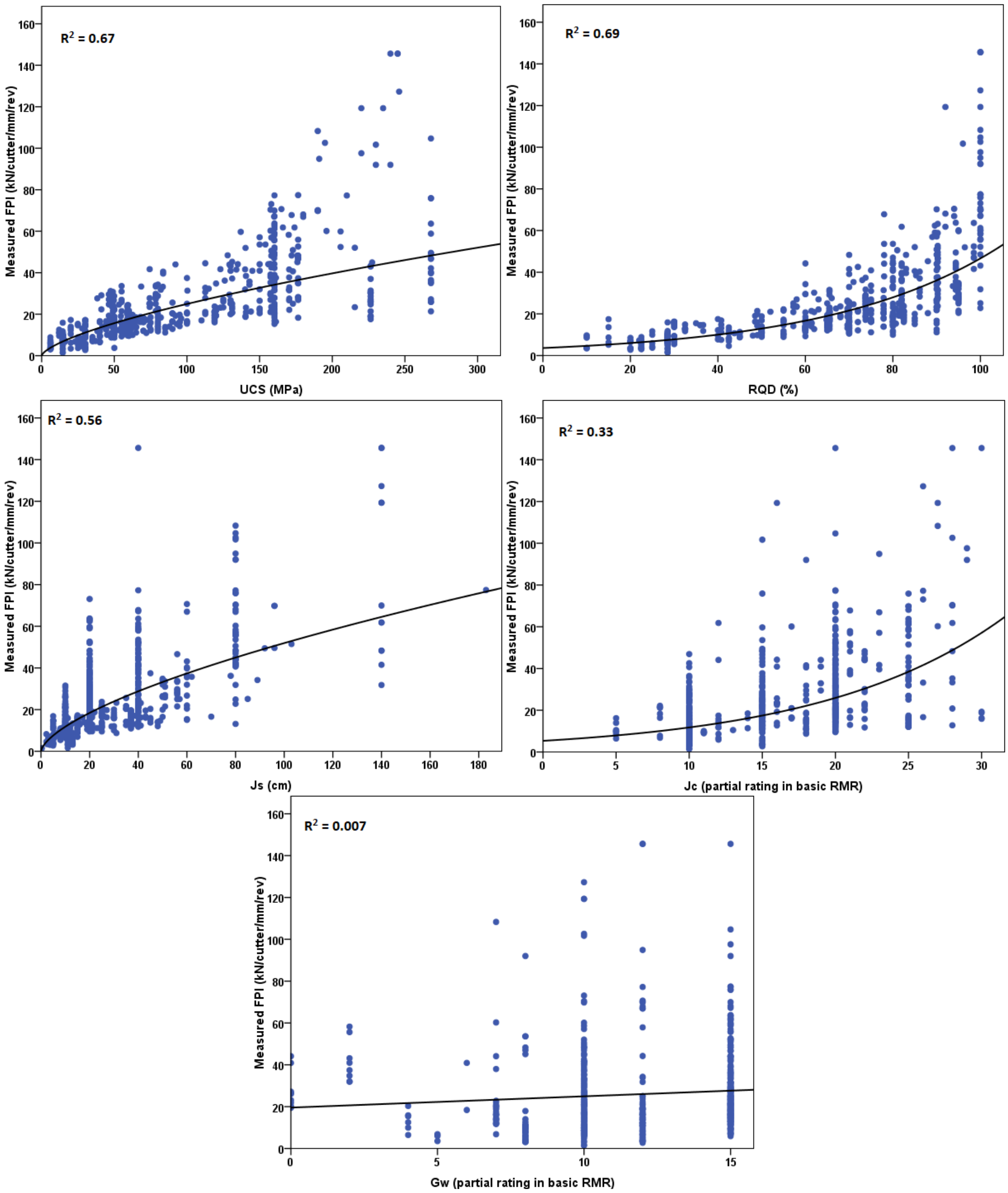

Figure 6.7: The relationship between measured FPI and Basic RMR five input parameters

Obviously, the use of a single parameter will provide a simple predictive model, but it lacks the impact of other important parameters. However, a single value classification system as the summed value of several parameters is also limited in establishing an accurate and reliable correlation with TBM performance which is basically due to the internal weighting system. For more illustration, Table 6.4 presents an example in which the RMR system measured for two rock masses. Upon assigning such ratings in a given condition, the same RMR value is calculated for both rock masses with different conditions of RMR input parameters. However, from the point of view of rock mass boreability, it is expected that the excavation of Rock mass 2 is much easier than that of Rock mass 1. The correlation between the RMR and penetration rate assumes the same trend as correlations between the penetration rate and these five parameters. This inherent assumption will decrease the accuracy of empirical equations. This was the reason for Sapigni et al. (2002) to suggest that several improvements should be made to the conventional RMR system.

Table 6.4: Comparison between the two different rock masses with the same basic RMR value

RMR input parameters	**Rock mass properties**		**Rating**	
	Rock mass 1	**Rock mass 2**	**Rock mass 1**	**Rock mass 2**
Uniaxial compressive strength (MPa)	180	70	12	8
RQD (%)	90	50	18	10
Spacing of discontinuities (m)	1	0.5	14	10
Condition of discontinuities	Slightly rough and moderately to highly weathered, wall rock surface separation 1 < mm	Rough and slightly weathered, wall rock surface separation <1 mm	20	25
Groundwater condition	Dripping	Completely dry	4	15
Basic RMR			68	68

The study of correlations between the individual independent variables in the basic RMR and the actual measured FPI shows that, *RQD* offers the highest R^2 value of 0.69, followed by the *UCS* (0.67), *Js* (0.56), *Jc* partial rating in RMR (0.33). *Gw* is practically neutral relative to TBM penetration rate and therefore it can be concluded that the groundwater condition has negligible effects on the TBM FPI. All of these results are almost in good agreement with those of Ribacchi and Lembo-Fazio (2005) and Hassanpour et al. (2009). Ribacchi and Lembo-Fazio (2005) stated that the TBM specific penetration is best fitted with modified RMR index indicated as RMRP, for which a fixed partial rating value of 15 is assigned to groundwater condition and no adjustment factor for joint orientation is applied. Hassanpour et al. (2009) used the same index and arrived at the same conclusion that, water condition has an indirect effect on the TBM performance with increasing alteration of the rock mass and decreasing strength parameters of the intact rock and joint surface condition. On the other hand, the water flow in rock mass decreases the rock brittleness, consequently decreases the penetration rate. The meaningless correlation between FPI and Gw condition may be described via this contradicting effect of water flow in the rock mass. However, it is necessary to note that, another reason for the as-built data showing the low influence of water ingress on TBM performance is because the solid rock TBMs in real unfavourable Gw conditions were not taken into account. This is not to say that there is no relationship between PR and Gw, it is that the available data do not clearly indicate the conclusive relationship (perhaps due to inconsistency of the data) and thus this factor was removed from the additional analysis and consideration in the study. As such, it can be considered as a new topic to be investigated by researchers in this field to examine the relationship between unfavourable groundwater conditions and TBM performance and its influence in terms of solid rock-TBMs.

The effect of groundwater condition on TBM performance was also studied by Nelson (1983) and Laughton (1998). They indicate that the groundwater mostly impacts the advance rate, through machine utilization, rather than penetration rate. Tunnel instability accidents always occur with the inflow of groundwater. This is also the basis for the inclusion of the groundwater condition in the RMR system. Given that the rating (weight) for the Gw condition and UCS in the RMR system are identical, the influence of the two independent variables on the FPI is quite different and hence, is ignored.

6.6 Developing New Empirical Equations

In rock engineering practice, statistically-based empirical equations have been extensively used to predict target variables based on other operational or geological parameters. Empirical equations have great importance during the early stages of rock excavation and design works since they are more practical compared to extensive theoretical analyses. In this study, regression analyses were performed between TBM performance parameters and geomechanical parameters in the database. Both simple regression and multi-variable regression (linear and non-linear form) analyses were used to develop empirical equations.

6.6.1 Simple Regression Analysis

As mentioned in previous sections, among machine parameters, FPI shows better correlations with geological and geomechanical parameters. Table 6.5 lists the summary results of the correlation of FPI with rock mass parameters and related equations. Since groundwater condition (Gw) has a negligible impact on FPI, this parameter has been eliminated for further investigations.

Table 6.5: Summary results of the determination of regression coefficients of correlation between different geological and geomechanical parameters and FPI

Parameter	Regression Coefficient (R^2)	Regression type	Relationship	Eq. No.
Geological and Geomechanical				
UCS (MPa)	67	Power	$FPI = 1.097 UCS^{0.682}$	6.1
RQD (%)	69	Exponential	$FPI = 3.566 e^{0.026 RQD}$	6.2
Js (cm)	56	Power	$FPI = 2.597 Js^{0.658}$	6.3
Jc (partial rating in basic RMR)	33	Exponential	$FPI = 5.289 e^{0.08 Jc}$	6.4
Rock Mass Classifications				
Basic RMR	60	Power	$FPI = 0.002 RMR^{2.316}$	6.5
Q	41	Power	$FPI = 13.731 Q^{0.343}$	6.6
GSI	53	Exponential	$FPI = 2.356 e^{0.041 GSI}$	6.7

6.6.2 Principle Component Analysis (PCA)

To establish the predictive models and evaluate the effective parameters and their impacts, principal component analysis (PCA) was performed. PCA is a classical method that provides a sequence of the best linear approximations to a given high-dimensional observation. This method has received much attention in the literature in recent years for various applications. PCA is used frequently in different types of analysis (from neuroscience to computer graphics) because it is a simple, nonparametric method of extracting relevant information from confusing data sets. With minimal additional effort, PCA provides a roadmap on how to reduce a complex data set to a lower dimension. Fig.6.8 (a) represents a two-variable data set which has been measured in the X-Y coordinate system. The principal direction in which the data varies is shown by the U axis and the second most important direction is the V axis orthogonal to it. If one transforms each (X, Y) coordinate into its corresponding (U, V) value, the data is de-correlated, meaning that the co-variance between the U and V variables is zero. For a given set of data, PCA finds the axis system defined by the principal directions of variance (i.e., the U-V axis system in Fig. 6.8 (b)). The directions U and V are called the principal components. In this new reference frame, note that variance is greater along with axis U than it is on axis V. PCA computes new variables which are obtained as linear combinations of the original variables. These variables are found by calculating the covariance (or correlation) matrix of the data patterns (Jolliffe 1986; Engelbrecht 2007). In this study, PCA was performed on a set of output and input parameters, and the ratio of the variance of the first component to the total variance (variance ratio) were calculated. Accordingly, this ratio can be determined by the similarity among the output and a set of input factors.

As noted by Rostami (2016b), a cursory review of the parameters impacting TBM performance reveals that the most important geological features that impact TBM performance includes rock strength (UCS or BTS), joint frequency, orientation, and conditions, as well as rock abrasion. With the exception of the rock abrasivity that controls the disc cutter life and thus machine utilization, other parameters are the same as the parameters used in common rock mass classification systems. As such, it makes sense to assume that some versions of existing rock mass classifications can be used for the prediction of TBM performance. This means that perhaps a methodical selection of input parameters and different weight or rating schemes can be adopted to develop rock mass classifications that are pertinent and suitable for the prediction of TBM rate of penetration (ROP).

In this study, the PCA, R statistical computing software was applied to screen the input parameters (see Appendix). To quantify the performance of TBM, the Field Penetration Index (FPI) was computed from the raw data. Several analyses with two, three, and four input parameters, with special emphasis on input parameters of basic RMR, were performed to identify the influencing parameters on the TBM performance and check the capability and possibility of using basic RMR parameters as inputs for developing a new model for TBM PR studies. As can be seen from Fig.6.9, the factor containing four inputs (UCS, RQD, Js, Jc) was shown to be more effective and FPI has been expressed as a function of these inputs. Also, it is good to note that, although the difference in comparison with three factors, containing UCS, RQD, and Js is minimal, however, as expressed by Ribacchi & Lembo-Fazio (2005) in which the influence of different rock mass parameters on the performance of TBM in Varzo tunnel was analysed; even simple quality indexes, such as the partial rating of joint spacing in the RMR classification, had sound predictive value for penetration rate. Joint conditions proved to have a significant impact, though the most influencing feature is joint spacing.

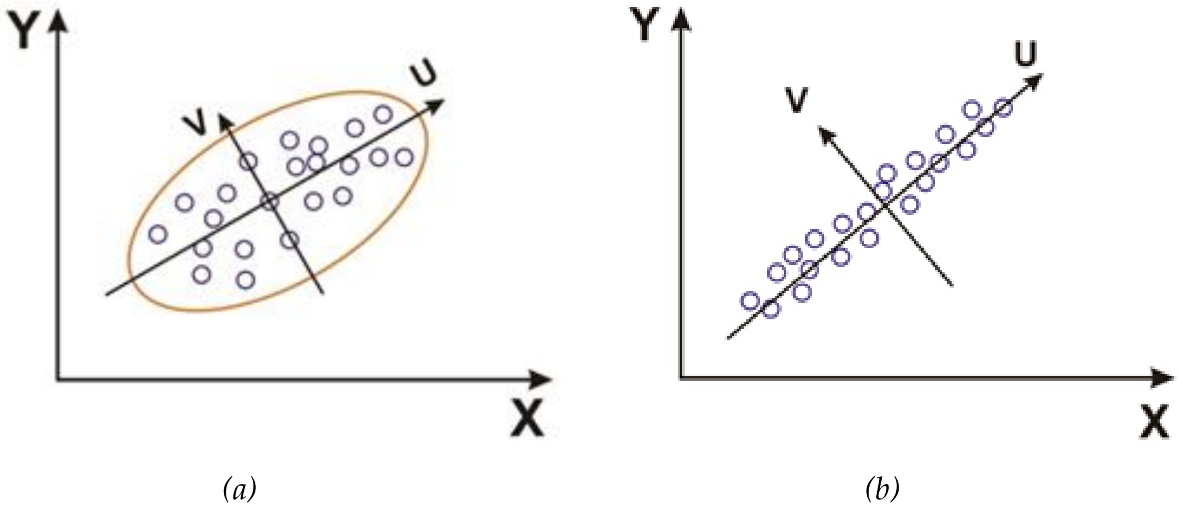

Figure 6.8: (a) Principal components for data representation; (b) Principal components for dimension reduction

For more clarification and assessing exactly what percentage of the variance was retained in these principal components, the proportion of variance explained (PVE) by the mth principal component is calculated using the equation:

$$PVE = \frac{\sum_{i=1}^{n}(\sum_{j=1}^{p}\phi jm\, x_{ij})^2}{\sum_{j=1}^{p}\sum_{i=1}^{n}x_{ij}^2} \tag{6.8}$$

Where ϕ is the principal component loading vector. It can be shown that the PVE of the mth principal component can be more simply calculated by taking the mth eigenvalue and dividing it by the number of principal components, p. The results of PVE is illustrated in Figure 6.10, while, the cumulative variance of the first four parameters is shown in Figure 6.11. As can be seen, together, the first three principal components explain 93% of the variability, and adding *Jc* results in a 100% explanation.

Besides that, Farrokh et al. (2012) considers Rock Type Code (RTC) as an input parameter in their model to estimate TBM PR. Since different rock textures (cementation and grain size and shape) affect the penetration rate, such properties should also be taken into account in PR studies. According to the results of sensitivity analysis and parametric study of common models conducted by Fatemi et al. (2016), consideration of RTC has a significant role to play in the estimation of rock mass boreability. For more clarification, Table 6.6 presents a comparison between different rock type categorizations with the same RMR value and TBM FPI. As can be seen from Table 6.6, despite the similar values are found between two types of rock, the boreability of rock masses are different.

Although, there are several factors which directly or indirectly can affect TBM performance, such as the angle between tunnel axis and discontinuity plane α (Alpha angle), crew experience, backup system, and so on, but from geological points of view, it can be expected that, the differences are due to the rock texture and cementation. Therefore, as expected, the boreability of rock masses is totally different based on rock texture and cementation (Salimi et al. 2019).

Table 6.6: Comparison between different rock type categorizations with the same basic RMR value and TBM FPI

RMR input parameters	Rock mass properties		Rating	
	Rock mass 1 (Amphibolite)	Rock mass 2 (Limestone)	Rock mass 1	Rock mass 2
Uniaxial compressive strength (MPa)	170	170	12	12
RQD (%)	95	95	20	20
Spacing of discontinuities (m)	0.8	0.8	15	15
Condition of discontinuities	Slightly rough and moderately to highly weathered, wall rock surface separation 1 < mm	Slightly rough and moderately to highly weathered, wall rock surface separation 1 < mm	20	20
Groundwater condition	Damp	Damp	10	10
Basic RMR			77	77
FPI (Field Penetration Index; kN/cutter/mm/rev)			46.81	38.48

Therefore, this parameter has been considered in this investigation as well. To such that, seven rock type categories, as proposed by Hoek and Brown (1980) and Stevenson (1999), were adopted.

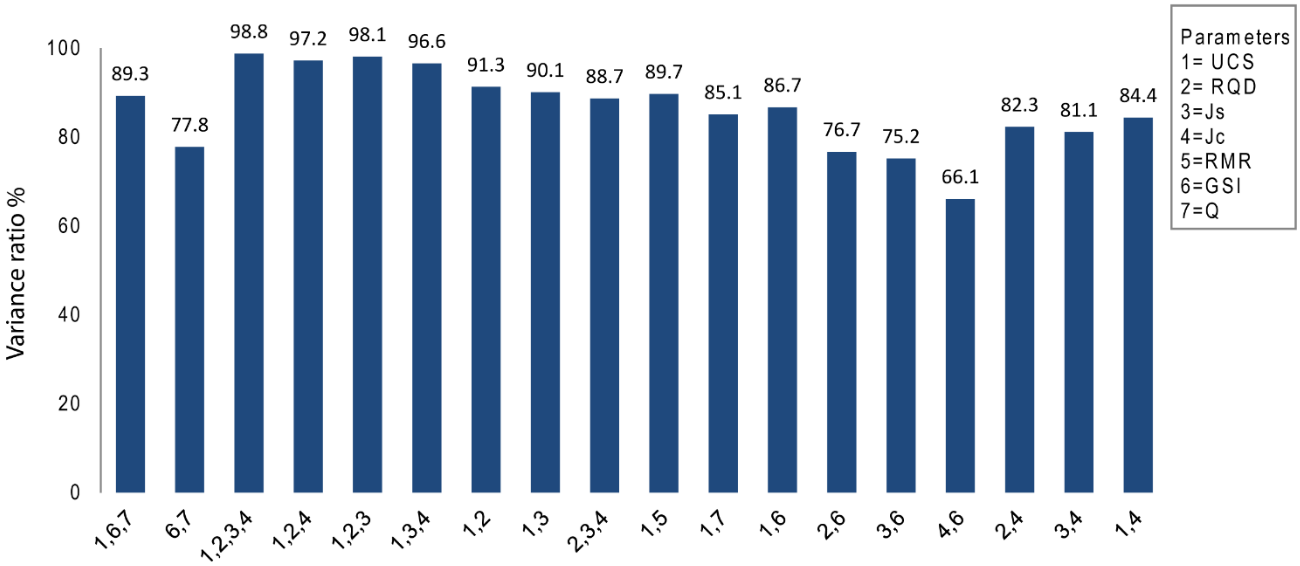

Figure 6.9: Results of some of the principal components analysis (PCA) for TBM performance analysis using various geotechnical input parameters

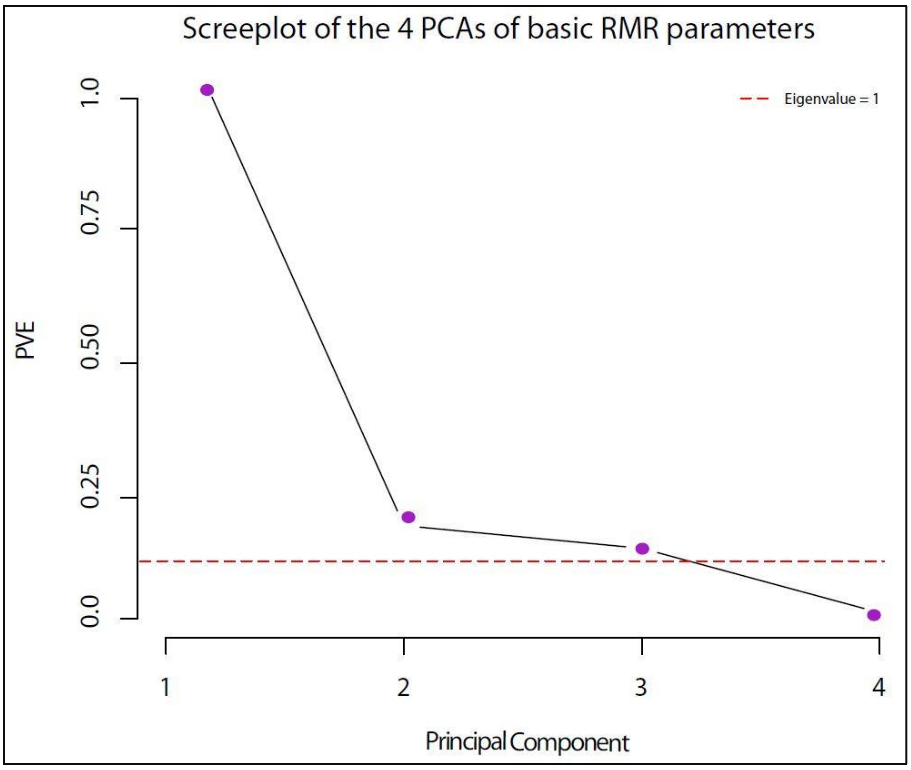

Figure 6.10: Proportion of Variance Explained (PVE) for the first four features (UCS, RQD, Js, Jc)

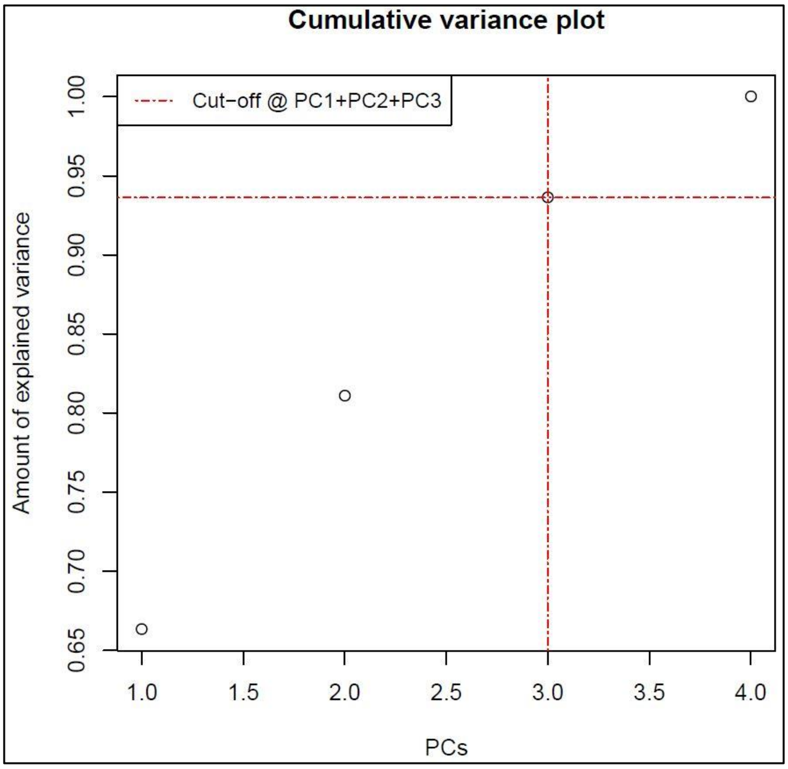

Figure 6.11: Cumulative variance of first four features (input parameters of basic RMR)

These rock types are listed in Table 6.7. The first four classes are for ''Sedimentary Rocks.'' The fifth, sixth, and seventh classes are for ''Metamorphic Rocks, Granitic Rocks, and Volcanic Rocks'' respectively. It should be mentioned, Gneiss (GN) is inherently metamorphic, but it is typically closer to granite in terms of its behaviour, especially where foliation is less pronounced. For this reason, it was categorized as GN in this analysis. As can be seen in Fig. 6.12, when the rock type is taken into consideration in the analysis, a good relationship can be established between rock strength and FPI. The graphs show that in general a lower FPI is achieved in sedimentary rocks, and a higher FPI is achieved in igneous rocks. These results are in agreement with the results proposed by Laughton (1998) and Robbins (1992) for different rock types.

Table 6.7: Rock-type categorization in the database (modified from Hoek and Brown, 1980)

Rock type	**Code**
Claystone, mudstone, marl, slate, phyllite, argillite	C
Sandstone, siltstone, conglomerate, quartzite	S
Limestone, chalk, dolomite, marble	L
Karstic Limestone	K
Metamorphic rocks such as gneiss and schist	M
Coarse igneous such as granite and diorite	G
Fine volcanic such as basalt, tuff, and andesite	V

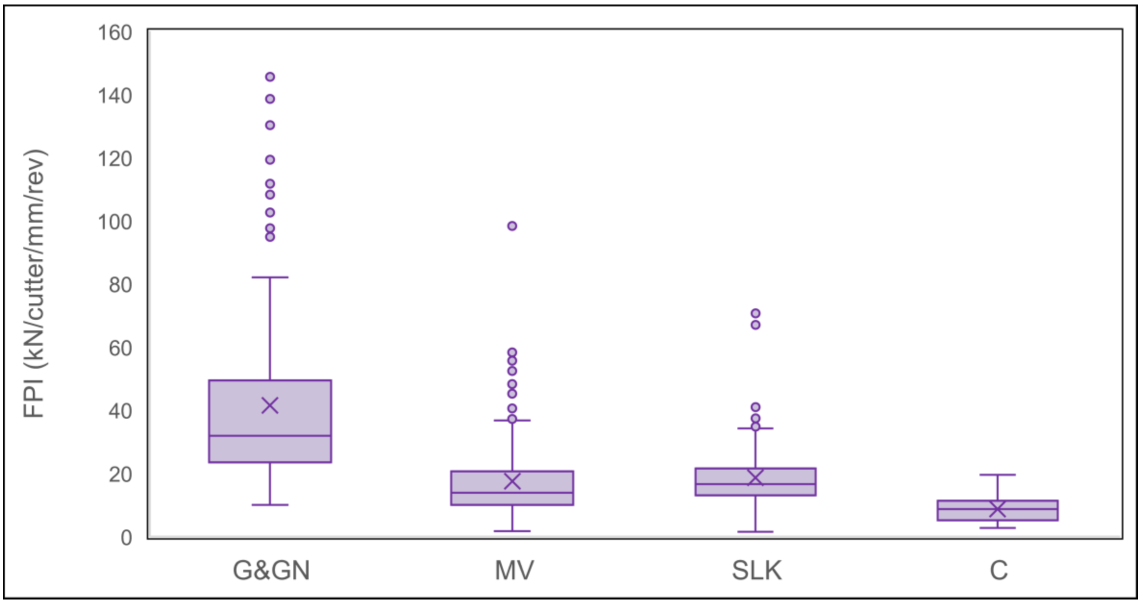

Figure 6.12: Rock type versus TBM FPI

To use rock type code as one of the selected input parameters for developing new models, code numbers including, 1 for G and GN, 2 for MV, 3 for SLK, 5 for C have been employed. Figure 6.13 shows the percentage distribution of different rock type codes in this investigation. The results of PCA grouped by RTC across the four selected features is presented in Figure 6.14.

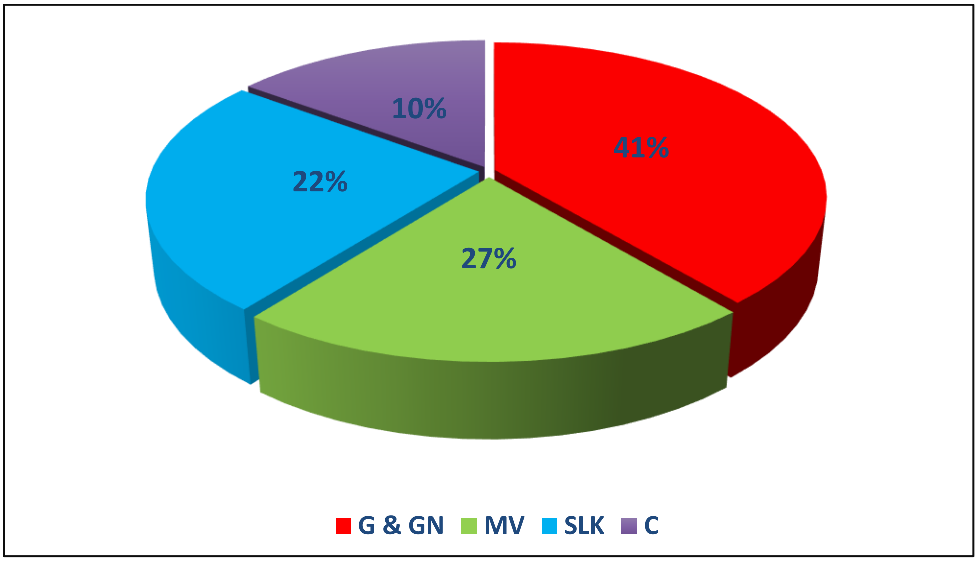

Figure 6.13: Percentage distribution of different rock type codes

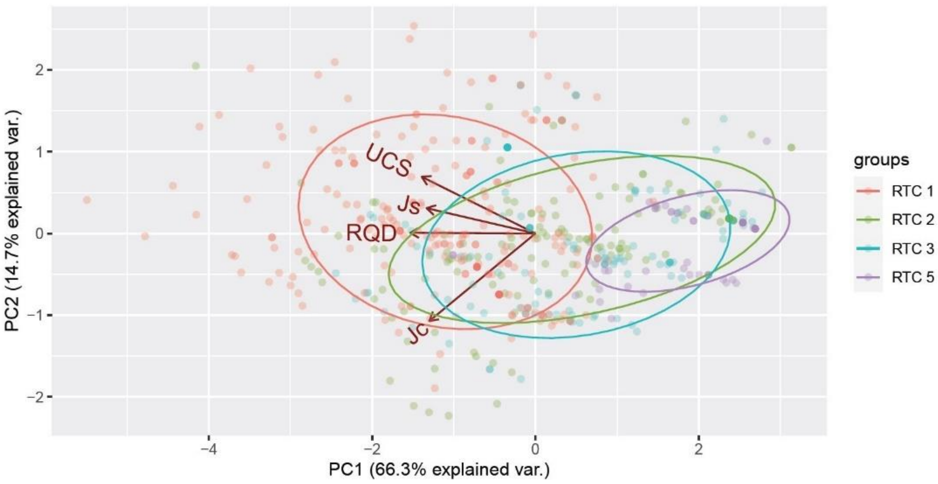

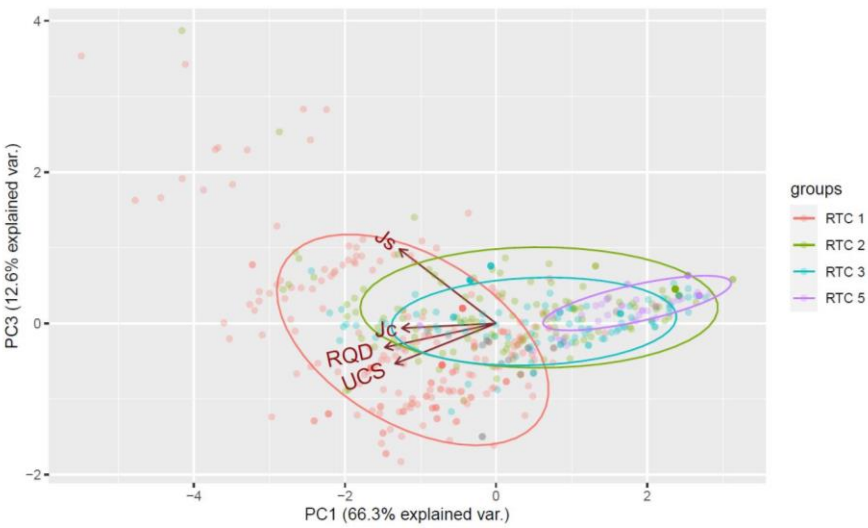

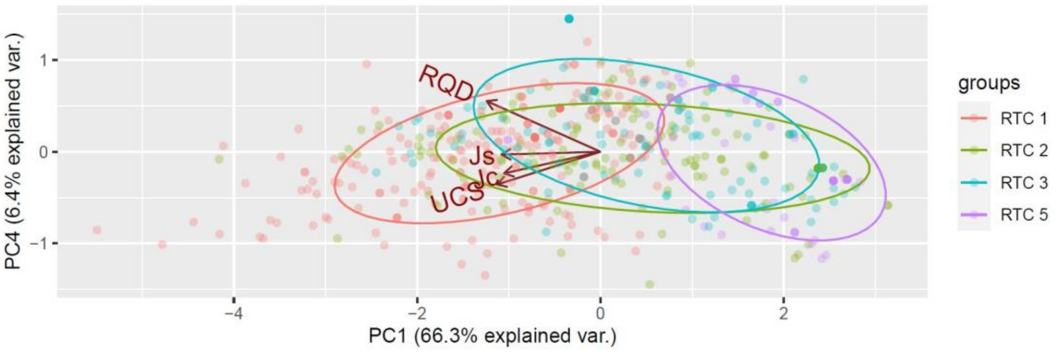

RQD
Js
Jc
UCS
PC4 (6.4% explained var.)
PC1 (66.3% explained var.)
groups
RTC 1
RTC 2
RTC 3
RTC 5

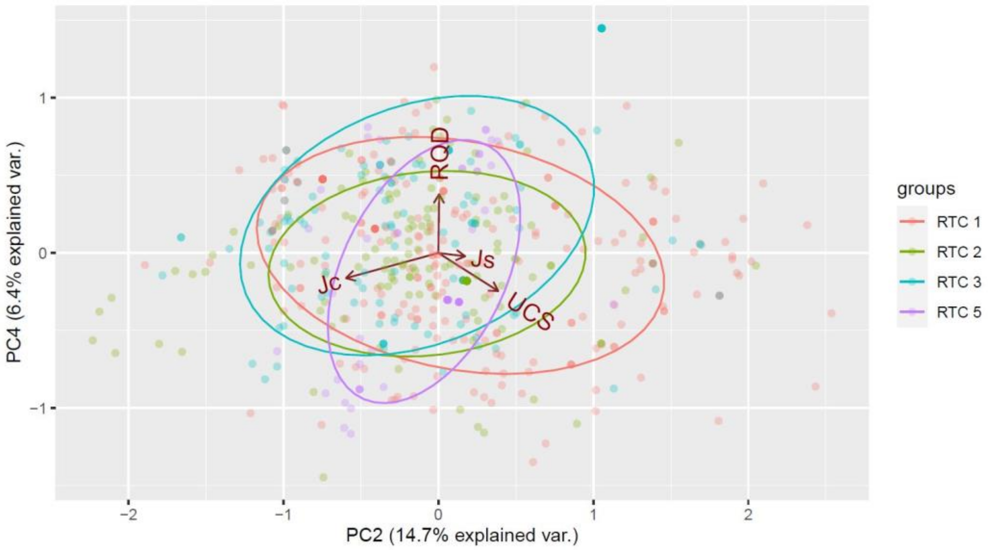

RQD
Js
Jc
UCS
PC4 (6.4% explained var.)
PC2 (14.7% explained var.)
groups
RTC 1
RTC 2
RTC 3
RTC 5

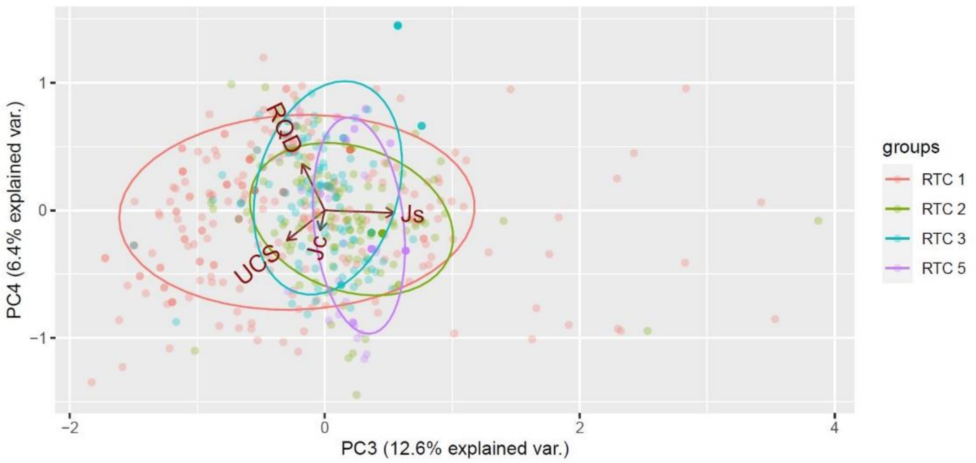

RQD
Js
Jc
UCS
PC4 (6.4% explained var.)
PC3 (12.6% explained var.)
groups
RTC 1
RTC 2
RTC 3
RTC 5

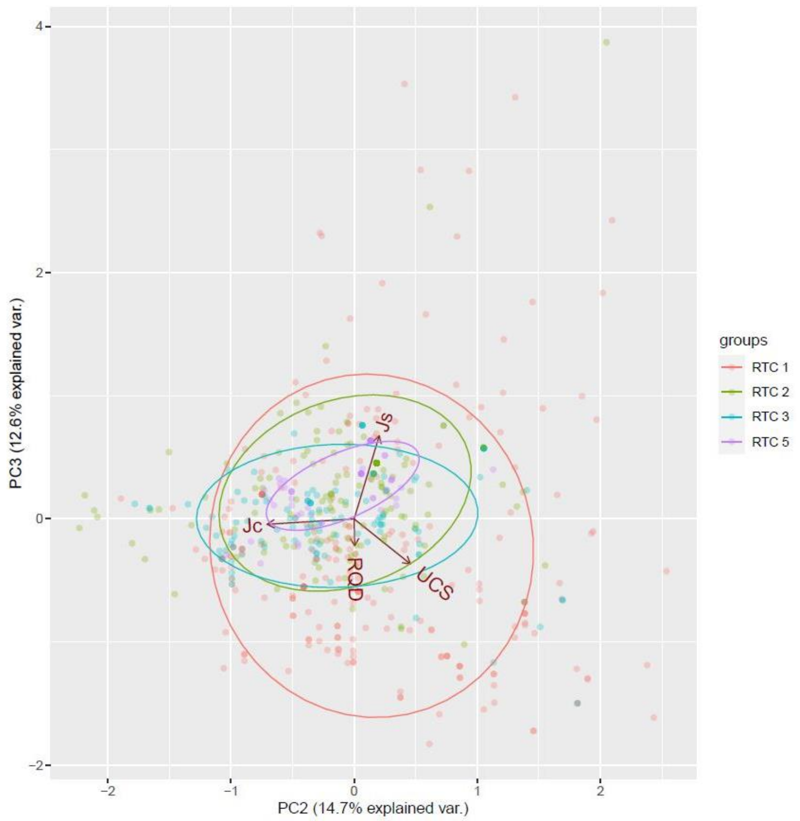

Figure 6.14: Results of scatter plot of PCA grouped by RTC across the four selected features

In brief, the four parameters of basic RMR containing UCS, RQD, Js, Jc as well as RTC were taken into consideration as input parameters for developing new models for FPI. To eliminate and examine the multicollinearity between the selected input parameters; tolerance analysis (VIF, variance inflation factor) was conducted. Tolerance values approaching zero indicate a high degree of multicollinearity among the independent variables. The effect of collinearity is to increase the standard error of the regression coefficients (and hence to increase the confidence intervals and decrease the P values). The standard error of a regression estimates of the variable j ($\hat{\beta}_j$) is given by:

$$se(\hat{\beta}_j) = \sqrt{\left(\frac{\sigma^2}{\sum x_j^2} \times \frac{1}{1-R_j^2}\right)} \tag{6.9}$$

Where R_j^2 is the R^2 found when regressing all other predictors onto the predictor j. Note that when there is only one variable in the regression equation, or when the correlation between the predictors is equal to zero, the value for the part of the equation $1/(1-R_j^2)$ is equal to 1. The term $1/(1-R_j^2)$ is known as the *variance inflation factor* (VIF). When the correlation changes from 0 (or when additional variables are added), the value of the VIF increases, and the value of the standard error of the regression parameter increases with the square root of the VIF. The reciprocal of the VIF is called *tolerance*. It is equal to $1-R_j^2$, where each predictor is regressed on all of the other predictors in the analysis. Table 6.8 is the summary of collinearity evaluation using the tolerance values calculated by statistical analysis of the input data and shows minimum to no multicollinearity between the selected input parameters.

Table 6.8: Summary of collinearity evaluations based on statistical analysis

Independent variable	**Tolerance**	**VIF (variance inflation factor)** *
UCS (MPa)	0.44	2.27
RQD (%)	0.355	2.819
Js (cm)	0.621	1.61
Jc (partial rating in basic RMR)	0.599	1.67
RTC	0.613	1.631

* VIF=1/Tolerance "Threshold is 10.0"

The distribution curve and frequency histogram of selected input parameters based on PCA results (UCS, RQD, Js, Jc) and TBM performance parameter (FPI & ROP) in the database is illustrated in Figure 6.15. As can be seen, the higher value of UCS (strength parameter) belongs to igneous rocks and the lower value associates to sedimentary ones. Similar pattern can be found in the other parameters such as RQD, Js and Jc, as well as TBM performance parameter, FPI, while the higher value of rate of penetration (ROP) seen in sedimentary rocks as it was expected.

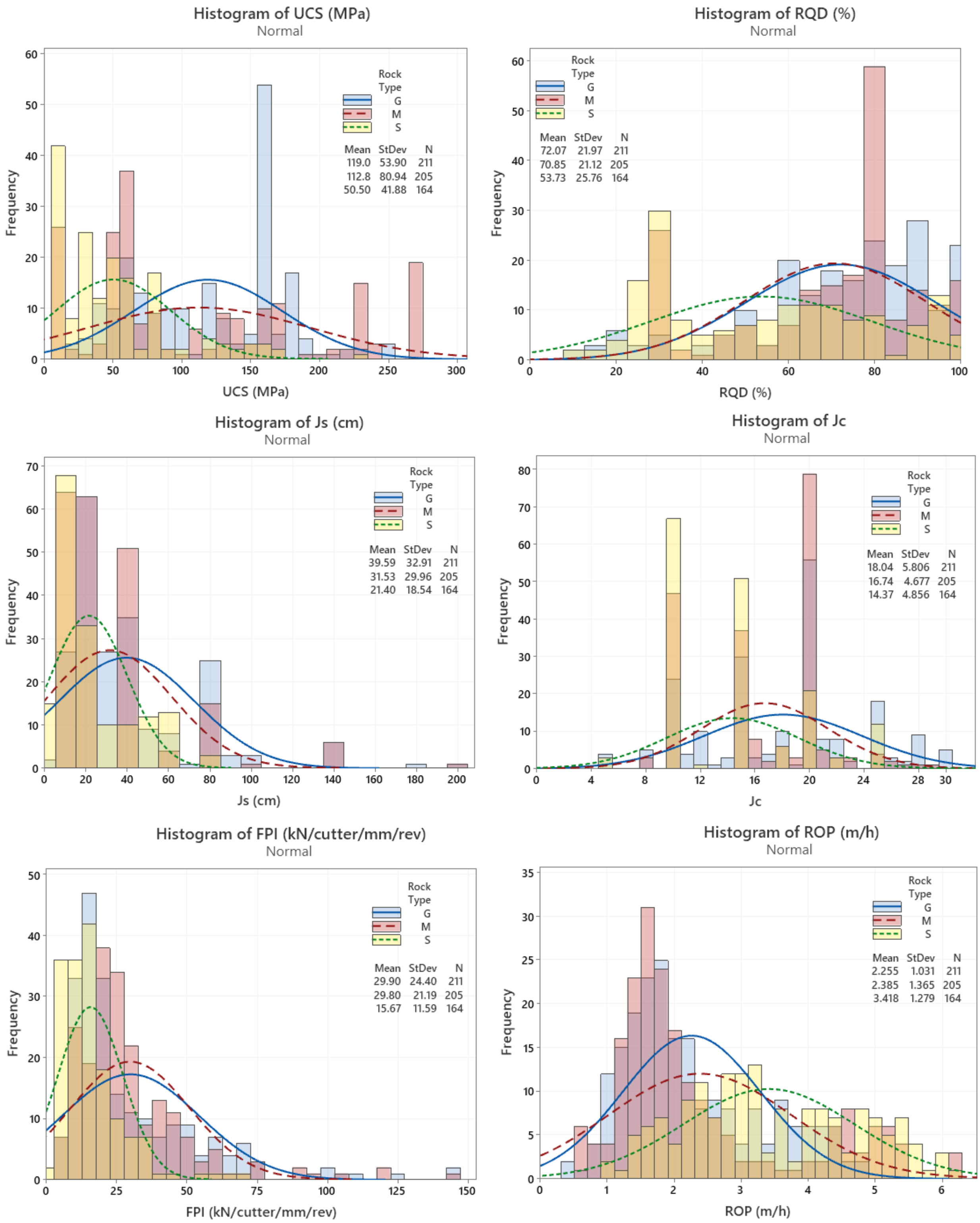

Figure 6.15: Distribution curve and frequency histogram of selected input parameters of basic RMR, FPI and ROP in the database grouped by rock type (G: Igneous rocks, M: Metamorphic rocks, S: Sedimentary rocks)

6.6.3 Multiple Linear Regression Analysis Model (MLRA)

Multivariate regression analysis (MVRA) is an extension of regression analysis which was firstly conducted by Pearson in 1908 (Yilmaz and Yuksek, 2009). The purpose of multiple regressions is to learn more about the relationship between several independent or predictor variables and a dependent or criterion variable. The goal of regression analysis is to determine the values of parameters for a function that cause the function to fit a set of data observations provided. In linear regression, the function is a linear (straight-line) equation. When there is more than one independent variable, then multivariate regression analysis is used to get the best-fit equation. The main form of MLRA is:

$$Y = \beta_0 + \beta_1 x_1 + \beta_2 x_2 + ... + \beta_n x_n \tag{6.10}$$

Where $\beta_1, \beta_2, ..., \beta_n$ are the coefficient of a regression model, β_0 is a constant value, Y is the dependent variable, and $x_1, x_2, ..., x_n$ are independent variables. The R statistical computing software (see Appendix) was used as a modelling tool to apply multiple linear regression analysis. In this regard, five independent variables including $UCS, RQD, Js, Jc \text{ and } RTC$ are considered as input parameters and FPI as an output. As a result, a new performance predictive equation was obtained as follows:

$$FPI = 1.102 + 0.129UCS + 0.071RQD + 0.314Js + 0.389Jc - 0.466RTC \tag{6.11}$$

where UCS is uniaxial compressive strength (MPa), Js is joint spacing (cm), RQD is rock quality designation, Jc is joint characteristic in basic RMR and RTC is rock type code; 1 for G and GN, 2 for MV, 3 for SLK, 5 for C. Correlation between the measured and predicted FPI via MLRA is illustrated in Fig.6.16 in which the correlation coefficient (R^2) is 0.68.

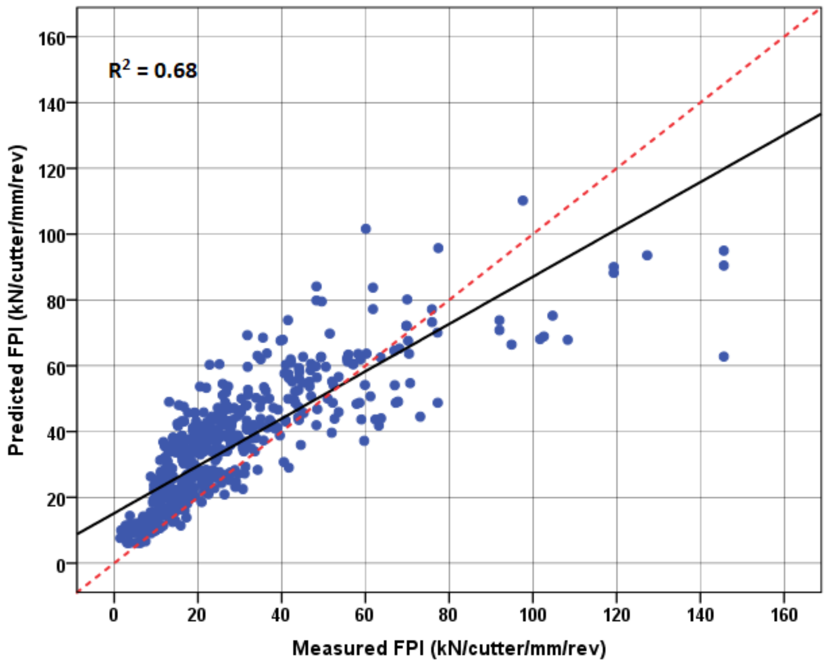

Figure 6.16: Comparison between the measured and predicted FPI from MLRA model

6.6.4 Multiple Non-linear Regression Analysis (MNLRA)

As stated by Davis (2002), most of the problems in geology involve complex and interacting forces, impossible to isolate and study individually. Non-linear multiple regression analyses have been utilized in rock engineering and engineering geology to solve complex problems. In fact, non-linear regression involves estimating the coefficients in a non-linear relationship between independent and dependent variables. The R Statistical Computing software (see Appendix) was used to apply multi-variable non-linear regression analysis. After a series of modelling, the best combination of rock mass parameters to predict the field penetration index (FPI) was found based on the established TBM performance database. As a result, a new predictive equation was empirically obtained as follows:

$$FPI = \exp(1.763 + 0.003UCS + 0.012\,RQD + 0.005\,Js + 0.008\,Jc - 0.091\,RTC) \tag{6.12}$$

A comparison between the measured and predicted results from Eq.6.12 is shown in Figure 6.17. Furthermore, the correlation and distribution between input parameters and output were found in 3-dimensional plots (Figure 6.18). The plots show that an increase in UCS and RQD value, UCS and Jc value, UCS and Js value results in a higher value of FPI, as does an increase in RQD and Jc value, RQD and Js value as well as Js and Jc. While the higher value of FPI respecting to RTC can be found in group one "G&GN" and it decreases to group five "C". This seems intuitive and is in an agreement with field observation and previous literature. In brief, the strength of rock material (*UCS*) and three parameters defining joint condition (*RQD*, *Js*, and *Jc*) as well as *RTC* which is representative of rock texture can be used for estimation of TBM FPI.

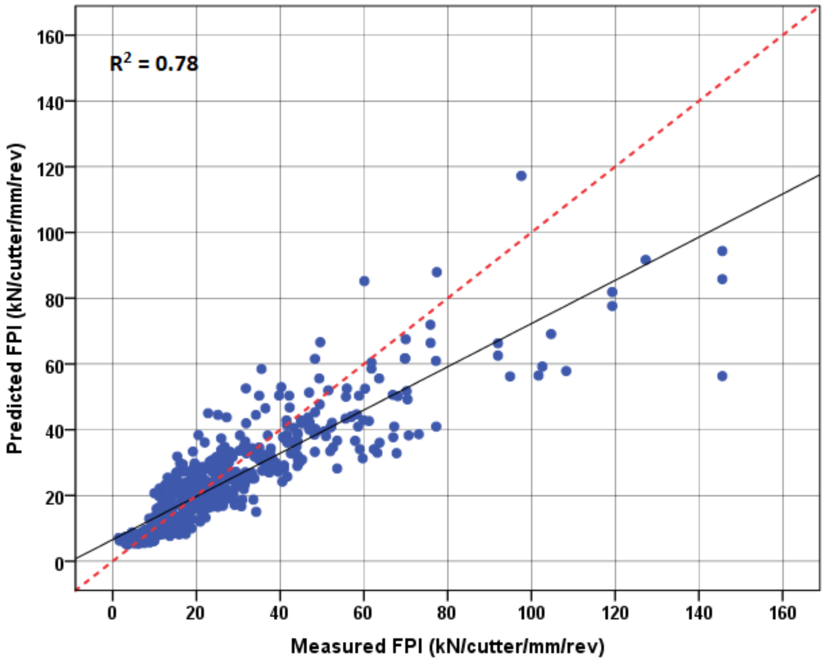

Figure 6.17: Comparison between the measured and predicted FPI from multivariable non-linear regression analysis

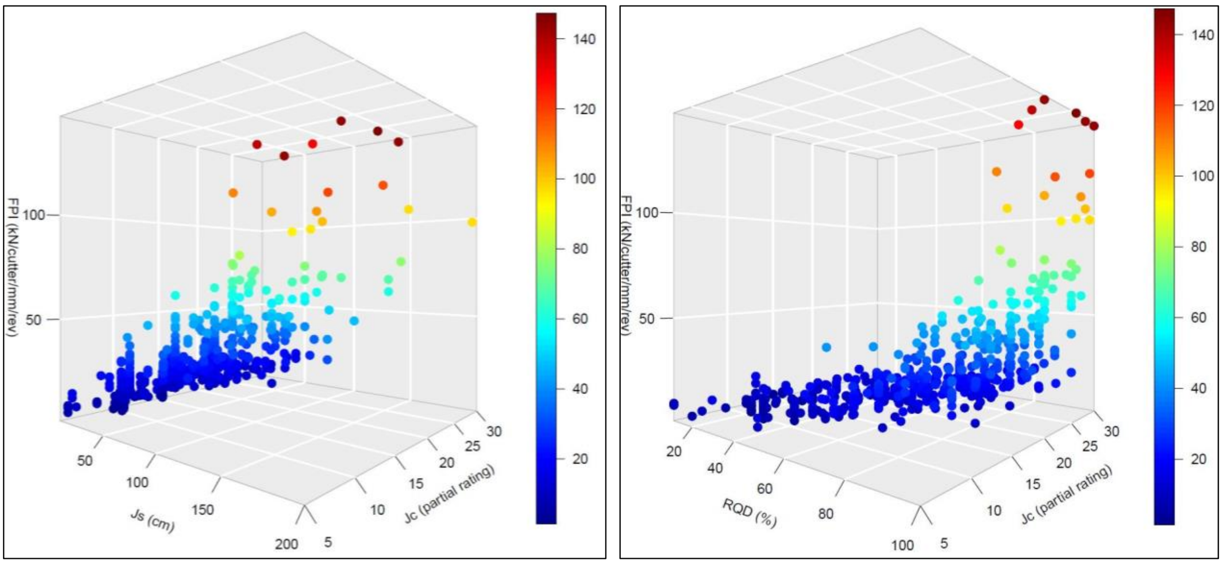

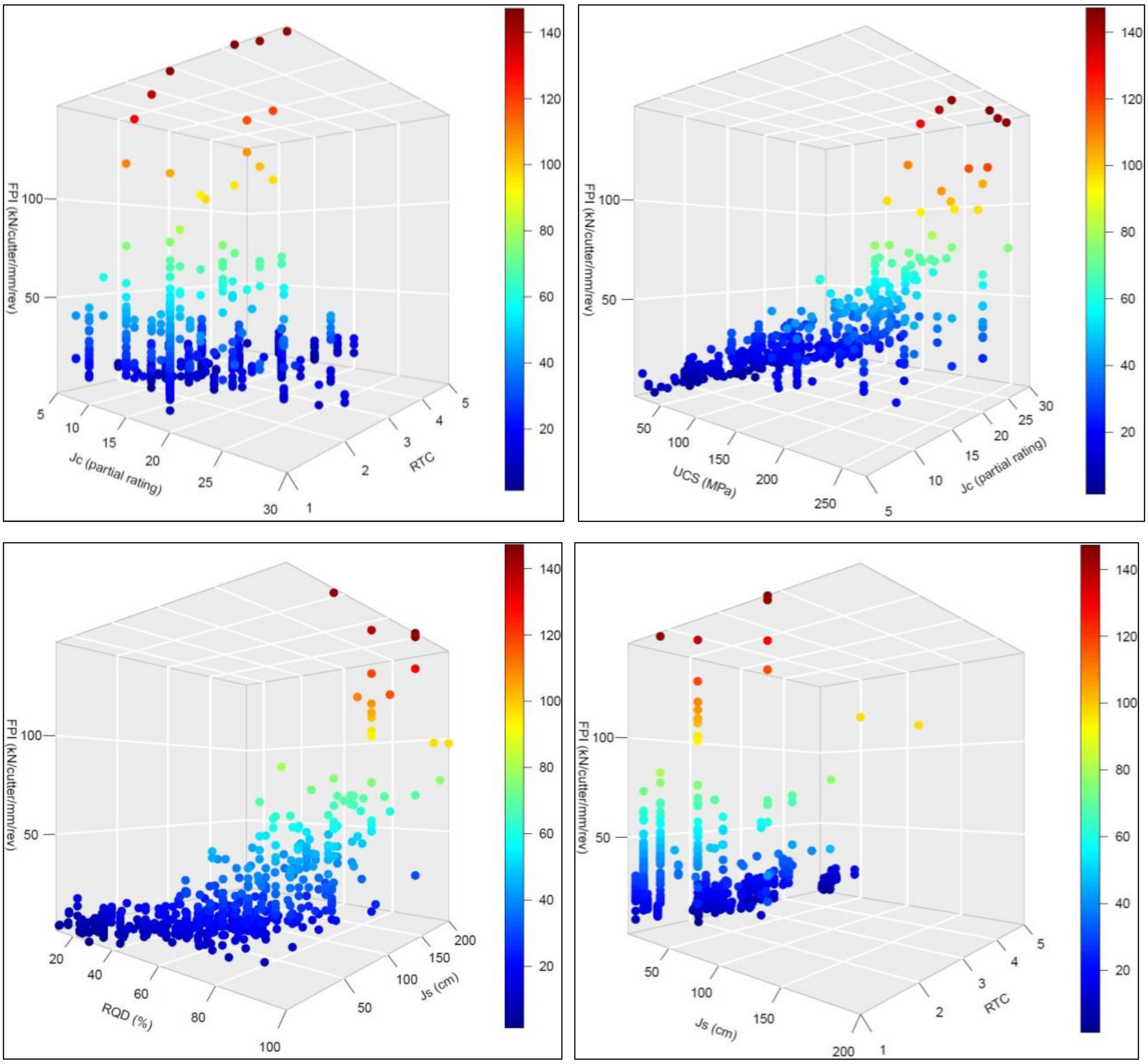
FPI (kN/cutter/mm/rev)
Jc (partial rating)
RTC
UCS (MPa)
RQD (%)
Js (cm)

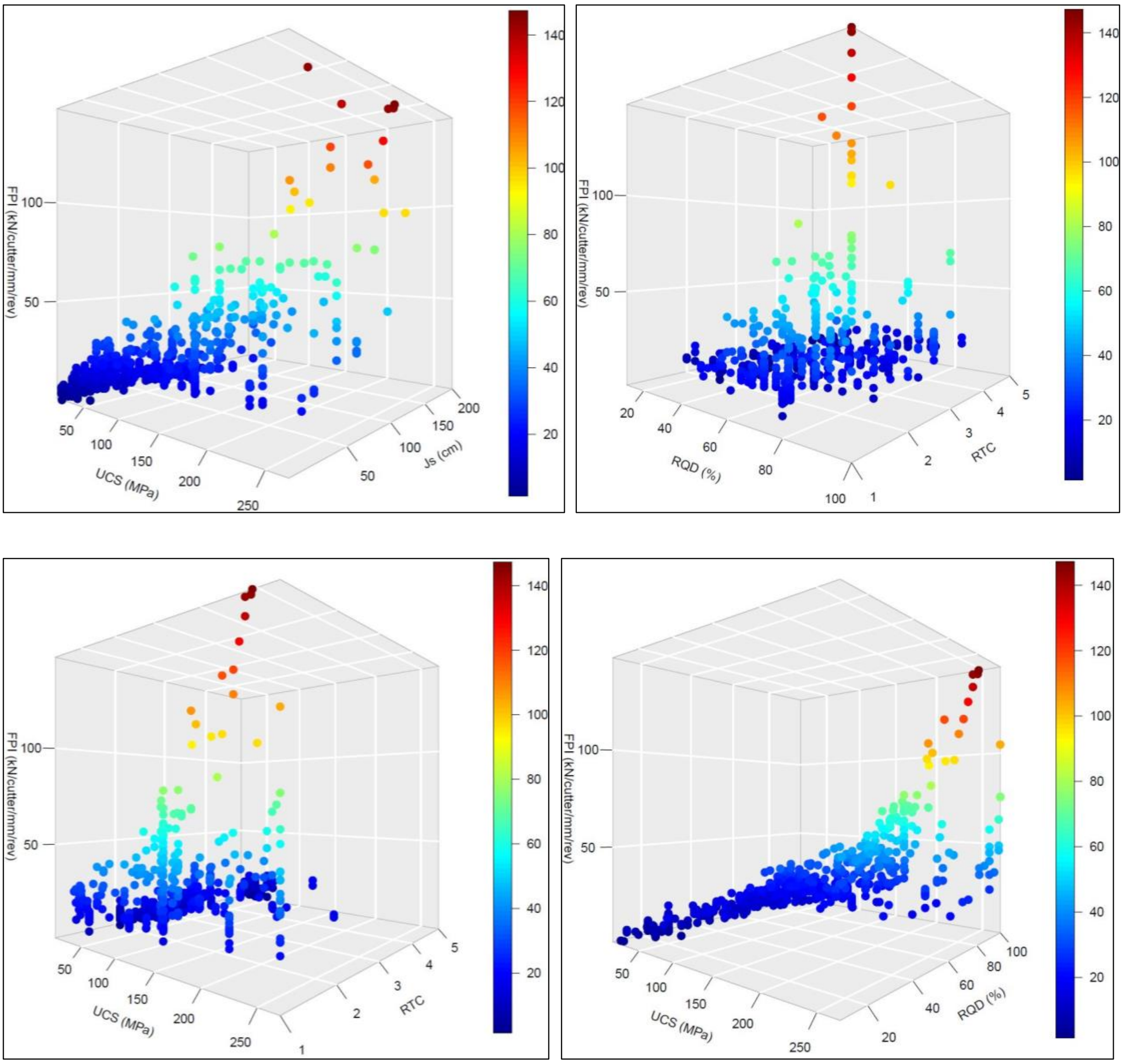

Figure 6.18: 3D graph showing the relationship of FPI with *UCS*, *RQD*, *Js*, *Jc* and *RTC*

Chapter 7 Artificial Intelligence Algorithms

7.1 Introduction

Apart from empirical and theoretical models, the use of artificial intelligence (AI) techniques has received attention in various aspects of geotechnical engineering. Several techniques, such as an artificial neural network (ANN), fuzzy logic, adaptive neuro-fuzzy inference system (ANFIS), particle swarm optimization (PSO) and support vector machine (SVM) in approximating TBM performance parameters like penetration rate (PR) and advance rate (AR) have been highlighted by many scholars. The flexible nature of the AI techniques makes them powerful tools in approximating and solving engineering problems more specifically when the problem is highly complex and nonlinear. Although AI techniques such as ANN are considered as powerful techniques in approximating TBM performance parameters, they are known as "black-box" methods and there is no clear knowledge about their internal procedures or reuse of the algorithm by others in their estimations. Therefore, in this study for the first time, two different AI models, including Classification & Regression Tree (CART) and Genetic Programming (GP) have been considered to develop a system for predicting TBM performance through offering pertinent graphs (diagrams) and mathematical equations, respectively.

7.2 Artificial Intelligence Methods & TBM Performance

One of the early works in this field was by Alvarez Grima et. al (2000) where a neuro-fuzzy method for TBM performance prediction was introduced. Benardos and Kaliampakos (2004) proposed an ANN model by using data of 1077 m of Athens Metro tunnel in Greece. Simoes and Kim (2006) employed two fuzzy inference system (FIS) types namely rule-based and parametric based to predict utilization index (UI) using data of three TBM projects. Yagiz et al. (2009) applied ANN to predict TBM PR using 7.5 km data of Queens Water Tunnel in the USA. Gholamnejad and Tayarani (2010) conducted ANN for estimation of TBM PR using data collected from three different TBM projects (the Queens Water Tunnel, USA, the Karaj-Tehran water transfer tunnel, Iran, and the Gilgel Gibe II hydroelectric project, Ethiopia. Besides, a fuzzy logic model was developed to predict the penetration rate based on collected data from one hard rock TBM tunnel (the Queens Water Tunnel in New York City, USA (Ghasemi et al. 2014) while the support vector regression (SVR) was performed by Mahdevari et al. (2014) for the same dataset collected and compiled by Yagiz (2008). Furthermore, Armaghani et al. (2017) applied two different hybrid intelligent models, containing particle swarm optimization (PSO)-artificial neural network (ANN) and imperialism competitive algorithm (ICA)-ANN and also simple ANN for predicting the TBM penetration rate in the Pahang- Selangor Raw Water Transfer (PSRWT) tunnel in Malaysia. Several works of TBM performance prediction using AI techniques have been summarized in Table 7.1.

While the domain method applied by researchers for estimation of TBM performance is ANN, the author in 2016 (Salimi et al. 2016) conducted two common AI methods, including support vector regression (SVR) and adaptive neuro-fuzzy inference system (ANFIS) using data collected from two tunnelling projects in Iran, named Zagros lot 1B and 2 for a total length of 14.3 km. In ANFIS, both of the learning capabilities of neural networks and reasoning capabilities of fuzzy logic were combined in order to enhance prediction capabilities in comparison with using a single methodology alone. Takagi-Sugeno method was considered because of its computational efficiency and higher reliability for developing a systematic approach to build fuzzy rules from the input-output dataset and among different membership functions, the Gaussian membership function was used. (see figures 7.1; 7.2 as well as Table 7.2). On the other hand, a support vector machine (SVM) "was developed for solving both classification and regression problems", which maximizes predictive accuracy and avoids over-fitting simultaneously was also employed. This is similar to a neural network; however, a neural network's solution is based on empirical risk minimization. In contrast, SVR introduces structural risk minimization into the regression and thereby achieves a global optimization, while a neural network achieves only a local minimum. The details of the topology selected for the SVR model are listed in Table 7.3. The variation of FPI with two input parameters (UCS , Js) in the form of a surface graph based on the results of SVR is shown in figure 7.3.

The results of most of these studies have been a ''black/opaque box'' programs that show a high level of accuracy and correlation between their predicted rates and actual machine performance but cannot be used by others in a similar way of using empirical models in estimating machine performance in other projects, since the end-user need to be expert in programming as well as has a good knowledge of AI methodology. In this respect, two machine learning algorithms, containing classification and regression tree (CART) and genetic programming (GP) have been utilized to assess the TBM performance which are not acting as ''black box'' and can be easily applied in other projects in the form of graph and a mathematical equation, respectively.

Table 7.1: Several investigations of TBM performance prediction using AI techniques

Reference	Technique	Input	Output	Description
Alvarez Grima et al. (2000)	ANN, ANFIS	CFF; UCS, RPM, Dc, TF	PR, AR	A database containing 640 TBM projects
Benardos and Kaliampakos (2004)	ANN	N, RQD, UCS, RMR, overburden, permeability, WTS, rock mass weathering	AR	Data collected from an interstation section of the Athens metro tunnel
Yavari and Mahdavi (2005)	ANN	Dc, UCS, Qu, TPC, Rock-type	PR	Data of 251 sections of Gavshan tunnel, Iran
Simoes and Kim (2006)	FIS	RMR, RQD, machine diameter, groundwater inflow rate	UI	Using data of three TBM projects in South Korea, USA, and New Zealand
Yagiz et al. (2009)	ANN	DPW, UCS, BI, α	PR	151 datasets collected from the Queens Water Tunnel, USA
Mikaeil et al. (2009)	FIS	DPW, UCS, BTS, α , PSI	PR	Using dataset presented by Yagiz (2008)
Gholamnejad and Tayarani (2010)	ANN	UCS, RQD, DPW	PR	185 datasets collected from three TBM projects
Eftekhari et al. (2010)	ANN	UCS, Rock Type, Qu, BTS, RQD, RMR, TF, CT, Rs	PR	Using 10 km data excavated in Zagros tunnel, Iran
Yagiz and Karahan (2011)	PSO	UCS, BTS, BI, DPW, α	PR	151 datasets collected from the Queens Water Tunnel, USA
Oraee et al. (2012)	ANFIS	RQD, DPW, UCS	PR	Using 177 datasets obtained from two tunnel projects
Gholami et al. (2012)	ANN	UCS, RQD, Js, Jc	PR	Data of 121 tunnel sections
Salimi and Esmaeili (2013)	ANN	PSI, UCS, BTS, DPW, α	PR	Data of 46 sections of the Karaj–Tehran water supply tunnel
Torabi et al. (2013)	ANN	UCS, C, φ , ν	PR, UI	Data of 39 sections of Tehran–Shomal highway project
Shao et al. (2013)	ELM	PSI, UCS, BTS, DPW, α	PR	153 datasets of Queens Water Tunnel, USA

Reference	Technique	Input	Output	Description
Mahdevari et al. (2014)	SVR	UCS, BTS, BI, DPW, α , SE, TF, CP, CT	PR	150 data points pertaining to the Queens Water Tunnel, USA
Ghasemi et al. (2014)	FIS	DPW, UCS, BI, α	PR	151 datasets collected from the Queens Water Tunnel, USA
Salimi et al. (2016)	ANFIS, SVR	UCS, Js	PR (FPI)	Zagros lot 1B and 2, Iran (75 datasets)
Armaghani et al. (2017)	ANN, PSO-ANN, ICA-ANN	UCS, BTS, RQD, RMR, WZ, TF, RPM	PR	1286 data points of a water transfer tunnel in Malaysia

The distance between planes of weakness (DPW); rock brittleness (BI); the angle between the plane of weakness and TBM-driven direction (α); rock quality designation (RQD); rock mass rating (RMR); core fracture frequency (CFF); revolution per minute (RPM); penetration rate (PR); advance rate (AR); utilization index (UI); cutter diameter (Dc); particle swarm optimization (PSO); peak slope index (PSI) also refers to rock brittleness; quartz percentage (Qu); the rotational speed of TBM (Rs); joint spacing (Js); joint condition (Jc); cohesion (C); friction angle (φ); Poisson's ratio (ν); specific energy (SE); thrust force (TF); cutterhead power (CP); cutterhead torque (CT); extreme learning machine (ELM); overload factor (N); uniaxial compressive strength (UCS); water table surface (WTS); differential evolution (DE); field penetration index (FPI); imperialism competitive algorithm (ICA), fuzzy inference system (FIS), support vector regression (SVR), adaptive neuro-fuzzy inference system (ANFIS).

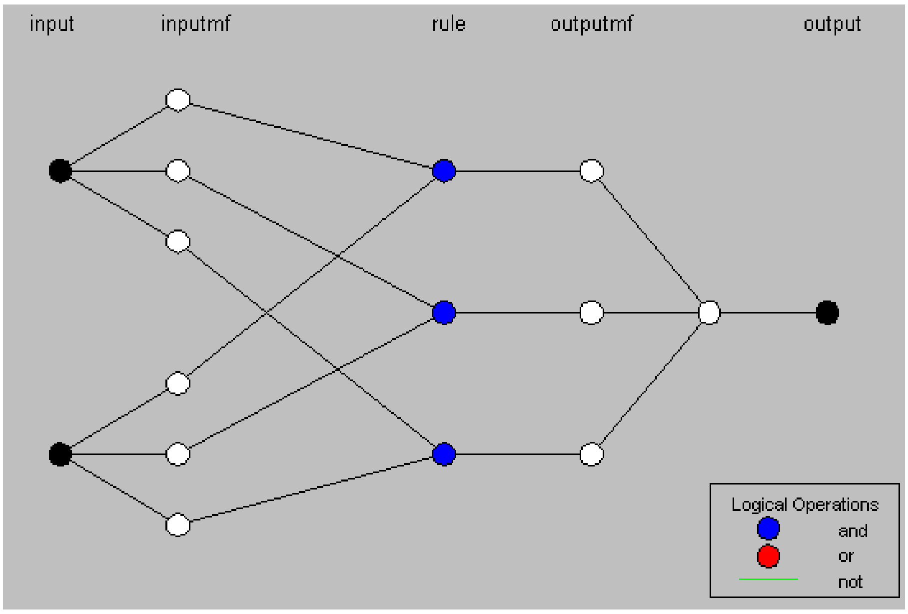

Figure 7.1: ANFIS model structure for FPI prediction (Salimi et al. 2016a)

(a)

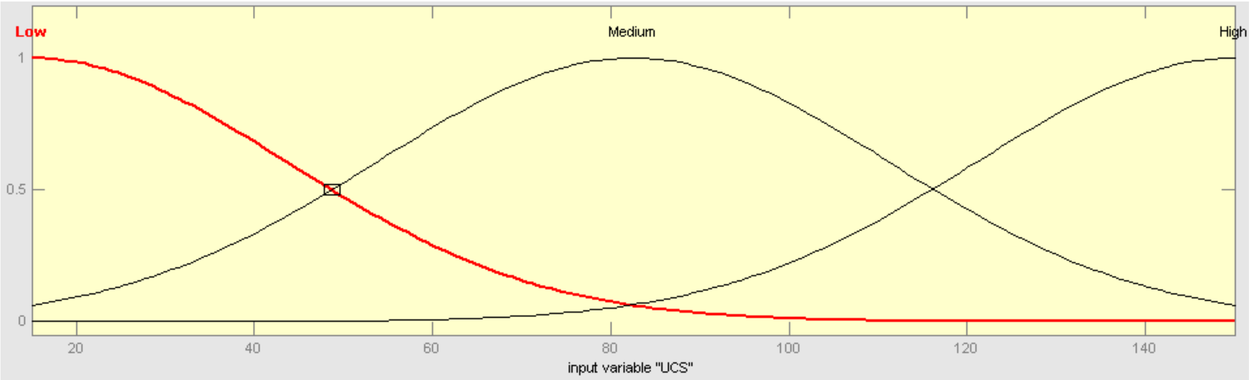

(b)

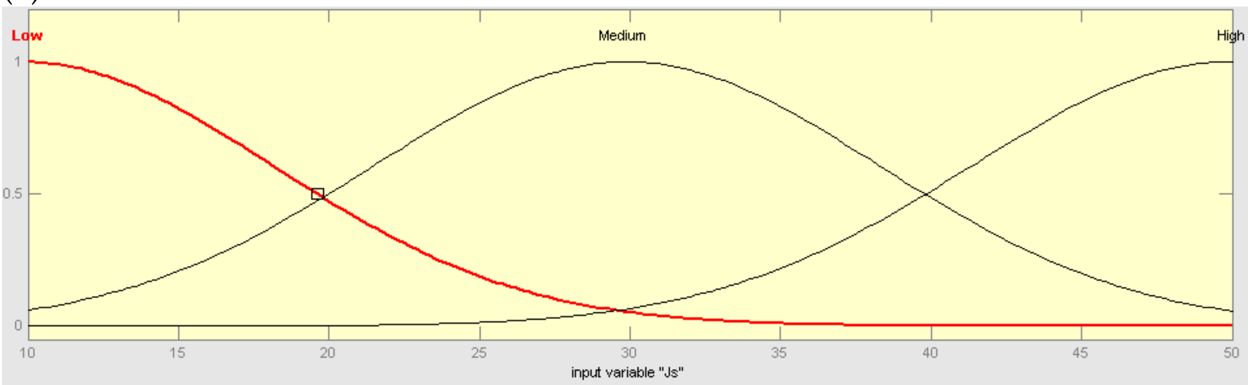

Figure 7.2: TSK membership function plot for input (a) ''Uniaxial compressive strength (UCS)'', (b) ''Joint spacing (Js)'' (Salimi et al. 2016a)

Table 7.2: The ANFIS information used for developing a model for estimation of TBM FPI (Salimi et al. 2016a)

ANFIS parameter type	**Value**
MF type	Gaussian
Number of MFs	3
Number of fuzzy rules	3
Output function	Linear
Number of nodes	23
Number of linear parameters	9
Number of nonlinear parameter	12
Total number of parameters	21
Training RMSE	2.43

Table 7.3: Parameters of the SVR model for estimation of TBM FPI (Salimi et al. 2016a)

Parameter	Value
Type	ε-SVR
Kernel	Radial basis function (RBF)
Degree	2
γ	1
ε	0.1
C	25
Tolerance of stopping criterion	0.0001

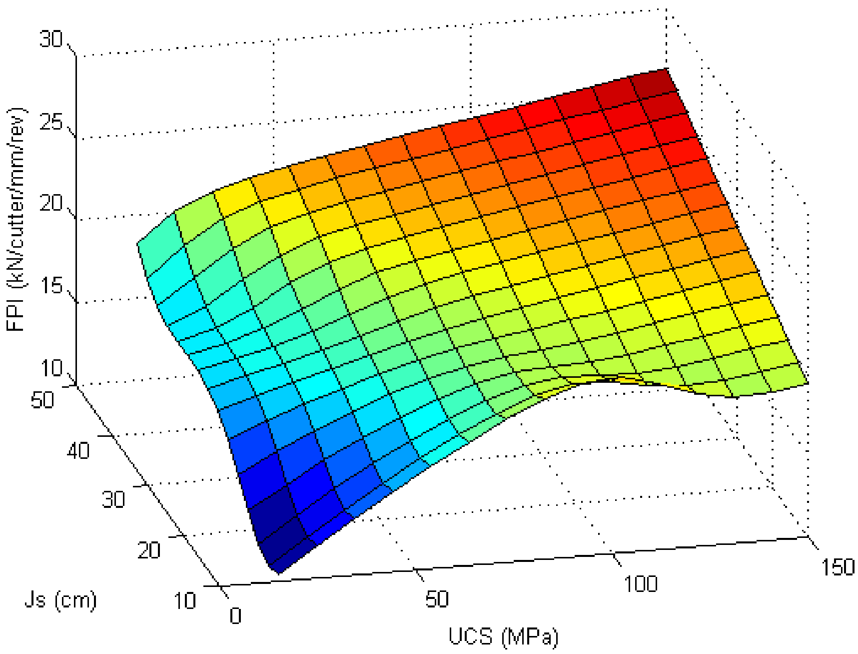

Figure 7.3: Surface graph generated by SVR showing relationship of FPI with *UCS* and *Js* (Salimi et al. 2016a)

7.2.1 TBM Performance Prediction by Regression Tree

One of the most popular techniques in data mining (analysis) is a DT (decision tree) in which a simple and comprehensible structure is used that can be utilized for classification, recognition, decision making as well as prediction of certain target parameters. In comparison to other ML algorithms such as ANNs or SVRs which have a complex structure and known as a black box, meaning that, they can be applied to predict the value of a target variable depending on data, but the rules or implicit patterns within the model cannot be interpreted. Therefore, the application of a DT for a prediction scheme is usually preferred for its simplicity, explicability, and low computational costs. Thus, the main advantage of using DT algorithms is that the tree structure can be presented, easily interpreted, and defined as a white box. There are several kinds of DT methods, including CART (classification & regression tree), chi-squared automatic interaction detector (CHAID), exhaustive CHAID (E-CHAID), quick, unbiased, efficient statistical tree (QUEST), random forest regression and classification (RFRC), and boosted tree classifiers and regression (BTCR). According to the literature review, among the above six different DT methods, CART has been widely conducted with a high level of accuracy and performance for predicting problems in different engineering fields. CART is a rule-based method introduced by Breiman et al. (1984) and is based on whether the dependent variable is qualitative or quantitative; as such it can be categorized as a classification tree (CT) or regression tree (RT), respectively. The fact is that, this technique is recommended for use in situations where the form of the relationships between the dependent variable (response) and independent variables (predictors) is not exactly known before building a predictive model (Breiman et al. 1984). Besides, in CART analysis, there is no need to consider prior suppositions about the relationship between variables.

An RT can perform recursive partitioning (aka recursive partitioning) as an alternative method to the traditional multiple regressions. In the case of a database with a complex of variables and nonlinear interactions, constructing a single global predictive model can be arduous and confusing. Therefore, partitioning or subdividing the space into smaller regions where the interactions become more manageable and can be considered as an alternative to mitigate the problem.

Decision trees are represented by a set of questions that splits the learning sample into smaller and smaller parts. CART asks only yes/no questions. CART algorithm will search for all possible variables and all possible values in order to find the best split – the question that splits the data into two parts with maximum homogeneity. The process is then repeated for each of the resulting data fragments. A DT includes a root node, interior nodes, branches, and terminal nodes (see Fig. 7.4) in which the root node contains a complete dataset and is divided into two sub-nodes with left and right branches while each node represents a variable; the branches indicate a specific range of input variables. A sequence of elements of the root node, branches, and interior nodes forms a leaf (Breiman et al. 1984).

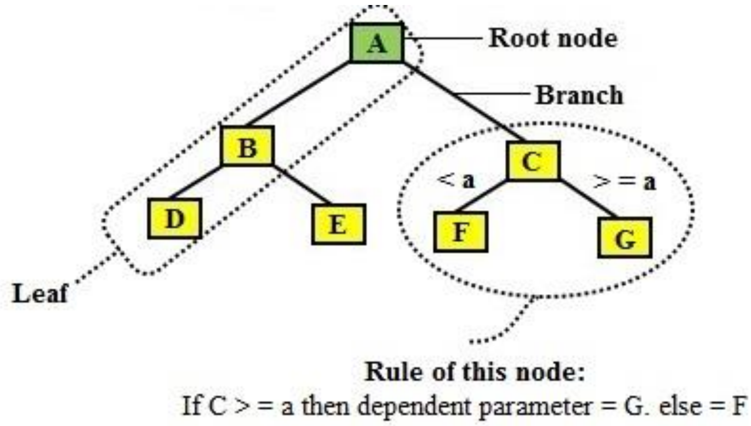

Figure 7.4: Structure of a decision tree

7.2.1.1 Classification Tree

Classification trees are used when for each observation of the learning sample, we know the class in advance. Classes in the learning sample may be provided by a user or calculated in accordance with some exogenous rule. For example, for a stock trading project, the class can be computed as subject to a real change of asset price. Let t_p be a parent node and t_l, t_r -respectively left and right child nodes of a parent node t_p. Consider the learning sample with a variable matrix X with M a number of variables x_j and N observations. Let the class vector Y consist of N observations with the total amount of K classes. The classification tree is built in accordance with the splitting rule - the rule that performs the splitting of learning samples into smaller parts. We already know that each time data has to be divided into two parts with maximum homogeneity:

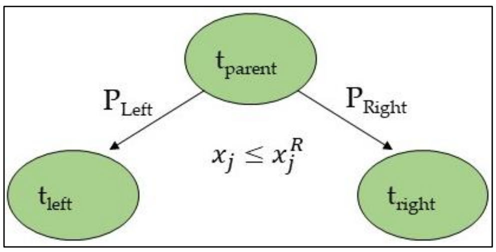

Figure 7.5: Splitting algorithm of CART

Where t_p, t_l, t_r -parent, left and right nodes; x_j -variable j; x_j^R is the best splitting value of a variable x_j. Maximum homogeneity of child nodes is defined by the so-called *impurity function* $i(t)$. Since the impurity of the parent node t_p is constant for any of the possible splits $x_j \le x_j^R$, $j = 1,\dots,M$, the maximum homogeneity of left and right child nodes will be equivalent to the maximization of change of impurity function $\Delta i(\mathrm{t})$:

$$\Delta i(\mathrm{t}) = i(t_p) - E\left[i(t_c)\right]$$
(7.1)

Where t_c -left and right child nodes of the parent node t_p. Assuming that the P_l, P_r -probabilities of right and left nodes, we get:

$$\Delta i(\mathrm{t}) = i(t_p) - \mathrm{P}_l\, i(t_l) - P_r\, i(t_r) \tag{7.2}$$

Therefore, at each node CART solves the following maximization problem:

$$\text{argmax} \quad x_j \le x_j^R,\ j = 1,\dots,M \quad \left[i(t_p) - P_l i(t_l) - P_r i(t_r)\right] \tag{7.3}$$

Equation 7.3 implies that CART will search through all possible values of all variables in the matrix X for the best split question $x_j \le x_j^R$ which will maximize the change of impurity measure $\Delta i(\mathrm{t})$.

RT algorithms use a binary-dividing procedure that splits the dataset from a root node (parent node) based on yes/no questions of the independent variables in which the created sub-nodes (child or interior nodes) are purer than the parent node. During this process, candidates are searched to reach the optimum split which results in a tree with high purity. The next important question is how to define the impurity function $i(\mathrm{t})$. In theory, there are several impurity functions. Some of the most frequent ones are gain ratio (Quinlan, 1993), Gini Index (Breiman et al. 1984), and chi-square (Mingers, 1989). In RT, usually, the Gini index is used for selecting the best split. Gini splitting rule (or Gini index) is the most broadly used rule. It uses the following impurity function $i(\mathrm{t})$:

$$i(t) = \sum_{k \ne l} p(k|t)\, p(l|t) \tag{7.4}$$

where $k, l \quad 1,\dots,K$ -index of class; $p(k|t)$ is a conditional probability of class k provided we are in a node t. Applying the Gini impurity function (7.4) to the maximization problem (7.3). we will get following change of impurity measure $\Delta i(\mathrm{t})$:

$$\Delta i(\mathrm{t}) = -\sum_{k=1}^{K} p^2(k \mid \mathrm{t}_p) + P_l \sum_{k=1}^{K} p^2(k \mid t_l) + P_r \sum_{k=1}^{K} p^2(k \mid t_r) \tag{7.5}$$

Therefore, Gini algorithm will solve the following problem:

argmax

$$x_j \le x_j^R \ , j = 1,\ldots,M \ \left[-\sum_{k=1}^{K} p^2(k \mid t_p) + P_l \sum_{k=1}^{K} p^2(k \mid t_l) + P_r \sum_{k=1}^{K} p^2(k \mid t_r) \right] \tag{7.6}$$

Gini algorithm will search in the learning sample for the largest class and isolate it from the rest of the data. Gini works well for noisy data.

7.2.1.2 Regression Tree

Regression trees do not have classes. Instead, there are a response vector Y which represents the response values for each observation in variable matrix X. Since regression trees do not have pre-assigned classes, classification splitting rules like Gini 7.6. Consider we have a continuous response variable Y and two inputs X_1 and X_2. The recursive partitioning results in three regions (R_1, R_2, R_3) where the model predicts Y with constant \$c_m\$ for region R_m:

$$\hat{f}(X) = \sum_{m=1}^{3} c_m I(X_1, X_2) \in R_m \tag{7.7}$$

However, an important question remains of how to grow a regression tree. It's important to realize the partitioning of variables is done in a top-down, greedy fashion. This just means that a partition performed earlier in the tree will not change based on later partitions. The model begins with the entire data set S and searches every distinct value of every input variable to find the predictor and split value that partitions the data into two regions $(R_1, \text{and}\, R_2)$ such that the overall sums of squares error are minimized:

$$\text{minimize}\left\{ SSE = \sum_{i \in R_1} (y_i - c_1)^2 + \sum_{i \in R_2} (y_i - c_2)^2 \right\} \tag{7.8}$$

Having found the best split, we partition the data into the two resulting regions and repeat the splitting process on each of the two regions. This process is continued until some stopping criterion is reached.

The process of partitioning in RT algorithms is repeated until achieving the stop condition that was previously assigned. Several criteria can be considered, such as the minimum number of observations for the node split, the minimum number of observations in a leaf, the maximum tree depth, the number of intervals, and the complexity of parameters. The main goal of these parameters is to reduce computational time by pruning off the splits which do exhibit no worth. The structural complexity of the trees is related to the minimum number of observations; therefore, increasing the number of minimum observations in nodes leads to the less complexity of the model. To prevent the overgrowth of trees and over-fitting of the problems as well as achieve the predictive model with the highest accuracy and lowest estimation error, the optimum number of these parameters should be determined. Each leaf, or final node, represents a simple regression which is dedicated to that node. Pruning can be implemented in order to enhance the tree's generalization capacity, when the process of the tree's induction is fulfilled. The number of observations in nodes can be taken into consideration as pruning criteria.

The CART algorithm is able to detect the outliers in the dataset and eliminate them during the partitioning procedure. Furthermore, a CART uses inherent principal component analysis (PCA) to identify the most important parameters in the modeling (Michael and Gordon 1997; Kiers et al. 2000; Myles et al. 2004; MATLAB, 2006). Further information regarding the algorithm and its mathematical logic can be found in Breiman et al. (1984).

In order to build the CART model, the R statistical computing software "rpart" was used (see Appendix). Similar data which has been employed in linear and non-linear regression models are used, i.e., 580 as-built data with a total length of 60.63 km tunnel length. It is worth noting that the CART model has the ability to deem qualitative variables as well as descriptive parameters such as rock type, RTC in the analysis. The suggested interval software for maximum ''tree depth'' and the ''number of the intervals'' were [2–10] and [1–10], respectively. The higher in-depth, the model becomes more complicated and harder for production of the tree; and low three depth means lower accuracy which some parameters may be omitted. Hence, the related tree depth was reduced to [3–8] and several CART models with different controlling parameters were created by trial and error. There is often a balance to be achieved in the depth and complexity of the tree to optimize predictive performance on some unseen data. To find this balance, we typically grow a very large tree as defined in the previous section and then prune it back to find an optimal subtree. The optimal subtree can be found by using a *cost complexity parameter* that penalizes our objective function in 7.8 for the number of terminal nodes of the tree as in equation 7.9.

$$\text{minimize}\left\{SSE + \alpha''\left|T''\right|\right\} \tag{7.9}$$

For a given value of the smallest pruned tree that has the lowest penalized error can be achieved. As with these regularization methods, smaller penalties tend to produce more complex models, which result in larger trees. Whereas larger penalties result in much smaller trees. Consequently, as a tree grows larger, the reduction in the SSE must be greater than the cost complexity penalty. Behind the scenes "rpart" is automatically applying a range of cost complexity (α") values to prune the tree. To compare the error for each α" value, "rpart" performs 10-fold cross-validation so that the error associated with a given α" value is computed.

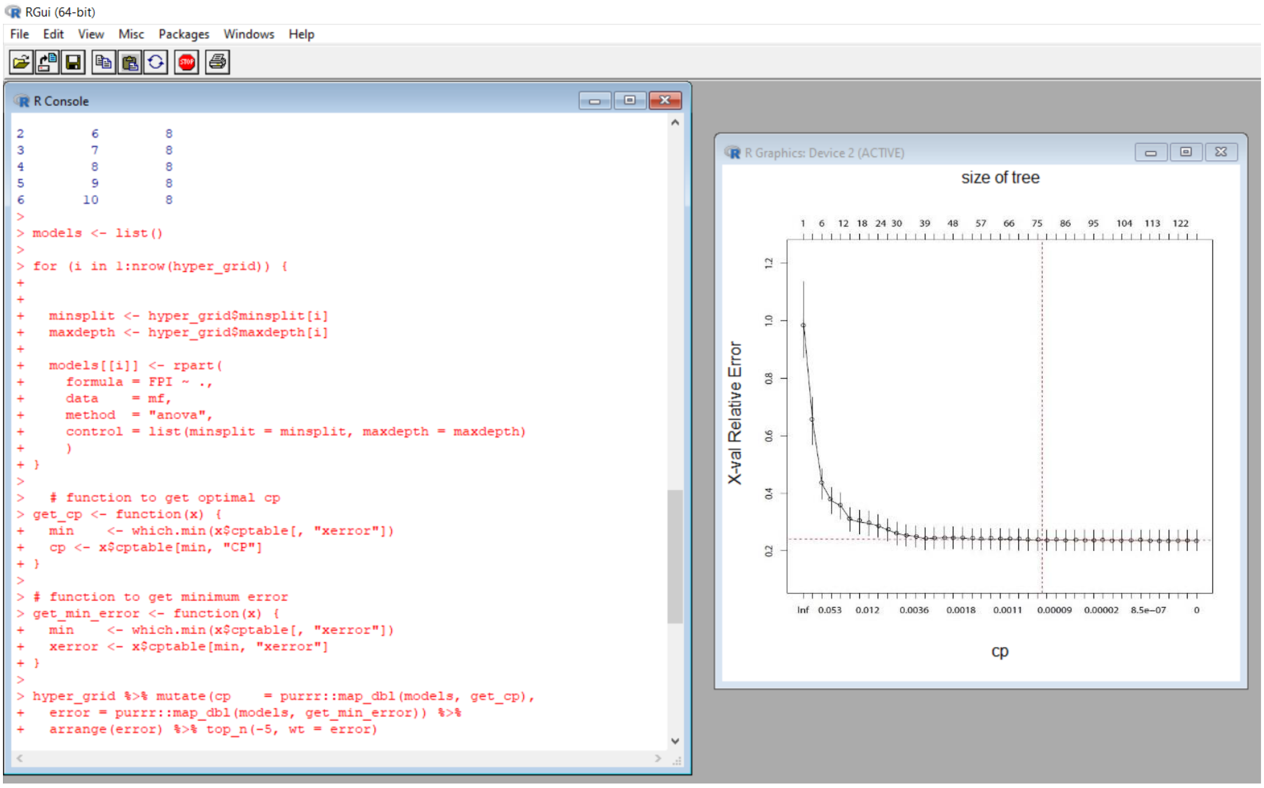

Figure 7.6: Cost complexity in terms of optimum tree size generated by "rpart"

In brief, given a set of samples, CART identifies one input variable and one break-point, before partitioning the samples into two child nodes. Starting from the entire set of available samples (root node), a recursive binary partition is performed for each node until no further split is possible or a certain terminating criterion is satisfied. At each node, the best split is identified by exhaustive search, i.e., all potential splits on each input variable and each break-point are tested, and the one corresponding to the minimum deviations by respectively predicting two child nodes of samples with their mean output variables is selected. After the tree growing procedure, typically an overly large tree is constructed, resulting in a lack of model generalization to unseen samples. A procedure of pruning is employed to remove sequentially the splits contributing insufficiently to training accuracy. The tree is pruned from the maximal-sized tree all the way back to the root node, resulting in a sequence of candidate trees. Each candidate tree is tested on an independent validation sample set and the one corresponding to the lowest prediction error is selected as the final tree (Breiman, 2001).

To analyse the performance of the models, root-mean-square-error (RMSE) has been calculated and used to quantify the errors generated by each model. It should be mentioned that, the values of the maximum tree depth, number of intervals, minimum number of the parent node, the minimum number of the child node, and the *cost complexity parameter* (cp) related to the best model are 7, 7, 3, 2 and 0.0001, respectively. The best final tree was scripted via C++ programming language and visualized/depicted by "FigTree software - v1.4.0" (http://tree.bio.ed.ac.uk/software/figtree/) (Figure 7.7). Figure 7.8 illustrates the preferable tree. The developed tree model has 153 nodes which are specified by squares and their related numbers and the name of variable related to the node and interval changes are shown. The optimum size of the tree (number of terminal nodes) is 77. The detailed information regarding the structure of the tree is presented in Table 7.4. The relationship between measured and predicted values obtained from the CART model is shown in Fig. 7.9. The correlation coefficient (R^2) between measured and predicted FPI by the CART model is 0.91.

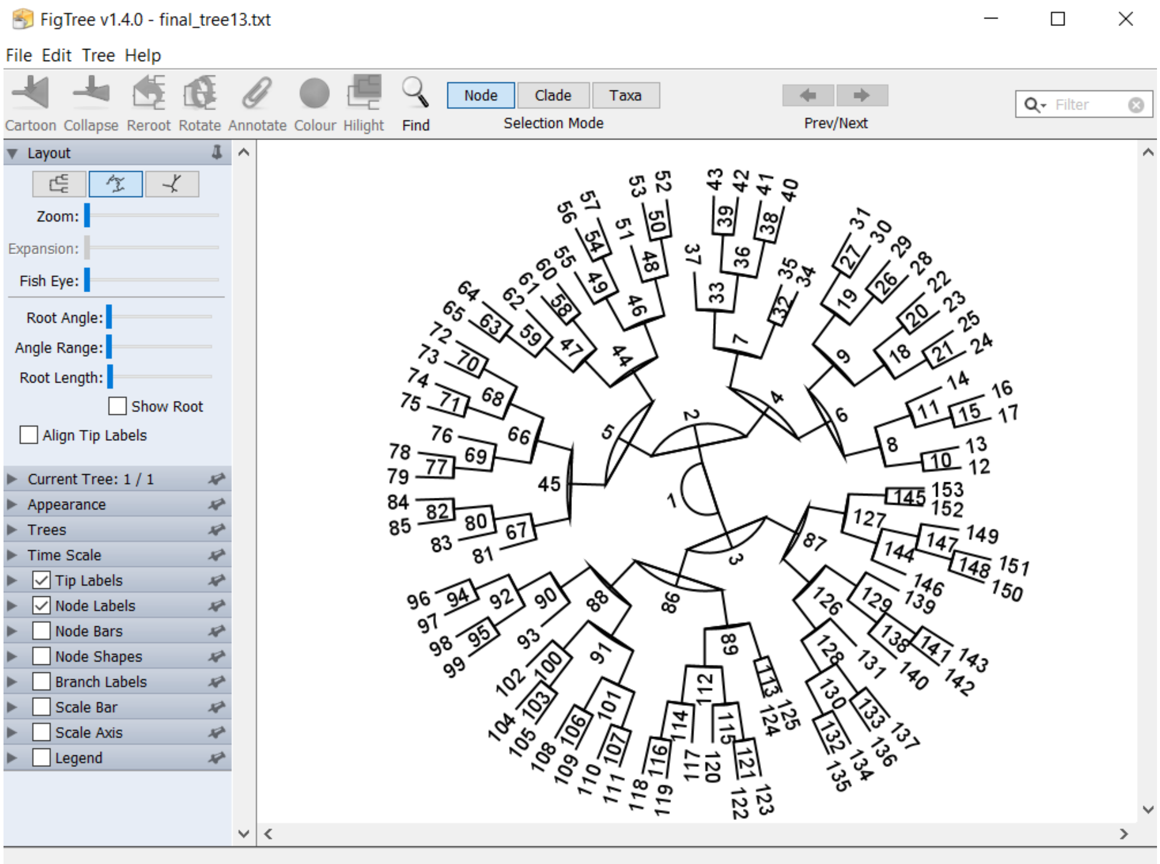

Figure 7.7: FigTree software - v1.4.0 "circle version of developed CART model"

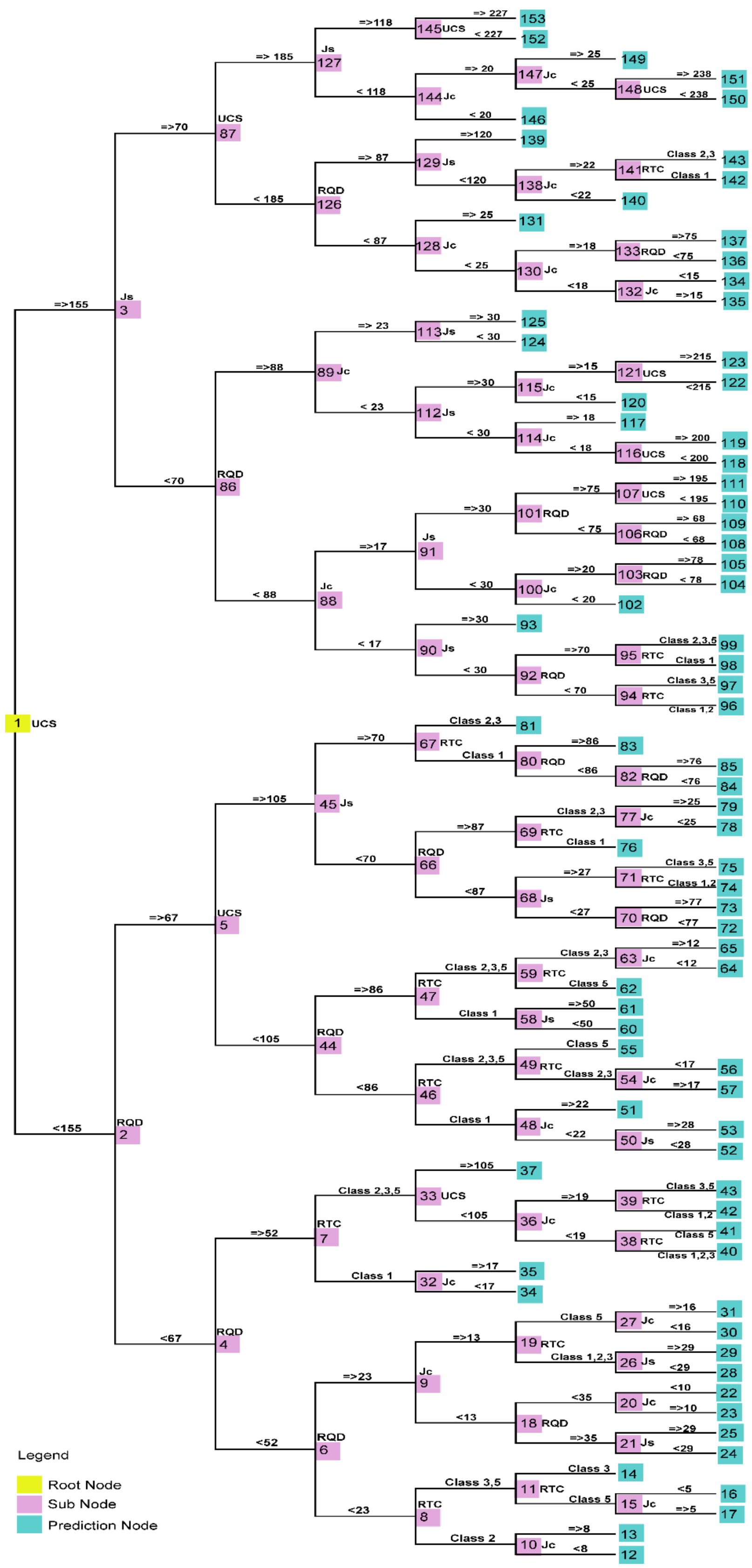

Figure 7.8: Regression tree developed for FPI prediction

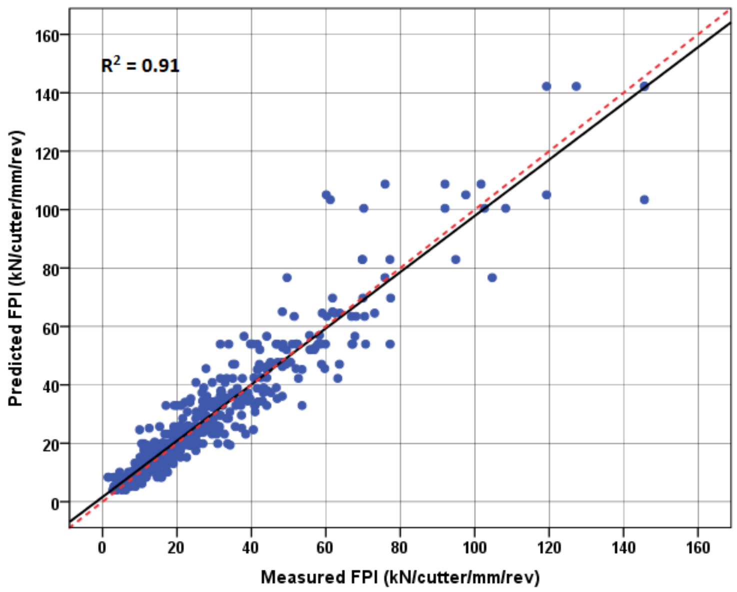

Figure 7.9: Comparison between the measured and predicted FPI from CART model

Table 7.4: Information related to each node in the CART model generated via "rpart"

Node	Fre-quency	Split variable	Value	Pre-dicted	Node	Fre-quency	Split variable	Value	Pre-dicted
1	580	-	-	26.49	78	8	Jc	[20, 25]	23.80
2	421	UCS	[6, 155]*	17.67	79	6	Jc	[25, 30]	37.31
3	159	UCS	[155, 267.9]	49.86	80	8	RTC	class 1	45.53
4	223	RQD	[10, 67]	11.54	81	4	RTC	class 2, 3	30.77
5	198	RQD	[67, 100]	24.56	82	6	RQD	[67, 86]	43.12
6	155	RQD	[10, 52]	9.27	83	2	RQD	[86, 100]	52.75
7	68	RQD	[52, 67]	16.72	84	2	RQD	[67, 76]	38.85
8	33	RQD	[10, 23]	6.28	85	4	RQD	[76, 86]	45.25
9	122	RQD	[23, 52]	10.08	86	110	Js	[10, 70]	38.52
10	5	RTC	class 2	11.60	87	49	Js	[70, 200]	75.33
11	28	RTC	class 3, 5	5.34	88	65	RQD	[50, 88]	30.12
12	2	Jc	[5, 8]	9.12	89	45	RQD	[88, 100]	50.65
13	3	Jc	[8, 12]	13.25	90	36	Jc	[8, 17]	23.67
14	6	RTC	class 3	7.14	91	29	Jc	[17, 30]	38.14
15	22	RTC	class 5	4.84	92	33	Js	[10, 30]	22.72
16	15	Jc	[5, 12]	4.04	93	3	Js	[30, 70]	34.03
17	7	Jc	[12, 15]	5.22	94	15	RQD	[49, 70]	20.08
18	81	Jc	[5, 13]	9.03	95	18	RQD	[70, 100]	24.92
19	41	Jc	[13, 21]	12.16	96	11	RTC	class 1, 2	21.10
20	59	RQD	[23, 35]	8.52	97	4	RTC	class 3, 5	17.27
21	22	RQD	[35, 52]	10.38	98	16	RTC	class 1	25.72

Node	Fre-quency	Split variable	Value	Pre-dicted	Node	Fre-quency	Split variable	Value	Pre-dicted
22	2	Jc	[5, 10]	8.36	99	2	RTC	class 2, 3, 5	18.55
23	57	Jc	[10, 30]	13.08	100	17	Js	[10, 30]	33.57
24	20	Js	[2.2, 29]	10.12	101	12	Js	[30, 70]	44.62
25	2	Js	[29, 37]	12.94	102	3	Jc	[15, 20]	32.01
26	32	RTC	class 1, 2, 3	12.78	103	14	Jc	[20, 30]	40.82
27	9	RTC	class 5	9.94	104	7	RQD	[50, 78]	29.59
28	29	Js	[5, 29]	10.68	105	7	RQD	[78, 100]	34.44
29	3	Js	[29, 41]	13.00	106	6	RQD	[50, 75]	33.93
30	5	Jc	[12, 16]	6.17	107	6	RQD	[75, 88]	55.32
31	4	Jc	[16, 21]	14.66	108	4	RQD	[50, 68]	32.29
32	8	RTC	class 1	23.22	109	2	RQD	[68, 100]	37.20
33	60	RTC	Class 2, 3, 5	15.86	110	3	UCS	[155, 195]	51.01
34	4	Jc	[10, 17]	20.46	111	3	UCS	[195, 267.9]	57.00
35	4	Jc	[17, 22]	25.98	112	39	Jc	[10, 23]	46.52
36	55	UCS	[6, 105]	15.33	113	6	Jc	[23, 30]	77.50
37	5	UCS	[105, 155]	21.71	114	14	Js	[10, 30]	39.35
38	43	Jc	[10, 19]	14.63	115	25	Js	[30, 70]	50.53
39	12	Jc	[19, 28]	17.83	116	8	Jc	[10, 18]	37.20
40	34	RTC	class 1, 2, 3	15.22	117	6	Jc	[18, 30]	42.22
41	9	RTC	class 5	12.40	118	5	UCS	[155, 200]	36.10
42	3	RTC	class 1, 2	19.38	119	3	UCS	[200, 267.9]	39.04
43	9	RTC	class 3, 5	13.21	120	2	Jc	[10, 15]	35.31
44	131	UCS	[6, 105]	21.49	121	23	Jc	[15, 30]	51.86
45	67	UCS	[105, 155]	30.57	122	16	UCS	[155, 215]	47.06
46	110	RQD	[67, 86]	20.28	123	7	UCS	[215, 267.9]	54.00
47	21	RQD	[86, 100]	27.81	124	4	Js	[10, 30]	64.56
48	48	RTC	class 1	23.19	125	2	Js	[30, 70]	103.40
49	62	RTC	class 2, 3, 5	18.03	126	28	UCS	[155, 185]	54.19
50	45	Jc	[10, 22]	22.37	127	21	UCS	[185, 267.9]	103.52
51	3	Jc	[22, 28]	35.38	128	13	RQD	[60, 87]	47.45

Node	Frequency	Split variable	Value	Predicted	Node	Frequency	Split variable	Value	Predicted
52	26	Js	[10, 28]	19.29	129	15	RQD (%)	[87, 100]	60.03
53	19	Js	[28, 80]	24.63	130	11	Jc	[10, 25]	44.25
54	58	RTC	class 2, 3	18.43	131	2	Jc	[25, 30]	65.05
55	4	RTC	class 5	12.28	132	5	Jc	[10, 18]	40.67
56	23	Jc	[10, 17]	17.10	133	6	Jc	[18, 30]	42.43
57	35	Jc	[17, 30]	20.05	134	3	Jc	[10, 15]	47.23
58	5	RTC	class 1	35.64	135	2	Jc	[15, 30]	38.03
59	16	RTC	class 2, 3, 5	25.36	136	2	RQD	[60, 75]	46.26
60	3	Js	[20, 50]	34.14	137	4	RQD	[75, 100]	47.71
61	2	Js	[50, 140]	37.90	138	12	Js	[70, 120]	57.60
62	4	RTC	class 5	18.41	139	3	Js	[120, 200]	69.72
63	12	RTC	class 2, 3	27.67	140	5	Jc	[15, 22]	52.05
64	9	Jc	[10, 12]	25.15	141	7	Jc	[22, 30]	61.57
65	3	Jc	[12, 25]	28.50	142	5	RTC	class 1	63.43
66	55	Js	[10, 70]	28.38	143	2	RTC	class 2, 3	56.94
67	12	Js	[70, 140]	40.61	144	14	Js	[70, 118]	92.13
68	36	RQD	[67, 87]	25.51	145	7	Js	[118, 200]	126.29
69	19	RQD	[87, 100]	33.80	146	3	Jc	[15, 20]	87.60
70	21	Js	[10, 27]	22.65	147	11	Jc	[20, 30]	108.74
71	15	Js	[27, 70]	29.52	148	7	Jc	[20, 25]	80.26
72	4	RQD	[67, 77]	20.55	149	4	Jc	[25, 30]	100.45
73	17	RQD	[77, 100]	23.15	150	4	UCS	[185, 238]	76.72
74	11	RTC	class 1, 2	32.92	151	3	UCS	[238, 267.9]	82.93
75	4	RTC	class 3, 5	20.16	152	3	UCS	[185, 227]	105.07
76	5	RTC	class 1	45.58	153	4	UCS	[227, 267.9]	142.20
77	14	RTC	class 2, 3	29.59					

*The software keeps the left bracket open

7.2.2 TBM Performance Prediction by Genetic Programming

Genetic programming (GP) is an automatic programming technique modeled on Darwin's theory of 'survival of the fittest' and natural evolution that was first invented by Cramer (1985) and then developed in the true mathematical formulation by Koza (1992).

GP is a branch of evolutionary algorithms (EAs) which is obtained from the development of genetic algorithm (GA) (Ferreira, 2001). Nevertheless, genetic programming differs from the other Evolutionary Algorithm (EA) disciplines in its application area. While the other EAs normally pertain to optimization problems, GP is related to machine learning. GP is utilized to discover systems (Fig.7.10a), while most of the other EAs generally seek for input to optimize the solution to the system (Fig.7.10b).

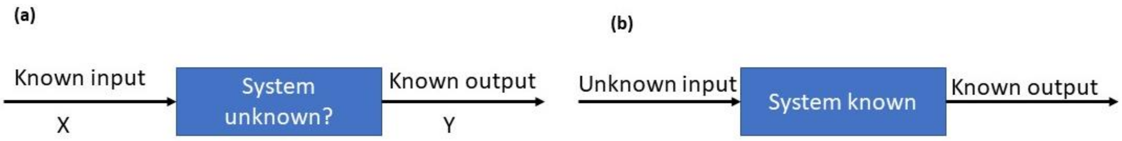

Figure 7.10: Process of modelling and optimization problems

The main difference between GP and other EAs like GA is related to the structure of the problem solutions (individuals). Individuals in GA are linear coded binary strings of a fixed length that known as chromosomes, whereas in GP individuals are the computer programs which follow LISP language. LISP is an acronym of the processing list and can be applied for executing the data strings. The programs are called symbolic expression (s-Expression) and can be presented in the form of a tree structure with different sizes and shapes. The population in GP is initialized with randomly generated the programs which are composed of the terminal set (T) and function set (F). The fact is that, if the terminal and function set are not selected appropriately for the problem, the desired results cannot be achieved.

Terminals are input (independent) variables of the model and a set of constant values that assigned as GP designers according to the nature of the problem. The function set is arithmetical, logical, Booleans, or user-defined functions (e.g., +, -, *, /, ^2, ^3, Q, sin, cos, tan, ln, and, or, not, nor, etc.). A typical program, presenting the expression is demonstrated in Fig. 7.11. In this example, the function set (F) is consisted of multiplication, division, addition, subtraction and the tangent function, F = {×, /, +, -, tan} and the terminal set (T) is consisted of N = 3 variable as T = {a, b, c}.

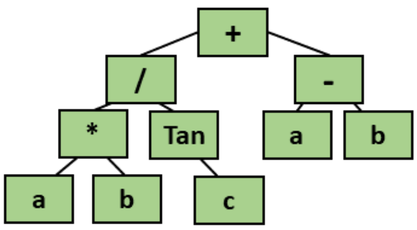

Figure 7.11: A typical parse tree structure of the function ab/ (tan(c)) + (a - c)

As discussed before, genetic algorithms (GA) typically apply biologically inspired evolutionary operators to a fixed-length binary character. Genetic programming (GP) extends this by increasing the complexity of the structure that undergoes adaption to broad hierarchical computer programs with dynamically varying from and sizes. In the classical GP, the structure is typically comprised of the set of N_{func} functions from the function set $F = \{f_1, f_2, ..., f_{Nfunc}\}$ and the set of N_{term} the terminal from the terminal set $T = \{a_1, a_2, ..., a_{Nterm}\}$ forming the combined set $C = F \cup T$.

Definition 1: the **terminal set** consists of all the inputs and the constants supplied to the GP algorithm together with the zero-argument functions with side-effects executed by GP.

Definition 2: the **function set** consists of all operators, statements, and functions supplied to the GP algorithm.

Definition 3: the combined set is the union of the terminal set and function set, i.e., $C = F \cup T$.

There are two important notes which need to be considered in the procedure of terminal and function set.

Closure Property:

It is desired that, the terminal set and the function set in the genetic programming satisfy the closure property. The closure property requires that all the functions $f \in F$ can accept as their arguments any terminal $a \in T$ and any data type returned by any function $f \in F$. For example, for the arithmetic operation such as, division by zero or mathematical function such as, the logarithm of non-positive numbers, the closure property is not satisfied. If the closure property is not met, the individuals will need to be discarded if they don't evaluate to an acceptable result.

Sufficiency Property:

It is incumbent that, some composition of terminal $a \in T$ and functions $f \in F$ will yield a solution to the problem. This is known as the sufficiency property, where it is required to identify functions and terminals with sufficient power to solve a particular problem. Determining the repertoire of primitive functions and terminals is considered one of the most important preparatory steps in GP, but it is common to virtually every problem in science and other machine learning paradigms.

The flowchart of the GP system is shown in Fig. 7.12. As can be seen, the process of the GP algorithm starts with a random generation of the first population of CPs.

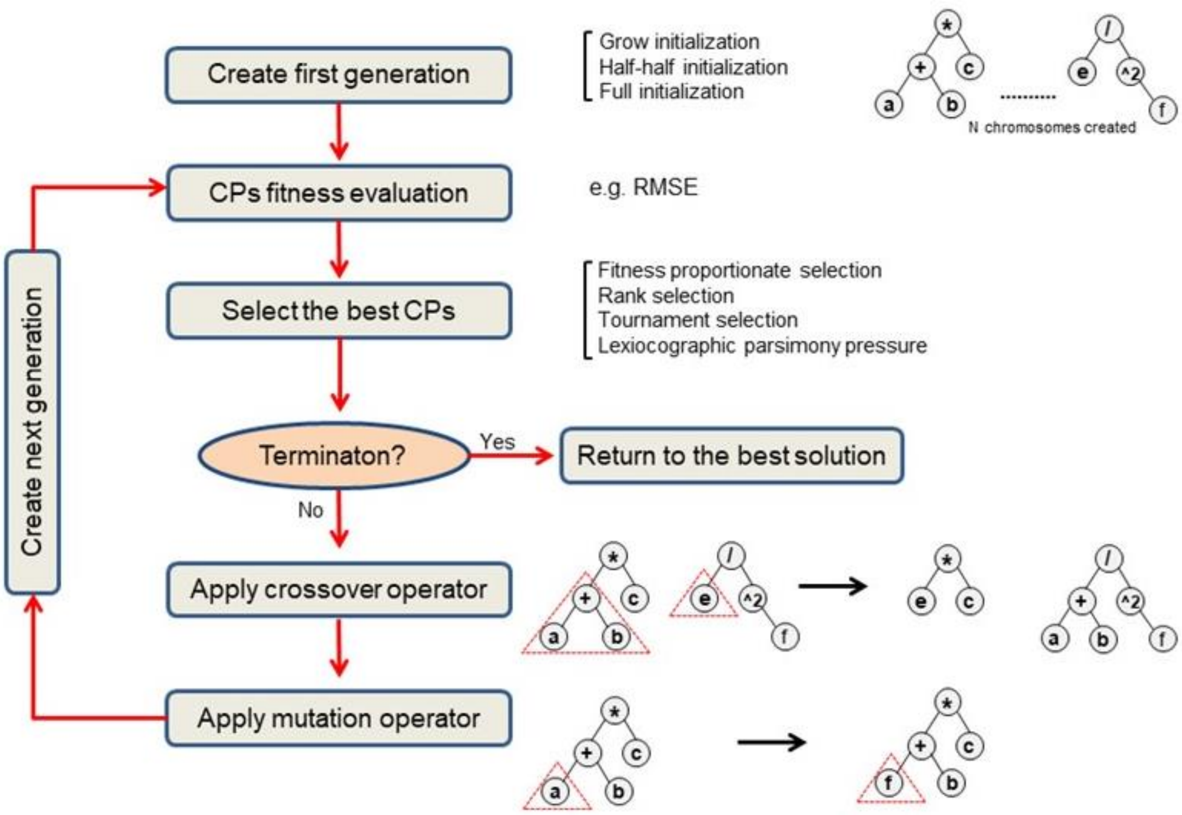

Figure 7.12: A general flowchart for GP (Salimi et al. 2017)

Initialization

The initial population is created by randomly generating individual S-expression of a rooted, point-labeled tree with order branches. Using a uniform random probability distribution, the selection of the root of the tree is restricted to a function $f \in F$, there will be $a(f_i)$ lines radiating out from the respective node, where $a(f_i)$ returns the arity of f_i (or the number of arguments f_i takes). For each of these radiated lines, an element is randomly selected from $C = F \cup T$ using a uniform random probability distribution to be the endpoint of the radiating line. If a function is chosen, then the above steps are recursively iterated. However, if a terminal is selected for that point, that point becomes the endpoint for the tree and the generating process is consequently terminated. There exist three main generative process implementation methods which are discussed in the following text (Kosa, 1992).

Full Method

The ***FULL*** method restricts the selection of nodes n at a depth less than the maximum depth $(d(n)<D_{\max})$ to a function $f \in F$ and nodes at the maximum depth to a terminal

$a \in T$. The depth of a node $d(n)$ is the length or number of branches connecting the specific node to the root node and the depth of a tree is defined as the length of the longest non-backtracking node from the root to the endpoint. The maximum depth of any rooted point-labelled tree with ordered branches is denoted by $D_{\max}$. The full method produces a full parse tree, where the tree is fully balanced the left and right-hand side of the root node has the same amount of nodes and the same depth. For more illustration, in this method, the initial individuals are generated so that they do not exceed a user-specified maximum depth. The depth of a node is the number of edges that need to be traversed to reach the node starting from the tree's root node (which is assumed to be at depth 0). The depth of a tree is the depth of its deepest leaf (e.g., the tree in Figure 7.13 has a depth of 2). In the full method (so named because it generates full trees, i.e., all leaves are at the same depth) nodes are taken at random from the function set until the maximum tree depth is reached. (Beyond that depth, only terminals can be chosen.) Figure 7.13 shows a series of snapshots of the construction of a full tree of depth 2. The children of the * and / nodes must be leaves or otherwise, the tree would be too deep. Thus, at both steps t = 3, t = 4, t = 6 and t = 7 a terminal must be chosen (x, y, 1 and 0, respectively).

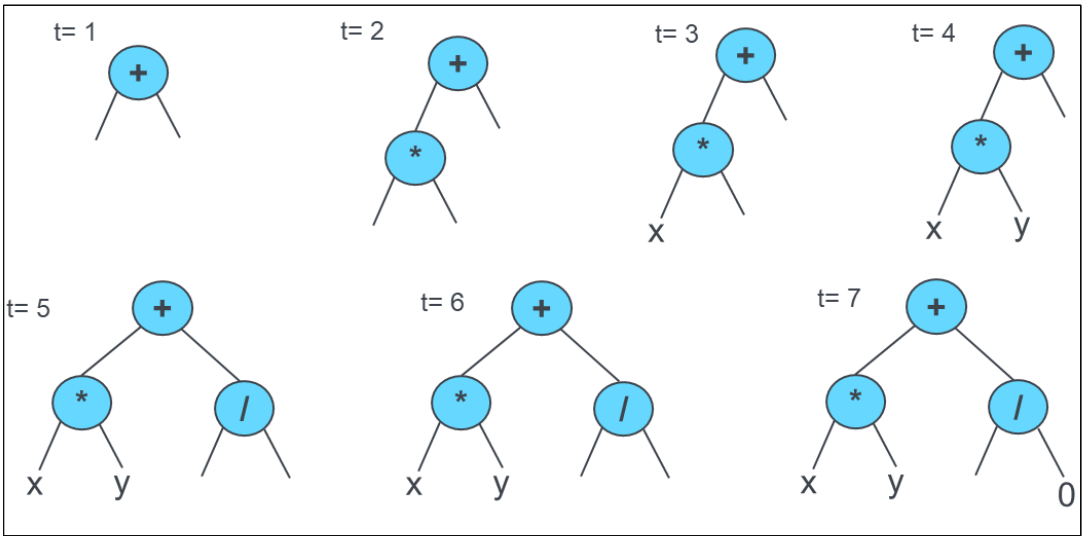

Figure 7.13: Creation of a full tree having maximum depth 2 using the full initialization method (t = time) (modified from Poli et al. 2008)

Although, the full method generates trees where all the leaves are at the same depth, this does not necessarily mean that all initial trees will have an identical number of nodes (often referred to as the size of a tree) or the same shape. This only happens, in fact, when all the functions in the primitive set have an equal arity. Nonetheless, even when mixed-arity primitive sets are used, the range of program sizes and shapes produced by the full method may be rather limited.

GROW Method

As opposed to the full method, the ***GROW*** method generates random trees that are variably shaped. Each node n at the depth less than the maximum depth $(d(n)<D_{\max})$ is randomly selected from the combined set $C=F\cup T$, where nodes at maximum depth $(d(n)<D_{\max})$ are restricted to a terminal $a\in T$. The trees produced are not balanced and are variably different in shape and size. on the contrary to the full method, the grow method allows for the creation of trees of more varied sizes and shapes. Nodes are selected from the whole primitive set (i.e., functions and terminals) until the depth limit is reached. Once the depth limit is reached only terminals may be chosen (just as in the full method). Figure 7.14 illustrates this process for the construction of a tree with a depth limit of 2. Here the first argument of the + root node happens to be a terminal. This closes off that branch preventing it from growing any more before it reached the depth limit. The other argument is a function (-), but its arguments are forced to be terminals to ensure that the resulting tree does not exceed the depth limit.

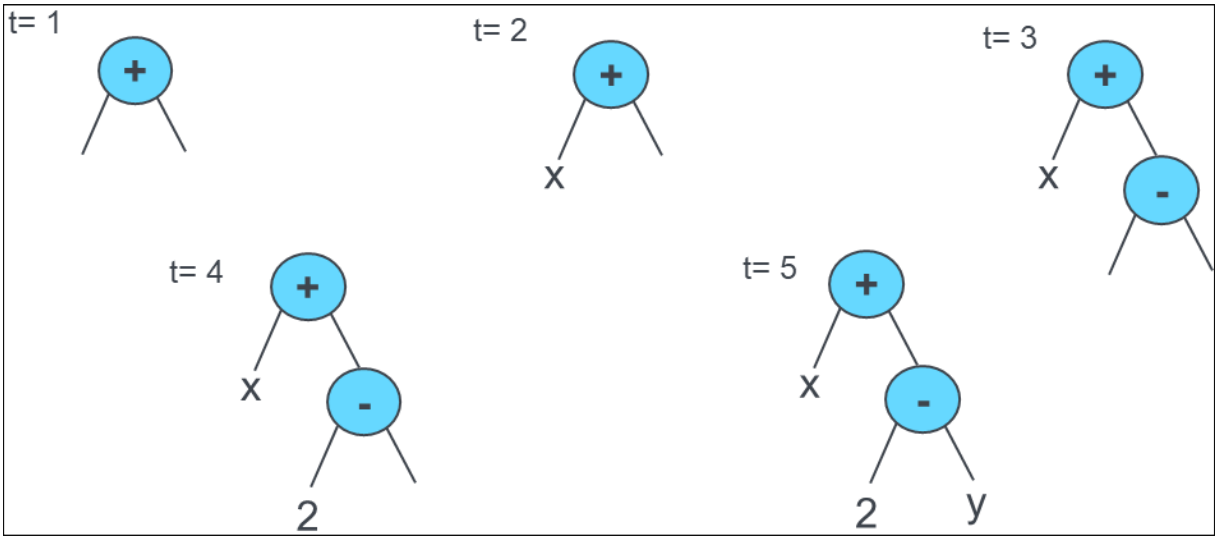

Figure 7.14: Creation of a five-node tree using the grow initialization method with a maximum depth of 2 (t = time). A terminal is chosen at t = 2, causing the left branch of the root to be closed at that point even though the maximum depth had not been reached (modified from Poli et al. 2008)

Ramped Half-and-Half Method

Because neither the grow nor full method provides a very wide array of sizes or shapes on their own, Koza (1992) proposed a combination called ramped half-and-half. Half the initial population is constructed using full and half is constructed using grow. This is done using a range of depth limits (hence the term "ramped") to help ensure that we generate trees having a variety of sizes and shapes. The *Ramped Half-and-Hal*f method is the most popular method in GP and is a mixture of the previous methods. It incorporates both the *GROW* method and *FULL* method by generating equal numbers of trees from each of the methods and thereby maximizing the variety of trees in the population. The depth of the tree ranging from 2 to $D_{\max}$ is used as a parameter to create trees. To illustrate, if the maximum specified depth is 6, 20% of the trees will have depth 2, 20% will have depth 3, and so forth up to depth 6. Then, for each value of depth, 50% of the trees are created via the full method and 50% of the trees are produced via the growing method. More information about each of these initialization methods can be found in Koza (1992).

After generating the initial population, the fitness of each individual will be evaluated by a fitness function. The prevalent fitness function is the root mean square error (RMSE), which is used for this investigation, and then if the stopping conditions (best solution; selected RMSE value or number of generation) are not attained, the process will continue. In another word, the best individuals of the first generation will be selected by means of the selection operator to reproduce into the next generation using the reproduction operator. It is good to note that, three important genetic operators (primary operators), containing reproduction, crossover, and mutation respectively, are applied in the GP algorithm.

The reproduction operator, a primary operation, is an asexual operator which takes one parental S-expression and creates only one offspring S-expression. This operation is conducted in two steps in which an individual is selected and then copied without any alteration into the new population. Unlike the other genetic programming (crossover and mutation), in reproduction, the "offspring" in the next generation cannot be worse in terms of fitness than the original "parent". For this reason, only the fittest individuals in the population at each generation are selected for reproduction. This is important as it ensures that the evolutionary search produces individuals in the next generation that are at least as fit as individuals from the previous generation.

In the GP algorithm, there are four common selection schemes (i.e., fitness proportionate selection, rank selection, tournament selection, and Lexicographic parsimony pressure selection), where they mimic Darwinian natural selection and pick individuals based on their fitness values (Koza, 1992).

Fitness Proportionate Selection (FPS) which also called *Roulette Wheel Selection* is the most popular and the simplest selection technique among the others. In this method, individuals are selected based on their fitness on the roulette wheel the chance factor. Any individual having a lower fitness proportion passes into a new population. Each individual of the population is allocated a section of an imaginary roulette wheel, which is proportionate to its fitness. The fittest candidate has the biggest section of the wheel and the weakest candidate has the smallest. The wheel is then spun n number of times, where n is the population size and every time the individual associated with the winning section is selected. To explain the way this method works assume that $f(s_i(t))$ denotes the fitness belonging to the individual s_i at the t[th] generation. When the reproduction operation is applied, the individual s_i will be then passed to the subsequent generation with the probability of $P(S_j(t))$

$$P(S_j(t)) = \frac{f(s_i(t))}{\sum_{j=1}^{m} f(s_j(t))} \tag{7.10}$$

Where $\sum_{j=1}^{m} f(s_j(t))$ indicates the sum of fitness values for m chromosomes. The fittest candidate has the biggest section of the wheel and the weakest candidate has the smallest. The wheel is then spun n number of times, where n is the population size and every time the individual associated with the winning section is selected.

No.	Fitness (fx)	% of total
1	6.82	31
2	1.11	5
3	8.48	38
4	2.57	12
5	3.08	14
Total	22.05	100

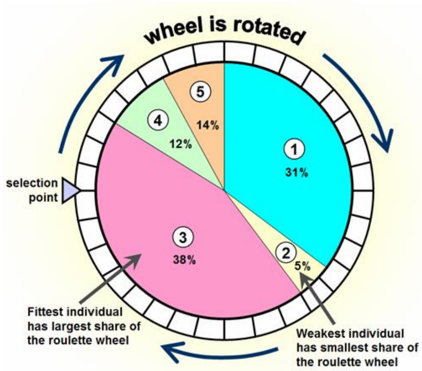

Figure 5.15: Fitness Proportionate Selection (FPS), "Roulette wheel selection" (Dalton, 2007)

As can be seen from Figure 5.15, the fittest candidate has the biggest section of the wheel and the weakest candidate has the smallest. The wheel is then spun n number of times, where n is the population size and every time the individual associated with the winning section is selected. As the wheel is spun N times and each time selecting a member of the population, picked by the selection pointer. In this example, the 3th individual has higher fitness, hence would be selected more than others. The probability of selecting an individual in the roulette wheel method is the ratio of the fitness value of that individual to the total fitness values of all individuals as depicted in the figure. Fitness f(x) of individual no.3 is the fittest and no.2 is the weakest. Strongest individual a value of 38% and the weakest 5%. These percentage fitness values can then be used to configure the roulette wheel and the number of times the roulette wheel is spun is equal to the size of the population. Each time the wheel stops it gives the fitter individual the greater chance of being selected for the next generation (and subsequent mating pool) That means that, individual no.3 will become more prevalent in the general population because it is fitter. The observation is that the individual with higher fitness values will guard the other to be selected for mating. This leads to a lesser diversity and hence fewer scope toward exploring the alternative solution and also premature convergence or early convergence with a local optimal solution.

Tournament Selection A very popular and often used method based on ranked selection is tournament selection, which is also applied in this research. The method is suggested for quick convergence. In this method, usually, a special group of individuals (generally two) will be selected randomly from a population and the individuals with a better fitness (i.e., lower fitness) will be selected. This selection technique uses n sets of individuals (also known as tournament sets; for $n = 2$ the selection technique is referred to as binary tournament selection shown in Figure). These sets are filled with a number (typically smaller than the size of the parent population) of uniformly randomly picked individuals from the parent population. From all tournaments, the fittest individuals are then chosen into the mating pool for breeding. The popularity of tournament selection is due to its computational efficiency and statistical properties. Due to the independent random selection (individuals may be picked more than once into a tournament) of individuals for the tournament sets the parent population does not need to be ordered (no preprocessing of the population is required) which makes this selection method fast. By altering the tournament size, the selective pressure can be varied. A low tournament size corresponds to a low selective pressure. In fact, a tournament size of 1 would result in uniformly random selection while a large tournament size allows more individuals from the parent population to be compared to find the fittest and hence increases the selective pressure. Having a large tournament size will generally find fitter programs more quickly and the evolution process will tend to converge to a solution in less time. A smaller tournament size will likely maintain more diversity in the population as more programs are given a chance to evolve and the population may find a better solution at the expense of taking longer. This is known as selection pressure, and your choice here may be governed by the computation time. Note that, tournament size (n) can be used to vary the selection pressure.

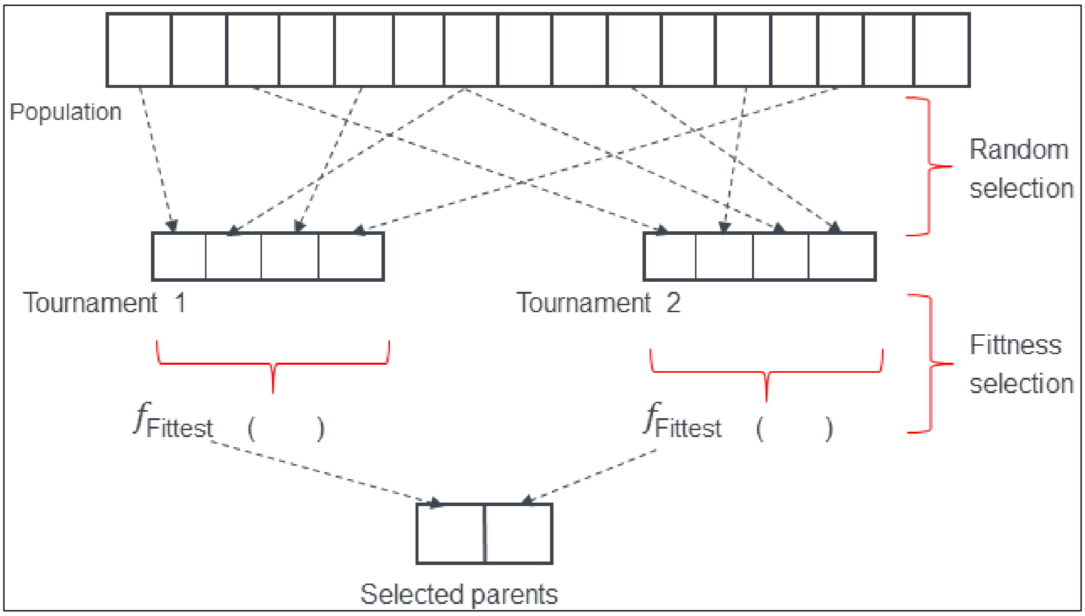

Figure 7.16: Binary tournament selection (modified from Poli et al. 2008)

Rank Selection addresses the drawbacks of FPS by maintaining a constant selection pressure. If the best individual fitness is 90%, its circumference occupies 90% of the Roulette wheel, and then other individuals have too few chances to be selected. To overcome the problem with Roulette-Wheel selection, a rank-based selection scheme has been proposed. The basic idea is that, first rank the population and every individual receives fitness, it means that, the worst have the fitness 1 and the best will have the fitness N (number of individuals in a population) (Figure 7.17). The process of ranking selection consists of two steps:

1. Individuals are arranged in an ascending order of their fitness values. The individual, which has the lowest value of fitness is assigned rank 1, and other individuals are ranked accordingly. (the best)
2. The proportionate based selection scheme is then followed based on the assigned rank.

Note that, the % area to be occupied by a particular individual i, is given by $\frac{r_i}{\sum_{i=1}^{N} r_i} \times 100$ where r_i indicates the rank of i-th individual. Two or more individuals with the same fitness values should have the same rank. For example, continuing with the population of 4 individuals with fitness values: $f_1 = 0.40; f_2 = 0.05; f_3 = 0.03; f_4 = 0.02$. Their proportionate area on the wheel are: 80%, 10%, 6%, and 4% (Figure 7.18). Comparison of two types of selection method (Roulette wheel & Rank selection) also depicted in Figure 7.18. It is evident that expectation counts have been improved compared to Roulette-Wheel selection. As such, a rank-based selection is expected to perform better than the Roulette-Wheel selection

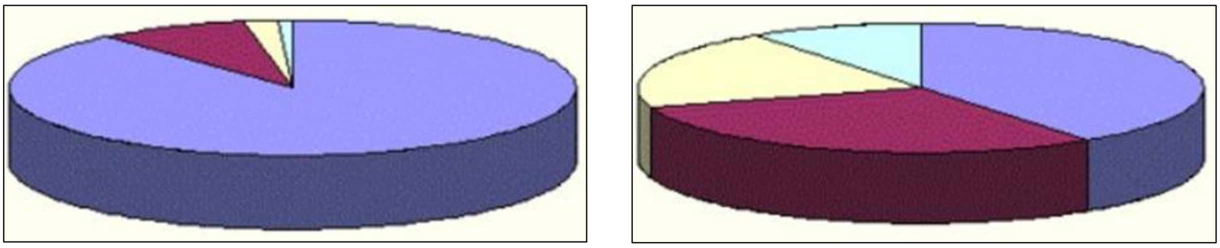

Figure 7.17: Rank selection method, left: (Situation before ranking (graph of fitness), right: Situation after ranking (graph of order number) (Obitko, 1998)

Individual (i)	**Fitness (fi)**	**RW (Area)**	**Rank**	**RS (Area)**
1	0.4	80%	4	40%
2	0.05	10%	3	30%
3	0.03	6%	2	20%
4	0.02	4%	1	10%

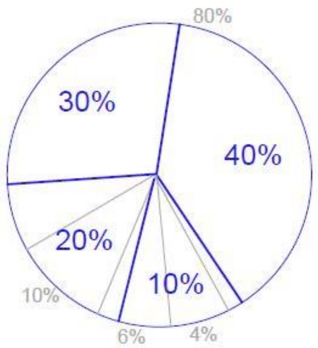

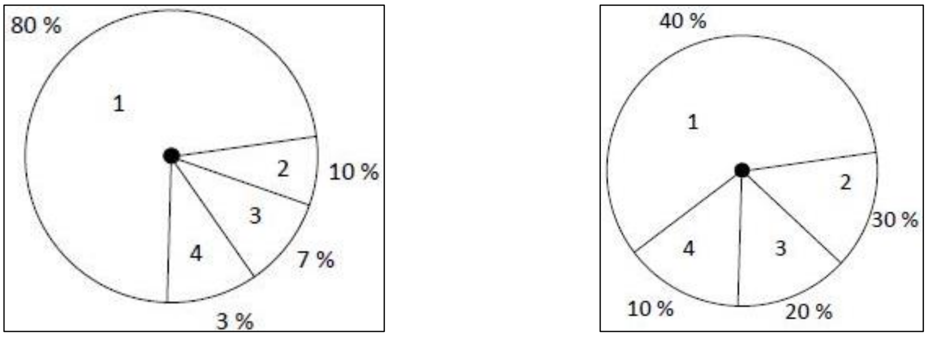

Individual	**% Area**	**fi**	**Rank (ri)**	**% Area**
1	80%	0.4	4	40
2	10%	0.05	3	30
3	7%	0.03	2	20
4	4%	0.02	1	10

Figure 7.18: Rank selection method & the distinction with Roulette wheel selection method

In brief, when the difference between the individual's fitness is considerable, the use of two previous methods is not suggested and the rank selection methods are suitable.

This selection method is similar to fitness proportionate selection, but the numerical values are replaced by a ranking, therefore, the main advantage of rank selection is that it exploits the small differences between individuals, maintaining population diversity and avoiding premature convergence.

Lexicographic Parsimony Pressure method is similar to tournament procedure and is able to optimize the fitness and the parse tree sizes. Lexicographic parsimony pressure is a straightforward multi-objective technique for optimizing both fitness and tree size, by treating fitness as the primary objective and tree size as a secondary objective in a lexicographic ordering. The fact is that, the procedure does not assign a new fitness value, but instead uses a modified tournament selection operator to consider the size. To select an individual, two individuals are chosen at random, and their finesses are compared. If an individual has superior fitness, it is selected. If the finesses are the same, then sizes are compared, and the smaller individual is selected. If both fitness and size are the same, an individual is selected at random. It can be thought that, the procedure is attractive because it is based on the relative rank of individuals in a population rather than their explicit fitness values, thus, specific differences in fitness are immaterial. All that matters is that one fitness is greater than another. Additionally, plain lexicographic parsimony pressure has nothing to tune. However, the procedure only works well in environments/biology which have a large number of individuals with identical fitness (see Figure 7.19). As shown, two GP-trees with the same fitness value but, the left one has size 6 and the right one has size 4, as such this method selects the right one which includes less size.

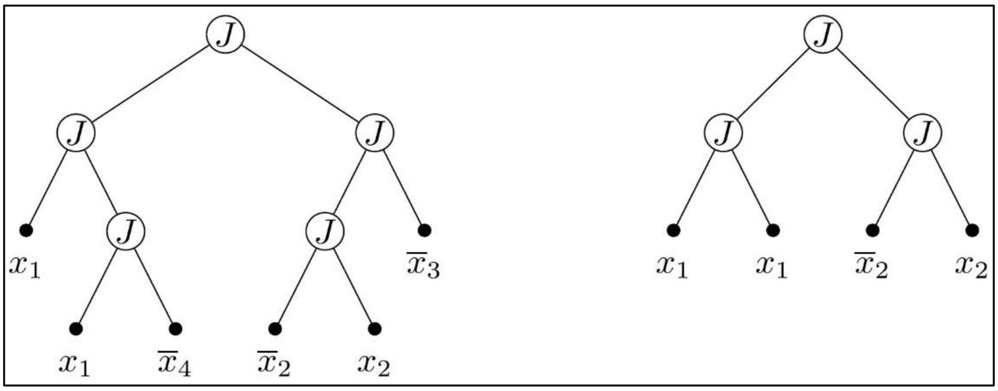

Figure 7.19: Lexicographic parsimony pressure; two GP-trees with the same fitness; the left one has size 6, whereas the right one has size 4 (Kötzing et al. 2019)

Further information about the mentioned methods can be found in Koza (1992).

Crossover or the sexual recombination is another predominant search operator, where it produces new offspring by swapping genetic material between the selected parents, as depicted in Figure 7.20. This operator is highly stochastic. It is a binary operator, where it selects two S-expression probabilistically and produces two new S-expression. In selecting the crossover point, a higher probability P_{ip} is given to the internal (function) points of the tree. This distribution promotes the recombination of the much larger structure. The crossover fragment of each parent is itself a rooted subtree, with its root being crossover point. The offspring is created in a symmetric manner, where the crossover fragments of the first parent is deleted and the crossover point of the other parent is inserted at the crossover point of the first parent. As it is required for all functions to comply with the closure property and the entire subtree are exchanged, this genetic operation creates syntactically legal LISP S-expression. The maximum depth of a tree during the evolution $D_{evolution}$ limits the maximum permissible size of the tree. If the crossover operation results in offspring of impermissible size, the crossover operation is aborted and one of its parents is arbitrarily selected to be reproduced. Usually, the general range of (0, 1) is considered for this operator.

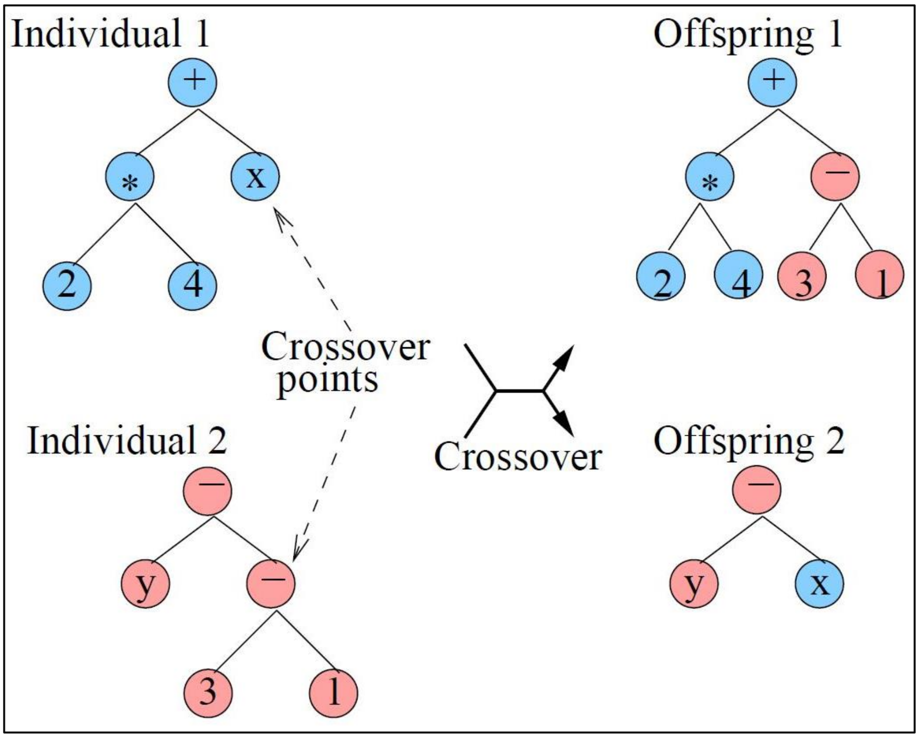

Figure 7.20: Crossover operator in GP

Mutation is another genetic operator which is an unary operator, introduces random changes in the individual. Mutation selects randomly individuals and can occur on any operational and final nodes of parse trees (Figure 7.21). If the selected node is an operational node, it changes with another node with sub-trees that contain a new function otherwise if the selected node is a final node; it substitutes just with another node. The range of (0, 1) is suggested usually as the rate of this operator.

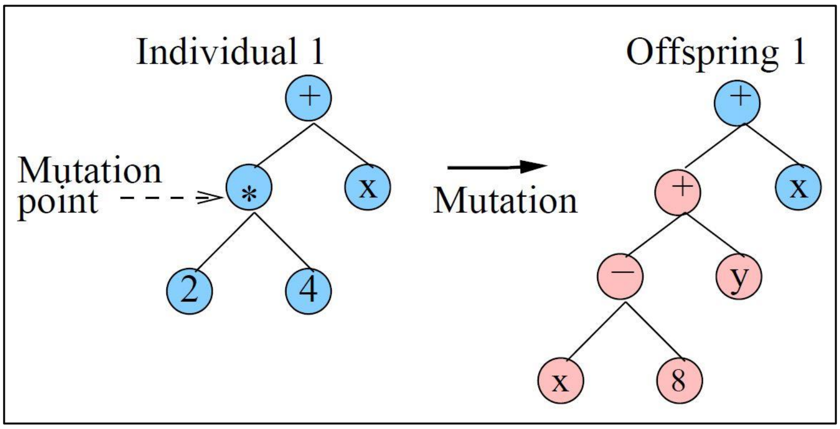

Figure 7.21: Mutation operator in GP

After applying these genetic operators, new programs with modified structures will be created as the second generation. This process continues to achieve the maximum generation (Koza, 1992; Silva and Almeida 2003a; Salimi et al. 2017).

In fact, reproduction, crossover, and mutation are considered as primary genetic operators and there is a secondary genetic operator that is known as ***Elitism*** which prevents the loss of the fittest individual within the population by ensuring that, the current fittest individual always survives and is kept in the population. Thus, the fittest of the best individual is an increasing function. Besides that, the Elitism controls the *"bloating"* in genetic programming which is defined as the increase in mean program size without a corresponding improvement in fitness. The phenomenon of uncontrolled growth in the size of an individual without any significant improvement in fitness is known as bloat. Mostly, it is suggested 10 % of the population size is considered as elitism size (Poli et al. 2008).

The fact is that, genetic programming has been applied to a variety of problem domains. For example, Johari et al. (2006) have successfully applied GP for the prediction of the soil-water characteristic curve. Moreover, Javadi et al. (2006) introduced a new technique based on genetic programming (GP), for the determination of liquefaction-induced lateral spreading. Also, genetic programming has been employed by Nguyen Thi et al. (2020) for storm surge forecasting.

The GP domain addressed in this work is symbolic regression. Classical mathematical regression techniques typically utilize a regression model (e.g., linear, non-linear, parametric) pre-specified by a user according to the requirements of the problem domain. While conventional regression techniques seek to optimize the parameters for a pre-specified model structure, symbolic regression avoids imposing prior assumptions, and instead infers the model from the data. In other words, it attempts to discover both model structures and model parameters, thus it has more potential in terms of accurate modelling than conventional regression methods.

According to Fig. 7.22, to develop a mathematical equation in order to predict TBM FPI, GP modeling can be summarized in five major steps as below:

i. Determining the set of terminals which are appropriate to solve the given problem.
ii. Identifying the set of primitive functions.
iii. Formulating and establishing the fitness function.
iv. Adjusting the values for genetic operators and population size.
v. Defining the initialization and selection methods and termination criterion.

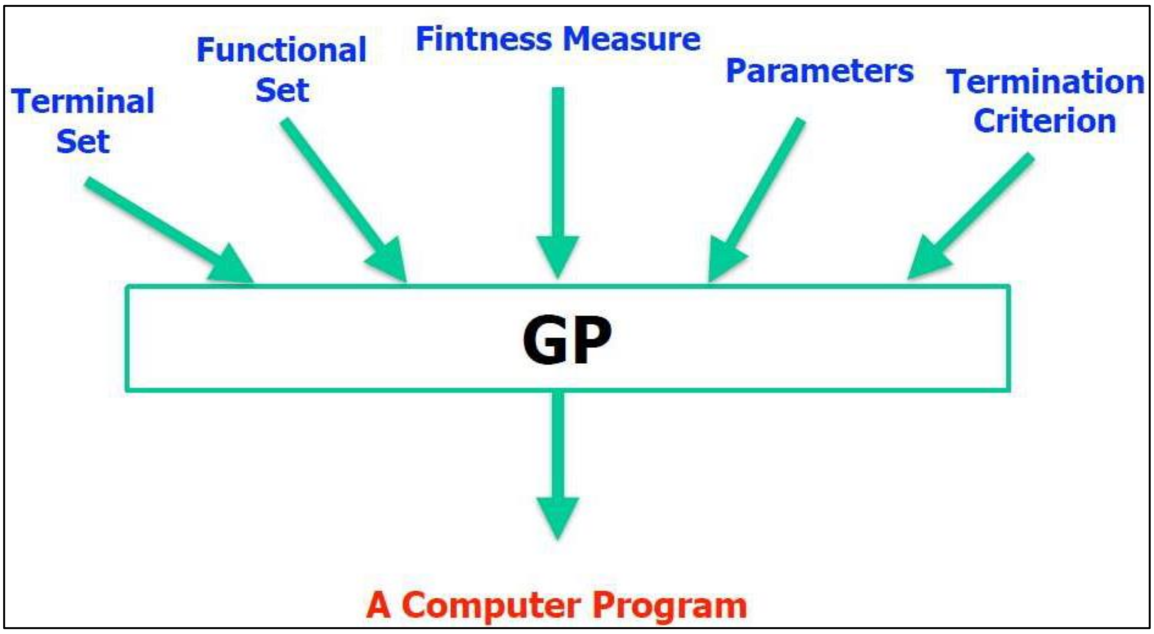

Figure 7.22: Five preparatory steps for GP

As mentioned before, unlike to other evolutionary algorithms, GP is able to develop mathematical functions for the dependent variables. To such that, the same input parameters, including UCS, RQD, Js, Jc, and RTC are considered as terminal set and FPI is the output parameter. The final aim of GP modeling is the development of an equation in the form of $FPI = f(UCS, RQD, Js, Jc, RTC)$. Besides, to improve the ability of GP in function finding, 6 random constants ranging from -10 to +10 were defined. Therefore, the used terminal sets include as follow:

$$F = \{UCS; RQD; Js; Jc; RTC; 5.655; -8.096; -6.813; 0.833; 8.307; -3.484\} \tag{7.11}$$

In the modeling procedure of GP,

The problem was solved by using the popular suite of machine learning software written in C# known as GPdoNET v5 (Hrnjica and Danandeh Mehr, 2018). To minimize the error and maximize correlation coefficient (R^2), the most common functions suggested by other researchers were taken into consideration and used as follow:

$$F = \left\{+, -, \times, /, \wedge 2, \wedge 3, \tfrac{1}{x}, Sqrt, Sin, Tan, Exp, Ln\right\} \tag{7.12}$$

The fitness of each individual parameter was evaluated by RMSE. It is well-recognized that if RMSE=0, an idealized fit can be obtained. Remember that the fitness value and efficiency are directly proportional to each other consequently, it is impossible to directly employ this index as the fitness function. Thus, a modified equation, i.e., Equation 7.13 was considered as the fitness function.

$$RMSE' = \frac{1}{1 + RMSE} \times 1000 \tag{7.13}$$

where $RMSE'$ signifies a value in the interval from 0 to 1000; where 1000 represents the ideal state.

It is worth to note that in addition to genetic operators which need to be arranged, several important parameters composed of the number of populations, the initialization method, selection method, number of generations, maximum tree depth, etc. are necessary to be assigned. As noted by Koza (1992), the mutation plays a minor role in GP and, therefore this genetic operator is fixed as a value of 0.05 (suggested by literature review). Besides that, among different initialization methods and pressure methods, the ramped-half-and-half initialization method and tournament selection method are more favorable by the scholars (based on literatures review) and frequently used and, thus got more attention in this study. Also, since the maximum tree depth has a key role in initialization, a range of (3, 10) is defined to achieve the best tree depth. Considering that a small tree depth causes the elimination of some input parameters in the developed models and in another side, the large value for tree depth increases the complexity of the model and decreases its performance. Besides, the probability of GP operators of crossover in the range of (0, 1) and (0, 0.5) for reproduction are taken into account. In order to determine the proper values of other parameters, several models with different conditions were evaluated based on a trial-and-error procedure considering the literature's suggestions. The optimum combination of GP parameters is obtained as listed in Table 7.5. The program is evolved through 3000 generations and equation 7.14 is the mathematical phrase of the best-generated computer program by GP; where UCS is uniaxial compressive strength (MPa), Js is joint spacing (cm), RQD is rock quality designation (%), Jc is joint characteristic in basic RMR and RTC is rock type code; 10 for G and GN, 20 for MV, 30 for SLK, 50 for C. Tree structure of the best GP model for TBM performance prediction is depicted in Fig. 7.23. Figure 7.24 displays the fitness progression of the evolved chromosomes during 3000 generations. The relationship between measured and predicted values obtained from the GP model is shown in Fig. 7.25. The correlation coefficient (R^2) between measured and predicted FPI by GP model is 0.86. Moreover, the variation of FPI with 5 selected input parameters generated by GP in the form of a surface graph is shown in Fig. 7.26. It can clearly be seen the variation of output (FPI) with inputs is found to be in agreement with previous literatures. Increasing the uniaxial compressive strength, joint spacing, RQD, and Jc increases the FPI as anticipated, while the low value of FPI respected to RTC is obtained in rock type category "C or 50" and the higher one in "G&GN or 10".

$$\frac{\left[\left(\left(\frac{Js}{5.65}\right)-RQD\right)-12.138\right]-\left[\frac{\left(\left(UCS-Jc\right)/5.65\right)}{\left(\left(Js/RTC\right)-RTC\right)}\right]}{\left[\left[\left(Sin\left(UCS\right)\right)\cdot\left(\frac{UCS}{8.3}\right)\right]\Big/\left(\frac{68.89}{\left(RQD/RTC\right)}\right)\right]-5.65}+\frac{\left[\left(\frac{Js}{-1.2}\right)-\left[\left(\frac{RQD}{RTC}\right)-\left(\frac{Js}{5.65}\right)\right]\right]-\left[\frac{\left(\left(Js/8.3\right)-Jc\right)}{\left(\left(RQD/RTC\right)-10.29\right)}\right]}{\left[\frac{8.3}{\left(\left(UCS/5.65\right)/-6.81\right)}\right]} \tag{7.14}$$

Table 7.5: GP parameters for constructed model

GP parameters	Values
Terminal set	UCS, RQD, Js, Jc, RTC
Fitness function	RMSE
Number of populations	500
Number of generations	3000
Initialization method	Half
Selection method	Tournament
Tour size	5
Crossover	0.89
Mutation	0.05
Reproduction	0.2
Elitism size	50
Max. Tree depth	
Initialize depth	5
Operation depth	6

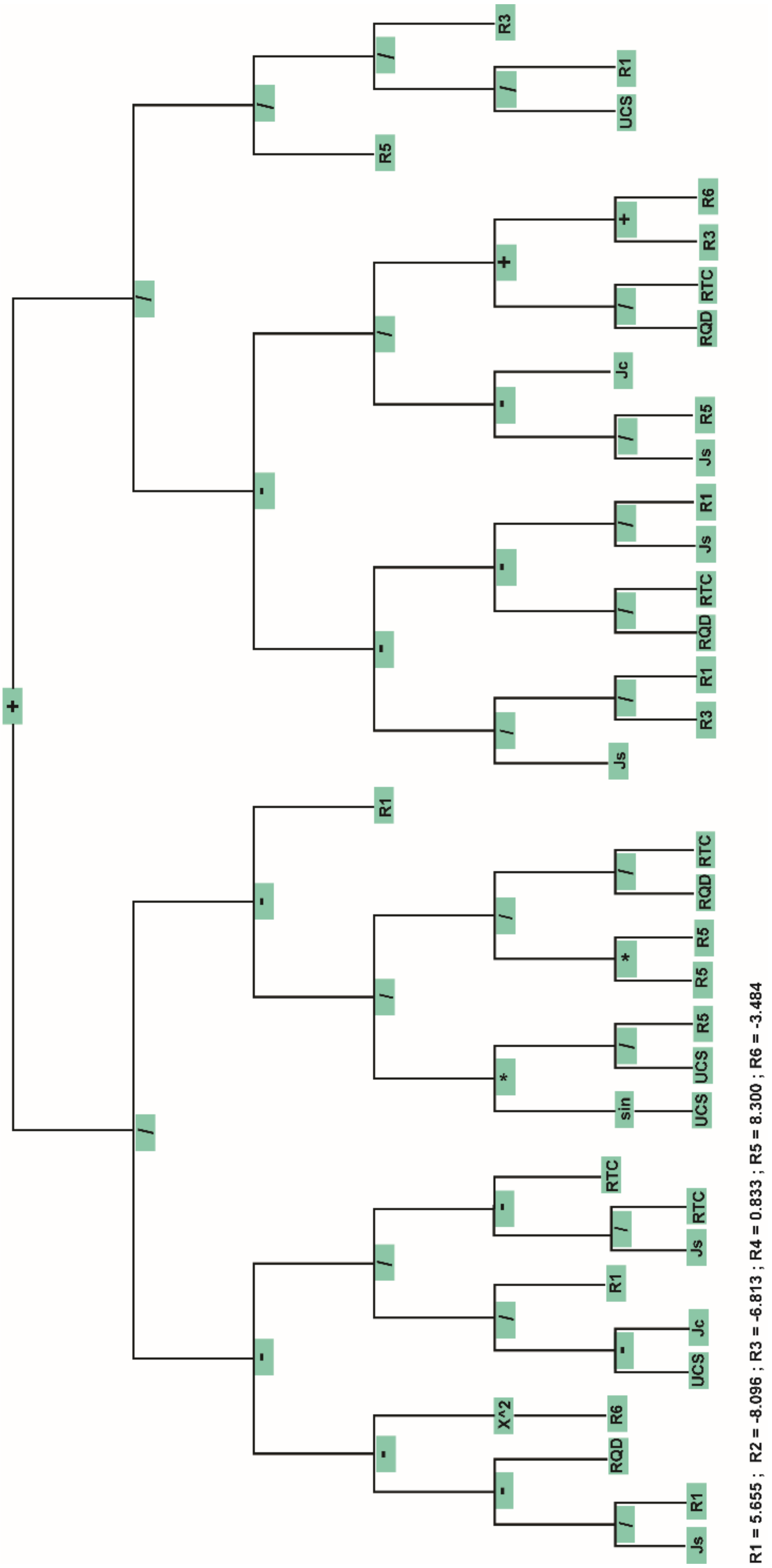

Figure 7.23: Tree structure of the best GP model

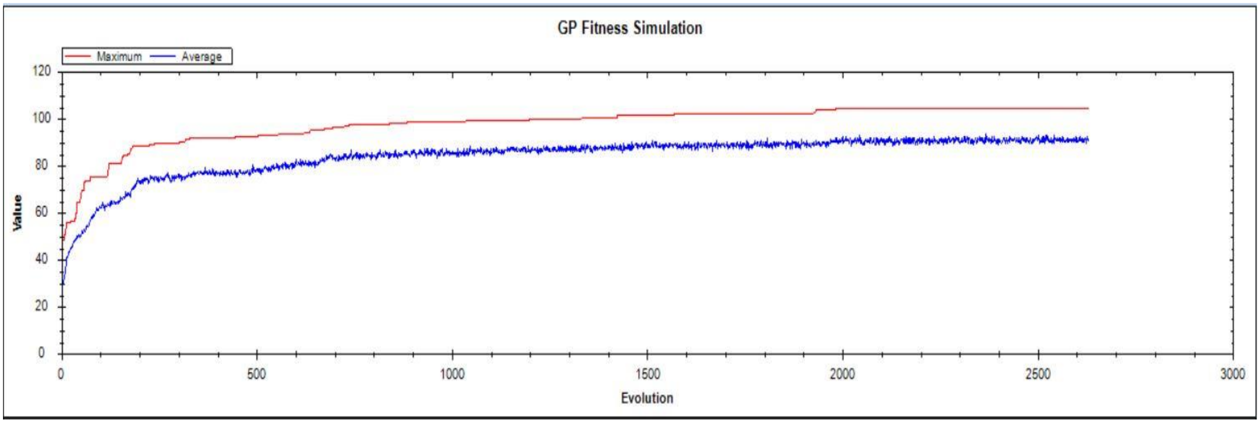

Figure 7.24: Fitness progression of the evolved chromosomes during 3000 generations

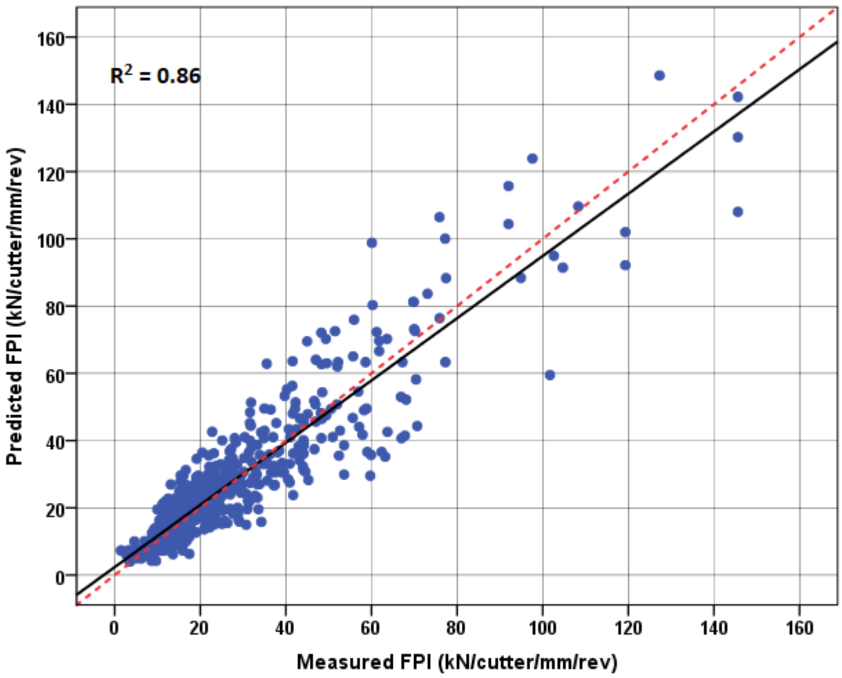

Figure 7.25: Comparison between the measured and predicted FPI from the GP model

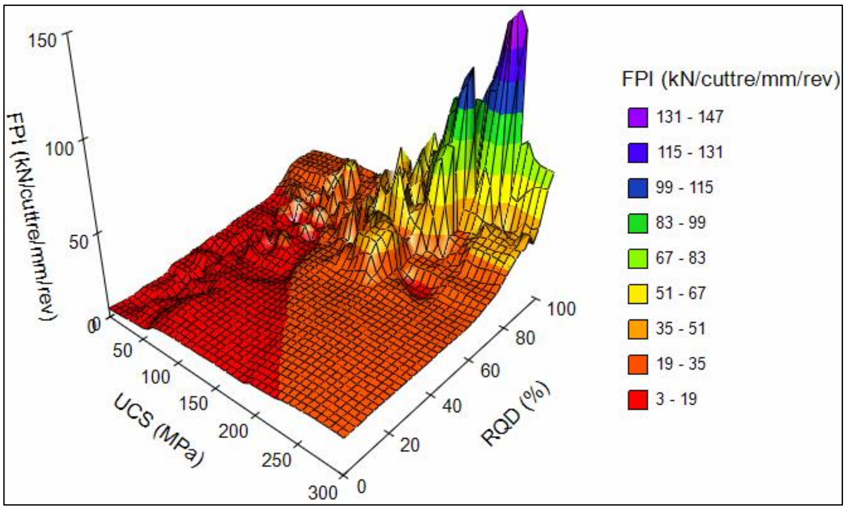
150
100
50
0
FPI (kN/cuttre/mm/rev)
50
100
150
200
250
300
UCS (MPa)
0
20
40
60
80
100
RQD (%)
FPI (kN/cuttre/mm/rev)
131 - 147
115 - 131
99 - 115
83 - 99
67 - 83
51 - 67
35 - 51
19 - 35
3 - 19

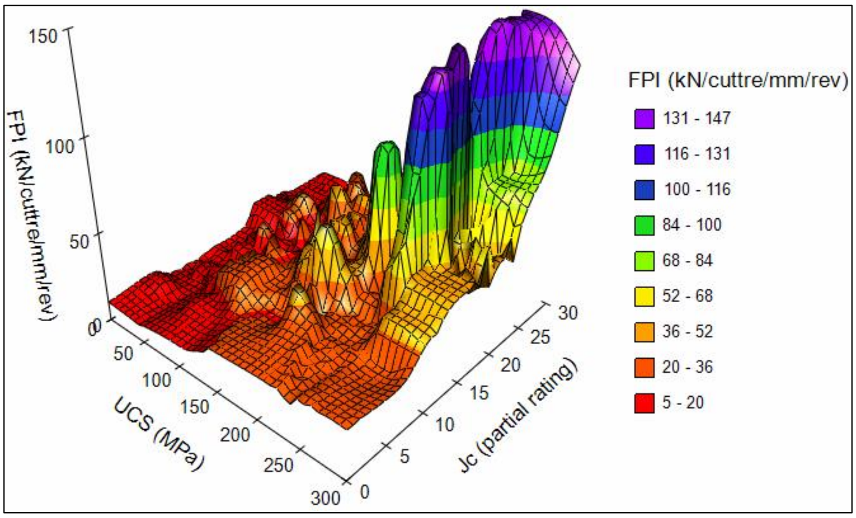
150
100
50
0
FPI (kN/cuttre/mm/rev)
50
100
150
200
250
300
UCS (MPa)
0
5
10
15
20
25
30
Jc (partial rating)
FPI (kN/cuttre/mm/rev)
131 - 147
116 - 131
100 - 116
84 - 100
68 - 84
52 - 68
36 - 52
20 - 36
5 - 20

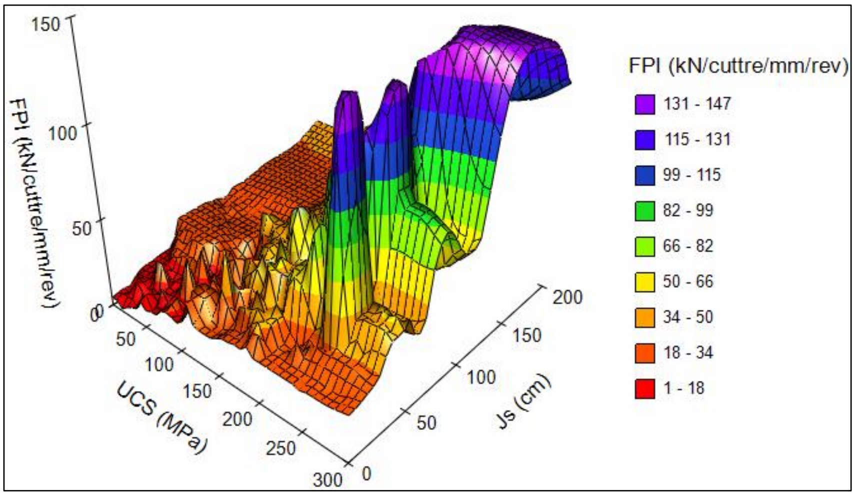
150
100
50
0
FPI (kN/cuttre/mm/rev)
50
100
150
200
250
300
UCS (MPa)
0
50
100
150
200
Js (cm)
FPI (kN/cuttre/mm/rev)
131 - 147
115 - 131
99 - 115
82 - 99
66 - 82
50 - 66
34 - 50
18 - 34
1 - 18

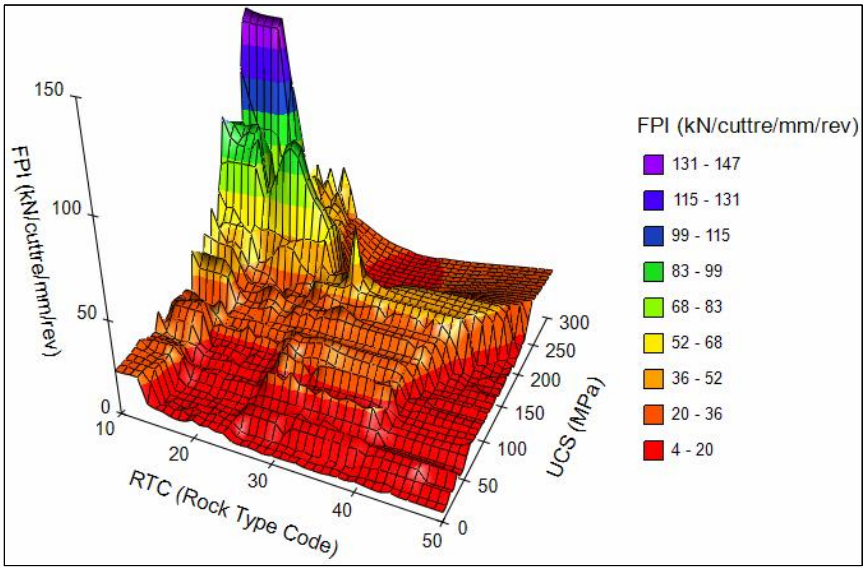
FPI (kN/cuttre/mm/rev)
131 - 147
115 - 131
99 - 115
83 - 99
68 - 83
52 - 68
36 - 52
20 - 36
4 - 20
RTC (Rock Type Code)
UCS (MPa)

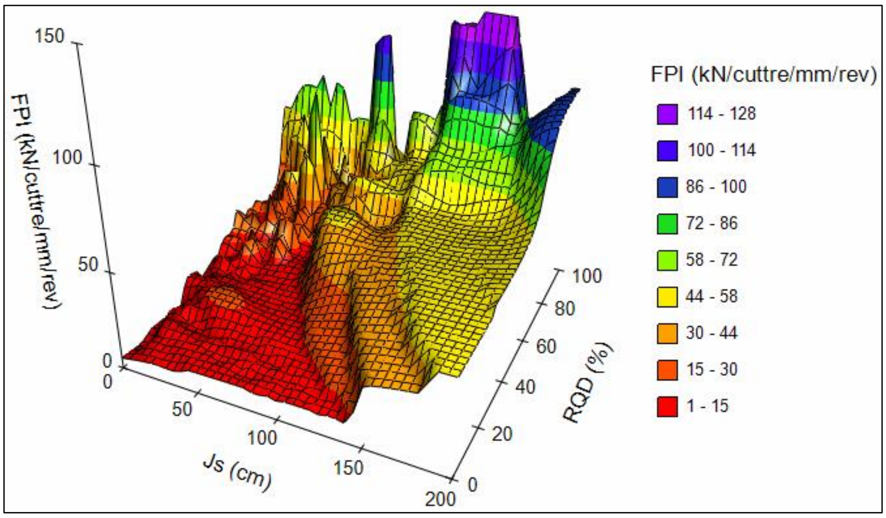
FPI (kN/cuttre/mm/rev)
114 - 128
100 - 114
86 - 100
72 - 86
58 - 72
44 - 58
30 - 44
15 - 30
1 - 15
Js (cm)
RQD (%)

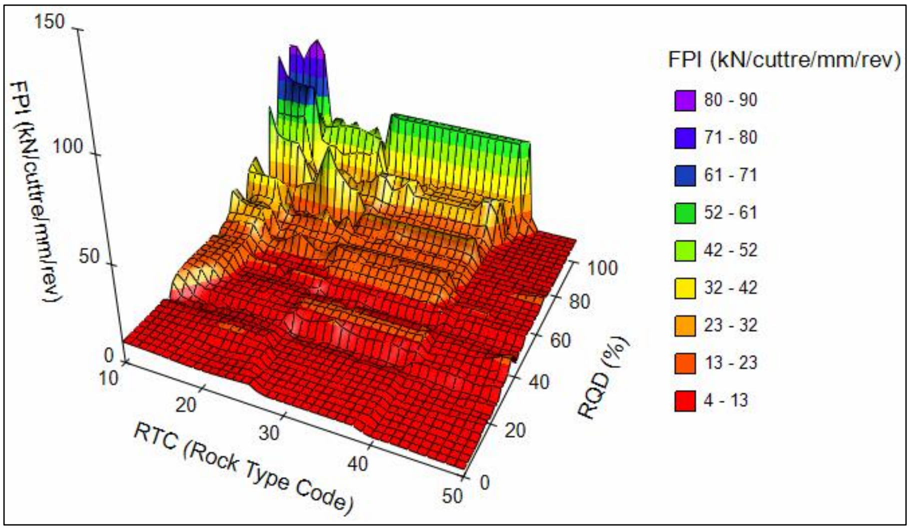
FPI (kN/cuttre/mm/rev)
80 - 90
71 - 80
61 - 71
52 - 61
42 - 52
32 - 42
23 - 32
13 - 23
4 - 13
RTC (Rock Type Code)
RQD (%)

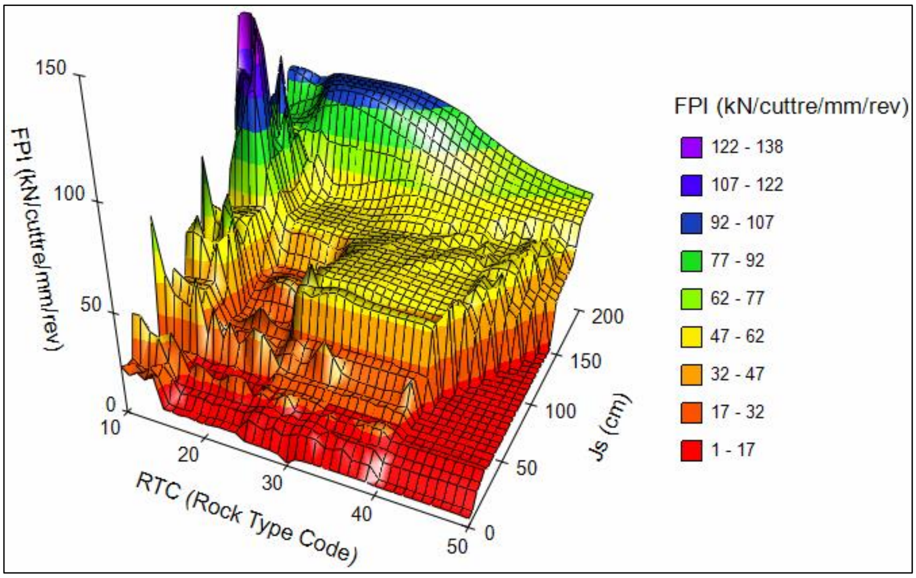
150
100
50
0
FPI (kN/cuttre/mm/rev)
10
20
30
40
50
RTC (Rock Type Code)
0
50
100
150
200
Js (cm)
FPI (kN/cuttre/mm/rev)
122 - 138
107 - 122
92 - 107
77 - 92
62 - 77
47 - 62
32 - 47
17 - 32
1 - 17

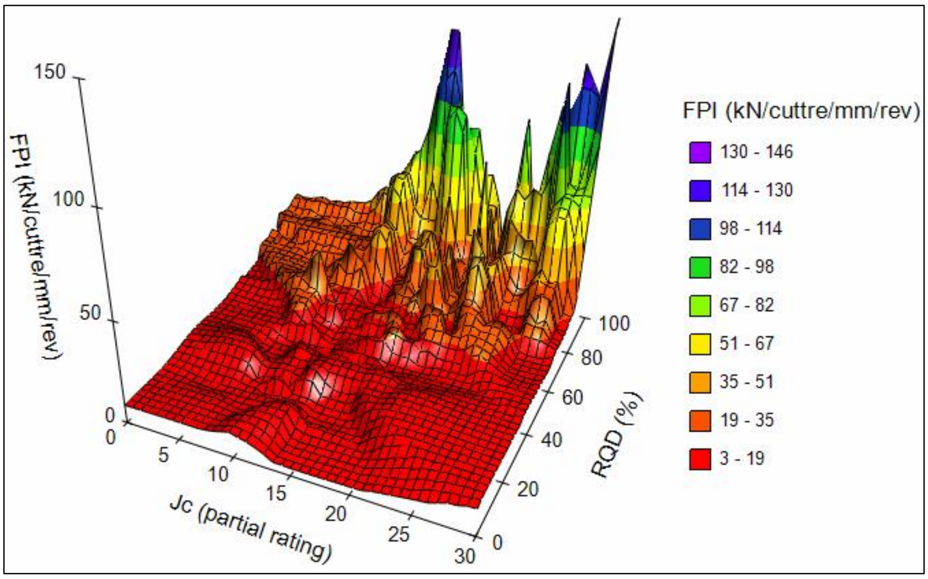
150
100
50
0
FPI (kN/cuttre/mm/rev)
0
5
10
15
20
25
30
Jc (partial rating)
0
20
40
60
80
100
RQD (%)
FPI (kN/cuttre/mm/rev)
130 - 146
114 - 130
98 - 114
82 - 98
67 - 82
51 - 67
35 - 51
19 - 35
3 - 19

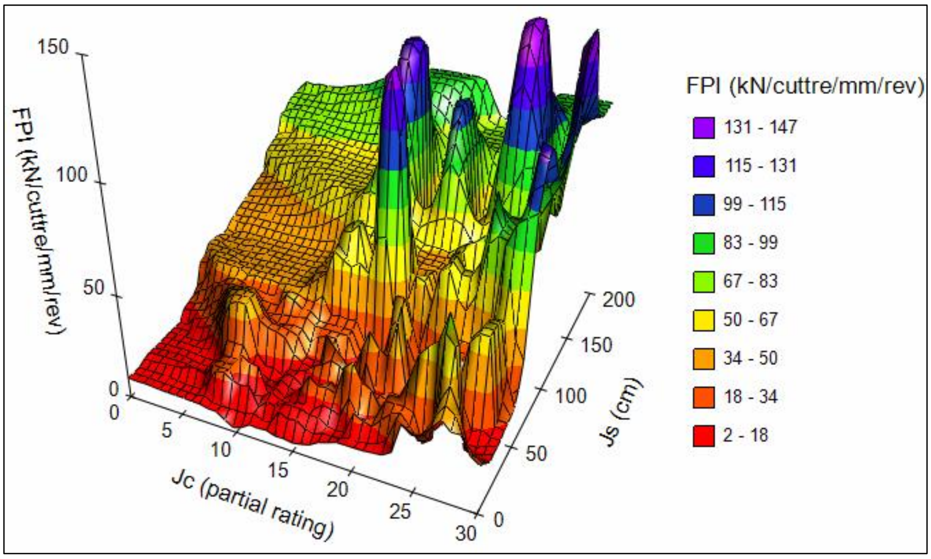
150
100
50
0
FPI (kN/cuttre/mm/rev)
0
5
10
15
20
25
30
Jc (partial rating)
0
50
100
150
200
Js (cm)
FPI (kN/cuttre/mm/rev)
131 - 147
115 - 131
99 - 115
83 - 99
67 - 83
50 - 67
34 - 50
18 - 34
2 - 18

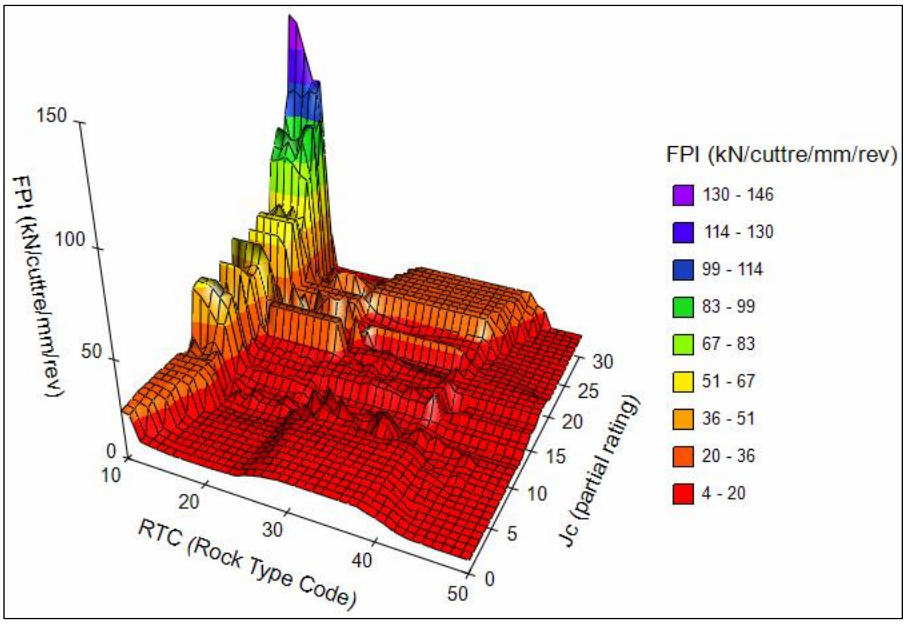

Figure 7.26: Surface graph generated by GP showing the relationship of FPI with *UCS*, *RQD*, *Js*, *Jc and RTC*

Chapter 8 Evaluation & Validation of Developed Models

8.1 Introduction

A wide variety of performance prediction methods and principles are proposed and used to estimate the performance (penetration and advance rate) of a TBM in hard rock. Different models are used in different countries, contractors, engineers, and by various TBM manufacturers based on their experience and available information. While some of the methods are based mainly on one or two rock parameters (for example uniaxial compressive strength and a rock abrasion parameter) the others are based on a combination of comprehensive laboratory, field, and machine parameters.

To fulfill the main goal of this study, which is developing new and more accurate models for prediction and penetration rate of TBMs in rock tunneling, seven TBM tunneling projects with 61.09 km available data were compiled and analyzed. The models have been developed based on the input parameters of rock mass classification system such as, rock mass rating (RMR), which is often available in tunneling projects. The statistical analysis as well as artificial intelligence algorithm, including classification and regression tree (CART), genetic programming (GP) were used to analyze the compiled field data. In this chapter, the performance and accuracy of the proposed models are evaluated based on different statistical indices. In addition, sensitivity analysis is conducted for non-linear regression, CART, and GP models to examine of the effects of variability of the input parameters on the results of the developed models. Finally, in order to validate and assess the performance/efficiency of the proposed models, the data from Zagros water conveyance tunnel lot 2 (5-15 km) was used. The data from this section of the Zagros tunnel had not been employed for the development of the proposed model, hence it is used for testing and validation. For comparison, the results of proposed models are compared with the results of three world-wide prognosis models, including the CSM model (Rostami 1997), the NTNU (Bruland 1998), and Q_{TBM} (Barton 2000). Eventually, the limitations of developed model (CART) are being proposed and discussed.

8.2 Comparison of the Developed Models

The performance of the proposed models was evaluated according to statistical criteria such as correlation coefficient (R^2), the root mean square error (RMSE), mean absolute deviation (MAD), mean absolute percentage error (MAPE), mean square error (MSE) and variance account for (VAF).

Description of these statistical parameters can be found in textbooks and statistical software tutorials. The results of applying these models are summarized in Table 8.1.

Table 8.1: Performance indices for developed models

Model	R^2	MAD	MSE	RMSE	MAPE	VAF
Linear	0.68	11.048	217.168	14.736	58.436	0.678
Non-linear	0.78	6.780	138.734	11.778	26.382	0.744
GP	0.86	5.787	71.514	8.456	23.017	0.863
CART	0.91	4.194	44.470	6.668	20.146	0.912

8.3 Model Evaluation via Sensitivity Analysis

Sensitivity analysis examines the variability of the outputs of a model by changing the input variables within a prescribed range. This process allows for a better understanding of the relationship between the input parameters and the output results and facilitates the recognition of possible errors caused by models when the input parameters vary beyond an intended range. In addition, this analysis accommodates validating the results and identification of critical or uninfluential parameters in the models. The simplest form of sensitivity analysis is to change one variable by keeping other variables constant and investigating the effect of the change of isolated input parameter on the model results. This is known as a one-way sensitivity analysis. One-way sensitivity analysis can be done by different methods, each of which is applicable for certain purposes. While one-way sensitivity analysis is useful for demonstrating the effect of one parameter in the model, sometimes it is necessary to investigate the effect of changes in two or several parameters simultaneously. Multi variable sensitivity analysis allows for this possibility, through which the effect of changes in the possible combinations of influential parameters is evaluated in their range of variations. Note that the interpretation and demonstration of multivariable sensitivity analysis would become complex and difficult with an increased number of parameters. In the probabilistic sensitivity analysis, instead of allocating a certain value to each parameter, a distribution is used to allow variation all of the parameters available in the model. The distribution of the model inputs is assigned through either fitting a curve to a set of data or by using a mean, standard deviation, and using a normal distribution.

In this study, the multiway sensitivity analysis is used by simultaneous variation of different parameters on the developed model conducted by non-linear regression analysis, CART GP model (see below).

The probabilistic sensitivity analysis method was implemented by using a set of initial values for each of the influential variables affecting the output. For each combination of input values, the output was calculated based on these values. The output is recalculated by the newly selected values and eventually, the output distribution curve was obtained based on the values calculated in each replication. It is worth to be noted that, the whole range (distribution) of the input parameters and respected output has been taken into the consideration for the analysis. The results of sensitivity analysis are shown by tornado diagrams, allowing the ranking of the effect of the distribution of input parameters on the output results. The input with the greatest impact on the output is the largest (and highest) bar in the diagram. To demonstrate the extent of the effect of each parameter on the output, the input values were divided into groups with equal size, from the lowest input value to the highest. In a multiway sensitivity analysis, a group of different input parameters are selected simultaneously and randomly changed, and then the variation in output results is calculated in numerous iterations and recorded.

The difference between the maximum and minimum value of the output calculated in the range of variations of each output variable represents the length of the bar in the tornado diagram. Figure 8.1 illustrates the tornado diagram for the developed non-linear regression model. Based on this diagram, the lowest sensitivity of the model is to Jc (joint characteristics), while the other inputs have a great impact on the sensitivity of the model. This could be attributed to the limited range of Jc (it changes between 0 to 30) in the original database or this parameter is shadowed by the other inputs such as UCS or RQD. Figure 8.2 shows tornado diagram for the developed GP model. As can be seen, again the lowest sensitivity of the model is to Jc and the other parameters have a significant impact on the sensitivity of the model. Figure 8.3 illustrates tornado diagram for the CART model. Again, similar results were obtained in which Jc shows the lowest sensitivity of the model.

The results of sensitivity analysis can also be illustrated by a spider diagram. A spider diagram indicates variations in the output in relation to the percentage of changes in each of the input variables. The percentage of changes in input variables is shown in the horizontal axis and the extent of changes in the output results corresponding with the given inputs is indicated in the vertical axis. The higher the slope of the line for an input, the greater its impact on the output. The spider diagram contains more information than the tornado diagram. A tornado diagram only shows the overall change of output values, whereas the spider diagram also shows the rate of changes in the output value per changes in the given range of input parameters. Figure 8.4, 8.5, and 8.6 reveal changes in the field penetration index (FPI) value in terms of the percentage of variations in the input parameters in the MNLRA, GP, and CART model, respectively.

The tornado diagram of sensitivity for the MNLRA model indicates that the difference between the effects of different parameters is not similar. This shows that the MNLRA model is equally affected by input variables (with exception of *Jc*), The extent of difference in the effect of the most important input parameter and the least important parameter in MNLRA models is not considerable, revealing suitable selected parameters and their weights for the model. The tornado diagram of the sensitivity of the GP model demonstrates that the distinctness between the effects of various parameters is not identical. This expresses that the GP model is equally affected by input variables (with exception of *Jc*). Besides, similar results have been obtained from the tornado diagram of the CART model, meaning the CART model also is equally affected by input variables.

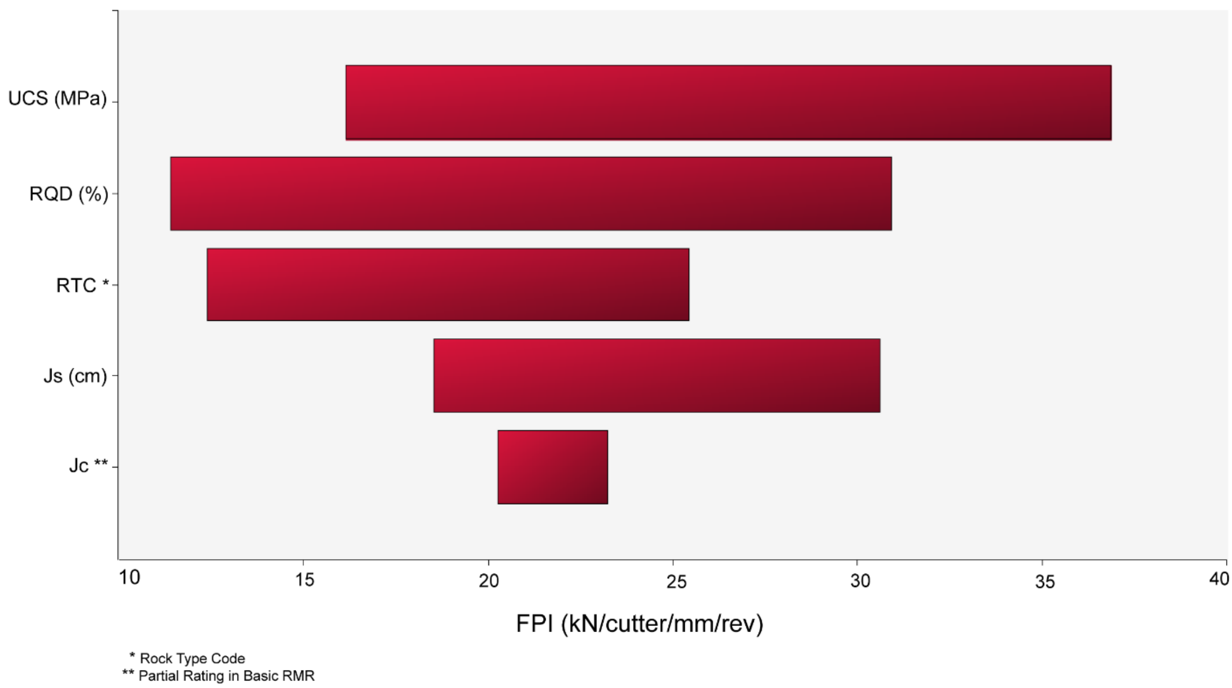

Figure 8.1: Tornado graph resulted of sensitivity analysis of MNLRA model

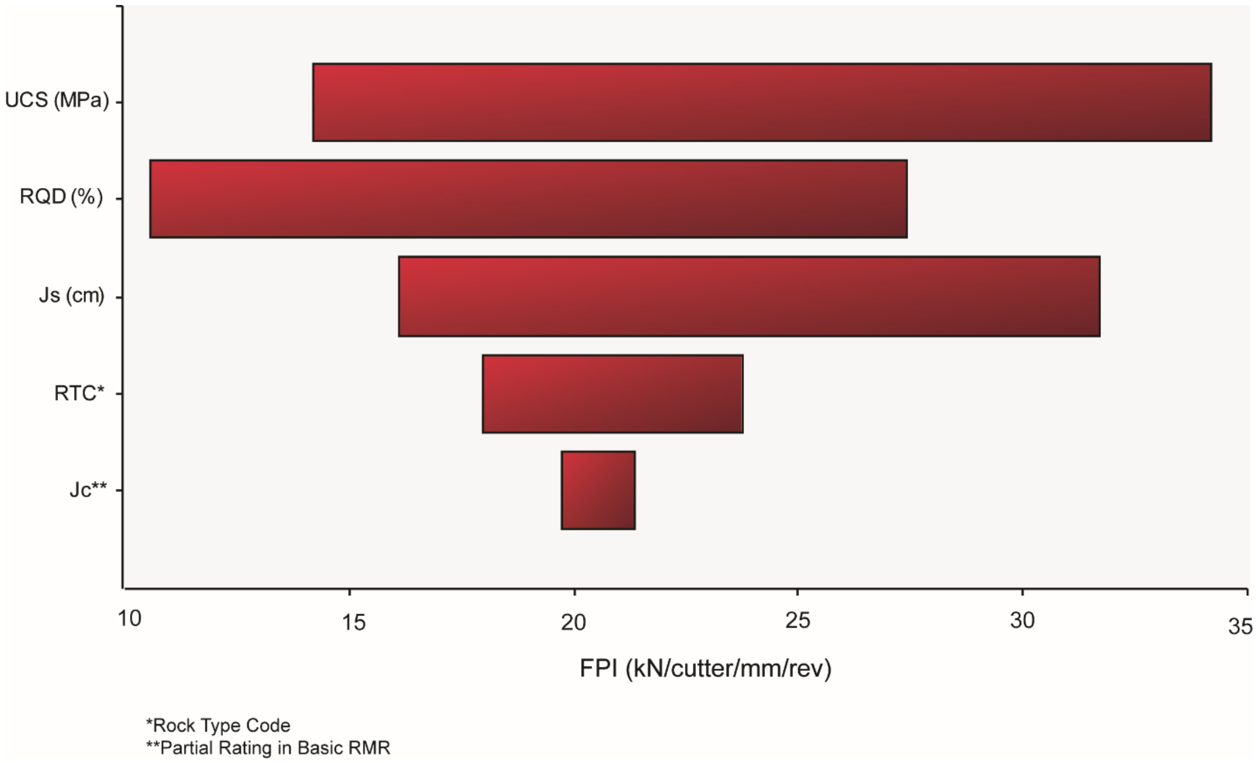

Figure 8.2: Tornado graph resulted of sensitivity analysis of GP model

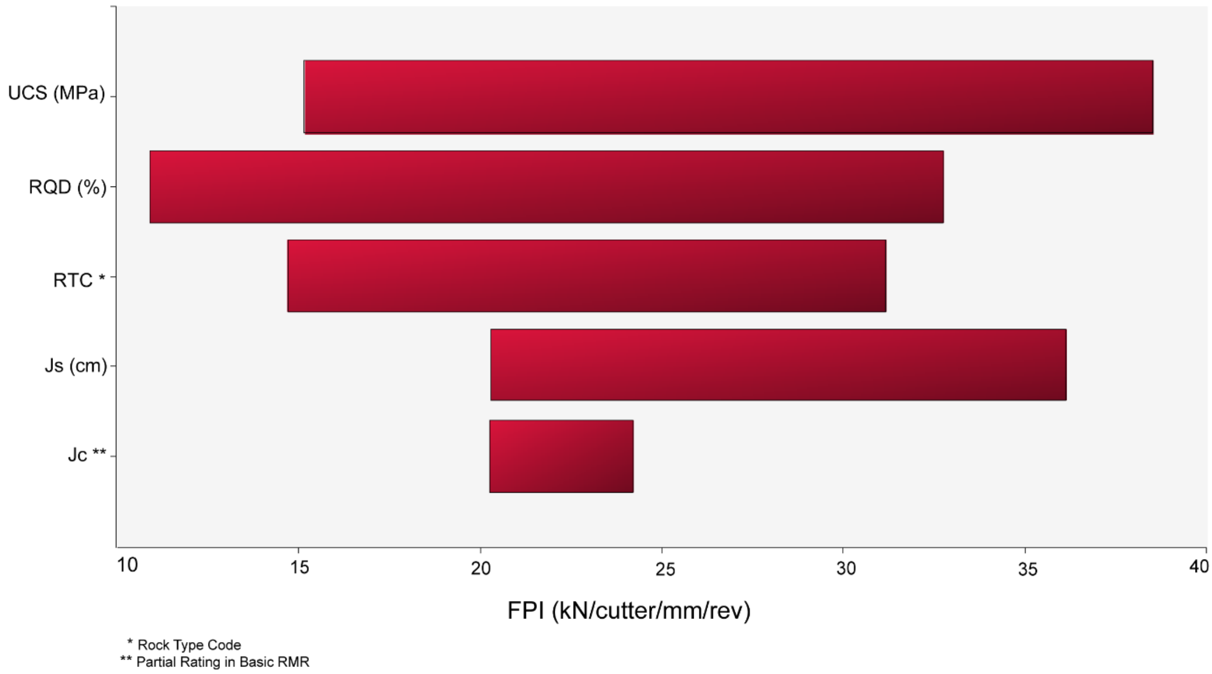

Figure 8.3: Tornado graph resulted of sensitivity analysis of CART model

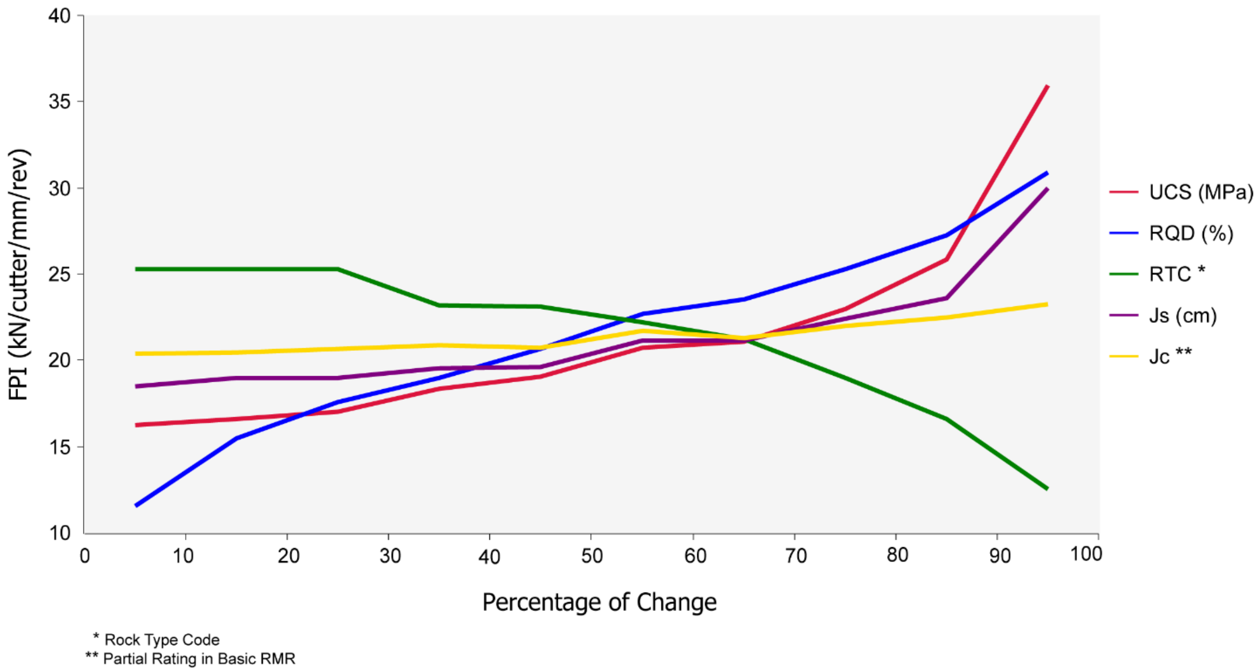

Figure 8.4: Changes in the penetration value by change of input parameters in MNLRA model

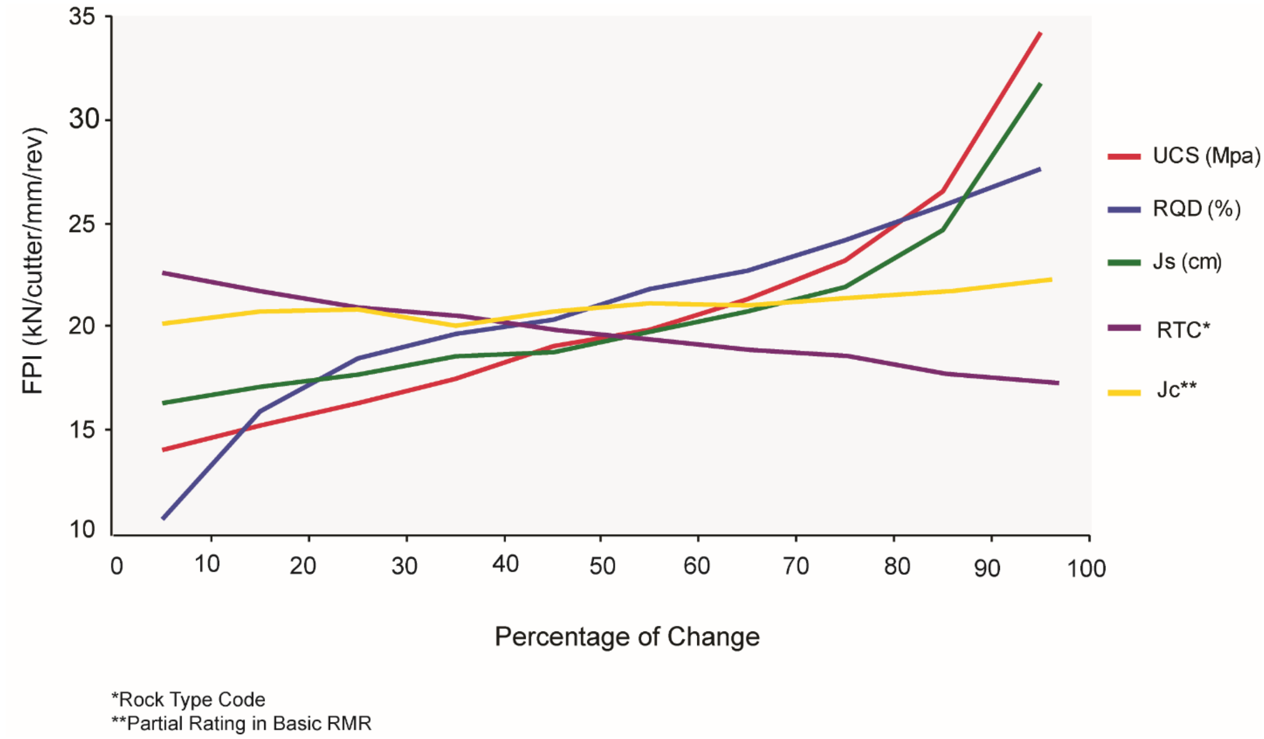

Figure 8.5: Changes in the penetration value by change of input parameters in GP model

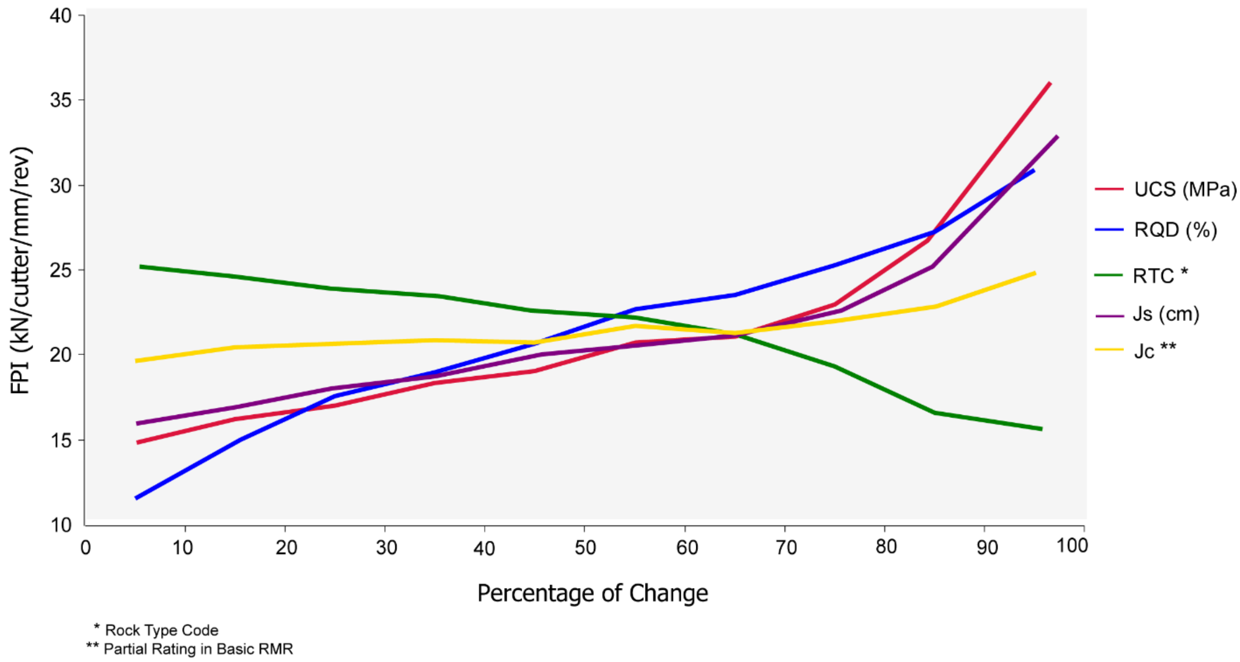

Figure 8.6: Changes in the penetration value by change of input parameters in CART model

8.4 Validation of the Proposed Models

In order to validate/evaluate the capability of the proposed models, the data from Zagros water conveyance tunnel lot 2 which had not been used in the earlier analysis and development of the models, was used for validation.

The geological profile of this section of the tunnel is shown in Fig. 8.7, including the distribution of various stratigraphic units along the tunnel. Pictures (a) to (c) of Fig. 8.8 illustrate different identified engineering geological units in outcrops and tunnel faces. Due to the considerable difference in the engineering properties of the stratigraphic units, they can be considered as different engineering geological units.

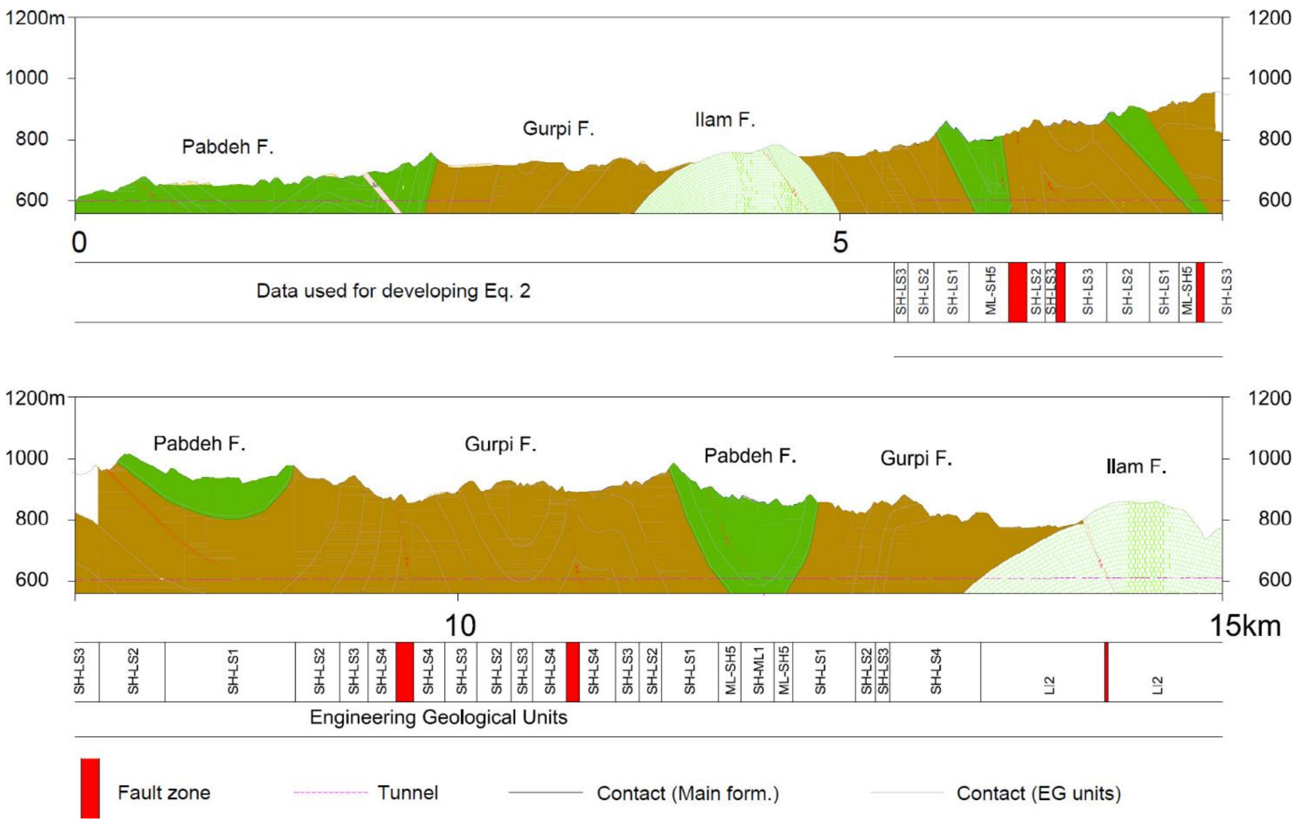

Figure 8.7: Geological cross-section along the ZWCT2 (Hassanpour et al. 2016)

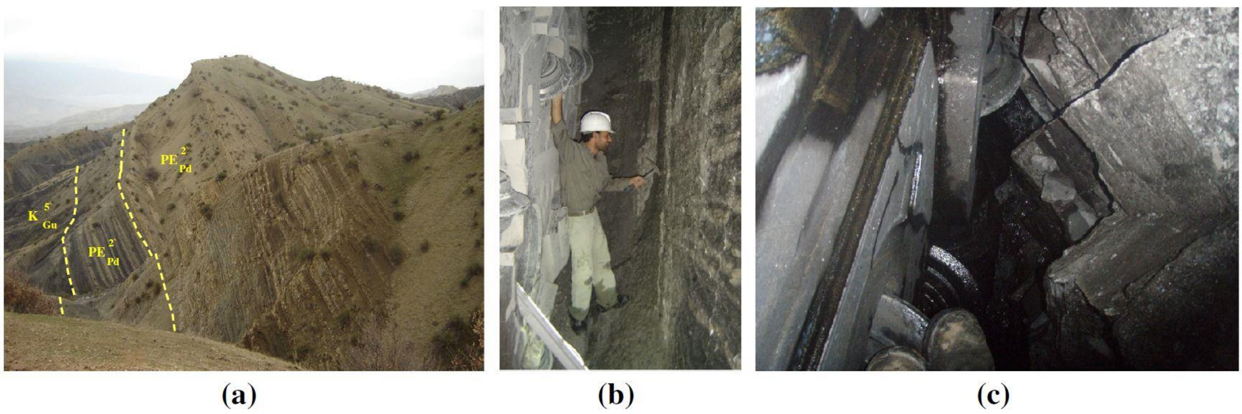

Figure 8.8: (A) A view of Pabdeh and Gurpi contact and stratigraphic units identified along the tunnel alignment, (b) alteration of shale and shaly limestone in tunnel face, (c) views of limestone blocks in tunnel face (Hassanpour et al. 2016)

The main petrographic, physical, and mechanical characteristics of these lithotypes are summarized in chapter 5, Table 5.4. To determine drillability indices, 12 sets of Norwegian tests were performed by the SINTEF laboratory on samples taken from different boreholes along the tunnel alignment. Also, a series of tests were performed using devices in a local laboratory. (Hassanpour, 2009; Hassanpour et al. 2016). The selected area for assessment of the proposed models is focused on TBM performance for the chainage from 5.3 km to 15 km at the southern section of the ZWCT Lot 2 project (~ 9.5 km) while, the first 5 km of the tunnel used before for development of the models.

As mentioned earlier, the main objective of this section was the evaluation of the accuracy of developed models and comparison of the most common TBM performance prediction models in a given geological condition encountered at this site. The normal range of ROP was 1.6-4 m/h with an average of 2.6 m/h for the total length of bored section. Graphs presented in Fig.8.9. shows the variations of the RPM, penetration rate (m/h), and total TBM thrust at different identified geological units along the bored section of the tunnel used in this section, respectively. Average values of rock mass parameters and intact rock properties have been used to determine geomechanical conditions of the identified engineering geological units by some empirical rock mass classification systems (See Figure 8.10). Besides that, the joint spacing encountered along the tunnel in the study area has an average of 0.21 m, ranging from 0.05 to 0.35 m.

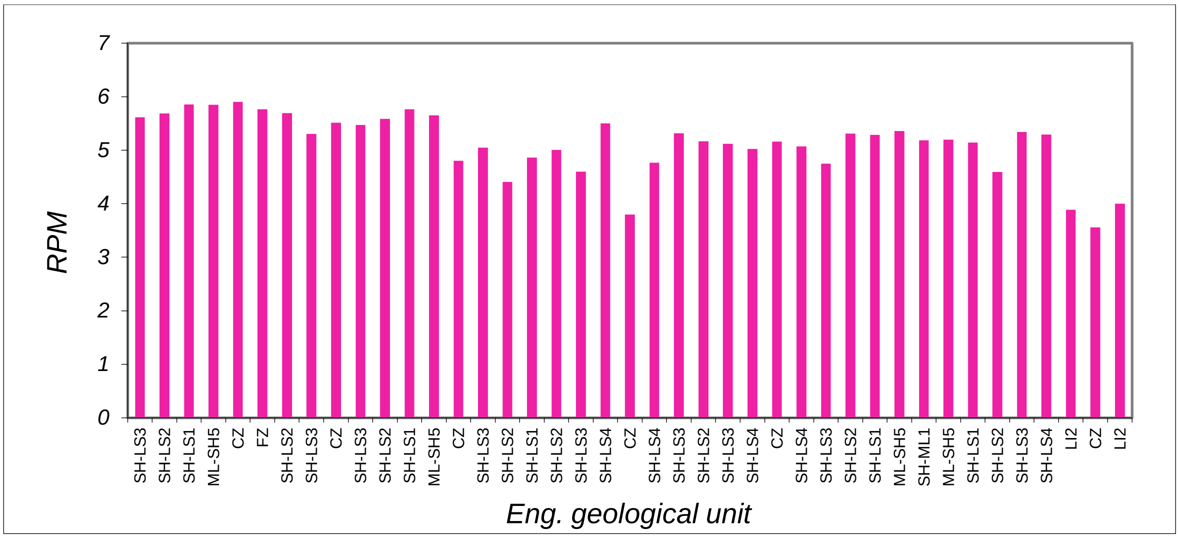

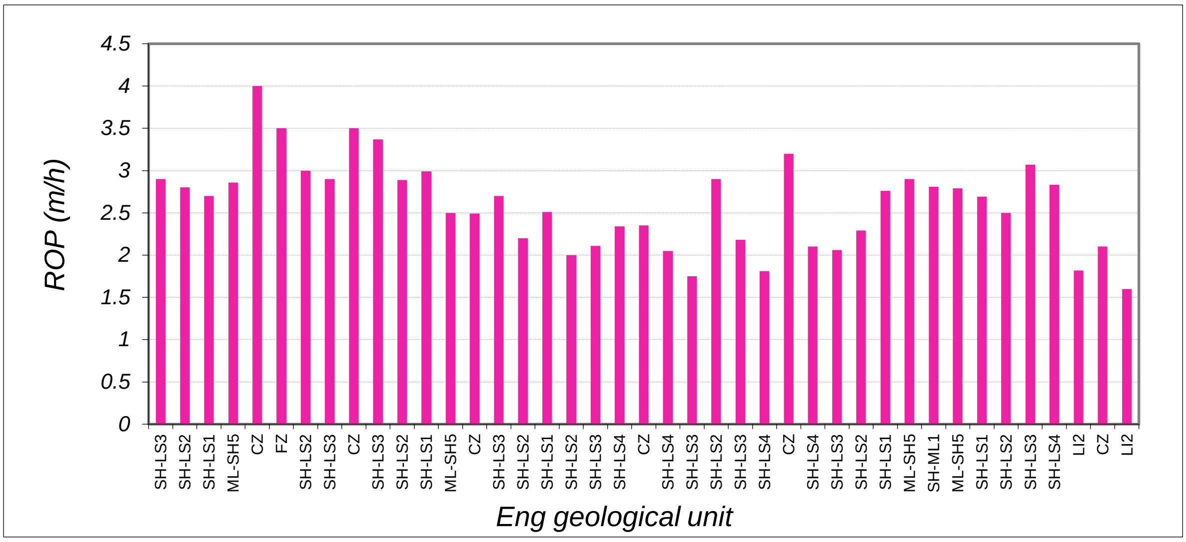

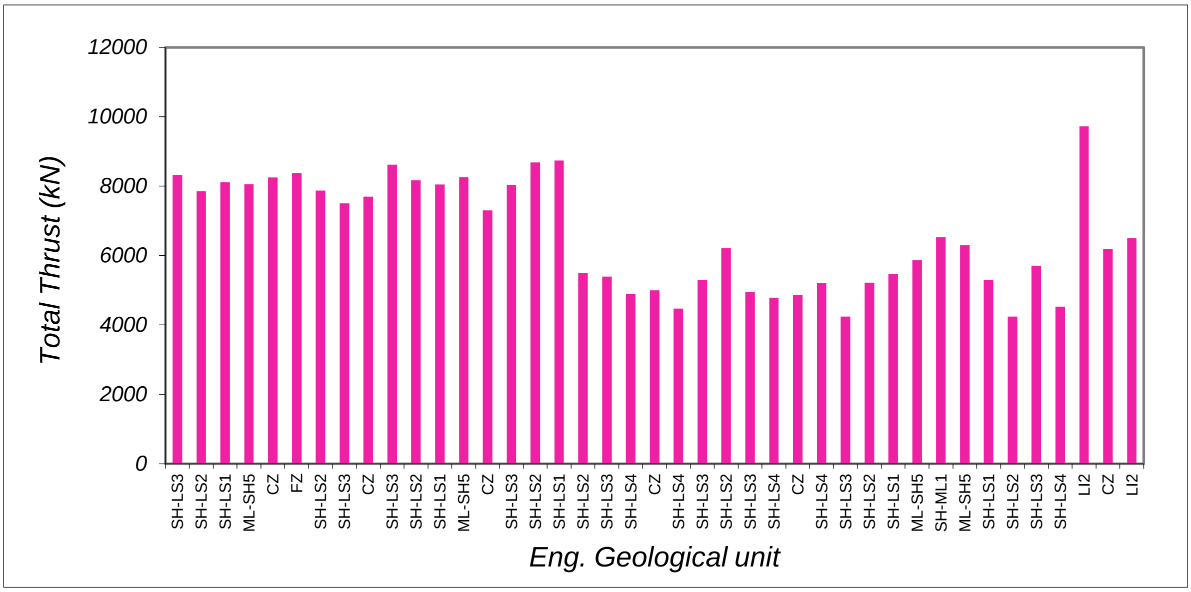

Figure 8.9: Variations of average TBM performance parameters (ROP, RPM, Total Thrust) along the tunnel

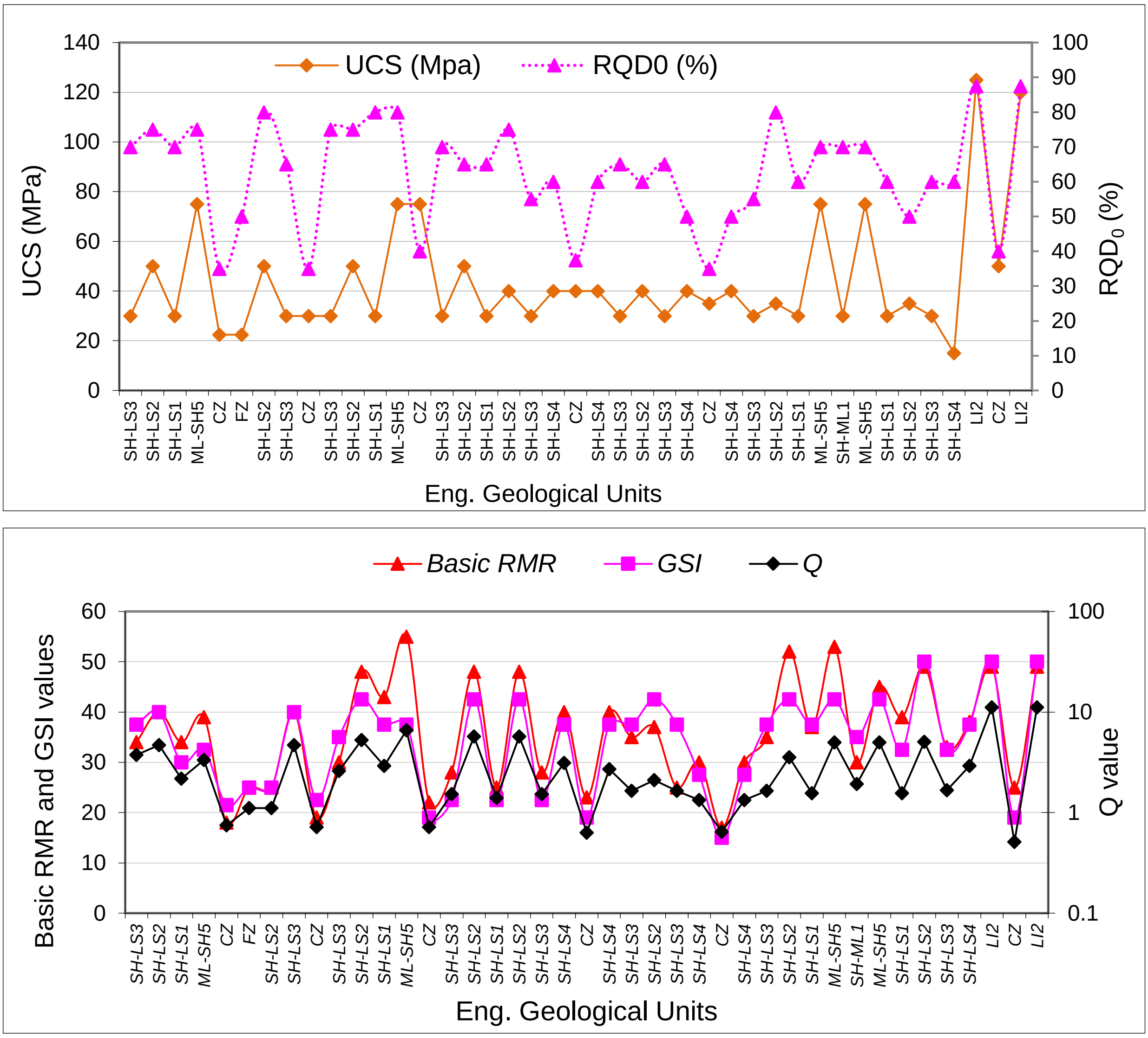

Figure 8.10: Variations of UCS, RQD_0 and rock mass parameters of engineering units identified along the tunnel alignment

8.4.1 Estimation of TBM Performance using CSM, NTNU, Q_{TBM} & CART Models

Among the models presented and discussed in Chapter 4, three of them including CSM, NTNU, and Q_{TBM} are the most commonly used prognosis models applied in the tunnel industry. As such, based on the arranged data and data-collection, the rate of penetration at each tunnel sections are calculated and recorded in a new separate file defined as the results of performance prediction by different models. Table 8.2 presents an overview and calculation procedure of each mentioned model, containing CSM, NTNU, and Q_{TBM}. Since among the developed models in this investigation, CART shows better results comparing to the others (Non-linear regression & GP), therefore, the CART model is adopted to assess the results efficiency/ accuracy of TBM PR contrasting to CSM, NTNU, Q_{TBM} as well as the actual recorded one. Also, the following formula can be used to calculate ROP (m/h) from the FPI.

$$ROP(m/h) = \frac{0.06 \cdot F_n \cdot RPM}{FPI} \tag{8.1}$$

Where F_n is the average cutter load (kN/cutter), RPM is cutterhead speed (revolution per minute), and FPI is field penetration index (kN/cutter/rev/min). Figure 8.11 shows estimated ROP m/h) for the TBM in each unit using the above-mentioned prediction models, while Figure 8.12 presents the actual and estimated ROP in scatter-plot. Moreover, variations of absolute error or $E(\%)$ for each model in each tunnel section, are shown in graphs of Figure 8.13. The absolute error $E(\%)$ can be calculated according to the following formulae:

$$E(\%) = 100 \cdot \left| \frac{Actual\ ROP - Estimated\ ROP}{Actual\ ROP} \right| \tag{8.2}$$

A summary of the statistical analysis performed on calculated rates and respected error are presented in Table 8.3. The results show that CART had the lowest total error and thus offers a more accurate prediction of the TBM performance for this project.

Table 8.2: Overview of CSM, NTNU, Q_{TBM} and CART prediction models

Prediction model	Required input parameters		Output parameter	Limitations
	Rock mass parameters	**Machine parameters**		
CSM	Uniaxial compressive strength (UCS), Brazilian tensile strength (BTS), Cerchar Abrasivity Index (CAI)	Cutter load capacity, cutter spacing, cutter diameter, cutter tip width, TBM thrust, and torque.	Penetration	The original model is based only on intact rock properties
NTNU	Fracturing: frequency & orientation, Drilling Rate Index (DRI), Bit Wear Index (BWI), Cutter Life Index (CLI), and the other parameters	Cutter thrust, cutter spacing, cutter diameter	Penetration rate, advance rate, utilization factor, tunnel cost	Determination of input parameters needs special tests
Q_{TBM}	RQD_0, Jn, Jr, Iw, SRF, rock mass strength, cutter life index (CLI), UCS, induced biaxial stress	Average cutter load, TBM diameter	Penetration rate, advance rate	The model uses many parameters, input parameters determination needs special tests, some inputs parameters are overlapped
CART (Salimi et al. 2019)	UCS, RQD, joint spacing (Js), joint characteristics (partial rating in basic RMR), Rock Type Code (RTC)	Thrust, rotation speed of cutterhead, number of disc cutters	Penetration rate	Unstable blocky ground, Mixed face conditions,

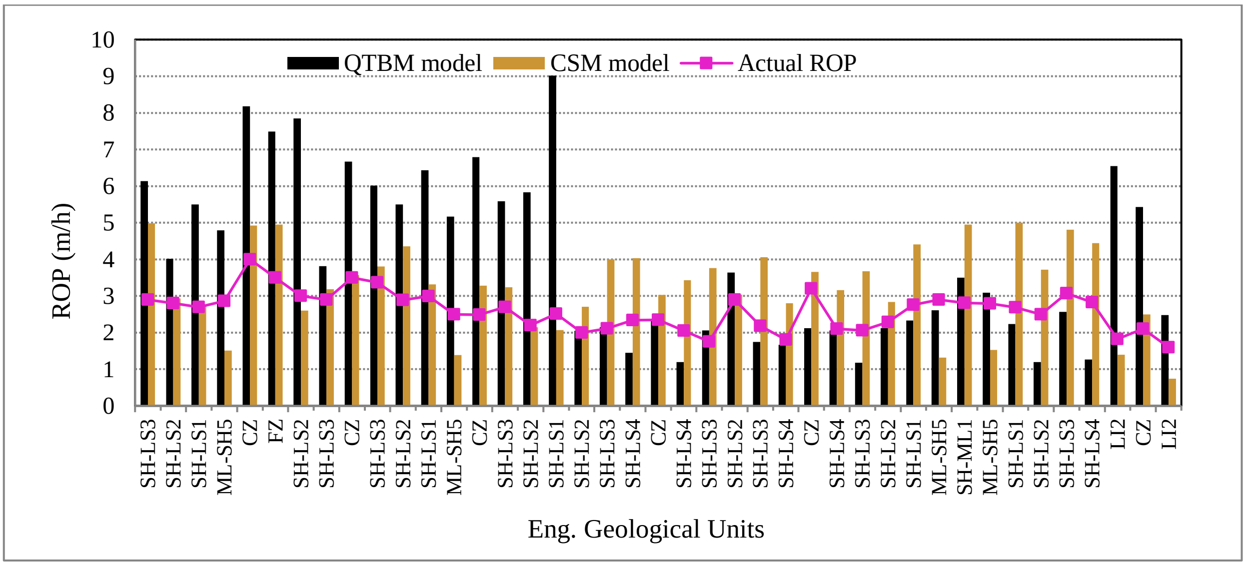

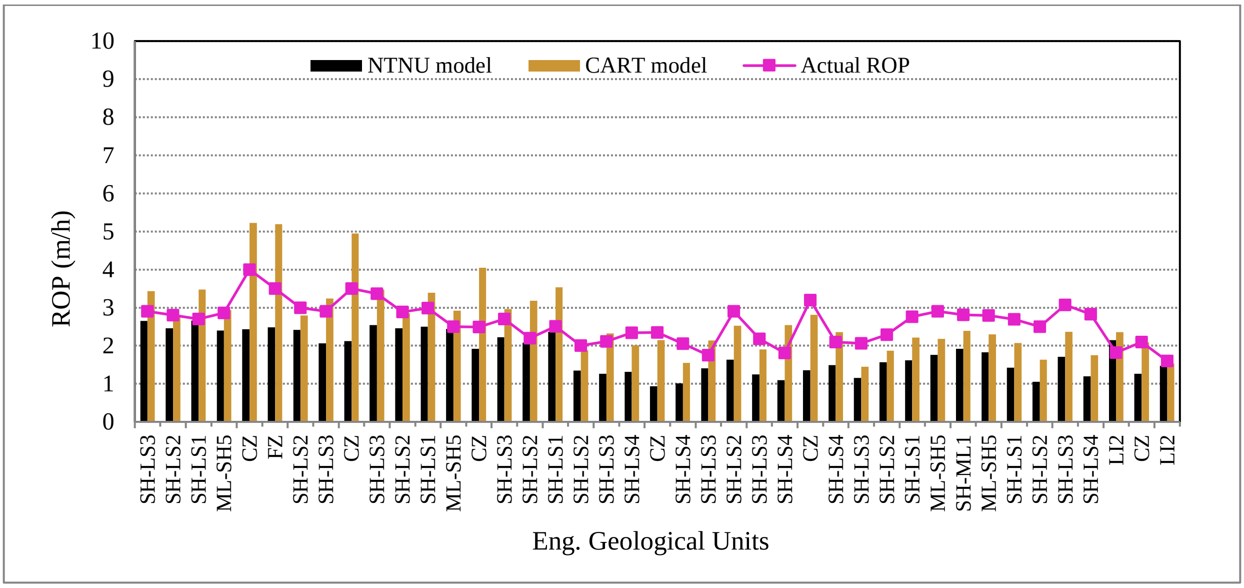

Figure 8.11: Comparison of measured and calculated ROP using CSM, Q_{TBM}, NTNU & CART models

Table 8.3: Descriptive statistics of absolute errors (E) estimated for the prediction models

Models	N	Range	Minimum	Maximum	Mean	Std. Deviation
NTNU	41	58.75	1.55	60.30	30.74	16.43
CSM	41	112.94	2.09	115.03	41.66	28.60
Q_{TBM}	41	258.72	1.00	259.72	69.26	66.59
CART	41	61.77	0.68	62.45	20.40	14.58

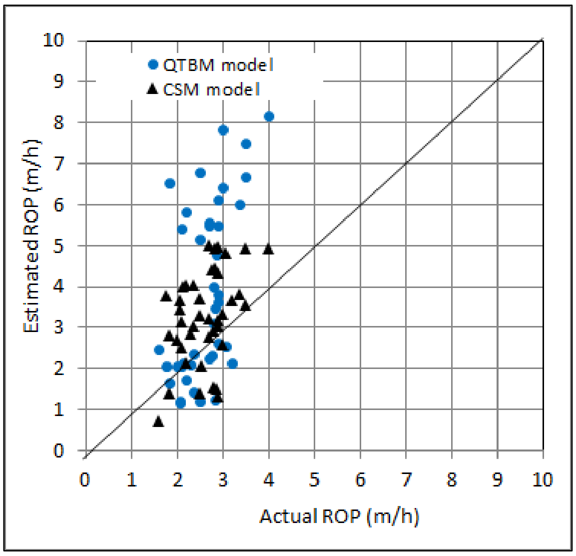

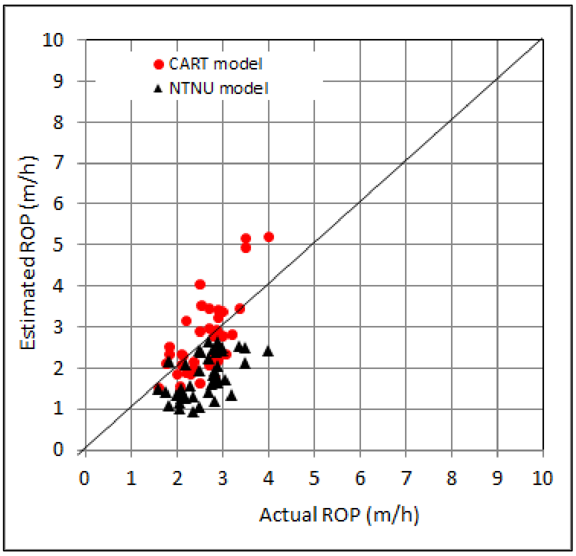

Figure 8.12: Comparison between actual and estimated ROP from Q_{TBM}, CSM, CART, and NTNU model

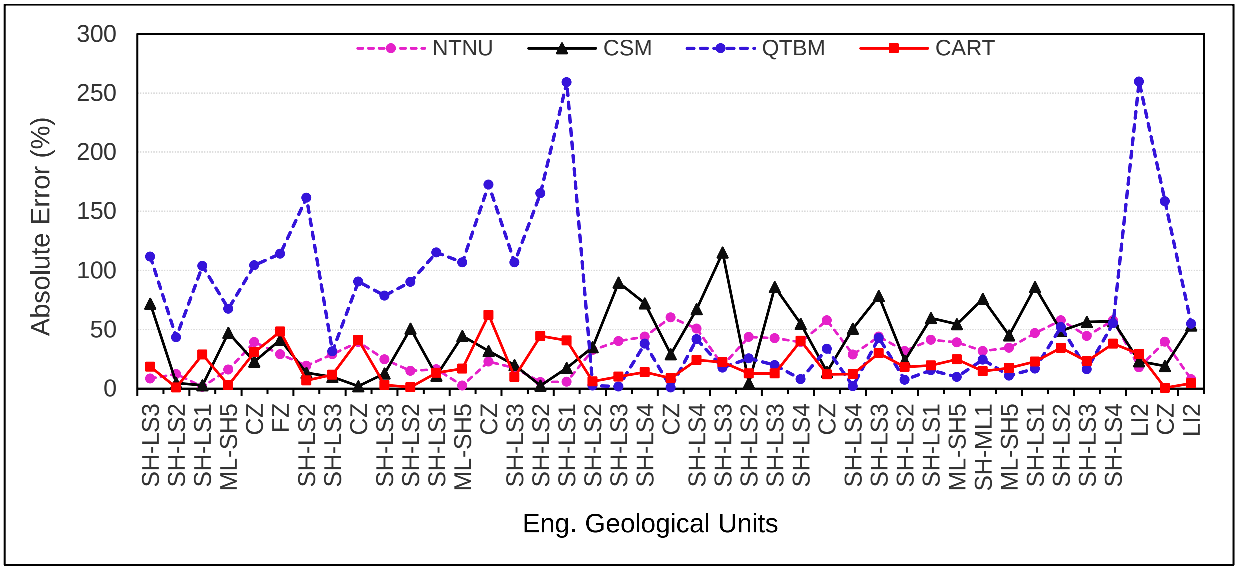

Figure 8.13: Variations of absolute error estimated for different models in each geological unit along the tunnel alignment

8.4.2 Comparison with compatible model, (CART vs Hassanpour et al. (2011))

Among the different models which have been presented and discussed in chapter 4, the model proposed by Hassanpour et al. (2011) was developed based on the FPI model. As such, in this section, the results of the calculated ROP via the CART model is compared with Hassanpour's model. Similar data has been used for model assessment, i.e., the chainage from 5.3 km to 15 km at the southern section of the ZWCT Lot 2 project (~ 9.5 km). Figure 8.14 displays estimated ROP (m/h) for the TBM in each unit respecting to CART and Hassanpour et al. 2011 models, while Figure 8.15 illustrates the actual and estimated ROP in scatter plot. Besides that, variations of absolute error or $E(\%)$ for the above-mentioned models in each section tunnel section are depicted in Figure 8.16. Also, a summary of statistical analysis executed on the calculated rate and respected error shown in Table 8.4. As can be seen, the CART model shows slightly less error and better accuracy in contrast to Hassanpour et al. (2011) model.

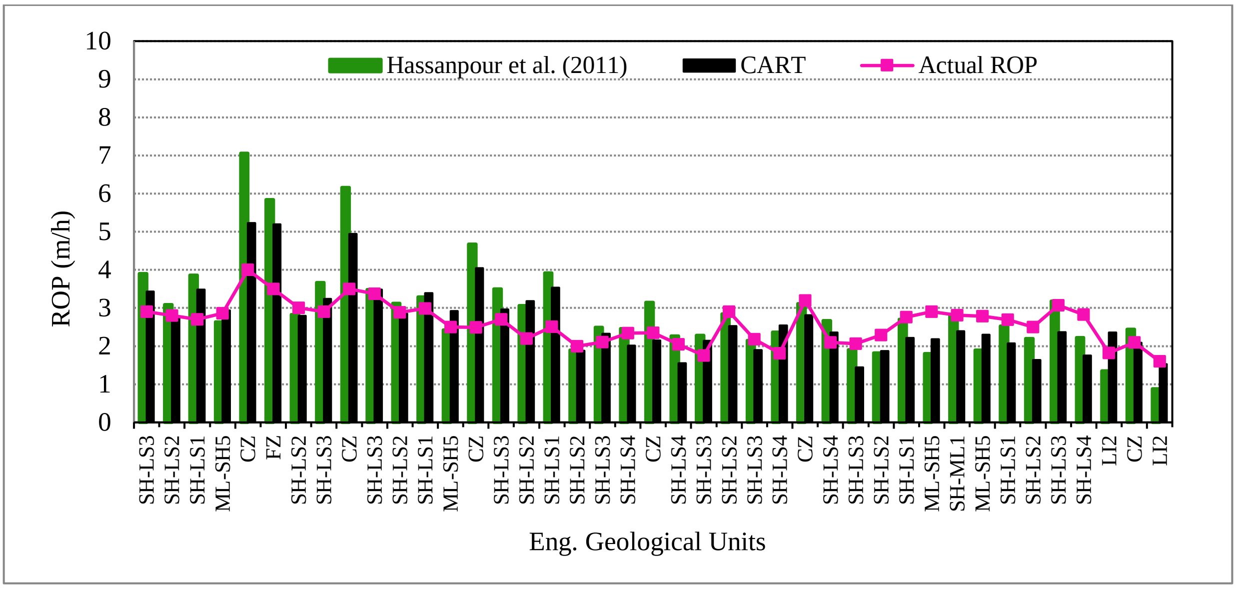

Figure 8.14: Comparison of measured and calculated ROP using CART & Hassanpour et al. 2011 models

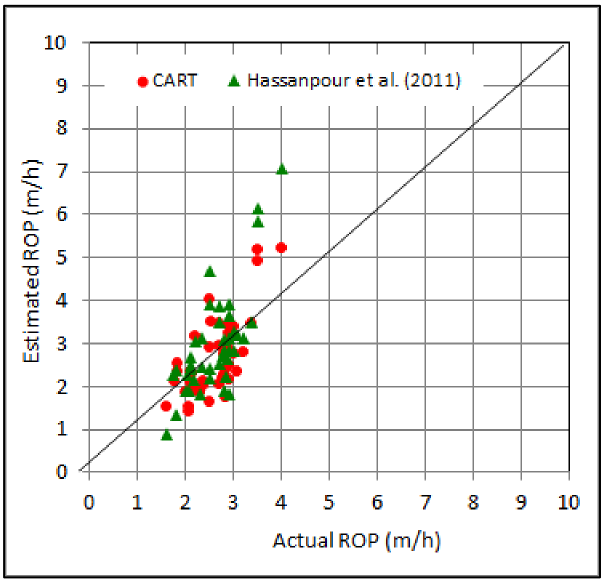

Figure 8.15: Comparison between actual and estimated ROP from CART and Hassanpour et al. (2011) model

Table 8.4: Descriptive statistics of absolute error (E) estimated from CART and Hassanpour et al. (2011) models

Models	N	Range	Minimum	Maximum	Mean	Std. Deviation
CART	41	61.77	0.68	62.45	20.40	14.58
Hassanpour et al. (2011)	41	87.23	0.45	87.68	23.92	22.78

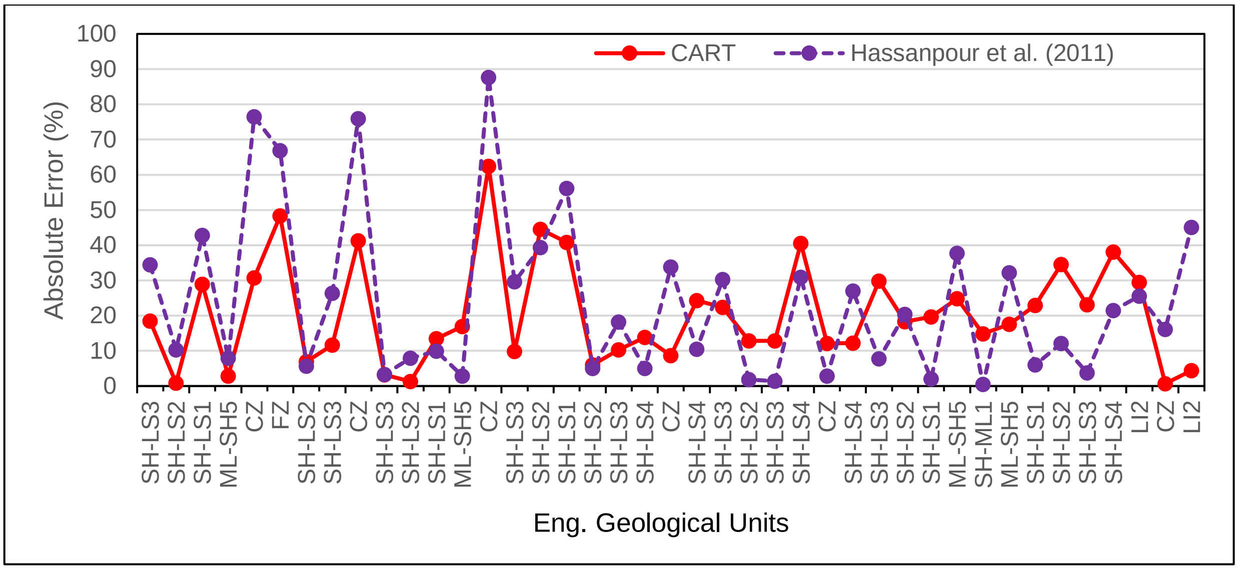

Figure 8.16: Variations of absolute error estimated for CART & Hassanpour et al. (2011) models in each geological unit along the tunnel alignment

8.5 Limitations of the developed CART model

The CART model developed in this investigation has some limitation in its application, similar to any other empirical model, and that is the applicability within the range of parameters in the original database and the best results for the range of data with substantial number of data points. The additional limitations are with respect to machine parameters, mainly associated with the cutter diameter & spacing used on the machines used in this study, mostly 432 mm (17 inch) disc cutters. Although the thrust force per cutter is a normalized value by cutter number in the developed model, the concentrated stress acting on the rock face at the contact point which initiates the fracture propagation is still greatly affected by cutter diameter and cutter tip width even if the force per cutter is the same as noted by Gong & Zhao (2009). Although, these machines have different diameters, they are similar in most of their specifications, particularly in cutterhead design and cutters arrangement i.e., all of these machines used 17-inch constant cross section (CCS) disc cutters with almost similar geometry; and the average spacing of disc cutters in all cutterheads was in the range of 60-90 mm. Consequently, when the machine parameters are changed (especially cutter dimeter, cutter width and spacing), the model need to be used with consideration of the effects of these parameters. Perhaps existing models such as CSM formula which allows for variation of these parameters can be used for developing adjustment factors to extend the use of the proposed FPI numbers to the cases where disc diameter and tip width or spacing is outside the range of the available database.

On the other hand, the estimated FPI and machine performance is dependent upon geological characteristics of the sites and hence, there are some limitations in the range of geosocial parameters for the use of the proposed formulas that can be listed as follows:

- Transitional working conditions: In general, the estimated penetration rate by any performance prediction models is not applicable to machines operating in transition zones which could be Mixed Face Conditions where dissimilar material is cut at the face. The mixed face describes a tunnel face exhibiting two or more rock materials, interface between rock and fault zone, fault and soil, etc. with significantly different boreability properties.

- Unstable Blocky Ground: "blocky rock conditions" is a term associated in the literature to face instabilities in jointed/blocky rock masses, in which the combined effect of rock mass structure and in-situ stresses may lead to a degradation process of the tunnel face that may lead to face failure in the "blocky" ground. In this type of ground, intersection of discontinuity sets forms rock blocks which could detach from tunnel face and cause cutterhead jamming, increase required torque and cause damage to disc cutters.

- Squeezing Ground Conditions: Operation of TBMs involves tremendous difficulties in weak and deformable grounds, typically encountered within zones exhibiting ground squeezing behaviours such as highly tectonic zones or weak ductile rocks at great depth. The high tunnel deformation phenomenon is called 'squeezing ground' in which large time-dependent and anisotropic deformations occur. The potential hazards associated with squeezing ground concern both the ma-chine (sticking of the cutter head, jamming of the shield) and the back-up area (in-admissible convergences of the bored profile, damage to the support). But the main issue is that the cutterload delivered to the cutters at the face are unpredictable, due to the unknown level of frictional forces between the walls and the TBM shield.

In addition to the above-mentioned conditions which needs ample amount of caution to apply the developed CART model, the use of model in boundary conditions of rock mass also requires more scrutiny. This refers to rock masses with high in-situ stress and groundwater. While groundwater in principle does not impact penetration rates, it surely can affect the advance rate. Many tunnel instability incidents are linked to groundwater inflow. High in-situ stress influences both advance rate and penetration rate. As noted by Liu et al. (2002), if the in-situ stress is insufficient to cause stress slabbing at the face, it may still limit or enhance crack propagation and consequently affect penetration rate.

At higher in-situ stress levels where stress slabbing can occur, over-stressed burst may occur that impacts the machine utilization but, in some cases, this can also affect TBM penetration rate (U. S. Army Corps of Engineer, 1997; Boniface, 2000). In either scenario, if elevated levels of in-situ stresses are encountered, the use of models based on normal TBM operation conditions may yield less accurate estimates of machine performance. The CART model offered in this study is no exception.

Chapter 9 Discussion & Conclusion

9.1 Introduction

As mentioned in chapter 1, the main goal of this investigation was to develop new models for more accurate prediction of penetration rate for rock TBM, based on rock mass conditions. For this purpose, data from different tunneling projects using TBMs were compiled in a database, which included different rock mass conditions. The database of TBM field performance includes 7 tunnel projects with a total length of 70.73 km, including rock properties, and TBM operational parameters. Statistical analyses were used to seek correlations between rock/ground characteristics and TBM operational parameters, and the resulting TBM performance. Based on the recent experiences with TBM performance prediction models, field penetration index (FPI) was selected to represent TBM performance due to its scalability and the fact that it accounts for TBM diameter, RPM, and applied cutterload.

To find the most effective parameters in the prediction of FPI, principal component analysis (PCA) was used, followed by developing some models using linear & non-linear regression analysis, as well as artificial intelligence algorithms including, classification and regression tree (CART) & genetic programming (GP).

In this chapter the main results are highlighted, conclusions are summarized, and some recommendations for future follow-up studies are proposed.

9.2 Discussion & Conclusion

The machine penetration rate is represented by a unit of m/h or penetration rate per rotation (PRev i.e., mm/rev). There are various approaches to estimate the TBM penetration rate that has been introduced over the past few decades. Parameters such as specific penetration (SP), the normalized index of the penetration rate per unit value of cutter load, and the field penetration index (FPI), which is the inverse of specific penetration, are used for this purpose. The main advantage of these indices is to account for machine diameter, rotational speed (RPM), and cutter load (or machine thrust) through normalization of the objective parameter, ROP, which allows for a head-to-head comparison between machine performance in two different ground conditions (Gong and Zhao 2009; Farrokh et al. 2012; Salimi et al. 2016a).

While various empirical models for TBM performance prediction have been introduced, many lack the correct reflection of the geotechnical input parameters to allow for proper accounting of the impacts of such parameters. As such, rock mass classifications have been used to represent rock mass conditions in TBM performance prediction, often with low correlations since they were originally developed for estimation of rock load and ground support design and not TBM excavation. Among the most commonly used classification systems, Rock Mass Rating (RMR), Rock Mass Quality Index (Q), and Geological Strength Index (GSI) have been used more frequently in TBM performance prediction. However, the use of RMR classification systems, while better than the other options, it has offered limited success in providing an accurate estimation of TBM penetration rate.

Meanwhile, it is known that the parameters that determine rock mass classification do influence TBM performance. This includes rock strength and jointing parameters. The most frequent input parameters used in the previous studies for prediction of TBM performance are: the uniaxial compressive strength and tensile strength of intact rock (used by 70% of the models), distance and the orientation of discontinuities (used by 50% of the models), the assumed thrust per cutter (used by 40% of the models) and the cutter diameter (used by 30% of the models).

The current study focused on developing a new model for estimation of TBM performance represented by FPI, based on input parameters from rock mass classification systems. As such, input parameters of the RMR system, which are often available for various projects, have been used as input parameters for the estimation of FPI. This includes UCS, RQD, Js, and Jc, with the addition of Rock Type to replace Gw which was clearly shown to have no measurable impact on FPI. Seven tunneling projects used in the current study and related ground characteristics, machine's operational parameters, and recorded performance data were compiled in a database for subsequent analysis. The use of the PCA method has allowed for the selection of the input parameters with the maximum impact on the FPI. Based on the results of the PCA method, statistical analysis of the TBM field performance was conducted using linear and non-linear regression on the parameters identified to the highest impact on machine performance. As a result, bivariate or multivariate empirical equations have been presented for TBM performance in different selected tunneling projects.

Apart from the empirical and theoretical models, artificial intelligence (AI) techniques have also been used for developing models to predict penetration rate (PR) in hard rock conditions in the past.

In this investigation, two different AI models including classification and regression tree (CART) and genetic programming (GP) have been examined to develop new models for estimation of FPI based on input parameters of the RMR system (without the Gw and with the addition of rock type code). The CART model demonstrates better accuracy for TBM performance estimation compared to other methods. The model and formulas developed based on GP analysis while offer better results than the empirical formulas based on regression analysis, they are more complex and include components that does not offer a coherent physical meaning.

It is prudent to apply three methods (MNLRA, CART, GP) for TBM performance prediction and compare the results, perhaps use the average value for FPI for prediction and hence calculation of TBM rate of penetration.

The following is the summary of the most important highlights and findings of this study:

- Among the common rock mass classification systems, basic RMR shows a better correlation with TBM penetration rate.
- FPI is a flexible and reliable TBM performance index that is a better representative for TBM performance as it incorporates machine size (by RPM) and applied thrust or cutterload.
- The analysis of variations in TBM operational parameters as well as rock mass properties and resulting TBM performance in this investigation shows that, higher thrust, torque, and higher cutterhead RPM were needed or used in the excavation of harder rock, while lower penetration rates were experienced. In Contrast, in fractured formation as well as in softer rock, higher penetration rate and lower cutterhead RPM along with lower thrust forces were required. Besides, better correlations were found between rock mass parameters, e.g., RQD with TBM operational parameters, as compared to rock properties such as UCS in jointed rocks. However, the overall performance of TBM not only influenced by factors related to geology or machine specifications, the experience and skills of the crew and especially TBM operators, and site organization also impacts the outcome. This can be seen in the difference between machine performance in different shifts, but is often not directly incorporated in the analysis of TBM field performance data.

- The study of correlations between the individual independent variables in the basic RMR and the actual FPI measured in the field shows that *RQD* offers the highest R^2 value of 0.69, followed by the *UCS* (0.67), *Js* (0.56), *Jc* partial rating in RMR (0.33), and *Gw* shows no correlation with TBM performance (0.0074).
- The results of PCA, which is done independent of the correlation studies, confirm the findings of the statistical analysis and indicated that the most effective parameters for the determination of FPI are *UCS* , *RQD* , *Js* , and *Jc* .
- Since different rock textures (cementation and grain size and shape) affect the penetration rate, such properties need to be taken into account in PR studies. For this purpose, rock type code (*RTC*) was considered to reflect this aspect of rock characteristics.
- As discussed before, the use of statistical analysis alone cannot offer satisfactory results, and the application of artificial intelligent (AI) methods can improve the result of regression analysis. This is while the formulas developed based on multi-variable regression analysis in this study have offered slight improvements over the formulas that were published in the existing literature.
- Study of various statistical and AI analysis showed that CART offers the best results for the estimation of FPI based on the input parameters that was listed in the above sections. This system is based on a simple tree that can be followed by anyone to estimate FPI and subsequently to estimate PR.
- Sensitivity analysis conducted on the developed multivariable non-linear regression analysis (MNLRA) and GP, as well as CART, clearly indicates that, the lowest sensitivity of the model is to *Jc* (joint characteristics), while the other inputs have a significant impact on the output of the model. This could be attributed to the limited range of *Jc* (it changes between 5 to 30) in basic RMR classification or this parameter is shadowed by other inputs such as *UCS* , and *Js* . Besides, it demonstrates the model is equally affected by main input variables (with exception of *Jc*); revealing the suitability of selected parameters and their weights for the model. The results have a good agreement with PCA results.
- Various statistical indices, including correlation coefficient (R^2), the root mean square error (RMSE), mean absolute deviation (MAD), mean absolute percentage error (MAPE), mean square error (MSE), and variance account for (VAF) have been used to assess the performance of the proposed models for predicting FPI. The results show that the prediction capability and accuracy of the CART model is better than other models.

- As noted before, the result of GP analysis which was a series of formulas was deemed not suitable since the formulas incorporates a series of quotients that do not have any physical meaning and are dimensionally incorrect.

Furthermore, to examine the accuracy/ efficiency of the CART model, the operating and as-built geological data collected during the construction phase of the lot 2 of Zagros water conveyance tunnel (ZWCT), chainage 5 to 15 km, which has not been utilized for model development, was used to compare the calculated machine performance by common prediction models such as Q_{TBM} and NTNU as well as CSM models. Following conclusions can be made based on the comparison of the results of the proposed model with those of existing TBM performance prediction models.

- As shown, ΔROP or difference between predicted penetration rates by CSM, NTNU, and Q_{TBM} models and the recorded penetration rates are high, exceeding 100% in some tunnel sections. The NTNU model seems to underestimate, while CSM and notably Q_{TBM} seem to overestimate the ROP.

- The results of the Q_{TBM} model were often higher than the actual values. The main reason could be the consideration of some parameters such as, in-situ stress in the model which its influence on TBM performance in the Zagros Lot #2 project used for validation purposes.

- The results achieved from the original CSM model don't match the measured ROP values, perhaps because, the CSM model has been fundamentally developed for massive rocks with no significant fracturing. So, where the rock mass is massive it works better, but when the rock mass is fractured to intensely fractured, the estimated values of ROP are far from actual values.

- Among the three models, including NTNU, Q_{TBM}, and CSM, NTNU seems to offer more reasonable and relatively good matches with the actual results, for the test dataset. This is because, the NTNU model applies rock mass parameters.

- Among the studied models, the best results were obtained from the CART model, which has been developed based on data analysis of 61.03 km bored tunnels in various rock types & different rock mass as well as ground conditions.

- The estimated ROP by CART model reveals a slightly lower error rate in comparison with the Hassanpour et al. (2011) model. This can be attributed to the partial similarity in data-compilation for model developments. However, it can be expected that, in strong massive rock masses, the developed CART model indicates higher accuracy contrasting to Hassanpour et al. (2011) model, since in the CART model allows for incorporating joint spacing (Js) and joint condition (Jc) in the calculations. As such, the limitation of the Hassanpour model for strong massive rock masses (less fractured) is mitigated by the presented CART model. Moreover, the impact of rocks with similar RQD and UCS but different joining conditions cannot be captured by the Hassanpour model but can be distinguished by the CART model.

- In brief, it can be concluded that, for the selection of an empirical model to predict TBM performance in a new project, one should pay attention to the application range of the model and geological conditions that the original model was based on to produce the most reasonable estimates.

9.3 Recommendations for Future Research

Based on the findings and conclusions of this study, the following recommendations are offered for further study of performance prediction of hard-rock TBMs in the future.

- One of the main findings of this research is that rock type would be one of the best parameters that can be used for the distinction of various geological settings of the job sites, and it could contribute to the development of more accurate performance estimation formulas. There is a need for further investigation of this parameter, either by including the rock type code in the analysis or by averaging the performance of TBMs on the basis of different rock types.
- It is well known that the orientation of discontinuities (bedding and joint planes) can play a significant role in the TBM boring process, but, due to lack of detailed and relevant information, this factor has not been used in this study. Therefore, this parameter can be used for future investigation.
- Rock abrasiveness is recognized as an important parameter in cutter wear prediction and one of the common indexes that are used to predict the wear is Cerchar Abrasivity Index (CAI). Thus, it is recommended to consider this parameter or quartz content for future investigations. Further study would be needed to come up with a cutter wear and cutter consumption evaluation using detailed data and to account for the impact of rock structure on cutter consumption/life. This mainly impacts machine utilization due to the need for frequent cutter change, but it also impacts the FPI since worn cutters have a wider tip and take more force to penetration a certain amount into the rock surface.

- Since the CSM model was basically established for massive rock, additional work is needed to incorporate factors related to joint conditions and make the model applicable in rock masses. This allows for using the inherent strength of the CSM model, which is including machine design features such as cutter size, tip width, and cutterhead design, and extend it to the jointed rock masses where the joints can dominate machine performance.

- It is recommended that a universal recording system used for TBM data collection (onboard computer) be used to compile machine operational parameters and the information to be linked to back-mapping to join the machine operation and ground condition information. This can lead to the forming of a consistent set of data and a uniform/homogenous database which can be used in the future studies.

Bibliography

Aeberli, U., Wanner, W.J. On the influence of discontinuities at the application of tunnelling machines. In: Proceedings of the 3rd International Congress IAEG, Madrid. 7-14. 1978.

Afrasiabi, N., Rafiee, R., Noroozi, M. Investigating the effect of discontinuity geometrical parameters on the TBM performance in hard rock. Int. J. Tunnelling and Underground Space Technology 84, 326-333. 2019.

Alber, M. Advance rates of hard rock TBMs and their effects on project economics. Tunnell. Undergr. Space Technol. 15 (1), 55-64. 2000.

Alber, M. Classifying TBM contracts. Tunnelling and Tunnelling International Dec., 41-43. 1996.

Alvarez Grima, M., Bruines, P.A., Verhoef, P.N.W. Modeling tunnel boring machine performance by Neuro-Fuzzy method. Int. J. Tunnell. Undergr. Space Technol., 259-269. 2000.

Armaghani, D.J., Mohamad, E.T., Narayanasamy, M.S., Narita, N., Yagiz, S. Development of hybrid intelligent models for predicting TBM penetration rate in hard rock condition. 63, 29-43. 2017.

Barla, G., Pelizza, S. TBM tunnelling in difficult conditions, GeoEng 2000, International Conference on Geotechnical & Geological Engineering. 2000.

Barton, N. TBM performance estimation in rock using Q_{TBM}. Tunnels and Tunneling International. 31 (9), 1999.

Barton, N. TBM tunnelling in jointed and faulted rock. Balkema, Rotterdam. 2000.

Barton, N., Lien, R., Lunde, J. Engineering classification of rock masses for the design of rock support. Rock Mec. 6, 189-236. 1974.

BBT-SE Company. https://www.bbt-se.com/en/.

Benardos, A.G., Kaliamakos, D.C. Modelling TBM performance with artificial neural networks. Tunnell. Undergr. Space Technol. 19 (6), 597-605. 2004.

Benato, A., Oreste, P. Prediction of penetration per revolution in TBM tunneling as a function of intact rock and rock mass characteristics. Int. J. Rock Mech. Min. Sci. 74, 119-127. 2015.

Bieniawski, Z.T. Engineering classification of jointed rock masses. Trans. S. Afr. Inst. Civ. Eng. 15 (12), 335-344. 1973.

Bieniawski, Z.T. Engineering Rock Mass Classifications. John Wiley & Sons, New York. 1989.

Bieniawski, Z.T., Celada, B., Galera, J.M. Prediction TBM excavatability. Tunnels and Tunnelling International. 2007a.

Bieniawski, Z.T., Celada, B., Galera, J.M., Alvarez, M. Rock Mass Excavability (RME) Indicator: New Way to Selecting the Optimum Tunnel Construction Method, ITA World Tunnelling Congress, Seoul, South Korea. 2006.

Blindheim, O.T. TBM performance prediction models. Tunnels and Tunneling Int., December 2004.

Blindheim, O.T., Bruland, A. Boreability testing. Norwegian TBM tunnelling. Norwegian Tunnelling Society, Oslo. 1998.

Boniface, A. Tunnel boring machine performance in basalts of the Lesotho formation. Int. J. Tunnel Underground Space Technology. 15 (1), 49-54. 2000.

Breiman, L. Statistical modeling: The two cultures. Statistical Science, 16 (3), 199–231 .2001.

Breiman, L., Friedman, J.H., Olshen, R.A., Stone, C.J. Classification and regression trees. Wadsworth, Belmont, CA. 1984.

Bruland, A. Hard rock tunnel boring. Ph.D. Thesis. Norwegian University of Science and Technology, Trondheim. 1998.

Bruland, A. Hard Rock Tunnel Boring. Norwegian University of Science and Technology. 10 volumes (Dr. ingeniøravhandling). Trondheim, 2000.

Büchi, E. Einfluss Geologischer Parameter auf die Vortriebsleistung einer Tunnelbohrmaschine PhD Thesis. University of Bern. 1984.

Cheema, S. Develoment of a rock mass boreability index for the perfroamnce of tunnel boring machnies. PhD Thesis, Colorado School of Mines, Golden, Co. 1999.

Cho, J.W., Jeon, S., Jeong, H.Y., Chang, S.H. Evaluation of cutting efficiency during TBM disc cutter excavation within a Korean granitic rock using linear-cutting-machine testing and photogrammetric measurement. Tunn Undergr Space Technol. 35; 37-54. 2006.

Cigla, M., Ygiz, S., Ozdemir, L. Application of tunnel boring machines in underground mine development. 17th International mining Congress & Exhibition of Turkey, IMCET. Ankara, Turkey.155-164. 2001.

Cook, N.G.W., Hood, M., Tsai, F. Observations of crack growth in hard rock loaded by an indenter. Int. J. Rock Mech. Mining Sci. Geomech. Abstr. 21, 97–107. 1984.

Cramer, N.L. A representation for the adaptive generation of simple sequential programs. In: Proceedings of the international conference on genetic algorithms and their applications. Carnegie-Mellon University, Pittsburgh, PA, 183-187. 1985.

Cssinelli, F., Cina, S., Innaurato, N., Mancini, R., Sampaolo, A. Power consumption and metal wear in tunnel-boring machines: analysis of tunnelboring operation in hard rock. Tunnelling ‘82, London. Inst. Min. Metall., 73-81. 1982.

Dahl, F., Bruland, A., Jakobsen, P.D., Nilsen, B., Grov, E. Classifications of properties influencing the drillability of rocks, based on the NTNU/SINTEF test method. Tunn. Undergr. Space Technol. 28:150-158. 2012.

Dalton, J. Genetic Algorithms. Newcastle Engineering Design Centre, Merz Court, Newcastle University. http://www.edc.ncl.ac.uk/highlight/rhjanuary2007g02.php. 2007.

Davis, J.C. Statistics and data analysis in geology, 3rd edn. Wiley, New York ,638. 2002.

Deere, D.U., Deere, D.W. The rock quality designation (RQD) index in practice, Rock Classification Systems for Engineering Purposes. ASTM STP. American Society for Testing and Materials, Philadelphia, 91–101. 1988.

Deere, D.U., Hendron, A.J., Patton, F.D., Cording, E.J. Design of surface and near surface construction in rock. Proc. 8th U.S. Symp. Rock Mech. AIME, New York. 237-302. 1967.

Deere, D.W., Keis, S., Watts, C. The Manapouri Tailrace Tunnel No. 2 construction – a very large TBM Tunnel in very strong rock, in: Ozdemir, L. (Ed.), North American Tunnelling, 421-432. 2004.

Delisio, A. Field and numerical studies on the causes and effects of blocky rock conditions on TBM tunneling. Ph.D. Thesis. École Polytechnique Fédérale de Lausanne, Laboratoire de Mécanique des Roches. Unpublished. 2014.

Delisio, A., Zhao, J. A new model for TBM performance prediction in blocky rock conditions. Int. J. Tunnell. Undergr. Space Technol. 43, 440-452. 2014.

Delisio, A., Zhao, J., Einstein, H.H. Analysis and prediction of TBM performance in blocky rock conditions at the Lötschberg Base Tunnel. Int. J. Tunnell. Undergr. Space Technol. 33, 131-142. 2013.

Edelbro, C., Sjoberg, J., Nordlund, E. A quantitative comparison of strength criteria for hard rock masses. Tunnel. Undergr. Space Technol. 22, 57-68. 2006.

Eftekhari, M., Baghbanan, A., Bayati, M. Predicting penetration rate of a tunnel boring machine using artificial neural network. In: ISRM International Symposium-6th Asian Rock Mechanics Symposium. International Society for Rock Mechanics,1-7. 2010.

Engelbrecht, A.P. Computational Intelligence: An Introduction. John Wiley & Sons, New York. 2007.

Entacher, M. Measurement and interpretation of disc cutting forces in mechanized tunneling. Ph.D. Thesis. Montanuniversität Leoben, Austria. 2013.

Farmer, I.W., Glossop, N.H. Mechanics of disc cutter penetration. Tunnels Tunnell. Int. 12 (6), 22-25. 1980.

Farrokh, E., Rostami, J. Correlation of tunnel convergence with TBM operational parameters and chip size in the Ghomroud tunnel, Iran. J. Tunnell. Undergr. Space Technol. 23, 700-710.

Farrokh, E., Rostami, J., Laughton, C. Study of various models for estimation of penetration rate of hard rock TBMs. Tunn Undergr Space Technol 30, 110-123. 2012.

Fatemi, S.A. Prediction of TBM penetration rate by rock mass classification system. Ph.D. Thesis, Tarbiat Modares University, Tehran, Iran. Unpublished. 2016.

Fatemi, S.A., Ahmadi, M., Rostami, J. Evaluation of TBM performance prediction models and sensitivity analysis of input parameters. Int. J. Bull. Eng. Geol. Environ. DOI: 10.1007/s10064-016-0967-2. 2016.

Ferreira, C. Gene expression programming: a new adaptive algorithm for solving problems. Complex Syst. 13(2):87-129. 2001.

Franklin, J.A. Safety and economy in tunnelling. Proc. 10th Int. Can. Rock Mech. Symp. Queens University, Kingston, Canada, 27-53. 1975.

Gerhing, K. Leistungs-und Verschleissprognosen in maschinellen Tunnelbau. Felsbau 13 (6). 1995.

German Committee for Underground Construction (DAUB). Recommendations for static Analysis of Shield Tunnelling Machines. 2005.

Ghasemi, E., Yagiz, S., Ataei, M. Predicting penetration rate of hard rock tunnel boring machine using fuzzy logic. Bull. Eng. Geol. Environ. 73, 23-35. 2014.

Gholami, M., Shahriar, K., Sharifzadeh, M., Hamidi, J.K. A comparison of artificial neural network and multiple regression analysis in TBM performance prediction. In: ISRM Regional Symposium-7th Asian Rock Mechanics Symposium. International Society for Rock Mechanics. 2012.

Gholamnejad, J., Tayarani, N. Application of artificial neural networks to the prediction of tunnel boring machine penetration rate. Mining Sci. Technol. (China) 20 (5), 727-733. 2010.

Gong, Q.M., Jiao, Y.Y., Zhao, J. Numerical modelling of the effect of joint spacing on rock fragmentation by TBM cutters. J. Tunnel. Under. Space Techno. 21, 46-55. 2006.

Gong, Q.M., Zhao, J. Development of a rock mass characteristics model for TBM penetration rate prediction. Int. J. Rock Mech. Min. Sci. 46 (1), 8-18. 2009.

Gong, Q.M., Zhao, J. Influence of rock brittleness on TBM penetration rate in Singapore granite. J. Tunnel. Under. Space Techno. 22. 317-324. 2007.

Gong, Q.M., Zhao, J., Hefny, A.M. Numerical simulation of rock fragmentation process induced by two TBM cutters and cutter spacing optimization. Int. J. Tunnel. Undergr. Space Technol .21. 2006.

Gong, Q.M., Zhao, J., Jiang, Y. In situ TBM penetration tests and rock mass boreability analysis in hard rock tunnels. Int. J. Tunnel. Undergr. Space Technol. 22(3):303-316. 2007.

Gong, Q.M., Zhao, J., Jiao, Y.Y. Numerical modeling of the effects of joint orientation on rock fragmentation by TBM cutters. J. Tunnell. Undergr. Space Technol. 20, 183-191. 2005.

Graham, P.C. Rock exploration for machine manufacturers. In: Bieniawski, Z.T. (Ed.), Exploration for Rock Engineering. Balkema, Johannesburg.173-180. 1976.

Grandori, R., Sem, M., Lembo-Fazio, A., Ribacchi, R. Tunnelling by double shield TBM in the Hong Kong granite. In: Proceedings of the 8th ISRM Congress. 1, 569-574. 1995.

Guglielmetti, V., Grasso, P., Mahtab, A., Xu, Sh. Mechanized tunnelling in urban areas: design methodology and construction control. Taylor & Francis Group, London, UK, 2008.

Bejari, H., Kakaie, R., Mohammad, A., Khademi-Hamidi, J. Simultaneous effects of joint spacing and joint orientation on the penetration rate of a single disc cutter. Int. J. Mining Science and Technology (China). 21; 507-512. 2011.

Hamidi, J.K., Shahriar, K., Rezai, B., Rostami, J. Performance prediction of hard rock TBM using Rock Mass Rating (RMR) system. J. Tunnelling and Underground Space Technology 25, 333-345. 2010.

Hassanpour, J. Investigation of the effect of enginnering geological parameters on TBM performance and modifications to existing prediction models. Ph.D. Thesis, Tarbiat Modares University, Tehran, Iran. Unpublished. 2009.

Hassanpour, J., Ghaedi Vanani, A.A., Rostami, J., Cheshomi, A. Evaluation of common TBM performance prediction models based on field data from the second lot of Zagros water conveyance tunnel (ZWCT2). Tunnel Under. Space Technol. 52, 147-1456. 2016.

Hassanpour, J., Rostami, J., Khamehchiyan, M., Bruland, A. Developing new equations for TBM performance prediction in carbonate-argillaceous rocks: a case history of Nowsood water conveyance tunnel. Geomech. Geoeng.: Int. J. 4, 287-297. 2009.

Hassanpour, J., Rostami, J., Khamehchiyan, M., Bruland, A., Tavakoli, H. TBM performance analysis in pyroclastic rocks: a case history of Karaj water conveyance tunnel. Rock Mech Rock Eng 43(4):427-445. 2010.

Hassanpour, J., Rostami, J., Zhao, J. A new hard rock TBM performance prediction model for project planning, J. Tunnel. Under. Space Techno. 26. 595–603. 2011.

Heydari, S., Khademi Hamidi, J., Monjezi, M., Eftekhari, A. An investigation of the relationship between muck geometry, TBM performance, and operational parameters: A case study in Golab II water transfer tunnel. J. Tunnel. Under. Space Techno. DOI: 10.1016/j.tust.2018.11.043. 2019.

Herrenknecht, M., Rehm, U. "Hard rock technology ", Lecture at Colorado School of Mines, Golden, CO, 2006. www.mines.edu/academic/mining/research/emi/papers/seminar/01_hard_tbms.pdf.

Herrenknecht Company. https://www.herrenknecht.com/de/;

Hien Thi, N., Tran, C.T., et. al. Genetic Programming for storm surge forecasting. Int. J. Ocean Engineering. DOI: 10.1016/j.oceaneng.2020.107812. 2020.

Hoek, E. Rock engineering, course notes by Evert Hoek. 2007. Available from: http:\\www.Rocscience.com.

Hoek, E., Kaiser, P.K., Bawden, W.F. Support of underground excavations in hard rock. Balkema, Rotterdam. 1995.

Hoek, E. Strength of rock masses. News J. ISRM 2 (2), 4-16. 1994.

Hoek, E., Brwon, E.T. Underground excavations in rock. London: The Institute of Mining and Metallurgy. 1980.

Hoek, E., Wood, D. and Shah, S. A modified Hoek-Brown criterion for jointed rock masses. In: Hudson J.A. (ed.) Proceedings of the rock mechanics symposium. International Society of Rock Mechanics Eurock' 92, British Geotechnical Society (1992), London, pp 209-214. 1992.

Hrnjica, B., Danandeh Mehr, A. Optimized Genetic Programming Applications: Emerging Research and Opportunities: Emerging Research and Opportunities. IGI Global, ISBN: 1522560068, DOI:10.4018/978-579 1-5225-6005-0. 2018.

Hughes, H.M. The relative cuttability of coal measures rock. Min. Sci. Technol. 3, 95-109. 1986.

Imensazan Consulting Engineers (ICE). Golab water transfer tunnel engineering geology studies, Unpublished. 2009.

Innaurato, N., Mancini, R., Rondena, E., Zaninetti, A. Forecasting and effective TBM performances in a rapid excavation of a tunnel in Italy. In: Proceedings of the Seventh International Congress ISRM, Aachen. 1009-1014. 1991.

Innaurato, N., Oggeri, C., Oreste, P., Vinai, R. Laboratory tests to study the influence of rock stress confinement on the performances of TBM discs in tunnels. Int. J. Miner. Metall. Mater. 18, 253-259. 2011.

ISRM International Society for Rock Mechanics. Suggested methods for the quantitative description of discontinuities in rock masses. – Commission on Standardization of Laboratory and Field Tests, Document No. 4, International Journal of Rock Mechanics & Mining Science, Vol. 15, pp 319-368. 1978

ISRM International Society for Rock Mechanics. Suggested method for determining the uniaxial compressive strength and deformability of rock materials. International Journal of Rock Mechanics & Mining Science, Vol. 15, pp 137-140. 1979

ISRM. Basic geotechnical description of rock masses. Int. J. Rock Mech. Min. Sci. 18, 85-110. 1981.

ITA-AITES. Recommendations and guidelines for Tunnel Boring Machines (TBMs). Working Group N. 14 "Mechanized Tunnelling". Towards an improved use of underground space. 2000.

Jain, P. Evaluation of engineering geological and geotechnical properties for the performance of a tunnel boring machine in Deccan traps rocks-a case study From Mumbai, India. Ph.D. thesis, Indian Institute of Technology Bombay, India (Unpublished). 2014.

Jain, P., Naithani, A.K., Singh, T.N. Performance characteristics of tunnel boring machine in basalt and pyroclastic rocks of Deccan traps—a case study. Int. J. Rock Mech. Geotech. Eng. 6, 36-47. 2014.

Japan Society of Civil Engineers (JSCE). Standard Specifications for Tunneling - Shield Tunnels. 2007.

Javadi, A.A., Rezania, M., Nezhad, M.M. Evaluation of liquefaction induced lateral displacements using genetic programming. Computers and Geotechnics 33 (4–5),222–233. 2006.

Johari, A., Habibagahi, G., Ghahramani, A. Prediction of soil-water characteristic curve using genetic programming. Journal of Geotechnical and Geo-environmental Engineering132(5),661–665. 2006.

Jolliffe, I.T. Principal Component Analysis. Springer, New York. 1986.

Khraman, S. Correlation of TBM and drilling machine performance with rock brittleness. Journal of Engineering Geology. 65 (4), 269-283. 2002.

Kiers, H.A.L., Rasson, J.P., Groenen, P.J.F., Schader, M. Data analysis classification and related methods. In: International Federation of Classification Societies (IFCS), Namur, Belgium, 428. 2000.

Klein, S., Schmoll, M., Avrey, T. TBM performance at four hard rock tunnels in California. In Williamson & Gowering (eds), Proc. RETC. San Francisco, CA. Littleton, CO: Soc. For Mining, Metallurgy and Exploration; Inc. 1995.

Koza, J.R. Genetic programming: on the programming of computers by means of natural selection. MIT Press, Cambridge. 1992.

Kötzing, T., GregorLagodzinski, J.A., Lengler, J., Melnichenko, A. Destructiveness of lexicographic parsimony pressure and alleviation by a concatenation crossover in genetic programming. International Journal of Theoretical Computer Science. DOI: 10.1016/j.tcs.2019.11.036. 2019.

Kramer, Steven R., McDonald, William J., Thomson, James C. An Introduction to Trenchless Technology. Copyright © 1992 by Springer Science+Business Media New York, US. DOI: 10.1007/978-1-4615-3058-9. 1992.

Labra, C., Rojek, J., Onate, E. Discrete/Finite Element Modelling of Rock Cutting with a TBM Disc Cutter. Rock Mech. Rock Eng. 50: 621–638, 2017.

Laubscher, D.H. Class distinction in rock masses. Coal, Gold Base Min. Southern Africa 23, 37–50. 1975.

Laubscher, D.H. Geomechanics classification of jointed rock masses-mining applications. Trans. Inst. Min. Metall. A86, A1-A8. 1977.

Lauffer, H. Classification for tunnel construction. Geol. Bauwesen 24 (1), 46-51 (in German). 1958.

Laughton, C. Evaluation and prediction of tunnel boring machine performance in variable rock masses. Ph.D. Thesis, The University of Texas, Austin, USA. 1998.

Lin, Q., Cao, P., Cao, R. Experimental investigation of jointed rock breaking under a disc cutter with different confining stresses. Int. J. Comptes Rendus Mecanique. DOI: 10.1016/j.crme.2018.06.012. 2018.

Li, X.F., Li, H.B., Liu, Y.Q., Zhou, Q.C., Xia, X. Numerical simulation of rock fragmentation mechanisms subject to wedge penetration for TBMs. Int. J. Tunn. Undergr. Space Technol. 53, 96-108. 2016.

Li, G., Wang, w., Jing, Z., Zuo, L., Wang, F., Wei, Z. Mechanism and numerical analysis of cutting rock and soil by TBM cutting tools. Tunnelling and Underground Space Technology 81, 428-437. 2018.

Liu, J., Cao, P., Li, K. A study on isotropic rock breaking with TBM cutters under different confining stresses. Geotech. Geol. Eng. 33, 1379-1394. 2015.

Liu, H.Y., Kou, S.Q., Lindqvist, P.A., Tang, C.A. Numerical simulation of the rock fragmentation process induced by indenters. Int. J. Rock Mech. Min. Sci. 39, 491-505. 2002.

Ma, H., Gong, Q., Wang, J., Yin, L., Zhao, X. Study on the influence of confining stress on TBM performance in granite rock by linear cutting test. Int. J. Tunn. Undergr. Space Technol. 57, 145-150. 2016.

Ma, H., Yin, L., Ji, H. Numerical study of the effect of confining stress on rock fragmentation by TBM cutters. Int. J. Rock Mech. Min. Sci. 48, 1021-1033. 2011.

Macias, F.J. Hard Rock Tunnel Boring Performance Predictions and Cutter Life Assessments. Norwegian University of Science and Technology. PhD thesis. Trondheim, 2016

Mahdevari, S., Shahriar, K., Yagiz, S., Akbarpour Shirazi, M. A support vector regression model for predicting tunnel boring machine penetration rates. Int. J. Rock Mech. Min. Sci. 72, 214-229. 2014.

Maidl, B., Herrenknecht, M., and Anheuser, L. Mechanised shield tunnelling: Ernst & Sohn. 1996.

Maidl, B., Herrenknecht, M., Maidl, U., Wehrmeyer, G. Mechanised shield tunneling. Ernst & Sohn A Wiley Company. 2012

Maidl, B., Schmid, W., Ritz, W., Herrenknecht, M. Hardrock Tunnel Boring Machines. Ernst & Sohn A Wiley Company. 2008.

Maidl, B., Thewes, M., Maidl, U. Handbook of Tunnel Engineering Volume I: Structures and Methods. Ernst, Wilhelm & Sohn. ISBN 978-3-433-03048-6. 2013.

Marinos, V., Marinos, P. and Hoek, E. The geological strength index: applications and limitations. Bulletin of Engineering Geology and Environment, Vol. 64 (2005), pp. 55-65. 2005.

Marinos, P. and Hoek, E. GSI – A geologically friendly tool for rock mass strength estimation. In proceedings of the GeoEngineering 2000 Conference. Melbourne, Australia, 2000.

Marinos, P. and Hoek, E. Estimating the geotechnical properties of heterogeneous rock masses such as flysch. Bulleting of Engineering Geology and the Environment, Vol. 60 (2001), pp 82-92. 2001.

Matern von, N., Hjelmer, A. Forsok med pagrus (''Tests with Chippings''), Medelande nr. 65, Statens vaginstitut, Stockholm (English summary, 56-60). 1943.

MATLAB. Statistics toolbox for use with MATLAB, User's guide version 5. The MathWorks, Inc. 2006.

Matula, M., Holzer, R. Engineering typology of rock masses. Proc. Felsmekanik Kolloquium, Grundlagen und Andwendung der Felsmekanik. Karlsruhe, Germany, 107-121. 1978.

Ma, H., Yin, L., Ji, H. Numerical study of the effect of confining stress on rock fragmentation by TBM cutters. Int. J. Rock Mech. Min. Sci. 48, 1021–1033. 2011.

Michael, J.A., Gordon, S.L. Data mining technique: for marketing, sales and customer support. Wiley, New York. 1997.

Mikaeil, R., Naghadehi, M.Z., Sereshki, F. Multifactorial fuzzy approach to the penetrability classification of TBM in hard rock conditions. Int. J. Tunnell. Undergr. Space Technol. 24 (5), 500-505. 2009.

Mingers, J. An empirical comparison of selection measures for decision-tree induction. Mach. Learn. 3, 319-342. 1989.

Mitaini, S., Iwai, T., Isahai, H. Relations between conditions of rock mass and TBM's feasibility. Proc. 6th ISRM congress, Montreal. Rotterdam: Balkema. 1: 701-704. 1987.

Monvikel, T., Johannessen, O. Geological parameters for hard rock tunnel boring. Tunnels & Tunnelling, UK: British Tunnelling Society. April 1986.

Munchener Ruck, Munich Re Group. Underground transportation systems, chances and risks from the reinsurer's point of view. 2004.

Myles, A.J., Feudale, R.N., Liu, Y., Wood, N.A., Brwon, S.D. An introduction to decision tree modelling. J Chemometr 18:275-285. 2004.

Nelson, P., O´Rourke, T.D., Kulhawy, F.H. Factors affecting TBM penetration rates in sedimentary rocks. In: Proceeding, 24th US Symposium on Rock Mechanics, Texas A&M, College Station, TX., 227–237. 1983.

Nelson, P.P. TBM performance analysis with reference to rock properties. In: Hudson, J.A. (Ed.), Comprehensive Rock Engineering, Excavation, support and monitoring, vol. 4. Oxford, Pergamon Press, pp. 261–291. 1993.

Nelson, P.P. Tunnel boring machine performance in sedimentary rock. Ph.D. Thesis, Cornell University, Ithaca, NY. 1983.

Obitko, M. Introduction to genetic algorithm. Hochschule für Technik und Wirtschaft Dresden. https://www.obitko.com/tutorials/genetic-algorithms/index.php. 1998.

Okubo, S., Kfukui, K., Chen, W. Expert system for applicability of tunnel boring machines in Japan. Rock Mech. Rock Eng. 36 (4), 305-322. 2003.

Oraee, K., Khorami, M.T., Hosseini, N. Prediction of the penetration rate of TBM using adaptive neuro fuzzy inference system (ANFIS). In: Proceeding of SME Annual

Meeting & Exhibit, From the Mine to the Market, Now It's Global, Seattle, WA, USA, 297-302. 2012.

Ozdemi, L. Development of theoretical equations for predicting tunnel boreability. Ph.D., Thesis. Colorado School of Mines, Geolden, Co., 1977.

Ozdemi, L., Miller, R.J., Wang, F.D. Mechanical tunnel boring prediction and machine design, "NSF APR73-07776-A03, Colorado School of Mines, Golden Co, USA. 1978.

Palmström, A. RMi- a rock mass characterization system for rock engineering purposes. PhD thesis, Oslo University, Norway. 1995.

Palmström, A. The volumetric joint count- a useful and simple measure of the degree of rock mass jointing. Proc. 4th IAEG Congress, New Delhi. V: Theme 2, 221-228. 1982.

Patching, T.H., Coates, D.F. A recommended of rock classifications for rock mechanics purposes. CIM Bull. 1195-1197. 1968.

Perras, M.A., Diederichs, M.S. & Besaw, D. Geological and geotechnical observations from the Niagara Tunnel Project. Bull Eng. Geo.l Environ. 73, 1303–1323. 2014.

R. Poli, W. B. Langdon, and N. F. McPhee. A field guide to genetic programming. Published via http://lulu.com. (With contributions by J. R. Koza). 2008.

Quinlan, J.R. C4.5 Programs for Machine Learning ,1 st edn. Morgan Kaur- mann, San Mateo, CA. 1993.

Rabcewicz, L.V. The New Austrian Tunnelling Method-Part 2. Water Power 19-24. 1965.

Rabcewicz, L.V.The New Austrian Tunnelling Method-Part 1. Water Power 511-515. 1964.

Ramezanzadeh, A. Performance analysis and development of new models for performance prediction of hard rock TBMs in rock mass, Ph.D. Thesis, INSA, Lyon, France, 2005.

Ribacchi, R., Lembo-Fazio, A. Influence of rock mass parameters on the performance of a TBM in a gneissic formation (Varzo Tunnel). Rock Mech. Rock Eng. 38 (2), 105-127. 2005.

RobbinsCompany. http://www.therobbinscompany.com/en/our products/tunnelboring-machines.

Robbins, R.J. Large diameter hard rock boring machines: state-of-the-art and development in view of alpine base tunnels. Felsbau 10 (2), 56-62. 1992.

Robbins, R.J. Mechanized Tunnelling - progress and expectations, London: Institution of mining and metallurgy. 1976.

Robbins, R.J. Present trends and future directions in tunnelling. In: The Yugoslav Symp. on Rock Mechanics and Underground Actions, p. 11. 1980.

Robbins, R.J. Tunnel machines in hard rock. Butterworth, London. 1990.

Romana, M. New adjustment ratings for application of Bieniawski classification to slopes. Proceedings of the Int. Symp. on the Role of Rock Mech., Zacatecas, 49-53. 1985.

Rostami, J. Development of a force estimation model for rock fragmentation with disc cutters through theoretical modelling and physical measurement of crushed zone pressure. Ph.D. Thesis. Colorado School of Mines, Golden, Colorado, USA. 1997.

Rostami, J. Study of pressure distribution within the crushed zone in the contact area between rock and disc cutters. International Journal of Rock Mechanics & Mining Sciences. 57: 172-186, 2013.

Rostami, J. Performance prediction of hard rock Tunnel Boring Machines (TBMs) in difficult ground. Tunn. Undergr. Space Technol. 57:173–182, 2016a.

Rostami, J. Role of rock mass classification in TBM performance prediction, Where Are We Now, Where Are We Heading. International Conference on Tunnel Boring Machines in Difficult Grounds (TBM-DiGs). Istanbul-Turkey. 2016b.

Rostami, J., Ozdemir, L. A new model for performance prediction of hard rock TBM. In: Bowerman, L.D. et al. (Eds.), Proceedings of RETC, Boston, MA,793-809. 1993.

Rostami, J., Ozdemir, L., Bjorn, N. Comparison Between CSM and NTH Hard Rock TBM Performance Prediction Models, ISDT, Las Vegas. 1996.

Sala, A., Wick, R. Gotthard Base Tunnel – Technical project overview. Geomechanics and Tunnelling. Ernst & Sohn; Volume 9, Issue 2. 2016.

Salimi, A., Esmaeili, M. Utilizing of linear and non-linear prediction tools for evaluation of penetration rate of tunnel boring machine in hard rock condition. Int. J. Min. Miner. Eng. 4 (3), 249-264. 2013.

Salimi, A., Faradonbeh, R.S., Monjezi, M., Moormann, C. TBM performance estimation using a classification and regression tree (CART) technique. Int. J. Bull. Eng. Geol. Environ. DOI: 10.1007/s10064-016-0969-0. 2016c.

Salimi, A., Moormann, C., Rostami, J. Study of TBM performance prediction using rock mass classification". World Tunnel Congress (WTC), San Fransisco, USA. 22-28 April. 2016b.

Salimi, A., Rostami, J., Moormann, C., Hassanpour, J. Examining Feasibility of Developing a Rock Mass Classification for Hard Rock TBM Application Using Nonlinear Regression, Regression Tree and Generic Programming. Geotech. Geol. Eng. DOI: 10.1007/s10706-017-0380-z. 2017.

Salimi, A., Rostami, J., Moormann, C., Delisio, A. Application of non-linear regression analysis and artificial intelligence algorithms for performance prediction of hard rock TBMs. Int. J. Tunnell. Undergr. Space Technol. 58, 236-246. 2016a.

Salimi, A., Rostami, J., Moormann, C. Development of a new models for prediction of TBM performance in hard rock condition based on rock type. 4th International Conference on Tunnel Boring Machines in Difficult Grounds (TBM-DiGs), Colorado School of Mines Golden, Colorado USA. 2019.

Sanio, H.P. Prediction of the performance of disc cutters in anisotropic rock. Int. J. Rock Mech. Min. Sci. Geomech. 22, 153-161. 1985.

Sapigni, M., Berti, M., Behtaz, E., Busillo, A., Cardone, G. TBM performance estimation using rock mass classification. Int. J. Rock Mech. Min. Sci. 39, 771- 788. 2002.

SCE Company,Geological and Engineering Geological Report for Ghomrood Water Conveyance Tunnel Project (Lots 3 & 4), Unpublished report. 2004.

SCE Company. Geological and Engineering Geological Report for Karaj Water Conveyance Tunnel Project (Lot1), Unpublished report. 2006.

Shao, C., Li, X., Su, H. Performance prediction of hard rock TBM based on extreme learning machine. In: Intelligent Robotics and Applications. Springer, Berlin Heidelberg, 409-416. 2013.

Skuk, S., Schierl, H. Brenner Base Tunnel: First results of the exploratory tunnels from a geological and geomechanical point of view. Geomechanics and Tunnelling. Volume 10, Issue 3. 2017.

Skuk, S., Wegscheider, D. Brenner Base Tunnel – a 10.5 km double shield TBM drive in granite. Geomechanics and Tunnelling. Volume 8, Issue 3. 2015.

Silva, S., Almeida, J. Dynamic maximum tree depth-a simple technique for avoiding bloat in tree-based GP. In: Cantu-Paz E, Foster JA, Deb K (eds) Proceedings of the GECC0. Springer, Berlin, 1776-1787. 2003a.

Simoes, M.G., Kim, T. Fuzzy modelling approaches for the prediction of machine utilization in hard rock tunnel boring machines. In: Industry Applications Conference, 2006. 41st IAS Annual Meeting. Conference Record of the 2006 IEEE. IEEE, pp. 947–954. 2006.

Singh, B., Goel, R.K. Engineering Rock Mass Classification. Butterworth-Heinemann is an imprint of Elsevier 225 Wyman Street, Waltham, MA 02451, USA. 2011.

Singh, J., Ramamurthy, T., Rao, G.V. Strength anisotropies in rocks. Indian Geotech. J. 19, pp 147-166. 1989.

Snowdon, R.A., Ryley, M.D., Temporal, J. A study of disc cutting in selected British rocks. Int. J. Rock Mech. Min. Sci. Geomech. 19, 107-121. 1982.

Stack, B. Handbook of Mining and Tunnelling Machinery. Wiley, Chichester. 1982.

Satck, B. Encyclopaedia of tunnelling, mining and drilling equipment. Hobart, Tasmania: Muden Pub. Co. 1995.

Stevenson Garry, W. Empirical estimates of TBM performance in hard rock. In: Proc. RETC, AIME, 993-1006. 1999.

Sundaram, N.M., Rafek, A.G. The influence of rock mass properties in the assessment of TBM performance. In: Proceedings of the 8th IAEG Congress, Vancouver. 3553-3559. 1998.

Tarkoy, P.J., Marconi, M. Difficult rock comminution and associated geological conditions. In: Proceedings, 6th Congress Tunnelling, IMM, London, 195-207. 1991.

Terzaghi, K. Rock defect sand loads on tunnel supports. In: Proctor, R.V., White, T.L. (Eds.), Rock Tunneling with Steel Supports, 1. Commercial Shearingand Stamping Company, Youngstown, OH, 17-99. 1946.

The Niagara Tunnel Project (2012). Retrieved July 12, 2012 from http://www.niagarafrontier.com

Thuro, K., Plinninger, R.J. Hard rock tunnel boring, cutting, drilling and blasting: rock parameters for excavatability. ISRM 2003-Technology roadmap for rock mechanics, South African Institute of Mining and Metallurgy. 1-7. 2003.

Torabi, S.R., Shirazi, H., Hajali, H., Monjezi, M. Study of the influence of geotechnical parameters on the TBM performance in Tehran-Shomal highway project using ANN and SPSS. Arab. J. Geosci. 6 (4), 1215-1227. 2013.

Tumac, D., Balci, C. Investigations into the cutting characteristics of CCS type disc cutters and the comparison between experimental, theoretical and empirical force estimations. Tunn Undergr Space Technol.45: 84–98, 2015.

U. S. Army Corps of Engineer. Engineering and Design- Tunnels and Shafts in Rock, CECW-EG Engineer manual. Appendix C: Tunnel boring machine performance concepts and performance prediction. pp.C1-14. 1997.

Villeneuve, M.C. Examination of geological influence on machine excavation of highly stressed tunnels in massive hard rock. PhD thesis. Queen's University, Kingston, 2008.

Wallis, P (2011). Breakthrough ends Tortured Journey at Niagara. Tunneltalk. Retrieved from http://www.tunneltalk.com.

Watts, C., McMorran, T., Eldred, N., Howard, M. Manapouri Power Station. Second Tailrace Tunnel-Engineering Geological Construction Report. Unpublished Report. 2003.

Wickham, G.E., Tiedemann, H.R., Skinner, E.H. Support determination based on geologic predictions. Proc. Rapid Excav. Tunneling Conf. AIME, New York, 43-64. 1972.

Wilfing, L.S. The Influence of Geotechnical Parameters on Penetration Prediction in TBM Tunneling in Hard Rock. Ph.D. Thesis. Technical University of Munich, Germany, 2016

Wiliamson, D.A. Uniform rock classification for geotechnical engineering purposes. Trans. Res. Rec. 783, 9-14. 1980.

Witten, I., Frank, E., Hall, M. Data Mining: Practical Machine Learning Tools and Techniques, 3rd edn. Elsevier, Amsterdam. 2011.

Xia, Y.M., Guo, B., Cong, G.Q., Zhang, X.H., Zeng, G.Y. Numerical simulation of rock fragmentation induced by a single TBM disc cutter close to a side free surface. International Journal of Rock Mechanics & Mining Sciences 91, 40-48. 2017.

Yagiz, S. Assessment of brittleness using rock strength and density with punch penetration test. 24, 66-74. 2009

Yagiz, S. Development of rock fracture and brittleness indices to quantify the effects of rock mass fractures and toughness in the CSM Model basic penetration for hard rock tunnelling machines, Ph.D. Thesis, Department of Mining and Earth Systems Engineering, Colorado School of Mines, Golden, Colorado, USA, 2002.

Yagiz, S. Utilizing rock mass properties for predicting TBM performance in hard rock condition. Tunnell. Undergr. Space Technol. 23 (3), 326-339. 2008.

Yagiz, S., Gokceoglu, C., Sezar, E., Iplikci, S. Application of two non-linear prediction tools to the estimation of tunnel boring machine performance. Eng. Appl. Artif. Intell. 22 (4), 808-814. 2009.

Yagiz, S., Karahan, H. Prediction of hard rock TBM penetration rate using particle swarm optimization. Int. J. Rock Mech. Min. Sci. 48 (3), 427-433. 2011.

Yavari, M., Mahdavi, S. Prediction of penetration rate of TBM using ANN. In: National Mining Conference, 1-3 Feb 2005, Iran, 1-10. 2005.

Yilmaz, I., Yuksek, G. Prediction of the strength and elasticity modulus of gypsum using multiple regression, ANN, and ANFIS models. Int. J. Rock Mech. Min. Sci. 46(4):803-810. 2009.

Yin, L.J., Gong, Q.M., Ma, H.S., Zhao, J., Zhao, X.B. Use of indentation tests to study the influence of confining stress on rock fragmentation by a TBM cutter. Int. J. Rock Mech. Min. Sci. 72, 261-276. 2014a.

Yin, L.J., Gong, Q.M., Zhao, J. Study on rock mass boreability by TBM penetration test under different in situ stress conditions. Int. J. Tunn. Undergr. Space Technol. 43, 413-425. 2014b

Z.T. Bieniawski, B. Celada, J.M. Galera. TBM Excavability: Prediction and machine-rock interaction,1118-1130. 2007b.

Zhao, J. Tunnelling in rocks – present technology and future challenges. Keynote lectures. In: ITA-AITES World Tunnel Congress & 33rd ITA General Assembly, Prague, 22-32. 2007.

Zhao, Y., Gong, Q., Tian, Z., Zhou, Sh., Jiang, H. Torque fluctuation analysis and penetration prediction of EPB TBM in rock–soil interface mixed ground. Int. J. Tunnelling and Underground Space Technology. DOI: 10.1016/j.tust.2019.103002.

Zhao, Y., Yang, H., Chen, Z., Chen, X., Huang, L., Liu, Sh. Effects of Jointed Rock Mass and Mixed Ground Conditions on the Cutting Efficiency and Cutter Wear of Tunnel Boring Machine. Int. J. Rock Mechanics and Rock Engineering. DOI: 10.1007/s00603-018-1667-y. 2018.

Ziegler, H.J., Giovanoli, F., Isler, A. Basistunnel Steg/Raron Geologischer Bericht. Raron-Ferden, Lötschberg Basistunnel Schlussdokumentation, Unpublished Report. 2008.

Appendix A

```
#r script developed and modified by Salimi A. for my Ph.D. in Uni Stuttgart
# welcome back ...
##################################################################
#import TBM dataset
#working directory

#getwd()

setwd("C://Users//admin//Desktop//Ali")
load('Ali_R_PhD.r')



#load libraries

library(vegan)
library(RFtools)
library(pairwiseAdonis)

mf = read.table('PCA_noname.csv', header = FALSE, sep=",")
mf

TTnames <- c('UCS','RQD','Js','Jc','FPI','RTC')
colnames(mf) <- TTnames
```

```
mf4 = read.table('mf4.csv', header = FALSE, sep=",")
TTnames4 <- c('UCS','RQD','Js','Jc','RTC','basic_RMR', 'Q', 'GSI', 'ROP', 'P', 'FPI')
colnames(mf4) <- TTnames4

gene <- 'Result'
pip <- 'R'
pr <- 'Distribution Pattern'

#Distribution analysis
#GSI vs RMR
pdf(file=paste('GSI.basic RMR',gene,pip,pr,'pdf',sep='.'))
plot(mf4$GSI,mf4$basic_RMR,xlim=c(13,90),ylim=c(20,90),xlab='GSI',ylab='basic
RMR',pch=21,bg='orange')
abline(v=30,h=40, col="red")
dev.off()

pdf(file=paste('GSI.Q',gene,pip,pr,'pdf',sep='.'))
plot(mf4$GSI,mf4$Q,xlim=c(13,90),ylim=c(0.10,166),xlab='GSI',ylab='Q',pch=21,bg='or-
ange')
abline(v=30,h=0.09, col="red")
dev.off()

pdf(file=paste('Q.basic RMR',gene,pip,pr,'pdf',sep='.'))
plot(mf4$Q,mf4$bacis_RMR,xlim=c(0.10,166),ylim=c(10,90),xlab='Q',ylab='basic
RMR',pch=21,bg='orange')
abline(v=0.09,h=20, col="red")
dev.off()

#UCS vs RQD
pdf(file=paste('UCS.RQD',gene,pip,pr,'pdf',sep='.'))
```

```
plot(mf$UCS,mf$RQD,xlim=c(1,270),ylim=c(1,100),xlab='UCS MPa',ylab='RQD %',pch=21,bg='orange')
abline(v=20,h=20, col="red")
dev.off()

#Js vs UCS
pdf(file=paste('UCS.Js',gene,pip,pr,'pdf',sep='.'))
plot(mf$Js,mf$UCS,xlim=c(0.3,201),ylim=c(1,270),ylab='UCS MPa',xlab='Js cm',pch=21,bg='orange')
abline(v=5,h=5, col="red")
dev.off()

#UCS vs Jc
pdf(file=paste('UCS.Jc',gene,pip,pr,'pdf',sep='.'))
plot(mf$UCS,mf$Jc,xlim=c(1,270),ylim=c(2,31),xlab='UCS MPa',ylab='Jc partial rating in RMR basic',pch=21,bg='orange')
abline(v=25,h=9, col="red")
dev.off()

#RQD vs Js
pdf(file=paste('RQD.Js',gene,pip,pr,'pdf',sep='.'))
plot(mf$RQD,mf$Js,xlim=c(1,100),ylim=c(0.3,201),xlab='RQD %',ylab='Js cm',pch=21,bg='orange')
abline(v=20,h=5, col="red")
dev.off()

#RQD vs Jc
pdf(file=paste('RQD.Jc',gene,pip,pr,'pdf',sep='.'))
```

```
plot(mf$RQD,mf$Jc,xlim=c(1,100),ylim=c(2,31),xlab='RQD %',ylab='Jc partial rating in RMR basic',pch=21,bg='orange')

abline(v=20,h=9, col="red")

dev.off()


#Js vs Jc

pdf(file=paste('Js.Jc',gene,pip,pr,'pdf',sep='.'))

plot(mf$Js,mf$Jc,xlim=c(0.3,201),ylim=c(2,31),xlab='Js cm',ylab='Jc partial rating in RMR basic',pch=21,bg='orange')

abline(v=5,h=9, col="red")

dev.off()


####################################################################################
#good job!
#Lets calculate the PCA for basic RMR variables


library(devtools)

#install_github("vqv/ggbiplot")

library(ggbiplot)


#PCAs

TBMrmr.pca <- prcomp(mf[,c(1:4)], center = TRUE,scale. = TRUE)


summary(TBMrmr.pca)

str(TBMrmr.pca)


#Importance of components:

                    PC1    PC2    PC3     PC4

#Standard deviation     1.6288 0.7679 0.7089 0.50485

#Proportion of Variance 0.6632 0.1474 0.1256 0.06372
```

```
#Cumulative Proportion  0.6632 0.8106 0.9363 1.00000

#List of 5
# $ sdev    : num [1:4] 1.629 0.768 0.709 0.505
# $ rotation: num [1:4, 1:4] -0.5 -0.55 -0.479 -0.466 0.528 ...
#  ..- attr(*, "dimnames")=List of 2
#  .. ..$ : chr [1:4] "UCS" "RQD" "Js" "Jc"
#  .. ..$ : chr [1:4] "PC1" "PC2" "PC3" "PC4"
# $ center  : Named num [1:4] 97.4 66.5 31.6 16.5
#  ..- attr(*, "names")= chr [1:4] "UCS" "RQD" "Js" "Jc"
# $ scale   : Named num [1:4] 68.79 24.15 29.3 5.36
#  ..- attr(*, "names")= chr [1:4] "UCS" "RQD" "Js" "Jc"
# $ x       : num [1:580, 1:4] -1.882 -1.864 -0.789 -2.133 -1.235 ...
#  ..- attr(*, "dimnames")=List of 2
#  .. ..$ : NULL
#  .. ..$ : chr [1:4] "PC1" "PC2" "PC3" "PC4"
# - attr(*, "class")= chr "prcomp"

#PCA for characters 1 vs 2
TBMrmr.pca = prcomp(mf[,c(1:4)], center = TRUE,scale. = TRUE)
pdf(file=paste('PCA1&2',gene,pip,pr,'pdf',sep='.'),width=6,height=6)
ggbiplot(TBMrmr.pca, choices = 1:2, scale = 1, obs.scale=1 , var.scale=1 , pc.biplot =
  TRUE, var.axes=10, varname.size=3, varname.abbrev=TRUE, varname.adjust = 1.5,
  labels.size=3, pch=2, cex=4, main='PCA Plot of TBM data', cex.lab=1.5,
  cex.axis=1.5, cex.main=1.5, cex.sub=1.5, alpha = 0.2)
dev.off()

#PCA for characters 1 vs 3
TBMrmr.pca = prcomp(mf[,c(1:4)], center = TRUE,scale. = TRUE)
pdf(file=paste('PCA2&3',gene,pip,pr,'pdf',sep='.'),width=6,height=6)
ggbiplot(TBMrmr.pca, choices = 2:3, scale = 1, obs.scale=1 , var.scale=1 , pc.biplot =
```

```
  TRUE, var.axes=10, varname.size=3, varname.abbrev=TRUE, varname.adjust = 1.5,
  labels.size=3, pch=2, cex=4, main='PCA Plot of TBM data', cex.lab=1.5,
  cex.axis=1.5, cex.main=1.5, cex.sub=1.5, alpha = 0.2)
dev.off()

#PCA for characters 1 vs 4
TBMrmr.pca = prcomp(mf[,c(1:4)], center = TRUE,scale. = TRUE)
pdf(file=paste('PCA1&4',gene,pip,pr,'pdf',sep='.'),width=6,height=6)
ggbiplot(TBMrmr.pca, choices = c(1,4), scale = 1, obs.scale=1 , var.scale=1 , pc.biplot =
  TRUE, var.axes=10, varname.size=3, varname.abbrev=TRUE, varname.adjust = 1.5,
  labels.size=3, pch=2, cex=4, main='PCA Plot of TBM data', cex.lab=1.5,
  cex.axis=1.5, cex.main=1.5, cex.sub=1.5, alpha = 0.2)
dev.off()

#PCA for characters 2 vs 3
TBMrmr.pca = prcomp(mf[,c(1:4)], center = TRUE,scale. = TRUE)
pdf(file=paste('PCA2&3',gene,pip,pr,'pdf',sep='.'),width=6,height=6)
ggbiplot(TBMrmr.pca, choices = c(2,3), scale = 1, obs.scale=1 , var.scale=1 , pc.biplot =
  TRUE, var.axes=10, varname.size=3, varname.abbrev=TRUE, varname.adjust = 1.5,
  labels.size=3, pch=2, cex=4, main='PCA Plot of TBM data', cex.lab=1.5,
  cex.axis=1.5, cex.main=1.5, cex.sub=1.5, alpha = 0.2)
dev.off()

#PCA for characters 2 vs 4
TBMrmr.pca = prcomp(mf[,c(1:4)], center = TRUE,scale. = TRUE)
pdf(file=paste('PCA2&4',gene,pip,pr,'pdf',sep='.'),width=6,height=6)
ggbiplot(TBMrmr.pca, choices = c(2,4), scale = 1, obs.scale=1 , var.scale=1 , pc.biplot =
  TRUE, var.axes=10, varname.size=3, varname.abbrev=TRUE, varname.adjust = 1.5,
  labels.size=3, pch=2, cex=4, main='PCA Plot of TBM data', cex.lab=1.5,
  cex.axis=1.5, cex.main=1.5, cex.sub=1.5, alpha = 0.2)
dev.off()
```

```
#PCA for characters 3 vs 4
TBMrmr.pca = prcomp(mf[,c(1:4)], center = TRUE,scale. = TRUE)
pdf(file=paste('PCA3&4',gene,pip,pr,'pdf',sep='.'),width=6,height=6)
ggbiplot(TBMrmr.pca, choices = c(3,4), scale = 1, obs.scale=1 , var.scale=1 , pc.biplot =
  TRUE, var.axes=10, varname.size=3, varname.abbrev=TRUE, varname.adjust = 1.5,
  labels.size=3, pch=2, cex=4, main='PCA Plot of TBM data', cex.lab=1.5,
  cex.axis=1.5, cex.main=1.5, cex.sub=1.5, alpha = 0.2)
dev.off()

#PCA for characters 1 vs 3
TBMrmr.pca = prcomp(mf[,c(1:4)], center = TRUE,scale. = TRUE)
pdf(file=paste('PCA1&3',gene,pip,pr,'pdf',sep='.'),width=6,height=6)
ggbiplot(TBMrmr.pca3, choices = c(1,3), scale = 1, obs.scale=1 , var.scale=1 , pc.biplot =
  TRUE, var.axes=10, varname.size=3, varname.abbrev=TRUE, varname.adjust = 1.5,
  labels.size=3, pch=2, cex=4, main='PCA Plot of TBM data', cex.lab=1.5,
  cex.axis=1.5, cex.main=1.5, cex.sub=1.5, alpha = 0.2)

dev.off()
#####################################################################
#PCA for test
TBMrmr.pca = prcomp(mf[,c(1:4)], center = TRUE,scale. = TRUE)
pdf(file=paste('colortest',gene,pip,pr,'pdf',sep='.'),width=6,height=6)
ggbiplot(TBMrmr2.pca, choices = c(1,3), scale = 1, obs.scale=1 , var.scale=1 , pc.biplot =
  FALSE, var.axes=10, varname.size=3, varname.abbrev=TRUE, varname.adjust = 1.5,
  labels.size=3, pch=2, cex=4, main='PCA Plot of TBM data', cex.lab=1.5,
  cex.axis=1.5, cex.main=1.5, cex.sub=1.5, alpha = 0.4)+
  geom_point(aes(color = mf2Tunnel) +
scale_color_viridis(option = "D")
ggplot(TBMrmr.pca, aes(x = PC1, y = PC2, colour = mf$RTC)) +
  stat_ellipse(level = 0.95, size = 2, show.legend = FALSE) +
  geom_point(size = 3) +
```

```
  geom_segment(aes(x = 0, y = 0, xend = (PC1), yend = (PC2)),
     arrow = arrow(length = unit(1/2, "picas")), color = "black") +
 geom_text( aes(label = Variables, x = (PC1), y = (PC2)),
    color = "black", size = 4, angle = TBMrmr.pca$Angle) +
      theme_classic() +
      theme(legend.justification = c(1,1), legend.position = c(1,1))

dev.off()


ggplot(PCAvalues, aes(x = PC1, y = PC2)) +
  stat_ellipse(level = 0.95, size = 2, show.legend = FALSE) +
  geom_point(size = 3)+
  geom_segment(data = PCAloadings, aes(x = 0, y = 0, xend = (PC1), yend = (PC2)),
     arrow = arrow(length = unit(2, "picas")), color = "black")+
  geom_text(data = PCAloadings, aes(label = Variables, x = (PC1), y = (PC2)),
    color = "black", size = 4, angle = PCAloadings$Angle, hjust =
    PCAloadings$Offset) +
      theme_classic() +
      theme(legend.justification = c(1,1), legend.position = c(1,1))

pdf(file=paste('PCA1&4 for characters grouped by Tun-
nels',gene,pip,pr,'pdf',sep='.'),width=8,height=8)
 ggbiplot(TBMrmr2.pca, choices = c(1,4), scale = 0, obs.scale=1 , var.scale=1 , pc.biplot =
TRUE, var.axes=10, varname.size=5, varname.abbrev=TRUE, varname.adjust = 1.5,
labels.size=5, pch=2, cex=4, main='PCA Plot of TBM data', cex.lab=1.5,
cex.axis=1.5, cex.main=1.5, cex.sub=1.5, alpha = 0.3, groups=mf2$RTC, col=c25, ellipse =
TRUE,
arrow.color = green, arrow.linetype = solid, arrow.alpha = 1)
dev.off()
#################################################################################
#################
```

```
#PCA for characters grouped by RTC factor

library(devtools)
library(ggbiplot)
library(viridis)
#Main
#PCA grouped by RTC 1vs2
pdf(file=paste('PCA1&2 for characters grouped by RTC factor',gene,pip,pr,'pdf',sep='.'),width=8,height=8)
 ggbiplot(TBMrmr.pca, choices = c(1,2), scale = 0, obs.scale=1 , var.scale=1 , pc.biplot =
TRUE, var.axes=10, varname.size=5, varname.abbrev=TRUE, varname.adjust = 1.5,
labels.size=5, pch=2, cex=4, main='PCA Plot of TBM data', cex.lab=1.5,
cex.axis=1.5, cex.main=1.5, cex.sub=1.5, alpha = 0.3, groups=mf$RTC, col=c25, ellipse =
TRUE,
arrow.color = green, arrow.linetype = solid, arrow.alpha = 1)

dev.off()

#PCA grouped by RTC 1vs3
pdf(file=paste('PCA1&3 for characters grouped by RTC factor',gene,pip,pr,'pdf',sep='.'),width=8,height=8)
 ggbiplot(TBMrmr.pca, choices = c(1,3), scale = 1, obs.scale=1 , var.scale=1 , pc.biplot =
TRUE, var.axes=10, varname.size=5, varname.abbrev=TRUE, varname.adjust = 1.5,
labels.size=5, pch=2, cex=4, main='PCA Plot of TBM data', cex.lab=1.5,
cex.axis=1.5, cex.main=1.5, cex.sub=1.5, alpha = 0.3, groups=mf$RTC, col=c25, ellipse =
TRUE,
arrow.color = green, arrow.linetype = solid, arrow.alpha = 1)
dev.off()

#PCA grouped by RTC 1vs4
pdf(file=paste('PCA1&4 for characters grouped by RTC factor',gene,pip,pr,'pdf',sep='.'),width=8,height=8)
```

```
 ggbiplot(TBMrmr.pca, choices = c(1,4), scale = 1, obs.scale=1 , var.scale=1 , pc.biplot =
TRUE, var.axes=10, varname.size=5, varname.abbrev=TRUE, varname.adjust = 1.5,
labels.size=5, pch=2, cex=4, main='PCA Plot of TBM data', cex.lab=1.5,
cex.axis=1.5, cex.main=1.5, cex.sub=1.5, alpha = 0.3, groups=mf$RTC, col=c25, ellipse =
TRUE,
arrow.color = green, arrow.linetype = solid, arrow.alpha = 1)
dev.off()

#PCA grouped by RTC 2vs3
pdf(file=paste('PCA2&3 for characters grouped by RTC factor',gene,pip,pr,'pdf',sep='.'),width=8,height=8)
 ggbiplot(TBMrmr.pca, choices = c(2,3), scale = 1, obs.scale=1 , var.scale=1 , pc.biplot =
TRUE, var.axes=10, varname.size=5, varname.abbrev=TRUE, varname.adjust = 1.5,
labels.size=5, pch=2, cex=4, main='PCA Plot of TBM data', cex.lab=1.5,
cex.axis=1.5, cex.main=1.5, cex.sub=1.5, alpha = 0.3, groups=mf$RTC, col=c25, ellipse =
TRUE,
arrow.color = green, arrow.linetype = solid, arrow.alpha = 1 )
dev.off()

#PCA grouped by RTC 2vs4
pdf(file=paste('PCA2&4 for characters grouped by RTC factor',gene,pip,pr,'pdf',sep='.'),width=8,height=8)
 ggbiplot(TBMrmr.pca, choices = c(2,4), scale = 1, obs.scale=1 , var.scale=1 , pc.biplot =
TRUE, var.axes=10, varname.size=5, varname.abbrev=TRUE, varname.adjust = 1.5,
labels.size=5, pch=2, cex=4, main='PCA Plot of TBM data', cex.lab=1.5,
cex.axis=1.5, cex.main=1.5, cex.sub=1.5, alpha = 0.3, groups=mf$RTC, col=c25, ellipse =
TRUE,
arrow.color = green, arrow.linetype = solid, arrow.alpha = 1)
dev.off()

#PCA grouped by RTC 3vs4
```

```
pdf(file=paste('PCA3vs4 for characters grouped by RTC factor',gene,pip,pr,'pdf',sep='.'),width=8,height=8)
 ggbiplot(TBMrmr.pca, choices = c(3,4), scale = 1, obs.scale=1 , var.scale=1 , pc.biplot =
TRUE, var.axes=10, varname.size=5, varname.abbrev=TRUE, varname.adjust = 1.5,
labels.size=5, pch=2, cex=4, main='PCA Plot of TBM data', cex.lab=1.5,
cex.axis=1.5, cex.main=1.5, cex.sub=1.5, alpha = 0.3, groups=mf$RTC, col=c25, ellipse = TRUE,
arrow.color = green, arrow.linetype = solid, arrow.alpha = 1)
dev.off()

##################################################################################
#############
#Multi_color
#PCA grouped by RTC 1vs2
pdf(file=paste('PCA1&2 multicol for characters grouped by RTC factor',gene,pip,pr,'pdf',sep='.'),width=8,height=8)
 ggbiplot(TBMrmr.pca3, choices = c(1,2), scale = 0, obs.scale=1 , var.scale=1 , pc.biplot =
TRUE, var.axes=10, varname.size=5, varname.abbrev=TRUE, varname.adjust = 1.5,
labels.size=5, pch=2, cex=4, main='PCA Plot of TBM data', cex.lab=1.5,
cex.axis=1.5, cex.main=1.5, cex.sub=1.5, alpha = 0.3, groups=mf3$RTC, col=c25, ellipse = TRUE,
arrow.color = green, arrow.linetype = solid, arrow.alpha = 1)

dev.off()


#PCA grouped by RTC 1vs3
pdf(file=paste('PCA1&3 multicol for characters grouped by RTC factor',gene,pip,pr,'pdf',sep='.'),width=8,height=8)
 ggbiplot(TBMrmr.pca3, choices = c(1,3), scale = 1, obs.scale=1 , var.scale=1 , pc.biplot =
TRUE, var.axes=10, varname.size=5, varname.abbrev=TRUE, varname.adjust = 1.5,
labels.size=5, pch=2, cex=4, main='PCA Plot of TBM data', cex.lab=1.5,
```

cex.axis=1.5, cex.main=1.5, cex.sub=1.5, alpha = 0.3, groups=mf3$RTC, col=c25, ellipse = TRUE,

arrow.color = green, arrow.linetype = solid, arrow.alpha = 1)

dev.off()

#PCA grouped by RTC 1vs4

pdf(file=paste('PCA1&4 multicol for characters grouped by RTC factor',gene,pip,pr,'pdf',sep='.'),width=8,height=8)

ggbiplot(TBMrmr.pca3, choices = c(1,4), scale = 1, obs.scale=1 , var.scale=1 , pc.biplot =

TRUE, var.axes=10, varname.size=5, varname.abbrev=TRUE, varname.adjust = 1.5,

labels.size=5, pch=2, cex=4, main='PCA Plot of TBM data', cex.lab=1.5,

cex.axis=1.5, cex.main=1.5, cex.sub=1.5, alpha = 0.3, groups=mf3$RTC, col=c25, ellipse = TRUE,

arrow.color = green, arrow.linetype = solid, arrow.alpha = 1)

dev.off()

#PCA grouped by RTC 2vs3

pdf(file=paste('PCA2&3 multicol for characters grouped by RTC factor',gene,pip,pr,'pdf',sep='.'),width=8,height=8)

ggbiplot(TBMrmr.pca3, choices = c(2,3), scale = 1, obs.scale=1 , var.scale=1 , pc.biplot =

TRUE, var.axes=10, varname.size=5, varname.abbrev=TRUE, varname.adjust = 1.5,

labels.size=5, pch=2, cex=4, main='PCA Plot of TBM data', cex.lab=1.5,

cex.axis=1.5, cex.main=1.5, cex.sub=1.5, alpha = 0.3, groups=mf3$RTC, col=c25, ellipse = TRUE,

arrow.color = green, arrow.linetype = solid, arrow.alpha = 1)

dev.off()

#PCA grouped by RTC 2vs4

pdf(file=paste('PCA2&4 multicol for characters grouped by RTC factor',gene,pip,pr,'pdf',sep='.'),width=8,height=8)

ggbiplot(TBMrmr.pca3, choices = c(2,4), scale = 1, obs.scale=1 , var.scale=1 , pc.biplot =

TRUE, var.axes=10, varname.size=5, varname.abbrev=TRUE, varname.adjust = 1.5,

```
labels.size=5, pch=2, cex=4, main='PCA Plot of TBM data', cex.lab=1.5,
cex.axis=1.5, cex.main=1.5, cex.sub=1.5, alpha = 0.3, groups=mf3$RTC, col=c25, ellipse = TRUE,
arrow.color = green, arrow.linetype = solid, arrow.alpha = 1)
dev.off()

#PCA grouped by RTC 3vs4
pdf(file=paste('PCA3vs4 multicol for characters grouped by RTC factor',gene,pip,pr,'pdf',sep='.'),width=8,height=8)
 ggbiplot(TBMrmr.pca3, choices = c(3,4), scale = 1, obs.scale=1 , var.scale=1 , pc.biplot =
TRUE, var.axes=10, varname.size=5, varname.abbrev=TRUE, varname.adjust = 1.5,
labels.size=5, pch=2, cex=4, main='PCA Plot of TBM data', cex.lab=1.5,
cex.axis=1.5, cex.main=1.5, cex.sub=1.5, alpha = 0.3, groups=mf3$RTC, col=c25, ellipse = TRUE,
arrow.color = green, arrow.linetype = solid, arrow.alpha = 1)
dev.off()

####################################################################################################
#Screen plots
library("PCAtools")

pdf(file=paste('Screeplot of the first 4 PCAs',gene,pip,pr,'pdf',sep='.'),width=6,height=6)
screeplot(tbmpcr, type = "l", npcs = 4, main = "Screeplot of the first 4 PCAs")
abline(h = 1.5, col="red", lty=5)
legend("topright", legend=c("Eigenvalue = 1.5"),
      col=c("red"), lty=5, cex=0.6)
            dev.off()

#Cumulative plot
pdf(file=paste('Cumulative variance plot',gene,pip,pr,'pdf',sep='.'),width=6,height=6)
cumpro <- cumsum(tbmpcr$sdev^2 / sum(tbmpcr$sdev^2))
```

```
plot(cumpro[0:4], xlab = "PCs", ylab = "Amount of explained variance", main = "Cumu-
lative variance plot")
abline(v = 3, col="red", lty=6)
abline(h = 0.9362, col="red", lty=6)
legend("topleft", legend=c("Cut-off @ PC1+PC2+PC3"),
    col=c("red"), lty=6, cex=0.9)
        dev.off()

##############################################################################
#####
#new PCA (playing around)

tbmpcr <- prcomp(mf[c(1:4)], center = TRUE, scale = TRUE)
> summary(tbmpcr)
#Importance of components:
                        PC1    PC2    PC3     PC4
#Standard deviation     1.6288 0.7679 0.7089 0.50485
#Proportion of Variance 0.6632 0.1474 0.1256 0.06372
#Cumulative Proportion  0.6632 0.8106 0.9363 1.00000

#install PCAtools
  if (!requireNamespace('BiocManager', quietly = TRUE))
    install.packages('BiocManager')

  BiocManager::install('PCAtools')

plot(tbmpcr$x[,1],tbmpcr$x[,2], xlab="PC1 (66.32%)", ylab = "PC2 (14.74%)", main = "PC1
/ PC2 - plot")

library("factoextra")
fviz_pca_ind(tbmpcr, geom.ind = "point", pointshape = 21,
```

```
          pointsize = 2,
          fill.ind = "green",
          col.ind = "black",
          palette = "jco",
          addEllipses = TRUE,
          label = "var",
          col.var = "black",
          repel = TRUE,
          legend.title = "Diagnosis") +
  ggtitle("2D PCA-plot from 30 feature dataset") +
  theme(plot.title = element_text(hjust = 0.5))

#screen plot
PVEplot <- plot(PVE[c(1:4)]) +
  geom_line() +
  xlab("Principal Component") +
  ylab("PVE") +
  ggtitle("Screen Plot") +
  ylim(0, 1)

 #PCAtools
   if (!requireNamespace('BiocManager', quietly = TRUE))
      install.packages('BiocManager')

   BiocManager::install('PCAtools')

  if (!requireNamespace("BiocManager", quietly = TRUE))
   install.packages("BiocManager")

BiocManager::install("GEOquery")
```

```
 library(Biobase)
  library(GEOquery)
    library(PCAtools)

 p <- pca(mf, mf = mf(c[1:4]), removeVar = 0.1)
  x <- exprs(mf(c[1:4]))

  screeplot(TBMrmr.pca,
    components = getComponents(tbmpcr(c[1:4])),
    vline = c(horn$n, elbow)) +
    geom_text(aes(horn$n + 1, 50, label = "Horn's", vjust = -1)) +
    geom_text(aes(elbow + 1, 50, label = "Elbow", vjust = -1))

################################################################################
#########
#Multiple Regression analysis and graphs

fit <- lm(mf$FPI ~ mf$UCS + mf$RQD + mf$Js + mf$Jc + mf$RTC)

summary(fit)

#Call:
#lm(formula = mf$FPI ~ mf$UCS + mf$RQD + mf$Js + mf$Jc + mf$RTC)

#Residuals:
   Min      1Q  Median      3Q     Max
#-30.467  -7.876   0.303   4.693  90.160

#Coefficients:
#           Estimate Std. Error t value Pr(>|t|)
#(Intercept)  1.10239    2.82769  -1.880   0.0606 .
```

```
#mf$UCS      0.12944    0.01170  10.893   <2e-16 ***
#mf$RQD      0.07116    0.03709   1.838   0.0666 .
#mf$Js       0.31468    0.02315  13.591   <2e-16 ***
#mf$Jc       0.38983    0.12884   3.002   0.0028 **
#mf$RTC     -0.46621    0.54362  -1.286   0.1989
#---
#Signif. codes:  0 ‘***’ 0.001 ‘**’ 0.01 ‘*’ 0.05 ‘.’ 0.1 ‘ ’ 1

#Residual standard error: 12.87 on 574 degrees of freedom
#Multiple R-squared:  0.6779,    Adjusted R-squared:  0.6751
#F-statistic: 241.6 on 5 and 574 DF,  p-value: < 2.2e-16

coef(fit)

#(Intercept)     mf$UCS     mf$RQD      mf$Js      mf$Jc     mf$RTC
#1..1029169  0.12943574  0.07115533  0.31467594  0.3893486 -0.46621387

#fit <- lm(mf$ln(FPI) ~ mf$UCS + mf$RQD + mf$Js + mf$Jc + mf$RTC)

##################################################################################
####
#nonLinear multiple regression analysis
FPI2 = log (mf$FPI)
fit <- lm(FPI2 ~ mf$UCS + mf$RQD + mf$Js + mf$Jc + mf$RTC)
fit2 <- lm(FPI2 ~ mf$UCS + mf$RQD + mf$Js + mf$Jc + mf$RTC)
summary(fit2)

#Call:
#lm(formula = FPI2 ~ mf$UCS + mf$RQD + mf$Js + mf$Jc + mf$RTC)

#Residuals:
```

```
#     Min       1Q   Median       3Q      Max
#-1.60547 -0.20584  0.01632  0.21321  0.85817

#Coefficients:
#             Estimate Std. Error t value Pr(>|t|)
#(Intercept)  1.7635334  0.0707257  24.723  < 2e-16 ***
#mf$UCS       0.0032486  0.0002926  11.102  < 2e-16 ***
#mf$RQD       0.0123444  0.0009277  13.306  < 2e-16 ***
#mf$Js        0.0052290  0.0005791   9.029  < 2e-16 ***
#mf$Jc        0.0079601  0.0032226   2.470   0.0138 *
#mf$RTC      -0.0912347  0.0135970  -6.489 1.87e-10 ***
#---
#Signif. codes:  0 '***' 0.001 '**' 0.01 '*' 0.05 '.' 0.1 ' ' 1

#Residual standard error: 0.3218 on 574 degrees of freedom
#Multiple R-squared:  0.7791,    Adjusted R-squared:  0.7776
#F-statistic: 519.9 on 5 and 574 DF,  p-value: < 2.2e-16

#Regression graphs
 x = mf$UCS + mf$RQD + mf$Js + mf$Jc + mf$RTC
 y = FPI2

 pdf(file=paste('Multiple linear Regression',gene,pip,pr,'pdf',sep='.'),width=6,height=6)
ggplot(mf, aes(x = x , y = y)) +
  geom_point() +
  geom_point(colour="purple")+
  geom_smooth(method = "lm", se = FALSE, size = 0.5) +
  labs(x = "Variables", y = "FPI",
       title = "lm(FPI ~ UCS, Js, Jc, RTC, RQD)")

dev.off()
```

```
library(dplyr)
mf$FPI2 <- factor(mf$FPI2)
mf$FPI2 <- recode(mf$FPI2, "0" = "Automatik", "1" = "Schaltgetriebe")

mod2 <- lm(FPI2 ~ x)

library(ggplot2)
library(broom)
pdf(file=paste('Multiple linear Regression coloured',gene,pip,pr,'pdf',sep='.'),width=6,height=6)
ggplot(augment(mod2), aes(x = x, y = y, color = FPI2)) +
  geom_point() +
  geom_line(aes(y = .fitted)) +
  labs(x = "Variables", y = "FPI",
       title = "lm(FPI ~ UCS, Js, Jc, RTC, RQD)")
            dev.off()

# Zwei Regressionsgeraden mit Interaktionseffekt

mod2b <- lm(y ~ x )
summary(mod2b)
pdf(file=paste('Multiple linear Regressionsgeraden mit Interaktionseffekt',gene,pip,pr,'pdf',sep='.'),width=6,height=6)
ggplot(mf, aes(x = x, y = y, color = x)) +
  geom_point() +
  geom_smooth(method = "lm", se = FALSE) +
  labs(x = "Variables", y = "FPI",
       title = "lm(FPI ~ UCS, Js, Jc, RTC, RQD)")

dev.off()
```

```
pdf(file=paste('Multiple linear Regressionsgeraden mit Inter-
aktionseffekt2',gene,pip,pr,'pdf',sep='.'),width=6,height=6)

ggplot(augment(mod2b), aes(x = x, y = y, color = y)) +
  geom_point() +
  geom_line(aes(y = .fitted), size = 1) +
  labs(x = "Variables",
       y = "FPI",
       title = "lm(FPI ~ UCS, Js, Jc, RTC, RQD)")

dev.off()

################################################################################
#
#3D surface plots
install.packages("plot3D")
library("plot3D")

#3D surface plot for variables UCS and RQD
pdf(file=paste('3D surface plot for variables UCS and
RQD',gene,pip,pr,'pdf',sep='.'),width=8,height=8)
scatter3D(UCS, RQD, FPI, phi = 0, bty = "g",pch = 20, cex = 2, ticktype = "detailed",
xlab="UCS (MPa)", ylab="RQD (%)", zlab="FPI (kN/cutter/mm/rev)")
dev.off()

#3D surface plot for variables UCS and Js
pdf(file=paste('3D surface plot for variables UCS and
Js',gene,pip,pr,'pdf',sep='.'),width=8,height=8)
scatter3D(UCS, Js, FPI, phi = 0, bty = "g",pch = 20, cex = 2, ticktype = "detailed", xlab="UCS
(MPa)", ylab="Js (cm)", zlab="FPI (kN/cutter/mm/rev)")
dev.off()
```

```
#3D surface plot for variables UCS and Jc

pdf(file=paste('3D surface plot for variables UCS and Jc',gene,pip,pr,'pdf',sep='.'),width=8,height=8)

scatter3D(UCS, Jc, FPI, phi = 0, bty = "g",pch = 20, cex = 2, ticktype = "detailed", xlab="UCS (MPa)", ylab="Jc (partial rating)", zlab="FPI (kN/cutter/mm/rev)")

dev.off()


#3D surface plot for variables RQD and Js

pdf(file=paste('3D surface plot for variables RQD and Js',gene,pip,pr,'pdf',sep='.'),width=8,height=8)

scatter3D(RQD, Js, FPI, phi = 0, bty = "g",pch = 20, cex = 2, ticktype = "detailed", xlab="RQD (%)", ylab="Js (cm)", zlab="FPI (kN/cutter/mm/rev)")

dev.off()


#3D surface plot for variables RQD and Jc

pdf(file=paste('3D surface plot for variables RQD and Jc',gene,pip,pr,'pdf',sep='.'),width=8,height=8)

scatter3D(RQD, Jc, FPI, phi = 0, bty = "g",pch = 20, cex = 2, ticktype = "detailed", xlab="RQD (%)", ylab="Jc (partial rating)", zlab="FPI (kN/cutter/mm/rev)")

dev.off()


#3D surface plot for variables Js and Jc

pdf(file=paste('3D surface plot for variables Js and Jc',gene,pip,pr,'pdf',sep='.'),width=8,height=8)

scatter3D(Js, Jc, FPI, phi = 0, bty = "g",pch = 20, cex = 2, ticktype = "detailed", xlab="Js (cm)", ylab="Jc (partial rating)", zlab="FPI (kN/cutter/mm/rev)")

dev.off()


#3D surface plot for variables UCS and RTC

pdf(file=paste('3D surface plot for variables UCS and RTC',gene,pip,pr,'pdf',sep='.'),width=8,height=8)

scatter3D(UCS, RTC, FPI, phi = 0, bty = "g",pch = 20, cex = 2, ticktype = "detailed", xlab="UCS (MPa)", ylab="RTC", zlab="FPI (kN/cutter/mm/rev)")
```

```
dev.off()


#3D surface plot for variables RQD and RTC
pdf(file=paste('3D surface plot for variables RQD and RTC',gene,pip,pr,'pdf',sep='.'),width=8,height=8)
scatter3D(RQD, RTC, FPI, phi = 0, bty = "g",pch = 20, cex = 2, ticktype = "detailed", xlab="RQD (%)", ylab="RTC", zlab="FPI (kN/cutter/mm/rev)")
dev.off()


#3D surface plot for variables Js and RTC
pdf(file=paste('3D surface plot for variables Js and RTC',gene,pip,pr,'pdf',sep='.'),width=8,height=8)
scatter3D(Js, RTC, FPI, phi = 0, bty = "g",pch = 20, cex = 2, ticktype = "detailed", xlab="Js (cm)", ylab="RTC", zlab="FPI (kN/cutter/mm/rev)")
dev.off()


#3D surface plot for variables Jc and RTC
pdf(file=paste('3D surface plot for variables Jc and RTC',gene,pip,pr,'pdf',sep='.'),width=8,height=8)
scatter3D(Jc, RTC, FPI, phi = 0, bty = "g",pch = 20, cex = 2, ticktype = "detailed", xlab="Jc (partial rating)", ylab="RTC", zlab="FPI (kN/cutter/mm/rev)")
dev.off()


##################################################################################################
#go ahead!
#Classification and Regression tree


#install and load following libraries:


install.packages("rsample")
install.packages("dplyr")
```

```
install.packages("rpart")
install.packages("rpart.plot")
install.packages("ipred")
install.packages("caret")

library(rsample)    # data splitting
library(dplyr)      # data wrangling
library(rpart)      # performing regression trees
library(rpart.plot) # plotting regression trees
library(ipred)      # bagging
library(caret)      # bagging


m1 <- rpart(formula = FPI ~ UCS + Js + RQD + Jc + RTC, data = mf, method  = "anova")
rpart.plot(m1)
plotcp(m1)

m2 <- rpart(formula = FPI ~ .,data    = mf, method  = "anova", control = list(cp = 0, xval = 10))

pdf(file=paste('Regression tree (Tree size evaluation)',gene,pip,pr,'pdf',sep='.'),width=8,height=8)
plotcp(m2)
abline(v = 25, lty = "dashed", col="red")
dev.off()

m1$cptable


m3 <- rpart(FPI ~ UCS + Js + RQD + Jc + RTC, data = mf, method  = "anova",
control = list(minsplit = 12, maxdepth = 7, xval = 10))
```

```
m3$cptable

hyper_grid <- expand.grid(minsplit = seq(5, 20, 1),maxdepth = seq(8, 15, 1))

head(hyper_grid)

models <- list()

for (i in 1:nrow(hyper_grid)) {


  minsplit <- hyper_grid$minsplit[i]
  maxdepth <- hyper_grid$maxdepth[i]

  models[[i]] <- rpart(
    formula = FPI ~ .,
    data    = mf,
    method  = "anova",
    control = list(minsplit = minsplit, maxdepth = maxdepth)
    )
}

  # function to get optimal cp
get_cp <- function(x) {
  min    <- which.min(x$cptable[, "xerror"])
  cp <- x$cptable[min, "CP"]
}

# function to get minimum error
get_min_error <- function(x) {
```

```
  min    <- which.min(x$cptable[, "xerror"])
  xerror <- x$cptable[min, "xerror"]
}

hyper_grid %>% mutate(cp    = purrr::map_dbl(models, get_cp),
  error = purrr::map_dbl(models, get_min_error)) %>%
  arrange(error) %>% top_n(-5, wt = error)

  optimal_tree <- rpart(formula = FPI ~ .,data    = mf, method  = "anova",
    control = list(minsplit = 11, maxdepth = 7, cp = 0.0001))

pred <- predict(optimal_tree, newdata = ames_test)
RMSE(pred = pred, obs = mf$FPI)



bagged_m1 <- bagging(formula = FPI ~ .,data    = mf,coob    = TRUE)

bagged_m1

ntree <- 10:50

# create empty vector to store OOB RMSE values
rmse <- vector(mode = "numeric", length = length(ntree))

for (i in seq_along(ntree)) {
  # reproducibility
  set.seed(123)

  # perform bagged model
  model <- bagging(
  formula = FPI ~ .,
```

```
  data    = mf,
  coob    = TRUE,
  nbagg   = ntree[i]
)
  # get OOB error
  rmse[i] <- model$err
}

plot(ntree, rmse, type = 'l', lwd = 2)
abline(v = 25, col = "red", lty = "dashed")

# Specify 10-fold cross validation
ctrl <- trainControl(method = "cv",  number = 10)

# CV bagged model
bagged_cv <- train(FPI ~ .,data = mf,method = "treebag",trControl = ctrl,
importance = TRUE)

# assess results

bagged_cv

## Bagged CART
##
## 2051 samples
##   80 predictor
##
## No pre-processing
## Resampling: Cross-Validated (10 fold)
## Summary of sample sizes: 1846, 1845, 1847, 1845, 1846, 1847, ...
## Resampling results:
```

```
##
## RMSE      Rsquared   MAE
## 36477.25  0.8001783  24059.85

###############################################################################
############
# plot most important variables

pdf(file=paste('Desicion tree, important variables',gene,pip,pr,'pdf',sep='.'),width=4,height=3)
plot(varImp(bagged_cv), 5)
dev.off()
###############################################################################
############
#pruning the trees
spac.tree = rpart(FPI ~ ., data = mf, cp = 10^(-6))
> spac.tree = rpart(FPI ~ ., data = mf, cp = 10^(-6))
> names(spac.tree)
 [1] "frame"       "where"       "call"
 [4] "terms"       "cptable"     "method"
 [7] "parms"       "control"     "functions"
[10] "numresp"     "splits"      "variable.importance"
[13] "y"           "ordered"
spac.tree$cptable[1:10, ]
spac.tree$cptable[dim(spac.tree$cptable)[1] - 9:0, ]
cp9 = which(spac.tree$cptable[, 2] == 9)
spac.tree9 = prune(spac.tree, spac.tree$cptable[cp9, 1])
print(spac.tree9)
rpart(formula = FPI ~ ., data = mf, cp = 10^(-6))

pdf("Regression tree.pdf", width = 40, height = 15)
```

```
post(spac.tree9, file = "", title. = "Classifying TBM FPI",
bp = 18)
dev.off()
save.image('Ali_R_PhD.r')
```

Appendix B

TBM performance database, Zagros tunnel lot 2 “Chainage 0 – 5.3 km”

No.	Station	UCS (MPa)	RQD0 (%)	Average joint spacing (m)	Jc (partial rating in basic RMR)	FPI (kN/cut-ter/mm/rev)	Lithotype
1	317	30	70	0.2	15	14.68720889	Shale
2	487	30	65	0.2	15	14.68612539	
3	646	70	80	0.25	18	18.29055061	Shaly limestone
4	717	20	55	0.15	10	10.47976953	Shale
5	740	25	45	0.15	10	8.848819053	
6	845	30	65	0.2	15	15.19343494	Limy shale
7	941	30	60	0.2	15	17.16555613	
8	1021	40	55	0.15	15	16.63565324	Limy shale
9	1203	40	60	0.15	15	16.36392305	
10	1428	30	65	0.2	15	17.09344926	Limy shale
11	1487	30	70	0.25	15	16.59278401	
12	1595	20	60	0.2	10	13.21121495	Shale
13	1705	20	60	0.2	10	12.30255319	
14	1926	50	65	0.15	10	16.13399821	Limy shale
15	2019	20	50	0.15	5	13.95513577	Shale
16	2128	20	55	0.15	10	17.24044408	Shale
17	2263	90	90	0.35	15	25.58909278	Shaly limestone
18	2287	90	80	0.35	15	20.46845126	Shaly limestone
19	2329	30	60	0.2	10	14.19428571	Shale
20	2532	50	60	0.2	15	15.59130518	Limy shale
21	2656	40	55	0.2	15	16.16841004	
22	2773	30	55	0.15	10	8.906495776	Shale
23	2921	30	60	0.15	10	11.29782837	
24	3108	30	72	0.2	15	12.08617213	Limy shale
25	3304	30	70	0.2	15	11.46791122	
26	3594	30	50	0.2	15	10.57219965	Limy shale
27	3874	120	80	0.4	20	23.11377948	Limestone
28	3923	125	95	0.5	20	26.08035714	
29	4233	125	95	0.4	20	27.15992003	
30	4485	120	75	0.4	20	21.87135142	
31	4510	120	65	0.4	20	19.43755152	
32	4595	150	90	0.5	20	26.47202223	
33	4625	100	70	0.35	20	20.29435789	
34	4970	60	72	0.2	15	21.05146155	Limy shale
35	5269	60	72	0.25	15	21.77958756	Limy shale

Curriculum Vitae

7 April 1983	Born in Babol, Iran
Nationality:	Iranian – German
Marital Status:	Married

Education:

2002 – 2007	B.Sc. student in Mining Engineering-Excavation, Azad university of Tehran; south branch
2007 - 2009	M.Sc. student in Mining Engineering-Excavation, Azad university of Tehran, south branch
2011 – 2013	Ph.D. student in Mining Engineering, TU- Bergakademie Freiberg, “Institut für Bergbau” (No closure)
2013 – 2019	Ph.D. student in Geotechnical Engineering, Institute of Geotechnical Engineering (IGS), University of Stuttgart

Mitteilung des Instituts für Geotechnik der Universität Stuttgart

Mitteilungen des Baugrundinstitutes Stuttgart
(Institut für Grundbau und Bodenmechanik) der Universität Stuttgart
Hrsg.: Prof. Dr.-Ing. Dr. h.c. U. Smoltczyk

Nr. 01	Thamm, B. R.	(1974)	Anfangssetzungen und Anfangsporenwasserüberdrücke eines normalverdichteten wassergesättigten Tones
Nr. 02	Gußmann, P.	(1975)	Einheitliche Berechnung von Grundbruch und Böschungsbruch
Nr. 03	Feeser, V.	(1975)	Die Bedeutung des Kalziumkarbonats für die bodenphysikalischen Eigenschaften vom Löß
Nr. 04	Du Thin, K.	(1976)	Standsicherheit von Böschungen: Programm-Dokumentation
Nr. 05	Smoltczyk, U./ Pertschi, O./ Hilmer, K.	(1976)	Messungen an Schleusen in der UDSSR. Schleusennorm der UDSSR (SN 30365)
Nr. 06	Hilmer, K.	(1976)	Erddruck auf Schleusenkammerwände
Nr. 07	Laumans, Q.	(1977)	Verhalten einer ebenen, in Sand eingespannten Wand bei nichtlinearen Stoffeigenschaften des Bodens
Nr. 08	Lächler, W.	(1977)	Beitrag zum Problem der Teilflächenpressung bei Beton am Beispiel der Pfahlkopfanschlüsse
Nr. 09	Spotka, H.	(1977)	Einfluß der Bodenverdichtung mittels Oberflächenrüttelgeräten auf den Erddruck einer Stützwand bei Sand

Nr. 10	Schad, H.	(1979)	Nichtlineare Stoffgleichungen für Böden und ihre Verwendung bei der numerischen Analyse von Grundbauaufgaben
Nr. 11	Ulrich, G./ Gußmann, P.	(1980)	Verschiebungs- und kraftgesteuerte Plattendruckversuche auf konsolidierenden Böden. Zum Modellgesetz der Konsolidation
Nr. 12	Salden, D.	(1980)	Der Einfluß der Sohlenform auf die Traglast von Fundamenten
Nr. 13	Seeger, H.	(1980)	Beitrag zur Ermittlung des horizontalen Bettungsmoduls von Böden durch Seitendruckversuche im Bohrloch
Nr. 14	Schmidt, H.H.	(1981)	Beitrag zur Ermittlung des Erddrucks auf Stützwände bei nachgiebigem Baugrund
Nr. 15	Smoltczyk, U./ Schweikert, O.	(1981)	Vorstudie über bauliche Alternativen für Durchgangsstraßen in Siedlungen
Nr. 16	Malcharek, K./ Smoltczyk, U.	(1981)	Vergleich nationaler Richtlinien für die Berechnung von Fundamenten
Nr. 17	Gruhle, H.D.	(1981)	Das Verhalten des Baugrundes unter Einwirkung vertikal gezogener Ankerplatten als räumliches Problem des Erdwiderstandes
Nr. 18	Kobler, W.	(1982)	Untersuchungen über Böschungs- und Grundbruch bei begrenzten Lastflächen
Nr. 19	Lutz,W.	(1983)	Tragfähigkeit des geschlitzten Baugrunds neben Linienlasten
Nr. 20	Smoltczyk, U.	(1983)	Studienunterlagen "Bodenmechanik und Grundbau"; überarbeitete Ausgabe 1993
Nr. 21	Schweikert, O.	(1984)	Der Einfluß des Böschungswinkels auf die Berechnung des aktiven Erddrucks
Nr. 22	Vogt, N.	(1984)	Erdwiderstandsermittlung bei monotonen und wiederholtenWandbewegungen in Sand
Nr. 23	Buchmaier, R.	(1985)	Zur Berechnung von Konsolidationsproblemen bei nichtlinearem Stoffverhalten
Nr. 24	Schad, H./ Smoltczyk, U./ Schad, H./ Zoller, P.	(1985)	Möglichkeiten der Böschungssicherung bei kleinen Baugruben Sonderkonstruktionen der Böschungssicherung kleinen Baugruben
Nr. 25	Gußmann, P.	(1986)	Die Methode der Kinematischen Elemente

Nr. 26	Steinmann, B.	(1985)	Zum Verhalten bindiger Böden bei monotoner einaxialer Beanspruchung
Nr. 27	Lee, S.D.	(1987)	Untersuchungen zur Standsicherheit von Schlitzen im Sand neben Einzelfundamenten

Mitteilungen des Instituts für Geotechnik der Universität Stuttgart
Hrsg.: Prof. Dr.-Ing. Dr. h.c. U. Smoltczyk

Nr. 28	Kolb, H.	(1988)	Ermittlung der Sohlreibung von Gründungskörpern unter horizontalem kinematischen Zwang
Nr. 29	Ochmann, H.	(1988)	Ebene Grenzzustände von Erdböschungen im stochastischen Sicherheitskonzept
Nr. 30	Breinlinger, F.	(1989)	Bodenmechanische Stoffgleichungen bei großen Deformationen sowie Be- und Entlastungsvorgängen
Nr. 31	Smoltczyk, U./ Breinlinger, F./ Schad, H./ Wittlinger, M.	(1989)	Beitrag zur Bemessung von Tunneln in offener Bauweise
Nr. 32	Gußmann, P./ Schanz, T./ Smoltczyk, U./ Willand, E.	(1990)	Beiträge zur Anwendung der KEM (Erddruck, Grundbuch, Standsicherheit von Böschungen)
Nr. 33	Gruhle, H.D.	(1990)	Der räumliche Erdwiderstand vor überwiegend horizontal belasteten Ankerplatten
Nr. 34	Henne, J.	(1995)	Zur Bewehrung von verformten Bodenschichten durch Einsatz zugfester Geokunststoffe
Nr. 35	Wittlinger, M.	(1994)	Ebene Verformungsuntersuchungen zur Weckung des Erdwiderstandes bindiger Böden
Nr. 36	Schad, H.	(1992)	Zeit- und geschwindigkeitsabhängiges Materialverhalten in der Geotechnik – Experimentelle Erfassung und numerische Analyse
Nr. 37	Belz, I.	(1992)	Zur Ermittlung dynamischer Bodenkennwerte in situ aus der Systemantwort des Erregers

Nr. 38	Ma, J.	(1994)	Untersuchungen zur Standsicherheit der durch Stützscheiben stabilisierten Böschungen
Nr. 39	Smoltczyk, U.	(1994)	Sonderheft: 25 Jahre Lehre und Forschung in der Geotechnik
Nr. 40	Rilling, B.	(1994)	Untersuchungen zur Grenztragfähigkeit bindiger Schüttstoffe am Beispiel von Lößlehm

Mitteilungen des Instituts für Geotechnik der Universität Stuttgart
Hrsg.: Prof. Dr.-Ing. Pieter A. Vermeer

Nr. 41	Vermeer, P.A.	(1996)	Deponiebau und Geotechnik
Nr. 42	Vermeer, P.A.	(1997)	Baugruben in Locker- und Festgestein
Nr. 43	Brinkmann, C.	(1998)	Untersuchungen zum Verhalten von Dichtungsübergängen im Staudammbau
Nr. 44	Fiechter-Scharr, I.	(1998)	Beeinflussung von Erdbaustoffen durch Beimischen eines organophilen Bentonits
Nr. 45	Schanz, T.	(1998)	Zur Modellierung des mechanischen Verhaltens von Reibungsmaterialien
Nr. 46	Akinrogunde, A.E.	(1999)	Propagation of Cement Grout in Rock Discontinuities Under Injection Conditions
Nr. 47	Vogt-Breyer, C.	(1999)	Experimentelle und numerische Untersuchungen zum Tragverhalten und zur Bemessung horizontaler Schraubanker
Nr. 48	Vermeer, P.A.	(1999)	Neue Entwicklungen in der Geotechnik
Nr. 49	Marcher, T.	(2002)	Resultate eines Versuchsprogramms an Beaucaire Mergel
Nr. 50	Marcher, T.	(2003)	Nichtlokale Modellierung der Entfestigung dichter Sande und steifer Tone
Nr. 51	Ruse, N.M.	(2004)	Räumliche Betrachtung der Standsicherheit der Ortsbrust beim Tunnelvortrieb
Nr. 52	Beutinger, P.H.	(2005)	Ein geotechnischer Beitrag zur Standsicherheit mobiler Baumaschinen
Nr. 53	Wehnert, M.	(2006)	Ein Beitrag zur drainierten und undrainierten Analyse in der Geotechnik
Nr. 54	Möller, S. C	(2006)	Tunnel induced settlements and forces in linings

Nr. 55	Benz, T.	(2007)	Small-Strain Stiffness of Soils and its Numerical Consequences
Nr. 56	Abed, A.	(2008)	Numerical Modeling of Expansive Soil Behavior
Nr. 57	Hintner, J.	(2008)	Analyse der Fundamentverschiebungen infolge vertikaler und geneigter Belastung
Nr. 58	Russelli, C.	(2008)	Probabilistic Methods applied to the Bearing Capacity Problem
Nr. 59	Peña Olarte, A.A.	(2008)	Influence of Particle Shape on the Global Mechanical Response of Granular Packings: Micromechanical Investigation of the Critical State in Soil Mechanics
Nr. 60	Neher, H.P.	(2008)	Zeitabhängiges Materialverhalten und Anisotropie von weichen Böden – Theorie und Anwendung
Nr. 61	Vermeer, P.A.	(2008)	Von der Forschung zur Praxis: Symposium anlässlich des 80. Geburtstags von Prof. U. Smoltczyk
Nr. 62	Syawal, S.	(2009)	Numerical Analysis and Design Criteria of Embankments on Floating Piles
Nr. 63	Lächler, A.	(2009)	Bedeutung herstellungsbedingter Einflüsse auf das Trag- und Verformungsverhalten von Schlitzwänden
Nr. 64	Möllmann, A.	(2009)	Probabilistische Untersuchung von Hochwasserschutzdeichen mit analytischen Verfahren und der Finite-Elemente-Methode

Mitteilungen des Instituts für Geotechnik der Universität Stuttgart
Hrsg.: Prof. Dr.-Ing. habil. Ch. Moormann

Nr. 65	Moormann, Ch.	(2011)	7. Stuttgarter Geotechnik-Symposium
Nr. 66	Beuth, L.	(2012)	Formulation and Application of a Quasi-Static Material Point Method
Nr. 67	Moormann, Ch./ Huber, M./ Proske, D.	(2012)	Proceedings of the 10th International ProbabilisticWorkshop

Nr. 68	Schneider, M.	(2013)	Zur energetischen Nutzung von Tunnelbauwerken – Messungen und numerische Berechnungen am Beispiel Fasanenhoftunnel
Nr. 69	Huber, M.	(2013)	Soil variability and its consequences in geotechnical engineering
Nr. 70	Hamad, F.	(2014)	Formulation of a Dynamic Material Point Method and Applications to Soil-Water-Geotextile Systems
Nr. 71	Klein, L.	(2019)	Untersuchungen zum räumlichen aktiven Erddruck bei Baugruben mit rechteckigem Grundriss
Nr. 72	Aschrafi, J.	(2019)	Beitrag zur Seitendruckbeanspruchung von Pfählen in bindigen Böden
Nr. 73	Buhmann, P.	(2019)	Energetisches Potenzial geschlossener Tunnelgeothermiesysteme
Nr. 74	Labenski, J.	(2020)	Untersuchungen zum Einbringverhalten und dem lateralen Tragverhalten unter monotoner Einwirkung von in nichtbindigen Böden vibrierend installierten Monopiles
Nr. 75	Knopp, J.	(2020)	Verwitterungsabhängige Entfestigungsvorgänge von veränderlich festen Ton- und Tonschluffsteinen am Beispiel von Keupergesteinen
Nr. 76	Salimi A.	(2021)	Investigation and Evaluation of Rock Mass Characteristics for Development of New TBM Performance Prediction Model in Hard Rock Conditions